

**Using Mechanistic Insight to Develop Living Polymerizations for Conjugated
Homopolymers and Conjugated/Olefin Copolymers**

by

Amanda Kim Leone

A dissertation submitted in partial fulfillment
of the requirements for the degree of
Doctor of Philosophy
(Chemistry)
in the University of Michigan
2018

Doctoral Committee:

Professor Anne J. McNeil, Chair
Professor Jinsang Kim
Professor Adam J. Matzger
Professor Melanie S. Sanford

Amanda K. Leone

akleone@umich.edu

ORCID iD: 0000-0002-4020-9453

© Amanda K. Leone 2018

Dedication

To my family, teammates, and labmates

Acknowledgements

First, I would like to thank my advisor Anne McNeil. Anne, thank you for letting me join your lab, for providing me with countless examples of how to think critically about chemistry, and for teaching me how to be a better mentor. You continue to inspire me to expand my interests beyond our field, which has helped me immensely throughout my time at Michigan and I am sure it will continue in the future as well. It is evident that you genuinely care about helping me and our labmates become better chemists. I will be forever grateful for the opportunities you gave me and your helpful suggestions and edits along the way.

Thank you to my committee, Jinsang Kim, Adam Matzger, and Melanie Sanford. Professor Kim your advanced materials course taught me how to think about designing polymers for applications. We also talked in the parking lot on my way to my 3M interview; your calming presence completely eased my nerves. Professor Matzger, thank you for letting me rotate in your lab. Your guidance in lab and on grant writing has helped me many times throughout graduate school. I also appreciate that when I have stopped you in the hallway to ask about you about paramagnetic and ^{13}C NMR spectroscopy that you have taken the time to answer my questions. Professor Sanford, you are a significant reason why I came to Michigan. You are my grandPI and when I met you at St. Olaf College you helped persuade me that Michigan would be the right program for me.

I would like to thank my undergraduate advisors Bob Hanson and Dipannita Kalyani for teaching me how to do research and encouraging me to apply for graduate school. Professor

Kalyani taught me how to “make it happen,” how to work in the glovebox, and completely prepared me for graduate school. Your countless hours of teaching me to write and how to be efficient in lab shaped me into the chemist I am today.

Thank you to the McNeil lab, past and present members. Specifically, those I currently work with: (in order of where we sit) Dr. Patrick Lutz, Han Kim, Justin Trammell Harris, Matthew Hannigan, Dr. Danielle Fagnani, Takunda Chazovachii, Oscar Mota, Kikel Sekoni, Bri Barbu, Emily Mueller, and Tomo Kubo. I love going to work every day and that is because of you. Special thank you to the Trap Room™ for entertaining (and distracting) me.

I would also like to thank members from other labs with whom I have had the pleasure of sharing countless chemistry and science conversations. Most notably, Eric Dahl, Nomaan Rezayee, Gesine Viets, Devin Ferguson, and Alyssa Miller. Every conversation helped me become a better scientist.

I would like to thank all of my coaches and teammates for teaching me how to collaborate, to learn from failures, and to try again. These have been some of the most important skills to have in graduate school.

Lastly, a special thank you to my family: Bob, Nora, Gina, and Janice. Words cannot describe your love and support.

Table of Contents

Dedication	ii
Acknowledgements	iii
List of Figures	viii
List of Tables	xxxi
List of Charts	xxxvi
List of Schemes	xxxvii
List of Appendices	xl
Abstract	xliii
Chapter 1 : Introduction – Matchmaking in Catalyst-Transfer Polymerization: Optimizing Catalysts based on Mechanistic Insight	1
1.1 Introduction	1
1.2 Ancillary Ligand	4
1.3 Reactive Ligand	10
1.4 Transition Metal	14
1.5 On Using Model Systems	15
1.6 Conclusion	17
1.7 Outlook	18
1.8 References	19

Chapter 2 : Ring-Walking in Catalyst-Transfer Polymerization	32
2.1 Introduction	32
2.2 Results and Discussion.....	35
2.3 Conclusion.....	41
2.4 Implications of These Discoveries – Developing Methods to Synthesize High-Performing Conjugated Polymers via CTP	42
2.5 References	42
Chapter 3 : Mechanistic Insight into Thiophene Catalyst-Transfer Polymerization Mediated by Nickel Diimine Catalysts	50
3.1 Introduction	50
3.2 Results and Discussion.....	53
3.2.1 Evaluating Ni Diimines for 3HT Polymerization.....	53
3.2.2 Chain-Growth Synthesis of P3HT with Precatalyst C ₃ Me.....	55
3.2.3 Propagation Mechanism	57
3.2.4 Fate of Catalysts during Propagation	57
3.2.5 Fate of Catalysts after Dissociation.....	59
3.3 Conclusion.....	62
3.4 Implications of These Discoveries – Synthesizing Thiophene/Olefin Block Copolymers.	62
3.5 References	64
Chapter 4 : Progress Towards Thiophene/Olefin Block Copolymers using an in-situ Ligand- Exchange Approach	71
4.1 Introduction	71
4.2 Results and Discussion.....	73

4.3 References	80
Chapter 5 : Outlook - The History of Palladium-catalyzed Cross-couplings Should Inspire the Future of Catalyst-Transfer Polymerization	84
5.1 Introduction	84
5.2 Mechanism.	86
5.3 Why CTP for organic electronics?	87
5.4 Why Palladium?	90
5.5 Identifying new catalysts.....	93
5.6 The most popular Pd-CTP precatalyst.	95
5.7 The future: Buchwald ligands.	97
5.8 The future: N-Heterocyclic Carbenes (NHCs).....	105
5.9 Reflection.	110
5.10 References.	111
Appendices.....	133

List of Figures

Figure 2-1. Percent ring-walking (% RW) versus degree of polymerization (m) for each catalyst and polymer.	38
Figure 2-2. (Top) Reaction conditions for 3DT end-capping experiments, involving x iterations of capping/scavenger reagents over y hours. (Bottom) MALDI-TOF/MS data for 3DT polymerization followed by end-capping. ⁴⁵ The observed and predicted m/z values for each labeled peak can be found in Appendix 1.	39
Figure 2-3. (Top) Reaction conditions for BHP end-capping experiments over y hours. (Bottom) MALDI-TOF/MS data for BHP polymerization followed by end-capping. ⁴⁵ The observed and predicted m/z values for each labeled peak can be found in Appendix 1.	41
Figure 3-1. (A) Plot of M_n (●) and D (○) versus percent conversion (theo $M_n = 13.3$ kDa). (B) Plot of M_n (●) and D (○) versus monomer/precatalyst ratio (50/1, 80/1, 125/1; monomer conversion >80%). (C, D) MALDI-TOF-MS spectra at 19% conversion. (Note that all polymerizations were run under the optimized conditions with precatalyst $C3_{Me}$ in THF at 0 °C, [monomer] = 10 mM, and [catalyst] = 0.08–0.19 mM.).....	56
Figure 3-2. (A) GPC traces from the initial (solid line) and final (dashed line) aliquot taken during the chain-extension experiments. (B) MALDI-TOF-MS spectrum of end-capping experiments with added vinyl Grignard. All polymerizations were run at 0 °C.	59
Figure 3-3. MALDI-TOF-MS data for polymerizations run in the presence of monomer analogue added either (A) before initiation or (B) after initiation.	61

Figure 4-1. (Top) Reaction conditions for 3DT polymerization followed by end-capping experiments. (Bottom) MALDI-TOF/MS data for 3DT polymerization followed by end-capping. The full MALDI-TOF/MS spectra can be found in Appendix 3.²⁵ 74

Figure 4-2. (left) MALDI-TOF/MS data and (right) GPC traces for 3DT polymerization followed by end-capping via a ligand-switched precatalyst. All M_n are reported in kg/mol. The full MALDI-TOF/MS spectra can be found in Appendix 3.^{25,26} 77

Figure 4-3. (A) Reaction conditions for ligand-switch copolymerization attempt. (B) GPC trace of the poly(olefin) macroinitiator before and after ligand-switch. (C) GPC traces showing the RI and UV curves of the final polymers. 80

Figure A1-1. ¹H and ¹³C NMR spectra for S1. ¹H NMR (400 MHz, CDCl₃) δ 6.82 (s, 4H), 3.90 (t, J = 6.6 Hz, 4H), 1.75 (dt, J = 14.7, 6.6 Hz, 4H), 1.50–1.39 (m, 4H), 1.38–1.26 (m, 8H), 0.98–0.80 (m, 6H). ¹³C NMR (176 MHz, CDCl₃) δ 153.34, 115.53, 68.80, 31.77, 29.53, 25.90, 22.77, 14.19. 139

Figure A1-2. ¹H and ¹³C NMR spectra for S2. ¹H NMR (500 MHz, CDCl₃) δ 7.08 (s, 2H), 3.95 (t, J = 6.5 Hz, 4H), 1.80 (dq, J = 8.3, 6.5 Hz, 4H), 1.52–1.43 (m, 4H), 1.38–1.31 (m, 8H), 0.95–0.87 (m, 6H). ¹³C NMR (176 MHz, CDCl₃) δ 150.22, 118.62, 111.28, 70.46, 31.63, 29.23, 25.76, 22.72, 14.16..... 140

Figure A1-3. GPC traces from Br/H–P3DT and end-capped–P3DT (left = zoomed, right = full GPC trace of the set of samples). Note that residual monomer elutes from 20.5–22 min, PhMe elutes at 23.1 min and BHT elutes at 23.8 min. 146

Figure A1-4. MALDI-TOF/MS spectra from Br/H–P3DT, end-capped–P3DT, and Br/H–P3DT combined with end-capped–P3DT in a 1:1 (wt/wt) ratio. Calculated using an average method, at signal-to-noise = 2. The degree of polymerization shown is 11. 147

Figure A1-5. ^1H NMR spectrum of Br/H-P3DT (relaxation delay = 3s). ^1H NMR (500 MHz, CDCl_3-d) δ 7.01–6.76 (m, 1H), 2.92–2.42 (m, 2H), 1.83–1.56 (m, 2H), 1.48–1.07 (m, 9H), 0.88 (t, J = 6.5 Hz, 3H). 148

Figure A1-6. ^1H NMR spectrum of end-capped-P3DT (relaxation delay = 3s). The ratios of each polymer are predicted based on MALDI-TOF/MS data (see above). ^1H NMR (500 MHz, CDCl_3-d) δ 7.39–7.31 (m, 0.25H), 7.25–7.19 (m, 0.23H), 7.06–6.77 (m, 1H), 3.54–3.44 (m, 0.25H), 2.93–2.52 (m, 2H), 2.44–2.34 (m, 0.36H), 1.80–1.59 (m, 2H), 1.46–1.17 (m, 8H), 0.87 (t, J = 6.4 Hz, 2H)..... 149

Figure A1-7. ^1H NMR spectrum of Br/H-P3DT combined with end-capped-P3DT in a 1:1 (wt/wt) ratio. The ratios of each polymer are predicted in accordance to diluting the end-capped-P3DT (ratios determined by “homopolymer” MALDI-TOF/MS, see above) with Br/H-P3DT. Relaxation delay = 3s. ^1H NMR (500 MHz, CDCl_3-d) δ 7.38–7.32 (m, 0.13H), 7.25–7.21 (m, 0.13H), 7.07–6.75 (m, 1H), 3.52–3.46 (m, 0.13H), 2.94–2.45 (m, 2H), 2.45–2.33 (m, 0.13H), 1.82–1.56 (m, 2H), 1.47–1.07 (m, 8H), 0.88 (t, J = 6.4 Hz, 2H)..... 150

Figure A1-8. (top) GPC trace of pre-precipitated P3DT synthesized via $\text{Ni}(\text{dppp})\text{Cl}_2$. M_n = 7.81 kg/mol, Đ = 1.12. (bottom) MALDI-TOF/MS spectrum of pre-precipitated P3DT synthesized via $\text{Ni}(\text{dppp})\text{Cl}_2$. Calculated using an exact method, nd = not detected at signal-to-noise = 1. The degree of polymerization shown is 23. 152

Figure A1-9. MALDI-TOF/MS spectra from end-capping control reactions for P3DT and $\text{Ni}(\text{IPr})(\text{PPh}_3)\text{Cl}_2$. Calculated using an exact mass method, nd = not detected at signal-to-noise = 1. The degree of polymerizations shown are 23, 24, 23 from the top figure to the bottom one. 156

Figure A1-10. MALDI-TOF/MS spectra from end-capping control reactions for P3DT and Pd(IPr)(3-Clpy)Cl ₂ . Calculated using an exact mass method, signal-to-noise = 1. The degree of polymerization shown is 23.	157
Figure A1-11. MALDI-TOF/MS spectra from end-capping control reactions for P3DT and Ni(dppp)Cl ₂ . Calculated using an average mass method, signal-to-noise = 2. The degree of polymerization shown is 16.	159
Figure A1-12. GPC traces from added Br/H-P3DT (left = zoomed, right = full GPC trace of the set of samples). Note that residual monomer elute from 20.5–22 min, PhMe elutes at 23.1 min and BHT elutes at 23.8 min. Mn = 4.09 kg/mol, Đ = 1.21.	165
Figure A1-13. GPC traces from P3HT (before end-capping cross-over experiments), end-capping cross-over experiment (ec), and end-capping cross-over control (only capping agent) experiments via Ni(IPr)(PPh ₃)Cl ₂ . (left = zoomed, right = full GPC trace of the set of samples). Note that M(0) scavenging agent and residual monomer elute from 20.5–22 min, PhMe elutes at 23.1 min and BHT elutes at 23.8 min.	165
Figure A1-14. GPC traces from P3HT (before end-capping cross-over experiments), end-capping cross-over experiment (ec), and end-capping cross-over control (only capping agent) experiments via Pd(IPr)(3-Clpy)Cl ₂ . (left = zoomed, right = full GPC trace of the set of samples). Note that M(0) scavenging agent and residual monomer elute from 20.5–22 min, PhMe elutes at 23.1 min and BHT elutes at 23.8 min.	166
Figure A1-15. GPC traces from P3HT (before end-capping cross-over experiments), end-capping cross-over experiment (ec), and end-capping cross-over control (only capping agent) experiments via Ni(dppp)Cl ₂ . (left = zoomed, right = full GPC trace of the set of samples). Note	

that M(0) scavenging agent and residual monomer elute from 20.5–22 min, PhMe elutes at 23.1 min and BHT elutes at 23.8 min. 166

Figure A1-16. MALDI-TOF/MS traces from the added Br/H–P3DT. Values calculated using average mass method at signal-to-noise = 1. The degree of polymerization shown is 13..... 167

Figure A1-17. MALDI-TOF/MS traces from P3HT macroinitiator (before end-capping), end-capping cross-over experiment, and end-capping cross-over control (only capping agent) experiments for Ni(IPr)(PPh₃)Cl₂. Values calculated using average mass method, nd = not detected at signal-to-noise = 1. The degrees of polymerization shown are 20 and 21 for P3HT and 15 for P3DT..... 168

Figure A1-18. MALDI-TOF/MS traces from P3HT macroinitiator (before end-capping), end-capping cross-over experiment, and end-capping cross-over control (only capping agent) experiments for Pd(IPr)(3-Clpy)Cl₂. Values calculated using average mass method at signal-to-noise = 1. The degrees of polymerization shown are 18 and 19 for P3HT and 13 for P3DT..... 169

Figure A1-19. MALDI-TOF/MS traces from P3HT macroinitiator (before end-capping), end-capping cross-over experiment, and end-capping cross-over control (only capping agent) experiments for Ni(dppp)Cl₂. Values calculated using average mass method, nd = not detected at signal-to-noise = 1. The degrees of polymerization shown are (left) 17 and 18 for P3HT and 13 for P3DT and (right) 28 and 29 for P3HT and 21 for P3DT. 170

Figure A1-20. GPC traces from P3DT (before end-capping), end-capping experiment, and end-capping control (only capping agent) experiments for Ni(IPr)(PPh₃)Cl₂ and P3DT (left = zoomed, right = full GPC trace from Run 1). 175

Figure A1-21. MALDI-TOF/MS traces from P3DT (before end-capping t = 5 min), P3DT (quenched at the final end-capping experiment quench t = 125 min), and end-capping control

(only capping agent) experiments for Ni(IPr)(PPh₃)Cl₂ and P3DT. Values calculated using average mass method, signal-to-noise = 1. The degree of polymerization shown is 24..... 176

Figure A1-22. MALDI-TOF/MS traces from end-capping experiments (ec1 and ec2) for Ni(IPr)(PPh₃)Cl₂ and P3DT. Values calculated using average mass method, signal-to-noise = 1. The degree of polymerization shown is 24 (left) and 25 (right). 177

Figure A1-23. GPC traces from P3DT (before end-capping), end-capping experiment (ec), and end-capping control (only capping agent) experiments for Pd(IPr)(3-Clpy)Cl₂ and P3DT t = 18 h. (Left = zoomed, right = full GPC trace from Run 1). Note that M(0) scavenging agent and residual monomer elute from 20.5–22 min, PhMe elutes at 23.1 min and BHT elutes at 23.8 min. 181

Figure A1-24. MALDI-TOF/MS traces from P3DT (before end-capping), end-capping experiment, and end-capping control (only capping agent) experiments for Pd(IPr)(3-Clpy)Cl₂ and P3DT (t = 18 h) from Run 1. Values calculated using average mass method, nd = not detected at signal-to-noise = 2. The degree of polymerization shown is 23..... 182

Figure A1-25. GPC traces from the control, end-capping control, and end-capping experiments for Pd(IPr)(3-Clpy)Cl₂ and P3DT. (Left = zoomed, right = full GPC trace from Run 1)..... 187

Figure A1-26. MALDI-TOF/MS traces from P3DT (before end-capping) and end-capping control (only capping agent) experiments for Pd(IPr)(3-Clpy)Cl₂ and P3DT from Run 1. Values calculated using an average mass method, nd = not detected at signal-to-noise = 2. The degree of polymerization shown is 18. 188

Figure A1-27. MALDI-TOF/MS traces from end-capping experiments (ec1, ec2, and ec3) for Pd(IPr)(3-Clpy)Cl₂ and P3DT from Run 1. Values calculated using an average mass method, signal-to-noise = 2. The degree of polymerization shown is 18. 189

Figure A1-28. MALDI-TOF/MS traces from end-capping experiments (ec4, ec5, ec6, and ec7) for Pd(IPr)(3-Clpy)Cl₂ and P3DT from Run 1. Values calculated using an average mass method, nd = not detected at signal-to-noise = 2. The degree of polymerization shown is 18. 190

Figure A1-29. GPC traces of P3DT (before end-capping), end-capping experiment, and end-capping control (only capping agent) (t = 1 h) experiments for Ni(dppp)Cl₂ and P3DT. (Left = zoomed, right = full GPC trace from Run 1). 193

Figure A1-30. MALDI-TOF/MS traces from P3DT (before end-capping), end-capping experiment, and end-capping control (only capping agent) experiments (t = 1 h) for Ni(dppp)Cl₂ and P3DT from Run 1. Values calculated using an average mass method, signal-to-noise = 2. The degree of polymerization shown is 15. 194

Figure A1-31. GPC traces from P3DT (before end-capping), end-capping experiment, and end-capping control (only capping agent) experiments (t = 18 h) for Ni(dppp)Cl₂ and P3DT. (Left = zoomed, right = full GPC trace from Run 1). 196

Figure A1-32. MALDI-TOF/MS traces from P3DT (before end-capping), end-capping experiment, and end-capping control (only capping agent) experiments (t = 18 h) for Ni(dppp)Cl₂ and P3DT from Run 1. Values calculated using average mass method, signal-to-noise = 2. The degree of polymerization shown is 27. 197

Figure A1-33. GPC traces from P3DT (before end-capping), end-capping control (only capping agent), end-capping (ec), and end-capping with hexane (ec (hex)) experiments for Ni(IPr)(PPh₃)Cl₂. (Left = zoomed, right = full GPC trace). Note that M(0) scavenging agent and residual monomer elute from 20.5–22 min, PhMe elutes at 23.1 min and BHT elutes at 23.8 min. 203

Figure A1-34. GPC traces from P3DT (before end-capping), end-capping control (only capping agent), end-capping (ec), and end-capping with hexane (ec (hex)) experiments for Pd(IPr)(3-Clpy)Cl₂. (Left = zoomed, right = full GPC trace). Note that M(0) scavenging agent and residual monomer elute from 20.5–22 min, PhMe elutes at 23.1 min and BHT elutes at 23.8 min. 203

Figure A1-35. GPC traces from P3DT (before end-capping), end-capping control (only capping agent), end-capping (ec), and end-capping with hexane (ec (hex)) experiments for Ni(dppp)Cl₂. (Left = zoomed, right = full GPC trace). Note that M(0) scavenging agent and residual monomer elute from 20.5–22 min, PhMe elutes at 23.1 min and BHT elutes at 23.8 min..... 204

Figure A1-36. MALDI-TOF/MS traces from P3DT (before end-capping), end-capping experiments (THF alone, and THF & hexanes), and end-capping control (only capping agent) experiments for Ni(IPr)(PPh₃)Cl₂. Values calculated using average mass method signal-to-noise = 2. The repeat unit shown is 22. (Note that to reach complete tol/tol-end capped polymers 2 iterations of CIMg–tol and M(0) scavenger should be used)..... 205

Figure A1-37. MALDI-TOF/MS traces from P3DT (before end-capping), end-capping experiments (THF alone, and THF & hexanes), and end-capping control (only capping agent) experiments for Pd(IPr)(3-Clpy)Cl₂. Values calculated using average mass method signal-to-noise = 2. The repeat unit shown is 19. (Note that to reach complete tol/tol-end capped polymers 6 iterations of CIMg–tol and M(0) scavenger should be used)..... 206

Figure A1-38. MALDI-TOF/MS traces from P3DT (before end-capping), end-capping experiments (THF alone, and THF & hexanes), and end-capping control (only capping agent) experiments for Ni(dppp)Cl₂. Values calculated using average mass method signal-to-noise = 2. The repeat unit shown is 14. 207

Figure A1-39. GPC traces from the polymerization of 3-decylthiophene at rt via Ni(IPr)(PPh ₃)Cl ₂ . (Left = zoomed, right = full GPC trace from Run 1).....	211
Figure A1-40. MALDI-TOF/MS traces from the polymerization of 3-decylthiophene at rt via Ni(IPr)(PPh ₃)Cl ₂ from Run 1. Values calculated using an average mass method, signal-to-noise = 2. The degree of polymerization shown is 23.	212
Figure A1-41. ¹ H NMR spectra from the polymerization of 3-decylthiophene at rt via Ni(IPr)(PPh ₃)Cl ₂ after 20 h (relaxation delay = 2 s). ¹ H NMR (700 MHz, CDCl ₃) δ 8.31 (s, 1H), 8.28 (s, 1H), 7.70–7.63 (m, 2H), 7.45–7.40 (m, 3H), 7.14–6.63 (multiple peaks, 23H), 6.29 (s, 1H), 6.23 (s, 1H), 4.06–4.01 (m, 2H), 3.59–3.54 (m, 2H), 3.49 (s, 1H), 2.95–2.15 (multiple peaks, 44H), 2.01–1.50 (multiple peaks, 41H), 1.50–1.01 (multiple peaks, 196H), 1.01–0.69 (multiple peaks, 45H).....	213
Figure A1-42. GPC traces from Br/H–PBHP and end-capped–PBHP (left = zoomed, right = full GPC trace of the set of samples). Note that residual monomer elutes from 20.5–22 min, PhMe elutes at 23.1 min and BHT elutes at 23.8 min.	219
Figure A1-43. MALDI-TOF/MS spectra from Br/H–PBHP, end-capped–PBHP, and Br/H–PBHP combined with end-capped–PBHP in a 1:1 wt/wt ratio. Calculated using an average method, at signal-to-noise = 2. The degree of polymerization shown is 16.	220
Figure A1-44. ¹ H NMR spectrum of Br/H–PBHP (relaxation delay = 3s). ¹ H NMR (500 MHz, CDCl ₃ - <i>d</i>) δ 7.18–6.78 (m, 1H), 4.10–3.68 (m, 2H), 1.91–1.59 (m, 2H), 1.51–1.02 (m, 4H), 1.02–0.65 (m, 2H).....	221
Figure A1-45. ¹ H NMR spectrum of end-capped–PBHP (relaxation delay = 3s). ¹ H NMR (500 MHz, CDCl ₃ - <i>d</i>) δ 7.54 (d, <i>J</i> = 7.5 Hz, 0.14H), 7.24 (d, <i>J</i> = 7.5 Hz, 0.14H), 7.15–6.93 (m, 1H),	

3.91 (q, $J = 5.8$ Hz, 2H), 2.41 (s, 0.21H), 1.83–1.58 (m, 2H), 1.45–1.02 (m, 5H), 0.86 (t, $J = 5.8$ Hz, 3H).....	222
Figure A1-46. ^1H NMR spectrum of Br/H–PBHP combined with end-capped–PBHP in a 1:1 (wt/wt) ratio (relaxation delay = 3s). ^1H NMR (500 MHz, CDCl_3-d) δ 7.54 (d, $J = 7.6$ Hz, 0.7H), 7.23 (apparent s, 0.7H), 7.18–6.78 (m, 1H), 3.91 (q, $J = 5.9, 5.2$ Hz, wH), 2.41 (s, 0.12H), 1.90–1.57 (m, 2H), 1.45–1.07 (m, 4H), 0.87 (t, $J = 6.4$ Hz, 2H).....	223
Figure A1-47. GPC trace of pre-precipitated PBHP synthesized via $\text{Ni}(\text{dppp})\text{Cl}_2$. $M_n = 5.13$ kg/mol, $\text{Đ} = 1.24$. (Left = zoomed, right = full GPC trace from the same sample).....	226
Figure A1-48. MALDI-TOF/MS spectrum of crude PBHP synthesized via $\text{Ni}(\text{dppp})\text{Cl}_2$. The 0.84 fractional corresponds to an unknown impurity. Values calculated using an average mass method, signal-to-noise = 1. The degree of polymerization shown is 16.	226
Figure A1-49. MALDI-TOF/MS spectra from end-capping control reactions for PBHP using $\text{Ni}(\text{IPr})(\text{PPh}_3)\text{Cl}_2$. The 0.84 fractional corresponds to an unknown impurity. Values calculated using an average mass method, signal-to-noise = 2. The degree of polymerization shown is 16.	230
Figure A1-50. MALDI-TOF/MS spectra from end-capping control reactions for PHBP and $\text{Pd}(\text{IPr})(3\text{Clpy})\text{Cl}_2$. Values calculated using average mass method, nd = not detected at signal-to-noise = 1. The degree of polymerization shown is 16.	233
Figure A1-51. MALDI-TOF/MS spectra from end-capping control experiments for PBHP and $\text{Ni}(\text{dppp})\text{Cl}_2$. Values calculated using an average mass method, nd = not detected at signal-to-noise = 1. The degree of polymerization shown is 16.	236

Figure A1-52. GPC traces from added Br/H–PBHP (left = zoomed, right = full GPC trace of the set of samples). Note that residual monomer elutes from 20.5–22 min, PhMe elutes at 23.1 min and BHT elutes at 23.8 min. 241

Figure A1-53. GPC traces from PBBP (before end-capping cross-over experiments), end-capping cross-over experiment (ec), and end-capping cross-over control (only capping agent) experiments via Ni(IPr)(PPh₃)Cl₂. Note that M(0) scavenging agent and residual monomer elute from 20.5–22 min, PhMe elutes at 23.1 min and BHT elutes at 23.8 min. 241

Figure A1-54. MALDI-TOF/MS traces from added Br/H–PBHP added polymer in cross-over experiment. Values calculated using average mass method at signal-to-noise = 2. The repeat unit shown is 21. 242

Figure A1-55. MALDI-TOF/MS traces from PBBP macroinitiator (before end-capping), end-capping cross-over experiment, and end-capping cross-over control (only capping agent) experiments for Ni(IPr)(PPh₃)Cl₂. Values calculated using average mass method at signal-to-noise = 2. The repeat unit shown is 26 for PBBP and 21 for PBHP..... 243

Figure A1-56. GPC traces from PBHP (before end-capping), end-capping experiment, and end-capping control (only capping agent) experiments for Ni(IPr)(PPh₃)Cl₂ and PBHP (t = 2 h). (Left = zoomed, right = full GPC trace from Run 1). 247

Figure A1-57. MALDI-TOF/MS traces from PBHP (before end-capping), end-capping experiment, and end-capping control (only capping agent) experiments (t = 2 h) for Ni(IPr)(PPh₃)Cl₂ and PBHP from Run 2. Values calculated using average mass method, signal-to-noise = 1. The degree of polymerization shown is 23. 248

Figure A1-58. GPC traces from PBHP (before end-capping), end-capping experiment, and end-capping control (only capping agent) experiments (t = 20 h) for Ni(IPr)(PPh₃)Cl₂ and PBHP. (Left = zoomed, right = full GPC trace from Run 2)..... 249

Figure A1-59. MALDI-TOF/MS traces from PBHP (before end-capping), end-capping experiment, and end-capping control (only capping agent) experiments (t = 20 h) for Ni(IPr)(PPh₃)Cl₂ and PBHP from Run 2. Values calculated using average mass method, nd = not detected at signal-to-noise = 1. The degree of polymerization shown is 23..... 250

Figure A1-60. GPC traces from PBHP (before end-capping), end-capping experiment (ec), and end-capping control (only capping agent) experiments for Pd(IPr)(3-Clpy)Cl₂ and PBHP. (Left = zoomed, right = full GPC trace from Run 2). 253

Figure A1-61. MALDI-TOF/MS traces from PBHP (before end-capping) and end-capping control (only capping agent) experiments for Pd(IPr)(3-Clpy)Cl₂ and PBHP from Run 2. Values calculated using an average mass method, nd = not detected at signal-to-noise = 2. The degree of polymerization shown is 17. 254

Figure A1-62. MALDI-TOF/MS traces from the end-capping experiment for Pd(IPr)(3-Clpy)Cl₂ and PBHP. The zoomed MALDI-TOF/MS traces represent low–high molecular weight peaks to show a distribution of *m* from Run 2. Values calculated using average mass method, nd = not detected at signal-to-noise = 1. The degrees of polymerization shown are 13, 17, and 21 (from left to right). 255

Figure A1-63. GPC traces from PBHP (before end-capping), end-capping experiment, and end-capping control (only capping agent) experiments for Ni(dppp)Cl₂ and PBHP. (Left = zoomed, right = full GPC trace from Run 2)..... 259

Figure A1-64. MALDI-TOF/MS traces from PBHP (before end-capping), end-capping experiment, and end-capping control (only capping agent) experiments for Ni(dppp)Cl₂ and PBHP from Run 2. Values calculated using average mass method signal-to-noise = 2. The degree of polymerization shown is 21..... 260

Figure A1-65. GPC traces from PBHP (before end-capping), end-capping control (only capping agent), end-capping (ec), and end-capping with hexane (ec (hex)) experiments for Ni(IPr)(PPh₃)Cl₂. (Left = zoomed, right = full GPC trace). Note that M(0) scavenging agent and residual monomer elute from 20.5–22 min, PhMe elutes at 23.1 min and BHT elutes at 23.8 min. 266

Figure A1-66. GPC traces from PBHP (before end-capping), end-capping control (only capping agent), end-capping (ec), and end-capping with hexane (ec (hex)) experiments for Pd(IPr)(3-Clpy)Cl₂. (Left = zoomed, right = full GPC trace). Note that M(0) scavenging agent and residual monomer elute from 20.5–22 min, PhMe elutes at 23.1 min and BHT elutes at 23.8 min. 266

Figure A1-67. GPC traces from PBBP (before end-capping), end-capping control (only capping agent), end-capping (ec), and end-capping with hexane (ec (hex)) experiments for Ni(dppp)Cl₂. (Left = zoomed, right = full GPC trace). Note that M(0) scavenging agent and residual monomer elute from 20.5–22 min, PhMe elutes at 23.1 min and BHT elutes at 23.8 min..... 267

Figure A1-68. MALDI-TOF/MS traces from PBHP (before end-capping), end-capping experiments (THF alone, and THF & hexanes), and end-capping control (only capping agent) experiments for Ni(IPr)(PPh₃)Cl₂ and PBHP. Values calculated using average mass method signal-to-noise = 2. The degree of polymerization shown is 20..... 268

Figure A1-69. MALDI-TOF/MS traces from PBHP (before end-capping), end-capping experiments (THF alone, and THF & hexanes), and end-capping control (only capping agent)

experiments for Pd(IPr)(3-Clpy)Cl ₂ and PBHP. Values calculated using an average mass method signal-to-noise = 2. The degree of polymerization shown is 15.....	269
Figure A1-70. MALDI-TOF/MS traces from PBBP (before end-capping), end-capping experiments (THF alone, and THF & hexanes), and end-capping control (only capping agent) experiments for Ni(dppp)Cl ₂ and PBBP. Values calculated using an average mass method signal-to-noise = 2. The degree of polymerization shown is 26.....	270
Figure A1-71. GPC traces from PBHP t = 90 min and t = 6.5 h via Pd(IPr)(3-Clpy)Cl ₂ . (Left = zoomed, right = full GPC trace from the same experiment).....	273
Figure A1-72. MALDI-TOF/MS traces from PBHP t = 90 min (left) and t = 6.5 h (right) via Pd(IPr)(3-Clpy)Cl ₂ . Values calculated using an average mass method signal-to-noise = 3.....	274
Figure A1-73. ¹ H NMR spectrum of PBHP generated via Pd(IPr)(3-Clpy)Cl ₂ (t = 6.5 h) relaxation delay = 2 s. ¹ H NMR (700 MHz, CDCl ₃) δ 7.51 (d, J = 6.5 Hz, 1H), 7.38 (d, J = 6.5 Hz, 1H), 7.31 (d, J = 6.5 Hz, 1H), 7.24–6.77 (multiple peaks, 45H), 6.43 (s, 1H), 4.07–3.80 (multiple peaks, 68H), 2.22 (s, 1H), 2.18 (s, 1H), 1.9–1.57 (multiple peaks, 73H), 1.56–1.09 (multiple peaks, 209H), 1.05–0.73 (multiple peaks, 103H).....	275
Figure A1-74. (Top) Reaction conditions for 3DT end-capping experiments, involving x iterations of capping/scavenger reagents over y hours. (Bottom) MALDI-TOF/MS data for 3DT polymerization followed by end-capping. (Values calculated using an average mass method signal-to-noise = 1 or 2).....	280
Figure A1-75. (Top) Reaction conditions for BHP end-capping experiments over y hours. (Bottom) MALDI-TOF/MS data for BHP polymerization followed by end-capping. (Values calculated using an average mass method signal-to-noise = 1 or 2. In the Ni(IPr) plot Br/Br was not detected).....	280

Figure A2-1. ^1H and ^{13}C NMR Spectra of S1. ^1H NMR (700 MHz, CDCl_3) δ 7.87 (d, $J = 8.2$ Hz, 2H), 7.54 (d, $J = 7.7$ Hz, 2H), 7.37 (t, $J = 7.7$ Hz, 2H), 7.25–7.20 (m, 4H), 6.94 (d, $J = 7.3$ Hz, 2H), 6.83 (d, $J = 7.3$ Hz, 2H), 1.39 (s, 18H). ^{13}C NMR (176 MHz, CDCl_3) δ 159.78, 150.50, 141.75, 139.27, 131.15, 129.14, 128.65, 127.64, 126.76, 126.66, 124.50, 123.86, 118.95, 35.48, 29.69..... 296

Figure A2-2. ^1H NMR Spectrum of C1_{tBu} . ^1H NMR (400 MHz, CD_2Cl_2 , rd = 0.005 s, at = 0.05 s) δ 22.83 (s, 1H), 21.82 (s, 1H), 18.46 (s, 1H), 12.14 (d, $J = 7.5$ Hz, 1H), 6.92–6.85 (m, 1H), 3.20 (s, 9H), 1.45 (s, 9H), 0.41 (broad s, 1H), –13.77 (s, 1H). Unaccounted for hydrogens (8 H) due to peak broadening..... 297

Figure A2-3. ^1H and ^{13}C NMR Spectra of S2. ^1H NMR (400 MHz, CDCl_3) δ 7.87 (d, $J = 8.3$ Hz, 2H), 7.38 (t, $J = 7.3$, 2H), 6.96 (s, 4H), 6.75 (d, $J = 7.3$ Hz, 2H), 2.36 (s, 6H), 2.07 (s, 12H). ^{13}C NMR (176 MHz, CDCl_3) δ 161.01, 146.73, 140.50, 132.76, 130.96, 129.67, 128.88, 128.72, 128.19, 124.55, 122.44, 20.92, 17.70..... 298

Figure A2-4. ^1H NMR Spectrum of C2. ^1H NMR (400 MHz, CD_2Cl_2 , rd = 0.005 s, at = 0.05 s) δ 33.77 (s, 6H), 27.54 (s, 12H), 24.49 (s, 4H), 23.93 (s, 2H), 17.35 (d, $J = 7.9$ Hz, 2H), 5.85 (s, 2H). 299

Figure A2-5. ^1H and ^{13}C NMR Spectra of S3. ^1H NMR (500 MHz, CDCl_3) δ 7.17 (s, 1H), 6.85 (dd, $J = 7.9, 1.9$ Hz, 1H), 6.80 (s, 2H), 6.47 (d, $J = 7.9$ Hz, 1H), 4.35 (q, $J = 7.3$ Hz, 1H), 3.12 (s, 2H), 2.30 (s, 3H), 2.19 (overlapping peaks, 9H), 1.61 (d, $J = 7.3$ Hz, 3H). ^{13}C NMR (126 MHz, CDCl_3) δ 142.48, 137.63, 136.58, 135.90, 130.75, 130.07, 128.43, 127.50, 127.24, 115.98, 36.17, 21.15, 21.03, 20.83, 17.43..... 300

Figure A2-6. ^1H and ^{13}C NMR spectra of S4. ^1H NMR (500 MHz, CDCl_3) δ 7.61 (d, $J = 8.2$ Hz, 2H), 7.47 (s, 2H), 7.18 (d, $J = 7.7$ Hz, 2H), 7.10 (t, $J = 7.7$ Hz, 2H), 6.90 (d, $J = 7.8$ Hz, 2H),

6.69 (d, $J = 7.2$ Hz, 2H), 5.97 (br s, 2H), 5.39 (br s, 2H), 4.60 (q, $J = 7.4$ Hz, 2H), 2.52 (s, 6H), 2.41 (br s 6H), 1.62 (br s, 6H), 1.58 (d, $J = 7.4$ Hz, 6H), 0.97 (s, 6H). ^{13}C NMR (126 MHz, CDCl_3) δ 161.00, 148.78, 141.11, 138.97, 136.22 (br), 134.46, 133.56, 132.70, 130.25, 129.80, 129.48, 128.78 (br), 127.85, 127.28, 126.57, 122.40, 117.77, 36.74, 21.84, 21.65 (br), 19.80, 16.80..... 301

Figure A2-7. ^1H NMR Spectrum of C3_{Me} . ^1H NMR (500 MHz CD_2Cl_2) δ 35.53 (s, 6H), 24.88 (s, 2H), 23.17 (s, 2H), 21.45 (br s, 2H), 20.14 (s, 2H), 14.03 (s, 2H), 6.27 (s, 2H), 4.82 (br s, 6H), 1.99 (s, 6H), 1.44 (s, 2H) 0.87 (s, 2H), 0.45 (s, 6H), -16.43 (br s, 2H). Unaccounted for hydrogens (6H) due to peak broadening. Spectrum matches literature precedent.³ 302

Figure A2-8. ^1H and ^{13}C NMR spectra of S5. ^1H NMR (500 MHz, CDCl_3) δ 7.02–6.98 (m, 1H), 6.80 (s, 2H), 6.64 (dd, $J = 8.5, 2.8$ Hz, 1H), 6.50 (d, $J = 8.5$ Hz, 1H), 4.38 (q, $J = 7.3$ Hz, 1H), 3.80 (s, 3H), 3.01 (s, 2H), 2.32–1.99 (m, 9H), 1.61 (d, $J = 7.3$ Hz, 3H). ^{13}C NMR (126 MHz, CDCl_3) δ 152.72, 138.69, 137.12, 136.44, 135.83, 131.81, 119.54, 116.45, 114.78, 111.18, 55.81, 36.23, 21.02, 20.66, 17.22..... 303

Figure A2-9. ^1H and ^{13}C NMR Spectra of S6. ^1H NMR (500 MHz, CD_2Cl_2) δ 7.63 (d, $J = 8.2$ Hz, 2H), 7.33–7.20 (m, 2H), 7.11 (ddd, $J = 8.2, 7.2, 1.2$ Hz, 2H), 6.95 (dd, $J = 8.2, 2.6$ Hz, 2H), 6.92–6.86 (m, 2H), 6.75–6.71 (m, 2H), 6.21–5.39 (m, 4H), 4.53 (q, $J = 7.4$ Hz, 2H), 3.94 (s, 6H), 2.61–1.62 (m, 12H), 1.56 (d, $J = 7.7$ Hz, 6H), 0.94 (s, 6H). ^{13}C NMR (126 MHz, CD_2CD_2) δ 160.71, 156.13, 144.39, 140.63, 140.63, 138.22, 135.44, 134.07, 130.00, 129.11, 127.49, 127.49, 126.17, 121.82, 117.97, 115.12, 110.75, 55.50, 36.47, 21.02, 19.07, 16.14..... 304

Figure A2-10. ^1H NMR Spectrum of C3_{OMe} . ^1H NMR (400 MHz, CD_2Cl_2 , rd = 0.005 s, at = 0.05 s) δ 23.31 (s, 2H), 20.80 (s, 2H), 20.46 (s, 2H), 14.04 (d, $J = 7.7$ Hz, 2H), 9.53 (s, 6H), 6.29 (s,

2H), 4.89 (s, 4H), 2.14 (s, 7H), 1.27 (d, $J = 4.1$ Hz, 6H), 0.87 (s, 1H), 0.49 (d, $J = 4.9$ Hz, 6H), - 17.60 (s, 2H). Unaccounted for hydrogens (6 H) due to peak broadening	305
Figure A2-11. ^1H and ^{13}C NMR Spectra of 1. ^1H NMR (400 MHz, CDCl_3) δ 2.11 (s, 6H). ^{13}C NMR (176 MHz, CDCl_3) δ 137.38, 107.68, 15.19.....	306
Figure A2-12. ^1H and ^{13}C NMR Spectra of S7. ^1H NMR (700 MHz, CDCl_3) δ 6.85 (s, 1H), 2.17 (s, 3H), 2.10 (s, 3H). ^{13}C NMR (176 MHz, CDCl_3) δ 137.50, 136.92, 120.39, 109.18, 15.98, 13.89.....	307
Figure A 2-13. ^1H and ^{13}C NMR Spectra of S8. ^1H NMR (500 MHz, CDCl_3) δ 7.31 (dd, $J = 4.4$, 1.9 Hz, 1H), 7.08–7.03 (multiple peaks, 2H), 2.28 (s, 3H), 2.14 (s, 3H). ^{13}C NMR (176 MHz, CDCl_3) δ 138.47, 136.01, 134.19, 130.93, 127.74, 126.52, 125.94, 108.28, 14.95, 14.86.....	308
Figure A2-14. ^1H and ^{13}C NMR Spectra of S9. ^1H NMR (700 MHz, CDCl_3) δ 7.30 (dd, $J = 5.2$, 1.3 Hz, 1H), 7.14–7.10 (m, 1H), 7.09–7.06 (m, 1H), 6.85 (s, 1H), 2.27 (s, 3H), 2.20 (s, 3H). ^{13}C NMR (176 MHz, CDCl_3) δ 139.10, 137.44, 134.25, 131.25, 127.64, 125.99, 125.38, 119.64, 15.82, 13.90.....	309
Figure A2-15. ^1H and ^{13}C NMR Spectra of 2. ^1H NMR (700 MHz, CDCl_3) δ 7.31 (d, $J = 5.2$ Hz, 2H), 7.14 (d, $J = 3.6$ Hz, 2H), 7.08 (dd, $J = 5.2$, 3.6 Hz, 2H), 2.31 (s, 6H). ^{13}C NMR (176 MHz, CDCl_3) δ 136.67, 135.49, 129.82, 127.76, 126.28, 125.64, 14.66.....	310
Figure A2-16. ^1H and ^{13}C NMR Spectra of 3. ^1H NMR (700 MHz, CDCl_3) δ 7.23 (d, $J = 5.1$ Hz, 1H), 7.17 (dd, $J = 3.6$, 1.1 Hz, 1H), 7.06 (d, $J = 3.8$ Hz, 1H), 7.03 (dd, $J = 5.1$, 3.6 Hz, 1H), 7.01 (d, $J = 3.8$ Hz, 1H), 6.97 (d, $J = 3.8$ Hz, 1H), 6.91 (d, $J = 3.8$ Hz, 1H). ^{13}C NMR (176 MHz, CDCl_3) δ 138.54, 136.80, 136.66, 135.01, 130.64, 127.89, 124.70, 124.53, 124.27, 123.87, 123.68, 110.99.....	311

Figure A2-17. ^1H and ^{13}C NMR Spectra of 4. ^1H NMR (700 MHz, CDCl_3) δ 6.99 (s, 2H), 6.98 (d, $J = 3.8$ Hz, 2H), 6.91 (d, $J = 3.8$ Hz, 2H). ^{13}C NMR (176 MHz, CDCl_3) δ 138.24, 135.49, 130.69, 124.53, 123.90, 111.29.....	312
Figure A2-18. GPC traces of poly(3-hexylthiophene) (P3HT) generated at rt via (diimine) NiBr_2 precatalysts C1_{tBu} , C2, C3_{Me} , C3_{OMe} , C4_{Me} , and C4_{CF_3}	315
Figure A2-19. MALDI-TOF-MS spectra of P3HT via C2 at rt, aliquot taken at 30 min.....	317
Figure A2-20. MALDI-TOF-MS spectra of P3HT via C3_{Me} at rt, aliquot taken at 30 min.	317
Figure A 2-21. MALDI-TOF-MS spectra of P3HT via C3_{OMe} at rt, aliquot taken at 30 min. ...	318
Figure A2-22. Plots of M_n versus conversion at 0 °C for polymerizations via precatalyst C3_{Me}	321
Figure A2-23. MALDI-TOF-MS data from M_n versus conversion at 0 °C for polymerizations via precatalyst C3_{Me} for the first two aliquots analyzed.	322
Figure A2-24. GPC traces from M_n versus conversion at 0 °C for polymerizations via precatalyst C3_{Me} with increasing monomer conversion from bottom to top of plots.....	323
Figure A2-25. Plots of M_n versus monomer/catalyst ratio from 0 °C polymerizations via precatalyst C3_{Me} ($M_n = \bullet$, $\text{D} = \circ$).....	325
Figure A2-26. Full ^1H NMR spectra from the reaction of 3, S8, and thiophene-2-ylmagnesium chloride with precatalyst C3_{Me} showing no formation of compound 2.	327
Figure A2-27. Zoomed-in regions of the ^1H NMR spectra (see Figure A2-26) from the reaction of 3, S8, and thiophene-2-ylmagnesium chloride with precatalyst C3_{Me} showing no formation of compound 2.....	328
Figure A2-28. ^1H NMR spectrum for the reaction of 1 with $i\text{PrMgCl}$. ^1H NMR (400 MHz, THF-d_8) δ 2.19 (s, 3H), 1.97 (s, 3H).....	330

Figure A2-29. ¹ H NMR spectra for the reaction of S11 with C3 _{Me} . Full spectrum (bottom), zoomed-in region (top). No observed pair of singlets at 2.19 and 1.97 suggests complete conversion of S11. Paramagnetic peaks (boxed in blue) indicate unreacted C3 _{Me} .	332
Figure A2-30. GPC traces of P3HT (<i>m</i> = 25, <i>n</i> = 50) chain-extension experiments at 0 °C via precatalyst C3 _{Me} .	337
Figure A2-31. GPC traces of P3HT (<i>m</i> = 10, <i>n</i> = 70) chain-extension experiments at 0 °C via precatalyst C3 _{Me} .	337
Figure A2-32. GPC traces from vinyl end-capping polymerizations at 0 °C via precatalyst C3 _{Me} .	339
Figure A2-33. MALDI-TOF-MS data from vinyl end-capping polymerizations at 0 °C via precatalyst C3 _{Me} .	341
Figure A2-34. MALDI-TOF-MS spectrum from the reaction of excess 2,5-dibromothiophene, 4, and (3-hexylthiophen-2-yl)magnesium chloride with precatalyst C3 _{Me} .	343
Figure A2-35. MALDI-TOF-MS spectra of the rt polymerization with monomer analogue 1 added before initiation via precatalyst C3 _{Me} .	347
Figure A2-36. MALDI-TOF-MS spectra of rt polymerizations via precatalyst C3 _{Me} after 8 min (control polymerization).	348
Figure A2-37. MALDI-TOF-MS spectra of rt polymerizations with monomer analogue (1) added after 90s at rt via precatalyst C3 _{Me} after 8 min.	349
Figure A2-38. MALDI-TOF-MS spectra of the polymerization of thiophene at rt via precatalyst C3 _{Me} after 90 s (top) and 8 min (bottom) (control polymerization).	350
Figure A2-39. Ni Mulliken Charge Calculations for C3 _{Me} and C3 _{OMe} .	351

Figure A3-1. ^1H and ^{13}C NMR Spectra of S1. ^1H NMR (400 MHz, CDCl_3) δ 7.87 (d, $J = 8.3$ Hz, 2H), 7.38 (t, $J = 7.3$ Hz, 2H), 6.96 (s, 4H), 6.75 (d, $J = 7.3$ Hz, 2H), 2.36 (s, 6H), 2.07 (s, 12H). ^{13}C NMR (176 MHz, CDCl_3) δ 161.01, 146.73, 140.50, 132.76, 130.96, 129.67, 128.88, 128.72, 128.19, 124.55, 122.44, 20.92, 17.70..... 363

Figure A3-2. ^1H NMR Spectrum of C2. ^1H NMR (400 MHz, CD_2Cl_2 , rd = 0.005 s, at = 0.05 s) δ 33.77 (s, 6H), 27.54 (s, 12H), 24.49 (s, 4H), 23.93 (s, 2H), 17.35 (d, $J = 7.9$ Hz, 2H), 5.85 (s, 2H). 364

Figure A3-3. ^1H and ^{13}C NMR Spectra of S2. ^1H NMR (500 MHz, CDCl_3) δ 7.17 (s, 1H), 6.85 (dd, $J = 7.9, 1.9$ Hz, 1H), 6.80 (s, 2H), 6.47 (d, $J = 7.9$ Hz, 1H), 4.35 (q, $J = 7.3$ Hz, 1H), 3.12 (s, 2H), 2.30 (s, 3H), 2.19 (overlapping peaks, 9H), 1.61 (d, $J = 7.3$ Hz, 3H). ^{13}C NMR (126 MHz, CDCl_3) δ 142.48, 137.63, 136.58, 135.90, 130.75, 130.07, 128.43, 127.50, 127.24, 115.98, 36.17, 21.15, 21.03, 20.83, 17.43..... 365

Figure A3-4. ^1H and ^{13}C NMR spectra of S3. ^1H NMR (500 MHz, CDCl_3) δ 7.61 (d, $J = 8.2$ Hz, 2H), 7.47 (s, 2H), 7.18 (d, $J = 7.7$ Hz, 2H), 7.10 (t, $J = 7.7$ Hz, 2H), 6.90 (d, $J = 7.8$ Hz, 2H), 6.69 (d, $J = 7.2$ Hz, 2H), 5.97 (br s, 2H), 5.39 (br s, 2H), 4.60 (q, $J = 7.4$ Hz, 2H), 2.52 (s, 6H), 2.41 (br s 6H), 1.62 (br s, 6H), 1.58 (d, $J = 7.4$ Hz, 6H), 0.97 (s, 6H). ^{13}C NMR (126 MHz, CDCl_3) δ 161.00, 148.78, 141.11, 138.97, 136.22 (br), 134.46, 133.56, 132.70, 130.25, 129.80, 129.48, 128.78 (br), 127.85, 127.28, 126.57, 122.40, 117.77, 36.74, 21.84, 21.65 (br), 19.80, 16.80..... 366

Figure A3-5. ^1H NMR Spectrum of S4. ^1H NMR (500 MHz, CD_2Cl_2) δ 35.53 (s, 6H), 24.88 (s, 2H), 23.17 (s, 2H), 21.45 (br s, 2H), 20.14 (s, 2H), 14.03 (s, 2H), 6.27 (s, 2H), 4.82 (br s, 6H), 1.99 (s, 6H), 1.44 (s, 2H) 0.87 (s, 2H), 0.45 (s, 6H), -16.43 (br s, 2H). Unaccounted for hydrogens (6H) due to peak broadening. Spectrum matches literature precedent.³ 367

Figure A3-6. GPC data from the polymerization of 3-decylthiophene at rt via Ni and Pd precatalysts before and after end-capping experiments (ec). Zoomed (left) and full traces (right) of the same experiment. Note that M(0) scavenging agent and residual monomer elute from 20.5–22 min, PhMe elutes at 23.1 min, and BHT elutes at 23.8 min. 371

Figure A3-7. MALDI-TOF/MS spectra the polymerization of 3-decylthiophene at rt via Ni(dppp)Cl₂ before and after end-capping experiments (ec). Full trace (left) zoomed image (right). Values calculated using average mass method, signal-to-noise = 2. The degree of polymerization shown is 27. 372

Figure A3-8. MALDI-TOF/MS spectra the polymerization of 3-decylthiophene at rt via Ni(IPr)(PPh₃)Cl₂ before and after end-capping experiments (ec). Full trace (left) zoomed image (right). Values calculated using average mass method, signal-to-noise = 2. The degree of polymerization shown is 22. 373

Figure A3-9. MALDI-TOF/MS spectra the polymerization of 3-decylthiophene at rt via Pd(IPr)(3-Clpyr)Cl₂ before and after end-capping experiments (ec). Full trace (left) zoomed image (right). Values calculated using average mass method, signal-to-noise = 2. The degree of polymerization shown is 18. 374

Figure A3-10. MALDI-TOF/MS spectra the polymerization of 3-decylthiophene at rt via Pd(IPent)(3-Clpyr)Cl₂ before and after end-capping experiments (ec). Full trace (left) zoomed image (right). Values calculated using average mass method, signal-to-noise = 2. The degree of polymerization shown is 11. 375

Figure A3-11. GPC data from the polymerization of 3-decylthiophene to evaluate IPr ligand-switching effectiveness before and after (ec) end-capping experiments. Zoomed (left) and full

traces (right) of the same experiment. Note that M(0) scavenging agent and residual monomer elute from 20.5–22 min, PhMe elutes at 23.1 min and BHT elutes at 23.8 min..... 381

Figure A3-12. MALDI-TOF/MS data from the polymerization of 3-decylthiophene using precatalyst C2 before and after (ec) end-capping experiments. Full traces (left) and zoomed (right) of the same experiment. Values calculated using average mass method, signal-to-noise = 2. The degree of polymerization shown is 11. 382

Figure A3-13. MALDI-TOF/MS data from the polymerization of 3-decylthiophene using precatalyst C2 treated with IPr before and after (ec) end-capping experiments. Full traces (left) and zoomed (right) of the same experiment. Values calculated using average mass method, signal-to-noise = 2. The degree of polymerization shown is 14. 383

Figure A3-14. MALDI-TOF/MS data from the polymerization of 3-decylthiophene using precatalyst C2 treated with IPr and PPh₃ before and after (ec) end-capping experiments. Full traces (left) and zoomed (right) of the same experiment. Values calculated using average mass method, signal-to-noise = 2. The degree of polymerization shown is 11. Note that the GPC trace indicates high molecular weight polymer was formed however these polymers did not ionize here..... 384

Figure A3-15. MALDI-TOF/MS data from the polymerization of 3-decylthiophene using precatalyst C2 treated with pyr and IPr before and after (ec) end-capping experiments. Full traces (left) and zoomed (right) of the same experiment. Values calculated using average mass method, signal-to-noise = 2. The degree of polymerization shown is 18. 385

Figure A3-16. MALDI-TOF/MS data from the polymerization of 3-decylthiophene in the presence of 1-hexene using precatalyst C2 treated with pyr and IPr before and after (ec) end-capping experiments. Full traces (left) and zoomed (right) of the same experiment. Values

calculated using average mass method, signal-to-noise = 2. The degree of polymerization shown is 21..... 386

Figure A3-17. GPC data from the attempted ligand-switch copolymerization. Zoomed (left) and full traces (right) of the same experiment. The solid line represents poly(1-pentene) macroinitiator before ligand-switch. The dashed line represents poly(1-pentene) macroinitiator after ligand-switch. The RI traces are shown, poly(olefin) does not absorb UV light. Note that BCF and residual monomer elute from 20.5–22 min, PhMe elutes at 23.1 min and BHT elutes at 23.8 min. 390

Figure A3-18. GPC data from the attempted ligand-switch copolymerization with thiophene monomer added (25 equiv.). Zoomed (left) and full traces (right) of the same experiment. The solid line represents the RI trace. The dashed line represents the UV trace. Note that BCF and residual monomer elute from 20.5–22 min, PhMe elutes at 23.1 min and BHT elutes at 23.8 min. 390

Figure A3-19. GPC data from the attempted ligand-switch copolymerization with thiophene monomer added (50 equiv.). Zoomed (left) and full traces (right) of the same experiment. The solid line represents the RI trace. The dashed line represents the UV trace. Note that BCF and residual monomer elute from 20.5–22 min, PhMe elutes at 23.1 min and BHT elutes at 23.8 min. 391

Figure A3-20. GPC data from the attempted ligand-switch copolymerization with thiophene monomer added (100 equiv.) 391

List of Tables

Table 3-1. Polymerization Data for Precatalysts C1–C4	54
Table A1-1. Percent P3DT with each end-group based on MALDI-TOF/MS.	145
Table A1-2. M_n and \bar{D} from Br/H–PBHP and end-capped–PBHP.....	145
Table A1-3. GC data from the polymerization of P3HT before end-capping cross-over experiments via Ni(IPr)(PPh ₃)Cl ₂ , Pd(IPr)(3-Clpy)Cl ₂ , and Ni(dppp)Cl ₂ . Initial ratio of Grignard isomers is 4:1 (major:minor).....	164
Table A1-4. M_n and \bar{D} from P3HT (before end-capping cross-over experiments), end-capping cross-over experiment (ec), and end-capping cross-over control (only capping agent) experiments via Ni(IPr)(PPh ₃)Cl ₂ , Pd(IPr)(3-Clpy)Cl ₂ , and Ni(dppp)Cl ₂	164
Table A1-5. GC data from the polymerization of P3DT before end-capping experiments via Ni(IPr)(PPh ₃)Cl ₂ . Initial ratio of Grignard isomers is major:minor (4:1).....	174
Table A1-6. M_n and \bar{D} from P3DT (before end-capping), end-capping experiment, and end-capping control (only capping agent) experiments for Ni(IPr)(PPh ₃)Cl ₂ and P3DT.....	175
Table A1-7. GC data from the polymerization of P3DT before end-capping experiments via Pd(IPr)(3-Clpy)Cl ₂ . Initial ratio of Grignard isomers is major:minor (4:1).	180
Table A1-8. M_n and \bar{D} from P3DT (before end-capping), end-capping experiment (ec), and end-capping control (only capping agent) experiments for Pd(IPr)(3-Clpy)Cl ₂ and P3DT.	180
Table A1-9. Vial preparation for capping/competition experiments with Pd(IPr)(3-Clpy)Cl ₂ and P3DT.....	184

Table A1-10. GC data from the polymerization of P3DT before end-capping experiments via Pd(IPr)(3-Clpy)Cl ₂ . Initial ratio of Grignard isomers is 4:1 (major:minor).	186
Table A1-11. <i>M_n</i> and Đ from the control, capping, and capping/competition experiments for Pd(IPr)(3-Clpy)Cl ₂ and P3DT.....	186
Table A1-12. GC data from the polymerization of P3DT before end-capping experiments via Ni(dppp)Cl ₂ . Initial ratio of Grignard isomers is 4:1 (major:minor).	192
Table A1-13. <i>M_n</i> and Đ from P3DT (before end-capping), end-capping experiment (ec), and end-capping control (only capping agent) (t = 1 h) experiments for Ni(dppp)Cl ₂ and P3DT.	193
Table A1-14. GC data from the polymerization of P3DT before end-capping experiments via Ni(dppp)Cl ₂ . Initial ratio of Grignard isomers is 4:1 (major:minor).	195
Table A1-15. <i>M_n</i> and Đ from P3DT (before end-capping), end-capping experiment (ec), and end-capping control (only capping agent) experiments (t = 18 h) for Ni(dppp)Cl ₂ and P3DT.	195
Table A1-16. GC data from the polymerization of P3DT before end-capping experiments via Ni(IPr)(PPh ₃)Cl ₂ , Pd(IPr)(3-Clpy)Cl ₂ , and Ni(dppp)Cl ₂ . Initial ratio of Grignard isomers is 4:1 (major:minor).....	202
Table A1-17. <i>M_n</i> and Đ from P3DT (before end-capping), end-capping control (capping agent only), end-capping (ec), and end-capping with hexanes (ec (hex)) experiments for Ni(IPr)(PPh ₃)Cl ₂ , Pd(IPr)(3-Clpy)Cl ₂ , and Ni(dppp)Cl ₂	202
Table A1-18. GC data from the polymerization of 3-decylthiophene at rt via Ni(IPr)(PPh ₃)Cl ₂ . Initial ratio of Grignard isomers is 4:1 (major:minor).	210
Table A1-19. <i>M_n</i> and Đ from the polymerization of 3-decylthiophene at rt via Ni(IPr)(PPh ₃)Cl ₂	210
Table A1-20. Percent PBHP end-groups based on MALDI-TOF/MS analysis.	218

Table A1-21. M_n and \bar{D} from Br/H–PBHP and end-capped–PBHP.....	219
Table A1-22. M_n and \bar{D} from PBBP (B = butyloxy) (before end-capping cross-over experiments), end-capping cross-over experiment (ec), end-capping cross-over control (only capping agent) experiment, and the added Br/H–PBHP via Ni(IPr)(PPh ₃)Cl ₂	240
Table A1-23. M_n , and \bar{D} from PBHP (before end-capping), end-capping experiment (ec), and end-capping control (only capping agent) experiments for Ni(IPr)(PPh ₃)Cl ₂ and PBHP.	247
Table A1-24. M_n , and \bar{D} from PBHP (before end-capping), end-capping experiment (ec), and end-capping control (only capping agent) experiments (t = 20 h) for Ni(IPr)(PPh ₃)Cl ₂ and PBHP.	249
Table A1-25. M_n and \bar{D} from PBHP (before end-capping), end-capping experiment (ec), and end-capping control (only capping agent) experiments (t = 2 h) for Pd(IPr)(3-Clpy)Cl ₂ and PBHP.	253
Table A1-26. M_n and \bar{D} from PBHP (before end-capping), end-capping experiment (ec), and end-capping control (only capping agent) experiments for Ni(dppp)Cl ₂ and PBHP.....	258
Table A1-27. GC data from the polymerization of PBAP before end-capping experiments via Ni(IPr)(PPh ₃)Cl ₂ , Pd(IPr)(3-Clpy)Cl ₂ , and Ni(dppp)Cl ₂	265
Table A1-28. M_n and \bar{D} from PBAP (before end-capping), end-capping control (only capping agent), end-capping (ec), and end-capping with hexanes (ec (hex)) experiments for Ni(IPr)(PPh ₃)Cl ₂ , Pd(IPr)(3-Clpy)Cl ₂ , and Ni(dppp)Cl ₂	265
Table A1-29. M_n and \bar{D} from PBHP t = 90 min and t = 6.5 h via Pd(IPr)(3-Clpy)Cl ₂	272
Table A2-1. GC and GPC data from the polymerization of 3-hexylthiophene at rt via (diimine)NiBr ₂ precatalysts (C1 _{tBu} , C2, C3 _{Me} , and C3 _{OMe}). Initial ratio of Grignard isomers is 4:1 (a:b).....	316

Table A2-2. GC and GPC data from the polymerization of 3-hexylthiophene at rt via (diimine)NiBr ₂ precatalysts (C ₄ _{Me} and C ₄ _{CF₃}). Initial ratio of Grignard isomers is 4:1 (a:b). ...	316
Table A2-3. GC and GPC data from the polymerization of 3-hexylthiophene at rt via C1 _{tBu} . Initial ratio of Grignard isomers is 4:1 (a:b).	319
Table A2-4. GC and GPC data from <i>M_n</i> versus conversion at 0 °C for polymerizations via precatalyst C3 _{Me} (monomer/catalyst = 80/1).	321
Table A2-5. Monomer/catalyst details, GC, and GPC data from 0 °C polymerizations via precatalyst C3 _{Me}	325
Table A2-6. Monomer conversion, <i>M_n</i> , and Đ of P3HT (<i>m</i> = 25, <i>n</i> = 50) chain-extension experiments at 0 °C via precatalyst C3 _{Me}	336
Table A2-7. Monomer conversion, <i>M_n</i> , and Đ of thiophene (<i>m</i> = 10, <i>n</i> = 70) chain-extension experiments at 0 °C via (diimine)NiBr ₂ precatalyst C3 _{Me}	336
Table A2-8. GPC data from vinyl end-capping polymerizations at 0 °C via precatalyst C3 _{Me} . ..	339
Table A2-9. GC data from the reaction of excess 2,5-dibromothiophene, 4, and (3-hexylthiophen-2-yl)magnesium chloride with precatalyst C3 _{Me} . Note that 2,5-dibromothiophene flies with solvent on the GC, hence conversion could not be measured.....	343
Table A2-10. GC and GPC data from rt polymerizations with and without monomer analogue 1 added prior to initiation via precatalyst C3 _{Me}	346
Table A2-11. GC and GPC data from rt polymerization via precatalyst C3 _{Me} with and without monomer analogue 1 added after 90s.	346
Table A3-1. GC data from the polymerization of 3-decylthiophene at rt via Ni and Pd precatalysts before end-capping experiments.	370

Table A3-2. GPC data from the polymerization of 3-decylthiophene at rt via Ni and Pd precatalysts before and after end-capping experiments.	371
Table A3-3. GC data from the polymerization of 3-decylthiophene to evaluate IPr ligand-switching effectiveness. GC data is acquired from the polymerizations before end-capping is done.	379
Table A3-4. GPC data from the polymerization of 3-decylthiophene to evaluate IPr ligand-switching effectiveness. GPC data is acquired from the polymerizations before and after end-capping is done.	380
Table A3-5. GC data from the ligand-switch copolymerization experiments.	389
Table A3-6. GPC data from the ligand-switch copolymerization experiments.	389

List of Charts

Chart 1-1. Representative Examples of Ni-Catalyzed CTP (Examples with DP > 15 and Đ < 1.5 in a Homopolymerization Are Included; Bolded References Report Đ ≤ 1.25) ^{4-6, 8-58}	4
Chart 1-2. Second-Generation Reactive Ligands ⁷³	13
Chart 1-3. Representative Examples of Pd-Catalyzed CTP (Examples with DP > 15 and Đ < 1.5 in a Homopolymerization Are Included; Bolded References Report Đ ≤ 1.25) ⁷⁵⁻⁸⁶	14
Chart 2-1. Precatalysts and Monomers Used Herein	34
Chart 2-2. Optimized Reagents and Reaction Conditions to Eliminate Intermolecular Reactivity ³⁴	36
Chart 3-1. Reported and New Nickel Diimine Precatalysts for CTP	52
Chart 4-1. Selected Ni and Pd precatalysts used for insertion and chain-walking or CTP.....	72
Chart 5-1. High-performing polymers synthesized via step-growth polymerization methods.....	88
Chart 5-2. The limited scope of ancillary ligands used in Pd-CTP since 2008. Each ligand was counted once per publication.	92
Chart 5-3. Select Buchwald precatalysts and ancillary ligands.	98
Chart 5-4. NHC-ligated Pd precatalysts.....	106
Chart 5-5. Examples of NHCs with varied electronic properties.	107
Chart 5-6. Select examples of CAACs and CAACs.....	107

List of Schemes

Scheme 1-1. CTP Mechanism.....	2
Scheme 1-2. Optimal Ancillary Ligand Depends on the Transmetalating Agent ^{9,10,12,18}	6
Scheme 1-3. Impact of the Ancillary Ligand on Phenylene Polymerization ⁵¹	7
Scheme 1-4. Support for an Intermediate Ni–Arene π -Complex ⁶⁴	8
Scheme 1-5. Influence of the Cone Angle on Ni-Mediated Phenylene Polymerization ⁴⁰	9
Scheme 1-6. Initiation through Preinitiation (top) or Use of Reactive Ligands (bottom)	11
Scheme 1-7. Effect of the Reactive Ligand on Initiation Rates and Phenylene Polymerization ⁷	12
Scheme 1-8. Comparison of Nickel- versus Palladium-Catalyzed Syntheses of Poly(p-phenylene vinylene) ⁷⁴	15
Scheme 1-9. (left) Two Pathways That Form Triarene; ⁹¹ (right) Small-Molecule Difunctionalization To Identify CTP for Thiophene-3-carboxylate. ²⁵	17
Scheme 1-10. Summary of Precatalyst Parameters and Their Impact.....	18
Scheme 2-1. Propagation via Ring-Walking versus Catalyst Dissociation during CTP	33
Scheme 2-2. In Situ End-Capping Experiment.....	35
Scheme 3-1. Initiation and Propagation Mechanisms for CTP.....	51
Scheme 3-2. Free Energy Landscape for Catalyst Dissociation versus Ring Walking for Precatalysts C3 _{Me} , C4 _{Me} , and C4 _{CF3}	55
Scheme 3-3. Intra- versus Intermolecular Competition Experiment	57
Scheme 3-4. Evaluating Oligomer versus Monomer Reactivity	60

Scheme 3-5. Proposed Mechanism for CTP with C ₃ Me.....	62
Scheme 3-6. Synthesizing poly(olefin)-block-poly(thiophene) copolymers via C ₃ Me-CH ₂ TMS	63
Scheme 4-1. Proposed ligand-switch approach for synthesizing insulating/conducting block copolymers.....	73
Scheme 5-1. CTP mechanism.....	86
Scheme 5-2. Identifying potential CTP precatalysts using small-molecule difunctionalization reactions.....	95
Scheme 5-3. (top) Ad ₃ P-ligated Pd-catalyzed small-molecule difunctionalization reaction of benzothiadiazole and fluorinated arenes. (bottom) High-performing polymer containing benzothiadiazole and fluorinated-thiophene units.....	97
Scheme 5-4. Generating block copolymers based on monomer reactivity differences using SPhos-ligated Pd.....	99
Scheme 5-5. (top) Synthesizing extended arene polymers using Buchwald ancillary ligand SPhos. (bottom) Example of an extended arene polymer in Li ion batteries.....	100
Scheme 5-6. (top) Matching Buchwald ligands to fluoroarene, boronic acids. (bottom) Example of a high-performing polymer with fluorine substituents.....	102
Scheme 5-7. (top) Identifying optimal Buchwald ligands for coupling arenes with coordinating atoms. (bottom) Examples of polymers containing N and reactive functional groups.....	104
Scheme 5-8. (top) HandaPhos-ligated Pd catalyzed difunctionalization reaction. (bottom) Examples of conjugated polymers that could be accessed through Sonogashira-CTP.....	104
Scheme 5-9. (top) IPent-ligated Pd-catalyzed difunctionalization reaction. (bottom) Examples of structurally diverse polymers containing carbazole for high performing organic electronics....	108

Scheme 5-10. (top) Examples of bulky yet flexible NHCs for cross-coupling N-containing and sterically hindered substrates. (bottom) Example of a conjugated polymer containing sterically encumbered side-chains.	109
Scheme 5-11. Generic depiction of routes to an AB-functionalized donor/acceptor monomer and potential starting reagents.	110

List of Appendices

Appendix 1: Supporting information for Chapter 2. Ring-Walking in Catalyst Transfer

Polymerization	134
A1.1 Materials	134
A1.2 General Experimental	135
A1.3 Synthetic Procedures	137
A1.4 NMR Spectra	139
A1.5 Thiophene	141
A1.5.1 Confirming MALDI-TOF/MS provides an accurate and quantitative description of end-group distributions for poly(3-alkylthiophene)	142
A1.5.2 Synthesis of H/Br-polymer for end-capping control reactions	151
A1.5.3 End-capping control reactions	153
A1.5.4. End-capping cross-over experiments to evaluate the impact of chain-entanglement for P3AT (A = alkyl)	160
A1.5.5 End-capping reactions	171
A1.5.6 3-Decylthiophene polymerization via Ni(IPr)(PPh ₃)Cl ₂ generating NHC/Br-polymers	208
A1.6 Phenylene	214
A1.6.1 Confirming MALDI-TOF/MS provides an accurate and quantitative description of end-group distributions for poly(2,5-bisalkoxyphenylene)	215

A1.6.2. Synthesis of H/Br-polymer for end-capping control reactions.....	224
A1.6.3. End-capping control reactions.....	227
A1.6.4. End-capping cross-over experiments to evaluate the impact of chain-entanglement for PBAP (A = alkoxy).....	237
A1.6.5. End-capping reactions	244
A1.6.6. 2,5-Bis(hexyloxy)phenylene polymerization via Pd(IPr)(3-Clpy)Cl ₂ generating NHC/Br-polymers	271
A1.7. Values for the %ring-walking charts.....	276
A1.8. Figures from the manuscript with found and predicted m/z.	280
A1.9 References	281
Appendix 2: Supporting Information for Chapter 3. Mechanistic Insight into Thiophene Catalyst- Transfer Polymerization Mediated by Nickel Diimine Catalysts.....	282
A2.1. Materials.....	282
A2.2. General experimental	282
A2.3. Synthetic procedures	285
A2.4. NMR Spectra.....	296
A2.5. Polymerizations at rt.....	313
A2.6. M_n versus conversion at 0 °C	320
A2.7. M_n versus Monomer/catalyst ratios at 0 °C.....	324
A2.8. Intramolecular competition experiment	326
A2.9. Chain-extension polymerizations at 0 °C.....	335
A2.10. Vinyl end-capped polymerizations at 0 °C.....	338
A2.11. Mono/terthiophene reactivity experiment	342

A2.12. Monomer analogue addition polymerizations at rt.....	344
A2.13. Computational Details.....	351
A2.14 References	352
Appendix 3: Supporting Information for Chapter 4. Progress Towards Thiophene/Olefin Block	
Copolymers using an in-situ Ligand-Exchange Approach.....	354
A3-1. Materials.....	354
A3.2 General Experimental.....	355
A3.3 Synthetic Procedures	358
A3.4 NMR Spectra	363
A3.5 Me-end capping experiments	368
A3.5.1 Precatalyst screen for ligand-switch.....	368
A3.5.2 Ligand Switch thiophene polymerization followed by end-capping.....	376
A3.6. Attempting copolymerization.....	387
A3.7 References	392

Abstract

Catalyst-transfer polymerization (CTP) is a useful living, chain-growth polymerization method for synthesizing conjugated polymers with targetable molecular weights, narrow dispersities, and controllable copolymer sequences—all properties that significantly influence their performance in devices. Several phosphine- and N-heterocyclic carbene (NHC)-ligated Ni- and Pd-based precatalysts have been shown to be effective in CTP. One current limitation is that these traditional CTP catalysts lead to nonliving, non-chain-growth behavior when polymerizing complex monomers. Because these monomers are found in high-performing materials, there is a need to identify alternative CTP catalysts. Mechanistic insight has laid the foundation for designing new CTP catalysts. Building off this insight, we have designed and implemented model systems to identify catalysts by understanding their mechanistic behaviors and systematically modifying catalyst structures to improve their chain-growth behavior.

In Chapter 1, we describe how each catalyst parameter influences CTP. Ancillary ligands can be used to promote the key intermediate (a metal–arene associative complex) and its reactivity. Reactive ligands can improve catalyst solubility and accelerate initiation. While most CTP catalysts contain nickel, palladium-based catalysts exhibit a higher functional group tolerance and broader substrate scope. Overall, we anticipate that applying the tools and lessons detailed in Chapter 1 to other monomers should facilitate a better “matchmaking” process that will lead to new CTPs.

Few studies have elucidated the impact of these identities on the stability and reactivity of the key intermediate, especially under polymerization-relevant conditions. In Chapter 2, we developed a simple experiment to identify catalyst stability and ring-walking ability using in situ-generated polymers. The combined results show that the ancillary ligand, metal, and polymer identity all play a crucial role. While each catalyst studied walks efficiently over large distances in poly(thiophene), the trends observed for poly(phenylene) highlight the differing roles of transition metal and ancillary ligand identities. The insights gained herein should be useful for extending CTP to other monomer and copolymer scaffolds.

Recently, diimine-ligated Ni complexes have been employed for CTP; however, in most cases nonliving pathways become dominant at high monomer conversions and/or low catalyst loading. In Chapter 3, we report an alternative Ni diimine catalyst that polymerizes 3-hexylthiophene in a chain-growth manner at low catalyst loading and high monomer conversion. In addition, we elucidate the chain-growth mechanism as well as one chain-transfer pathway. Overall, these studies provide insight into the mechanism of conjugated polymer synthesis mediated by Ni diimine catalysts.

There are a limited number of living polymerization methods for generating copolymers from dissimilar monomers. In Chapter 4 we describe a model system to identify potential precatalysts for synthesizing thiophene/olefin block copolymers. We identified a potential living copolymerization systems involving a ligand-switch from a diimine ancillary ligand to an NHC. Currently, this method generates homopolymers rather than the desired copolymers. Future efforts are focused on elucidating potential termination pathways to circumvent them and enable future copolymerizations.

In Chapter 5 we highlight palladium precatalysts with promise for polymerizing complex monomers. Palladium precatalysts demonstrate good functional group tolerance and can polymerize monomers with various transmetalating groups. Few ancillary ligands have been explored for palladium-catalyzed CTP. Here, we describe ancillary ligands used in small-molecule cross-couplings that should be evaluated for CTP. Precatalysts capable of cross-coupling motifs found in complex monomers are highlighted. We anticipate the mechanistic insight and precatalysts discussed herein should facilitate designing future CTPs.

Chapter 1: Introduction – Matchmaking in Catalyst-Transfer Polymerization: Optimizing Catalysts based on Mechanistic Insight

Portions of this chapter have been published:

Leone, A. K.; McNeil, A. J. Matchmaking in Catalyst-Transfer Polycondensation: Optimizing Catalysts based on Mechanistic Insight. *Acc. Chem. Res.* **2016**, *49*, 2822–2831.

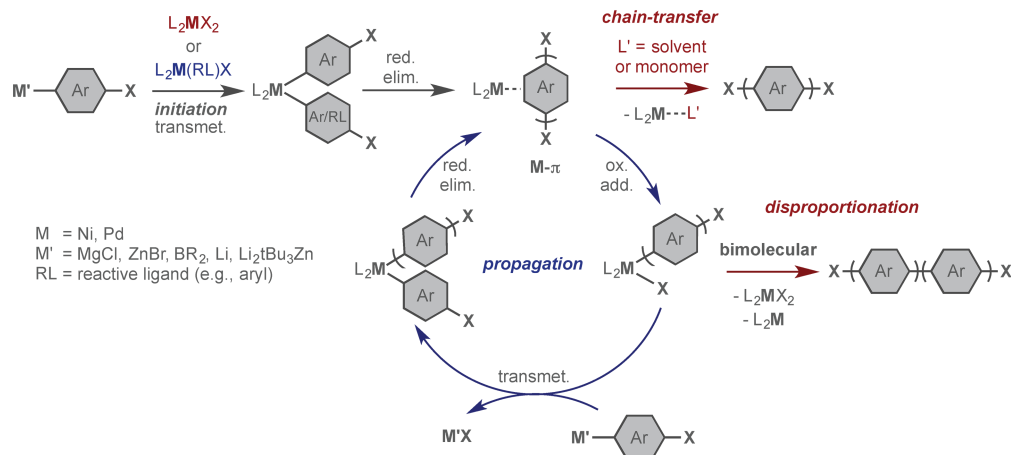
1.1 Introduction

Living, chain-growth polymerization methods are attractive because they provide a streamlined route to polymers with specific molecular weights, sequences, and end groups as well as narrow dispersities (i.e., \mathcal{D} approaching 1.00). These structural parameters influence the polymer's physical, optical, and morphological properties, ultimately impacting its performance in devices.¹ Living, chain-growth methods have been predominantly developed for monomers that can be polymerized via radical and anionic pathways. In contrast, for conjugated polymers, living, chain-growth methods are nascent and have a much narrower monomer scope.^{2,3}

Catalyst-transfer polymerization (CTP) is a living, chain-growth polymerization method used to generate conjugated (hetero)arene polymers using transition metal catalysis. The CTP reaction begins when a metal precatalyst reacts with 1–2 equiv of monomer to generate a bis(arene)-functionalized metal complex (Scheme 1-1). Subsequent biaryl reductive elimination generates a metal–biaryl associative intermediate, which then undergoes an intramolecular oxidative addition. The catalytic cycle continues as monomers are enchainned into the growing

polymer. This pathway is chain-growth because the intramolecular oxidative addition ensures catalyst association with the same chain throughout the polymerization.

Scheme 1-1. CTP Mechanism

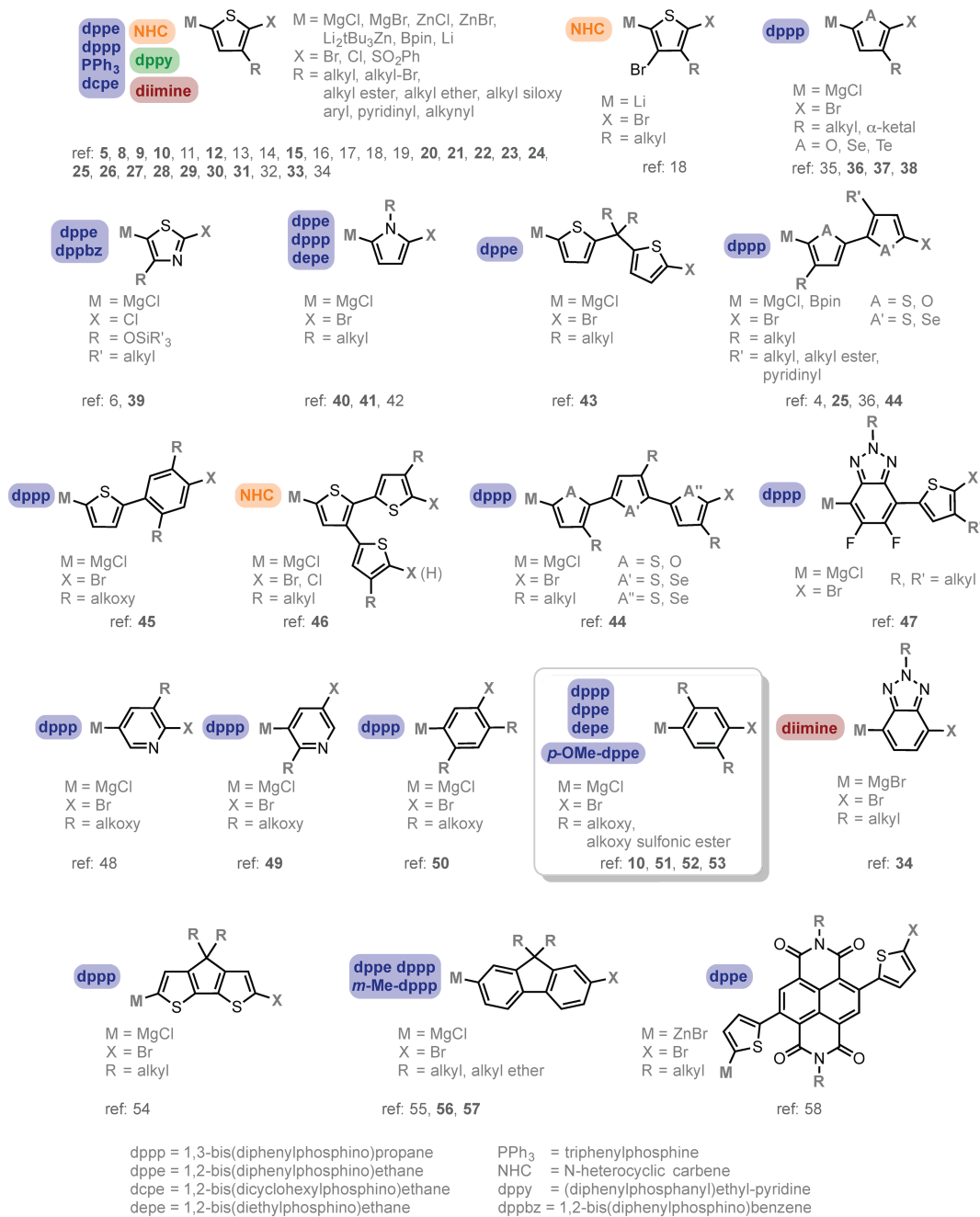


The CTP pathway can undergo unproductive reactions when the catalyst's electronic and steric properties are mismatched for a specific monomer (Scheme 1-1). For example, if the metal- π associative intermediate is weakly associated, other species in the reaction mixture (e.g., a coordinating solvent or un/activated monomer) can displace the growing polymer from the catalyst, resulting in chain-transfer.^{4,5} Alternatively, polymer chains can be exchanged between catalysts, producing two new active catalysts along with a polymer of twice the molecular weight via disproportionation.⁶ Finally, slow precatalyst initiation continuously generates new chains throughout the polymerization.⁷ All three pathways lead to undesirable, broad dispersities ($\mathcal{D} > 1.00$). Although some of these undesired reactions can be minimized by adjusting the catalyst concentration, solvent identity, or reaction temperature, a better approach is to modify the catalyst structure, as it has the largest influence over the living, chain-growth behavior.

Our studies have shown that instead of searching for a universal catalyst, one should tune the catalyst's electronic and steric properties for each monomer. Three parameters can be altered to tune a catalyst's reactivity: the ancillary ligand, the reactive ligand, and the transition metal.

We describe herein our efforts to understand how each parameter influences initiation, propagation, and the unproductive pathways. We have focused our efforts on bisphosphine-ligated nickel catalysts because they are widely utilized in CTP (cf. Chart 1-1), their steric and electronic properties are easily modified, and the catalyst resting state can be monitored in situ. We have developed both model systems and direct methods to interpret the effects of catalyst tuning and present general trends to assist future catalyst design.

Chart 1-1. Representative Examples of Ni-Catalyzed CTP (Examples with DP > 15 and Đ < 1.5 in a Homopolymerization Are Included; Bolded References Report Đ ≤ 1.25)^{4-6, 8-58}



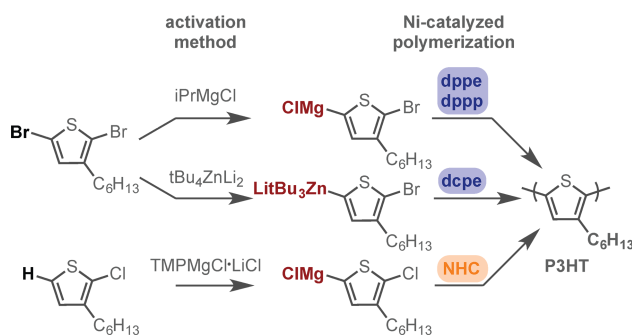
1.2 Ancillary Ligand

The ancillary ligand(s) often remains coordinated to the transition metal throughout the polymerization, influencing initiation, propagation, and the unproductive pathways. As described

in detail below, the ancillary ligand has the greatest impact on the turnover-limiting step (for both initiation and propagation) and on the stability/reactivity of the metal–polymer associative intermediate.

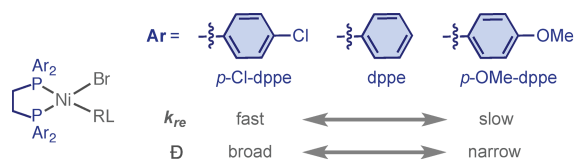
While carbene,^{18,25,46} diimine,^{19,34,59,60} and N/P⁵ ancillary ligands have been reported in Ni-mediated CTP, phosphine-based ligands are the most widely used (Chart 1-1). Of these ligands, both 1,3-bis(diphenylphosphino)propane (dppp) and 1,2-bis(diphenylphosphino)ethane (dppe) have been employed for many different monomers (Chart 1-1). As a consequence, many researchers use either dppe or dppp without further optimization. However, with some monomers, these ligands are not simply interchangeable. For example, different ancillary ligands were optimal for synthesizing poly(3-hexylthiophene) (P3HT) with narrow dispersities when only the transmetalating agents were different (Scheme 1-2). Other seemingly minor variations, such as changing the monomer side-chain length or identity⁵ as well as its location^{61,62} have also led to different optimized ancillary ligands. These results emphasize the need to understand how the properties of the ancillary ligand influence the polymerization mechanism for each specific monomer. To accomplish this goal, we examined the effects of the ancillary ligand on the chain-growth polymerization of 2,5-bis(hexyloxy)phenylene (hereafter referred to as “phenylene”) as a paradigm for new catalyst development.

Scheme 1-2. Optimal Ancillary Ligand Depends on the Transmetalating Agent^{9,10,12,18}



To evaluate the impact of ancillary ligand electronic properties, two modified dppe-based ligands were prepared by functionalizing the para position of the phenyl ring with electron-withdrawing or electron-donating groups (Scheme 1-3).⁵¹ We found that the most electron-withdrawing ancillary ligand (*p*-Cl-dppe) exhibited the highest polymerization rates. This trend is consistent with turnover-limiting reductive elimination, as removing electron density from Ni facilitates the formal reduction from Ni(II) to Ni(0).⁶³ Additional rate studies were consistent with turnover-limiting reductive elimination for all three ligands. Similar reactivity trends were observed during initiation, with the highest rates obtained from the most electron-withdrawing ancillary ligands. On the other hand, the most electron-donating ancillary ligand (*p*-OMe-dppe) led to the narrowest dispersities. This result is likely due to both a strengthened Ni–arene π interaction via metal– π^* back-donation and increased reactivity toward oxidative addition due to additional electron density on Ni. Overall, these results suggest that electron-rich ancillary ligands are more beneficial for CTP of phenylene.

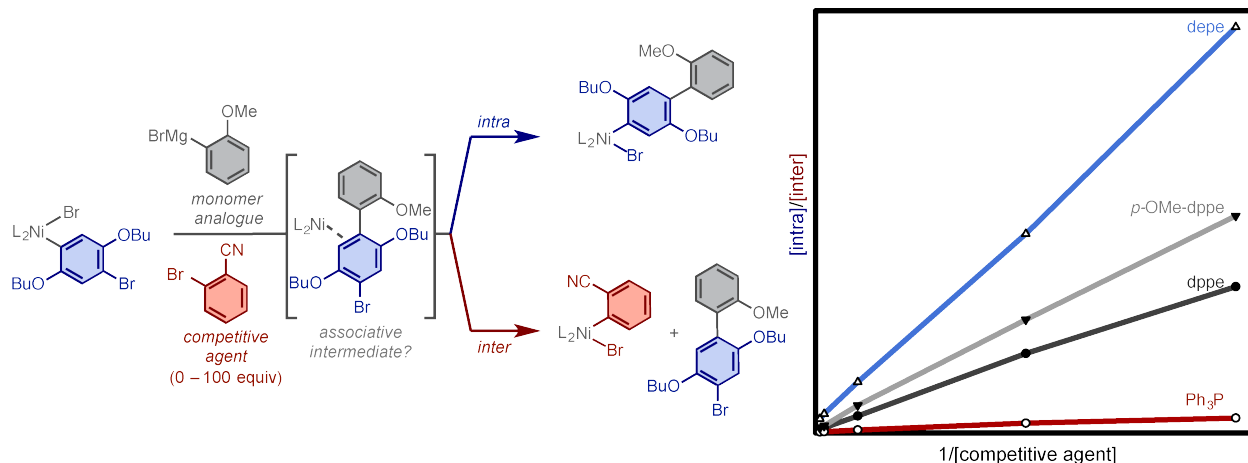
Scheme 1-3. Impact of the Ancillary Ligand on Phenylene Polymerization⁵¹



On the basis of these results, we designed a small-molecule model system to establish whether increasing the ancillary ligand's donating ability would promote Ni–arene π -complex formation and reactivity and, ultimately, improve CTP.⁶⁴ Although it is widely believed that CTP proceeds through this metal–arene intermediate,² it is difficult to observe in situ because of rapid intramolecular oxidative addition. Using a competition experiment, we can quantify the fractions of starting materials that proceed through the intra- and intermolecular pathways by measuring the product ratios (Scheme 1-4): The intramolecular pathway leads to a triaryl product via the Ni–arene π -complex, with a subsequent intracomplex oxidative addition and coupling with the Grignard reagent. The intermolecular pathway generates two biaryl products, one from dissociation and one from the competitive agent trapping the dissociated catalyst, followed by oxidative addition and coupling with the Grignard reagent. In all cases examined, the intramolecular product was dominant, providing strong evidence for an associative Ni–arene π intermediate. Significantly, the more electron-donating ancillary ligands gave the highest proportion of intramolecular products, implying stronger Ni–arene associative intermediates and/or increased reactivities in the subsequent oxidative additions. As an example, the most electron-donating ligand examined, 1,2-bis(diethylphosphino)ethane (depe), gave an 800-fold preference for the intramolecular products when low concentrations of competitive agent were used (i.e., most similar to the polymerization conditions). Finally, these studies revealed that bidentate phosphine ligands yield more intramolecular products than monodentate phosphine

ligands. These results align well with the improved chain-growth behavior observed in standard^{43,65} and surface-initiated CTP⁶⁶ with bidentate phosphines.

Scheme 1-4. Support for an Intermediate Ni–Arene π -Complex⁶⁴

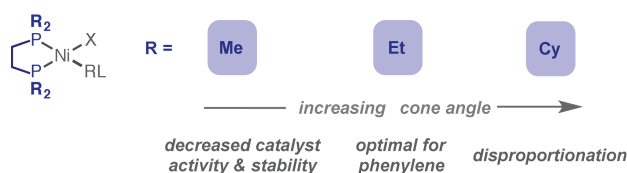


Having provided indirect support for π -associative intermediates in the small-molecule system, we evaluated the same ligands in phenylene polymerization by comparing the polymer dispersities.⁶⁴ This analysis is complicated, however, by the fact that precatalyst initiation rates also impact the dispersity.⁷ As a result, we compared the dispersities with and without the competitive agent. We expected that the intermolecular, chain-transfer process could be “turned on” with added competitive agent. Consistent with the small-molecule studies, we found that the most electron-donating ancillary ligand (depe) was the most resistant to the intermolecular reaction even at high competitive agent concentrations. Overall, these results indicate that stabilizing the Ni–arene π -complex and increasing its reactivity in the oxidative addition reduces the likelihood of chain transfer, improving CTP.

Given the effect of ancillary ligand electronic properties on the chain-growth behavior, we also investigated the impact of their steric properties (Scheme 1-5).⁴⁰ We anticipated that increasing the cone angle using 1,2-bis(dicyclohexylphosphino)ethane (dcpe) would hinder additional molecules from interfering with the Ni–arene π -complex, further reducing chain

transfer. Instead, we continuously observed Ni(dcppe)Cl₂ (along with other species) in the ³¹P NMR spectra during polymerization, stemming from either unreacted precatalyst or a process that regenerates it (e.g., disproportionation). In contrast, reducing the cone angle with 1,2-bis(dimethylphosphino)ethane (dmpe) resulted in decreased catalyst activity and stability during polymerization. In contrast to the results with phenylene, Higashihara found that dcppe gave the narrowest dispersity in Negishi-type CTP of 3-hexylthiophene compared with ligands with smaller cone angles (i.e., depe and dppe).¹² Combined, these experiments demonstrate that the ancillary ligand cone angle should be optimized for each monomer, with a dual focus on reducing catalyst decomposition and facilitating chain-growth behavior.

Scheme 1-5. Influence of the Cone Angle on Ni-Mediated Phenylene Polymerization⁴⁰



Although this work focuses on the specific case of phosphine-ligated catalysts in phenylene polymerizations, the lessons learned should be broadly applicable: (i) ancillary ligand electronic properties should be optimized to stabilize the π -complex and increase its subsequent reactivity in oxidative addition (note that a too-strong π -complex could inhibit chain walking and catalyst turnover⁵⁴) and (ii) ancillary ligand steric properties show a “goldilocks” effect (i.e., not too big and not too small) on the relative productive/unproductive pathways as well as on the catalyst stability. For phenylene polymerization, we found that a bisphosphine ancillary ligand that is electron-donating with a moderate cone angle (i.e., depe) led to the “matched” case with greatest chain-growth behavior. This ligand is not without limitations, however, as precatalyst initiation (with Ni(depe)Cl₂) is slower than propagation. Although reactive ligands can be

introduced to accelerate the initiation, the corresponding precatalyst structures are more challenging to synthesize and handle.

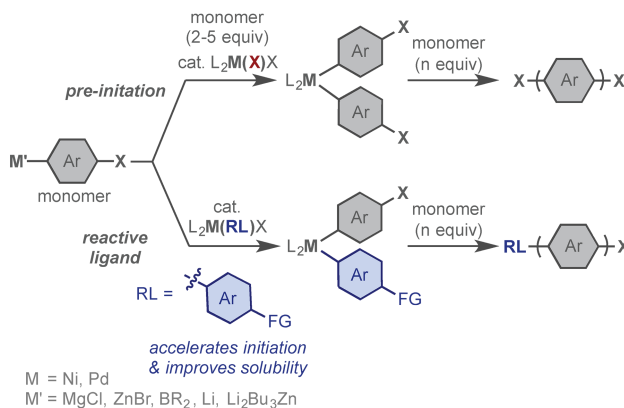
1.3 Reactive Ligand

The reactive ligand (RL), if present, is initially bound to the precatalyst but after one turnover becomes the ω -end of the polymer chain. As such, the reactive ligand can be used to tune precatalyst solubility, stability, and reactivity without influencing propagation. In addition, the reactive ligand can be used to selectively functionalize one chain end for postpolymerization use.⁶⁷

Precatalysts containing reactive ligands can be prepared either by aryl halide oxidative addition with Ni(0) or by reacting Ni(II) precursors with an organometallic reagent; however, in many cases a subsequent ligand exchange reaction is necessary to generate the desired precatalyst.^{66,68,69} The alternative one-step approach involves reacting aryl Grignard reagents directly with a dihalide precatalyst already containing the ancillary ligand. For chelating ancillary ligands, this approach requires an ortho substituent on the reactive ligand to prevent two consecutive transmetalations.⁷⁰ Ortho-substituted reactive ligands have become standard practice as they also improve precatalyst stability, generating polymers with the largest fraction of RL/H end groups.⁶⁸ This effect is caused by a favorable overlap between the ortho substituent's π^* orbital and the Ni d_{xy} orbitals.⁷¹ This interaction is further stabilized by the reactive ligand's restricted rotation due to steric interactions with the ancillary ligand.⁷² Precatalysts with tailored reactive ligands have been used for postpolymerization modification,⁶⁷ reaction monitoring,⁷ and synthesis of polymers directly off surfaces.^{65,66} However, designing reactive ligands specifically to accelerate initiation has been overlooked until recently.

The precatalyst initiation rate can have a significant influence on dispersities, polymer length, and sequence. Rate studies of several Ni-mediated polymerizations revealed that initiation and propagation proceed through the same turnover-limiting steps and that in many cases initiation was slower than propagation.⁵¹ In such cases, the ancillary ligand cannot be used to selectively accelerate initiation over propagation. Slow initiation by dihalide catalysts is attributed to poor catalyst solubility and, in some cases, unfavorable transmetalations due to monomer/monomer side-chain interactions.⁶¹ Preinitiation of dihalide catalysts with >2 equiv of monomer has been used to separate initiation from propagation^{8,10} (Scheme 1-6); nevertheless, precatalyst insolubility remains problematic. A superior approach is to design reactive ligands that selectively accelerate initiation and at the same time enhance the precatalyst stability and solubility (Scheme 1-6).

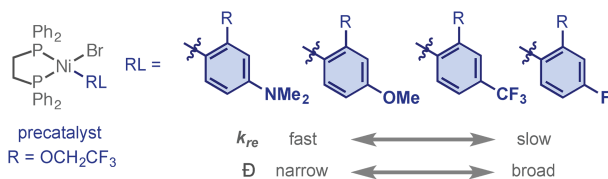
Scheme 1-6. Initiation through Preinitiation (top) or Use of Reactive Ligands (bottom)



We targeted reactive ligands that would selectively accelerate precatalyst initiation for phenylene polymerization. Our inspiration came from work by Hartwig,⁶³ who showed that electronically mismatched arenes exhibited the highest reductive elimination rates in Pt complexes. We began our studies with reactive ligands that were electronically dissimilar to the monomer and measured the rate of biaryl reductive elimination (Scheme 1-7).⁷ The reactive ligand contained an *o*-trifluoroethoxy group, which provides stability and enables reaction

monitoring by in situ ^{19}F NMR spectroscopy. The reactive ligand's electronic properties had a significant rate effect, with a 132-fold difference between the slowest (*p*-F) and fastest (*p*-NMe₂). The large range of rates that can be achieved simply by modifying the para-position of the reactive ligand is impressive and represents an easy target for future catalyst design.

Scheme 1-7. Effect of the Reactive Ligand on Initiation Rates and Phenylene Polymerization⁷

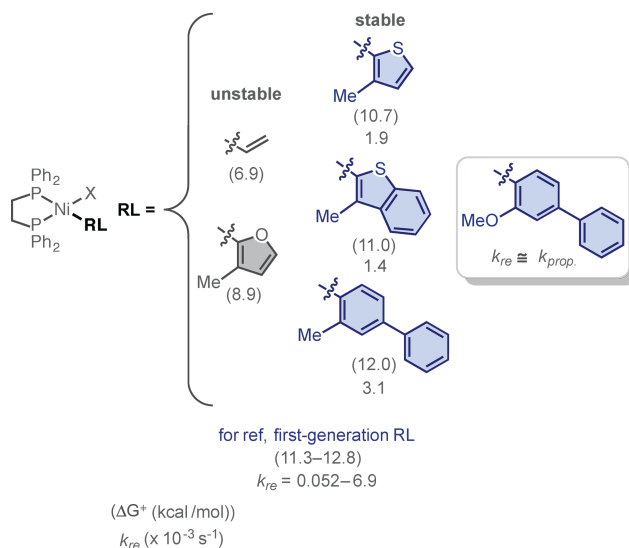


To understand these rate trends, computational studies were used to evaluate the activation barriers (ΔG^\ddagger) for reductive elimination as a function of reactive ligand structure through collaboration with Wheeler.⁷ We found that the determining factor for initiation rates is the change in charge redistribution between the RL and monomer in going from the ground state to the transition state, with the fastest-initiating precatalyst exhibiting the smallest change. Notably, this model is not consistent with the electronic-mismatch model proposed by Hartwig.⁶³ However, this trend is consistent with the rates observed from our model system, wherein resonance-based substituents facilitated charge delocalization in the ground state and resulted in accelerated reductive elimination. Combined, these results suggest that reactive ligand electronic properties should be “matched” to the specific monomer to minimize changes in charge delocalization and achieve the highest initiation rates.

Building on this foundation, we developed a streamlined approach to measure initiation and propagation rates simultaneously that, importantly, does not require F-labeling.⁷³ Using the computational model, we targeted a second-generation precatalyst to achieve even higher initiation rates (Chart 1-2). All of the precatalysts bearing reactive ligands with significantly lower reductive elimination barriers, however, were unstable during isolation. As a consequence,

we instead evaluated heteroaromatic ligands with activation barriers similar to those of the first-generation precatalysts, where the initiation rates approached those of propagation. We also analyzed ortho-substituted biphenyl ligands to more closely mimic the monomer/polymer reductive elimination occurring during propagation. The observed initiation rates were similar to those of our first-generation precatalysts.⁷ Next, we replaced the *o*-methyl with an *o*-methoxy because resonance-donating reactive ligands previously displayed the highest initiation rates. This substitution led to a dramatic increase in the initiation rate, now on par with the propagation rate.

Chart 1-2. Second-Generation Reactive Ligands⁷³

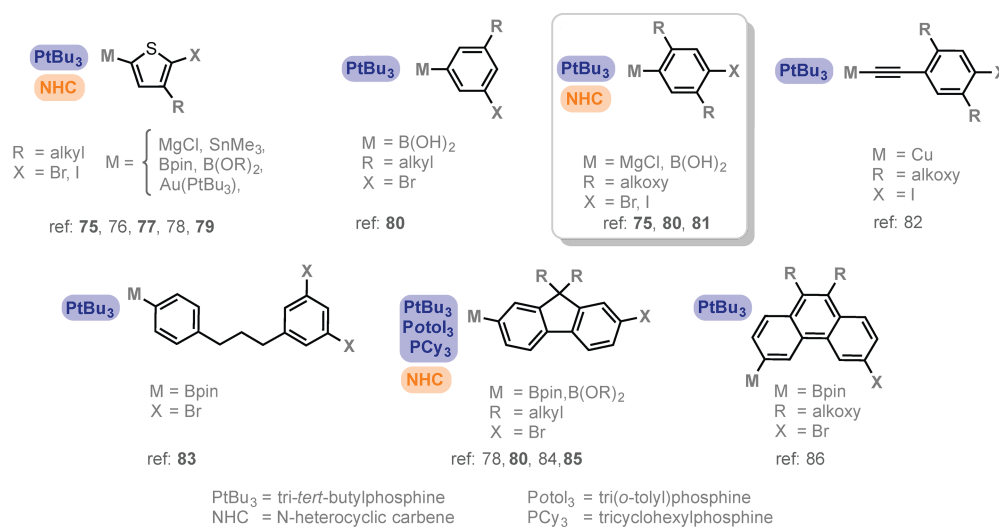


To summarize, by means of a combined experimental and computational approach, a precatalyst was identified that demonstrates the highest measured initiation rates for phenylene polymerization. Given the widespread interest in using reactive ligands to drive applications,^{65–67} future efforts should focus on identifying fast-initiating reactive ligands for these systems.

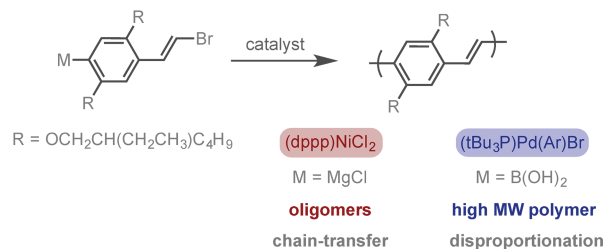
1.4 Transition Metal

Although the field largely focuses on nickel catalysts, palladium catalysts are more tolerant of other activation methods and functional groups and in some cases outperform Ni (Chart 1-3). For example, Yokozawa and co-workers reported that Pd-based catalysts generated high-molecular-weight poly(*p*-phenylene vinylene) while the Ni catalysts gave only oligomers (Scheme 1-8).⁷⁴ Nevertheless, even with Pd, the dispersities were quite broad, and end-group analysis revealed a disproportionation reaction. On the basis of our results, increasing the ancillary ligand's steric properties could minimize the disproportionation, although this hypothesis remains untested for this system.

Chart 1-3. Representative Examples of Pd-Catalyzed CTP (Examples with $DP > 15$ and $\mathcal{D} < 1.5$ in a Homopolymerization Are Included; Bolded References Report $\mathcal{D} \leq 1.25$)⁷⁵⁻⁸⁶



Scheme 1-8. Comparison of Nickel- versus Palladium-Catalyzed Syntheses of Poly(p-phenylene vinylene)⁷⁴



Although palladium-based catalysts are underdeveloped in CTP, their extensive use in small-molecule reactions can be a source of inspiration.⁸⁷ For example, we discovered a Pd–(NHC)PdCl₂(3-CIPy) catalyst for CTP⁷⁵ by noticing selective difunctionalization reactions reported by Larrosa and Goldup⁸⁸ and Hu.⁸⁹ In these cases, the statistically favored intermolecular pathway was outcompeted by an intramolecular pathway (presumably via a Pd–arene π -complex). We hypothesized that a similar intramolecular pathway (chain-growth) might be observed during polymerization. This approach of looking to the vast small-molecule literature is important as we aim to expand the monomer scope to more complex and electronically varied (hetero)arene-based monomers. Moreover, the expansive library of commercially available Pd precatalysts provides a rich and unexplored platform for CTP that we believe will expand its reach and impact.

1.5 On Using Model Systems

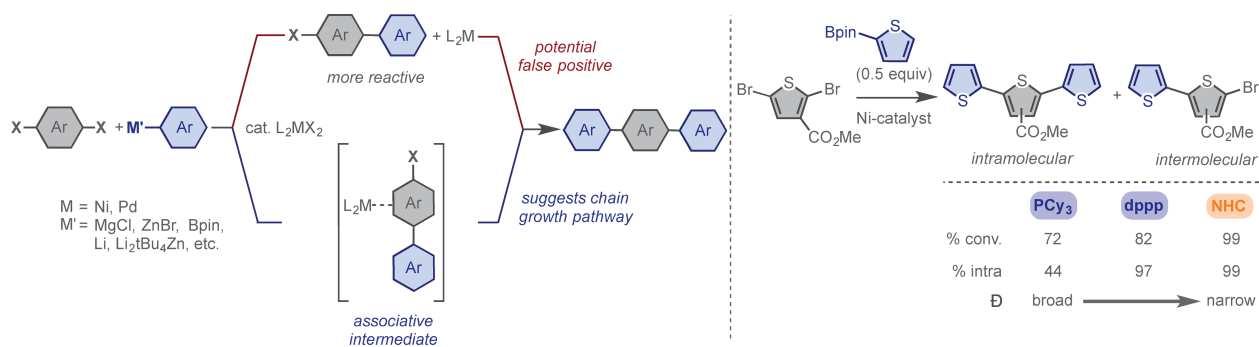
Small-molecule model systems can be found throughout the CTP literature. Advantages include providing a mechanistic window into otherwise unobservable processes and efficient screening of catalysts for evidence of an intramolecular process. However, users should proceed with caution by acknowledging that a model system provides information only about the model system. We can draw inferences and inspiration from the results, but they may not always translate to polymerizations and in some cases can be misleading. For example, we added PPh₃

to trap free Ni(0) generated in the model system when measuring initiation rates.⁷ Later, we discovered that the added PPh₃ also accelerated the reaction,⁷³ likely through the formation of a five-coordinate species in the reductive elimination transition state. Labile ligands are well-known for their ability to associate and dissociate from transition metals, changing their coordination number and geometry.⁹⁰ On the basis of these results, we suspect that PPh₃ may play a noninnocent role in other polymerizations when precatalysts are prepared in situ from PPh₃-ligated starting materials (e.g., (Ph₃P)₂Ni(Ar)X).^{68,69} At the same time, this observation hints at a relatively unexplored strategy to improve polymerizations by intentionally using additives.

Model systems for CTP have been primarily used to identify alternative catalysts.^{8,25,49,77} A common example is difunctionalization reactions, which evaluate catalysts by reacting a dihalide monomer with substoichiometric monofunctionalized, organometallic monomer. A potential chain-growth catalyst-monomer system is identified when more triarene (intramolecular) products than diarene (intermolecular) products are formed. Nevertheless, substantial triarene formation can be observed when the biaryl intermediate is simply more reactive than the intermediate dihalide (Scheme 1-9).⁹¹ One way to distinguish these “false positives” is to monitor triarene formation over time; the absence of triarene at low conversion suggests that its formation is due to reactivity differences and not an intramolecular pathway. An alternative approach is to add a competitive agent to trap the “free” catalyst after dissociation. With these caveats in mind, we still believe that small-molecule studies are essential tools to improve existing methods and to identify new catalysts for CTP. For example, Noonan and co-workers evaluated three ancillary ligands for Suzuki polycondensation of thiophene-3-carboxylate (Scheme 1-9).⁹⁵ Using dihalogen and monoborylated monomer analogues, they

found that strong σ -donating NHC-ligated Ni catalysts gave high triarene formation with nearly complete monomer conversion, indicating a good catalyst–monomer system. Consistent with these results, the NHC-ligated Ni catalysts generated polymers with the narrowest dispersity and fewest side reactions among the catalysts tested. Overall, the success of these model systems demonstrates their effectiveness as a simple method to screen catalysts for new CTP systems.

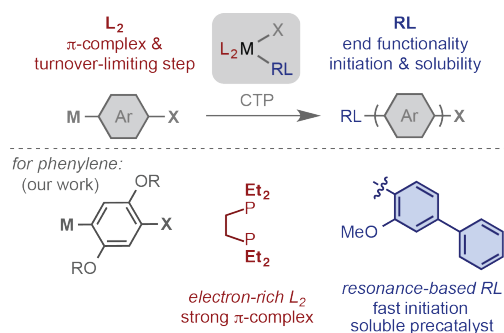
Scheme 1-9. (left) Two Pathways That Form Triarene;⁹¹ (right) Small-Molecule Difunctionalization To Identify CTP for Thiophene-3-carboxylate.²⁵



1.6 Conclusion

Overall, we have summarized our work on identifying effective catalysts for the living, chain-growth polymerization of phenylene by understanding the mechanistic impact of the ancillary and reactive ligand structures as well as the identity of the metal. We have used model systems to obtain unprecedented mechanistic insight that has facilitated systematic tuning of catalyst parameters (Scheme 1-10). We believe that the tools presented herein, and the lessons learned, will guide future catalyst development to tackle the field's biggest challenges: electron-deficient and/or structurally complex monomers. Although we are still a long way from achieving the efficiency and broad monomer scope displayed by other living, chain-growth polymerization methods, recent CTP developments forecast its increasing relevance to the synthesis and applications of conjugated polymers.

Scheme 1-10. Summary of Precatalyst Parameters and Their Impact



1.7 Outlook

The mechanistic understanding presented above demonstrates how catalyst design can influence the productive and unproductive pathways during CTP. Nevertheless, a strong understanding of the metal-polymer π -bound intermediate remained elusive. Therefore, in Chapter 2 of this thesis we designed a method to evaluate the metal-polymer π -bound intermediate and its ring-walking abilities. Using in situ end-capping, we could specifically identify the impact of the ancillary ligand, transition metal, and polymer identity. Three catalysts and two polymer scaffolds were evaluated and provide trends to facilitate designing future catalyst/monomer pairs.

As discussed in this introduction, phosphine-based ancillary ligands are the most frequently used ancillary ligands for CTP (cf. Chart 1-1 & 1-3). In Chapter 3 we explore an alternative class of ancillary ligands, α -diimines, for CTP. We identified a sterically encumbering ancillary ligand that outperforms previously used α -diimines. Evaluating the polymerization mechanism revealed that the α -diimine-ligated Ni precatalyst polymerizes via a pseudo-living, chain-growth method. Because α -diimine-ligated precatalysts also generate poly(olefin) in a living manner, this precatalyst was subsequently used to synthesize thiophene/olefin block copolymers in one-pot. A high barrier for sp^3/sp^2 reductive elimination

during mechanism-switching however resulted in dissociated, active catalysts that would initiate thiophene homopolymers.

In Chapter 4, we describe using a model system to develop a copolymerization method using catalysts that are efficient in sp^3/sp^2 reductive elimination. The model system simulates chain-extension from the olefin macroinitiator with thiophene by evaluating catalysts on their ability to end-cap in situ generated poly(thiophene) with methyl Grignard. While in practice, these models show promise for generating block copolymers, when applied to the copolymerization macroinitiator termination occurs.

Ultimately, this thesis aims to use mechanistic insight to enable CTP to be used for synthesizing high-performing materials. Chapters 2–4 elucidate mechanistic insight to facilitate catalyst design, identify alternative catalyst scaffolds for CTP, and attempt to generate high-performing materials in a streamlined, one-pot system. For CTP to continue to evolve, we believe additional precatalysts will need to be discovered. High-performing conjugated polymers with complex architectures are continually being developed, but have not been synthesized in a living manner. In Chapter 5, we provide insight on palladium precatalysts that have promise for generating these complex, high-performing polymers.

1.8 References

- (1) Grimsdale, A. C.; Chan, K. L.; Martin, R. E.; Jokisz, P. G.; Holmes, A. B. Synthesis of Light-Emitting Conjugated Polymers for Applications in Electroluminescent Devices. *Chem. Rev.* **2009**, *109*, 897–1091.

- (2) Bryan, Z. J.; McNeil, A. J. Conjugated Polymer Synthesis via Catalyst-Transfer Polycondensation (CTP): Mechanism, Scope, and Applications. *Macromolecules* **2013**, *46*, 8395–8405.
- (3) Yokozawa, T.; Ohta, Y. Transformation of Step-Growth Polymerization into Living Chain-Growth Polymerization. *Chem. Rev.* **2016**, *116*, 1950–1968.
- (4) Takagi, K.; Kawagita, E.; Kouchi, R. Synthesis and Characterization of Polythiophene Derivatives with Nitrogen Heterocycles on the Side Chain. *J. Polym. Sci., Part A: Polym. Chem.* **2014**, *52*, 2166–2174.
- (5) Schiefer, D.; Wen, T.; Wang, Y.; Goursot, P.; Komber, H.; Hanselmann, R.; Braunstein, P.; Reiter, G.; Sommer, M. Nickel Catalyst with a Hybrid P, N Ligand for Kumada Catalyst Transfer Polycondensation of Sterically Hindered Thiophenes. *ACS Macro Lett.* **2014**, *3*, 617–621.
- (6) Pammer, F.; Jager, J.; Rudolf, B.; Sun, Y. Soluble Head-to-Tail Regioregular Polythiazoles: Preparation, Properties, and Evidence for Chain-Growth Behavior in the Synthesis via Kumada-Coupling Polycondensation. *Macromolecules* **2014**, *47*, 5904–5912.
- (7) Lee, S. R.; Bloom, J. W. G.; Wheeler, S. E.; McNeil, A. J. Accelerating Ni(II) Precatalyst Initiation Using Reactive Ligands and its Impact on Chain-Growth Polymerizations. *Dalton Trans.* **2013**, *42*, 4218–4222.
- (8) Sheina, E. E.; Liu, J.; Iovu, M. C.; Laird, D. W.; McCullough, R. D. Chain Growth Mechanism for Regioregular Nickel-Initiated Cross-Coupling Polymerizations. *Macromolecules* **2004**, *37*, 3526–3528.

- (9) Iovu, M. C.; Sheina, E. E.; Gil, R. R.; McCullough, R. D. Experimental Evidence for the Quasi-“Living” Nature of the Grignard Metathesis Method for the Synthesis of Regioregular Poly(3-alkylthiophenes). *Macromolecules* **2005**, *38*, 8649–8656.
- (10) Lanni, E. L.; McNeil, A. J. Mechanistic Studies on Ni(dppe)Cl₂-Catalyzed Chain-Growth Polymerizations: Evidence for Rate-Determining Reductive Elimination. *J. Am. Chem. Soc.* **2009**, *131*, 16573–16579.
- (11) Yokoyama, A.; Miyakoshi, R.; Yokozawa, T. Chain-Growth Polymerization for Poly(3-hexylthiophene) with a Defined Molecular Weight and a Low Polydispersity. *Macromolecules* **2004**, *37*, 1169–1171.
- (12) Goto, E.; Nakamura, S.; Kawauchi, S.; Mori, H.; Ueda, M.; Higashihara, T. Precision Synthesis of Regioregular Poly(3-hexylthiophene) with Low Dispersity Using a Zincate Complex Catalyzed by Nickel with the Ligand of 1,2-bis(dicyclohexylphosphino)ethane. *J. Polym. Sci., Part A: Polym. Chem.* **2014**, *52*, 2287–2296.
- (13) Beryozkina, T.; Senkovskyy, V.; Kaul, E.; Kiriy, A. Kumada Catalyst-Transfer Polycondensation of Thiophene-Based Oligomers: Robustness of a Chain-Growth Mechanism. *Macromolecules* **2008**, *41*, 7817–7823.
- (14) Ohshimizu, K.; Ueda, M. Well-Controlled Synthesis of Block Copolythiophenes. *Macromolecules* **2008**, *41*, 5289–5294.
- (15) Fujita, K.; Sumino, Y.; Ide, K.; Tamba, S.; Shono, K.; Shen, J.; Nishino, T.; Mori, A.; Yasuda, T. Synthesis of Poly(3-substituted thiophene)s of Remarkably High Solubility in Hydrocarbon via Nickel-Catalyzed Deprotonative Cross-Coupling Polycondensation. *Macromolecules* **2016**, *49*, 1259–1269.

- (16) Tamba, S.; Fuji, T.; Nakamura, K.; Mori, A. Nickel(II)-Catalyzed Cross-Coupling Polycondensation of Thiophenes via C-S Bond Cleavage. *Organometallics* **2014**, *33*, 12–15.
- (17) Song, I. Y.; Kim, J.; Im, M. J.; Moon, B. J.; Park, T. Synthesis and Self-Assembly of Thiophene-Based All-Conjugated Amphiphilic Diblock Copolymers with a Narrow Molecular Weight Distribution. *Macromolecules* **2012**, *45*, 5058–5068.
- (18) Fuji, K.; Tamba, S.; Shono, K.; Sugie, A.; Mori, A. Murahashi Coupling Polymerization: Nickel(II)-N-Heterocyclic Carbene Complex-Catalyzed Polycondensation of Organolithium Species of (Hetero)arenes. *J. Am. Chem. Soc.* **2013**, *135*, 12208–12211.
- (19) Magurudeniya, H. D.; Sista, P.; Westbrook, J. K.; Ourso, T. E.; Nguyen, K.; Maher, M. C.; Alemseghed, M. G.; Biewer, M. C.; Stefan, M. C. Nickel(II) α -Diimine Catalyst for Grignard Metathesis (GRIM) Polymerization. *Macromol. Rapid Commun.* **2011**, *32*, 1748–1752.
- (20) Tamba, S.; Shono, K.; Sugie, A.; Mori, A. C-H Functionalization Polycondensation of Chlorothiophenes in the Presence of Nickel Catalyst with Stoichiometric or Catalytically Generated Magnesium Amide. *J. Am. Chem. Soc.* **2011**, *133*, 9700–9703.
- (21) Zhang, Y.; Tajima, K.; Hashimoto, K. Nanostructure Formation in Poly(3-hexylthiophene-block-3-(2-ethylhexyl)thiophene)s. *Macromolecules* **2009**, *42*, 7008–7015.
- (22) Vallat, P.; Lamps, J.-P.; Schosseler, F.; Rawiso, M.; Catala, J.-M. Quasi-Controlled Polymerization through a Nickel Catalyst Process of a Functionalized Thiophene Monomer: Kinetic Studies and Application to the Synthesis of Regioregular Poly(thiophene-3-acetic acid). *Macromolecules* **2007**, *40*, 2600–2602.
- (23) Mao, Y.; Wang, Y.; Lucht, B. L. Regiocontrolled Synthesis of Poly(3-alkylthiophene)s by Grignard Metathesis. *J. Polym. Sci., Part A: Polym. Chem.* **2004**, *42*, 5538–5547.

- (24) Holcombe, T. W.; Woo, C. H.; Kavulak, D. F. J.; Thompson, B. C.; Frechet, J. M. J. All-Polymer Photovoltaic Devices of Poly(3-(4'-noctyl)-phenylthiophene) from Grignard Metathesis (GRIM) Polymerization. *J. Am. Chem. Soc.* **2009**, *131*, 14160–14161.
- (25) Qiu, Y.; Worch, J. C.; Fortney, A.; Gayathri, C.; Gil, R. R.; Noonan, K. J. T. Nickel-Catalyzed Suzuki Polycondensation for Controlled Synthesis of Ester-Functionalized Conjugated Polymers. *Macromolecules* **2016**, *49*, 4757–4762.
- (26) Pan, C.; Sugiyasu, K.; Aimi, J.; Sato, A.; Takeuchi, M. Picket-Fence Polythiophene and its Diblock Copolymers that Afford Microphase Separations Comprising a Stacked and an Isolated Polythiophene Ensemble. *Angew. Chem. Int. Ed.* **2014**, *53*, 8870–8875.
- (27) Peeters, H.; Jivanescu, M.; Stesmans, A.; Pereira, L. M. C.; Dillemans, L.; Locquet, J.-P.; Van Bael, M. J.; Persoons, A.; Koeckelberghs, G. Influence of the Bulkiness of the Substituent on the Aggregation and Magnetic Properties of Poly(3-alkylthiophene)s. *J. Polym. Sci., Part A: Polym. Chem.* **2014**, *52*, 76–86.
- (28) Verswyvel, M.; Monnaie, F.; Koeckelberghs, G. AB Block Copoly(3-alkylthiophenes): Synthesis and Chiroptical Behavior. *Macromolecules* **2011**, *44*, 9489–9498.
- (29) Adachi, I.; Miyakoshi, R.; Yokoyama, A.; Yokozawa, T. Synthesis of Well-Defined Polythiophene with Oxyethylene Side Chain: Effect of Phosphine Ligands on Catalyst-Transfer Polycondensation. *Macromolecules* **2006**, *39*, 7793–7795.
- (30) Zhao, C.; Nagura, K.; Takeuchi, M.; Sugiyasu, K. Twisting Poly(3-substituted thiophene)s: Cyclopolymerization of Gemini Thiophene Monomers through Catalyst-Transfer Polycondensation. *Polym. J.* **2017**, *49*, 133–139.
- (31) Palermo, E. F.; van der Laan, H. L.; McNeil, A. J. Impact of π conjugated Gradient Sequence Copolymers on Polymer Blend Morphology. *Polym. Chem.* **2013**, *4*, 4606–4611.

- (32) Pammer, F.; Guo, F.; Lalancette, R. A.; Jakle, F. Synthesis, Structures, and Hydroboration of Oligo- and Poly(3-alkynylthiophene)s. *Macromolecules* **2012**, *45*, 6333–6343.
- (33) Brusso, J. L.; Lilliedal, M. R.; Holdcroft, S. π -Conjugated Polymers with Thermocleavable Substituents for Use as Active Layers in Organic Photovoltaics. *Polym. Chem.* **2011**, *2*, 175–180.
- (34) Bridges, C. R.; Yan, H.; Pollit, A. A.; Seferos, D. S. Controlled Synthesis of Fully π -conjugated Donor-Acceptor Block Copolymers Using a Ni(II) Diimine Catalyst. *ACS Macro Lett.* **2014**, *3*, 671–674.
- (35) Hollinger, J.; Jahnke, A. A.; Coombs, N.; Seferos, D. S. Controlling Phase Separation and Optical Properties in Conjugated Polymers through Selenophene–Thiophene Copolymerization. *J. Am. Chem. Soc.* **2010**, *132*, 8546–8547.
- (36) Qiu, Y.; Fortney, A.; Tsai, C.-H.; Baker, M. A.; Gil, R. R.; Kowalewski, T.; Noonan, K. J. T. Synthesis of Polyfuran and Thiophene-Furan Alternating Copolymers Using Catalyst-Transfer Polycondensation. *ACS Macro Lett.* **2016**, *5*, 332–336.
- (37) Bridges, C. R.; Guo, C.; Yan, H.; Miltenburg, M. B.; Li, P.; Li, Y.; Seferos, D. S. Conjugated Polymers with Switchable Carrier Polarity. *Macromolecules* **2015**, *48*, 5587–5595.
- (38) Ye, S.; Steube, M.; Carrera, E. I.; Seferos, D. S. What Limits the Molecular Weight and Controlled Synthesis of Poly(3-alkyltellurophene)s? *Macromolecules* **2016**, *49*, 1704–1711.
- (39) Smith, M. L.; Leone, A. K.; Zimmerman, P. M.; McNeil, A. J. Impact of Preferential π -Binding in Catalyst-Transfer Polycondensation of Thiazole Derivatives. *ACS Macro Lett.* **2016**, *5*, 1411–1415.
- (40) Lanni, E. L.; Locke, J. R.; Gleave, C. M.; McNeil, A. J. Ligand-Based Steric Effects in Ni-Catalyzed Chain-Growth Polymerizations Using Bis(dialkylphosphino)ethanes. *Macromolecules* **2011**, *44*, 5136–5145.

- (41) Yokoyama, A.; Kato, A.; Miyakoshi, R.; Yokozawa, T. Precision Synthesis of Poly(N-hexylpyrrole) and its Diblock Copolymer with Poly(*p*-phenylene) via Catalyst-Transfer Polycondensation. *Macromolecules* **2008**, *41*, 7271–7273.
- (42) Stefan, M. C.; Javier, A. E.; Osaka, I.; McCullough, R. D. Grignard Metathesis Method (GRIM): Toward a Universal Method for the Synthesis of Conjugated Polymers. *Macromolecules* **2009**, *42*, 30–32.
- (43) Wu, S.; Sun, Y.; Huang, L.; Wang, J.; Zhou, Y.; Geng, Y.; Wang, F. Grignard Metathesis Chain-Growth Polymerization for Poly-(bithienylmethylene)s: Ni Catalyst Can Transfer across the Nonconjugated Monomer. *Macromolecules* **2010**, *43*, 4438–4440.
- (44) Tsai, C.-H.; Fortney, A.; Qiu, Y.; Gil, R. R.; Yaron, D.; Kowalewski, T.; Noonan, K. J. T. Conjugated Polymers with Repeated Sequences of Group 16 Heterocycles Synthesized through Catalyst-Transfer Polycondensation. *J. Am. Chem. Soc.* **2016**, *138*, 6798–6804.
- (45) Ono, R. J.; Kang, S.; Bielawski, C. W. Controlled Chain-Growth Kumada Catalyst Transfer Polycondensation of a Conjugated Alternating Copolymer. *Macromolecules* **2012**, *45*, 2321–2326.
- (46) Murakami, K.; Tanaka, S.; Mori, A. Linear-Selective Cross-Coupling Polymerization of Branched Oligothiophene by Deprotonative Metalation and Cross-Coupling. *Polym. Chem.* **2015**, *6*, 6573–6578.
- (47) Todd, A. D.; Bielawski, C. W. Controlled Synthesis of an Alternating Donor–Acceptor Conjugated Polymer via Kumada Catalyst-Transfer Polycondensation. *ACS Macro Lett.* **2015**, *4*, 1254–1258.
- (48) Nanashima, Y.; Yokoyama, A.; Yokozawa, T. Synthesis of Novel Blue-Light-Emitting Polypyridine. *J. Polym. Sci., Part A: Polym. Chem.* **2012**, *50*, 1054–1061.

- (49) Nanashima, Y.; Yokoyama, A.; Yokozawa, T. Synthesis of Well-Defined Poly(2-alkoxypyridine-3,5-diyl) via Ni-Catalyst-Transfer Condensation Polymerization. *Macromolecules* **2012**, *45*, 2609–2613.
- (50) Ohshimizu, K.; Takahashi, A.; Higashihara, T.; Ueda, M. Synthesis of Poly(*m*-phenylene) and Poly(*m*-phenylene)-block-Poly(3-hexylthiophene) with Low Polydispersities. *J. Polym. Sci., Part A: Polym. Chem.* **2011**, *49*, 2709–2714.
- (51) Lee, S. R.; Bryan, Z. J.; Wagner, A. M.; McNeil, A. J. Effect of Ligand Electronic Properties on Precatalyst Initiation and Propagation in Ni-Catalyzed Cross-Coupling Polymerizations. *Chem. Sci.* **2012**, *3*, 1562–1566.
- (52) Miyakoshi, R.; Shimono, K.; Yokoyama, A.; Yokozawa, T. Catalyst-Transfer Polycondensation for the Synthesis of Poly(*p*-phenylene) with Controlled Molecular Weight and Low Polydispersity. *J. Am. Chem. Soc.* **2006**, *128*, 16012–16013.
- (53) Umezawa, K.; Oshima, T.; Yoshizawa-Fujita, M.; Takeoka, Y.; Rikukawa, M. Synthesis of Hydrophilic–Hydrophobic Block Copolymer Ionomers Based on Polyphenylenes. *ACS Macro Lett.* **2012**, *1*, 969–972.
- (54) Willot, P.; Govaerts, S.; Koeckelberghs, G. The Controlled Polymerization of Poly(cyclopentadithiophene)s and Their AllConjugated Block Copolymers. *Macromolecules* **2013**, *46*, 8888–8895.
- (55) Traina, C. A.; Bakus, R. C., II; Bazan, G. C. Design and Synthesis of Monofunctionalized, Water-Soluble Conjugated Polymers for Biosensing and Imaging Applications. *J. Am. Chem. Soc.* **2011**, *133*, 12600–12607.

- (56) Sui, A.; Shi, X.; Wu, S.; Tian, H.; Geng, Y.; Wang, F. Controlled Synthesis of Polyfluorenes via Kumada Catalyst Transfer Polycondensation with Ni(acac)₂/dppp as the Catalyst. *Macromolecules* **2012**, *45*, 5436–5443.
- (57) Sui, A.; Shi, X.; Wang, Y.; Geng, Y.; Wang, F. Kumada Catalyst Transfer Polycondensation for Controlled Synthesis of Polyfluorenes Using 1,3-bis(diarylphosphino)propanes as Ligands. *Polym. Chem.* **2015**, *6*, 4819–4827.
- (58) Senkovskyy, V.; Tkachov, R.; Komber, H.; Sommer, M.; Heuken, M.; Voit, B.; Huck, W. T. S.; Kataev, V.; Petr, A.; Kiriya, A. Chain-Growth Polymerization of Unusual Anion-Radical Monomers Based on Naphthalene Diimide: A New Route to Well-Defined n-Type Conjugated Copolymers. *J. Am. Chem. Soc.* **2011**, *133*, 19966–19970.
- (59) Bridges, C. G.; McCormick, T. M.; Gibson, G. L.; Hollinger, J.; Seferos, D. S. Designing and Refining Ni(II)diimine Catalysts Toward the Controlled Synthesis of Electron-Deficient Conjugated Polymers. *J. Am. Chem. Soc.* **2013**, *135*, 13212–13219.
- (60) Pollit, A. A.; Bridges, C. R.; Seferos, D. S. Evidence for the Chain-Growth Synthesis of Statistical π -Conjugated Donor–Acceptor Copolymers. *Macromol. Rapid Commun.* **2015**, *36*, 65–70.
- (61) Tkachov, R.; Senkovskyy, V.; Komber, H.; Kiriya, A. Influence of Alkyl Substitution Pattern on Reactivity of Thiophene-Based Monomers in Kumada Catalyst-Transfer Polycondensation. *Macromolecules* **2011**, *44*, 2006–2015.
- (62) Boyd, S. D.; Jen, A. K.-Y.; Luscombe, C. K. Steric Stabilization Effects in Nickel-Catalyzed Regioregular Poly(3-hexylthiophene) Synthesis. *Macromolecules* **2009**, *42*, 9387–9389.

- (63) Shekhar, S.; Hartwig, J. F. Distinct Electronic Effects on Reductive Eliminations of Symmetrical and Unsymmetrical Bis-Aryl Platinum Complexes. *J. Am. Chem. Soc.* **2004**, *126*, 13016–13027.
- (64) Bryan, Z. J.; McNeil, A. J. Evidence for a Preferential Intramolecular Oxidative Addition in Ni-Catalyzed Cross-Coupling Reactions and their Impact on Chain-Growth Polymerizations. *Chem. Sci.* **2013**, *4*, 1620–1624.
- (65) Senkovskyy, V.; Khanduyeva, N.; Komber, H.; Oertel, U.; Stamm, M.; Kuckling, D.; Kiriya, A. Conductive Polymer Brushes of Regioregular Head-to-Tail Poly(3-alkylthiophenes) via Catalyst-Transfer Surface-Initiated Polycondensation. *J. Am. Chem. Soc.* **2007**, *129*, 6626–6632.
- (66) Senkovskyy, V.; Tkachov, R.; Beryozkina, T.; Komber, H.; Oertel, U.; Horecha, M.; Bocharova, V.; Stamm, M.; Gevorgyan, S. A.; Krebs, F. C.; Kiriya, A. Hairy” Poly(3-hexylthiophene) Particles Prepared via Surface-Initiated Kumada Catalyst-Transfer Polycondensation. *J. Am. Chem. Soc.* **2009**, *131*, 16445–16453.
- (67) Fronk, S. L.; Mai, C.-K.; Ford, M.; Noland, R. P.; Bazan, G. C. End-Group-Mediated Aggregation of Poly(3-hexylthiophene). *Macromolecules* **2015**, *48*, 6224–6232.
- (68) Bronstein, H. A.; Luscombe, C. K. Externally Initiated Regioregular P3HT with Controlled Molecular Weight and Narrow Polydispersity. *J. Am. Chem. Soc.* **2009**, *131*, 12894–12895.
- (69) Doubina, N.; Ho, A.; Jen, A. K.-Y.; Luscombe, C. K. Effect of Initiators on the Kumada Catalyst-Transfer Polycondensation Reaction. *Macromolecules* **2009**, *42*, 7670–7677.
- (70) Senkovskyy, V.; Sommer, M.; Tkachov, R.; Komber, H.; Huck, W. T. S.; Kiriya, A. Convenient Route To Initiate Kumada CatalystTransfer Polycondensation Using Ni(dppe)Cl₂ or Ni(dppp)Cl₂ and Sterically Hindered Grignard Compounds. *Macromolecules* **2010**, *43*, 10157–10161.

- (71) Chatt, J.; Shaw, B. L. Alkyls and Aryls of Transition Metals. Part III. Nickel (II) Derivatives. *J. Chem. Soc.* **1960**, 1718–1729.
- (72) Hidai, M.; Kashiwagi, T.; Ikeuchi, T.; Uchida, Y. Oxidative Additions to Nickel(0): Preparation and Properties of a New Series of Aryl-Nickel(II) Complexes. *J. Organomet. Chem.* **1971**, *30*, 279–282.
- (73) Hall, A. O.; Lee, S. R.; Bootsma, A.; Bloom, J. W. G.; Wheeler, S. E.; McNeil, A. J. *J. Polym. Sci., Part A: Polym. Chem.* **2017**, *55*, 1530–1535.
- (74) Nojima, M.; Ohta, Y.; Yokozawa, T. Investigation of Catalyst-Transfer Condensation Polymerization for Synthesis of Poly(p-phenylenevinylene). *J. Polym. Sci., Part A: Polym. Chem.* **2014**, *52*, 2643–2653.
- (75) Bryan, Z. J.; Smith, M. L.; McNeil, A. J. Chain-growth Polymerization of Aryl Grignards Initiated by Stabilized NHC-Pd Precatalysts. *Macromol. Rapid Commun.* **2012**, *33*, 842–847.
- (76) Yokozawa, T.; Suzuki, R.; Nojima, M.; Ohta, Y.; Yokoyama, A. Precision Synthesis of Poly(3-hexylthiophene) from Catalyst-Transfer Suzuki-Miyaura Coupling Polymerization. *Macromol. Rapid Commun.* **2011**, *32*, 801–806.
- (77) Qiu, Y.; Mohin, J.; Tsai, C.-H.; Tristram-Nagle, S.; Gil, R. R.; Kowalewski, T.; Noonan, K. J. T. Stille Catalyst-Transfer Polycondensation Using Pd-PEPPSI-IPr for High-Molecular-Weight Regioregular Poly(3-hexylthiophene). *Macromol. Rapid Commun.* **2015**, *36*, 840–844.
- (78) Sui, A.; Shi, X.; Tian, H.; Geng, Y.; Wang, F. Suzuki–Miyaura Catalyst-Transfer Polycondensation with Pd(IPr)(OAc)₂ as the Catalyst for the Controlled Synthesis of Polyfluorenes and Polythiophenes. *Polym. Chem.* **2014**, *5*, 7072–7080.

- (79) Suraru, S.-L.; Lee, J. A.; Luscombe, C. K. Preparation of an Arylated Alkylthiophene Monomer via C–H Activation for Use in Pd-PEPPSI-IPr Catalyzed-Controlled Chain Growth Polymerization. *ACS Macro Lett.* **2016**, *5*, 533–536.
- (80) Zhang, H.-H.; Xing, C.-H.; Hu, Q.-S. Controlled Pd(0)/t-Bu₃P-Catalyzed Suzuki Cross-Coupling Polymerization of AB-Type Monomers with PhPd(t-Bu₃P)I or Pd₂(dba)₃/t-Bu₃P/ArI as the Initiator. *J. Am. Chem. Soc.* **2012**, *134*, 13156–13159.
- (81) Yokozawa, T.; Kohno, H.; Ohta, Y.; Yokoyama, A. Catalyst Transfer Suzuki–Miyaura Coupling Polymerization for Precision Synthesis of Poly(*p*-phenylene). *Macromolecules* **2010**, *43*, 7095–7100.
- (82) Kang, S.; Ono, R. J.; Bielawski, C. W. Controlled Catalyst Transfer Polycondensation and Surface-Initiated Polymerization of a *p*-Phenyleneethynylene-Based Monomer. *J. Am. Chem. Soc.* **2013**, *135*, 4984–4987.
- (83) Huang, W.; Su, L.; Bo, Z. Hyperbranched Polymers with a Degree of Branching of 100% Prepared by Catalyst Transfer Suzuki–Miyaura Polycondensation. *J. Am. Chem. Soc.* **2009**, *131*, 10348–10349.
- (84) Yokoyama, A.; Suzuki, H.; Kubota, Y.; Ohuchi, K.; Higashimura, H.; Yokozawa, T. Chain-Growth Polymerization for the Synthesis of Polyfluorene via Suzuki-Miyaura Coupling Reaction from an Externally Added Initiator Unit. *J. Am. Chem. Soc.* **2007**, *129*, 7236–7237.
- (85) Zhang, Z.; Hu, P.; Li, X.; Zhan, H.; Cheng, Y. Investigation of Suzuki–Miyaura Catalyst-Transfer Polycondensation of AB-type fluorene monomer using Coordination-Saturated Aryl Pd(II) Halide Complexes as Initiators. *J. Polym. Sci., Part A: Polym. Chem.* **2015**, *53*, 1457–1463.

- (86) Verswyvel, M.; Hoebbers, C.; De Winter, J.; Gerbaux, P.; Koeckelberghs, G. Study of the Controlled Chain-Growth Polymerization of Poly(3,6-phenanthrene). *J. Polym. Sci., Part A: Polym. Chem.* **2013**, *51*, 5067–5074.
- (87) Zhang, D.; Wang, Q. Palladium Catalyzed Asymmetric Suzuki–Miyaura Coupling Reactions to Axially Chiral biaryl Compounds: Chiral Ligands and Recent Advances. *Coord. Chem. Rev.* **2015**, *286*, 1–16.
- (88) Larrosa, I.; Somoza, C.; Banquy, A.; Goldup, S. M. Two Flavors of PEPPSI-IPr: Activation and Diffusion Control in a Single NHC-Ligated Pd Catalyst? *Org. Lett.* **2011**, *13*, 146–149.
- (89) Dong, C.-G.; Hu, Q.-S. Preferential Oxidative Addition in Palladium(0)-Catalyzed Suzuki Cross-Coupling Reactions of Dihaloarenes with Arylboronic Acids. *J. Am. Chem. Soc.* **2005**, *127*, 10006–10007.
- (90) Komiya, S.; Abe, Y.; Yamamoto, A.; Yamamoto, T. Phosphineinduced Reductive Elimination from Cis-arylmethylnickel(II) Complexes having a 1,2-Bis(dimethylphosphino)ethane Ligand. *Organometallics* **1983**, *2*, 1466–1468.
- (91) Bryan, Z. J.; Hall, A. O.; Zhao, C. T.; Chen, J.; McNeil, A. J. Limitations of Using Small Molecules to Identify Catalyst-Transfer Polycondensation reactions. *ACS Macro Lett.* **2016**, *5*, 69–72.

Chapter 2: Ring-Walking in Catalyst-Transfer Polymerization

Portions of this chapter have been published:

Leone, A. K.; Goldberg, P. K.; McNeil, A. J. Ring-Walking in Catalyst-Transfer Polymerization *J. Am. Chem. Soc.*, **2018**, *140*, 7846–7850.

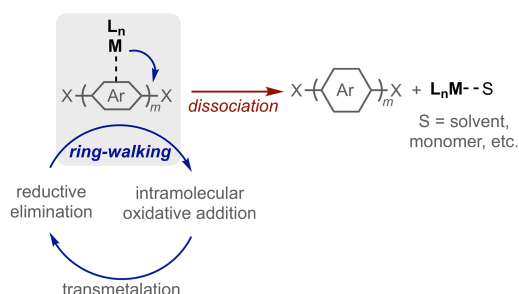
Goldberg, P. K ran preliminary experiments, identified the M(0) scavengers, and synthesized the phenylene monomer.

2.1 Introduction

Transition metal-catalyzed cross-coupling reactions are ubiquitous for forming carbon–carbon bonds.^{1–4} Decades of research on these reactions have informed researchers as to which transition metals, ancillary ligands, and reactive ligands are “optimal” for each substrate class.⁵ Far fewer studies have been done in the analogous (and newer^{6–8}) field of cross-coupling-based chain-growth polymerizations. Although the catalytic cycles are similar, the polymerizations rely on a key intermediate (i.e., a metal–polymer π -complex) to achieve chain-growth behavior.^{9–11} Catalyst ring-walking via this complex enables catalyst migration to the chain-end where intramolecular oxidative addition occurs (Scheme 2-1). These CTPs^{9–11} have enabled polymers with specified molecular weights¹² and end-groups to be synthesized,^{13,14} as well as provided access to alternating, random, block, and gradient copolymers,^{15–18} transforming the field. Both

the π -complex and its ring-walking process distinguish CTP from the more conventional metal-catalyzed step-growth polymerizations reported decades earlier.^{19,20}

Scheme 2-1. Propagation via Ring-Walking versus Catalyst Dissociation during CTP

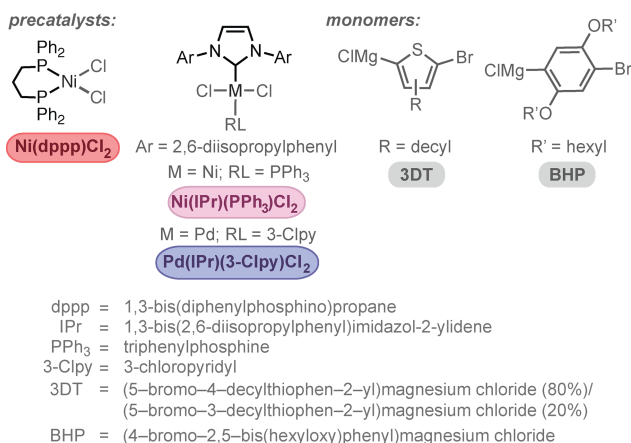


While previous efforts have elucidated the impact of ancillary ligand and monomer structure on reductive elimination and transmetalation rates,¹¹ little is known about the π -complex and ring-walking steps. Both experimental and computational studies have suggested that the metal–polymer π -complex stability influences the frequency of chain-growth (ring-walking) versus step-growth (dissociation) pathways.^{21–24} A complex that is too stable stalls propagation,²² while a complex that is unstable undergoes dissociation. Identifying the optimal catalyst has been challenging because the monomer, ancillary ligand, and metal identities all impact the π -complex stability.⁹ Moreover, little is known about how these parameters affect ring-walking. Therefore, we set out to elucidate the impact of the transition metal, ancillary ligand, and polymer identity on the π -complex’s stability and its ring-walking ability. We hypothesized that a generalizable approach to evaluate these π -complexes would facilitate matchmaking catalysts for future CTPs. For example, the efficient ring-walking catalysts identified herein have the potential to polymerize larger, heteroarene monomers while the inefficient ring-walking catalysts might be useful for unidirectional block copolymer synthesis. Previous efforts to probe π -complex stability and ring-walking have relied on small-molecule difunctionalization reactions.^{25–27} However, these reactions analyze ring-walking over simplified,

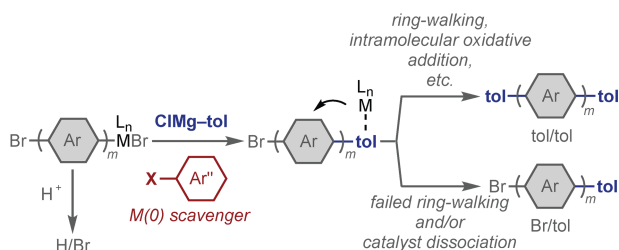
small molecules, limiting their insight and applicability to polymerizations.²⁸ Alternatively, polymerizations followed by end-group analysis using NMR spectroscopy have been used as evidence of catalyst ring-walking.^{29,30} However, these experiments can be misleading if a scavenging agent (i.e., a molecule that reacts with dissociated catalyst) is either not used or is not reactive enough to prevent intermolecular oxidative addition.³¹

We report herein a simple approach to analyze ring-walking over polymers using postpolymerization end-capping experiments (Scheme 2-2). To ensure this approach only elucidates ring-walking through intramolecular pathways, control experiments were used to exclude interchain pathways and to identify a scavenging agent and reaction conditions that prevent dissociated catalysts from reacting with polymers via an intermolecular process. Using this end-capping method, we analyzed the ring-walking abilities of three commonly utilized CTP catalysts⁹ with two distinct monomers (Chart 2-1). Analyzing the polymer end-groups by matrix-assisted laser desorption/ionization time-of-flight mass spectrometry (MALDI-TOF/MS) revealed how the ancillary ligand, transition metal, and polymer influence π -complex stability and ring-walking.

Chart 2-1. Precatalysts and Monomers Used Herein



Scheme 2-2. In Situ End-Capping Experiment



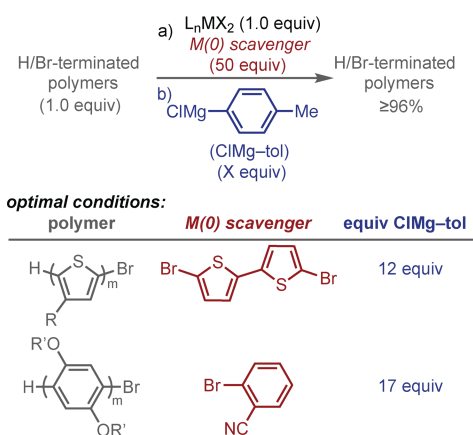
2.2 Results and Discussion

To confirm that MALDI-TOF/MS is a reliable method to quantitatively report polymer ratios, a sample of polymers with different end-groups were synthesized, combined, and analyzed by both MALDI-TOF/MS and ^1H NMR spectroscopy (Appendix 1). Regardless of end-group or monomer identities, the observed ratios were consistent between the two analytical techniques. As a consequence, the area ratios obtained via MALDI-TOF/MS should accurately reflect the experimental results.

Control experiments were performed to identify a scavenging agent as well as conditions where no intermolecular reactivity between dissociated catalysts and polymer chains is observed. A sample of isolated Br/H-terminated polymers was treated with catalyst, capping agent (*p*-tolylmagnesium chloride CIMg-tol),³² and scavenging agent (Chart 2-2). This capping agent was chosen because each set of possible end-groups is distinguishable by MALDI-TOF/MS. Each scavenging agent was selected to complement the polymer in terms of both structure and reactivity. Initially, similar conditions were used for each catalyst. While these conditions were satisfactory for PBHP, a significant amount P3DT had undergone capping. These undesired intermolecular processes were suppressed by both reducing the CIMg-tol equiv and increasing the scavenging agent equivalents. After optimizing the conditions, we found that $\geq 96\%$ of the Br/H-terminated polymers remained uncapped, indicating that these conditions inhibit catalysts

from reacting with dissociated polymers (Appendix 1).³³ These results also indicate that most ($\geq 96\%$) of the end-capped polymers observed in our studies have come from an intramolecular (ring-walking) pathway.

Chart 2-2. Optimized Reagents and Reaction Conditions to Eliminate Intermolecular Reactivity³⁴



A control experiment was performed to rule out a catalyst-transfer process involving entangled polymer chains. To distinguish inter- from intrachain reactions, polymers with different side-chain lengths were added to the end-capping experiments. As anticipated, the exogenous Br/H-terminated polymers remained uncapped while the macroinitiators (with catalysts bound) were end-capped with the same efficiency and product ratios as without the exogenous polymers (Appendix 1). These results indicate that the end-capped polymers generated herein form exclusively through an intramolecular ring-walking process involving a single polymer chain.

Our generalizable approach to evaluate π -complex stability and ring-walking begins with quantifying the amount of living, catalyst-bound chains by acid quenching an aliquot taken from the polymerization. Then, CIMg-tol and metal scavenging agent are added simultaneously (Scheme 2-2). One major polymer species is anticipated: tol/tol end-capped polymers. These polymers arise via two sequential capping events with efficient ring-walking over polymers of

length m in between. If any catalytic step during end-capping and/or ring-walking fails, polymers with alternative end-groups will be observed (i.e., Br/tol, Br/H, H/tol). If ring-walking fails because the catalyst dissociates or simply remains at the capped chain-end, Br/tol-terminated polymers will be generated. If the polymer-bound catalyst does not react completely with ClMg–tol, then H/Br- and tol/H-terminated polymers will be observed. To distinguish polymers that were simply uncapped due to lower reactivity, the in situ end-capping conditions were optimized until the H/Br-terminated polymer percentage did not change, indicating that all polymer-bound catalysts had reacted (Appendix 1).³⁵ The percent ring-walking was calculated by comparing the amount of tol/tol end-capped polymers (obtained via ring-walking) to the total number of polymers that arise from an active chain end at the start of the end-capping experiment (i.e., Br/tol- and tol/tol-terminated polymers) (eq 2-1). Each degree of polymerization (m) was analyzed in the mass spectrum (Appendix 1).

Equation 2-1. Percent ring-walking

$$\% \text{ ring-walking} = \frac{[\text{tol/tol}]}{[\text{tol/tol}] + [\text{tol/Br}]}$$

Remarkably, all three catalysts ring-walk over >35 repeat units at 100% efficiency for poly(3-decylthiophene) (P3DT) (Figure 2-1). These results demonstrate that thiophene forms a robust π -complex with both Ni and Pd regardless of the ancillary ligand. However, each catalyst varied in the end-capping conditions used, reflecting differences in their reactivities and stabilities.

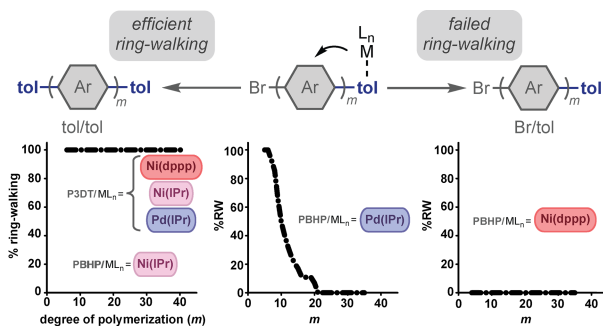


Figure 2-1. Percent ring-walking (% RW) versus degree of polymerization (m) for each catalyst and polymer.

For Ni(dppp)Cl₂, the end-capping experiments were run for >18 h, generating almost exclusively tol/tol end-capped polymers (Figures 2-1 and 2-2). These results are consistent with reports of Ni(dppp)Cl₂ as a viable catalyst for polymerizing thiophene monomers in a living, chain-growth manner.^{18,36–38} Analyzing ring-walking for Ni(IPr)(Ph₃P)Cl₂ over P3DT was complicated by an increasing percentage of NHC/Br-terminated polymers that become prevalent at low transmetalating agent concentrations (Figure 2-2 & Appendix 1).³⁹ This product is attributed to an instability of the polymer-bound catalyst, which undergoes ligand-based reductive elimination.^{40,41} To minimize this nonliving pathway in our experiment, a shortened end-capping time was used along with sequential cap/scavenger reagent additions. These modifications resulted in mostly tol/tol polymers and a few NHC/Br-polymers (3–12%), demonstrating that NHC-ligated Ni catalysts ring-walk successfully over large distances in P3DT.

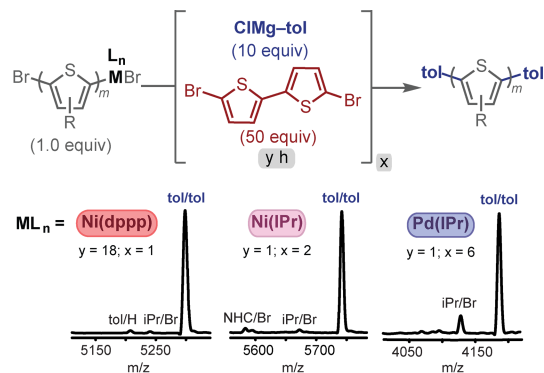


Figure 2-2. (Top) Reaction conditions for 3DT end-capping experiments, involving x iterations of capping/scavenger reagents over y hours. (Bottom) MALDI-TOF/MS data for 3DT polymerization followed by end-capping.⁴⁵ The observed and predicted m/z values for each labeled peak can be found in Appendix 1.

In contrast, the analogous Pd catalyst (i.e., Pd(IPr)(3-Clpy)Cl₂)^{42,43} generated far fewer NHC/Br-terminated polymers. Nevertheless, the major product from the end-capping experiments after 1 h was H/Br-terminated polymers rather than the expected tol/tol end-capped polymers (Appendix 1 Figure A1-27). Simply extending the capping times to 18 h led to NHC/Br-terminated polymers. Combined, these results indicate that catalysts are active at the chain-end but not reacting quickly enough with the CIMg-tol. Instead, CIMg-tol preferentially reacted with dissociated catalysts and scavenger. These results are consistent with those of Kiriy and co-workers, who showed that more hindered catalyst-bound reactive ligands undergo transmetalation slower than less hindered ones.⁴⁴ To overcome this reactivity difference, multiple iterations of the end-capping/scavenging agents were used, yielding almost exclusively tol/tol end-capped polymers (Figure 2-2). These results demonstrate that NHC-ligated Pd is a more stable (albeit less reactive) alternative to Ni for thiophene polymerization, as it does not undergo ancillary ligand-based reductive elimination within 6 h. This difference in NHC-based reductive elimination rates for Ni versus Pd can be rationalized by considering the smaller atomic radius of Ni, which will be more congested in the (IPr)Ni(bisthieryl) complex, accelerating the reductive elimination. This hypothesis is supported by the reactivity differences between Ni (5 min) and Pd

(15 min) in polymerization rates. Overall, we observed that both the transition metal and ancillary ligand identities influence catalyst stability and ring-walking with P3DT.

When we switched the monomer scaffold, the results highlighted the need for each catalyst to be “matched” to a monomer class. For instance, precatalyst Ni(dppp)Cl₂ generated none of the expected tol/tol end-capped polymers with BHP, suggesting that ring-walking fails even over short distances (Figures 2-1 & 2-3). These results are consistent with the previously reported challenging syntheses of block copolymers containing BHP.^{46,47} For example, when BHP was added to a poly(3-hexylthiophene) macroinitiator, BHP/BHP end-capped poly(3-hexylthiophene) was generated.⁴⁷ Combined, these results suggest that the ring-walking efficiency of dppp-ligated Ni(0) decreases with a decrease in a monomer’s π -basicity. Identifying catalysts that are proficient at ring-walking over dissimilar monomers will be necessary to expand the scope of CTP to synthesize more complex materials.

In contrast, NHC-ligated Ni and Pd catalysts both generated tol/tol end-capped polymers (Figures 2-1 and 2-3). However, the transition metal identity strongly influences the ring-walking efficiencies. For example, NHC-ligated Ni generates tol/tol end-capped polymers at all lengths measured, indicating a stable π -complex with efficient ring-walking. Conversely, the ring-walking efficiency for NHC-ligated Pd decreased with increasing chain length. Interestingly, the Ni NHC-based reductive elimination that was observed with P3DT was not observed for PBHP.⁴⁸ This difference could be due to a stabilizing electronic effect with BHP (i.e., due to R'O coordination to Ni). Overall, the NHC-ligated Ni catalyst forms a more robust π -complex with the PBHP and is less likely to dissociate during ring-walking or decompose relative to the analogous Pd. Nevertheless, the ability of the both NHC-ligated catalysts to ring-walk over both

P3DT and PBHP suggests these catalysts could have applications in synthesizing gradient and random sequence copolymers as well as polymerizing more complex monomers.⁴⁹

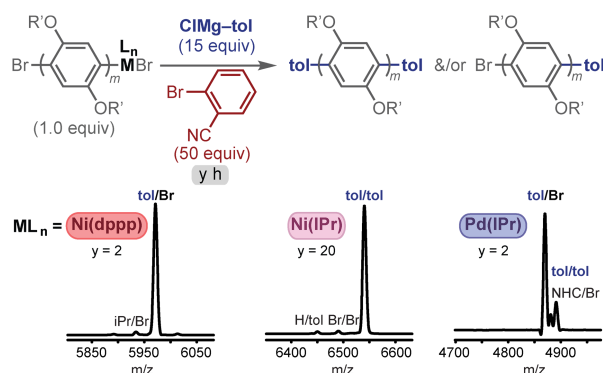


Figure 2-3. (Top) Reaction conditions for BHP end-capping experiments over y hours. (Bottom) MALDI-TOF/MS data for BHP polymerization followed by end-capping.⁴⁵ The observed and predicted m/z values for each labeled peak can be found in Appendix 1.

2.3 Conclusion

In summary, we designed a simple, in situ end-capping experiment to evaluate catalyst ring-walking across polymers under polymerization-relevant conditions. The combined results demonstrate that the ancillary ligand, transition metal, and polymer identity all play a crucial role in the π -complex stability and reactivity. Thiophene forms stable π -complexes⁵⁰ with all Ni and Pd catalysts evaluated, enabling ring-walking over impressively long distances. In contrast, phenylene forms less stable π -complexes,^{46,50} and consequently, the transition metal and ancillary ligand identities play a determining role. The strongly σ -donating NHC ligand⁵¹ promotes ring-walking, whereas the less σ -donating bisphosphine enables dissociation. Although dissociation is less likely with the NHC ligands, we observed detrimental ancillary ligand-based reductive elimination pathways when transmetalating agents were absent. Overall, these discoveries shed light on living, chain-growth pathways, catalyst stability, and how to systematically select catalysts for the next generation of CTP.

2.4 Implications of These Discoveries – Developing Methods to Synthesize High-Performing Conjugated Polymers via CTP

High-performing polymers consist of multiarene and/or fused-ring repeat units. Currently, these polymers are synthesized via step-growth methods, limiting the ability to target specific molecular weights, dispersities, and copolymer sequences. Because these polymer properties significantly influence device performance, we are working on developing catalyst/monomer pairs to generate these high-performing polymers via CTP. Our ring-walking studies presented above demonstrate that Ni and Pd catalysts are capable of traversing over many conjugated units. Inspired by the NHC-ligated precatalysts, current research efforts are underway to match NHC ancillary ligands with complex monomer scaffolds to ultimately synthesize these polymers via CTP.

2.5 References

- (1) Newton, C. G.; Wang, S-G.; Oliveira, C. C.; Cramer, N. Catalytic Enantioselective Transformations Involving C–H Bond Cleavage by Transition-Metal Complexes. *Chem. Rev.* **2017**, *117*, 8908–8976.
- (2) Ritleng, V.; Henrion, M.; Chetcuti, M. J. Nickel N-Heterocyclic Carbene-Catalyzed C–Heteroatom Bond Formation, Reduction, and Oxidation: Reactions and Mechanistic Aspects. *ACS Catal.* **2016**, *6*, 890–906.
- (3) Komiyama, T.; Minami, Y.; Hiyama, T. Recent Advances in Transition-Metal-Catalyzed Synthetic Transformations of Organosilicon Reagents. *ACS Catal.* **2017**, *7*, 631–651.
- (4) Hazari, N.; Melvin, P. R.; Beromi, M. M. Well-Defined Nickel and Palladium Precatalysts for Cross-Coupling. *Nat. Rev. Chem.* **2017**, *1*, 1–16.

- (5) For a recent example: Wu, K.; Doyle, A. G. Parameterization of Phosphine Ligands Demonstrates Enhancement of Nickel Catalysis via Remote Steric Effects. *Nat. Chem.* **2017**, *9*, 779–784.
- (6) Sheina, E. E.; Liu, J.; Iova, M. C.; Laird, D. W.; McCullough, R. D. Chain Growth Mechanism for Regioregular Nickel-Initiated Cross-Coupling Polymerizations. *Macromolecules* **2004**, *37*, 3526–3528.
- (7) Iovu, M. C.; Sheina, E. E.; Gil, R. R.; McCullough, R. D. Experimental Evidence for the Quasi-"Living" Nature of the Grignard Metathesis Method for the Synthesis of Regioregular Poly(3-alkylthiophenes). *Macromolecules* **2005**, *38*, 8649–8656.
- (8) Yokoyama, A.; Miyakoshi, R.; Yokozawa, T. Chain-Growth Polymerization for Poly(3-hexylthiophene) with a Defined Molecular Weight and a Low Polydispersity. *Macromolecules* **2004**, *37*, 1169–1171.
- (9) Leone, A. K.; McNeil, A. J. Matchmaking in Catalyst-Transfer Polycondensation: Optimizing Catalysts based on Mechanistic Insight. *Acc. Chem. Res.* **2016**, *49*, 2822–2831.
- (10) Yokozawa, T.; Ohta, Y. Transformation of Step-Growth Polymerization into Living Chain-Growth Polymerization. *Chem. Rev.* **2016**, *116*, 1950–1968.
- (11) Bryan, Z. J.; McNeil, A. J. Conjugated Polymer Synthesis via Catalyst-Transfer Polycondensation (CTP): Mechanism, Scope, and Applications. *Macromolecules* **2013**, *46*, 8395–8405.
- (12) Fujita, K.; Sumino, Y.; Ide, K.; Tamba, S.; Shono, K.; Shen, J.; Nishino, T.; Mori, A.; Yasuda, T. Synthesis of Poly(3-substituted thiophene)s of Remarkably High Solubility in Hydrocarbon via Nickel-Catalyzed Deprotonative Cross-Coupling Polycondensation. *Macromolecules* **2016**, *49*, 1259–1269.

- (13) Jeffries-El, M.; Sauv , G.; McCullough, R. D. Facile Synthesis of End-Functionalized Regioregular Poly(3-alkylthiophene)s via Modified Grignard Metathesis Reaction. *Macromolecules* **2005**, *38*, 10346–10352.
- (14) For a recent example see: Hall, A. O.; Lee, S. R.; Bootsma, A. N.; Bloom, J. W. G.; Wheeler, S. E.; McNeil, A. J. Reactive Ligand Influence on Initiation in Phenylene Catalyst-Transfer Polymerization. *J. Polym. Sci., Part A: Polym. Chem.* **2017**, *55*, 1530–1535.
- (15) Palermo, E. F.; McNeil, A. J. Impact of Copolymer Sequence on Solid-State Properties for Random, Gradient and Block Copolymers containing Thiophene and Selenophene. *Macromolecules* **2012**, *45*, 5948–5955
- (16) Palermo, E. F.; Darling, S. B.; McNeil, A. J. π -Conjugated Gradient Copolymers Suppress Phase Separation and Improve Stability in Bulk Heterojunction Solar Cells. *J. Mater. Chem. C* **2014**, *2*, 3401–3406.
- (17) Hardeman, T.; Koeckelberghs, G. The Synthesis of Poly(thiophene-co-fluorene) Gradient Copolymers. *Macromolecules* **2015**, *48*, 6987–6993.
- (18) Qiu, Y.; Fortney, A.; Tsai, C.-H.; Baker, M. A.; Gil, R. R.; Kow-alewski, T.; Noonan, K. J. T. Synthesis of Polyfuran and Thiophene-Furan Alternating Copolymers Using Catalyst-Transfer Polycondensation. *ACS Macro Lett.* **2016**, *5*, 332–336
- (19) Hu, Q.-S. Nontraditional Step-Growth Polymerization: Transition Metal Coupling. In *Synthetic Methods in Step-Growth Polymers*, Rogers, M. E., Long, T. E., Eds.; John Wiley & Sons, Inc.: Hoboken, New Jersey, 2003; pp 467–526.
- (20) For a recent step-growth example: Yu, J.; Yang, J.; Zhou, X.; Yu, S.; Tang, Y.; Wang, H.; Chen, J.; Zhang, S.; Guo, X. Phthalimide-Based Wide Bandgap Donor Polymers for Efficient Non-Fullerene Solar Cells. *Macromolecules* **2017**, *50*, 8928–8937.

- (21) He, W.; Patrick, B. O.; Kennepohl, P. η^2 bonded Nickel(0) Thio-phenene π -Complexes - Identifying the Missing Link in Catalyst Transfer Polymerization, 2018. DOI: 10.26434/chemrxiv.5758608.v1
- (22) Willot, P.; Koeckelberghs, G. Evidence for Catalyst Association in the Catalyst Transfer Polymerization of Thieno[3,2-b]thiophene. *Macromolecules* **2014**, *47*, 8548–8555.
- (23) Bryan, Z. J.; McNeil, A. J. Evidence for a Preferential Intramolecular Oxidative Addition in Ni-Catalyzed Cross-Coupling Reactions and their Impact on Chain-Growth Polymerizations. *Chem. Sci.* **2013**, *4*, 1620–1624.
- (24) Smith, M. L.; Leone, A. K.; Zimmerman, P. M.; McNeil, A. J. Impact of Preferential π -Binding in Catalyst-Transfer Polycondensation of Thiazole Derivatives. *ACS Macro Lett.* **2016**, *5*, 1411–1415.
- (25) Qiu, Y.; Worch, J. C.; Fortney, A.; Gayathri, C.; Gil, R. R.; Noonan, K. J. T. Nickel-Catalyzed Suzuki Polycondensation for Controlled Synthesis of Ester-Functionalized Conjugated Polymers. *Macromolecules* **2016**, *49*, 4757–4762.
- (26) Qiu, Y.; Mohin, J.; Tsai, C.-H.; Tristram-Nagle, S.; Gil, R. R.; Kowalewski, T.; Noonan, K. J. T. Stille Catalyst-Transfer Polycondensation Using Pd-PEPPSI-IPr for High-Molecular-Weight Regioregular Poly(3-hexylthiophene). *Macromol. Rapid Commun.* **2015**, *36*, 840–844.
- (27) Kosaka, K.; Uchida, T.; Mikami, K.; Ohta, Y.; Yokozawa, T. Am-Phos Pd-Catalyzed Suzuki–Miyaura Catalyst-Transfer Condensation Polymerization: Narrower Dispersity by Mixing the Catalyst and Base Prior to Polymerization. *Macromolecules* **2018**, *51*, 364–369.
- (28) Bryan, Z. J.; Hall, A. O.; Zhao, C. T.; Chen, J.; McNeil, A. J. Limitations of Using Small Molecules to Identify Catalyst-Transfer Polycondensation Reactions. *ACS Macro Lett.* **2016**, *5*, 69–72.

- (29) Tkachov, R.; Senkovskyy, V.; Komber, H.; Sommer, J-U.; Kiriya, A. Random Catalyst Walking along Polymerized Poly(3-hexylthiophene) Chains in Kumada Catalyst-Transfer Polycondensation. *J. Am. Chem. Soc.* **2010**, *132*, 7803–7810.
- (30) Mikami, K.; Nojima, M.; Masumoto, Y.; Mizukoshi, Y.; Takita, R.; Yokozawa, T.; Uchiyama, M. Catalyst-Dependent Intrinsic Ring-Walking Behavior on π -Face of Conjugated Polymers. *Polym. Chem.* **2017**, *8*, 1708–1713.
- (31) Leone, A. K.; Souther, K. D.; Vitek, A. K.; LaPointe, A. M.; Coates, G. W.; Zimmerman, P. M.; McNeil, A. J. Mechanistic Insight into Thiophene Catalyst-Transfer Polymerization Mediated by Nickel Diimine Catalysts. *Macromolecules* **2017**, *50*, 9121–9127.
- (32) Ortho-tolylmagnesium chloride should not be used because the ortho-substituent may prevent transmetalation. Senkovskyy, V.; Sommer, M.; Tkachov, R.; Komber, H.; Huck, W. T. S.; Kiriya, A. Convenient Route To Initiate Kumada Catalyst-Transfer Polycondensation Using Ni(dppe)Cl₂ or Ni(dppp)Cl₂ and Sterically Hindered Grignard Compounds. *Macromolecules* **2010**, *43*, 10157–10161.
- (33) As expected, tolyl end-capping of the H/Br-terminated polymers was observed when the scavenging agent was absent (Appendix 1).
- (34) Note that two extra equivalents of the CIMg-tol are used in this experiment to initiate the L_nMX₂, compared to the subsequent end-capping experiments.
- (35) Most end-capping experiments were performed in neat THF because it is the most commonly employed solvent for Kumada-based CTP. However, ring-walking was also evaluated with added hexanes. Each catalyst demonstrated the same ring-walking efficiencies in THF/hexanes and neat THF (Appendix 1).

- (36) Tsai, C.-H.; Fortney, A.; Qiu, Y.; Gil, R. R.; Yaron, D.; Kowalewski, T.; Noonan, K. J. T. Conjugated Polymers with Repeated Sequences of Group 16 Heterocycles Synthesized through Catalyst-Transfer Polycondensation. *J. Am. Chem. Soc.* **2016**, *138*, 6798–6804.
- (37) Brusso, J. L.; Lilliedal, M. R.; Holdcroft, S. π -Conjugated Polymers with Thermocleavable Substituents for Use as Active Layers in Organic Photovoltaics. *Polym. Chem.* **2011**, *2*, 175–180.
- (38) Verswyvel, M.; Monnaie, F.; Koeckelberghs, G. AB Block Copoly(3-alkylthiophenes): Synthesis and Chiroptical Behavior. *Macromolecules* **2011**, *44*, 9489–9498.
- (39) NHC (N-heterocyclic carbene) is used rather than “IPr” to distinguish ligand-terminated polymers from iPr-terminated polymers (ref 46).
- (40) NHC-based Ni/Ar reductive elimination example: Zell, T.; Fischer, P.; Schmidt, D.; Radius, U. C–Br Activation of Aryl Bromides at Ni⁰(NHC)₂: Stoichiometric Reactions, Catalytic Application in Suzuki–Miyaura Cross-Coupling, and Catalyst Degradation. *Organometallics* **2012**, *31*, 5065–5073.
- (41) NHC-based Pd/Ar reductive elimination example: Caddick, S.; Cloke, F. G. N.; Hitchcock, P. B.; Leonard, J.; Lewis, A. K. d. K.; McKerrecher, D.; Titcomb, L. R. The First Example of Simple Oxidative Addition of an Aryl Chloride to a Discrete Palladium N-Heterocyclic Carbene Amination Precatalyst. *Organometallics* **2002**, *21*, 4318–4319.
- (42) Suraru, S.-L.; Lee, J. A.; Luscombe, C. K. Preparation of an Arylated Alkylthiophene Monomer via C–H Activation for Use in Pd-PEPPSI-IPr Catalyzed-Controlled Chain Growth Polymerization. *ACS Macro Lett.* **2016**, *5*, 533–536.
- (43) Bryan, Z. J.; Smith, M. L.; McNeil, A. J. Chain-Growth Polymerization of Aryl Grignards Initiated by a Stabilized NHC-Pd Precatalyst. *Macromol. Rapid Commun.* **2012**, *33*, 842–847.

- (44) Tkachov, R.; Senkovskyy, V.; Komber, H.; Kiriya, A. Influence of Alkyl Substitution Pattern on Reactivity of Thiophene-Based Monomers in Kumada Catalyst-Transfer Polycondensation. *Macromolecules* **2011**, *44*, 2006–2015.
- (45) Note that the *i*Pr end-group likely arises via transmetalation with un-reacted *i*PrMgCl.
- (46) Miyakoshi, R.; Yokoyama, A.; Yokozawa, T. Importance of the Order of Successive Catalyst-transfer Condensation Polymerization in the Synthesis of Block Copolymers of Polythiophene and Poly(*p*-phenylene). *Chem. Lett.* **2008**, *37*, 1022–1023.
- (47) Wu, S.; Bu, L.; Huang, L.; Yu, X.; Han, Y.; Geng, Y.; Wang, F. Synthesis and Characterization of Phenylene-Thiophene All-Conjugated Diblock Copolymers. *Polymer* **2009**, *50*, 6245–6251.
- (48) Although slow transmetalation was an issue for (NHC)Pd with P3DT, it was not an issue with PBHP for several reasons: (1) A higher concentration of capping agent was present initially (15 equiv. for PBHP versus 10 equiv. for P3DT). (2) Fewer catalysts ring-walk efficiently to the chain-end with PBHP, where the second transmetalation would consume more capping agent. (3) The scavenging agent used for PBHP is less reactive than the one used with P3DT, hence a slower consumption of ClMg-tol.
- (49) For an example, see: Ashraf, R. S.; Meager, I.; Nikolka, M.; Kirkus, M.; Planells, M.; Schroeder, B. C.; Holliday, S.; Hurhangee, M.; Nielsen, C. B.; Siringhaus, H.; McCulloch, I. *J. Am. Chem. Soc.* **2015**, *137*, 1314–1321.
- (50) Sontag, S. K.; Bilbrey, J. A.; Huddleston, N. E.; Sheppard, G. R.; Allen, W. D.; Locklin, J. π -Complexation in Nickel-Catalyzed Cross-Coupling Reactions. *J. Org. Chem.* **2014**, *79*, 1836–1841.

(51) Díez-González, S.; Nolan, S. P. Stereoelectronic Parameters Associated with N-Heterocyclic Carbene (NHC) Ligands: A Quest for Understanding. *Coord. Chem. Rev.* **2007**, *251*, 874–883.

Chapter 3: Mechanistic Insight into Thiophene Catalyst-Transfer Polymerization Mediated by Nickel Diimine Catalysts

Portions of this chapter have been published:

Leone, A. K.; Souther, K. D.; Vitek, A. K.; LaPointe, A. M.; Coates, G. W.; Zimmerman, P. M.; McNeil, A. J. Mechanistic Insight into Thiophene Catalyst-Transfer Polymerization Mediated by Nickel Diimine Catalysts. *Macromolecules* **2017**, *50*, 9121–9127.

Souther, K. D. initially identified C3_{Me} as a potential CTP catalyst

Vitek, A. K. and Zimmerman, P. M conducted the computational experiments

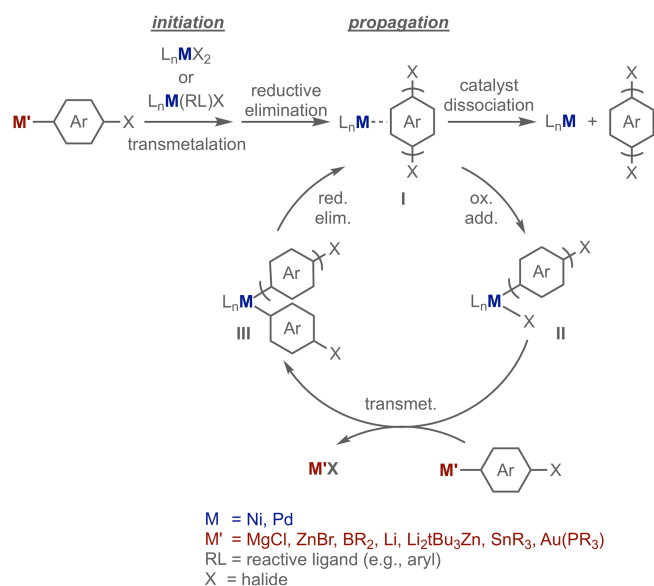
LaPointe, A. M. and Coates, G. W. provided C4_{Me} and C4_{CF3} and helpful guidance for working with diimine-ligated Ni catalysts

3.1 Introduction

Recent advances in tuning conjugated polymer parameters (molecular weights,¹ sequences,^{2,3} and end-group functionalities^{4,5}) via catalyst-transfer polymerization (CTP)^{6–9} have had a significant impact on their applications.^{10–13} For example, an organic solar cell with significantly improved thermal stability was obtained when a gradient sequence conjugated copolymer^{14,15} was used as an additive.^{16,17} Despite this progress, many monomers still cannot be polymerized via CTP (e.g., large, fused oligoarenes found in high-performing organic solar cells).^{18,19} One limitation is that the mechanistic underpinnings for failed chain-growth polymerizations are unknown.

Most catalyst-transfer polymerizations are initiated with a precatalyst that has either one (L_nMXRL) or two (L_nMX_2) halide reactive ligands ($X = \text{halide}$; $RL = \text{reactive ligand}$).^{6,8} Initiation from these complexes requires transmetalation by one or two monomers, followed by C–C bond forming reductive elimination (Scheme 3-1). The resulting species is an associative complex between $L_nM(0)$ and the generated biaryl (complex I).⁷ Subsequent ring-walking to the C–X terminus followed by an intramolecular oxidative addition generates a $L_nM(II)XAr$ species (complex II). Additional monomers are then added sequentially to the same growing polymer chain during propagation via consecutive transmetalation, reductive elimination, and oxidative addition. Unproductive pathways can occur when complex I is either too stable or unstable.^{20–26}

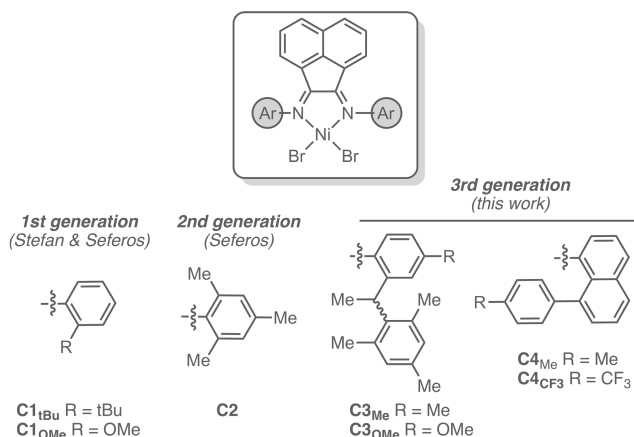
Scheme 3-1. Initiation and Propagation Mechanisms for CTP



Diimines^{27–31} have recently emerged as a promising alternative to bisphosphines or N-heterocyclic carbenes as ancillary ligands for CTP catalysts.⁸ Although these Ni diimine catalysts mediate chain-growth polymerizations, nonliving pathways become dominant at high monomer conversions and/or low catalyst loadings. For example, Stefan and co-workers used precatalyst $C1_{tBu}$ (Chart 3-1) to polymerize a 3-hexylthiophene (3HT) monomer.²⁷ Although a chain-growth

process was evident at low monomer conversions (<30%), a plateau in the number-average molecular weight (M_n) after 30% conversion and poor end-group control suggested that nonliving pathways dominated (e.g., catalyst dissociation). With an alternative diimine-ligated precatalyst (**C1_{OMe}**, Chart 3-1), Seferos and co-workers polymerized a benzotriazole monomer.²⁸ Again, only “quasi-living” behavior was observed: for example, a linear growth in M_n was only observed from 0–35% conversion. Even so, a single set of end-groups (i.e., H/Br) was observed after quenching, and most chains extended when a second aliquot of monomer was added. Combined, these results suggest that catalyst dissociation occurs, but reinsertion into existing chains gives the appearance of a living polymerization.

Chart 3-1. Reported and New Nickel Diimine Precatalysts for CTP



Using a different diimine scaffold (**C2**, Chart 3-1), Seferos and co-workers reported synthesizing block copolymers of benzotriazole with 3HT.²⁹ Although living, chain-growth behavior was observed in this system,³⁰ when a nonhalide reactive ligand (*o*-MeOPh) was used, a mixture of end-groups was observed after quenching.³¹ Some end-groups were consistent with a living, chain-growth process (i.e., MeOPh/H), and some end-groups were consistent with catalyst dissociation and termination (i.e., MeOPh/Br, Br/H, Br/Br, H/H). These unproductive pathways were dominant at low catalyst loadings (e.g., 2 mol %). Based on these data, precatalyst **C2**

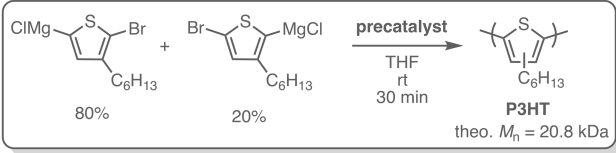
mediates a chain-growth polymerization, with both catalyst dissociation and initiation of new chains occurring.

We were inspired by the diimine-ligated Pd and Ni catalysts used for olefin polymerizations³²⁻³⁴ and began evaluating these precatalysts (e.g., **C3_{Me}**,³⁵⁻³⁹ **C4_{CF3}**,^{40, 41} and **C4_{Me}**⁴⁰) for conjugated polymer synthesis. From these known complexes, we discovered that precatalyst **C3_{Me}** polymerizes 3HT via a chain-growth process, even at high monomer conversion and low catalyst loading (<2 mol %). Detailed mechanistic studies revealed that the reaction proceeds via the expected associative intermediate (complex I in Scheme 1-1) with minimal catalyst dissociation. In addition, most of the dissociated catalysts preferentially react with a polymer chain due to a reactivity and a statistical preference, whereas the other dissociated catalysts either initiate new chains or decompose. Combined, these processes lead to a mechanism that is quasi-living and chain growth. Overall, these studies add mechanistic insight into CTP using diimine-ligated Ni complexes and highlight the role of ancillary ligand structure on reactivity.

3.2 Results and Discussion

3.2.1 Evaluating Ni Diimines for 3HT Polymerization

Our studies began by comparing each precatalyst (**C1–C4**, Chart 3-1) with the same monomer (3HT) under identical reaction conditions (Table 3-1).⁴² Complex **C3_{Me}** produced poly(3-hexylthiophene) (P3HT) with approximately the theoretical M_n (theo $M_n = 20.8$ kg/mol, measured $M_n = 23.8$ kg/mol) and a moderate dispersity ($\mathcal{D} = 1.75$), outperforming all other precatalysts. When the reaction was run at a lower temperature (0 °C), the resulting P3HT exhibited lower dispersity ($\mathcal{D} = 1.47$, Table A2-5), suggesting that **C3_{Me}** is a promising new catalyst for CTP.

Table 3-1. Polymerization Data for Precatalysts **C1–C4**^a

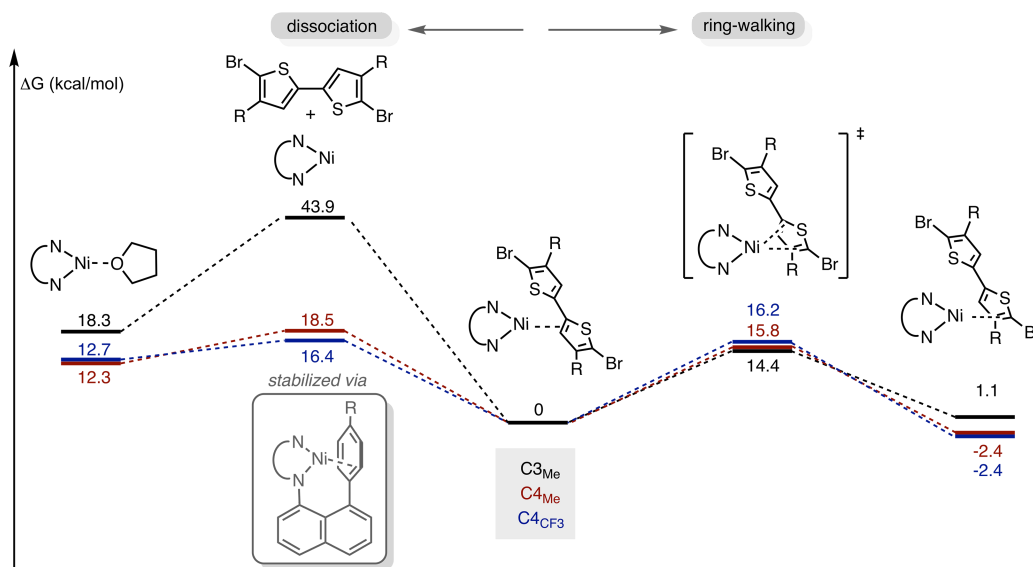
	C1_{tBu}	C2	C3_{Me}	C3_{OMe}	C4_{Me}^d	C4_{CF3}^d
conv. % ^b	19.1	77.3	79.0	73.3	45.2	16.3
<i>M_n</i> (kDa) ^c	1.20	14.0	23.8	22.3	0.26	0.24
Đ ^c	1.20	1.77	1.75	1.75	2.78	2.00

^aConditions: [monomer] = 15 mM; [catalyst] = 0.12 mM. ^bDetermined by GC relative to an internal standard. ^cDetermined by GPC relative to polystyrene standards.⁴³ ^d20–24 h.

The combined polymerization results demonstrate a “Goldilocks” effect regarding the ancillary ligand steric properties: both the less congested Ni centers (in **C1_{tBu}** and **C2**) as well as the more congested Ni centers (in **C4_{Me}** and **C4_{CF3}**) produce P3HT with a significantly lower than theoretical *M_n*. While **C1_{tBu}** generates thiophene oligomers with a narrow dispersity (Đ = 1.2), the molecular weight remains significantly below the theoretical *M_n*, generating only oligomers even after 20 h (Table A2-3). Consistent with results from Stefan,²⁷ these results suggest that catalyst dissociates from the polymer and then initiates new chains. To understand the impact of the more sterically encumbering diimine ligands, we computationally evaluated the productive (ring walking) and unproductive (dissociation) processes for precatalysts **C3_{Me}**, **C4_{Me}**, and **C4_{CF3}** (Appendix 2). Facile chain growth was observed for all three catalysts with barriers between 14.4 and 16.2 kcal/mol. However, for both **C4** derivatives, dissociation is competitive with ring walking (Scheme 3-2). When the polymer dissociates, an associative complex is observed between the Ni(0) center and the pendant arene on the diimine, stabilizing the Ni(0), likely giving rise to the low *M_n* and broad Đ observed experimentally for **C4_{Me}** and **C4_{CF3}**. A

similar Ni–ligand π interaction is less stabilizing for **C3_{Me}**, resulting in a less favorable dissociation pathway.

Scheme 3-2. Free Energy Landscape for Catalyst Dissociation versus Ring Walking for Precatalysts **C3_{Me}**, **C4_{Me}**, and **C4_{CF3}**



Additionally, an ancillary ligand with potentially greater electron-donating character (precatalyst **C3_{OMe}**, see Appendix 2 for Mulliken charges) was experimentally evaluated because electron-rich ligands have been shown to minimize catalyst dissociation during CTP.²³ No significant difference in M_n or \bar{D} was observed with **C3_{OMe}** compared to **C3_{Me}**. Nevertheless, precatalyst **C3_{Me}** gave higher conversions of the major 3HT regioisomer, leading to P3HT with higher regioregularities. Overall, these results suggest that precatalyst **C3_{Me}** is promising for CTP of 3HT. Both the M_n and \bar{D} data suggest that **C3_{Me}** undergoes more productive turnovers, with fewer side reactions, than the other precatalysts.

3.2.2 Chain-Growth Synthesis of P3HT with Precatalyst **C3_{Me}**

Under the optimized conditions, a linear relationship between M_n and monomer conversion was observed, even at high conversions (>90%, Figure 3-1A). In addition, the resulting M_n match those expected based on the catalyst-to-monomer ratios (Figure 3-1B).

Combined, these data are consistent with a chain-growth process, wherein each catalyst initiates and polymerizes a single chain. Nevertheless, we observe a modest increase in dispersity ($\Delta\bar{D} = 0.35$) with monomer conversion, suggesting that competing pathways occur later during propagation. Further evidence of these unproductive reactions came from the analysis of polymer end-groups. Polymerizations initiated from a L_nNiBr_2 precatalyst and quenched with acid should yield exclusively Br/H end-capped polymers, assuming complex I is not the catalyst resting state (Scheme 3-1). Instead, only 75% of polymer chains have Br/H end-groups after 19% monomer conversion. The other 25% have end-groups consistent with catalyst dissociation (e.g., Br/Br and iPr/Br^{44}) (Figure 3-1C,D). Combined, these data suggest most initiated catalysts undergo productive CTP while some catalysts dissociate during polymerization.

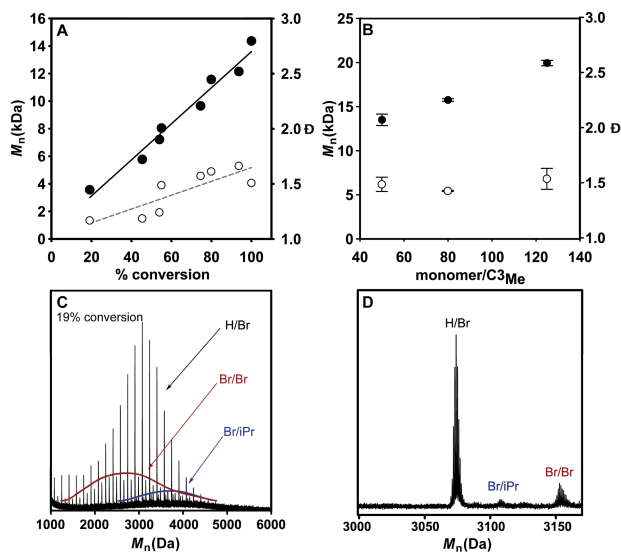
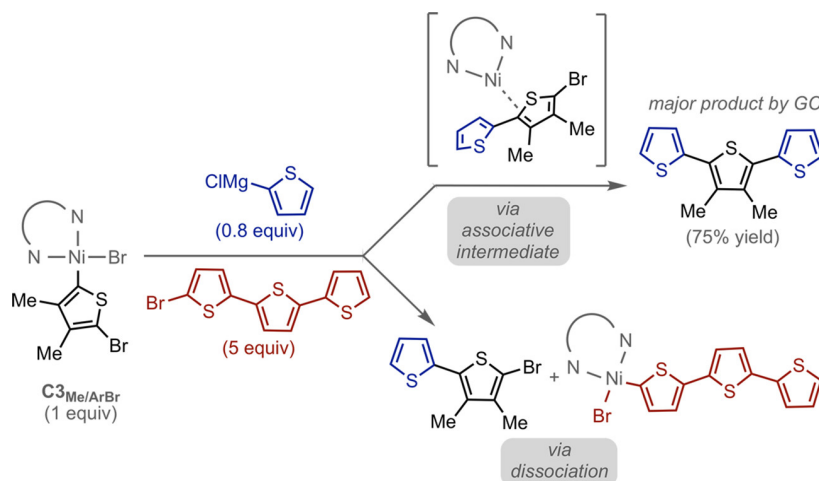


Figure 3-1. (A) Plot of M_n (●) and \bar{D} (○) versus percent conversion (theo $M_n = 13.3$ kDa). (B) Plot of M_n (●) and \bar{D} (○) versus monomer/precatalyst ratio (50/1, 80/1, 125/1; monomer conversion >80%). (C, D) MALDI-TOF-MS spectra at 19% conversion. (Note that all polymerizations were run under the optimized conditions with precatalyst $C3_{Me}$ in THF at 0 °C, [monomer] = 10 mM, and [catalyst] = 0.08–0.19 mM.)

3.2.3 Propagation Mechanism

Although the existence of an associative complex is well supported in CTP mediated by bisphosphine-ligated Ni complexes,^{23-25,45} it is unclear if this mechanism applies to other CTP catalysts. As a consequence, a competition experiment was used to indirectly probe whether the polymerization proceeds through an associative complex (Scheme 3-3).^{23,24} Indeed, the major product (75% yield) observed in this experiment was the dicoupled product, which can only be obtained via the associative complex, followed by intramolecular oxidative addition (top arrow in Scheme 3-3). Note that an excess of the competitive agent (Br-terthiophene) was used to “trap” any dissociated Ni(0) species. Extrapolating these results to the thiophene polymerization suggests that **C3_{Me}** primarily propagates via the conventional CTP mechanism.

Scheme 3-3. Intra- versus Intermolecular Competition Experiment



3.2.4 Fate of Catalysts during Propagation

Thus far, these data suggest that competitive mechanistic pathways are occurring: some catalysts stay associated with the initiated polymer chains while other catalysts dissociate during polymerization. Quantifying the extent of dissociation gave conflicting results using different methods: the dispersity data at high conversion suggest the overall extent of dissociation is low

(Figure 3-1A,B) while end-group analysis at low conversion suggests that the dissociation is high due to the significant amount of Br/Br and iPr/Br^{44} present (Figure 3-1C,D). One possible explanation for both results is that dissociated catalysts react preferentially with polymer chains rather than monomer. To provide support for this hypothesis, we ran a series of experiments to determine what fraction of chains are active and associated with a catalyst during polymerization.

A chain extension experiment, where a second aliquot of 3HT monomer is added after the first aliquot is mostly consumed, showed no new low molecular weight peaks in the GPC trace, suggesting that no new polymers were initiated from the second monomer addition (Figure 3-2A). Instead, most of the chains reach their theoretical M_n as evident by the peak shift from low (initial) to high (final) molecular weight with only a minor low molecular weight tail and a modest broadening in dispersity. Further support that most chains are active came from an end-capping experiment, wherein only catalyst-bound chains undergo capping. These experiments can be difficult to interpret due to complications arising from chain-walking and/or intermolecular reactions. However, McCullough and co-workers previously showed that employing vinyl Grignard as a capping agent minimizes these complications by trapping the Ni(0) after the first turnover.⁴⁶ Adding vinyl Grignard to our polymerizations resulted in >80% of chains terminated with a single vinyl group (Figure 3-2B). Combined, the less than 20% of inactive chains (in the chain-extension and end-capping experiments) suggest that **C3_{Me}** polymerizes 3HT in a mostly living, chain-growth fashion with some catalyst dissociation.

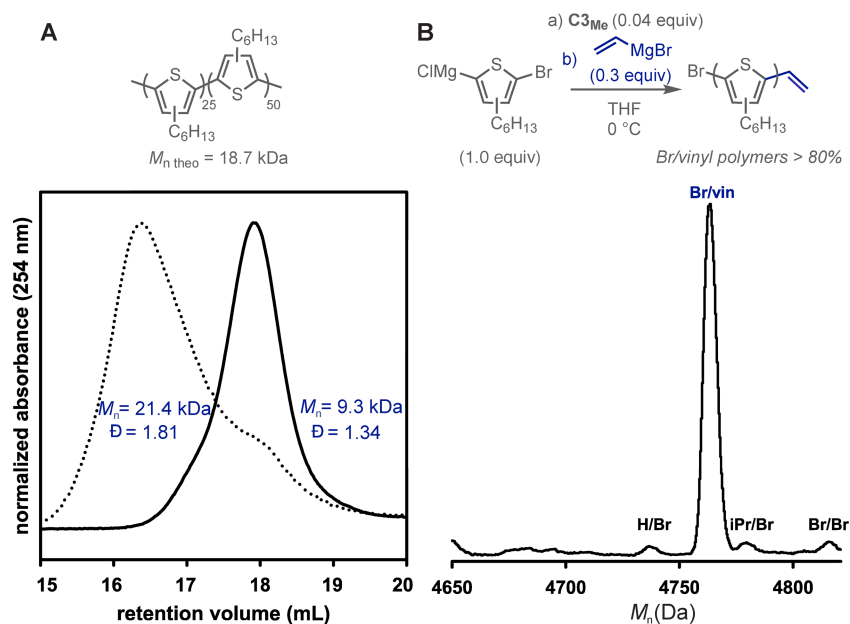


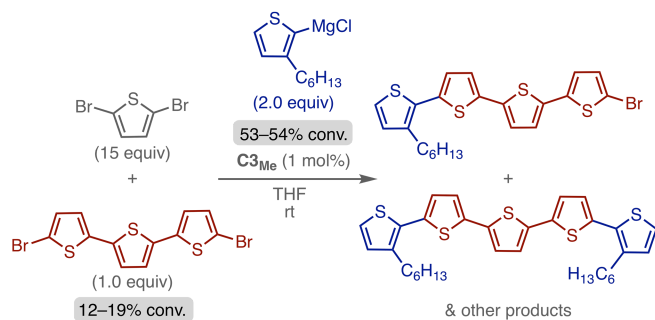
Figure 3-2. (A) GPC traces from the initial (solid line) and final (dashed line) aliquot taken during the chain-extension experiments. (B) MALDI-TOF-MS spectrum of end-capping experiments with added vinyl Grignard. All polymerizations were run at 0°C .

3.2.5 Fate of Catalysts after Dissociation

We hypothesized that most dissociated catalysts preferentially react with polymer chains rather than monomers to rationalize the observed moderate dispersities as well as the apparent living polymerization behavior at high conversion and low catalyst loadings. This preference for the polymer could be due to reactivity differences⁴⁷ and/or a statistical effect. To test this hypothesis, we ran a series of experiments aimed at elucidating if the preference is reactivity-based. Specifically, we evaluated whether 5,5''-dibromo-2,2':5',2''-terthiophene would preferentially react with C3_{Me} in the presence of excess monomer analogue (i.e., 2,5-dibromothiophene, Scheme 4). Indeed, between 12 and 19% of the terthiophene was converted to both di- and monofunctionalized products when $\sim 50\%$ of Grignard was consumed (Figure A2-34). The observed terthiophene conversion is significantly greater than what would be statistically

predicted (6%) if both thiophene species reacted equally.⁴⁸ Extrapolating these results to the polymerization suggests that reassociation into a polymer chain can occur even when it is present in lower concentrations than the monomer.

Scheme 3-4. Evaluating Oligomer versus Monomer Reactivity



To evaluate the reactivity hypothesis in the context of a polymerization, a different monomer analogue (i.e., 2,5-dibromo-3,4-dimethylthiophene) was added during polymerization (Figure 3-3). The reactivity/statistical model predicts that the dissociated catalysts should preferentially react with the polymer and not initiate a new chain by reacting with the monomer analogue. Indeed, regardless of whether the monomer analogue was present from the beginning of polymerization or added in the middle, less than 5% of it was consumed (Figure 3-3). The observed negligible incorporation suggests that catalysts preferentially reassociate with dissociated chains.

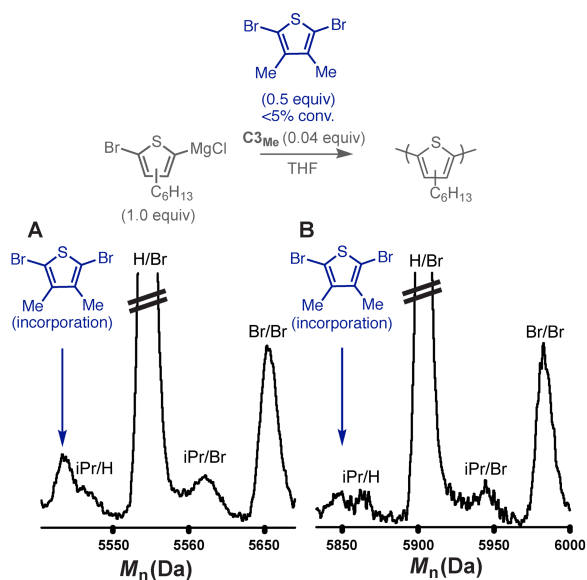
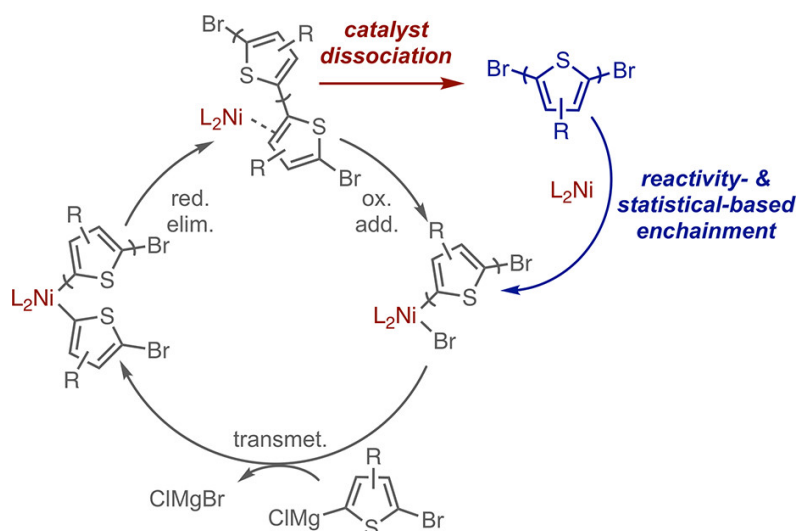


Figure 3-3. MALDI-TOF-MS data for polymerizations run in the presence of monomer analogue added either (A) before initiation or (B) after initiation.

Although there is strong evidence supporting a reactivity-based preference for reinsertion into growing chains, we cannot rule out the likely statistical preference for polymer association. The polymer can outcompete the monomer at the Ni(0) center based on having more available π -binding sites to form an associative complex prior to oxidative addition.^{49,50} Overall, we suspect that both reactivity and statistical effects contribute to the living, chain-growth polymerization of 3HT mediated by precatalyst **C3**_{Me} (Scheme 3-5).

Scheme 3-5. Proposed Mechanism for CTP with **C3_{Me}**



3.3 Conclusion

Diimine-ligated metal complexes have been underutilized in CTP. This work and others²⁷⁻³¹ suggest that such complexes are promising for generating conjugated polymers in a chain-growth manner. Herein, we reported a new precatalyst (**C3_{Me}**) for CTP of 3HT that outperforms the previously reported Ni diimine precatalysts. In addition, we demonstrated that the operative mechanism is similar to the conventional CTP mechanism with an associative complex forming after reductive elimination; the mechanism is different in that catalyst dissociation is followed by preferential reassociation with a growing polymer chain due to a reactivity- and statistical-based effect. Combined, these results suggest that diimine-ligated Ni catalysts warrant further investigation due to their potential to significantly expand the scope of materials accessible by CTP.³⁹

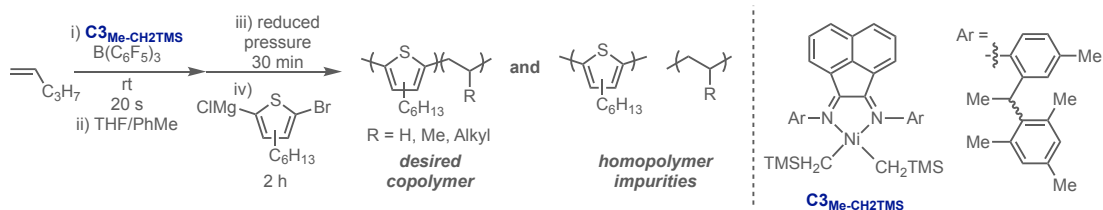
3.4 Implications of These Discoveries – Synthesizing Thiophene/Olefin Block Copolymers

Block copolymers containing conjugated and insulating segments have been explored as additives in organic electronic devices to improve device performance. The insulating segment

facilitates macromolecular formation of the conjugated segment, improving alignment and charge transfer. Synthesizing these copolymers is challenging, in most cases requiring multiple catalysts and purification steps. Because **C3_{Me}** polymerized thiophene in a chain-growth manner and is well known for polymerizing α -olefins through a living, chain-growth manner, we hypothesized that it could be used to generate thiophene/olefin block copolymers in one-pot.³⁹ Specifically, **C3_{Me}** precatalysts would initiate α -olefins polymerization to generate a poly(olefin) macroinitiator. Then, adding thiophene monomer would promote mechanism-switching and initiate CTP to generate the thiophene block.

To develop compatible conditions to promote mechanism-switching and subsequent polymerization required significant optimization. Ultimately, we used precatalyst **C3_{Me}-CH₂TMS** with a boron cocatalyst to generate the desired poly(olefin)-poly(thiophene) block copolymers albeit with both olefin and thiophene homopolymer impurities (Scheme 3-6). Using computational analysis, we identified a problematic high barrier for mechanism-switching (i.e., Csp²-Csp³ reductive elimination), which may facilitate off-cycle, undesired reactions to occur. In addition, if the Ni diimine dissociates during the copolymerization, there are few π -binding sites to reassociate with as the olefin segment has none. Combined, these studies demonstrate the challenges associated with developing a multitasking catalyst, and provide good insight into obstacles to consider when designing these systems.³⁹

Scheme 3-6. Synthesizing poly(olefin)-block-poly(thiophene) copolymers via **C3_{Me}-CH₂TMS**



3.5 References

- (1) For a recent example see: Zhang, H.-H.; Peng, W.; Dong, J.; Hu, Q.-S. t-Bu₃P-Coordinated 2-Phenylaniline-Based Palladacycle Complex/ArBr as Robust Initiators for Controlled Pd(0)/t-Bu₃P-Catalyzed Suzuki Cross-Coupling Polymerization of AB-Type Monomers. *ACS Macro Lett.* **2016**, *5*, 656–660.
- (2) For a recent example see: Qiu, Y.; Worch, J. C.; Fortney, A.; Gayathri, C.; Gil, R. R.; Noonan, K. J. T. Nickel-Catalyzed Suzuki Polycondensation for Controlled Synthesis of Ester-Functionalized Conjugated Polymers. *Macromolecules* **2016**, *49*, 4757–4762.
- (3) For a recent example see: Tsai, C.-H.; Fortney, A.; Qiu, Y.; Gil, R. R.; Yaron, D.; Kowalewski, T.; Noonan, K. J. T. Conjugated Polymers with Repeated Sequences of Group 16 Heterocycles Synthesized through Catalyst-Transfer Polycondensation. *J. Am. Chem. Soc.* **2016**, *138*, 6798–6804.
- (4) For a recent example see: Sun, H.; Zhang, S.; Yang, Y.; Li, X.; Zhan, H.; Cheng, Y. Excellent Control of Perylene Diimide End Group in Polyfluorene via Suzuki Catalyst Transfer Polymerization. *Macromol. Chem. Phys.* **2016**, *217*, 2726–2735.
- (5) For a recent example see: Hall, A. O.; Lee, S. R.; Bootsma, A. N.; Bloom, J. W. G.; Wheeler, S. E.; McNeil, A. J. Reactive Ligand Influence on Initiation in Phenylene Catalyst-Transfer Polymerization. *J. Polym. Sci., Part A: Polym. Chem.* **2017**, *55*, 1530–1535.
- (6) Yokozawa, T.; Ohta, Y. Transformation of Step-Growth Polymerization into Living Chain-Growth Polymerization. *Chem. Rev.* **2016**, *116*, 1950–1968.
- (7) Bryan, Z. J.; McNeil, A. J. Conjugated Polymer Synthesis via Catalyst-Transfer Polycondensation (CTP): Mechanism, Scope, and Applications. *Macromolecules* **2013**, *46*, 8395–8405.

- (8) Leone, A. K.; McNeil, A. J. Matchmaking in Catalyst-Transfer Polycondensation: Optimizing Catalysts based on Mechanistic Insight. *Acc. Chem. Res.* **2016**, *49*, 2822–2831.
- (9) Verheyen, L.; Leysen, P.; Van Den Eede, M.-P.; Ceunen, W.; Hardeman, T.; Koeckelberghs, G. Advances in the Controlled Polymerization of Conjugated Polymers. *Polymer* **2017**, *108*, 521–546.
- (10) Grimsdale, A. C.; Chan, K. L.; Martin, R. E.; Jokisz, P. G.; Holmes, A. B. Synthesis of Light-Emitting Conjugated Polymers for Applications in Electroluminescent Devices. *Chem. Rev.* **2009**, *109*, 897–1091.
- (11) Yassar, A.; Miozzo, L.; Gironda, R.; Horowitz, G. Rod-coil and All-Conjugated Block Copolymers for Photovoltaic Applications. *Prog. Polym. Sci.* **2013**, *38*, 791–844.
- (12) Jørgensen, M.; Norrman, K.; Gevorgyan, S. A.; Tromholt, T.; Andreasen, B.; Krebs, F. C. Stability of Polymer Solar Cells. *Adv. Mater.* **2012**, *24*, 580–612.
- (13) Wang, J.; Higashihara, T. Synthesis of All-Conjugated Donor– Acceptor Block Copolymers and their Application in All-Polymer Solar Cells. *Polym. Chem.* **2013**, *4*, 5518–5526.
- (14) Palermo, E. F.; van der Laan, H. L.; McNeil, A. J. Impact of π Conjugated Gradient Sequence Copolymers on Polymer Blend Morphology. *Polym. Chem.* **2013**, *4*, 4606–4611.
- (15) Palermo, E. F.; McNeil, A. J. Impact of Copolymer Sequence on Solid-State Properties for Random, Gradient and Block Copolymers containing Thiophene and Selenophene. *Macromolecules* **2012**, *45*, 5948–5955.
- (16) Amonoo, J. A.; Li, A.; Purdum, G. E.; Sykes, M. E.; Huang, B.; Palermo, E. F.; McNeil, A. J.; Shtein, M.; Loo, Y.-L.; Green, P. F. An All-Conjugated Gradient Copolymer Approach for Morphological Control of Polymer Solar Cells. *J. Mater. Chem. A* **2015**, *3*, 20174–20184.

- (17) Palermo, E. F.; Darling, S. B.; McNeil, A. J. π -Conjugated Gradient Copolymers Suppress Phase Separation and Improve Stability in Bulk Heterojunction Solar Cells. *J. Mater. Chem. C* **2014**, *2*, 3401–3406.
- (18) Lu, L.; Zheng, T.; Wu, Q.; Schneider, A. M.; Zhao, D.; Yu, L. Recent Advances in Bulk Heterojunction Polymer Solar Cells. *Chem. Rev.* **2015**, *115*, 12666–12731.
- (19) Holliday, S.; Li, Y.; Luscombe, C. K. Recent Advances in High Performance Donor-Acceptor Polymers for Organic Photovoltaics. *Prog. Polym. Sci.* **2017**, *70*, 34–51.
- (20) Takagi, K.; Kawagita, E.; Kouchi, R. Synthesis and Characterization of Polythiophene Derivatives with Nitrogen Heterocycles on the Side Chain. *J. Polym. Sci., Part A: Polym. Chem.* **2014**, *52*, 2166–2174.
- (21) Schiefer, D.; Wen, T.; Wang, Y.; Goursot, P.; Komber, H.; Hanselmann, R.; Braunstein, P.; Reiter, G.; Sommer, M. Nickel Catalyst with a Hybrid P, N Ligand for Kumada Catalyst Transfer Polycondensation of Sterically Hindered Thiophenes. *ACS Macro Lett.* **2014**, *3*, 617–621.
- (22) Lee, S. R.; Bryan, Z. J.; Wagner, A. M.; McNeil, A. J. Effect of Ligand Electronic Properties on Precatalyst Initiation and Propagation in Ni-Catalyzed Cross-Coupling Polymerizations. *Chem. Sci.* **2012**, *3*, 1562–1566.
- (23) Bryan, Z. J.; McNeil, A. J. Evidence for a Preferential Intramolecular Oxidative Addition in Ni-Catalyzed Cross-Coupling Reactions and their Impact on Chain-Growth Polymerizations. *Chem. Sci.* **2013**, *4*, 1620–1624.
- (24) Bryan, Z. J.; Hall, A. O.; Zhao, C. T.; Chen, J.; McNeil, A. J. Limitations of Using Small Molecules to Identify Catalyst-Transfer Polycondensation Reactions. *ACS Macro Lett.* **2016**, *5*, 69–72.

- (25) Willot, P.; Koeckelberghs, G. Evidence for Catalyst Association in the Catalyst Transfer Polymerization of Thieno[3,2-b]thiophene. *Macromolecules* **2014**, *47*, 8548–8555.
- (26) Smith, M. L.; Leone, A. K.; Zimmerman, P. M.; McNeil, A. J. Impact of Preferential π -Binding in Catalyst-Transfer Polycondensation of Thiazole Derivatives. *ACS Macro Lett.* **2016**, *5*, 1411–1415.
- (27) Magurudeniya, H. D.; Sista, P.; Westbrook, J. K.; Ourso, T. E.; Nguyen, K.; Maher, M. C.; Alemseghed, M. G.; Biewer, M. C.; Stefan, M. C. Nickel(II) α -Diimine Catalyst for Grignard Metathesis (GRIM) Polymerization. *Macromol. Rapid Commun.* **2011**, *32*, 1748–1752.
- (28) Bridges, C. R.; McCormick, T. M.; Gibson, G. L.; Hollinger, J.; Seferos, D. S. Designing and Refining Ni(II)diimine Catalysts Toward the Controlled Synthesis of Electron-Deficient Conjugated Polymers. *J. Am. Chem. Soc.* **2013**, *135*, 13212–13219.
- (29) Bridges, C. R.; Yan, H.; Pollit, A. A.; Seferos, D. S. Controlled Synthesis of Fully π -conjugated Donor-Acceptor Block Copolymers Using a Ni(II) Diimine Catalyst. *ACS Macro Lett.* **2014**, *3*, 671–674.
- (30) Pollit, A. A.; Bridges, C. R.; Seferos, D. S. Evidence for the Chain-Growth Synthesis of Statistical π -Conjugated Donor–Acceptor Copolymers. *Macromol. Rapid Commun.* **2015**, *36*, 65–70.
- (31) Pollit, A. A.; Obhi, N. K.; Lough, A. J.; Seferos, D. S. Evaluation of an External Initiating Ni(II) Diimine Catalyst for Electron-deficient π -Conjugated Polymers. *Polym. Chem.* **2017**, *8*, 4108–4113.
- (32) Guo, L.; Dai, S.; Sui, X.; Chen, C. Palladium and Nickel Catalyzed Chain Walking Olefin Polymerization and Copolymerization. *ACS Catal.* **2016**, *6*, 428–441.

- (33) Carrow, B. P.; Nozaki, K. Transition-Metal-Catalyzed Functional Polyolefin Synthesis: Effecting Control through Chelating Ancillary Ligand Design and Mechanistic Insights. *Macromolecules* **2014**, *47*, 2541–2555.
- (34) O'Connor, K. S.; Lamb, J. R.; Vaidya, T.; Keresztes, I.; Klimovica, K.; LaPointe, A. M.; Daugulis, O.; Coates, G. W. Understanding the Insertion Pathways and Chain Walking Mechanisms of α -Diimine Nickel Catalysts for α -Olefin Polymerization: A ^{13}C NMR Spectroscopic Investigation. *Macromolecules* **2017**, *50*, 7010–7027.
- (35) Cherian, A. E.; Rose, J. M.; Lobkovsky, E. B.; Coates, G. W. A C_2 -Symmetric, Living α -Diimine Ni(II) Catalyst: Regioblock Copolymers from Propylene. *J. Am. Chem. Soc.* **2005**, *127*, 13770–13771.
- (36) Rose, J. M.; Cherian, A. E.; Coates, G. W. Living Polymerization of α -Olefins with an α -Diimine Ni(II) Catalyst: Formation of Well-Defined Ethylene–Propylene Copolymers through Controlled Chain-Walking. *J. Am. Chem. Soc.* **2006**, *128*, 4186–4187.
- (37) Rose, J. M.; Deplace, F.; Lynd, N. A.; Wang, Z.; Hotta, A.; Lobkovsky, E. B.; Kramer, E. J.; Coates, G. W. C_2 -Symmetric Ni(II) α -Diimines Featuring Cumyl-Derived Ligands: Synthesis of Improved Elastomeric Regioblock Polypropylenes. *Macromolecules* **2008**, *41*, 9548–9555.
- (38) Ruiz-Orta, C.; Fernandez-Blazquez, J. P.; Anderson-Wile, A. M.; Coates, G. W.; Alamo, R. G. Isotactic Polypropylene with (3,1) Chain-Walking Defects: Characterization, Crystallization, and Melting Behaviors. *Macromolecules* **2011**, *44*, 3436–3451.
- (39) Souther, K. D.; Leone, A. K.; Vitek, A. K.; Palermo, E. F.; LaPointe, A. M.; Coates, G. W.; Zimmerman, P. M.; McNeil, A. J. Trials and Tribulations of Designing Multitasking Catalysts for Olefin/ Thiophene Block Copolymerizations. *J. Polym. Sci., Part A: Polym. Chem.* **2018**, *56*, 132–137.

- (40) Vaidya, T.; Klimovica, K.; LaPointe, A. M.; Keresztes, I.; Lobkovsky, E. B.; Daugulis, O.; Coates, G. W. Secondary Alkene Insertion and Precision Chain-Walking: A New Route to Semicrystalline “Polyethylene” from α -Olefins by Combining Two Rare Catalytic Events. *J. Am. Chem. Soc.* **2014**, *136*, 7213–7216.
- (41) O’Connor, K. S.; Watts, A.; Vaidya, T.; LaPointe, A. M.; Hillmyer, M. A.; Coates, G. W. Controlled Chain Walking for the Synthesis of Thermoplastic Polyolefin Elastomers: Synthesis, Structure, and Properties. *Macromolecules* **2016**, *49*, 6743–6751.
- (42) Note that both regioisomers of 3HT are consumed, leading to polymers with low regioregularity (Tables A2-1 and A2-2).
- (43) Note that the GPC overestimates the actual polymer molecular weight because of the different hydrodynamic volume of P3HT relative to the polystyrene calibration standards.
- (44) Note that the iPr end-group likely forms via transmetalation of unreacted iPrMgCl with a Ni species either during initiation or propagation or via oxidative addition of dissociated $L_nNi(0)$ into the generated iPrBr.
- (45) Nanashima, Y.; Yokoyama, A.; Yokozawa, T. Synthesis of Well-Defined Poly(2-alkoxypyridine-3,5-diyl) via Ni-Catalyst-Transfer Condensation Polymerization. *Macromolecules* **2012**, *45*, 2609–2613.
- (46) Jeffries-El, M.; Sauve, G.; McCullough, R. D. Facile Synthesis of End-Functionalized Regioregular Poly(3-alkylthiophene)s via Modified Grignard Metathesis Reaction. *Macromolecules* **2005**, *38*, 10346–10352.
- (47) Hardeman, T.; Koeckelberghs, G. The Synthesis of Poly-(thiophene-co-fluorene) Gradient Copolymers. *Macromolecules* **2015**, *48*, 6987–6993.

(48) The estimated “statistical” conversion was determined as follows: First, we assumed that each molecule (terthiophene and thiophene) would only undergo a single cross-coupling event (to simplify the calculations). With 50% conversion of the Grignard, based on the 15 equiv of thiophene and 1 equiv of terthiophene in the reaction mixture, the likelihood it would react with a terthiophene molecule then is 6.25% ($1/16 \times 100$).

(49) Sontag, S. K.; Bilbrey, J. A.; Huddleston, N. E.; Sheppard, G. R.; Allen, W. D.; Locklin, J. π -Complexation in Nickel-Catalyzed Cross-Coupling Reactions. *J. Org. Chem.* **2014**, *79*, 1836–1841.

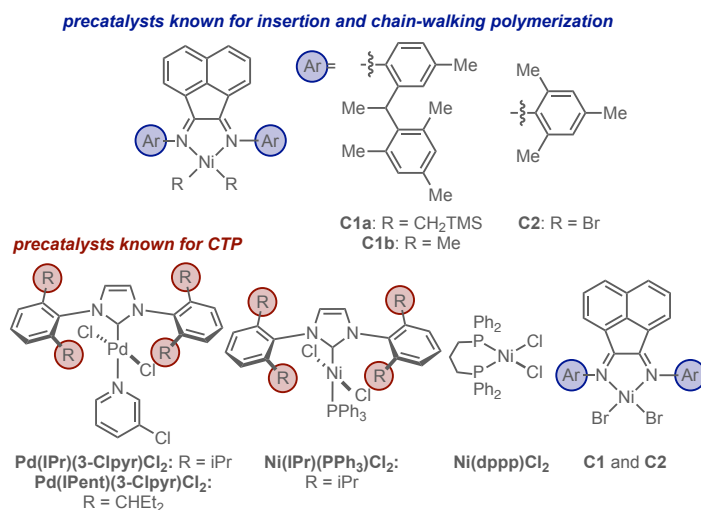
(50) Yoshikai, N.; Matsuda, H.; Nakamura, E. Ligand Exchange as the First Irreversible Step in the Nickel-Catalyzed Cross-Coupling Reaction of Grignard Reagents. *J. Am. Chem. Soc.* **2008**, *130*, 15258–15259.

Chapter 4: Progress Towards Thiophene/Olefin Block Copolymers using an in-situ Ligand-Exchange Approach

4.1 Introduction

Block copolymers containing conducting and insulating segments have been used in organic field effect transistors to improve charge mobility.^{1,2} Because each segment is synthesized through a different polymerization method, generating these copolymers, often requires multi-step routes with multiple catalysts, post-polymerization modifications, and purification steps.¹⁻⁴ Both segments, however, can be synthesized through Ni and Pd-catalyzed living, chain-growth polymerization methods which involve similar M(II) intermediates (cf. Chart 4-1). Conjugated polymers can be efficiently synthesized using catalyst-transfer polymerization (CTP).⁵⁻⁷ Insulating polymers with various topologies and functional groups can be polymerized using an insertion and chain-walking method.⁸⁻¹⁰ We anticipated that if a single catalyst scaffold could undergo both methods efficiently, switching between mechanisms could be facile and provide a streamlined approach toward these block copolymers.

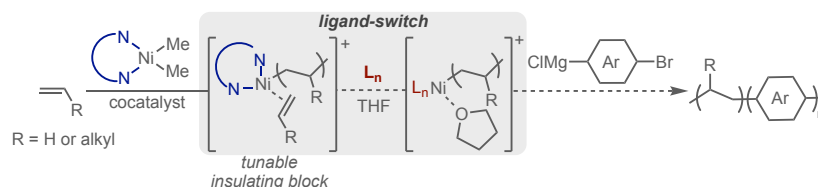
Chart 4-1. Selected Ni and Pd precatalysts used for insertion and chain-walking or CTP.



Diimine-ligated Ni precatalysts polymerize olefins via the insertion and chain-walking mechanism^{8–10} and have recently been investigated for polymerizing conjugated monomers^{9–16} (Chart 4-1). Despite identifying a diimine-ligated Ni precatalyst (**C1a**) efficient in both polymerization mechanisms, a high barrier for sp^3/sp^2 reductive elimination during mechanism-switching resulted in catalyst dissociation when synthesizing poly(1-pentene)-*block*-poly(3-hexylthiophene).¹⁷ As such homopolymer impurities were formed in addition to the desired block-copolymers. Many ancillary ligands can promote couple sp^3/sp^2 reductive elimination,^{18,19} but are not known for polymerizing olefins in a living, chain-growth manner. To design a versatile copolymerization method we envisioned an approach involving a ligand-switch, such that ancillary ligands could be matched for each monomer and switched during the polymerization. Ligand-switching has been used for catalysis where air-stable precatalysts are premixed with an optimized ancillary ligand before adding starting material.²⁰ To enable ligand-switching, the added ancillary ligand is more σ -donating than the initial ancillary ligand. We hypothesized that a similar ligand-switch approach could be used to polymerize conjugated-*block*-olefin copolymers. First, a diimine-ligated precatalyst would be used to generate a

poly(olefin) macroinitiator through the insertion and chain-walking mechanism. Then, adding a strongly σ -donating ligand would displace the diimine ancillary ligand, rendering the metal-center ready for CTP (Scheme 4-1).

Scheme 4-1. Proposed ligand-switch approach for synthesizing insulating/conducting block copolymers



4.2 Results and Discussion

Phosphine and N-heterocyclic carbene (NHC) ancillary ligands are stronger sigma-donating²¹⁻²³ than diimine ancillary ligands and make efficient CTP catalysts when ligated to Ni or Pd.⁵ Therefore, we began by evaluating bisphosphine- and NHC-ligated catalysts to determine an optimal ancillary ligand for coupling the poly(olefin) macroinitiator to thiophene through sp^2/sp^3 reductive elimination. To identify a catalyst scaffold capable of mediating this reductive elimination we designed a simple model system to evaluate poly(thiophene)/olefin coupling (Figure 4-1).²⁴ First, precatalysts were used to polymerize thiophene monomers via CTP. Subsequently, methyl Grignard end-capping reagent was added to evaluate the catalysts ability to couple poly(thiophene) with an sp^3 carbon. Concurrently, excess halogenated arene is added to scavenge M(0) generated after reductive elimination. The resulting polymers are then analyzed by MALDI-TOF/MS to determine the percentage of methyl-end capped poly(thiophene). For efficient sp^2/sp^3 reductive elimination we anticipate observing Me-end capped polymers. The catalyst that generates the most Me-terminated polymers will be the most efficient at coupling poly(thiophene) with an sp^3 carbon. Furthermore, the Me/Me-terminated polymers suggest that the catalyst ring-walks the length of the polymer between end-capping, rather than dissociating.

In contrast, polymers that remain un-capped suggest the catalyst is less efficient for sp^3/sp^2 reductive elimination and could lead to homopolymer impurities if applied to a copolymerization.

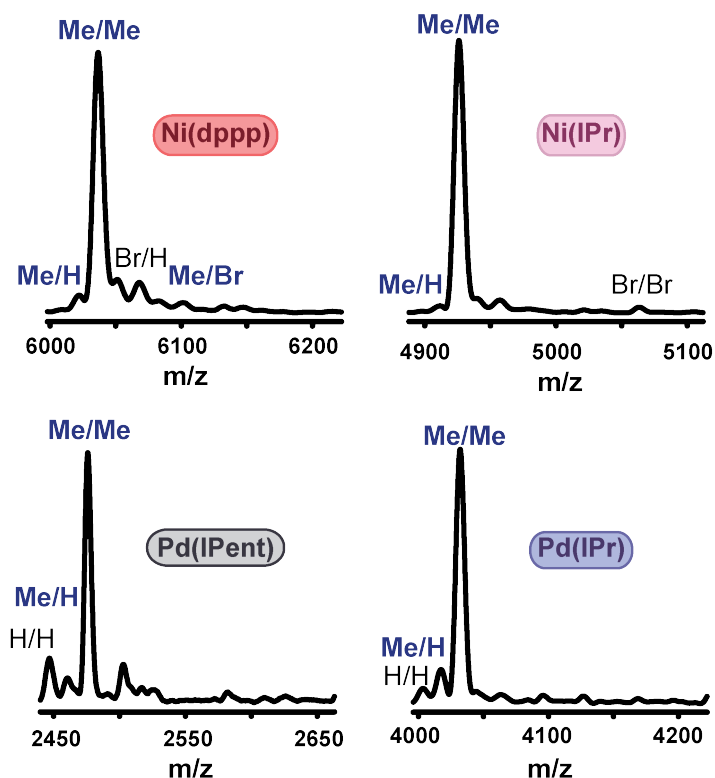
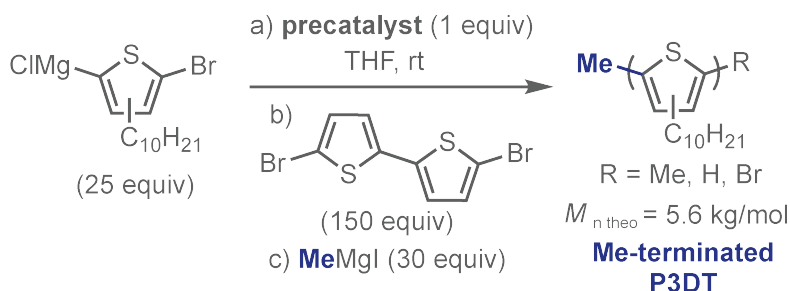


Figure 4-1. (Top) Reaction conditions for 3DT polymerization followed by end-capping experiments. (Bottom) MALDI-TOF/MS data for 3DT polymerization followed by end-capping. The full MALDI-TOF/MS spectra can be found in Appendix 3.²⁵

We evaluated three commonly used CTP precatalysts⁵ ($Ni(dppp)Cl_2$, $Ni(IPr)(PPh_3)Cl_2$, and $Pd(IPr)(3-Clpyr)Cl_2$) and a palladium precatalyst with a more sterically hindered ancillary

ligand (Pd(IPent)(3-Clpyr)Cl₂), hypothesizing that the increased steric properties could facilitate sp²/sp³ reductive elimination. The Ni precatalysts outperformed the Pd precatalysts generating 97–99% Me-terminated polymers. The NHC-ligated Ni precatalyst generated 99% Me-terminated polymers with gave 95% having Me/Me end-groups. In contrast, the bisphosphine-ligated Ni precatalyst, 97% of polymers were Me-terminated (3% remaining Br/H). Of the Me-terminated polymers, only 88% contained Me/Me end-groups, with the remaining 12% consisting of Me/H- and Me/Br-terminated polymers. Observing polymers with only one methyl group indicates that the catalyst failed to ring-walk the length of the polymer (Me/Br-terminated polymers) or was quenched before a second capping event occurred (Me/H-terminated polymers). The increased percentage of Me/Me-terminated polymers via the NHC-ligated precatalyst suggests it is more efficient at the sp³/sp² coupling than the bisphosphine-ligated precatalyst. The sterically hindered precatalyst, Pd(IPent)(3-Clpyr)Cl₂, generated polymers with a relatively broad dispersity ($\bar{M}_w/\bar{M}_n = 1.76$) and the fewest Me-terminated polymers (Figures 1, A3-7, & A3-11). These results could be attributed to sluggish turnover caused by the increased steric properties at Pd or unproductive pathways which generate inactive catalysts.

Having identified a potential ancillary ligand (IPr) and metal (Ni) for mechanism-switching and CTP, we next optimized the ligand-switching step. To evaluate ligand-switching, a second methyl-end capping model system was used (Figure 4-2). First, a diimine-ligated Ni precatalyst is treated with IPr to initiate ligand-switching and prepare the catalyst for CTP, which begins when the thiophene monomer is added. Then, methyl Grignard and the M(0) scavenger are added. Under optimized ligand-switch conditions, we expect to observe similar Me-end capping results, indicating that the sp³/sp² reductive elimination occurs with the same efficiency after ligand-switching as with the commercially available precatalysts. Treating the diimine-

ligated Ni precatalyst (**C2**) with IPr before initiating thiophene polymerization and subsequent end-capping, however, generated no detectable Me end-capped polymers (Figure 4-2). Furthermore, as demonstrated by GPC, the resulting polymer was multimodal suggesting that polymerizations were occurring through disparate pathways, either through multiple catalytic species or that the formed catalysts were undergoing unproductive pathways. Combined these results suggest displacing the diimine ancillary ligand with IPr alone will not be sufficient. One significant difference between initiating CTP with IPr-treated **C2** versus the commercial precatalyst, Ni(IPr)(PPh₃)Cl₂, is the stabilizing ligand, PPh₃. Treating **C2** with IPr and PPh₃ however generated polymers with an extremely broad dispersity ($\mathcal{D} = 17.1$) (Figure 4-2). In this case, both PPh₃ and IPr are stronger σ -donating ligands than the initial diimine ancillary ligand, enabling both added ligands to displace the diimine. Coupled with the multimodal GPC trace and broad dispersity, these results suggest various Ni species are present and polymerizing thiophene.

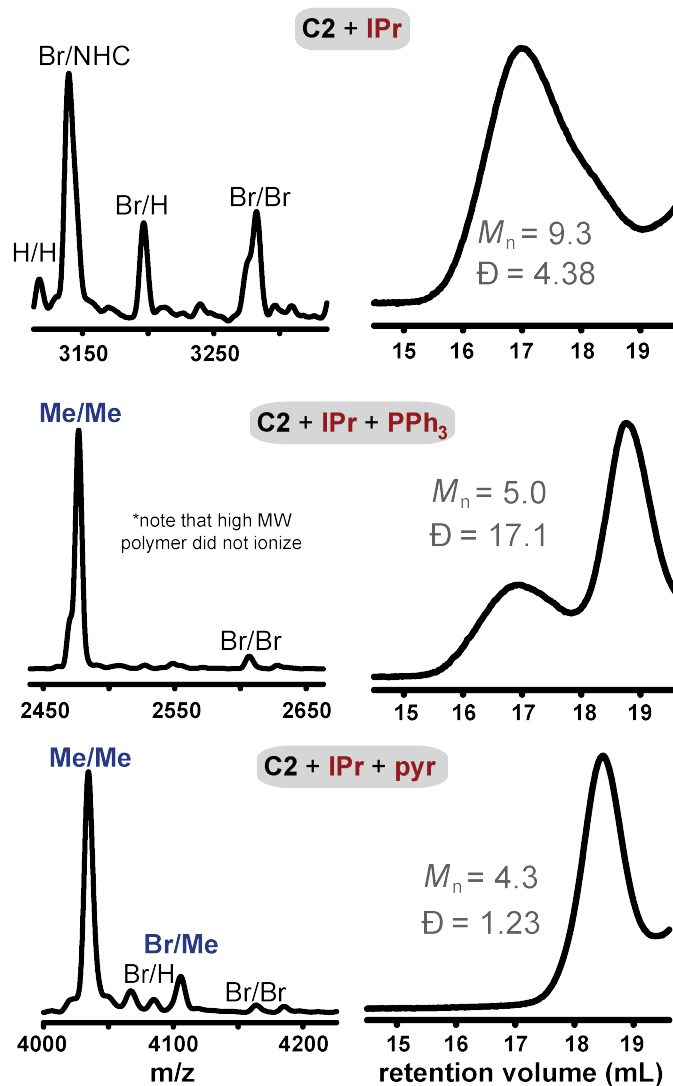
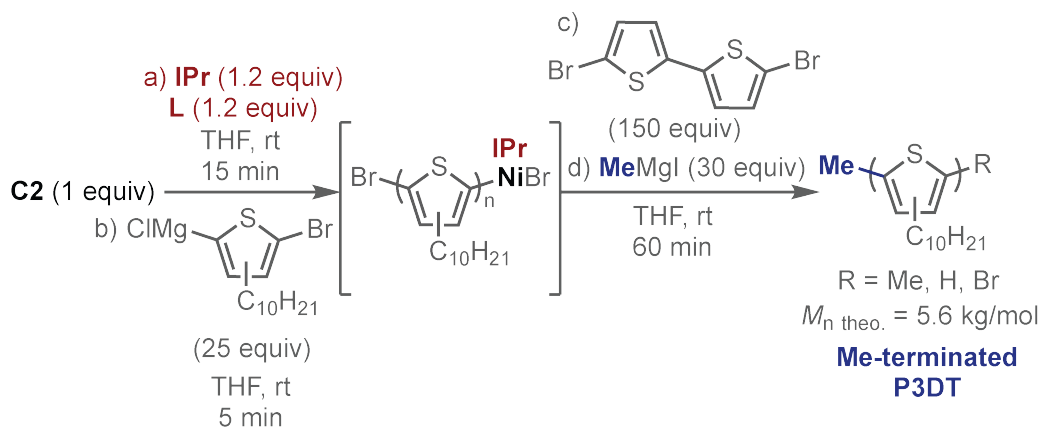


Figure 4-2. (left) MALDI-TOF/MS data and (right) GPC traces for 3DT polymerization followed by end-capping via a ligand-switched precatalyst. All M_n are reported in kg/mol. The full MALDI-TOF/MS spectra can be found in Appendix 3.^{25,26}

To avoid generating multiple catalytic species, we next evaluated adding a stabilizing ligand that would not displace the diimine ancillary ligand. Diimines are known to displace pyridine from Ni,²⁷ suggesting that pyridine would not displace the diimine ancillary ligand. In addition, pyridine derivatives have precedent as stabilizing ligands for IPr-ligated precatalysts.^{28,29} Adding both IPr and pyridine to **C2** prior to initiating thiophene polymerization and subsequent end-capping resulted in polymers with a narrow dispersity and efficient (90%) Me-end capping, suggesting ligand-switch, mechanism switching, and thiophene polymerization could all work in a multitasking catalyst system using IPr and pyridine (Figure 2). For our initial **C1a**-based multitasking catalyst system, 1-hexene was a competitive π -binding agent during CTP, which resulted in chain-transfer reactions and thiophene oligomers.¹⁷ This trend was not observed with IPr as the ancillary ligand, which promoted CTP and efficient end-capping (91% Me-terminated polymers) even in the presence of 1-hexene (Figure A3-17). In addition, the polymers generated using IPr and pyridine-treated **C2** are approximately the theoretical molecular weight and narrow dispersities ($M_{\text{theo}} = 5.6$ kg/mol and $M_n = 4.3\text{--}4.4$ kg/mol; $\mathcal{D} = 1.2$). These results suggest that the IPr ancillary ligand enable Ni to resist chain-transfer pathways instigated by excess olefin.

Having optimized ligand-switch conditions we next attempted copolymerization. We previously identified that a boron cocatalyst ($\text{B}(\text{C}_6\text{F}_5)_3$) activates (diimine)Ni(bisalkyl) complexes for polymerizing olefins and concomitantly does not disrupt CTP.¹⁷ Using this same catalyst system, **C1b** was activated to generate a poly(1-pentene) macroinitiator in neat 1-pentene (Figure 4-3A). Then, THF is added to bind to Ni's open coordination site and stall propagation.¹⁷ Ligand-switching was induced by adding both pyridine and the IPr ancillary

ligand. Evaluating the GPC traces before (PO_i) and after ligand-switching (PO_{LS}) indicates no further olefin insertion occurs after adding THF (Figure 4-3B). The Grignard thiophene monomer was subsequently added and a color change indicative of poly(thiophene) enchainment was observed. If chain-extension with thiophene monomers had occurred, an increase in molecular weight from the poly(olefin) macroinitiator to the final polymer should be evident. Instead, the RI trace does not shift to higher molecular weight suggesting that chain-extension did not occur. In addition, if chain-extension with thiophene monomers had occurred, the final UV and RI traces should overlay. Here, the final RI and UV traces do not overlay. Because no chain-extension occurs, the UV trace represents only poly(thiophene) and has a lower molecular weight than the poly(olefin) macroinitiator (Figure 4-3C).

If ligand-switching had not occurred the Ni would still be ligated with the initial diimine ancillary ligand, which can only generate thiophene oligomers in the presence of 1-hexene.¹⁷ Using this ligand-switch copolymerization approach, we observed that increasing the relative ratio of thiophene to Ni did increase the poly(thiophene)'s MW, suggesting the ancillary ligand switching step was not the mechanistic flaw (Figures A3-17–A3-20). Coupled with low thiophene monomer conversion, these data suggest catalyst dissociates from the poly(olefin) macroinitiator after ligand switching, generating mostly inactive catalyst species. After dissociating from the olefin macroinitiator, some catalysts do remain active and initiate CTP through oxidative addition into a thiophene C–Br bond. We hypothesized that although the IPr ancillary ligand switch enables living, chain-growth thiophene polymerization, it may be promoting olefin chain-termination pathways through β -hydride elimination.

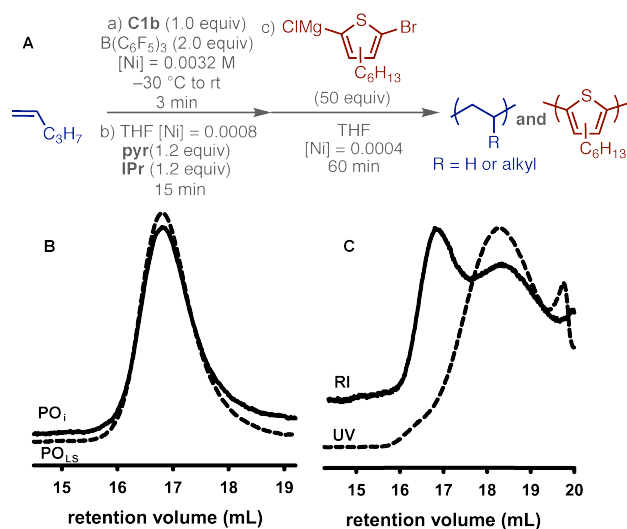


Figure 4-3. (A) Reaction conditions for ligand-switch copolymerization attempt. (B) GPC trace of the poly(olefin) macroinitiator before and after ligand-switch. (C) GPC traces showing the RI and UV curves of the final polymers.

In summary, here we present our progress towards developing a generalizable approach for generating poly(olefin)-*block*-poly(thiophene) copolymers. We developed a ligand-switching method that can be used to efficiently polymerize conjugated monomers. However, the strong σ -donating IPr ancillary ligand appears to promote chain-termination with poly(olefins). Currently, this ligand-switch only generates homopolymers, but with further optimization there is potential for developing a facile method for synthesizing copolymers.

4.3 References

- (1) Yu, X.; Xiao, K.; Chen, J.; Lavrik, N. V.; Hong, K.; Sumpter, B. G.; Geohegan, B. D. High-Performance Field-Effect Transistors Based on Polystyrene-*b*-Poly(3-hexylthiophene) Diblock Copolymers. *ACS Nano* **2011**, *5*, 3559–3567.
- (2) Lo, C-T.; Lin, C-J.; Lee, J-Y.; Tung, S-H.; Tsai, J-C.; Chen, W-C. Molecular stacking structure and field-effect transistor characteristics of crystalline poly-(3-hexylthiophene)-*block*-syndiotactic polypropylene through solvent selectivity. *RSC Adv.* **2014**, *4*, 23002–23009.

- (3) Radano, C. P.; Scherman, O. A.; Stingelin-Stutzmann, N.; Müller, C.; Breiby, D. W.; Smith, P.; Janssen, R. A. J.; Meijer, E. W. Crystalline–Crystalline Block Copolymers of Regioregular Poly(3-hexylthiophene) and Polyethylene by Ring-Opening Metathesis Polymerization. *J. Am. Chem. Soc.* **127**, 36, 12502–12503.
- (4) Moon, H. C.; Anthonysamy, A.; Lee, Y.; Kim, J. K. Facile Synthesis of Well-Defined Coil–Rod–Coil Block Copolymer Composed of Regioregular Poly(3-hexylthiophene) via Anionic Coupling Reaction. *Macromolecules* **2010**, 4, 1747–1752.
- (5) Leone, A. K.; McNeil, A. J. Matchmaking in Catalyst-Transfer Polycondensation: Optimizing Catalysts based on Mechanistic Insight. *Acc. Chem. Res.* **2016**, 49, 2822–2831.
- (6) Bryan, Z. J.; McNeil, A. J. Conjugated Polymer Synthesis via Catalyst-Transfer Polycondensation (CTP): Mechanism, Scope, and Applications. *Macromolecules* **2013**, 46, 8395–8405
- (7) Yokozawa, T.; Ohta, Y. Transformation of Step-Growth Polymerization into Living Chain-Growth Polymerization. *Chem. Rev.* **2016**, 116, 1950–1968.
- (8) Guo, L.; Dai, S.; Sui, X.; Chen, C. Palladium and Nickel Catalyzed Chain Walking Olefin Polymerization and Copolymerization. *ACS Catal.* **2016**, 6, 428–441.
- (9) Carrow, B. P.; Nozaki, K. Transition-Metal-Catalyzed Functional Polyolefin Synthesis: Effecting Control through Chelating Ancillary Ligand Design and Mechanistic Insights. *Macromolecules* **2014**, 47, 2541–2555.
- (10) O'Connor, K. S.; Lamb, J. R.; Vaidya, T.; Keresztes, I.; Klimovica, K.; LaPointe, A. M.; Daugulis, O.; Coates, G. W. Understanding the Insertion Pathways and Chain Walking Mechanisms of α -Diimine Nickel Catalysts for α -Olefin Polymerization: A ^{13}C NMR Spectroscopic Investigation. *Macromolecules* **2017**, 50, 7010–7027.

- (11) Leone, A. K.; Souther, K. D.; Vitek, A. K.; LaPointe, A. M.; Coates, G. W.; Zimmerman, P. M.; McNeil, A. J. Mechanistic Insight into Thiophene Catalyst-Transfer Polymerization Mediated by Nickel Diimine Catalysts. *Macromolecules* **2017**, *50*, 9121–9127.
- (12) Magurudeniya, H. D.; Sista, P.; Westbrook, J. K.; Ourso, T. E.; Nguyen, K.; Maher, M. C.; Alemseghed, M. G.; Biewer, M. C.; Stefan, M. C. Nickel(II) α -Diimine Catalyst for Grignard Metathesis (GRIM) Polymerization. *Macromol. Rapid Commun.* **2011**, *32*, 1748–1752.
- (13) Bridges, C. R.; McCormick, T. M.; Gibson, G. L.; Hollinger, J.; Seferos, D. S. Designing and Refining Ni(II)diimine Catalysts Toward the Controlled Synthesis of Electron-Deficient Conjugated Polymers. *J. Am. Chem. Soc.* **2013**, *135*, 13212–13219.
- (14) Bridges, C. R.; Yan, H.; Pollit, A. A.; Seferos, D. S. Controlled Synthesis of Fully π -conjugated Donor-Acceptor Block Copolymers Using a Ni(II) Diimine Catalyst. *ACS Macro Lett.* **2014**, *3*, 671–674.
- (15) Pollit, A. A.; Bridges, C. R.; Seferos, D. S. Evidence for the Chain-Growth Synthesis of Statistical π -Conjugated Donor–Acceptor Copolymers. *Macromol. Rapid Commun.* **2015**, *36*, 65–70.
- (16) Pollit, A. A.; Obhi, N. K.; Lough, A. J.; Seferos, D. S. Evaluation of an External Initiating Ni(II) Diimine Catalyst for Electron-deficient π -Conjugated Polymers. *Polym. Chem.* **2017**, *8*, 4108–4113.
- (17) Souther, K. D.; Leone, A. K.; Vitek, A. K.; Palermo, E. F.; LaPointe, A. M.; Coates, G. W.; Zimmerman, P. M.; McNeil, A. J. Trials and Tribulations of Designing Multitasking Catalysts for Olefin/ Thiophene Block Copolymerizations. *J. Polym. Sci., Part A: Polym. Chem.* **2018**, *56*, 132–137.

- (18) Valente, C.; Calimsiz, S.; Hoi, K. H.; Mallik, D.; Sayah, M.; Organ, M. G. The Development of Bulky Palladium NHC Complexes for the Most-Challenging Cross-Coupling Reactions. *Angew. Chem. Int. Ed.* **2012**, *51*, 3314–3332.
- (19) Kantchev, E. A. B.; Brien, C. J. O.; Organ, M. G. Palladium complexes of N-heterocyclic carbenes as catalysts for cross-coupling reactions - A synthetic chemist's perspective. *Angew. Chem. Int. Ed.* **2007**, *46*, 2768–2813.
- (20) Shields, J. D.; Gray, E. E.; Doyle, A. G. A Modular, Air-Stable Nickel Precatalyst. *Org. Lett.* **2015**, *17*, 2166–2169.
- (21) Setiawan, D.; Kalescky, R.; Kraka, E.; Cremer, D. Direct Measure of Metal–Ligand Bonding Replacing the Tolman Electronic Parameter. *Inorg. Chem.* **2016**, *55*, 2332–2344.
- (22) Hans J. Reich. 2001. Bordwell pKa Table (Acidity in DMSO). [ONLINE] Available at: <https://www.chem.wisc.edu/areas/reich/pkatable/index.htm>. [Accessed 2 August 2018]
- (23) Antonova, N. S.; Carbo, J. J.; Poblet, J. M. Quantifying the Donor-Acceptor Properties of Phosphine and N-Heterocyclic Carbene Ligands in Grubbs' Catalysts Using a Modified EDA Procedure Based on Orbital Deletion. *Organometallics* **2009**, *28*, 4283–4287.
- (24) For a similar model system: Leone, A. K.; Goldberg, P. K.; McNeil, A. J. Ring-Walking in Catalyst-Transfer Polymerization. *J. Am. Chem. Soc.* **2018**, *140*, 7846–7850.
- (25) Unlabeled peaks correspond to unidentified masses.
- (26) As anticipated the poly(thiophene) generated via **C2** alone showed no Me-terminated polymers (Figure A3-13).
- (27) Palmer, W. N.; Zarate, C.; and Chirik, P. J. Benzyltriboronates: Building Blocks for Diastereoselective Carbon–Carbon Bond Formation. *J. Am. Chem. Soc.* **2017**, *139*, 2589–2592.

Chapter 5: Outlook - The History of Palladium-catalyzed Cross-couplings Should Inspire the Future of Catalyst-Transfer Polymerization

This work has been done in collaboration with Mueller, E. A. who significantly contributed to the history of CTP, device performance, and Pd-catalyzed CTP sections of this perspective.

5.1 Introduction

Designing novel materials for fuel cells, batteries, and solar panels is central to meeting society's growing needs for alternative energy sources. Semiconducting polymers are widely explored in these applications due to their inherent ability to absorb light and conduct charge. These polymers can be accessed through either oxidative coupling or transition-metal catalyzed polymerization. For the latter approach, the polymerizations proceed either through a step-growth^{1,2} or chain-growth³⁻⁶ mechanism. Living, chain-growth polymerizations are ideal because monomers are sequentially added to the polymer without termination, which enables polymers with precise molecular weights, dispersities, sequences, and end-groups to be synthesized.⁷ Despite the promise of this approach, advances in catalyst-transfer polymerization (CTP) have been slow relative to other polymerization types.

Transition-metal catalyzed syntheses for conjugated polymers were first reported as early as 1978.⁸ Remarkably, the chain-growth mechanism of some of these transformations was not revealed until 26 years later.^{9,10} Thiophene polymerization catalyzed by Ni(dppp)Cl₂ was first reported by Heeger and Wudl in 1984.¹¹ Eight years later, McCullough demonstrated that this polymerization yielded regioregular poly(3-alkylthiophene).¹² However, it was not until 2004 that McCullough⁹ and Yokozawa¹⁰ concurrently reported that this polymerization was living and

chain-growth. These seminal reports revealed for the first time that conjugated polymers have the potential to be synthesized with control over their length, sequence and end-group functionality – an exciting advancement in the field. These discoveries lured the corresponding authors and several others to start exploring the method's potential.

This metal-catalyzed chain-growth method for synthesizing conjugated polymers is referred to as CTP. To date, CTP is still most frequently used to polymerize simple thiophene monomers with Ni(dppp)Cl₂.³⁻⁵ Over the last decade, the majority of advances in CTP have been mechanistic in nature: demonstrating how the ancillary ligands, reactive ligands, and transition metal identity influence initiation and propagation.^{8,9,15-19} In contrast, during the same time period most of the advances in organic electronic materials have been in structural diversification: developing new monomers to optimize optical and conductive properties as well as solid-state packing.^{1,2,20-26} There is an enormous mismatch between the mechanistic insight gained for CTP and its ability to polymerize state-of-the-art, structurally diverse monomers.

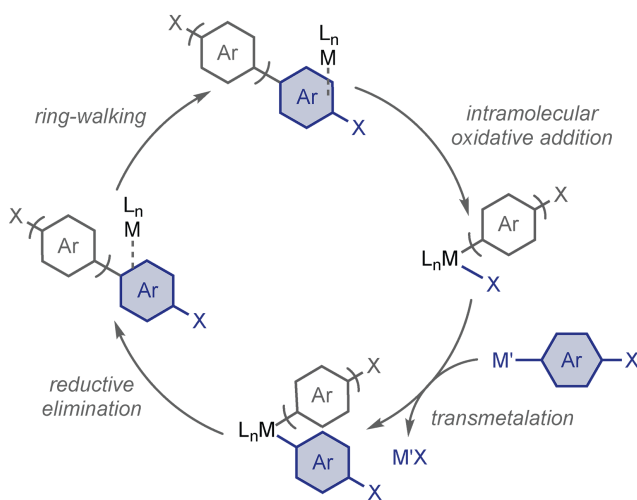
To overcome this limitation, we draw inspiration from the delayed “discovery” of CTP and urge the catalysis community to ask: what are we overlooking? What potential ligands and precatalysts for CTP might *already* exist in the small-molecule or polymerization literature? Fortunately, the mechanistic insight developed over the last decade provides a detailed road map for how to identify precatalysts for CTPs. This Perspective highlights what we think should be the path forward. We begin by describing the CTP mechanism and how it enables conjugated polymers to be systematically tuned. Then, we outline why we consider palladium precatalysts the most promising mediators for advancing CTP. Finally, ancillary ligands that have already been explored for Pd-mediated CTP are highlighted and used as inspiration to identify

precatalysts from the small-molecule literature that we believe should be explored in future polymerizations.

5.2 Mechanism.

In CTP, propagation proceeds through a M(0)/M(II) catalytic cycle, including transmetalation, reductive elimination, and oxidative addition (Scheme 5-1). The biggest difference between CTP and step-growth polymerizations is ring-walking,^{28,29} wherein the catalyst forms a metal–polymer π -bound intermediate that migrates to the C–X terminus. Intramolecular oxidative addition at the C–X bond primes the catalyst for subsequent monomer transmetalation. The cycle continues until all monomers have been added to the polymer chain. Ring-walking enables each catalyst to enchain monomers along a single polymer; therefore, polymers with targeted molecular weights, sequences, and narrow dispersities can be obtained. For propagation to proceed without unproductive pathways (e.g., chain-transfer²⁷ and/or termination), the catalyst and monomer identities must be matched sterically and electronically to promote stable, yet reactive, π -complexes which can efficiently ring-walk for many turnovers.

Scheme 5-1. CTP mechanism

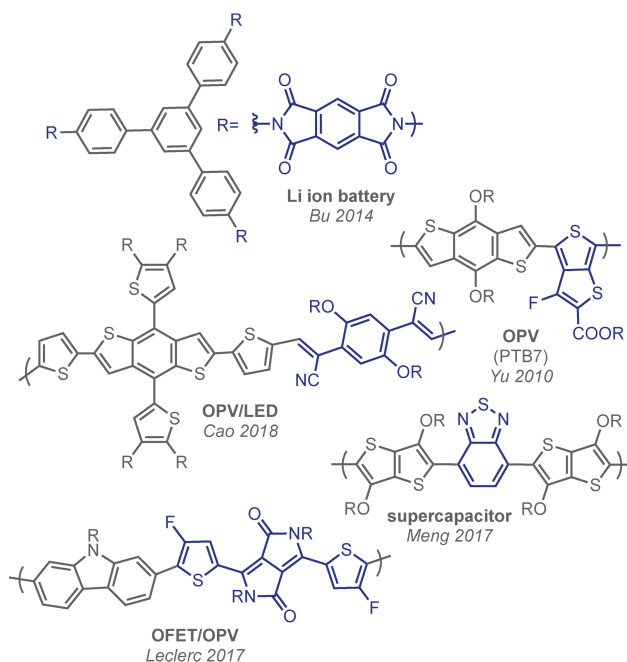


5.3 Why CTP for organic electronics?

CTP is advantageous for organic electronics because it enables polymers with specific molecular weights,²⁸ narrow dispersities, and precise sequences to be synthesized reproducibly.⁷ Each of these properties can significantly impact performance, but the degree to which each parameter affects different devices is less well understood. In the past, conjugated polymers have been predominantly used in organic light-emitting diodes (OLEDs),^{29,30} organic photovoltaics (OPVs),^{29,25,31} and organic field-effect transistors (OFETs).^{32,33,34} More recently, research efforts are focused on using conjugated polymers for energy storage applications such as supercapacitors,^{35,36,37,38} and batteries^{20,39,40,41} (Chart 5-1). The highest-performing conjugated polymers in these applications are almost exclusively synthesized via step-growth methods. These methods suffer from batch-to-batch variability⁴² and the researcher has little control over the polymer molecular weight, dispersity, and sequence. Nevertheless, these variables can have an enormous impact in organic electronic applications.

It is well established that increasing polymer molecular weight correlates with improved organic electronic device performance, especially for OFETs and OPVs.^{43,44} McGeehee and coworkers showed that increasing the M_n of regioregular poly(3-hexylthiophene)'s by 10 times increased charge mobility in OFETs by 10,000 times.⁴⁵ Similar trends have been observed in high-performing donor–acceptor polymers.²³ However, to synthesize high molecular weight donor–acceptor polymers using step-growth methods, long reaction times,⁴⁶ precise monomer stoichiometry,⁴⁷ and polymer purification⁴⁸ are required. In contrast, simply altering the initial catalyst-to-monomer ratio with CTP would enable high molecular weight polymers to be targeted and obtained.

Chart 5-1. High-performing polymers synthesized via step-growth polymerization methods



Similarly, it is challenging to target precise dispersities using step-growth methods, and therefore difficult to parse their influence on device performance. However, recent examples have shown that a broad dispersity correlates to decreased device performance. Yu and coworkers found that doubling polymer dispersity decreased device efficiency by 65% in PTB7-based OPVs (c.f., Chart 5-1).⁴⁹ They proposed that undesired homocoupled oligomers, containing donor–donor or acceptor–acceptor couplings, act as charge-trapping sites and facilitate charge recombination. The identities of these homocoupled defects were confirmed by analyzing low-performing batches using matrix assisted laser desorption-ionization time of flight mass spectrometry (MALDI-TOF-MS).⁵⁰ These homocoupled oligomer defects are challenging to remove from product mixtures even with time- and labor-intensive purifications. Identifying an optimal CTP catalyst for synthesizing donor–acceptor polymers would reduce these oligomeric contaminants and instead yield predominantly high molecular weight polymers. In

addition, by initiating with a precatalyst containing an aryl reactive ligand (e.g., $L_nM(X)(Ar)$), one can eliminate homocoupled defects altogether.⁵¹

Hawker and coworkers evaluated the effect of dispersity on emission by meticulously purifying thiophene oligomers to obtain monodisperse samples.⁵² To evaluate dispersity effects, emission spectra from pure ($\mathcal{D} = 1.0$) and blended ($\mathcal{D} = 1.1\text{--}1.4$) samples with the same effective molecular weight were compared. The blended samples exhibited red-shifted emission, suggesting that using conjugated polymers with even moderate dispersities could result in OLEDs with reduced color precision compared to the monodisperse samples. Combined, these select examples suggest that dispersity is directly related to organic electronic device performance. With CTP, narrow dispersities can be achieved without arduous purifications. As researchers begin to expand CTP to more complex scaffolds, it will be fascinating to see the full effect of dispersity on device performance.

Polymer sequence dramatically influences charge mobility, active layer morphology, and device longevity.^{53,54,55} However, because non-alternating sequences are challenging to target with step-growth methods, there have been limited examples evaluating the effect of sequence (e.g., random, block, gradient) in high-performing devices.⁵⁰ Currently, organic electronics are susceptible to performance decreases over time due to phase separation.⁵⁶ We used CTP to synthesize thiophene-based block, random, and gradient sequence copolymers as stabilizing additives in OPVs.^{57,58} Adding 2 wt% copolymer to a poly(3-hexylthiophene):fullerene blend suppressed phase separation to varying degrees depending on copolymer sequence. The random sequence copolymer was the best additive, improving initial device power conversion efficiency (PCE) by 29% and maintaining 75% of initial device performance after annealing for 90 min.⁵⁷

Here, we found that sequence had a profound effect on the stability of OPVs, even for an additive present only in 2 wt% of the overall blend.

Overall, these examples stress that there should be a collective effort towards identifying CTP catalysts to synthesize the latest and best conjugated polymers in organic electronics. Then, both monomer structures and polymer sequences can be simultaneously and systematically tuned to enhance performance and longevity for specific devices.

5.4 Why Palladium?

Although CTP has many advantages, it has been largely limited to polymerizing monocyclic, electron-rich monomers.^{4,5} As organic-electronics have advanced, polymers with fused-arene repeat units, electron-rich (“donor”) and -deficient (“acceptor”) moieties, and various functional groups (e.g., F, CN) have become the new standard for devices (Chart 5-1). As such, until the monomer scope of CTP expands to include monomers with diverse functional groups and electronic properties, these complex copolymers with targeted sequences will be out of reach. It is therefore essential to identify CTP catalysts for each monomer’s specific structural demands (e.g., functional groups, fused arenes, disparate electronic properties, extended π -systems).

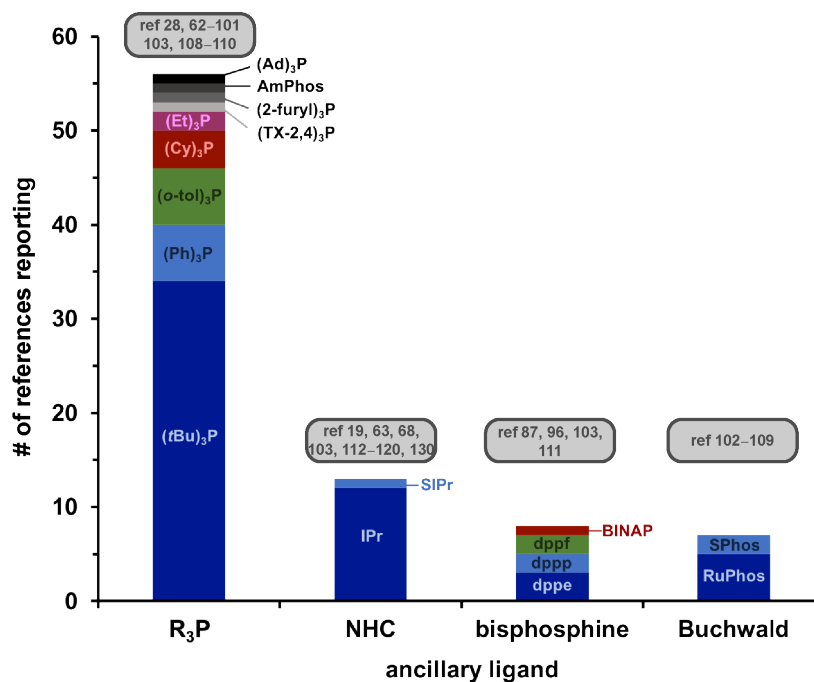
Palladium precatalysts are promising candidates to expand CTP’s monomer scope because they are ubiquitous in the small-molecule literature for coupling an array of electronically and sterically diverse substrates.^{59,60,61,62,63} Contrasting this precatalyst library with that of CTP⁵ begs the question, why haven’t most of these precatalysts been evaluated for polymerizing conjugated monomers? Most high-performing donor–acceptor polymers are commonly synthesized from two difunctionalized monomers (e.g., a dihalide and a distannane) using tetrakis(triphenyl)phosphine palladium ($\text{Pd}(\text{PPh}_3)_4$).^{54,55} Similar to the infancy of

palladium-catalyzed small-molecule cross-coupling,^{56,57} Pd(PPh₃)₄ is the workhorse precatalyst for conjugated polymers and is often used despite forming undesired products (e.g., homocoupled products). In Pd-catalyzed small-molecule cross-coupling, however, significant developments in catalyst design have now enabled electron-deficient and -rich substrates with unprotected functional groups to be synthesized with few side products.^{59,60,61} While hundreds of ancillary ligands have been screened and optimized for these small-molecule cross-coupling reactions, comparatively few have been explored for synthesizing conjugated polymers, leaving a vast range of potential Pd-precatalysts for CTP (Chart 5-2)^{19,28,68–126} These ligands have been specifically optimized for Pd and, as such, will likely be more successful on Pd than on Ni for CTP.¹²⁷ Herein, we highlight select examples of catalysts used in small-molecule cross-couplings as inspiration for expanding CTP.

In addition to the many potential CTP precatalysts, Pd is advantageous because it has been reported to have lower ring-walking barriers than commonly used Ni catalysts.¹⁹ This lower barrier to ring-walking could be favorable for polymerizing high-performing monomers, where the catalyst will be required to ring-walk over multiple π -bonds without dissociating. We recently developed a simple method to evaluate ring-walking over polymers and found that both Ni and Pd precatalysts demonstrated efficient ring-walking over electron-rich polymers.¹⁸ Compared to the analogous Ni precatalysts, however, Pd precatalysts were less likely to undergo unproductive pathways (i.e., ancillary ligand-based reductive elimination) at high monomer conversions when polymerizing thiophene. Additional computational evaluation by Yokozawa and coworkers indicated that Pd(IPr)(3-Clpyr)Cl₂ has lower ring-walking barriers than Ni(dppp)Cl₂, Pd(dppp)Cl₂, or Ni(IPr)PPh₃Cl₂.¹⁹ Combined with the small-molecule precedent for coupling electron-deficient and functionalized arenes, these ring-walking mechanistic studies all

suggest that Pd precatalysts should be capable of ring-walking over and polymerizing fused-arene repeat units, especially when catalyst stability is a determining factor.

Chart 5-2. The limited scope of ancillary ligands used in Pd-CTP since 2008. Each ligand was counted once per publication.



Although rare, there are some reports of Pd precatalysts outperforming commonly used Ni precatalysts in CTP. In one example, Kiriya and coworkers screened various commercial Ni and Pd precatalysts for polymerizing a fused-arene monomer, fluorene.⁷⁵ The phosphine-ligated Ni precatalyst ($Ni(dppp)Cl_2$) undergoes unproductive reactions, whereas the phosphine-ligated Pd precatalyst (tBu_3PPdX_2) proceeded through a chain-growth pathway. Yokozawa and coworkers found that Pd outperforms Ni when synthesizing poly(*p*-phenylenevinylene) (PPV). They hypothesized that the Ni became ‘trapped’ on the C=C bond in a π -complex that was too stable.^{70,72} Similarly, Koeckelberghs and coworkers showed that a tBu_3P -ligated Pd precatalyst could polymerize thieno[3,2-*b*]thiophene where Ni precatalysts with a variety of ancillary ligands (e.g., $dppp$, $dppe$, $depe$, IPr) failed.⁷⁴ This failed polymerization was attributed to Ni

trapping via a strong π -complex with the thienothiophene dimer formed in the initial reductive elimination. These examples highlight how Pd precatalysts are particularly advantageous for polymerizing repeat units that bind too strongly with Ni precatalysts.

Many complex polymers contain coordinating atoms such as N and O (c.f., Chart 5-1), which are rarely present in monomers polymerized by CTP.^{93,128,130–133} Previous efforts to polymerize N-containing monomers via CTP led to deleterious chain-transfer events.^{27,93} Palladium has reduced oxophilicity relative to Ni which should reduce both its affinity to N and O and could therefore promote CTP. Therefore, we anticipate that palladium precatalysts will be useful for polymerizing monomers with coordinating atoms.

Below, we highlight recent examples of Pd-catalyzed CTP and use small-molecule cross-coupling examples as inspiration for future CTP catalyst testing. It is our hope that this Perspective will encourage polymer chemists to evaluate these precatalysts for CTP of complex monomer scaffolds, and at the same time, encourage the small-molecule catalysis community to attempt polymerizations when developing new precatalysts.

5.5 Identifying new catalysts.

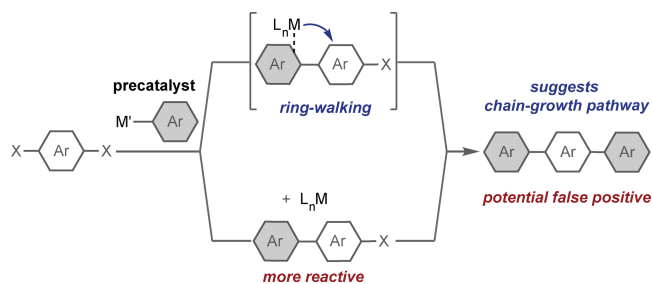
We and others have used small-molecule cross-coupling as inspiration for identifying new CTP precatalysts.^{116,124,126,139} Specifically, we view difunctionalization of polyhalogenated substrates as indicative of potential CTP precatalysts. For example, in 2012 we were inspired by a report by Goldup and Larrosa showing that Pd(IPr)(3-Clpyr)Cl₂ sequentially couples two PhMgBr to various dihalogenated arenes.¹³⁵ Because PhMgBr was the limiting reagent, these results suggested that the catalyst couples the arenes via ring-walking without dissociating. Had dissociation occurred, mono-functionalized starting material would have been observed. By expanding these difunctionalization studies to the analogous polymerization, we found that the

same precatalyst polymerizes both thiophene and phenylene monomers in a living, chain-growth manner.¹²⁶

Difunctionalization reactions can be misleading, however, if excess organometallic coupling partner is used or if a reactivity bias preferentially generates difunctionalized products (Scheme 5-2).¹³⁶ In both cases, difunctionalized products can form even if the catalyst does not proceed through a metal–arene π -bound intermediate. When screening catalysts to polymerize a phenylene ethynylene monomer we used a small-molecule difunctionalization model system. Although one precatalyst formed di- to mono-functionalized products in a 98:2 ratio, the resulting polymerization proceeded in a step-growth manner.¹³⁶ Here, dissociated catalysts preferentially reacted with the mono-functionalized intermediate because it was more reactive than the initial dihalogenated arene. Translating these small-molecule results to polymerizations, catalyst dissociation results in a step-growth mechanism rather than the desired chain-growth CTP.

To help ensure difunctionalized products are formed through ring-walking and *intramolecular* oxidative addition, a few precautionary steps should be taken. First, using substoichiometric organometallic coupling partner can reduce the number of false positives. However, reactivity differences can still lead to difunctionalized products.¹³⁷ In addition, we recommend adding a M(0) scavenger to stop dissociated catalysts from further reacting.¹⁸ These protocols should facilitate identifying potential CTP catalysts through small-molecule difunctionalization reactions.

Scheme 5-2. Identifying potential CTP precatalysts using small-molecule difunctionalization reactions.



5.6 The most popular Pd-CTP precatalyst.

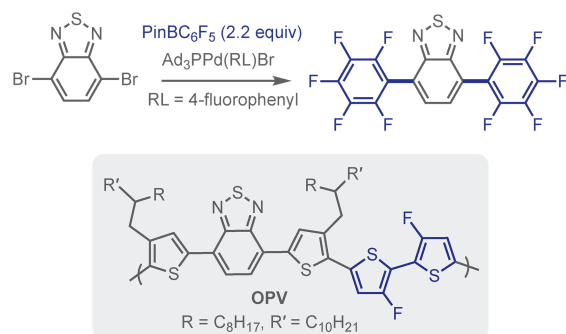
Most Pd-CTP examples use tBu_3P as the ancillary ligand for Suzuki polymerization.^{5,6} The reactive ligands in tBu_3P -ligated Pd precatalysts can be easily modified, providing an accessible handle for post-polymerization modification, or tuning the polymer's electronic properties.^{28,83,85} Nevertheless, tBu_3P -ligated Pd suffers from inconsistent initiation^{28,83,85,87,90,101} and turnover stability during propagation.⁷⁷ Unproductive pathways become especially detrimental if copolymer syntheses are attempted because inactive chains lead to oligomeric and/or homopolymer impurities, which are difficult to separate from the product mixture.¹³⁷ To circumvent these shortcomings, recent research efforts have been directed towards identifying alternative ancillary ligand scaffolds.

Tris(1-adamantyl)phosphine (Ad_3P) was identified as a promising ancillary ligand for Pd-catalyzed Suzuki-CTP of fluorene- and phenylene-based monomers with a range of steric properties.¹¹⁹ The Ad_3P ancillary ligand is sterically similar to tBu_3P but it is more Lewis basic.¹³⁸ This property could improve CTP relative to tBu_3P because increased electron-donation has been shown to stabilize the metal-polymer π -bound intermediate and promote productive CTP pathways.^{13,14} Using an Ad_3P -Pd precatalyst, polymers with approximately theoretical molecular weights could be synthesized with narrow dispersities, suggesting that the

polymerization proceeds via CTP.¹¹⁴ Furthermore, polymers could be end-capped in situ to generate a single detectable set of end-groups, indicating the catalyst was still polymer-bound and stable at high monomer conversions. These initial results using Ad₃P-ligated Pd to polymerize a relative range of monomers indicate potential for synthesizing structurally diverse polymers. Nevertheless, alternative electronically diverse monomer scaffolds have yet to be explored with this precatalyst.

A small-molecule cross-coupling precedent also supports the potential that Ad₃P-ligated Pd precatalysts have for polymerizing diverse monomer scaffolds. Carrow and coworkers generated an air-tolerant Ad₃P-ligated precatalyst that was used to synthesize various fluorinated bi- and triaryls under mild, Suzuki conditions (Scheme 5-3).¹³⁹ Heteroarenes could be difunctionalized with fluorinated arenes in excellent yields (>95%). Although these difunctionalization experiments were done using excess ArF[B], these methods were expanded to various fluorinated substrates, which could translate to fluorinated monomers for CTP. Fluorine-functionalized monomers are important in organic electronics because the fluorine substituents lower the polymer's highest occupied molecular orbital (HOMO) levels, which facilitates charge transfer. For example, Yan and coworkers developed a benzothiadiazole/thiophene polymer with fluorinated thiophenes for OPVs which resulted in an overall PCE of 10.8% (c.f., Scheme 5-3).¹⁴⁰

Scheme 5-3. (top) Ad₃P-ligated Pd-catalyzed small-molecule difunctionalization reaction of benzothiadiazole and fluorinated arenes. (bottom) High-performing polymer containing benzothiadiazole and fluorinated-thiophene units.



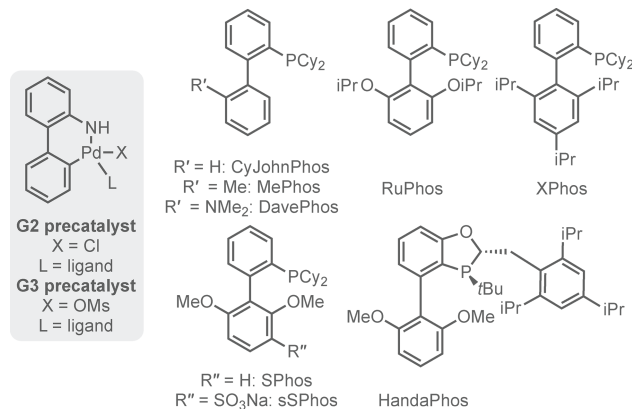
The Ad_3P ligand is one example of how modifying ancillary ligand electronic properties may significantly improve polymerization efficiency and potentially expand monomer scope. However, Ad_3P -ligated Pd is relatively nascent even for small-molecule cross-coupling.^{138,139} In contrast, there have been decades of research on biarylphosphine (Buchwald ligands)⁵⁹ and N-heterocyclic carbenes (NHCs).⁶¹ Many modifications to the original compounds have been made to optimize their small-molecule cross-coupling efficiency.^{59,60} Nevertheless, these ancillary ligands have scarcely been used in CTP. Based on preliminary CTP examples (discussed below), it is evident that these tunable ligands could be exactly what is needed to match catalyst/monomer pairings and significantly advance CTP.

5.7 The future: Buchwald ligands.

Dialkylbiarylphosphine ancillary ligands developed by Buchwald and co-workers are widely used for cross-coupling sterically hindered and/or electronically dissimilar small molecules.⁵⁹ Buchwald ancillary ligand modularity has enabled them to be designed to meet the demands of various substrates, promoting highly efficient cross-coupling systems (Chart 5-2). We expect that Buchwald ancillary ligands could also promote CTP of electron-poor and complex monomers. The few examples using Buchwald-type ligands in CTP^{108–113} should inspire

both the small-molecule and polymer communities to start evaluating more of these catalysts for CTP.

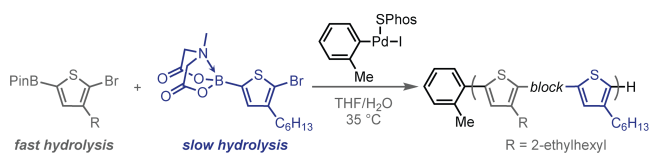
Chart 5-3. Select Buchwald precatalysts and ancillary ligands.



Recently, Choi and coworkers showed that both RuPhos and SPhos G3 Pd precatalysts outperformed XPhos- or tBu₃P-ligated Pd precatalysts when polymerizing BPin-thiophene monomers.¹⁰⁸ Mechanistic analysis revealed that when ligated to Pd, both RuPhos and SPhos mediated a living, chain-growth polymerization, affording polymers with consistently narrow dispersities ($\mathcal{D} \geq 1.16$), and excellent end-group fidelity (>95%), indicating each catalyst polymerizes a single polymer and is stable throughout polymerization. In addition, an SPhos-ligated Pd precatalyst was also used to polymerize MIDA-boronate-based thiophene monomers. For Suzuki-CTP to occur using a protected boron-transmetalating agent (e.g., BPin or MIDA boronate), the protecting group must be hydrolyzed. The resulting boronic acid is then capable of transmetalating to the precatalyst. In small-molecule cross-coupling, there are examples of using boron-transmetalating groups that hydrolyze at different rates to control the coupling order.¹⁴¹ Similarly, Choi and coworkers used these rate differences to generate block copolymers in one pot (i.e., without sequential monomer addition). Here, adding SPhos-ligated Pd to a solution of MIDA boronate-thiophene and BPin-thiophene resulted in block copolymers because BPin-thiophene hydrolyzes faster and is polymerized first (Scheme 5-4). Then, the MIDA boronate-

thiophene hydrolyzes and is added to the polymer chain. Although these examples are limited to thiophene monomers, they use relatively unexplored precatalysts and copolymerization methods. Future efforts should focus on exploring the versatility of these hydrolysis rate-dependent methods with alternative monomer scaffolds.

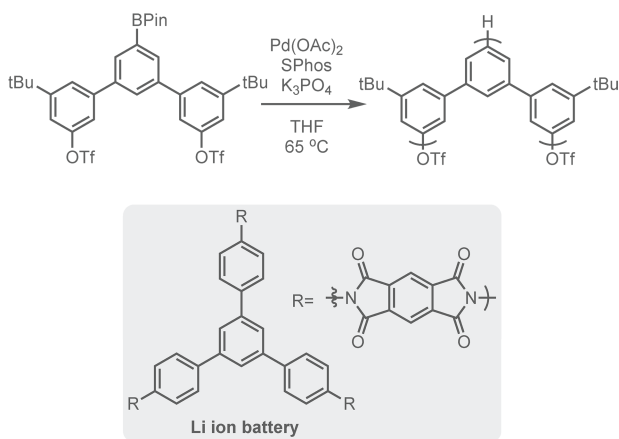
Scheme 5-4. Generating block copolymers based on monomer reactivity differences using SPhos-ligated Pd.



There are also several examples using Buchwald ancillary ligands in the postulated “preferential oxidative addition” chain-growth polymerizations.^{109–113} Here, after reductive elimination the catalyst is believed to dissociate from the polymer but preferentially undergo oxidative addition back into a polymer’s terminal C–X bond due to reactivity differences between the polymer and monomer. The dissociated catalysts react with polymers rather than monomers because of either “monomer deactivation” or diffusion control. In the monomer deactivation approach, the monomer’s electron-rich metal-carbon bond decreases the reactivity of the neighboring C–Br bond towards oxidative addition with Pd. In contrast, the polymers no longer have a deactivating Zn–C bond, enabling the catalyst to react more quickly with the C–Br bond. The monomer-deactivation approach has been used by Koeckelberghs and coworkers to synthesize homopolymers, diblock, and triblock copolymers consisting of various combinations of thiophene, selenophene, and fluorene via a RuPhos-ligated Pd catalyst.^{110–113} In the diffusion control mechanism, immediately after dissociating, the Pd(0) species is closer to polymer than monomer and therefore preferentially reacts with and continues extending the polymer. Moore and coworkers used an SPhos-ligated Pd catalyst to polymerize an extended arene monomer via the diffusion method which yields a hyperbranched polymer (Scheme 5-5).¹⁰⁹ Similar branched,

porous polymers are advantageous for Li ion battery cathodes (Scheme 5-5).²⁰ In both the monomer deactivation and diffusion control examples, Buchwald ancillary ligands outperformed others (e.g., PPh₃, dppf, P(o-tolyl)₃, IPr) for promoting pseudo-chain growth behavior. If the catalyst does dissociate, Buchwald ligands are advantageous because they can stabilize the Pd(0) center before re-association and continue monomer enchainment on the active polymer chain.

Scheme 5-5. (top) Synthesizing extended arene polymers using Buchwald ancillary ligand SPhos. (bottom) Example of an extended arene polymer in Li ion batteries.

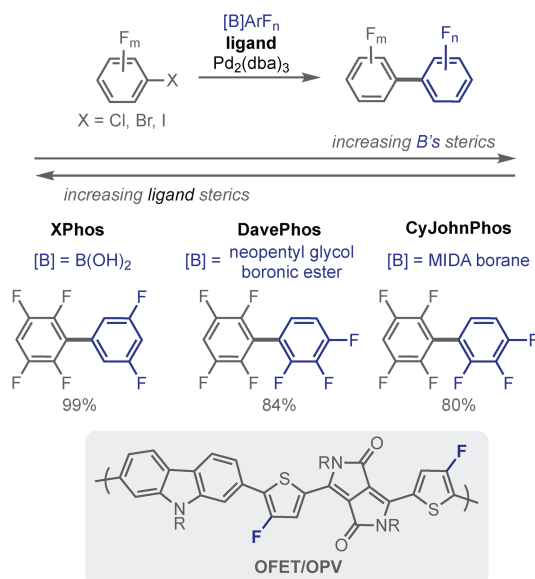


While these examples both expand the Pd-CTP ancillary ligand scope and generate interesting polymer sequences/architectures, they are still limited to polymerizing electron-rich monomers. To polymerize donor–acceptor monomers, it will be important to identify precatalysts capable of polymerizing monomers with diverse electronic properties. For this, we turn to the small-molecule literature for inspiration.

Electron deficient units are desirable for organic electronics but they are challenging to couple in both the polymer and small molecule literature. Since most Pd-catalyzed CTPs are Suzuki-type polymerizations, we looked to the Suzuki coupling small molecule literature for inspiration. A key challenge for Suzuki cross-coupling is that electron-deficient boronates are prone to protodeborylation.^{142,143} Precatalysts that quickly couple electron-deficient boronates result in fewer undesired byproducts and, therefore, are promising candidates for improving CTP

of electron-deficient monomers. In a select small-molecule example, Huber and Bulfield found that strong σ -donating Buchwald ancillary ligands with cyclohexyl (c.f., see Chart 5-3) could enable Pd-catalyzed cross-coupling of perfluoroarene boronic acids in high yields with few undesired products.¹⁴³ This method could be extended to neopentyl glycol boronic esters and MIDA-boronates as well (Scheme 5-6). The more sterically demanding and slower-hydrolyzing boron nucleophiles required less sterically encumbered ancillary ligands (e.g., DavePhos, CyJohnPhos, and MePhos) to achieve high yields. Similarly, the less hindered ancillary ligands DavePhos and CyJohnPhos were optimal for coupling *ortho*- or *meta*-substituted substrates. These examples demonstrate how matching the ancillary ligand steric and electronic properties to the substrate resulted in successful cross-couplings for challenging substrates. These ancillary ligand trends should be considered when designing hydrolysis-rate dependent copolymerizations¹⁰⁸ and polymerizing fluorinated monomers, which feature prominently in high-performing OVPs and OFETs. For example, adding fluorine to a carbazole/thieno[3,2-b]thiophene-diketopyrrolopyrrole-based monomer increased charge mobility in OFETs as well as PCE in OPVs by >2 times.³¹ Combined with the increasing number of fluorinated high-performing materials, these cross-coupling examples suggest that Buchwald ligands could promote polymerizing fluorinated units via CTP.

Scheme 5-6. (top) Matching Buchwald ligands to fluoroarene, boronic acids. (bottom) Example of a high-performing polymer with fluorine substituents.



Polymers with nitrogen-containing repeat units are used in organic electronics (e.g., battery anodes¹⁴⁴) but have been challenging to polymerize via CTP^{128–133} because the standard Ni-based precatalysts are susceptible to chain-transfer.^{27,93} In contrast, Buchwald-ligated Pd-precatalysts have been used extensively to couple nitrogen-containing small molecules.¹⁴⁵ The sterically encumbering ancillary ligands SPhos and XPhos are both efficient at coupling halogenated pyridine and indole moieties with boronic acids and varying electronic parameters in good to excellent yields (Scheme 5-7). When the N-containing heterocycle is the nucleophilic coupling partner (either boron- or zinc-based), the more sterically hindered XPhos ligand improves coupling efficiency.¹⁴⁶ Accordingly, SPhos- and/or XPhos-ligated Pd provide potential routes to polymerize N-containing monomers via CTP.

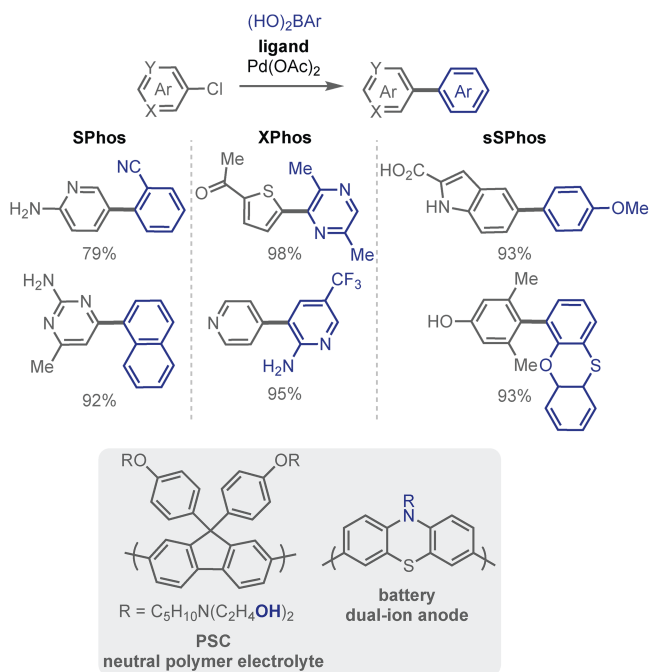
For Suzuki cross-coupling reactions, water is typically added to facilitate transmetalation.¹⁴⁷ but can be disadvantageous for catalyst stability. Adding sulfonate groups to ligands improves their solubility in aqueous solutions. The sulfonated-SPhos (sSPhos)-ligated Pd-precatalyst efficiently couple substrates containing various unprotected functional groups in

excellent yields.¹⁴⁸ These small-molecule cross-coupling examples with sSPhos-ligated Pd suggests that monomers with reactive functional groups (e.g., OH) could be polymerized without protection in a living, chain-growth manner, eliminating the need for post-polymerization modifications.

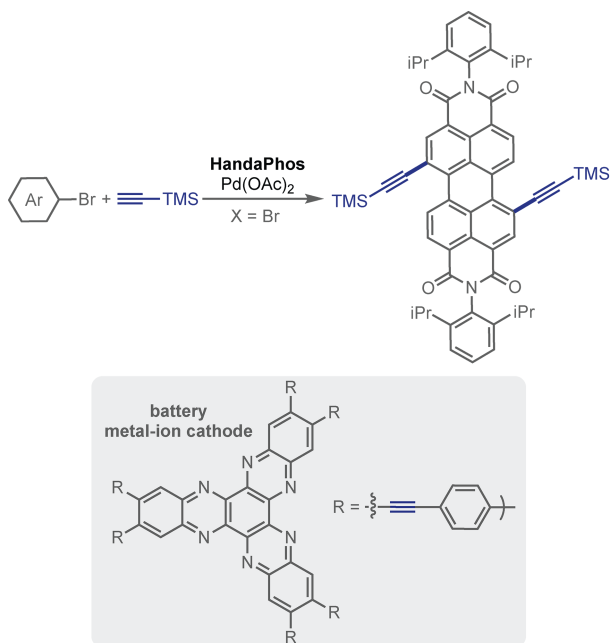
Sonogashira-^{76,115,136} and Heck⁷⁸-CTP examples are rare; however, alkynyl and alkenyl moieties are found in organic electronics. One challenge when polymerizing these functionalities is catalyst trapping at the triple or double bond. A mechanistic study conducted by Yokozawa and coworkers suggested that Pd precatalysts were less likely to get trapped on these π -bonds than Ni precatalysts.⁷² However, when applying tBu₃P-ligated Pd, disproportionation occurred. Using more sterically encumbering Buchwald ancillary ligands could destabilize these Pd- π interactions and facilitate ring-walking. Recently, a HandaPhos-ligated Pd precatalyst was used in di- and tri-functionalization reactions (Scheme 5-8).¹⁴⁹ Although excess alkynyl-coupling partner was used, these results suggest HandaPhos could be a good ancillary ligand for Sonogashira-CTP.

Overall, these select examples demonstrate the versatility and promise of Buchwald ancillary ligands for polymerizing electron-deficient and N-containing monomers as well as those with reactive functionalized groups.

Scheme 5-7. (top) Identifying optimal Buchwald ligands for coupling arenes with coordinating atoms. (bottom) Examples of polymers containing N and reactive functional groups.



Scheme 5-8. (top) HandaPhos-ligated Pd catalyzed difunctionalization reaction. (bottom) Examples of conjugated polymers that could be accessed through Sonogashira-CTP.



5.8 The future: N-Heterocyclic Carbenes (NHCs).

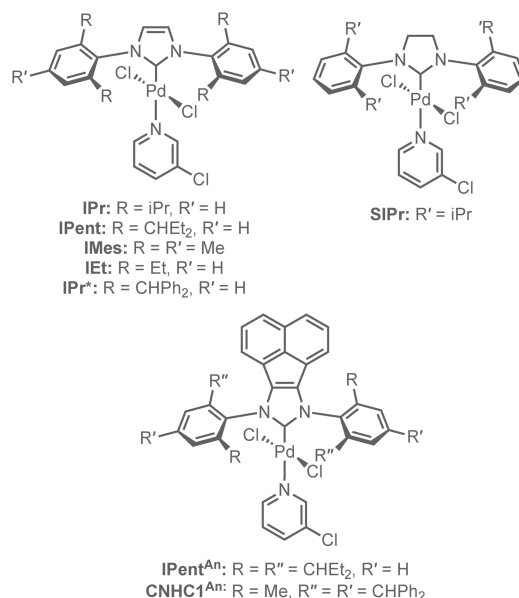
N-heterocyclic carbenes are promising ancillary ligands for CTP because their tunable properties have enabled sterically hindered and electronically dissimilar small molecules to be coupled.^{62,151} The steric and electronic properties of N-heterocyclic carbene ligands can be easily modified, which has resulted in a library of compounds with a range of Tolman electronic parameters and buried volumes (Chart 5-4).^{152,153} In most cases, NHCs are more Lewis basic (electron-donating) than phosphines¹⁵⁴ which indicates, based on previous mechanistic insight,^{13,14} that NHCs should be good ancillary ligands for CTP. There are even fewer NHC than Buchwald ligand examples that exist in the CTP literature. We believe that this area is ripe for further exploration.

Currently, the only NHC ancillary ligands used in Pd-CTP are IPr^{18,19,74,126,119,120–125} and SIPr.¹¹⁹ The unsaturated analogue, IPr, promotes CTP of various simple monomer scaffolds including a range of transmetalating agents (e.g., magnesium, boron, and tin). Additionally, AuPtBu₃ and ZnCl-based thiophene have been polymerized, but these systems deviate from living, chain-growth behavior at high monomer conversions.¹²⁵ As the field advances towards complex monomer scaffolds, this versatility in transmetalating-agent nucleophilicity will be advantageous for polymerizing electrophilic functional groups. In addition, IPr-ligated Pd precatalysts are often air-stable, which is an advantageous yet relatively unexplored property in the CTP field. The saturated analogue, SIPr, outperformed IPr in Murahashi-CTP of thiophene, however this result has not been explored further.¹¹⁹

Polymerizing alternative monomers with a more expansive range of electronic properties will likely require tuning the NHCs' electronic and steric properties. For example, altering σ -donating and π -accepting abilities of the ancillary ligand could have a dramatic impact on the

stability and reactivity of the metal-polymer π -complex. When studying ring-walking, we observed that increasing electron density in the metal/ancillary ligand pair promoted ring-walking along higher molecular weight polymers.¹⁸ Despite this data and other mechanistic insight,^{13,14,17,19} the orbital-electronic demands during ring-walking and propagation remain relatively undefined.

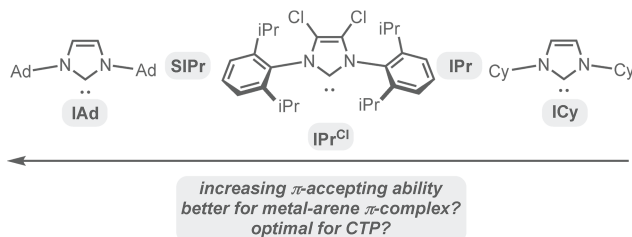
Chart 5-4. NHC-ligated Pd precatalysts



Designing precatalysts for CTP based on their π -accepting ability alone is unexplored, but ligands with these properties have already been synthesized. For example, Cavello and coworkers have deconstructed the effects of both π -accepting and σ -donating properties for many NHCs (Chart 5-5).¹⁵⁵ Alternatively, replacing one N with a quaternary carbon yields cyclic (alkyl)(amino)carbene (CAACs) which have both increased σ -donating and π -accepting properties relative to most NHC ancillary ligands, both of which could be advantageous for ring-walking (Chart 5-6).¹⁵⁶ Replacing the alkyl substituent in CAACs with an aryl group yields cyclic (aryl)(amino)carbene (CAArCs), which demonstrate similar electronic but different steric properties relative to CAACs.¹⁵⁷ Combined, both CAACs and CAArCs provide a range of

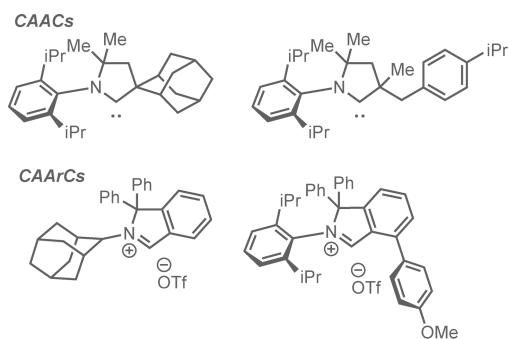
ancillary ligand parameters for both small-molecule cross-coupling and CTP that have yet to be explored by either communities (Chart 5-6).

Chart 5-5. Examples of NHCs with varied electronic properties.



Fully conjugated block copolymers have been underutilized in organic electronics in part because they are inaccessible through step-growth methods. In addition, block copolymer synthesis via CTP has been mostly limited to electronically similar monomers. However, the IPr-ligated Pd precatalyst Pd(IPr)(3-Clpyr)Cl₂ has shown promise for copolymerizing electronically diverse monomers. For example, block copolymers of thiophene and phenylene have been synthesized using this precatalyst¹²⁶ a process for which bisphosphine-Ni precatalysts fail.¹⁵⁸ The ability of IPr-ligated Pd to transition between monomers with different electronic properties suggests it could polymerize donor–acceptor monomers or gradient sequence copolymers.

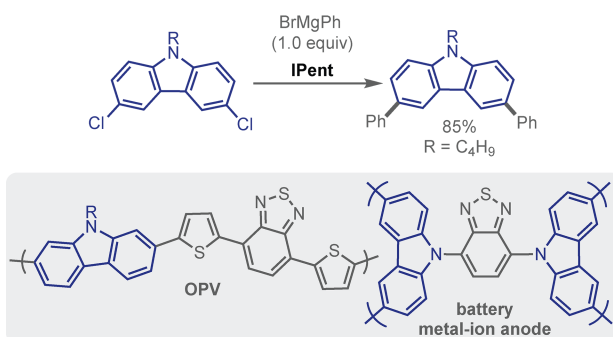
Chart 5-6. Select examples of CAACs and CAACs.



In light of these promising initial results with a single NHC ancillary ligand, we have identified alternative NHC scaffolds with potential for CTP. For example, Goldup and Larrosa have demonstrated that in addition to IPr-ligated Pd, increasing the steric encumbrance around

Pd using IPent results in a precatalyst optimal for difunctionalizing a range of substrates with substoichiometric PhMgBr, outperforming IPr, IMes, IEt, and IPr* (c.f., Chart 5-4 and Scheme 5-9).¹⁵⁹ One particularly promising example formed difunctionalized carbazole, a commonly used motif in high-performing polymers,^{2,21} in 85% yield. These experiments suggest IPent-ligated Pd forms a stable π -bound intermediate and should be evaluated for CTP.

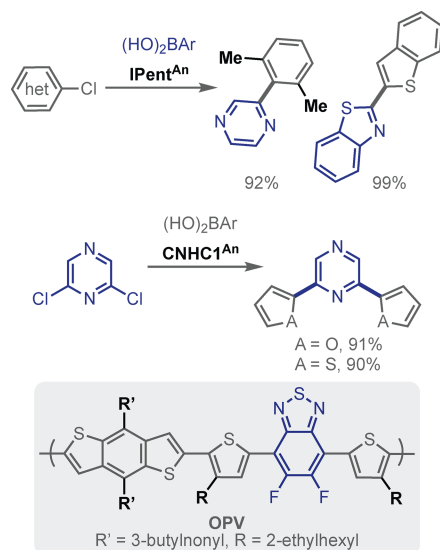
Scheme 5-9. (top) IPent-ligated Pd-catalyzed difunctionalization reaction. (bottom) Examples of structurally diverse polymers containing carbazole for high performing organic electronics.



When selecting an ancillary ligand, it is critical to identify steric properties that will match each monomer's demands. The IPr-ligated Pd precatalyst has precedent for polymerizing both 3HT regioisomers¹⁸ which suggests that NHC ancillary ligands could polymerize monomers with bulky side-chains. Side-chains are used to solubilize high molecular weight polymers and influence solid-state packing.^{2,141-143} Furthermore, adding functional groups (e.g., thiophenes,²² esters,²⁴ cyanides²⁵) to side-chains can improve device performance or stability.⁵⁷ In some cases, electron-deficient monomers are less soluble than analogous electron-rich monomers and therefore require sterically encumbering, branched side chains.²⁷ Here, we highlight a potential precatalyst that has demonstrated efficient coupling of sterically hindered arenes. Liu and coworkers recently reported an NHC-ligated precatalyst (IPent^{An}) that demonstrated similar steric properties but increased electron-donating ability relative to IPr.¹⁴⁴ Although no difunctionalization reactions were reported, IPent^{An} coupled various heteroaromatic and

sterically encumbered substrates in high yields. When coupling two, bis-ortho-substituted substrates, IPent^{An} generated the desired product in 92% yield whereas using IPr or IPent ancillary ligands resulted in considerably less efficient systems (0% and 50% yield, respectively), suggesting that increased electron-donation could facilitate sterically encumbered couplings. Further increasing the NHC's steric properties yields CNHC1^{An} (c.f., Chart 5-4), which affords difunctionalized heteroaromatic compounds in excellent yields via Suzuki cross-coupling, albeit using excess boron-coupling partners (Scheme 5-10).¹⁶⁵ Combined, these results suggest that increasing the steric encumbrance around Pd could facilitate CTP of more hindered and even N-containing monomers. This progression in NHC ligand design also demonstrates how modest adjustments to the ancillary ligand framework can significantly influence reaction outcomes.

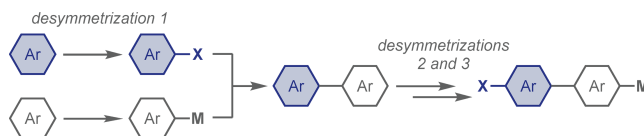
Scheme 5-10. (top) Examples of bulky yet flexible NHCs for cross-coupling N-containing and sterically hindered substrates. (bottom) Example of a conjugated polymer containing sterically encumbered side-chains.



5.9 Reflection.

This Perspective was borne out of frustration. Fourteen years after the initial discovery, CTP is still extraordinarily limited in its scope.⁷ All the mechanistic insight gained during this time has not translated efficiently into better catalysts. We wrote this call-to-action with the hope that it will inspire others to work on these challenges with us. Why not just do it ourselves? The reality is that synthesizing the more complex monomers for evaluating a potential precatalyst is challenging and time-consuming. For example, to synthesize a donor–acceptor monomer, each unit needs to first be desymmetrized (to prevent oligomerization or polymerization) and then coupled (Scheme 5-11). Then, another desymmetrization needs to take place so that a reactive C–X bond and a transmetalating agent can be located on opposing ends. The cartoon version seems simple, but the challenges lie in both over- or under-functionalization, and its resulting impact on the subsequent polymerization.

Scheme 5-11. Generic depiction of routes to an AB-functionalized donor/acceptor monomer and potential starting reagents.



The vast and impressive work in ligand design and evaluation performed by the small-molecule cross-coupling community serves as inspiration for the future of CTP. Here, we presented ways to find these catalysts and we matched specific Pd-precatalysts with high-performing monomers. Great strides will be necessary to develop these polymerizations. We encourage the catalysis field, small-molecule and polymer chemists alike, to help us develop the next generation of CTP. The impact of this collective effort will be enormous. Polymer macrostructure impacts device performance, with molecular weight, dispersity, and sequence each playing a significant role. Developing living, chain-growth methods for accessing these

materials should enable polymers to be optimized for each device. Someday we imagine commercial, conjugated polymer-based devices that help meet the world's growing energy demands.

5.10 References.

- 1) Holliday, S.; Li, Y.; Luscombe, C. K. Recent advances in high performance donor-acceptor polymers for organic photovoltaics. *Prog. Polym. Sci.* **2017**, *70*, 34–51.
- 2) Lu, L.; Zheng, T.; Wu, Q.; Schneider, A. M.; Zhao, D.; Yu, L. Recent Advances in Bulk Heterojunction Polymer Solar Cells. *Chem. Rev.* **2015**, *115*, 12666–12731.
- 3) Bryan, Z. J.; McNeil, A. J. Conjugated Polymer Synthesis via Catalyst-Transfer Polycondensation (CTP): Mechanism, Scope, and Applications. *Macromolecules* **2013**, *46*, 8395–8405.
- 4) Yokozawa, T.; Ohta, Y. Transformation of Step-Growth Polymerization into Living Chain-Growth Polymerization. *Chem. Rev.* **2016**, *116*, 1950–1968.
- 5) Leone, A. K.; McNeil, A. J. Matchmaking in Catalyst-Transfer Polycondensation: Optimizing Catalysts based on Mechanistic Insight. *Acc. Chem. Res.* **2016**, *49*, 2822–2831.
- 6) Baker, M. A.; Tsai, C.-H.; Noonan, K. J. T. Diversifying Cross-Coupling Strategies, Catalysts and Monomers for the Controlled Synthesis of Conjugated Polymers. *Chem. Eur. J.* **2018**. DOI: 10.1002/chem.201706102.
- 7) Lutz, J. P.; Hannigan, M. D.; McNeil, A. J.; Polymers synthesized via catalyst-transfer polymerization and their applications. *Coord. Chem. Rev.* **2018**, *376*, 225–247.
- 8) Yamamoto, T.; Hayashi, Y.; Yamamoto, A. A Novel Type of Polycondensation Utilizing Transition Metal-Catalyzed C–C Coupling. I. Preparation of Thermostable Polyphenylene Type Polymers. *Bull. Chem. Soc. Jpn.* **1978**, *51*, 2091–2097.

- 9) Sheina, E. E.; Liu, J.; Iovu, M. C.; Laird, D. W.; McCullough, R. D. Chain Growth Mechanism for Regioregular Nickel-Initiated Cross-Coupling Polymerizations. *Macromolecules* **2004**, *37*, 3526–3528.
- 10) Yokoyama, A.; Miyakoshi, R.; Yokozawa, T. Chain-Growth Polymerization for Poly(3-hexylthiophene) with a Defined Molecular Weight and a Low Polydispersity. *Macromolecules* **2004**, *37*, 1169–1171.
- 11) Kobayashi, M.; Chen, J.; Chung, T.-C.; Moraes, F.; Heeger, A. J.; Wudl, F. Synthesis and properties of chemically coupled poly(thiophene). *Synth. Met.* **1984**, *9*, 77–86.
- 12) McCullough, R. D.; Lowe, R. D. Enhanced Electrical Conductivity in Regioselectively Synthesized Poly(3-alkylthiophenes). *J. Chem. Soc., Chem. Commun.* **1992**, *0*, 70–72.
- 13) Lee, S. R.; Bryan, Z. J.; Wagner, A. M.; McNeil, A. J. Effect of Ligand Electronic Properties on Precatalyst Initiation and Propagation in Ni-Catalyzed Cross-Coupling Polymerizations. *Chem. Sci.* **2012**, *3*, 1562–1566.
- 14) Bryan, Z. J.; McNeil, A. J. Evidence for a Preferential Intramolecular Oxidative Addition in Ni-Catalyzed Cross-Coupling Reactions and their Impact on Chain-Growth Polymerizations. *Chem. Sci.* **2013**, *4*, 1620–1624.
- 15) Leone, A. K.; Souther, K. D.; Vitek, A. K.; LaPointe, A. M.; Coates, G. W.; Zimmerman, P. M.; McNeil, A. J. Mechanistic Insight into Thiophene Catalyst-Transfer Polymerization Mediated by Nickel Diimine Catalysts. *Macromolecules* **2017**, *50*, 9121–9127.
- 16) Hall, A. O.; Lee, S. R.; Bootsma, A. N.; Bloom, J. W. G.; Wheeler, S. E.; McNeil, A. J. Reactive Ligand Influence on Initiation in Phenylene Catalyst-Transfer Polymerization. *J. Polym. Sci., Part A: Polym. Chem.* **2017**, *55*, 1530–1535.

- 17) Lanni, E. L.; McNeil, A. J. Mechanistic Studies on Ni(dppe)Cl₂-Catalyzed Chain-Growth Polymerizations: Evidence for Rate-Determining Reductive Elimination. *J. Am. Chem. Soc.* **2009**, *131*, 16573–16579.
- 18) Leone, A. K.; Goldberg, P. K.; McNeil, A. J. Ring-Walking in Catalyst-Transfer Polymerization. *J. Am. Chem. Soc.* **2018**, *140*, 7846–7850.
- 19) Mikami, K.; Nojima, M.; Masumoto, Y.; Mizukoshi, Y.; Takita, R.; Yokozawa, T.; Uchiyama, M. Catalyst-dependent intrinsic ring-walking behavior on π -face of conjugated polymers. *Polym. Chem.* **2017**, *8*, 1708–1713.
- 20) Tian, D.; Zhang, H.-Z.; Zhang, D.-S.; Chang, Z.; Han, J. Gao, X.-P.; Bu, X.-H. Li-ion storage and gas adsorption properties of porous polyimides (PIs). *RSC Adv.*, **2014**, *4*, 7506–7510.
- 21) Schon, T. B.; McAllister, B. T.; Li P.-F.; Seferos, D. S. The rise of organic electrode materials for energy storage. *Chem. Soc. Rev.* **2016**, *45*, 6345–6404.
- 22) Li, S.; Ye, L.; Zhao, W.; Yan, H.; Yang, B.; Liu, D.; Li, W.; Ade, H.; Hou, J. A Wide Band Gap Polymer with a Deep Highest Occupied Molecular Orbital Level Enables 14.2% Efficiency in Polymer Solar Cells *J. Am. Chem. Soc.* **2018**, *140*, 7159–7167.
- 23) Bartelt, J. A.; Douglas, J. D.; Mateker, W. R.; El Labban, A.; Tassone, C. J.; Toney, M. F.; Fréchet, J. M. J.; Beaujuge, P. M.; McGehee, M. D. Controlling Solution-Phase Polymer Aggregation with Molecular Weight and Solvent Additives to Optimize Polymer-Fullerene Bulk Heterojunction Solar Cells. *Adv. Mater.* **2014**, *4*, 1301733.
- 24) Liang, Y.; Xu, Z.; Xia, J.; Tsai, S.-T.; Wu, Y.; Li, G.; Ray, C.; Yu, L. For the Bright Future—Bulk Heterojunction Polymer Solar Cells with Power Conversion Efficiency of 7.4%. *Adv. Mater.* **2010**, *22*, E135–E138

- 25) Cao, C.; Xiao, M.; Yang, X.; Zhang, J.; Huang F.; Cao, Y. Cyanovinylene-Based Copolymers by Tin-free Knoevenagel Polycondensation for High Efficiency Polymer Solar Cells. *J. Mater. Chem. C* **2018**, *6*, 8020–8027.
- 26) Grimsdale, A. C.; Chan, K. L.; Martin, R. E.; Jokisz, P. G.; Holmes, A. B. Synthesis of Light-Emitting Conjugated Polymers for Applications in Electroluminescent Devices. *Chem. Rev.* **2009**, *109*, 897–1091.
- 27) Smith, M. L.; Leone, A. K.; Zimmerman, P. M.; McNeil, A. J. Impact of Preferential π -Binding in Catalyst-Transfer Polycondensation of Thiazole Derivatives. *ACS Macro Lett.* **2016**, *5*, 1411–1415.
- 28) Zhang, H.-H.; Peng, W.; Dong, J.; Hu, Q.-S. *t*-Bu₃P-Coordinated 2-Phenylaniline-Based Palladacycle Complex/ArBr as Robust Initiators for Controlled Pd(0)/*t*-Bu₃P-Catalyzed Suzuki Cross-Coupling Polymerization of AB-Type Monomers. *ACS Macro Lett.* **2016**, *5*, 656–660.
- 29) Vandana, T.; Kannan, P. Blue and green light emitting polyarylpiperazines luminogens containing anthracene and thiophene units. *J. Photochem. Photobiol. A* **2018**, *359*, 64–72.
- 30) Hellerich, E. S.; Intemann, J. J.; Cai, M.; Liu, R.; Ewan, M. D.; Tlach, B. C.; Jeffries-EL, M.; Shinar, R.; Shinar, J. Fluorescent polymer guest:small molecule host solution-processed OLEDs. *J. Mater. Chem. C* **2013**, *1*, 5191–5199.
- 31) Bura, T.; Beaupré, S.; Ibraikulov, O. A.; Légaré, M.-A.; Quinn, J.; Lévêque, P.; Heiser, T.; Li, Y.; Leclerc, N.; Leclerc, M. New Fluorinated Dithienyldiketopyrrolopyrrole Monomers and Polymers for Organic Electronics. *Macromolecules* **2017**, *50*, 7080–7090.
- 32) Sirringhaus, H. 25th Anniversary Article: Organic Field-Effect Transistors: The Path Beyond Amorphous Silicon. *Adv. Mater.* **2014**, *26*, 1319–1335.

- 33) Ma, J.; Liu, Z.; Yao, J.; Wang, Z.; Zhang, G.; Zhang, X.; Zhang, D. Improving Ambipolar Semiconducting Properties of Thiazole-Flanked Diketopyrrolopyrrole-Based Terpolymers by Incorporating Urea Groups in the Side-Chains. *Macromolecules* **2018**, DOI: 10.1021/acs.macromol.8b01020.
- 34) Kim, Y.; Hwang, H.; Kim, N.-K.; Hwang, K.; Park, J.-J.; Shin, G.-I.; Kim, D.-Y. π -Conjugated Polymers Incorporating a Novel Planar Quinoid Building Block with Extended Delocalization and High Charge Carrier Mobility. *Adv. Mater.* **2018**, *30*, 1706557.
- 35) DiCarmino, P. M.; Schon, T. B.; McCormick, T. M.; Klein, P. P.; Seferos, D. S. Donor–Acceptor Polymers for Electrochemical Supercapacitors: Synthesis, Testing, and Theory. *J. Chem. Phys. C* **2014**, *118*, 8295–8307.
- 36) Ju, X.; Kong, L.; Zhao, J.; Bai, G. Synthesis and electrochemical capacitive performance of thieno[3,4-*b*] pyrazine-based Donor–Acceptor type copolymers used as supercapacitor electrode material. *Electrochim. Acta* **2017**, *238*, 36–48.
- 37) Guo, Y.; Li, W.; Yu, H.; Perepichka, D.; Meng, H. Flexible Asymmetric Supercapacitors via Spray Coating of a New Electrochromic Donor–Acceptor Polymer. *Adv. Energy Mater.* **2017**, *7*, 1601623.
- 38) Estrada, L. A.; Liu, D. Y.; Salazar, D. H.; Dyer, A. L.; Reynolds, J. R. Poly[Bis-EDOT-Isoindigo]: An Electroactive Polymer Applied to Electrochemical Supercapacitors. *Macromolecules* **2012**, *45*, 8211–8220.
- 39) Wu, J.; Rui, X.; Wang, C.; Pei, W.-B.; Lau, R.; Yan, Q.; Zhang, Q. Nanostructured Conjugated Ladder Polymers for Stable and Fast Lithium Storage Anodes with High-Capacity. *Adv. Energy Mater.* **2015**, *5*, 1402189.

- 40) Kim, Y. J.; Wu, W.; Chun, S.-E.; Whitacre, J. F.; Bettinger, C. J. Catechol-Mediated Reversible Binding of Multivalent Cations in Eumelanin Half-Cells. *Adv. Mater.* **2014**, *26*, 6572–6579.
- 41) Peterson, B. M.; Ren, D.; Shen, L.; Wu, Y.-C. M.; Ulgut, B.; Coates, G. W.; Abruña, H. D.; Fors, B. P. Phenothiazine-Based Polymer Cathode Materials with Ultrahigh Power Densities for Lithium Ion Batteries. *ACS App. Energy Mater.* **2018**, DOI: 10.1021/acsaem.8b00778.
- 42) Lee, S. M.; Park, K. H.; Jung, S.; Park, H.; Yang, C. Stepwise heating in Stille polycondensation toward no batch-to-batch variations in polymer solar cell performance. *Nat. Commun.* **2018**, *9*, 1867.
- 43) Kline, R. J.; McGehee, M. D.; Kadnikova, E. N.; Liu, J. Fréchet, J. M. J.; Toney, M. F. Dependence of Regioregular Poly(3-hexylthiophene) Film Morphology and Field-Effect Mobility on Molecular Weight. *Macromolecules* **2005**, *38*, 3312–3319.
- 44) Katsouras, A.; Gasparini, N.; Koulogiannis, C.; Spanos, M.; Ameri, T.; Brabec, C. J.; Chochos, C. L.; Avgeropoulos, A. Systematic Analysis of Polymer Molecular Weight Influence on the Organic Photovoltaic Performance. *Macromol. Rapid Commun.* **2015**, *36*, 1778–1797.
- 45) Kline, R. S.; McGehee, M. D.; Kadnikova, E. N.; Liu, J.; Fréchet, J. M. J. Controlling the Field-Effect Mobility of Regioregular Polythiophene by Changing the Molecular Weight. *Adv. Mater.* **2003**, *15*, 1519–1522.
- 46) Ma, P.; Wen, S.; Wang, C.; Guo, W.; Shen, L.; Dong, W.; Lu, J.; Ruan, S. Optimization of PDTS-DTffBT-Based Solar Cell Performance through Control of Polymer Molecular Weight. *J. Phys. Chem. C*, **2016**, *120*, 19513–19520.

- 47) Li, W.; Yang, L.; Tumbleston, J. R.; Yan, L.; Ade, H.; You, W. Controlling Molecular Weight of a High Efficiency Donor–Acceptor Conjugated Polymer and Understanding Its Significant Impact on Photovoltaic Properties. *Adv. Mater.* **2014**, *26*, 4456–4462.
- 48) Meager, I.; Shahid Ashraf, R.; Nielsen, C. B.; Donaghey, J. E.; Huang, Z.; Bronstein, H.; Durrant, J. R.; McCulloch, I. Power conversion efficiency enhancement in diketopyrrolopyrrole based solar cells through polymer fractionation. *J. Mater. Chem. C*, **2014**, *2*, 8593–8598.
- 49) Lu, L.; Zheng, T.; Xu, T.; Zhao, D.; Yu, L. Mechanistic Studies of Effect of Dispersity on the Photovoltaic Performance of PTB7 Polymer Solar Cells. *Chem. Mater.* **2015**, *27*, 537–543.
- 50) Vangerven, T.; Verstappen, P.; Drijkoningen, J.; Dierckx, W.; Himmelberger, S.; Salleo, A.; Vanderzande, D.; Maes, W.; Manca, J. V. Molar Mass versus Polymer Solar Cell Performance: Highlighting the Role of Homocouplings. *Chem. Mater.* **2015**, *27*, 3726–3732.
- 51) Bronstein, H. A.; Luscombe, C. K. *J. Am. Chem. Soc.* **2009**, *131*, 12894–12895.
- 52) Lawrence, J.; Goto, E.; Ren, J. M.; McDearmon, B.; Kim, D. S.; Ochiai, Y.; Clark, P. G.; Laitar, D.; Higashihara, T.; Hawker, C. J. A Versatile and Efficient Strategy to Discrete Conjugated Oligomers. *J. Am. Chem. Soc.* **2017**, *139*, 13735–13739.
- 53) Kipp, D.; Verduzco, R.; Ganesan, V.; Block copolymer compatibilizers for ternary blend polymer bulk heterojunction solar cells – an opportunity for computation aided molecular design. *Mol. Syst. Des. Eng.* **2016**, *1*, 353–369.
- 54) Yuan, K.; Chen, L.; Chen, Y. Nanostructuring compatibilizers of block copolymers for organic photovoltaics. *Polym. Int.* **2014**, *63*, 593–606.
- 55) Cheng, P.; Zhan, X. Versatile third components for efficient and stable organic solar cells. *Mater. Horiz.* **2015**, *2*, 462–485.

- 56) Rafique, S.; Abdullah, S. M.; Sulaiman, K.; Iwamoto, M. Fundamentals of bulk heterojunction organic solar cells: An overview of stability/degradation issues and strategies for improvement. *Renew. Sust. Energy Rev.* **2018**, *84*, 43–53.
- 57) Kong, C.; Song, B.; Mueller, E. A.; Kim, J.; McNeil, A. J. *Submitted*.
- 58) Palermo, E. F.; Darling, S. B.; McNeil, A. J. π -Conjugated gradient copolymers suppress phase separation and improve stability in bulk heterojunction solar cells. *J. Mater. Chem. C.* **2014**, *2*, 3401–3406.
- 59) Martin, R.; Buchwald, S. L. Palladium-Catalyzed Suzuki–Miyaura Cross-Coupling Reactions Employing Dialkylbiaryl Phosphine Ligands. *Acc. Chem. Res.* **2008**, *41*, 1461–1473.
- 60) Phan, N. T. S.; Van Der Sluys, M.; Jones, C. W. On the Nature of the Active Species in Palladium Catalyzed Mizoroki–Heck and Suzuki–Miyaura Couplings – Homogeneous or Heterogeneous Catalysis, A Critical Review. *Adv. Synth. Catal.* **2006**, *348*, 609–679.
- 61) Nasielski, J.; Hadei, N.; Achonduh, G.; Assen, E.; Kantchev, E. A. B.; O'Brien, C. J.; Lough, A.; Organ, M. G.; Structure–Activity Relationship Analysis of Pd–PEPPSI Complexes in Cross-Couplings: A Close Inspection of the Catalytic Cycle and the Precatalyst Activation Model. *Chem. Eur. J.* **2010**, *16*, 10844–10853.
- 62) Marion, N.; Nolan, S. P. Well-Defined N-Heterocyclic Carbenes-Palladium(II) Precatalysts for Cross-Coupling Reactions. *Acc. Chem. Res.* **2008**, *41*, 1440–1449.
- 63) Fu, G. C. The Development of Versatile Methods for Palladium-Catalyzed Coupling Reactions of Aryl Electrophiles through the Use of $P(t\text{-Bu})_3$ and PCy_3 as Ligands. *Acc. Chem. Res.* **2008**, *41*, 1555–1564.
- 64) Zhao, W.; Li, S.; Yao, H.; Zhang, S.; Zhang, Y.; Yang, B.; Hou, J. Molecular Optimization Enables over 13% Efficiency in Organic Solar Cells. *J. Am. Chem. Soc.* **2017**, *139*, 7148–7151.

- 65) Yamashita, Y.; Hinkel, F.; Marszalek, T.; Zajaczkowski, W.; Pisula, W.; Baumgarten, M.; Matsui, H.; Müllen, K.; Takeya, J. Mobility Exceeding $10 \text{ cm}^2/(\text{V}\cdot\text{s})$ in Donor–Acceptor Polymer Transistors with Band-like Charge Transport. *Chem. Mater.*, **2016**, *28*, 420–424.
- 66) Suzuki, A. Cross-Coupling Reactions of Organoboranes: An Easy Way to Construct C–C Bonds (Nobel Lecture). *Angew. Chem. Int. Ed.* **2011**, *50*, 6723–6737.
- 67) Miyaura, N.; Suzuki, A. Palladium-Catalyzed Cross-Coupling Reactions of Organoboron Compounds. *Chem. Rev.*, **1995**, *95*, 2457–2483.
- 68) Terayama, K.; Goto, E.; Higashihara, T. Nonstoichiometric Stille Coupling Polycondensation via an Intramolecular Pd(0) Catalyst Transfer Using Excess Phthalimide Monomer. *Macromol. Chem. Phys.* **2018**, *219*, 1800175.
- 69) Zhang, H.-H.; Zhu, Y.-X.; Wang, W.; Zhu, J.; Bonnesen, P. V.; Hong, K. Controlled synthesis of *ortho*, *para*-alternating linked polyarenes via catalyst-transfer Suzuki coupling polymerization. *Polym. Chem.* **2018**, *9*, 3342–3346.
- 70) Nojima, M.; Kamigawara, T.; Ohta, Y.; Yokozawa, T. Catalyst-Transfer Suzuki–Miyaura Condensation Polymerization of Stilbene Monomer: Different Polymerization Behavior Depending on Halide and Aryl Group of $\text{ArPd}(t\text{Bu}_3\text{P})\text{X}$ Initiator. *J. Polym. Sci. A. Polym. Chem.* **2018**, DOI: 10.1002/pola.29169.
- 71) Kang, S.; Todd, A. D.; Paul, A.; Lee, S. Y.; Bielawski, C. W. Controlled Syntheses of Poly(phenylene ethynylene)s with Regiochemically-Tuned Optical Band Gaps and Ordered Morphologies. *Macromolecules* **2018**. DOI: 10.1021/acs.macromol.8b00728.
- 72) Nojima, M.; Ohta, Y.; Yokozawa, Y. Investigation of catalyst-transfer condensation polymerization for synthesis of poly(*p*-phenylenevinylene) *J. Polym. Sci. Part A. Polym. Chem.* **2014**, *52*, 2643–2653.

- 73) Nojima, M.; Saito, R.; Ohta, Y.; Yokozawa, T. Investigation of Mizoroki-Heck Coupling Polymerization as Catalyst-Transfer Condensation Polymerization for Synthesis of Poly(*p*-phenylenevinylene). *J. Polym. Sci. A. Polym. Chem.* **2015**, *53*, 543–551.
- 74) Willot, P.; Koeckelberghs, G. Evidence for Catalyst Association in the Catalyst Transfer Polymerization of Thieno[3,2-*b*]thiophene. *Macromolecules* **2014**, *47*, 8548–8555.
- 75) Tkachov, R.; Senkovskyy, V.; Beryozkina, T.; Boyko, K.; Bakulev, V.; Lederer, A.; Sahre, K.; Voit, B.; Kiriy, A. Palladium-Catalyzed Chain-Growth Polycondensation of AB-type Monomers: High Catalyst Turnover and Polymerization Rates. *Angew. Chem. Int. Ed.* **2014**, *53*, 2402–2407.
- 76) Kang, S.; Ono, R. J.; Bielawski, C. W. Controlled Catalyst Transfer Polycondensation and Surface-Initiated Polymerization of *p*-Phenyleneethynylene-Based Monomer. *J. Am. Chem. Soc.* **2013**, *135*, 4984–4987.
- 77) Verswyvel, M.; Hoebers, C.; De Winter, J.; Gerbaux, P.; Koeckelberghs, G. Study of the Controlled Chain-Growth Polymerization of Poly(3,6-phenanthrene). *J. Polym. Sci. A. Polym. Chem.* **2013**, *51*, 5067–5074.
- 78) Kamigawara, T.; Sugita, H.; Mikami, K.; Ohta, Y.; Yokozawa, T. Intramolecular Transfer of Pd Catalyst on Carbon–Carbon Triple Bond and Nitrogen–Nitrogen Double Bond in Suzuki–Miyaura Coupling Reaction. *Catalysts* **2017**, *7*, 195.
- 79) Grisorio, R.; Suranna, G. P. Impact of Precatalyst Activation on Suzuki-Miyaura Catalyst-Transfer Polymerizations: New Mechanistic Scenarios for Pre-transmetalation Events. *ACS Macro Lett.* **2017**, *6*, 1251–1256.

- 80) Nojima, M.; Ohta, Y.; Yokozawa, T. Additive-controlled Switching from Abnormal to Normal Unstoichiometric Suzuki–Miyaura Polycondensation for Poly(biphenylenevinylene). *Chem. Lett.* **2017**, *46*, 35–37.
- 81) Tokita, Y.; Katoh, M.; Ohta, Y.; Yokozawa, T. Mechanistic Investigation of Catalyst-Transfer Suzuki–Miyaura Condensation Polymerization of Thiophene–Pyridine Biaryl Monomers with the Aid of Model Reactions. *Chem. Eur. J.* **2016**, *22*, 17436–17444.
- 82) Nojima, M.; Kosaka, K.; Kato, M.; Ohta, Y.; Yokozawa, T. Alternating Intramolecular and Intermolecular Catalyst-Transfer Suzuki–Miyaura Condensation Polymerization: Synthesis of Boronate-Terminated π -Conjugated Polymers Using Excess Dibromo Monomers. *Macromol. Rapid Commun.* **2016**, *37*, 79–85.
- 83) Zhang, H.-H.; Hu, Q.-S.; Hong, K. Accessing conjugated polymers with precisely controlled heterobifunctional chain ends *via* post-polymerization modification of the OTf group and controlled Pd(0)/*t*-Bu₃P-catalyzed Suzuki cross-coupling polymerization. *Chem. Commun.* **2015**, *51*, 14869–14872.
- 84) He, L.-Y.; Urrego-Riveros, S.; Gates, P. J.; Näther, C.; Brinkmann, M.; Abetz, V.; Staubitz, A. Synthesis of poly(thiophene-*alt*-pyrrole) from a difunctionalized thienylpyrrole by Kumada polycondensation. *Tetrahedron* **2015**, *71*, 5399–5406.
- 85) Zhang, H.-H.; Xing, C.-H.; Hu, Q.-S.; Hong, K. Controlled Pd(0)/*t*-Bu₃P-Catalyzed Suzuki Cross-Coupling Polymerization of AB-Type Monomers with ArPd(*t*-Bu₃P)X or Pd₂(dba)₃/*t*-Bu₃P/ArX as the Initiator. *Macromolecules* **2015**, *48*, 967–978.
- 86) Nojima, M.; Ohta, Y.; Tokozawa, T. Structural Requirements for Palladium Catalyst Transfer on a Carbon–Carbon Double Bond. *J. Am. Chem. Soc.* **2015**, *137*, 5682–5685.

- 87) Grisorio, R.; Mastrorilli, P.; Suranna, G. P. A Pd(AcO)₂/*t*-Bu₃P/K₃PO₄ catalytic system for the control of Suzuki cross-coupling polymerization. *Polym. Chem.* **2014**, *5*, 4304–4310.
- 88) Kosaka, K.; Ohta, Y.; Yokozawa, T. Influence of the Boron Moiety and Water on Suzuki–Miyaura Catalyst-Transfer Condensation Polymerization. *Macromol. Rapid Commun.* **2015**, *36*, 373–377.
- 89) Tkachov, R.; Komber, H.; Rauch, S.; Lederer, A.; Oertel, U.; Häußler, L.; Voit, B.; Kiriy, A. One-Pot Synthesis of All-Conjugated Block-Like Bisthiophene–Naphthalenediimide/Fluorene Copolymer. *Macromolecules* **2014**, *47*, 4994–5001.
- 90) Zhang, H.-H.; Xing, C.-H.; Hu, Q.-S. Controlled Pd(0)/*t*-Bu₃P-Catalyzed Suzuki Cross-Coupling Polymerization of AB-Type Monomers with PhPd(*t*-Bu₃P)I or Pd₂(dba)₃/*t*-Bu₃P/ArI as the Initiator. *J. Am. Chem. Soc.* **2012**, *134*, 13156–13159.
- 91) Elmalem, E.; Biedermann, F.; Johnson, K.; Friend, R. H.; Huck, W. T. S. Synthesis and Photophysics of Fully π -Conjugated Heterobis-Functionalized Polymeric Molecular Wires via Suzuki Chain-Growth Polymerization. *J. Am. Chem. Soc.* **2012**, *134*, 17769–17777.
- 92) Huddleston, N. E.; Sontag, S. K.; Bilbrey, J. A.; Sheppard, G. R.; Locklin, J. Palladium-Mediated Surface-Initiated Kumada Catalyst Polycondensation: A Facile Route Towards Oriented Conjugated Polymers. *Macromol. Rapid Commun.* **2012**, *33*, 2115–2120.
- 93) Nanashima, Y.; Shibata, R.; Miyakoshi, R.; Yokoyama, A.; Yokozawa, T. Investigation of Catalyst-Transfer Condensation Polymerization for the Synthesis of *n*-Type π -Conjugated Polymer, Poly(2-dioxaalkylpyridine-3,6-diyl). *J. Polym. Sci., A: Polym. Chem.* **2012**, *50*, 3628–3640.

- 94) Yokozawa, T.; Suzuki, R.; Nojima, M.; Ohta, Y.; Yokoyama, A. Precision Synthesis of Poly(3-hexylthiophene) from Catalyst-Transfer Suzuki–Miyaura Coupling Polymerization. *Macromol. Rapid Commun.* **2011**, *32*, 801–806.
- 95) Elmalem, E.; Kiriy, A.; Huck, W. T. S. Chain-Growth Suzuki Polymerization of n-Type Fluorene Copolymers. *Macromolecules* **2011**, *44*, 9057–9061.
- 96) Yokozawa, T.; Kohno, H.; Ohta, Y.; Yokoyama, A. Catalyst-Transfer Suzuki–Miyaura Coupling Polymerization for Precision Synthesis of Poly(*p*-phenylene). *Macromolecules* **2010**, *43*, 7095–7100.
- 97) Huang, W.; Su, L.; Bo, Z. Hyperbranched Polymers with a Degree of Branching of 100% Prepared by Catalyst Transfer Suzuki–Miyaura Polycondensation. *J. Am. Chem. Soc.* **2009**, *131*, 10348–10349.
- 98) Beryozkina, T.; Boyko, K.; Khanduyeva, N.; Senkovskyy, V.; Horecha, M.; Oertel, U.; Simon, F.; Stamm, M.; Kiriy, A. Grafting of Polyfluorene by Surface-Initiated Suzuki Polycondensation. *Angew. Chem. Int. Ed.* **2009**, *48*, 2695–2698.
- 99) Yokoyama, A.; Suzuki, H.; Kubota, Y.; Ohuchi, K.; Higashimura, H.; Yokozawa, T. Chain-Growth Polymerization for the Synthesis of Polyfluorene via Suzuki–Miyaura Coupling Reaction from an Externally Added Initiator Unit. *J. Am. Chem. Soc.* **2007**, *129*, 7236–7237.
- 100) Michinori, S.; Hiroyoshi, N.; Masahiro, M. Synthesis and Helical Structure of Oligo(quinoline-2,3-diyl)s. *Chem. Lett.* **2007**, *36*, 1036–1037.
- 101) Zhang, S.; Zhang, Z.; Fu, H.; Li, X.; Zhan, H.; Cheng, Y. Synthesis of polyfluorene containing simple functional end group with aryl palladium(II) complexes as initiators. *J. Organometal. Chem.* **2016**, *825–826*, 100–113.

- 102) Mao, Y.; Wang, Y.; Lucht, B. L. Regiocontrolled Synthesis of Poly(3-alkylthiophene)s by Grignard Metathesis. *J. Polym. Sci., A: Polym. Chem* **2004**, *42*, 5538–5547.
- 103) Zhang, Z.; Hu, P.; Li, X.; Zhan, H.; Cheng, Y. Investigation of Suzuki–Miyaura catalyst-transfer polycondensation of AB-type fluorene monomer using coordination-saturated aryl Pd(II) halide complexes as initiators. *J. Polym. Sci., Part A: Polym. Chem.* **2015**, *53*, 1457–1463.
- 104) Goto, E.; Ando, S.; Ueda, M.; Higashihara, T. Nonstoichiometric Stille Coupling Polycondensation for Synthesizing Naphthalene-Diimide-Based π -Conjugated Polymers. *ACS Macro Lett.* **2015**, *4*, 1004–1007.
- 105) Grisorio, R.; Suranna, G. P.; Mastroilli, P. Chain-Growth Versus Step-Growth Mechanisms for the Suzuki–Heck Polymerisation of Fluorenyldibromides with Potassium Vinyl Trifluoroborate. *Chem. Euro. J.* **2010**, *16*, 8054–8061.
- 106) Sun, H.; Zhang, S.; Yang, Y.; Li, X.; Zhan, H.; Cheng, Y. Excellent Control of Perylene Diimide End Group in Polyfluorene via Suzuki Catalyst Transfer Polymerization. *Macromol. Chem. Phys.* **2016**, *217*, 2726–2735.
- 107) Fu, H.; Li, J.; Zhang, Z.; Zhan, H.; Li, X.; Cheng, Y. Synthesis of novel polyfluorene with defined group in the center using aryl dipalladium complex as an initiator. *J. Organomet. Chem.* **2013**, *738*, 55–58.
- 108) Seo, K.-B.; Lee, I.-H.; Lee, J.; Choi, I.; Choi, T.-L. A Rational Design of Highly Controlled Suzuki–Miyaura Catalyst-Transfer Polycondensation for Precision Synthesis of Polythiophenes and their Block Copolymers: Marriage of Palladacycle Precatalysts with MIDA-boronates. *J. Am. Chem. Soc.* **2018**, *140*, 4335–4343.
- 109) Xue, Z.; Finke, A. D.; Moore, J. S. Synthesis of Hyperbranched Poly(*m*-phenylene)s via Suzuki Polycondensation of a Branched AB₂ Monomer. *Macromolecules* **2010**, *43*, 9277–9282

110) Verswyvel, M.; Verstappen, P.; De Cremer, L.; Verbiest, T.; Koeckelberghs, G. Development of a Universal Chain-Growth Polymerization Protocol of Conjugated Polymers: Toward a Variety of All-Conjugated Block-Copolymers. *J. Polym. Sci., A: Polym. Chem.* **2011**, *49*, 5339–5349.

111) Willot, P.; Steverlynck, J.; Moerman, D.; Leclère, P.; Lazzaroni, R.; Koeckelberghs, G. Poly(3-alkylthiophene) with tuneable regioregularity: synthesis and self-assembling properties. *Polym. Chem.* **2013**, *4*, 2662–2671.

112) Verswyvel, M.; Steverlynck, J.; Mohamed, S. H.; Trabelsi, M.; Champagne, B.; Koeckelberghs, G. All-Conjugated ABC-*block*-copolymer Formation with a Varying Sequence via an Unassociated Catalyst. *Macromolecules* **2014**, *47*, 4668–4675.

113) Hardeman, T.; Koeckelberghs, G. The Synthesis of Poly(thiophene-*co*-fluorene) Gradient Copolymers. *Macromolecules* **2015**, *48*, 6987–6993

¹Dong, J.; Guo, H.; Hu, Q.-S. Controlled Pd(0)/Ad3P-Catalyzed Suzuki Cross-Coupling Polymerization of AB-Type Monomers with Ad3P-Coordinated Acetanilide-Based Palladacycle Complex as Initiator. *ACS Macro Lett.* **2017**, *6*, 1301–1304.

114) Su, M.; Liu, N.; Wang, Q.; Wang, H.; Yin, J.; Wu, Z.-Q. Facile Synthesis of Poly(phenyleneethynylene)-*block*-Polyisocyanide Copolymers via Two Mechanistically Distinct, Sequential Living Polymerizations Using a Single Catalyst. *Macromolecules* **2016**, *49*, 110–119.

115) Kosaka, K.; Uchida, T.; Mikami, K.; Ohta, Y.; Yokozawa, T. AmPhos Pd-Catalyzed Suzuki–Miyaura Catalyst-Transfer Condensation Polymerization: Narrower Dispersity by Mixing the Catalyst and Base Prior to Polymerization *Macromolecules* **2018**, *51*, 364–369.

- 116) Bhatt, M. P.; Magurudeniya, H. D.; Sista, P.; Sheina, E. E.; Jeffries-EL, M.; Janesko, B. G.; Mccullough, R. D.; Stefan, M. C Role of the transition metal in Grignard metathesis polymerization (GRIM) of 3-hexylthiophene. *J. Mater. Chem. A*. **2013**, *1*, 12841–12849.
- 117) Fuji, K.; Tamba, S.; Shono, K.; Sugie, A.; Mori, A. Murahashi Coupling Polymerization: Nickel(II)–N-Heterocyclic Carbene Complex-Catalyzed Polycondensation of Organolithium Species of (Hetero)arenes. *J. Am. Chem. Soc.* **2013**, *135*, 12208–12211.
- 118) Shono, K.; Sumino, Y.; Tanaka, S.; Tamba, S.; Mori, A. Polythiophene synthesis via halogen dance. *Org. Chem. Front.*, **2014**, *1*, 678–682.
- 119) Sui, A.; Shi, X.; Tian, H.; Geng, Y.; Wang, F. Suzuki–Miyaura Catalyst-Transfer Polycondensation with Pd(IPr)(OAc)₂ as the Catalyst for the Controlled Synthesis of Polyfluorenes and Polythiophenes. *Polym. Chem.* **2014**, *5*, 7072–7080.
- 120) Qiu, Y.; Mohin, J.; Tsai, C.-H.; Tristram-Nagle, S.; Gil, R. R.; Kowalewski, T.; Noonan, K. J. T. Stille Catalyst-Transfer Polycondensation Using Pd-PEPPSI-IPr for High-Molecular-Weight Regioregular Poly(3-hexylthiophene). *Macromol. Rapid Commun.* **2015**, *36*, 840–844.
- 121) Zhang, H-H.; Ma, C.; Bonnesen, P. V.; Zhu, J.; Sumpter, B. G.; Carrillo, J-M. Y.; Yin, P.; Wang, Y.; Li, A-P.; Hong, K. Helical Poly(5-alkyl-2,3-thiophene)s: Controlled Synthesis and Structure Characterization. *Macromolecules*, **2016**, *49*, 4691–4698.
- 122) Suraru, S.-L.; Lee, J. A.; Luscombe, C. K. Preparation of an Aurylated Alkylthiophene Monomer via C–H Activation for Use in Pd-PEPPSI-iPr Catalyzed-Controlled Chain Growth Polymerization. *ACS Macro Lett.* **2016**, *5*, 533–536.
- 123) Qiu, Y.; Worch, J. C.; Fortney, A.; Gayathri, C.; Gil, R. R.; Noonan, K. J. T. Nickel-Catalyzed Suzuki Polycondensation for Controlled Synthesis of Ester-Functionalized Conjugated Polymers. *Macromolecules* **2016**, *49*, 4757–4762.

- 124) Hardeman, T.; Koeckelberghs, G.; Synthesis of conjugated copolymers by combining different coupling reactions. *Polym. Chem.*, **2017**, *8*, 3999–4004.
- 125) Bryan, Z. J.; Smith, M. L.; McNeil, A. J. Chain-Growth Polymerization of Aryl Grignards Initiated by A Stabilized NHC-Pd Precatalyst. *Macromol. Rapid Commun.* **2012**, *33*, 842–847.
- 126) Wu, K.; Doyle, A. G. Parameterization of phosphine ligands demonstrates enhancement of nickel catalysis via remote steric effects. *Nat. Chem.* **2017**, *9*, 779–784.
- 127) Pammer, F.; Passlack, U. Head-to-Tail Regioregular Polythiazole Prepared via Kumada-Coupling Polycondensation. *ACS Macro Lett.* **2014**, *3*, 170–174.
- 128) Senkovskyy, V.; Tkachov, R.; Komber, H.; John, A.; Sommer, J.-U.; Kiriya, A. Mechanistic Insight into Catalyst-Transfer Polymerization of Unusual Anion-Radical Naphthalene Diimide Monomers: An Observation of Ni(0) Intermediates. *Macromolecules* **2012**, *45*, 7770–7777.
- 129) Nanashima, Y.; Yokoyama, A.; Yokozawa, T. Synthesis of Novel Blue-Light-Emitting Polypyridine. *J. Polym. Sci., Part A: Polym. Chem.* **2012**, *50*, 1054–1061.
- 130) Senkovskyy, V.; Tkachov, R.; Komber, H.; Sommer, M.; Heuken, M.; Voit, B.; Huck, W. T. S.; Kataev, V.; Petr, A.; Kiriya, A. Chain-Growth Polymerization of Unusual Anion-Radical Monomers Based on Naphthalene Diimide: A New Route to Well-Defined n-Type Conjugated Copolymers. *J. Am. Chem. Soc.* **2011**, *133*, 19966–19970.
- 131) Wen, L.; Duck, B. C.; Dastoor, P. C.; Rasmussen, S. C. Poly(2,3-dihexylthieno[3,4-*b*]pyrazine) via GRIM Polymerization: Simple Preparation of a Solution Processable, Low-Band-Gap Conjugated Polymer. *Macromolecules* **2008**, *41*, 4576–4578.

132) Pammer, F.; Jäger, J.; Rudolf, B.; Sun, Y. Soluble Head-to-Tail Regioregular Polythiazoles: Preparation, Properties, and Evidence for Chain-Growth Behavior in the Synthesis via Kumada-Coupling Polycondensation. *Macromolecules* **2014**, *47*, 5904–5912.

133) Nanashima, Y.; Yokoyama, A.; Yokozawa, T. Synthesis of Well Defined Poly(2-alkoxypyridine-3,5-diyl) via Ni-Catalyst-Transfer Condensation Polymerization. *Macromolecules* **2012**, *45*, 2609–2613.

134) Larrosa, I.; Somoza, C.; Banquy, A.; Goldup, S. M. Two Flavors of PEPPSI-IPr: Activation and Diffusion Control in a Single NHC Ligated Pd Catalyst? *Org. Lett.* **2011**, *13*, 146–149

135) Bryan, Z. J.; Hall, A. O.; Zhao, C. T.; Chen, J.; McNeil, A. J. Limitations of Using Small Molecules to Identify Catalyst-Transfer Polycondensation reactions. *ACS Macro Lett.* **2016**, *5*, 69–72.

136) Souther, K. D.; Leone, A. K.; Vitek, A. K.; Palermo, E. F.; LaPointe, A. M.; Coates, G. W.; Zimmerman, P. M.; McNeil, A. J. Trials and Tribulations of Designing Multitasking Catalysts for Olefin/ Thiophene Block Copolymerizations. *J. Polym. Sci., A: Polym. Chem.* **2018**, *56*, 132–137.

137) Chen, L.; Ren, P.; Carrow, B. P.; Tri(1-adamantyl)phosphine: Expanding the Boundary of Electron Releasing Character Available to Organophosphorus Compounds. *J. Am. Chem. Soc.* **2016**, *138*, 6392–6395.

138) Chen, L.; Francis, H.; Carrow, B. P. An "On-Cycle" Precatalyst Enables Room-Temperature Polyfluoroarylation Using Sensitive Boronic Acids. *ACS Catal.* **2018**, *8*, 2989–2994.

- 139) Liu, Y.; Zhao, J.; Li, Z.; Mu, C.; Ma, W.; Hu, H.; Jiang, K.; Lin, H.; Ade, H.; Yan, H. Aggregation and morphology control enables multiple cases of high-efficiency polymer solar cells. *Nat. Commun.* **2014**, *5*, 5293.
- 140) Fyfe, J. W. B.; Fazakerley, N. J.; Watson, A. J. B. Chemoselective Suzuki–Miyaura Cross-Coupling via Kinetic Transmetalation. *Angew. Chem. Int. Ed.* **2017**, *56*, 1249–1253
- 141) Lennox, A. J. J.; Lloyd-Jones, G. C. Selection of boron reagents for Suzuki–Miyaura coupling. *Chem. Soc. Rev.*, **2014**, *43*, 412–443.
- 142) Bulfield, D.; Huber, S. M. Synthesis of Polyfluorinated Biphenyls; Pushing the Boundaries of Suzuki–Miyaura Cross Coupling with Electron-Poor Substrates. *J. Org. Chem.* **2017**, *82*, 13188–13203.
- 143) Yang, L.; Mihali, V.-A.; Brandell, D.; Strømme, M.; Sjödin, M. Conjugated Pyridine-Based Polymers Characterized as Conductivity Carrying Components in Anode Materials. *J. Phys. Chem. C*, **2014**, *118*, 25956–25963.
- 144) Billingsley, K. L.; Anderson, K. W.; Buchwald, S. L. A Highly Active Catalyst for Suzuki–Miyaura Cross-Coupling Reactions of Heteroaryl Compounds. *Angew. Chem. Int. Ed.* **2006**, *45*, 3484–3488.
- 145) Yang, Y.; Oldenhuis, N. J.; Buchwald, S. L. Mild and General Conditions for Negishi Cross-Coupling Enabled by the Use of Palladacycle Precatalysts. *Angew. Chem. Int. Ed.* **2013**, *52*, 615–619.
- 146) Thomas, A. A.; Denmark, S. E. Pre-transmetalation intermediates in the Suzuki–Miyaura reaction revealed: The missing link. *Science* **2016**, *352*, 329–332.

- 147) Anderson, K. W.; Buchwald, S. L. General Catalysts for the Suzuki–Miyaura and Sonogashira Coupling Reactions of Aryl Chlorides and for the Coupling of Challenging Substrate Combinations in Water. *Angew. Chem. Int. Ed.* **2005**, *44*, 6173–6177.
- 148) Handa, S.; Smith, J. D.; Zhang, Y.; Takale, B. S.; Gallou, F. Lipshutz, B. H. Sustainable HandaPhos-*ppm* Palladium Technology for Copper-Free Sonogashira Couplings in Water under Mild Conditions. *Org. Lett.* **2018**, *20*, 542–545.
- 149) Xu, F.; Chen, X.; Tang, Z.; Wu, D.; Fu, R.; Jiang, D. Redox-active conjugated microporous polymers: a new organic platform for highly efficient energy storage. *Chem. Commun.*, **2014**, *50*, 4788–4790.
- 150) Valente, C.; Çalimsiz, S.; Hoi, K. H.; Mallik, D.; Sayah, M.; Organ, M. G. The Development of Bulky Palladium NHC Complexes for the Most-Challenging Cross-Coupling Reactions. *Angew. Chem. Int. Ed.* **2012**, *51*, 3314–3332.
- 151) Nelson, D. J.; Nolan, S. P. Quantifying and understanding the electronic properties of *N*-heterocyclic carbenes. *Chem. Soc. Rev.*, **2013**, *42*, 6723–6753.
- 152) Gómez-Suárez, A.; Nelson, D. J.; Nolan, S. P. Quantifying and understanding the steric properties of *N*-heterocyclic carbenes. *Chem. Commun.*, **2017**, *53*, 2650–2660.
- 153) Antonova, N. S.; Carbó, J. J.; Poblet, J. M. Quantifying the Donor–Acceptor Properties of Phosphine and *N*-Heterocyclic Carbene Ligands in Grubbs’ Catalysts Using a Modified EDA Procedure Based on Orbital Deletion. *Organometallics* **2009**, *28*, 4283–4287.
- 154) Vummaleti, S. V. C.; Nelson, D. J.; Poater, A.; Gómez-Suárez, A.; Cordes, D. B.; Slawin, A. M. Z.; Nolan, S. P.; Cavallo, L. What can NMR spectroscopy of selenoureas and phosphinidenes teach us about the π -accepting abilities of *N*-heterocyclic carbenes? *Chem. Sci.* **2015**, *6*, 1895–1904.

- 155) Frey, G. D.; Dewhurst, R. D.; Kousar, S.; Donnadiou, B.; Bertrand, G. Cyclic (alkyl)(amino)carbene gold(I) complexes: A synthetic and structural investigation. *J. Organomet. Chem.* **2008**, *693*, 1674–1682.
- 156) Rao, B.; Tang, H.; Zeng, X.; Liu, L.; Melaimi, M.; Bertrand, G. Cyclic (Amino)(aryl)carbenes (CAArCs) as Strong σ -Donating and π -Accepting Ligands for Transition Metals. *Angew. Chem. Int. Ed.* **2015**, *54*, 14915–14919.
- 157) Miyakoshi, R.; Yokoyama, A.; Yokozawa, T. Importance of the Order of Successive Catalyst-transfer Condensation Polymerization in the Synthesis of Block Copolymers of Polythiophene and Poly(*p*-phenylene). *Chem. Lett.* **2008**, *37*, 1022–1023.
- 158) Groombridge, B. J.; Goldup, S. M.; Larrosa, I. Selective and general exhaustive cross-coupling of di-chloroarenes with a deficit of nucleophiles mediated by a Pd–NHC complex. *Chem. Commun.* **2015**, *51*, 3832–3834.
- 159) Zhang, S.; Huang, W.; Hu, P.; Huang, C.; Shang, C.; Zhang, C.; Yang R.; Cui, G. Conjugated microporous polymers with excellent electrochemical performance for lithium and sodium storage. *J. Mater. Chem. A*, **2015**, *3*, 1896–1901.
- 160) Liang, Y.; Feng, D.; Wu, Y.; Tsai, S.–T.; Li, G.; Ray, C.; Yu, L. Highly Efficient Solar Cell Polymers Developed via Fine-Tuning of Structural and Electronic Properties. *J. Am. Chem. Soc.* **2009**, *131*, 7792–7799.
- 161) Cabanetos, C.; El Labban, A.; Bartelt, J. A.; Douglas, J. D.; Mateker, W. R. Fréchet, J. M.; McGehee, M. D.; Beaujuge, P. M. Linear Side Chains in Benzo[1,2-*b*:4,5-*b'*]dithiophene–Thieno[3,4-*c*]pyrrole-4,6-dione Polymers Direct Self-Assembly and Solar Cell Performance *J. Am. Chem. Soc.* **2013**, *135*, 4656–4659.

162) Wang, X.; Deng, W.; Chen, Y.; Wang, X.; Ye, P.; Wu, X.; Yan, C.; Zhan, X.; Liu, F.; Huang, H. Fine-tuning solid state packing and significantly improving photovoltaic performance of conjugated polymers through side chain engineering *via* random polymerization. *J. Mater. Chem. A*, **2017**, *5*, 5585–5593.

163) Lu, D.-D.; He, X.-X.; Liu, F.-S. Bulky Yet Flexible Pd-PEPPSI-IPentAn for the Synthesis of Sterically Hindered Biaryls in Air. *J. Org. Chem.* **2017**, *82*, 10898–10911.

164) Ouyang, J-S.; Li, Y-F.; Huang, F-D.; Lu, D-D.; Liu, F-S. The Highly Efficient Suzuki–Miyaura Cross-Coupling of (Hetero)aryl Chlorides and (Hetero)arylboronic Acids Catalyzed by “Bulky-yet-Flexible” Palladium–PEPPSI Complexes in Air. *Chem. Cat. Chem.* **2018**, *10*, 371 – 375.

165) Stuart, A. C.; Tumbleston, J. R.; Zhou, H.; Li, W.; Liu, S.; Ade, H.; You, W. Fluorine Substituents Reduce Charge Recombination and Drive Structure and Morphology Development in Polymer Solar Cells. *J. Am. Chem. Soc.* **2013**, *135*, 1806–1815.

Appendices

Appendix 1: Supporting information for Chapter 2. Ring-Walking in Catalyst Transfer Polymerization

A1.1 Materials

Flash chromatography was performed on SiliCycle silica gel (40–63 μm). Thin layer chromatography was performed on Merck TLC plates (pre-coated with silica gel 60 F254). $i\text{PrMgCl}$ (2 M in THF) was purchased from Aldrich and titrated using salicylaldehyde phenylhydrazone.¹ $\text{Ni}(\text{IPr})(\text{PPh}_3)\text{Cl}_2$ (PPh_3 = triphenylphosphine, IPr = 1,3-bis(2,6-diisopropylphenyl)imidazol-2-ylidene) was purchased from TCI America. $\text{Pd}(\text{IPr})(3\text{-Clpy})\text{Cl}_2$ (3-Clpy = 3-chloropyridyl) was purchased from Sigma Aldrich. $\text{Ni}(\text{dppp})\text{Cl}_2$ (dppp = 1,3-bis(diphenylphosphinopropane)) was purchased from Strem Chemicals Inc. 2,5-Dibromo-3-decylthiophene (DB3DT) and 2,5-dibromo-3-hexylthiophene (DB3HT) were purchased from TCI America and purified by column chromatography with hexanes as the eluent. *p*-Toluenemagnesium chloride (2 M in THF) was purchased from Acros Organics. 5,5'-Dibromo-2,2'-bithiophene was purchased from Ark Pharm Inc. Compounds **S1**,² **S2**,² and **S3**² were prepared according to modified literature procedures. All other reagent grade materials and solvents were purchased from Aldrich, Acros, or Fisher and were used without further purification unless otherwise noted. Tetrahydrofuran (THF) and hexanes were dried and deoxygenated using an Innovative Technology (IT) solvent purification system composed of activated alumina, copper catalyst, and molecular sieves. The glovebox in which specified procedures were carried out was an MBraun LABmaster 130 with a N_2 atmosphere.

A1.2 General Experimental

NMR Spectroscopy: Unless otherwise noted, ^1H , and ^{13}C NMR spectra for all compounds were acquired at rt. Chemical shift data are reported in units of δ (ppm) relative to tetramethylsilane (TMS) and referenced with residual solvent. Multiplicities are reported as follows: singlet (s), doublet (d), doublet of doublets (dd), triplet (t), quartet (q), multiplet (m), broad resonance (br). Residual water is denoted by an asterisk (*).

Mass Spectrometry: High-resolution mass spectrometry data were obtained on a Micromass AutoSpec Ultima Magnetic Sector mass spectrometer.

Gel-Permeation Chromatography (GPC): Polymer molecular weights were determined by comparison with polystyrene standards (Varian, EasiCal PS-2 MW 580–377,400) at 40 °C in THF on a Malvern Viscotek GPCMax VE2001 equipped with two Viscotek LT- 5000L 8 mm (ID) \times 300 mm (L) columns and analyzed with Viscotek TDA 305 (with RI, UV-PDA Detector Model 2600 (190–500 nm), RALS/LALS, and viscometer). Data presented correspond to the absorbance at 254 nm normalized to the highest peak. Peaks are normalized to the polymer peak, when traces are presented in series, the normalized peaks are offset vertically. The peaks at ~21 min represent monomer which include unreacted, quenched Grignard monomers and/or unactivated dibromo monomer (see monomer activation procedures).

Polymer work-up for GPC: Polymerizations were quenched using aq. HCl (12 M). The organic layer was extracted with CHCl_3 , dried over MgSO_4 , and filtered through a PTFE filter (0.2 μm),

concentrated under reduced pressure to dryness and then redissolved in THF/toluene (99:1 v/v) with mild heating and filtered through a PTFE filter (0.2 μm) into a GPC vial.

Gas Chromatography: Gas chromatographic (GC) analysis was done using a Shimadzu GC 2010 containing a Shimadzu SHRX5 (crossbound 5% diphenyl – 95% dimethyl polysiloxane; 15 m, 0.25 mm ID, 0.25 μm df) column.

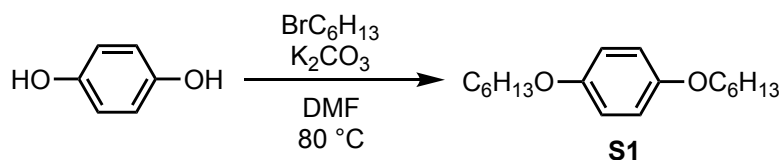
Polymer work-up for GC: Polymerizations were quenched using aq. HCl (12 M). The organic layer was extracted with CHCl_3 , dried over MgSO_4 , and filtered through a PTFE filter (0.2 μm) into a GC vial.

Matrix-Assisted Laser Desorption/Ionization Mass Spectrometry: Matrix-Assisted Laser Desorption/Ionization Mass Spectrometry (MALDI-TOF/MS) was done on a Bruker AutoFlex Speed MALDI-TOF in positive-ion reflectron mode using *trans*-2-[3-(4-*tert*-butylphenyl)-2-methyl-2-propenylidene]malononitrile (DCTB) as a matrix. Samples were prepared by mixing polymer dissolved in THF/toluene (99:1 v/v) (~1 mg polymer/1 mL THF) with DCTB dissolved in CHCl_3 (~1 M). Samples were diluted with varying polymer/DCTB ratios ([2.5–10 μL]/[2.5 μL] to ensure good signal/noise) and then spotted on a MALDI 96-well plate and air-dried. The data were analyzed using flexAnalysis. The MALDI-TOF/MS spectra shown represent the polymer distribution as well as a zoomed spectra from the center of the curve unless otherwise noted.

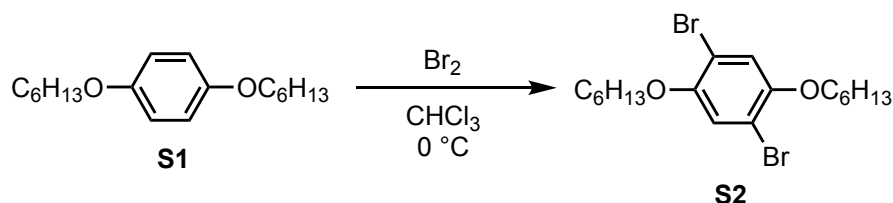
iPrMgCl titration:¹ In a glovebox, a precise amount of salicylaldehyde phenylhydrazone was dissolved in a precise amount of THF. For titration, iPrMgCl was added dropwise using a 100

μL syringe into the salicylaldehyde phenylhydrazone solution. Titration was complete when the solution turned bright orange.

A1.3 Synthetic Procedures



1,4-bis(hexyloxy)phenylene (S1).² To a 500 mL flask equipped with a stirbar, the following were added sequentially, hydroquinone (20. g, 0.18 mol, 1.0 equiv), DMF (120 mL), potassium carbonate (63 g, 0.46 mol, 2.6 equiv), and 1-bromohexane (63 mL, 0.45 mol, 2.5 equiv) and stirred under N_2 at 80 °C for 5 d. The reaction mixture was cooled to rt, then poured into DI H_2O (400 mL). The organic layer was extracted with hexanes (3 x 200 mL), washed with DI H_2O (2 x 200 mL), and brine (1 x 200 mL), dried over MgSO_4 , filtered, and concentrated under reduced pressure. The resulting oil was passed through silica gel using DCM as the eluent. Recrystallization from hot MeOH (minimal ~75 mL) gave a white, crystalline solid (29 g, 56% yield). HRMS (EI): $[M^+]$ Calcd. for $\text{C}_{18}\text{H}_{30}\text{O}_2$, 278.2246; found, 278.2242.



1,4-bis(hexyloxy)-2,5-dibromophenylene (S2).² To a 500 mL flask equipped with a stirbar was added S1 (24 g, 0.86 mol, 1.0 equiv) and CHCl_3 (98 mL). The flask was cooled to 0 °C using an ice/water bath and fitted with an addition funnel. Bromine (11 mL, 0.21 mol, 2.5 equiv) was added dropwise under N_2 over 10 min. The pressure was vented through an aq. solution of 10% Na_2SO_3 (150 mL). After 3 h, the reaction was quenched with sat. aq. Na_2SO_3 (150 mL) and vigorously stirred until colorless. The organic layer was extracted with DCM (3 x 100 mL),

washed with H₂O (2 x 100 mL) and brine (1 x 100 mL), dried over MgSO₄, filtered, and concentrated under reduced pressure. The residue was crystallized by dissolving in CHCl₃ (10 mL) and layering with MeOH (100 mL). The resulting solids were filtered to afford white crystals (29 g, 77% yield). HRMS (EI): [M⁺] Calcd. for C₁₈H₂₈Br₂O₂, 434.0451; found, 434.0455.

A1.4 NMR Spectra

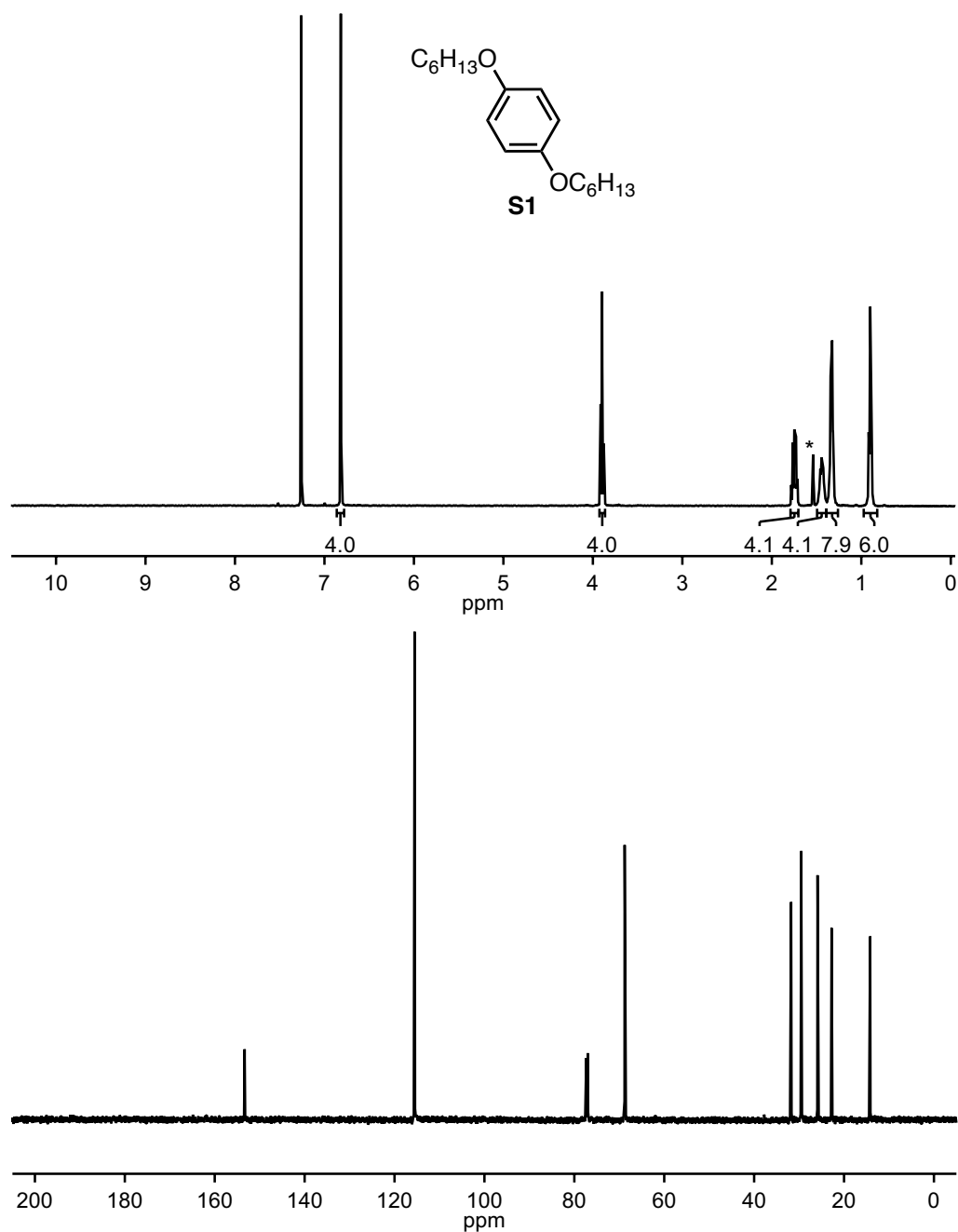


Figure A1-1. ^1H and ^{13}C NMR spectra for S1. ^1H NMR (400 MHz, CDCl_3) δ 6.82 (s, 4H), 3.90 (t, $J = 6.6$ Hz, 4H), 1.75 (dt, $J = 14.7, 6.6$ Hz, 4H), 1.50–1.39 (m, 4H), 1.38–1.26 (m, 8H), 0.98–0.80 (m, 6H). ^{13}C NMR (176 MHz, CDCl_3) δ 153.34, 115.53, 68.80, 31.77, 29.53, 25.90, 22.77, 14.19.

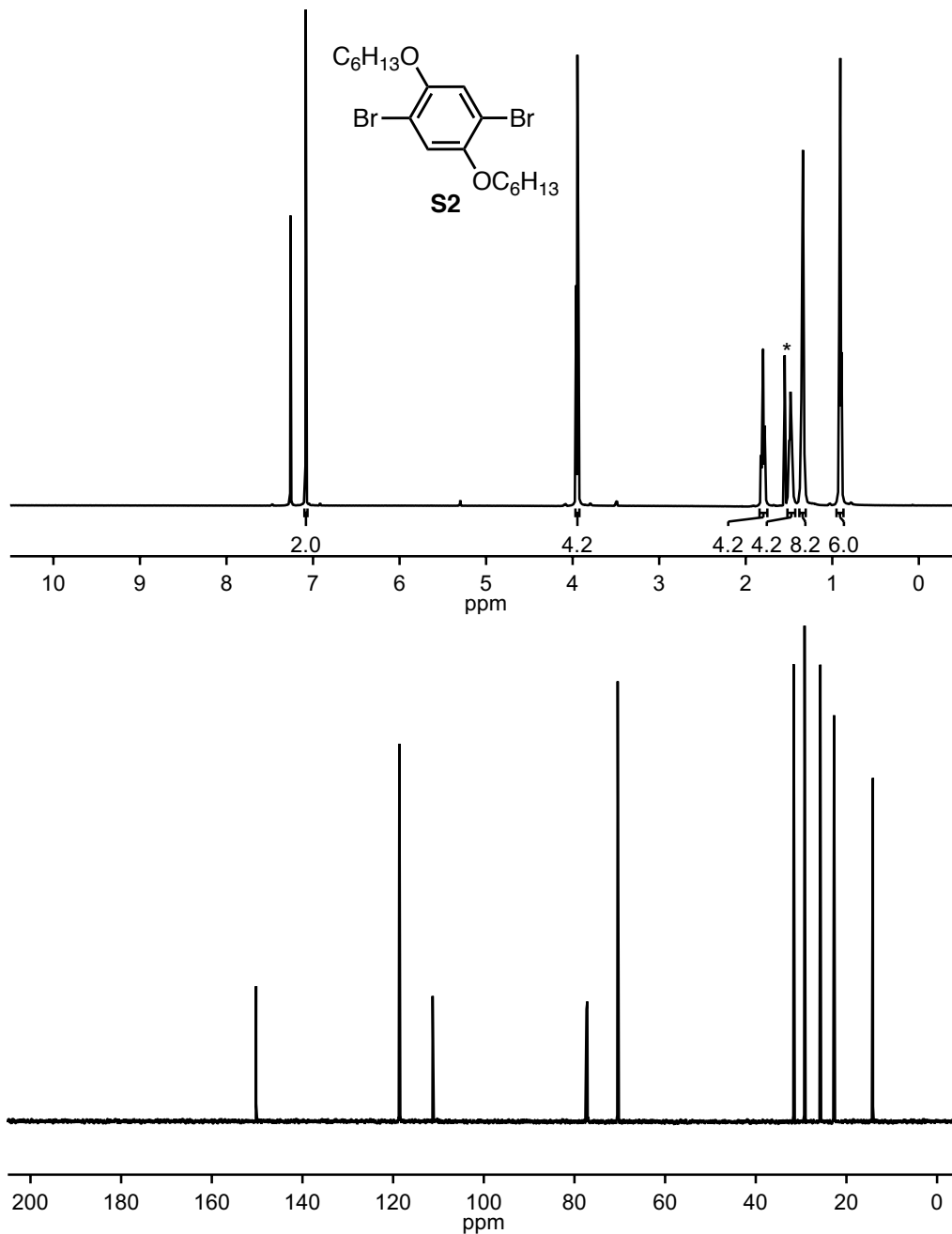


Figure A1-2. ¹H and ¹³C NMR spectra for **S2**. ¹H NMR (500 MHz, CDCl₃) δ 7.08 (s, 2H), 3.95 (t, J = 6.5 Hz, 4H), 1.80 (dq, J = 8.3, 6.5 Hz, 4H), 1.52–1.43 (m, 4H), 1.38–1.31 (m, 8H), 0.95–0.87 (m, 6H). ¹³C NMR (176 MHz, CDCl₃) δ 150.22, 118.62, 111.28, 70.46, 31.63, 29.23, 25.76, 22.72, 14.16.

A1.5 Thiophene

A1.5.1 Confirming MALDI-TOF/MS provides an accurate and quantitative description of end-group distributions for poly(3-alkylthiophene)

A1.5.2. Synthesis of H/Br-polymer for end-capping control reactions

A1.5.3. End-capping control reactions

i. Ni(IPr)(PPh₃)Cl₂ and Pd(IPr)(3-Clpy)Cl₂

ii. Ni(dppp)Cl₂

A1.5.4. Evaluating the effect of entangled chains

A1.5.5. End-capping reactions

i. Ni(IPr)(PPh₃)Cl₂ (2 iterations of end-capping conditions)

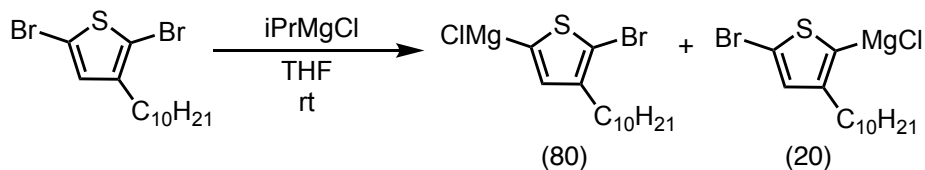
ii. Pd(IPr)(3-Clpy)Cl₂ (18 h end-capping and multiple iterations of end-capping conditions)

iii. Ni(dppp)Cl₂ (1 h and 18 h end-capping)

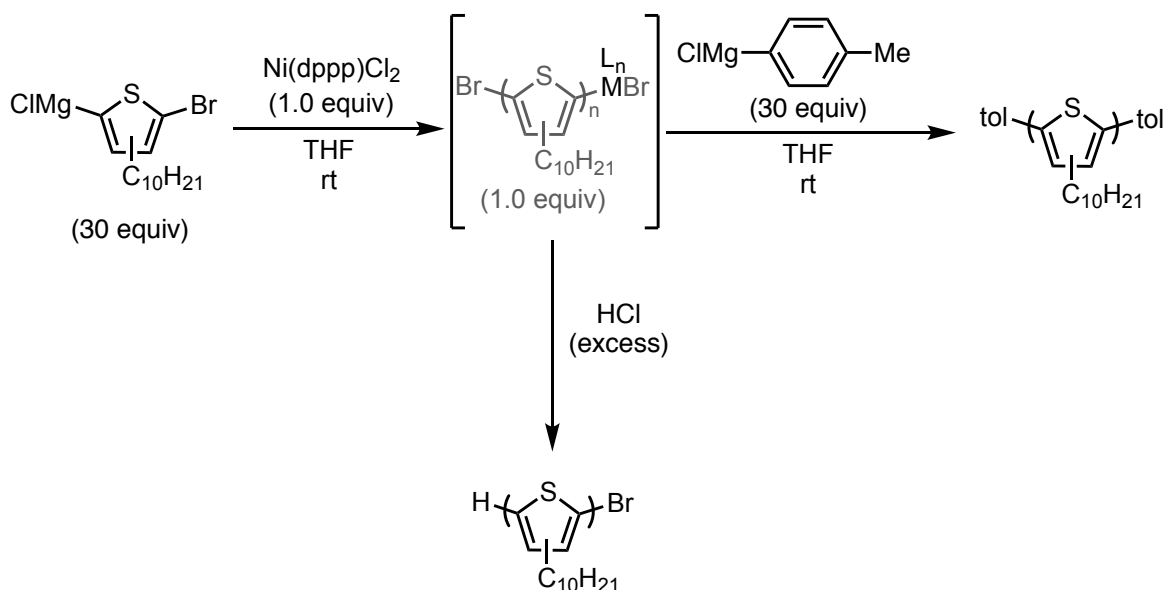
iv. Evaluating the effect of solvent (hexane) on end-capping

A1.5.6. 3-Decylthiophene Polymerization via Ni(IPr)(PPh₃)Cl₂ generating NHC/Br-polymers

A1.5.1 Confirming MALDI-TOF/MS provides an accurate and quantitative description of end-group distributions for poly(3-alkylthiophene)



Monomer activation: In a glovebox, iPrMgCl (2.2 M in THF, 118 μL , 0.260 mmol, 0.800 equiv) was added to a stirring solution of DB3DT (124.0 mg, 0.3240 mmol, 1.000 equiv) in THF (3.12 mL) and stirred for 30 min at rt.



Diluting monomer solution for polymerization: Activated monomer solution (3.10 mL, 0.248 mmol, 21.8 equiv) was diluted with THF (11.39 mL) for an overall monomer concentration of 0.017 M.

Polymerization: In a glovebox, to a 20 mL vial equipped with a stirbar was added precatalyst Ni(dppp)Cl₂ (6.2 mg, 0.011 mmol, 1.0 equiv). While stirring, a portion of the diluted-Grignard monomer solution (0.017 M in THF, 2.2 mL, 0.037 mmol, 3.3 equiv) was added to the catalyst.

The catalyst is preinitiated once all solids are dissolved (requires ~60 sec). Then, the remaining monomer solution was added to the preinitiated catalyst solution and stirred for 15 min at rt.

End-capping: An aliquot of the polymerization solution (7.0 mL, containing 0.00551 mmol catalyst, *new* 1.0 equiv Ni) was added to a 20 mL vial equipped with a stirbar containing *p*-toluenemagnesium chloride (1.11 M in THF, 0.149 mL, 0.165 mmol, 30.0 equiv relative to Ni added). The solution turned from red to dark purple after 3 min, and was stirred at rt for 30 min.

Quenching & work-up: The remaining (original) polymerization solution (c.f., 7.49 mL) was quenched outside of the glovebox with aq. HCl (12 M, 10 mL) immediately after removing the aliquot for end-capping, and stirred for 5 min during which time polymer precipitated generating a heterogeneous mixture of purple polymer in a clear supernatant. The quenched polymer was poured into two centrifuge tubes and diluted with MeOH (10 mL – per centrifuge tube). The polymers were spun on a centrifuge for 15 min. The resulting clear supernatant was decanted and the purple solid was washed with additional MeOH (10 mL – per centrifuge tube) and spun for an additional 15 min. The resulting clear supernatant was decanted and the purple solid collected by transferring to a 20 mL vial using CHCl₃ (5 x 1 mL). The polymer solution was concentrated under reduced pressure, yielding 12.9 mg of poly(3-decylthiophene) (Br/H–P3DT) (56% yield – relative to the predicted mmol remaining after the aliquot for end-capping was removed). The end-capped polymer was quenched by adding MeOH (15 mL) to the purple solution which precipitated the polymer. The polymers were spun on a centrifuge for 15 min. The resulting clear supernatant was decanted and the purple solid was washed with additional MeOH (10 mL – per centrifuge tube) and spun for an additional 15 min. The resulting clear supernatant was decanted

and the purple solid collected by transferring to a vial using CHCl_3 (5 x 1 mL). The polymer solution was concentrated under reduced pressure, yielding 22.7 mg of tol/tol-terminated poly(3-decylthiophene) (tol/tol-P3DT) (98% yield – relative to the predicted mmol removed for end-capping).

Polymer solutions for ^1H NMR spectroscopic analysis and MALDI-TOF/MS:

Br/H-P3DT (6.7 mg) was dissolved in CDCl_3 (2.68 mL), tol/tol-P3DT (3.0 mg) was dissolved in CDCl_3 (1.2 mL). The polymer solutions were combined by injecting an aliquot of each solution (0.3 mL) into a single NMR tube which was analyzed by ^1H NMR spectroscopy using a 3s relaxation delay. The NMR solution was used to prepare the MALDI-TOF/MS samples (see general experimental). The ^1H NMR spectrum and MALDI-TOF/MS are in agreement with the polymers being in equal 1:1 (wt/wt) concentration as prepared.

Table A1-1. Percent P3DT with each end-group based on MALDI-TOF/MS.

	Br/H-P3DT (%)	end-capped P3DT (%)	combined (theo.) (%)	combined (observed) (%)
H/H	0	6.12	3.06	3.13
Br/H	100	0	50	55.21
tol/H	0	23.47	11.74	11.46
tol/tol	0	70.40	35.20	30.20

Table A1-2. M_n and \mathcal{D} from Br/H-PBHP and end-capped-PBHP.

	M_n (kg/mol)	\mathcal{D}
Br/H-P3DT	4.09	1.21
end-capped-P3DT	4.30	1.17

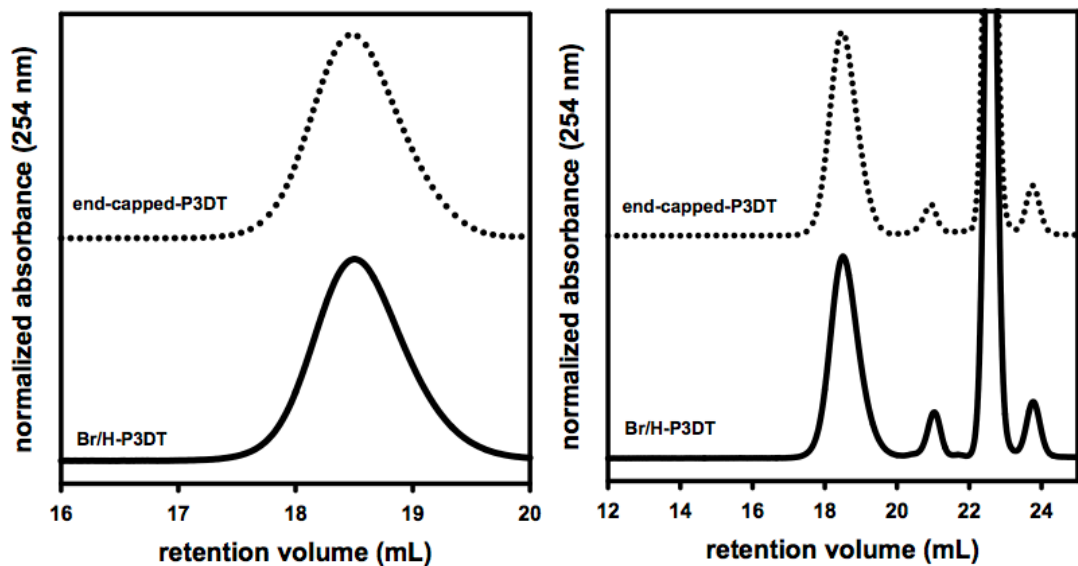


Figure A1-3. GPC traces from Br/H-P3DT and end-capped-P3DT (left = zoomed, right = full GPC trace of the set of samples). Note that residual monomer elutes from 20.5–22 min, PhMe elutes at 23.1 min and BHT elutes at 23.8 min.

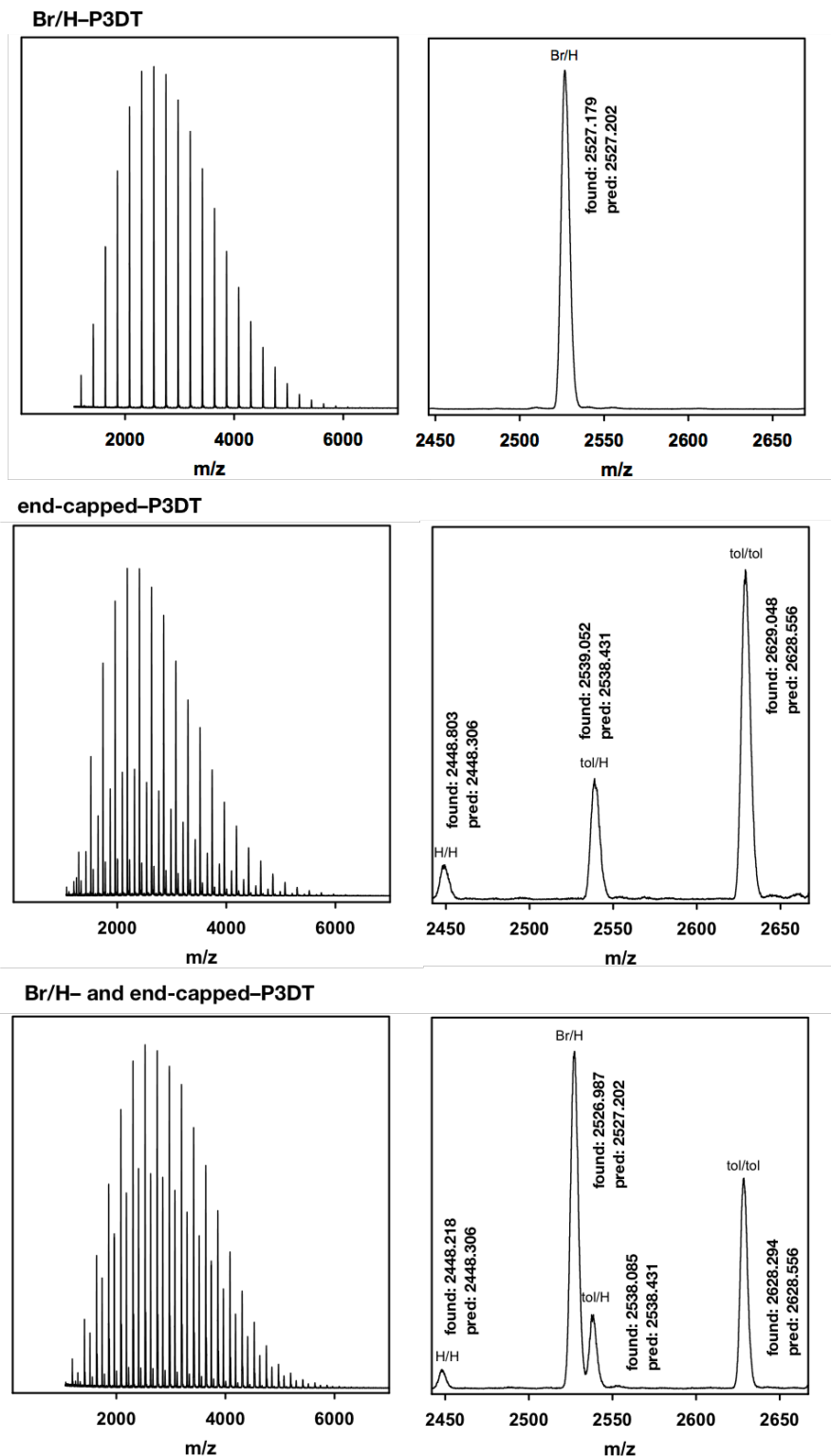


Figure A1-4. MALDI-TOF/MS spectra from Br/H-P3DT, end-capped-P3DT, and Br/H-P3DT combined with end-capped-P3DT in a 1:1 (wt/wt) ratio. Calculated using an average method, at signal-to-noise = 2. The degree of polymerization shown is 11.

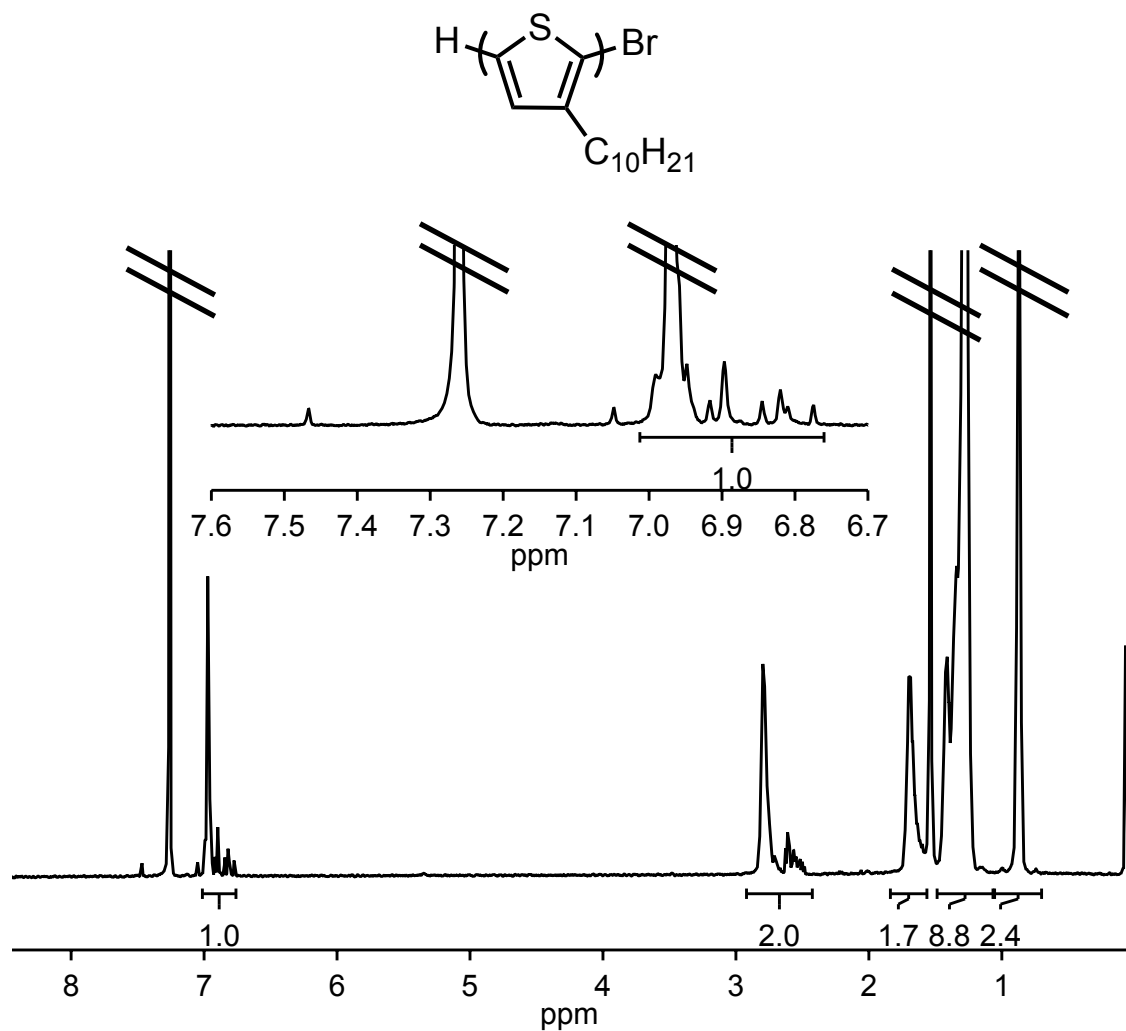


Figure A1-5. ¹H NMR spectrum of Br/H-P3DT (relaxation delay = 3s). ¹H NMR (500 MHz, CDCl₃-d) δ 7.01–6.76 (m, 1H), 2.92–2.42 (m, 2H), 1.83–1.56 (m, 2H), 1.48–1.07 (m, 9H), 0.88 (t, *J* = 6.5 Hz, 3H).

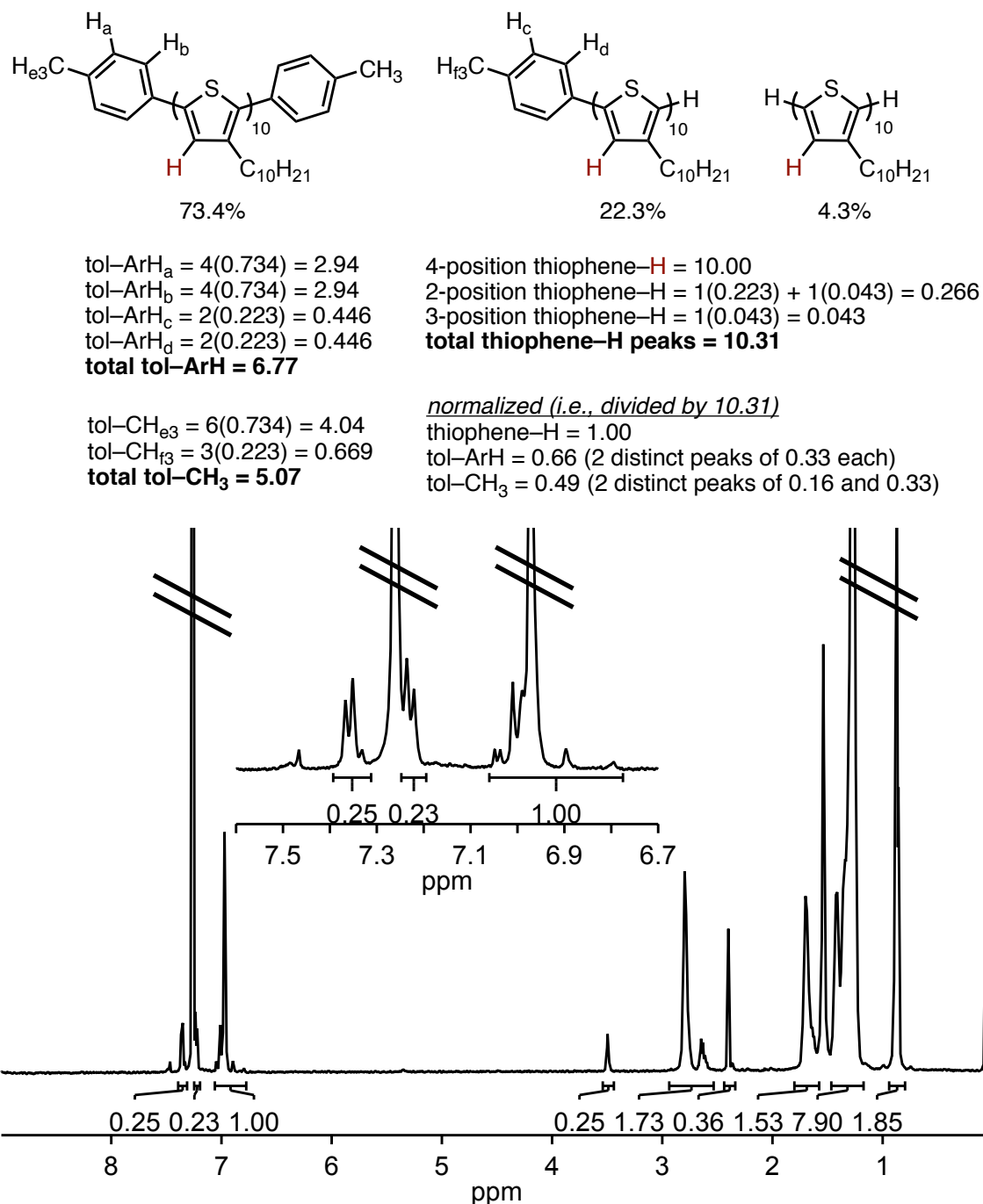
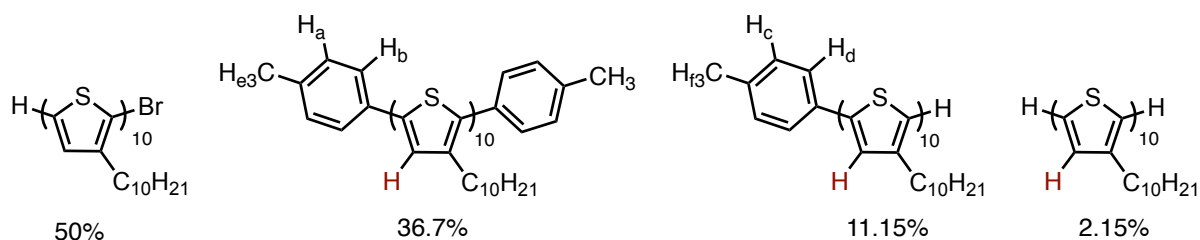


Figure A1-6. ^1H NMR spectrum of end-capped-P3DT (relaxation delay = 3s). The ratios of each polymer are predicted based on MALDI-TOF/MS data (see above). ^1H NMR (500 MHz, CDCl_3 -d) δ 7.39–7.31 (m, 0.25H), 7.25–7.19 (m, 0.23H), 7.06–6.77 (m, 1H), 3.54–3.44 (m, 0.25H), 2.93–2.52 (m, 2H), 2.44–2.34 (m, 0.36H), 1.80–1.59 (m, 2H), 1.46–1.17 (m, 8H), 0.87 (t, $J = 6.4$ Hz, 2H).



$$\begin{aligned}
 \text{tol-ArH}_a &= 4(0.367) = 1.47 & 4\text{-position thiophene-H} &= 10.00 \\
 \text{tol-ArH}_b &= 4(0.367) = 1.47 & 2\text{-position thiophene-H} &= 1(0.1115) + 1(0.0215) = 0.133 \\
 \text{tol-ArH}_c &= 2(0.1115) = 0.223 & 3\text{-position thiophene-H} &= 1(0.0215) = 0.0215 \\
 \text{tol-ArH}_d &= 2(0.1115) = 0.223 & \text{total thiophene-H peaks} &= \mathbf{10.15} \\
 \text{total tol-ArH} &= \mathbf{3.39} & & \\
 \\
 \text{tol-CH}_{e3} &= 6(0.367) = 2.02 & \text{normalized (i.e., divided by 10.15)} & \\
 \text{tol-CH}_{f3} &= 3(0.1115) = 0.335 & \text{thiophene-H} &= 1.00 \\
 \text{total tol-CH}_3 &= \mathbf{2.54} & \text{tol-ArH} &= 0.33 \text{ (2 distinct peaks of 0.17 each)} \\
 & & \text{tol-CH}_3 &= 0.25 \text{ (2 distinct peaks of 0.08 and 0.17)}
 \end{aligned}$$

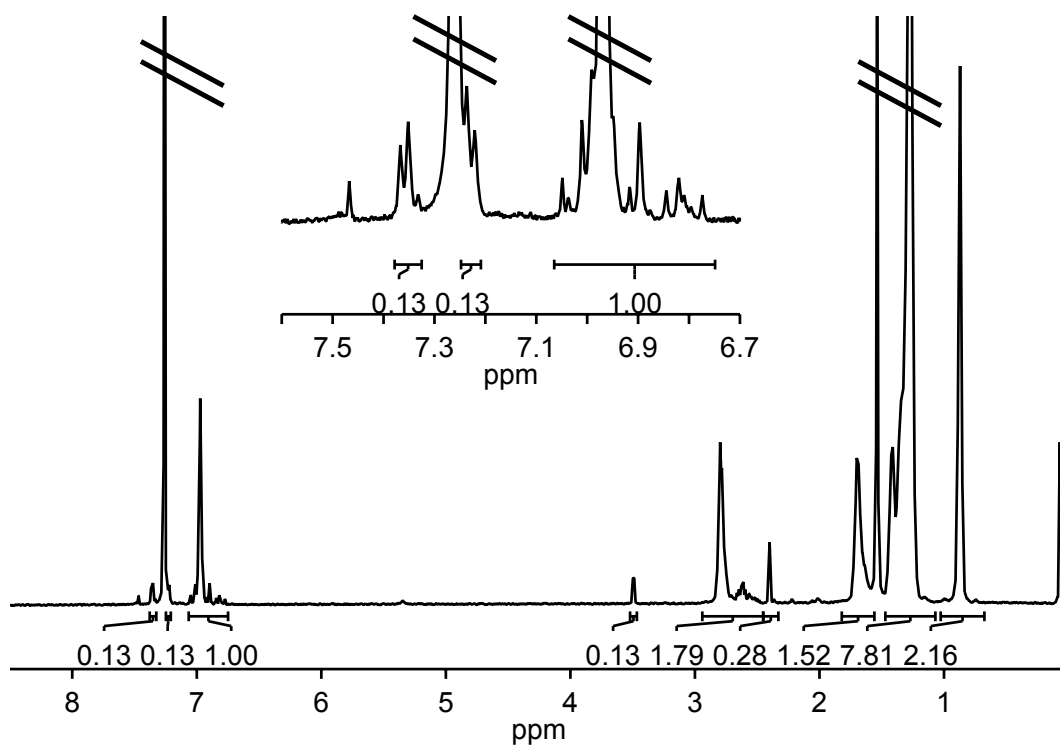
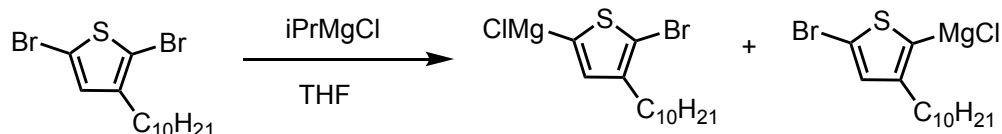
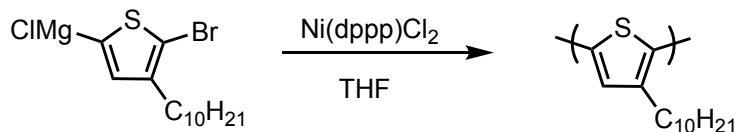


Figure A1-7. ^1H NMR spectrum of Br/H-P3DT combined with end-capped-P3DT in a 1:1 (wt/wt) ratio. The ratios of each polymer are predicted in accordance to diluting the end-capped-P3DT (ratios determined by “homopolymer” MALDI-TOF/MS, see above) with Br/H-P3DT. Relaxation delay = 3s. ^1H NMR (500 MHz, $\text{CDCl}_3\text{-}d$) δ 7.38–7.32 (m, 0.13H), 7.25–7.21 (m, 0.13H), 7.07–6.75 (m, 1H), 3.52–3.46 (m, 0.13H), 2.94–2.45 (m, 2H), 2.45–2.33 (m, 0.13H), 1.82–1.56 (m, 2H), 1.47–1.07 (m, 8H), 0.88 (t, J = 6.4 Hz, 2H).

A1.5.2 Synthesis of H/Br-polymer for end-capping control reactions



Monomer activation: In a glovebox, $iPrMgCl$ (1.85 M in THF, 0.368 mL, 0.681 mmol, 0.800 equiv) was added to a solution of DB3DT (326 mg, 0.852 mmol, 1.00 equiv) in THF (8.15 mL) and stirred for 30 min at rt. A portion of this Grignard monomer solution (0.08 M in THF, 8.0 mL, 0.64 mmol, 21 equiv – relative to $Ni(dppp)Cl_2$ below) was diluted with THF (32 mL) in a 50 mL round-bottom flask generating a [0.016 M] diluted-Grignard monomer solution.



Preinitiation of precatalyst $Ni(dppp)Cl_2$: In a glovebox, to a 20 mL vial equipped with a stirbar was added precatalyst $Ni(dppp)Cl_2$ (13.9 mg, 0.0256 mmol, 1.00 equiv). While stirring, a portion of the diluted-Grignard monomer solution (0.016 M in THF, 4.0 mL, 0.064 mmol, 2.5 equiv) was added to the catalyst. The catalyst is preinitiated once all solids are dissolved (requires ~30 sec).

Polymerization: In a glovebox, the preinitiated catalyst solution was added to the remaining diluted-Grignard monomer solution, using a syringe, and stirred for 20 min at rt. The polymerization was quenched outside of the glovebox with aq. HCl (12 M, 15 mL) and stirred for 5 min during which time polymer precipitated generating a heterogeneous mixture of purple polymer in a clear supernatant. An aliquot of the quenched polymer heterogeneous mixture (0.2 mL) was worked up for GPC analysis (see general experimental). The remaining quenched polymer was poured into four centrifuge tubes and diluted with MeOH (10 mL – per centrifuge

tube). The polymers were spun on a centrifuge for 15 min. The resulting clear supernatant was decanted and the purple solid was collected by transferring to a vial using CHCl_3 (8 mL). The polymer solution was concentrated under reduced pressure, yielding 78.9 mg of poly(3-decylthiophene) (P3DT) (55% yield).

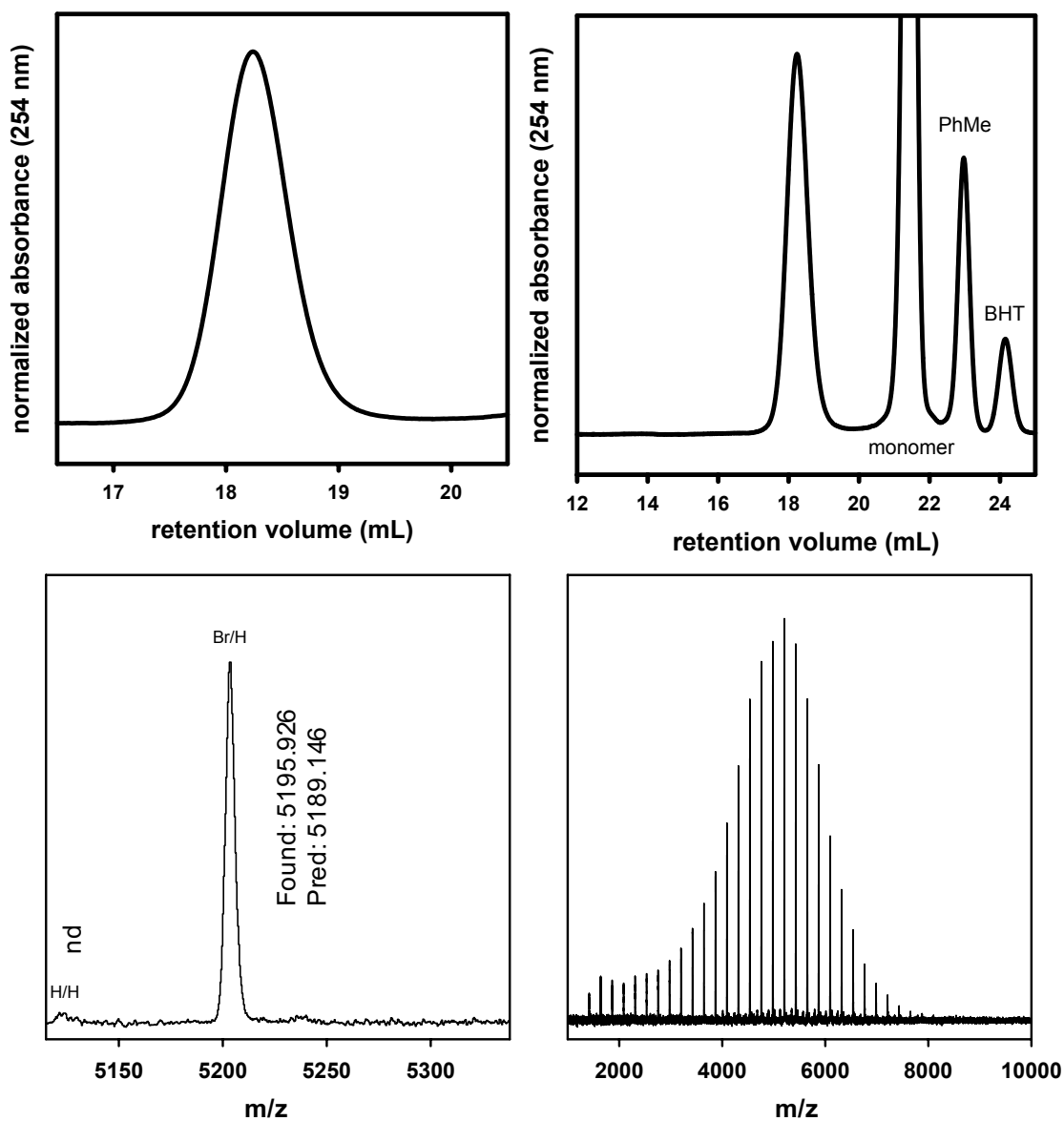


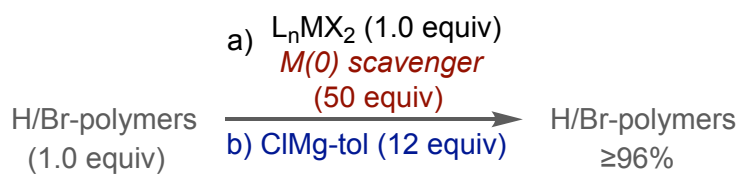
Figure A1-8. (top) GPC trace of pre-precipitated P3DT synthesized via $\text{Ni}(\text{dppp})\text{Cl}_2$. $M_n = 7.81$ kg/mol, $\bar{D} = 1.12$. (bottom) MALDI-TOF/MS spectrum of pre-precipitated P3DT synthesized via $\text{Ni}(\text{dppp})\text{Cl}_2$. Calculated using an exact method, nd = not detected at signal-to-noise = 1. The degree of polymerization shown is 23.

A1.5.3 End-capping control reactions

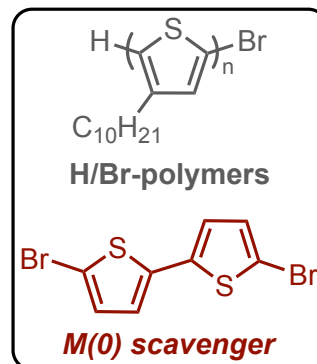
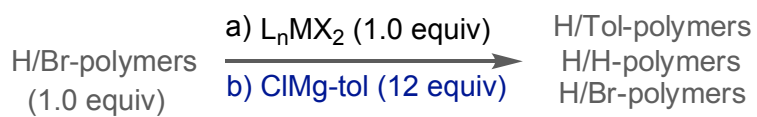
i. Ni(IPr)(PPh₃)Cl₂ and Pd(IPr)(3-Clpy)Cl₂

ii. Ni(dppp)Cl₂

end-capping experiment control



end-capping control (capping agent only)



i. Ni(PPh₃)IPrCl₂ and Pd(IPr)(3-Clpy)Cl₂ (the following takes place in the glovebox until noted)

Preparing stock solutions:

Ni(IPr)(PPh₃)Cl₂: In a 4 mL vial, Ni(IPr)(PPh₃)Cl₂ (9.4 mg, 0.012 mmol) was dissolved in THF (1.2 mL) for an overall concentration of 0.01 M.

Pd(IPr)(3-Clpy)Cl₂: In a 4 mL vial Pd(IPr)(3-Clpy)Cl₂ (11.0 mg, 0.0162 mmol) was dissolved in THF (1.62 mL) for an overall concentration of 0.01 M.

P3DT: In a 20 mL vial, P3DT (M_n by MALDI-TOF/MS = 5195.926 g/mol – repeat unit 222.16 g/mol, 6.6 mg, 0.030 mmol (relative to the repeat unit molecular weight)) was dissolved in THF (3.0 mL) with mild heating (35 °C) for an overall concentration of 0.01 M.

M(0) scavenger: To a 4 mL vial was added 5,5'-dibromo-2,2'-bithiophene (26.8 mg, 0.0827 mmol) and THF (3.3 mL) for an overall concentration of 0.025 M.

Experiment vial preparation:

End-capping experiment vial: 4 mL vials were prepared with 5,5'-dibromo-2,2'-bithiophene (0.025 M in THF, 0.460 mL, 0.0115 mmol, 50.0 equiv), P3DT (0.01 M in THF, 0.540 mL, 0.000230 mmol (relative to polymer molecular weight), 1.00 equiv), precatalyst (0.01 M in THF, 23 μL, 0.00023 mmol, 1.0 equiv), THF (0.23 mL), and a stirbar.

End-capping experiment control (capping agent only) vial: 4 mL vials were prepared with P3DT (0.01 M in THF, 0.540 mL, 0.000230 mmol (relative to polymer molecular weight), 1.00 equiv), precatalyst (0.01 M in THF, 23 μ L, 0.00023 mmol, 1.0 equiv), THF (0.69 mL) and a stirbar.

Experiments:

p-Toluenemagnesium chloride (0.26 M in THF, 10.6 μ L, 0.00276 mmol, 12.0 equiv) was added to each vial. The reactions were stirred for 1 h at rt before quenching outside of the glovebox with aq. HCl (12 M, 1 mL). Then, the organic layers were extracted with CHCl₃ (3 x 1 mL) and samples were worked up for MALDI-TOF/MS (see general experimental).

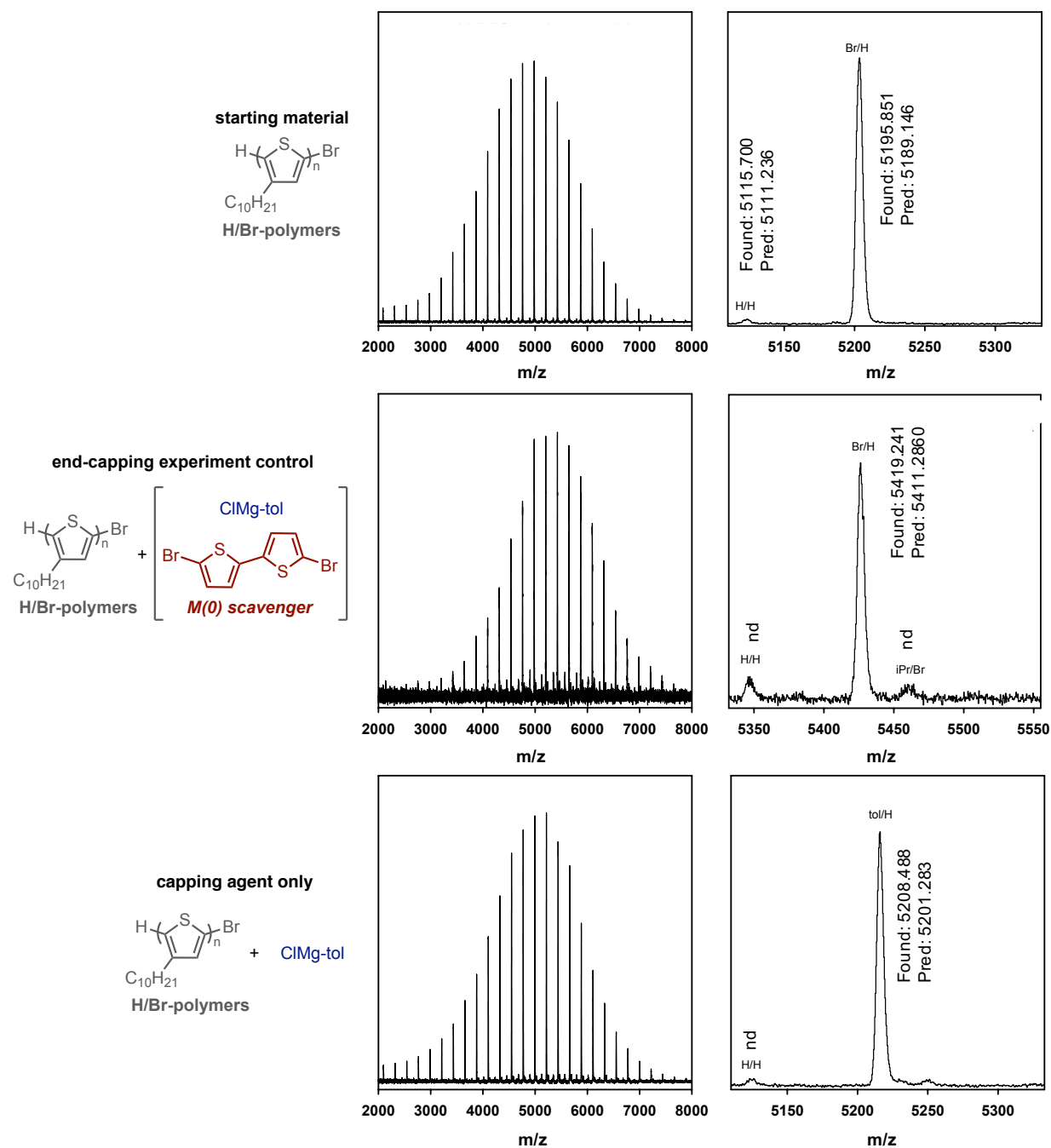


Figure A1-9. MALDI-TOF/MS spectra from end-capping control reactions for P3DT and $\text{Ni}(\text{IPr})(\text{PPh}_3)\text{Cl}_2$. Calculated using an exact mass method, nd = not detected at signal-to-noise = 1. The degree of polymerizations shown are 23, 24, 23 from the top figure to the bottom one.

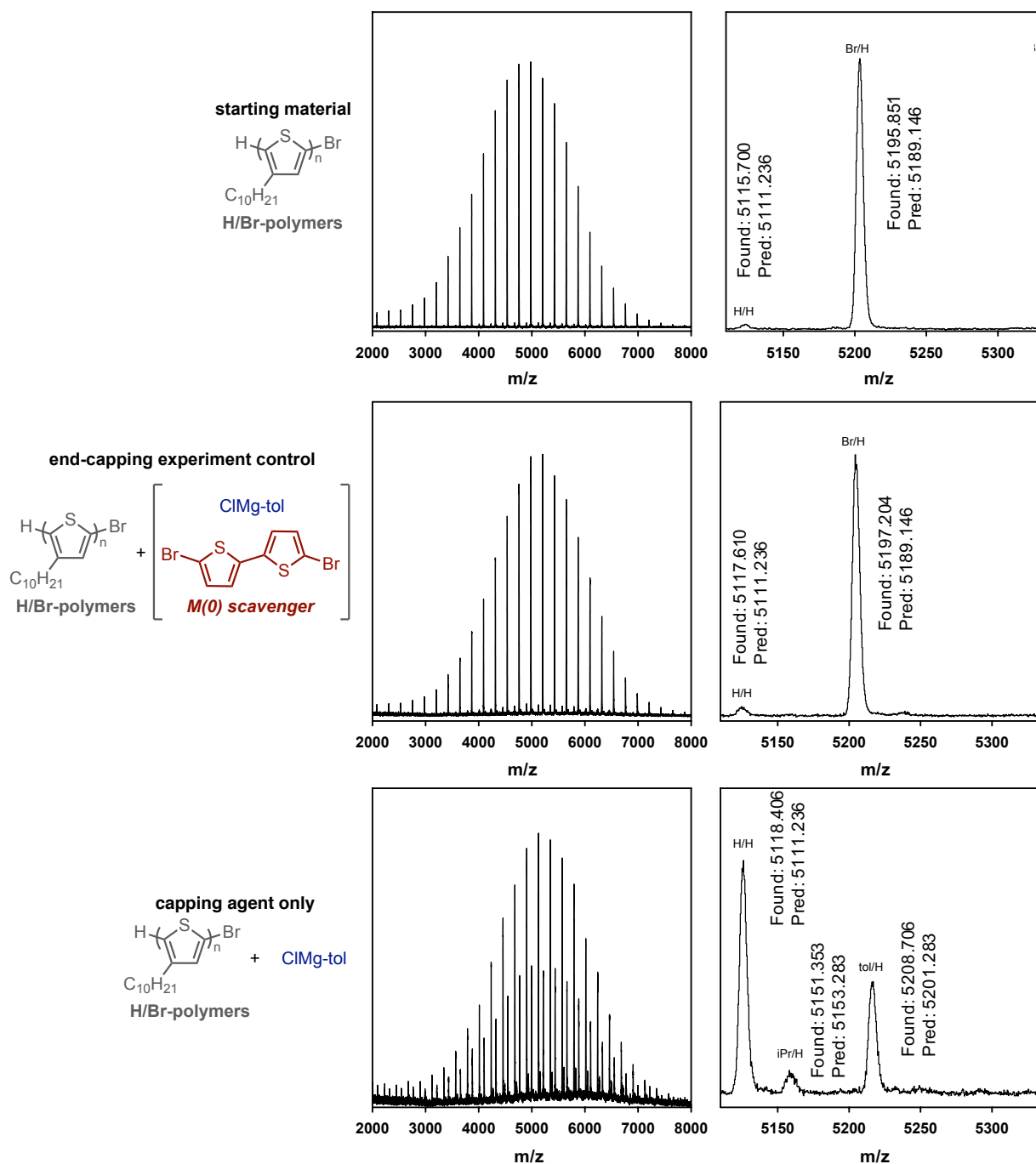


Figure A1-10. MALDI-TOF/MS spectra from end-capping control reactions for P3DT and Pd(IPr)(3-Clpy)Cl₂. Calculated using an exact mass method, signal-to-noise = 1. The degree of polymerization shown is 23.

ii. Ni(dppp)Cl₂ (the following takes place in the glovebox until noted)

P3DT stock solution: In a 20 mL vial, P3DT (M_n by MALDI-TOF/MS = 3861.530 g/mol – repeat unit 222.41 g/mol, 67.4 mg) was dissolved in THF (15.2 mL) with mild heating (40–60 °C for 2 min) for an overall concentration of 0.02 M relative to the monomer repeat unit.

Vial preparation:

End-capping experiment vial: To a 20 mL vial equipped with a stirbar was added Ni(dppp)Cl₂ (1.8 mg, 0.0033 mmol, 1.0 equiv), 5,5'-dibromo-2,2'-bithiophene (53.8 mg, 0.166 mmol, 50.0 equiv), P3DT (2.89 mL, 0.0033 mmol – relative to average M_n , 1.0 equiv), and THF (15.66 mL).

End-capping experiment control (capping agent only) vial: To a 20 mL vial equipped with a stirbar was added Ni(dppp)Cl₂ (1.8 mg, 0.0033 mmol, 1.0 equiv), P3DT (2.89 mL, 0.0033 mmol – relative to average M_n , 1.0 equiv), and THF (15.66 mL).

Experiments:

p-Toluenemagnesium chloride (0.26 M in THF, 153 μL, 0.0398 mmol, 12.0 equiv) was added to each vial. The reactions were stirred for 18 h at rt before quenching outside of the glovebox with aq. HCl (12 M, 1 mL). Then, the organic layer was extracted with CHCl₃ (3 x 1 mL). Samples were worked up for MALDI-TOF/MS (see general experimental).

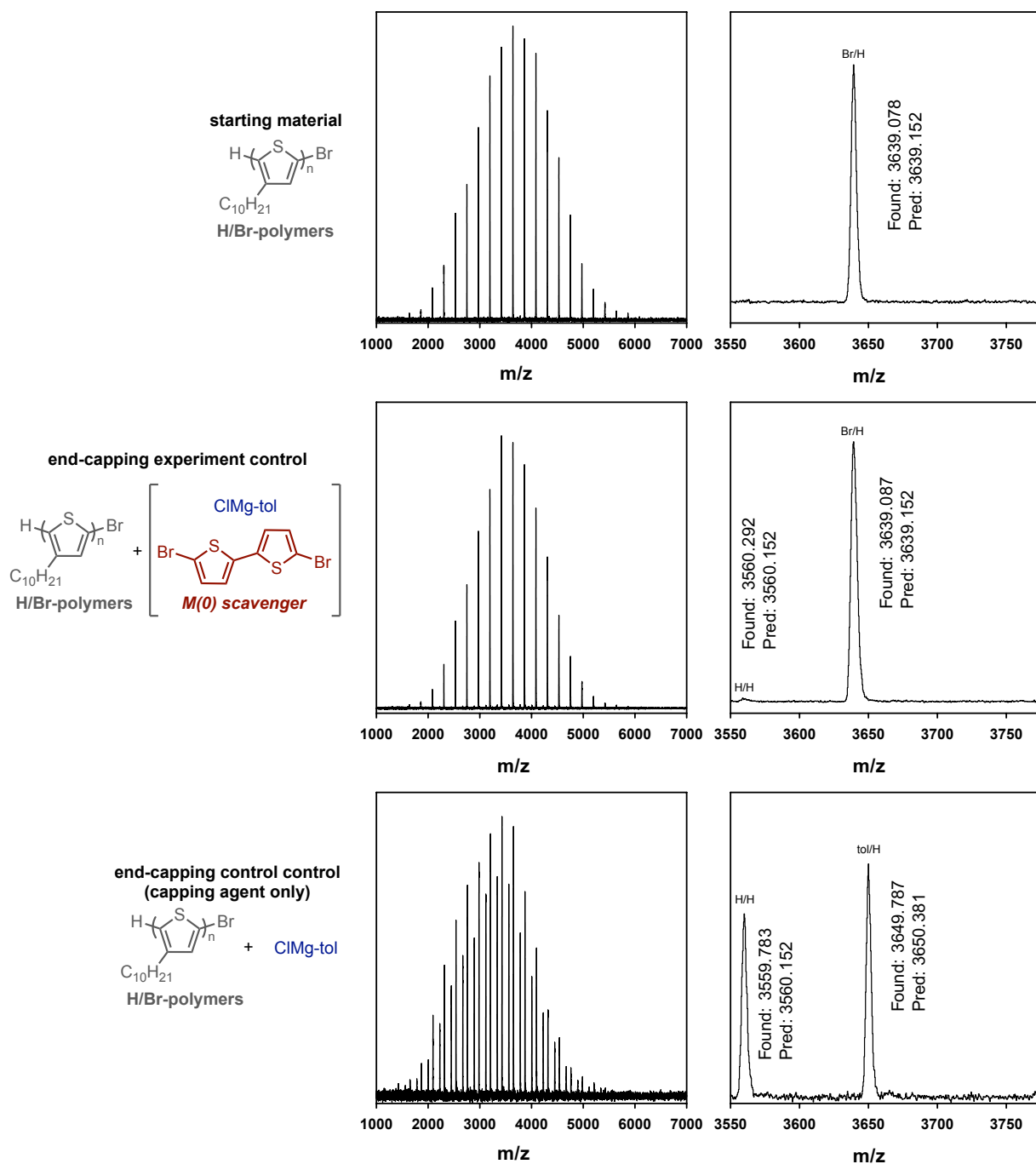
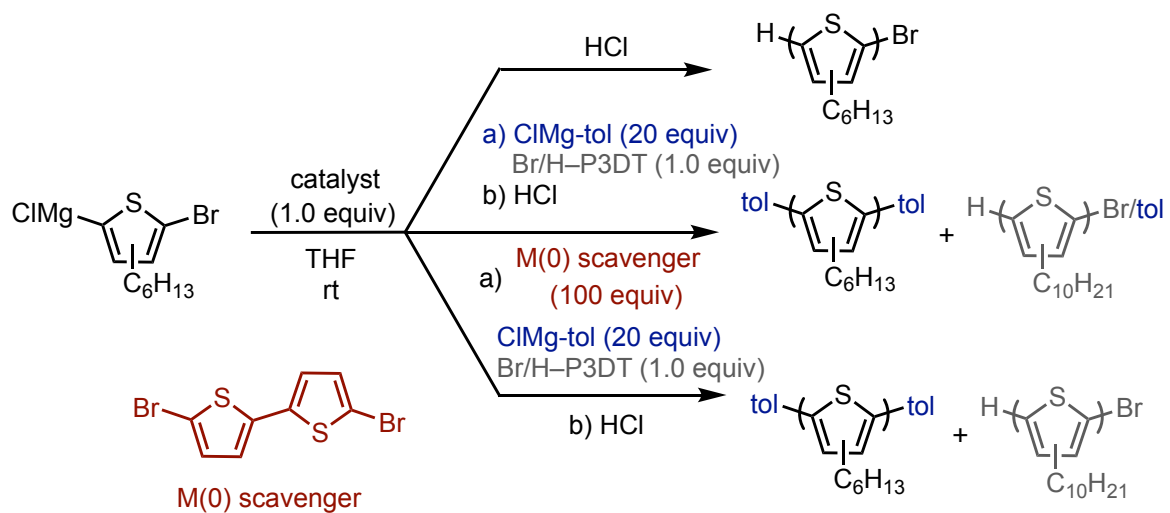
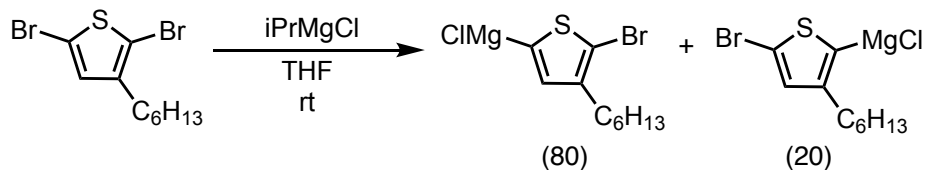


Figure A1-11. MALDI-TOF/MS spectra from end-capping control reactions for P3DT and Ni(dppp)Cl₂. Calculated using an average mass method, signal-to-noise = 2. The degree of polymerization shown is 16.

A1.5.4. End-capping cross-over experiments to evaluate the impact of chain-entanglement for P3AT (A = alkyl).





Monomer activation: In a glovebox, iPrMgCl (2.2 M in THF, 92.6 μ L, 0.204 mmol, 0.800 equiv) was added to a stirring solution of DB3HT (83.0 mg, 0.255 mmol, 1.00 equiv) in THF (2.46 mL) and stirred for 30 min at rt.

Precatalysts:

Ni(IPr)(PPh₃)Cl₂: Ni(IPr)(PPh₃)Cl₂ (7.2 mg, 0.0092 mmol) was weighed into a 4 mL vial and dissolved in THF (0.92 mL) for an overall concentration of 0.01 M.

Pd(IPr)(3-Clpy)Cl₂: Pd(IPr)(3-Clpy)Cl₂ (7.0 mg, 0.010 mmol) was weighed into a 4 mL vial and dissolved in THF (1.0 mL) for an overall concentration of 0.01 M.

Ni(dppp)Cl₂: Ni(dppp)Cl₂ (6.0 mg, 0.011 mmol) was weighed into a 4 mL vial with a stirbar.

Br/H-P3DT solution: Br/H-P3DT (average molecular weight by MALDI-TOF/MS = 2527.179 g/mol, 6.2 mg, 0.0025 mmol) was dissolved in THF (6.24 mL) for an overall 0.0004 M concentration.

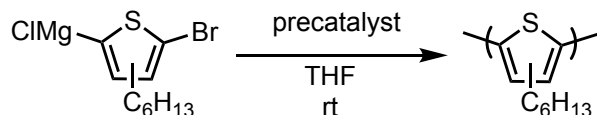
M(0) scavenger stock solution: 5,5'-Dibromo-2,2'-bithiophene (23.2 mg, 0.0716 mmol) was dissolved in THF (2.86 mL) in a 4 mL vial for an overall concentration of 0.025 M.

End-capping cross-over experiment vials:

End-capping cross-over experiment vials: *p*-Toluenemagnesium chloride (0.26 M in THF, 15.4 μ L, 0.0040 mmol, 20. equiv), 5,5'-dibromo-2,2'-bithiophene (0.025 M in THF, 0.80 mL, 0.020 mmol, 100 equiv), Br/H-P3DT (0.0004 M in THF, 0.50 mL, 0.0002 mmol, 1.0 equiv), and THF (0.36 mL) were added to a 4 mL vial equipped with a stirbar.

End-capping cross-over control (only capping agent) vial: *p*-Toluenemagnesium chloride (0.26 M in THF, 15.4 μ L, 0.0040 mmol, 20. equiv), Br/H-P3DT (0.0004 M in THF, 0.50 mL, 0.0002 mmol, 1.0 equiv), and THF (1.16 mL) were combined in a 4 mL vial equipped with a stirbar.

Polymerizations:



Polymerization procedure for precatalyst Ni(IPr)(PPh₃)Cl₂: In a glovebox, to a 20 mL vial equipped with a stirbar was added THF (3.41 mL), Grignard monomer solution (0.080 M in THF, 0.50 mL, 0.040 mmol, 25 equiv), and precatalyst (0.01 M in THF, 0.160 mL, 0.00160 mmol, 1.00 equiv) and stirred at rt for 5 min.

Polymerization procedure for precatalyst Pd(IPr)(3-Clpy)Cl₂: In a glovebox, to a 20 mL vial equipped with a stirbar was added THF (3.41 mL), Grignard monomer solution (0.080 M in THF, 0.50 mL, 0.040 mmol, 25 equiv), and precatalyst (0.01 M in THF, 0.160 mL, 0.00160 mmol, 1.00 equiv) and stirred at rt for 15 min.

Preinitiating precatalyst Ni(dppp)Cl₂: In a glovebox, Grignard monomer solution (0.080 M in THF, 0.55 mL, 0.044 mmol, 4.0 equiv) was added to the 4 mL vial containing precatalyst Ni(dppp)Cl₂ (6.0 mg, 0.011 mmol, 1.0 equiv) and a stirbar. Dissolving the precatalyst within 60 s.

Polymerization procedure for precatalyst Ni(dppp)Cl₂: In a glovebox, to a 20 mL vial equipped with a stirbar was added THF (3.34 mL), Grignard monomer solution (0.080 M in THF, 0.50 mL, 0.040 mmol, 26 equiv), and preinitiated-precatalyst (0.02 M in THF, 0.0769 mL, 0.00154 mmol, 1.00 equiv) and stirred at rt for 30 min.

In situ end-capping: After the designated time, aliquots of the polymerization solution (1.0 mL each containing 0.00040 mmol catalyst, 1.0 equiv) for the i) end-capping cross-over experiment and ii) end-capping cross-over control (capping agent only) reactions. The remaining polymerization solution was removed from the glovebox, quenched with aq. HCl (12 M, 1 mL), and worked up for analysis GC, GPC, and MALDI-TOF/MS analysis (see general experimental). The end-capping experiment/control reactions stirred for 1 h before quenching outside the glovebox with aq. HCl (12 M, 1 mL) and working up for GPC and MALDI-TOF/MS.

Table A1-3. GC data from the polymerization of P3HT before end-capping cross-over experiments via Ni(IPr)(PPh₃)Cl₂, Pd(IPr)(3-Clpy)Cl₂, and Ni(dppp)Cl₂. Initial ratio of Grignard isomers is 4:1 (major:minor).

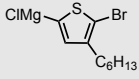
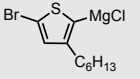
	 (% conv.)	 (% conv.)
Ni(IPr)(PPh₃)Cl₂	quant.	quant.
Pd(IPr)(3-Clpy)Cl₂	quant.	65%
Ni(dppp)Cl₂	71%	0%

Table A1-4. *M_n* and Đ from P3HT (before end-capping cross-over experiments), end-capping cross-over experiment (ec), and end-capping cross-over control (only capping agent) experiments via Ni(IPr)(PPh₃)Cl₂, Pd(IPr)(3-Clpy)Cl₂, and Ni(dppp)Cl₂.

Ni(IPr)(PPh ₃)Cl ₂	<i>M_n</i> (kg/mol)	Đ	Pd(IPr)(3-Clpy)Cl ₂	<i>M_n</i> (kg/mol)	Đ	Ni(dppp)Cl ₂	<i>M_n</i> (kg/mol)	Đ
P3HT	5.24	1.22	P3HT	5.25	1.21	P3HT	7.68	1.11
cap only	4.65	1.39	cap only	6.48	1.21	cap only	6.10	1.29
ec	6.13	1.28	ec	7.23	1.23	ec	8.15	1.35

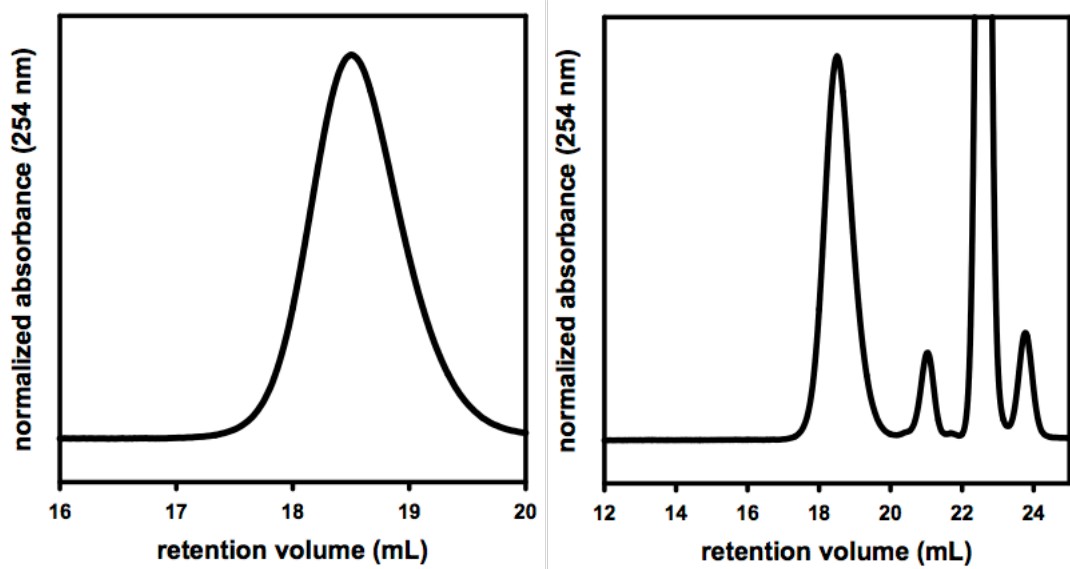


Figure A1-12. GPC traces from added Br/H-P3DT (left = zoomed, right = full GPC trace of the set of samples). Note that residual monomer elute from 20.5–22 min, PhMe elutes at 23.1 min and BHT elutes at 23.8 min. $M_n = 4.09$ kg/mol, $\bar{D} = 1.21$.

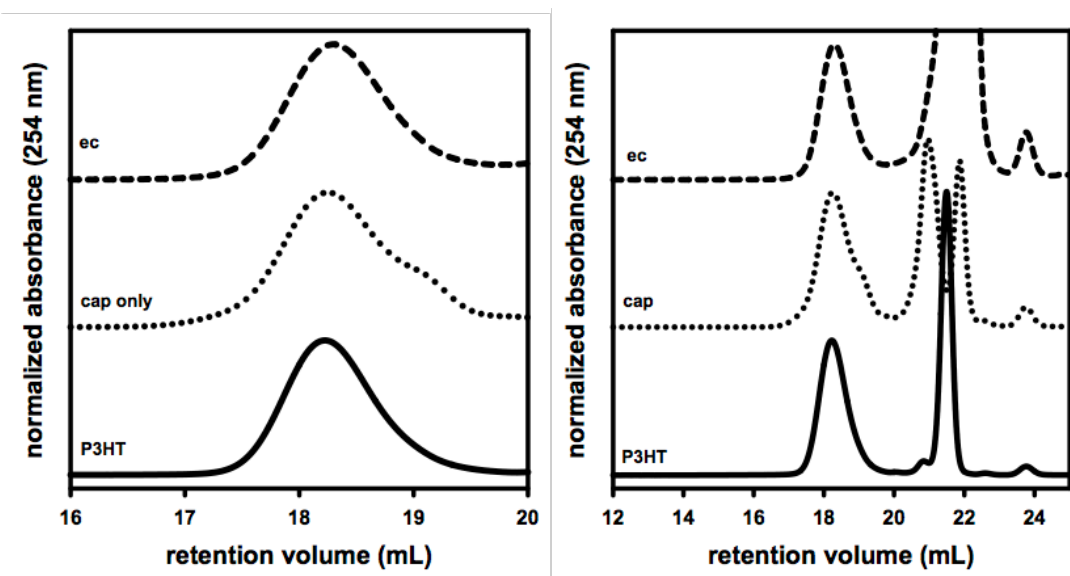


Figure A1-13. GPC traces from P3HT (before end-capping cross-over experiments), end-capping cross-over experiment (ec), and end-capping cross-over control (only capping agent) experiments via $\text{Ni}(\text{IPr})(\text{PPh}_3)\text{Cl}_2$. (left = zoomed, right = full GPC trace of the set of samples). Note that $M(0)$ scavenging agent and residual monomer elute from 20.5–22 min, PhMe elutes at 23.1 min and BHT elutes at 23.8 min.

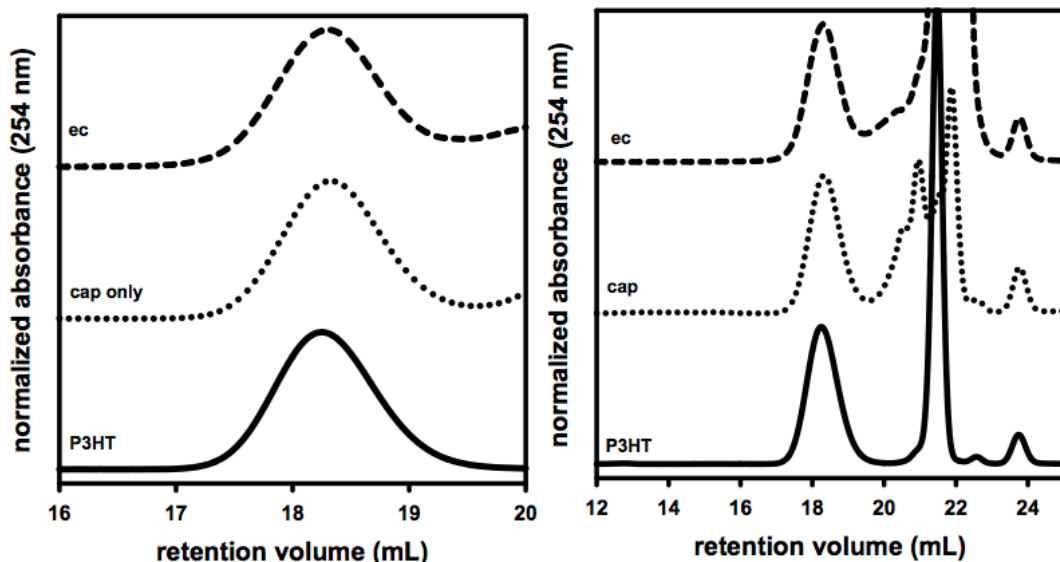


Figure A1-14. GPC traces from P3HT (before end-capping cross-over experiments), end-capping cross-over experiment (ec), and end-capping cross-over control (only capping agent) experiments via $\text{Pd}(\text{IPr})(3\text{-Clpy})\text{Cl}_2$. (left = zoomed, right = full GPC trace of the set of samples). Note that $\text{M}(0)$ scavenging agent and residual monomer elute from 20.5–22 min, PhMe elutes at 23.1 min and BHT elutes at 23.8 min.

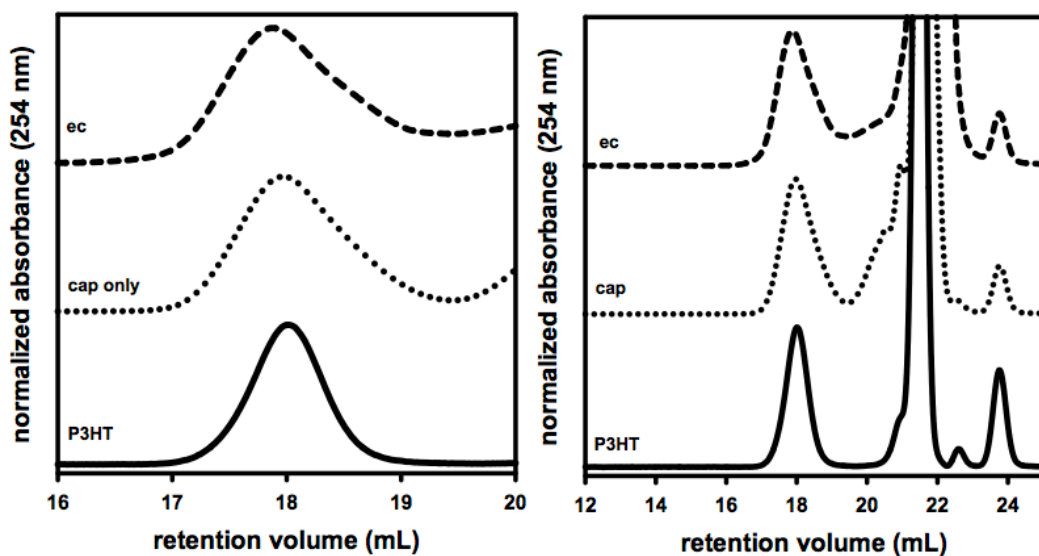


Figure A1-15. GPC traces from P3HT (before end-capping cross-over experiments), end-capping cross-over experiment (ec), and end-capping cross-over control (only capping agent) experiments via $\text{Ni}(\text{dppp})\text{Cl}_2$. (left = zoomed, right = full GPC trace of the set of samples). Note that $\text{M}(0)$ scavenging agent and residual monomer elute from 20.5–22 min, PhMe elutes at 23.1 min and BHT elutes at 23.8 min.

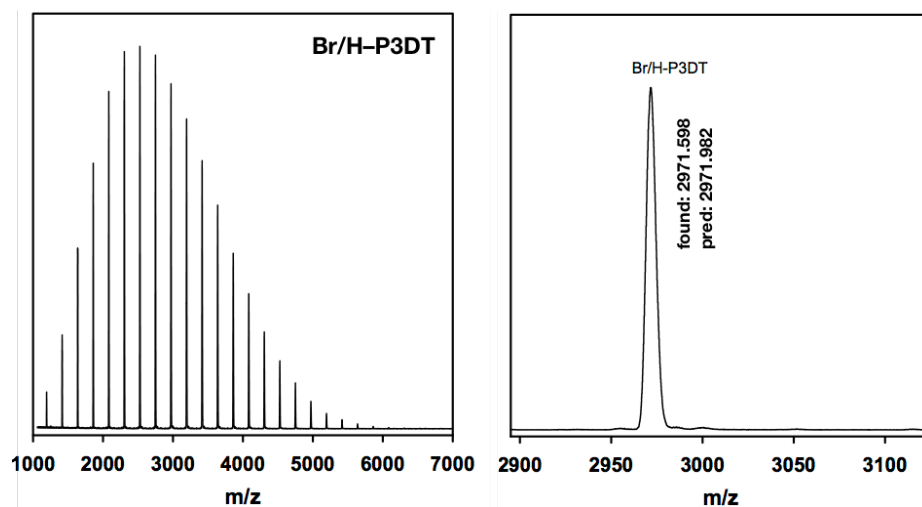


Figure A1-16. MALDI-TOF/MS traces from the added Br/H-P3DT. Values calculated using average mass method at signal-to-noise = 1. The degree of polymerization shown is 13.

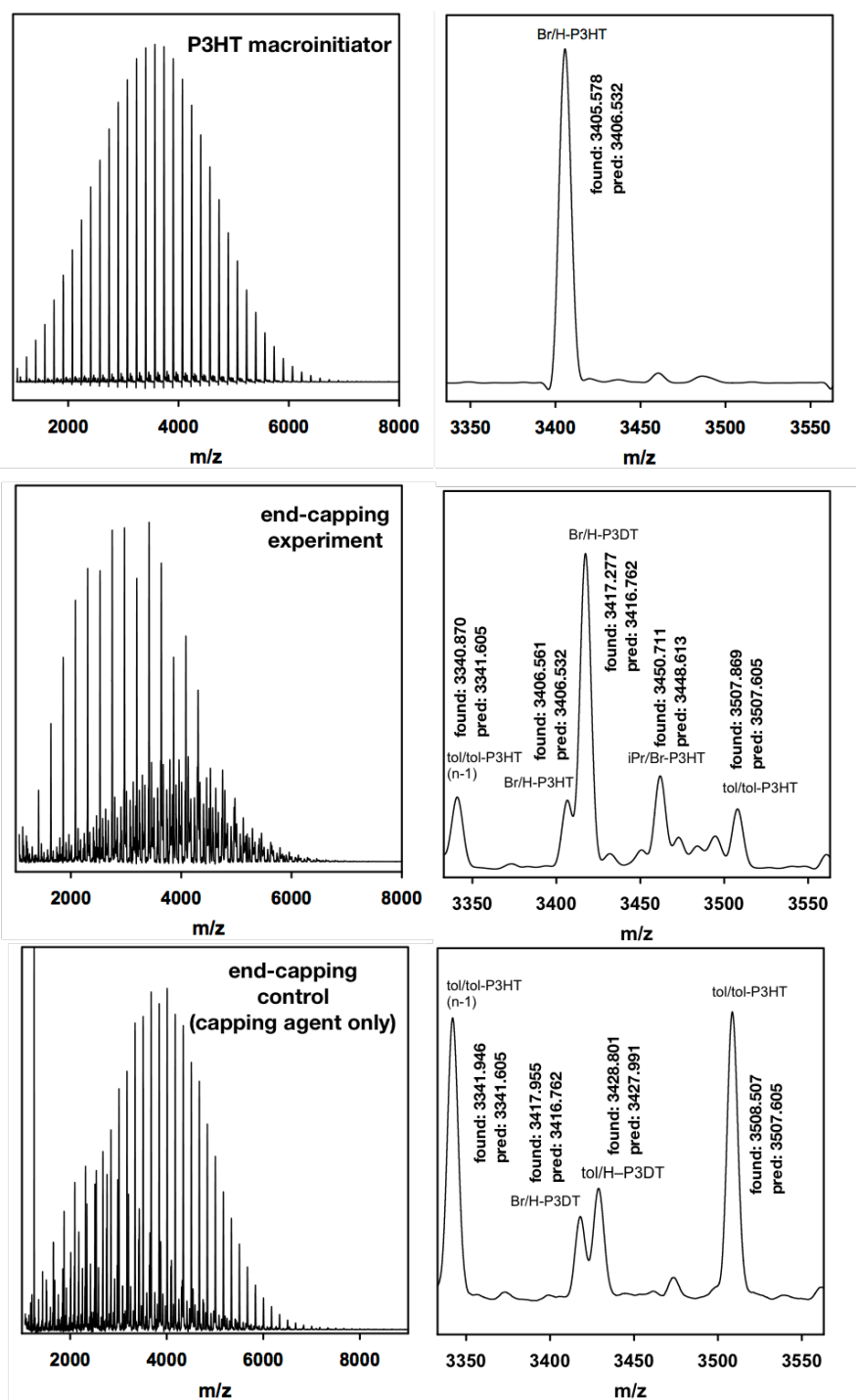


Figure A1-17. MALDI-TOF/MS traces from P3HT macroinitiator (before end-capping), end-capping cross-over experiment, and end-capping cross-over control (only capping agent) experiments for Ni(IPr)(PPh₃)Cl₂. Values calculated using average mass method, nd = not detected at signal-to-noise = 1. The degrees of polymerization shown are 20 and 21 for P3HT and 15 for P3DT.

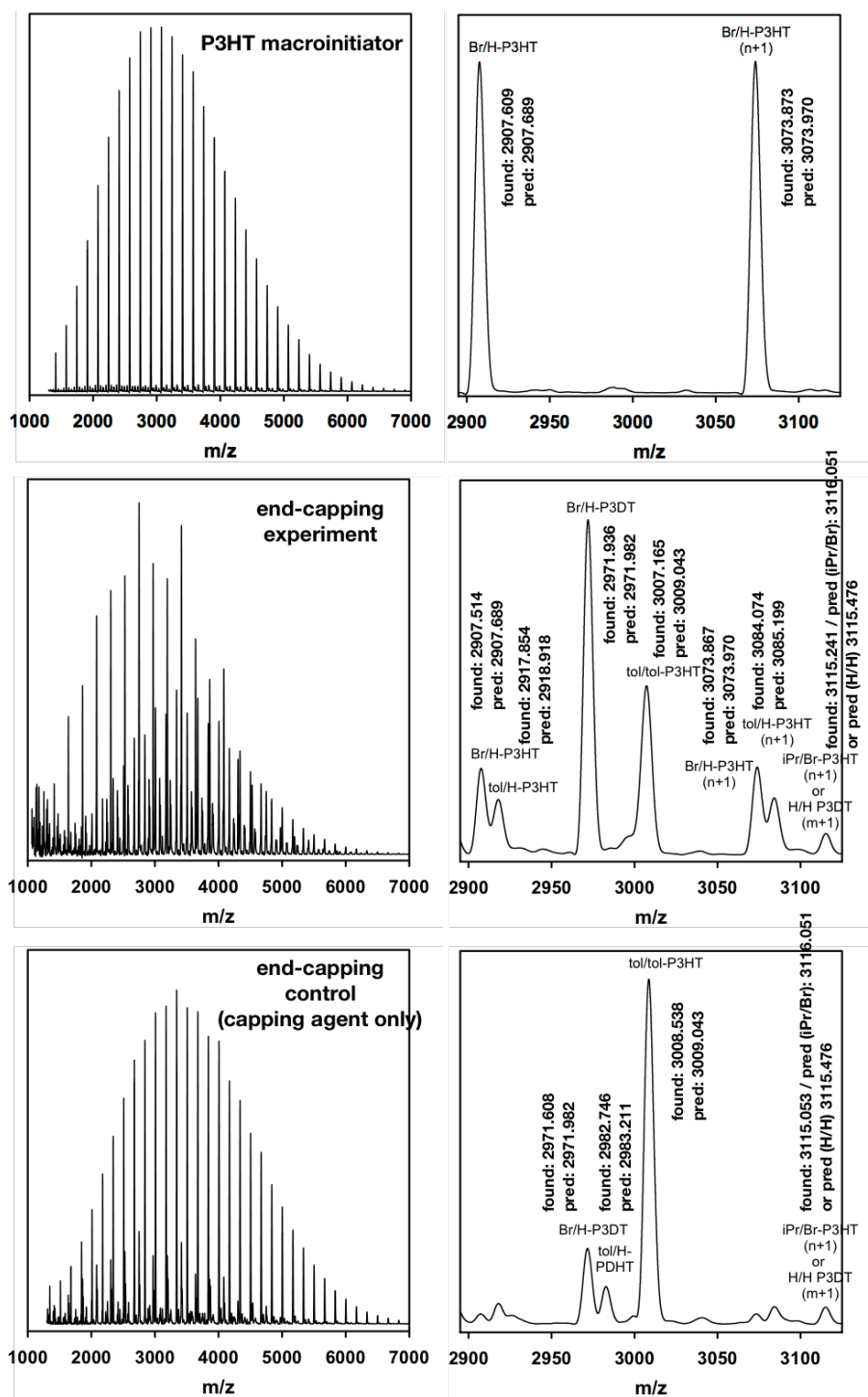
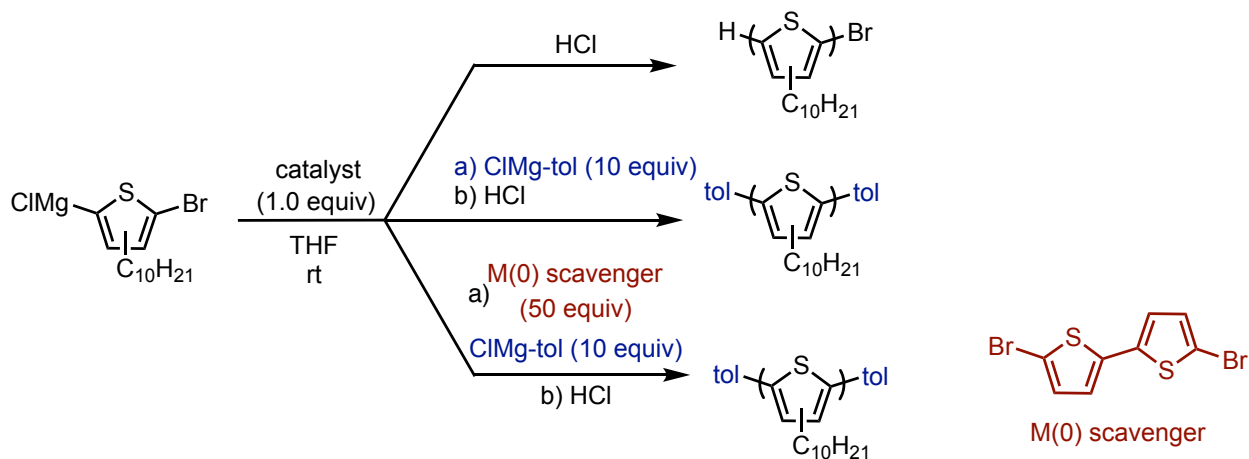


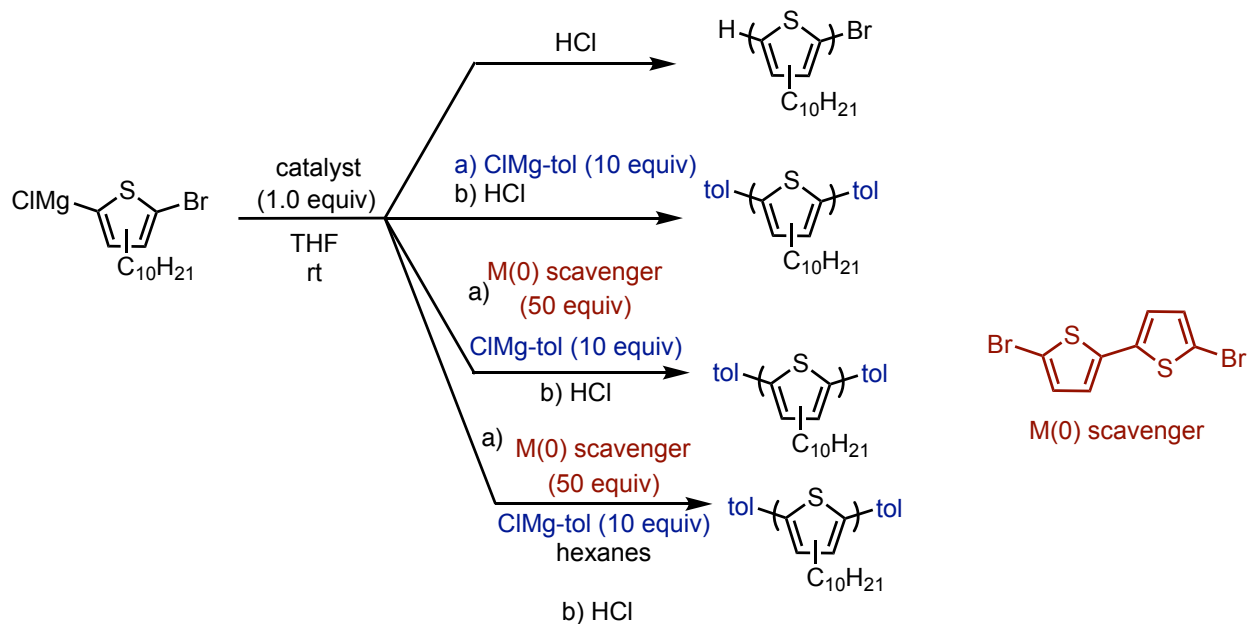
Figure A1-18. MALDI-TOF/MS traces from P3HT macroinitiator (before end-capping), end-capping cross-over experiment, and end-capping cross-over control (only capping agent) experiments for Pd(IPr)(3-Clpy)Cl₂. Values calculated using average mass method at signal-to-noise = 1. The degrees of polymerization shown are 18 and 19 for P3HT and 13 for P3DT.

A1.5.5 End-capping reactions

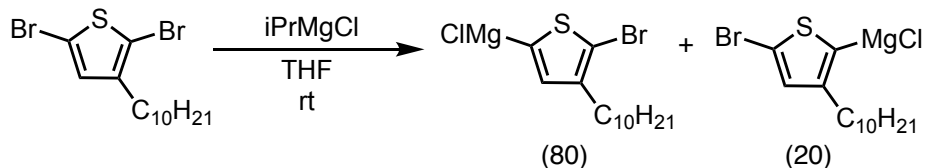
- i. Ni(IPr)(PPh₃)Cl₂ (2 iterations of end-capping conditions)
- ii. Pd(IPr)(3-Clpy)Cl₂ (18 h end-capping and multiple iterations of end-capping conditions)
- iii. Ni(dppp)Cl₂ (1 h and 18 h end-capping)



- iv. Evaluating the effect of solvent (hexane) on end-capping experiments



i. General procedure for Ni(IPr)(PPh₃)Cl₂ (2 iterations of end-capping conditions)



Monomer activation: In a glovebox, iPrMgCl (2.0 M in THF, 0.0774 mL, 0.155 mmol, 0.800 equiv) was added to a stirring solution of DB3DT (74.0 mg, 0.194 mmol, 1.00 equiv) and C₂₂H₄₆ (~2 mg, as an internal standard) in THF (1.86 mL) and stirred for 30 min at rt.

Preparing stock solutions:

Precatalyst stock solution: To a 4 mL vial was added Ni(IPr)(PPh₃)Cl₂ (3.5 mg, 0.0045 mmol) and THF (0.45 mL) for an overall concentration of 0.01 M.

M(0) scavenger stock solution: To a 4 mL vial was added 5,5'-dibromo-2,2'-bithiophene (25.5 mg, 0.0787 mmol) and THF (3.15 mL) for an overall concentration of 0.025 M.

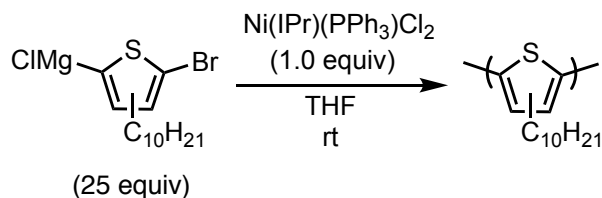
Experiment vials:

(equiv are relative to the catalyst/polymer (1.0 equiv) that will be added to each vial)

End-capping experiment – iteration 1 (**ec1**): p-Toluenemagnesium chloride (0.28 M in THF, 14 μL, 10. equiv, 0.0039 mmol), 5,5'-dibromo-2,2'-bithiophene (0.025 M in THF, 0.020 mmol, 0.79 mL, 50. equiv) and THF (0.36 mL)

End-capping experiment – iteration 2 (**ec2**): 5,5'-Dibromo-2,2'-bithiophene (0.025 M in THF, 0.364 mL, 0.0091 mmol, 50.0 equiv) and p-toluenemagnesium chloride (0.28 M in THF, 6.5 μL, 0.0018 mmol, 10. equiv)

End-capping experiment control (capping agent only): p-Toluenemagnesium chloride (0.28 M in THF, 14 μ L, 10. equiv, 0.0039 mmol) and THF (1.16 mL)



Polymerization: Freshly prepared Grignard monomer (0.08 M in THF, 0.50 mL, 0.040 mmol, 25 equiv) was diluted with THF (3.41 mL) in a 4 mL vial equipped with a stirbar. Then, precatalyst stock solution (0.01 M in THF, 0.16 mL, 0.0016 mmol, 1.0 equiv) was added and the polymerizations ran for 5 min at rt. Then, two aliquots (1.0 mL, containing 0.00039 mmol catalyst) were removed and added to a stirring 4 mL vial for i) end-capping experiment (**ec1**) or ii) end-capping experiment control (capping agent only). An aliquot of the remaining polymer solution (0.5 mL) was immediately removed from the glovebox and quenched with aq. HCl (12 M, 1 mL).

In situ end-capping: After 1 h, an aliquot (1.0 mL, 0.00018 mmol, 1.0 equiv catalyst) of the end-capping experiment (**ec1**) was added to a 4 mL vial containing second iteration of end-capping conditions (**ec2**), which was stirred for an additional hour. The remaining end-capping experiment –iteration 1 (**ec1**) was immediately quenched outside the glovebox with aq. HCl (12 M, 1 mL) and worked up for GPC and MALDI-TOF/MS. After a total time of 125 min (from the precatalyst initiation time zero) the remaining polymer solution, end-capping experiment (**ec2**) and end-capping control were quenched outside the glovebox with aq. HCl (12 M, 1 mL) and worked up for GC, GPC, MALDI-TOF/MS.

Table A1-5. GC data from the polymerization of P3DT before end-capping experiments via Ni(IPr)(PPh₃)Cl₂. Initial ratio of Grignard isomers is major:minor (4:1).

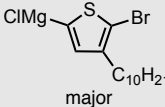
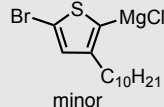
	 major (% conv.)	 minor (% conv.)
Run 1	98	quant.
Run 2	99	99

Table A1-6. M_n and \mathcal{D} from P3DT (before end-capping), end-capping experiment, and end-capping control (only capping agent) experiments for Ni(IPr)(PPh₃)Cl₂ and P3DT.

Run 1	M_n (kg/mol)	\mathcal{D}	Run 2	M_n (kg/mol)	\mathcal{D}
P3DT	8.41	1.16	P3DT	8.89	1.15
cap only	6.65	1.40	cap only	7.70	1.28
ec1	8.65	1.16	ec1*	6.45	1.31
ec2*	6.97	1.32	ec2*	4.42	1.54

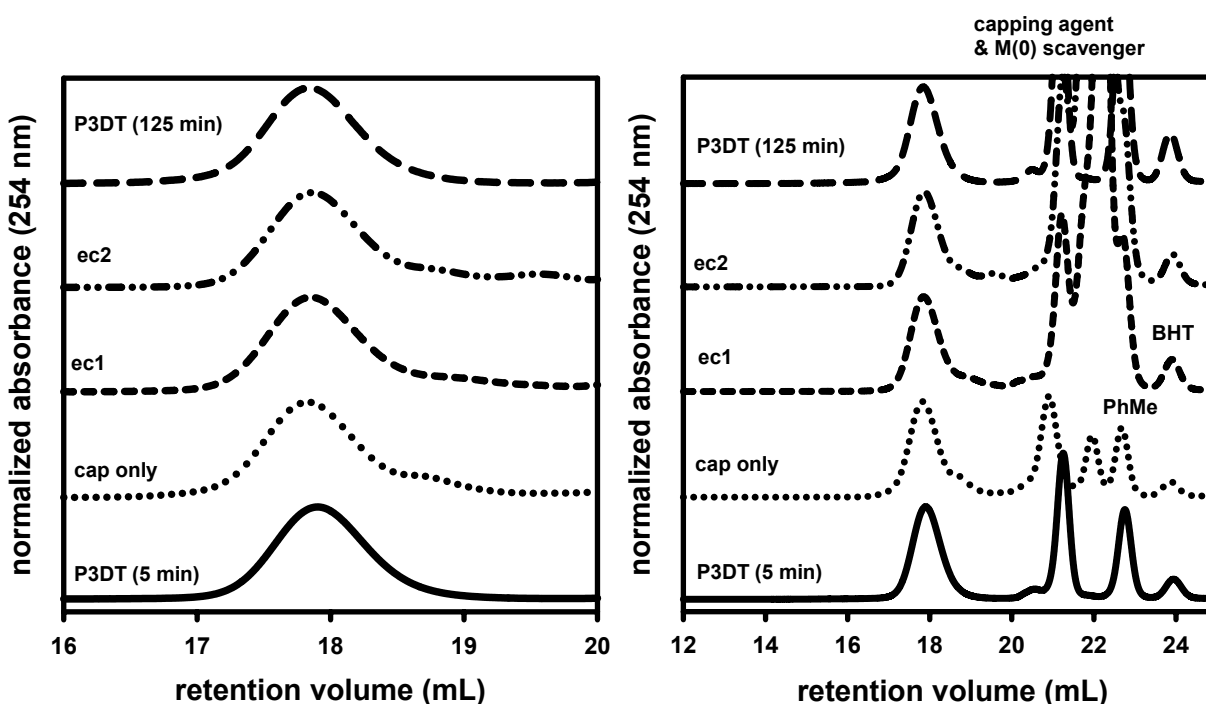


Figure A1-20. GPC traces from P3DT (before end-capping), end-capping experiment, and end-capping control (only capping agent) experiments for Ni(IPr)(PPh₃)Cl₂ and P3DT (left = zoomed, right = full GPC trace from Run 1).

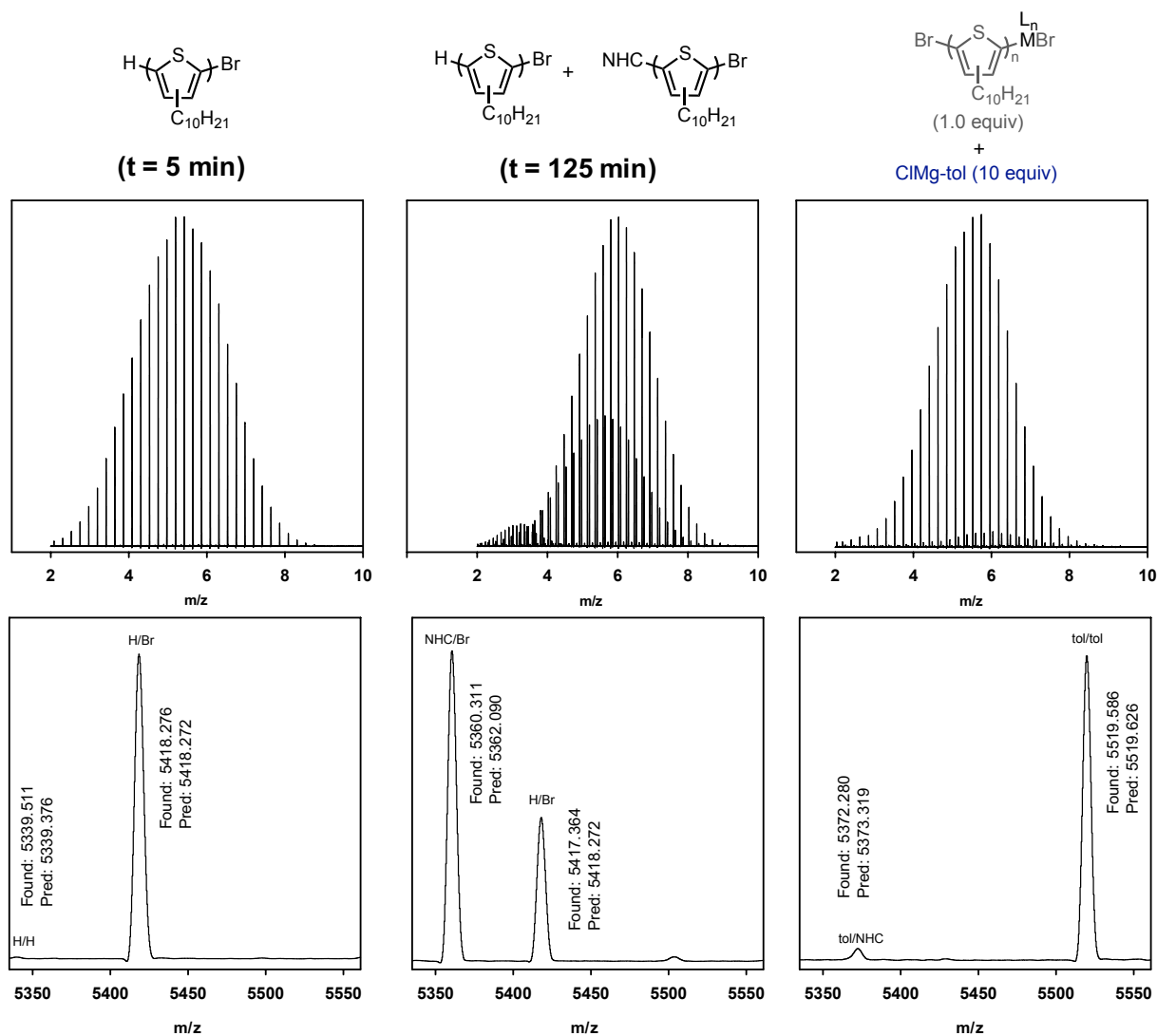


Figure A1-21. MALDI-TOF/MS traces from P3DT (before end-capping $t = 5$ min), P3DT (quenched at the final end-capping experiment quench $t = 125$ min), and end-capping control (only capping agent) experiments for $\text{Ni}(\text{IPr})(\text{PPh}_3)\text{Cl}_2$ and P3DT. Values calculated using average mass method, signal-to-noise = 1. The degree of polymerization shown is 24.

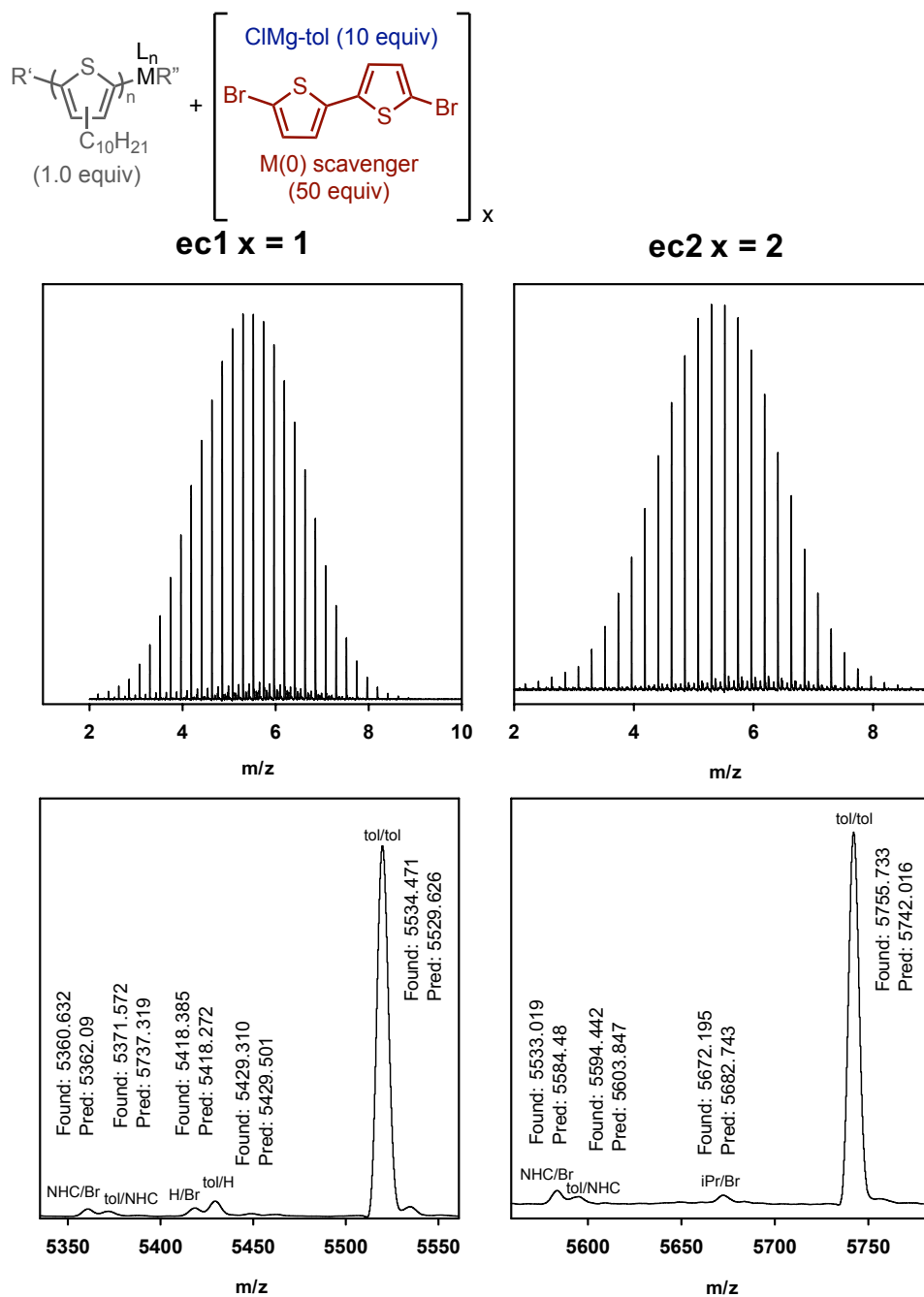
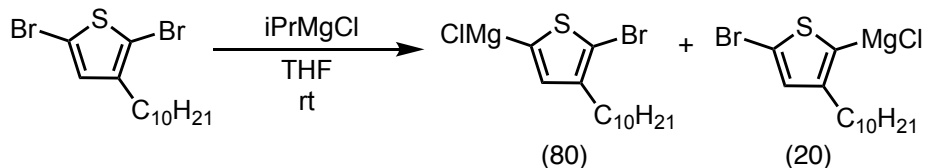


Figure A1-22. MALDI-TOF/MS traces from end-capping experiments (ec1 and ec2) for Ni(IPr)(PPh₃)Cl₂ and P3DT. Values calculated using average mass method, signal-to-noise = 1. The degree of polymerization shown is 24 (left) and 25 (right).

ii. General procedure for Pd(IPr)(3-Clpy)Cl₂ - 18 h end-capping experiments



Monomer activation: In a glovebox, iPrMgCl (2.0 M in THF, 72.2 μ L, 0.144 mmol, 0.800 equiv) was added to a stirring solution of DB3DT (69.0 mg, 0.180 mmol, 1.00 equiv) and C₂₂H₄₆ (~2 mg, as an internal standard) in THF (1.73 mL) and stirred for 30 min at rt.

Preparing stock solutions:

Precatalyst: Pd(IPr)(3-Clpy)Cl₂ (5.4 mg, 0.0079 mmol) was weighed into a 4 mL vial and dissolved in THF (0.79 mL) for an overall concentration of 0.01 M.

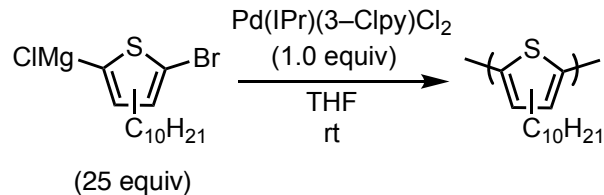
M(0) scavenger: 5,5'-Dibromo-2,2'-bithiophene (14 mg, 0.043 mmol) was dissolved in THF (1.7 mL) in a 4 mL vial for an overall concentration of 0.025 M.

Preparing reaction vials:

(equiv are relative to the catalyst/polymer (1.0 equiv) that will be added to each vial)

End-capping experiment vials: *p*-Toluenemagnesium chloride (0.26 M in THF, 7.7 μ L, 0.0020 mmol, 10. equiv) and 5,5'-dibromo-2,2'-bithiophene (0.025 M in THF, 0.40 mL, 0.010 mmol, 50. equiv) were dissolved in THF (0.18 mL) in an 8 mL vial equipped with a stirbar.

End-capping control (only capping agent) vial: *p*-Toluenemagnesium chloride (0.26 M in THF, 7.7 μ L, 0.0020 mmol, 10. equiv) was dissolved in THF (0.58 mL) in an 8 mL vial equipped with a stirbar.



Polymerization: In a glovebox, to a 4 mL vial equipped with a stirbar was added THF (2.48 mL), Grignard monomer solution (0.080 M in THF, 0.45 mL, 0.036 mmol, 30. equiv), and Pd(IPr)(3-Clpy)Cl₂ (0.01 M in THF, 0.120 mL, 0.00120 mmol, 1.00 equiv) and stirred at rt for 15 min.

In situ end-capping: Aliquots (0.50 mL each containing 0.00020 mmol catalyst, 1.0 equiv) for the i) end-capping experiment and ii) end-capping control (capping agent only) reactions. The remaining polymerization solution was removed from the glovebox, quenched with aq. HCl (12 M, 1 mL), and worked up for analysis GC, GPC, and MALDI-TOF/MS analysis (see general experimental). The end-capping experiment/control reactions stirred for 18 h before quenching outside the glovebox with aq. HCl (12 M, 1 mL) and working up for GC, GPC, MALDI-TOF/MS.

Table A1-7. GC data from the polymerization of P3DT before end-capping experiments via Pd(IPr)(3-Clpy)Cl₂. Initial ratio of Grignard isomers is major:minor (4:1).

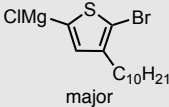
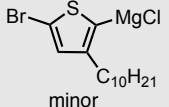
	 major (% conv.)	 minor (% conv.)
Run 1	quant.	quant.
Run 2	quant.	50

Table A1-8. M_n and \bar{D} from P3DT (before end-capping), end-capping experiment (ec), and end-capping control (only capping agent) experiments for Pd(IPr)(3-Clpy)Cl₂ and P3DT.

Run 1	M_n (kg/mol)	\bar{D}	Run 2	M_n (kg/mol)	\bar{D}
P3DT	8.70	1.16	P3DT	6.93	1.22
cap only	8.83	1.19	cap only	6.85	1.18
ec	8.26	1.17	ec	6.67	1.21

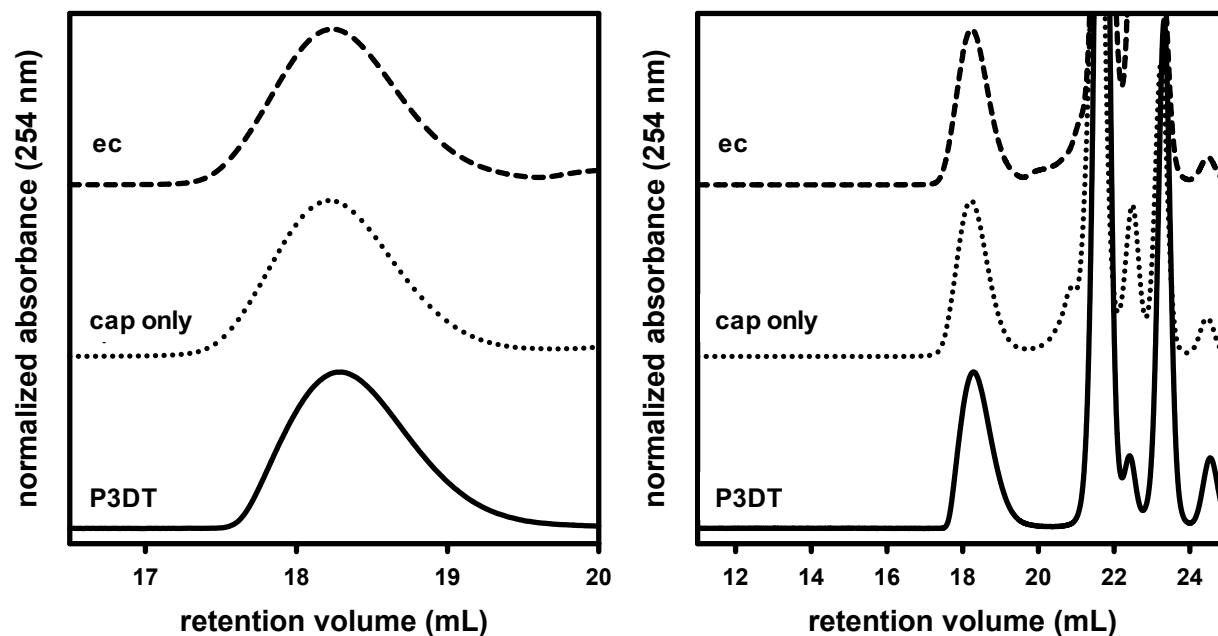


Figure A1-23. GPC traces from P3DT (before end-capping), end-capping experiment (ec), and end-capping control (only capping agent) experiments for Pd(IPr)(3-Clpy)Cl₂ and P3DT t = 18 h. (Left = zoomed, right = full GPC trace from Run 1). Note that M(0) scavenging agent and residual monomer elute from 20.5–22 min, PhMe elutes at 23.1 min and BHT elutes at 23.8 min.

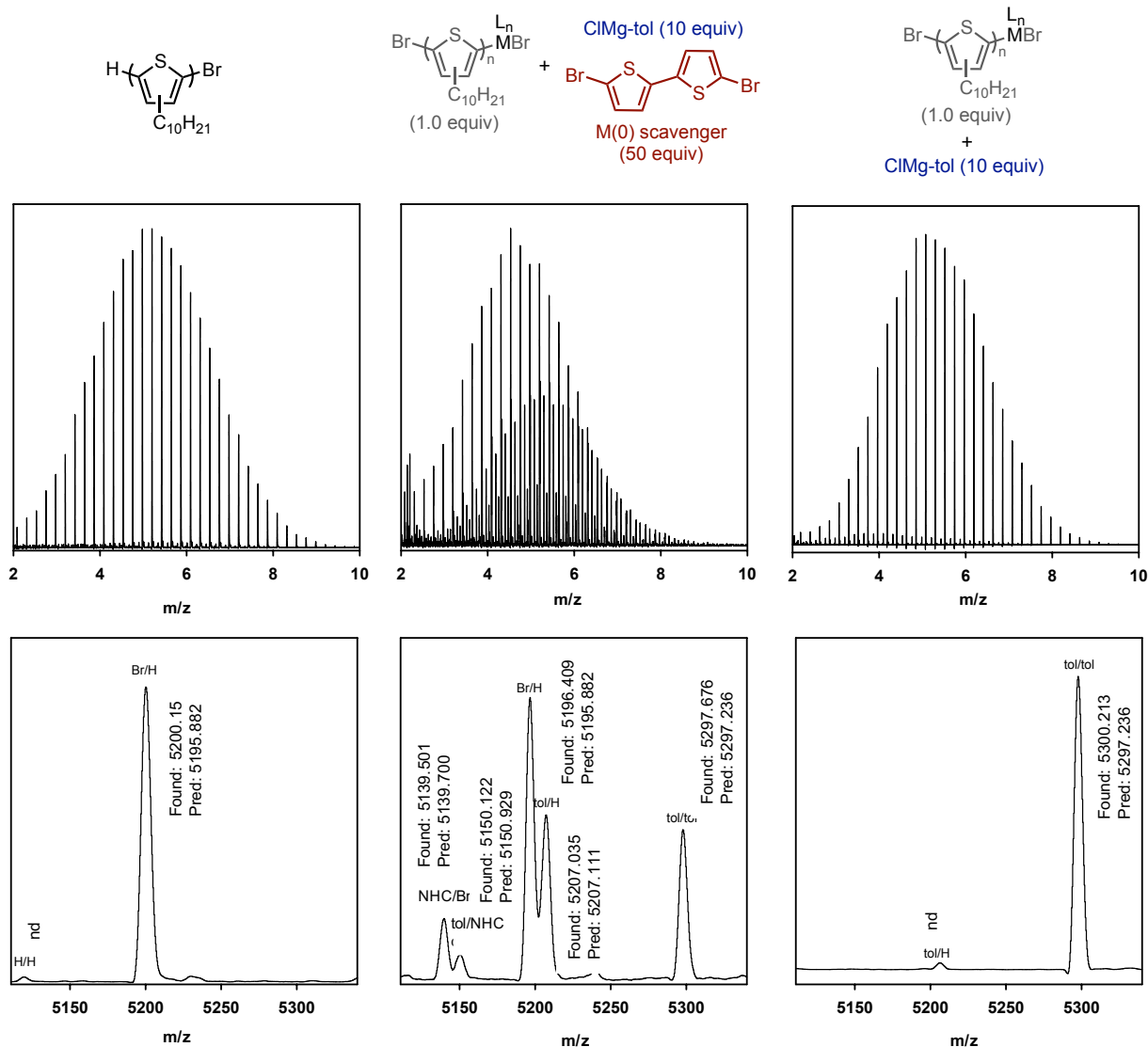
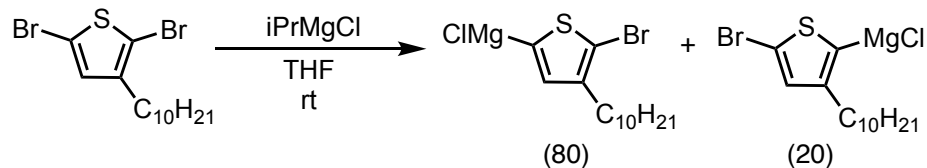


Figure A1-24. MALDI-TOF/MS traces from P3DT (before end-capping), end-capping experiment, and end-capping control (only capping agent) experiments for $Pd(I\text{Pr})(3\text{-Clpy})Cl_2$ and P3DT ($t = 18$ h) from Run 1. Values calculated using average mass method, nd = not detected at signal-to-noise = 2. The degree of polymerization shown is 23.

ii. General procedure for Pd(IPr)(3-Clpy)Cl₂ - multiple iterations of end-capping conditions



Monomer activation: In a glovebox, *i*PrMgCl (2.0 M in THF, 47.3 μ L, 0.0946 mmol, 0.800 equiv) was added to a stirring solution of DB3DT (45.2 mg, 0.118 mmol, 1.00 equiv) and C₂₂H₄₆ (~2 mg, as an internal standard) in THF (1.13 mL) and stirred for 30 min at rt.

Preparing stock solutions:

Precatalyst stock solution: Pd(IPr)(3-Clpy)Cl₂ (13.0 mg, 0.0191 mmol) was weighed into a 4 mL vial and dissolved in THF (1.91 mL) for an overall concentration of 0.01 M.

M(0) scavenger stock solution: 5,5'-Dibromo-2,2'-bithiophene (114.3 mg, 0.3526 mmol) was dissolved in THF (14.11 mL) in a 20 mL vial for an overall concentration of 0.025 M.

Preparing end-capping control/experiment vials:

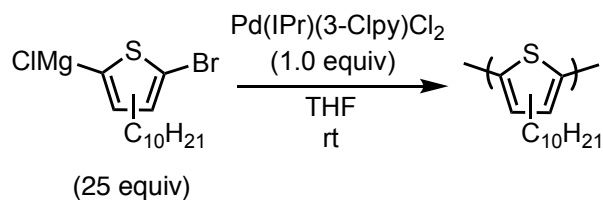
(equiv are relative to the catalyst/polymer (1.0 equiv) that will be added to each vial)

End-capping control (only capping agent) vial: *p*-Toluenemagnesium chloride (0.26 M in THF, 7.7 μ L, 0.0020 mmol, 10. equiv) was dissolved in THF (0.58 mL) in an 8 mL vial equipped with a stirbar.

End-capping experiment vials each equipped with a stirbar:

Table A1-9. Vial preparation for capping/competition experiments with Pd(IPr)(3-Clpy)Cl₂ and P3DT.

vial	<i>p</i>-toluenemagnesium chloride (0.26 M in THF) (μL, mmol) 10.0 equiv	5,5'-dibromo-2,2'- bithiophene (0.025 M in THF) (mL, mmol) 50.0 equiv	prev. soln. added (mL, mmol catalyst added) 1.0 equiv
ec1	46.2, 0.0120	2.4, 0.060 (and 1.08 mL THF)	3 mL orig. polym., 0.0012
ec2	30.8, 0.00801	1.6, 0.04	4.35 mL (of ec1), 0.0008
ec3	20.5, 0.00533	1.06, 0.0265	3.99 mL (of ec2), 0.000533
ec4	13.7, 0.00356	0.71, 0.018	3.38 mL (of ec3), 0.000356
ec5	9.1, 0.0024	0.47, 0.012	2.73 mL (of ec4), 0.000237
ec6	6.1, 0.0016	0.31, 0.0078	2.14 mL (of ec5), 0.000158
ec7	4.1, 0.0011	0.21, 0.0053	1.64 mL (of ec6), 0.000105



Polymerization: In a glovebox, to a 20 mL vial equipped with a stirbar was added THF (3.41 mL), activated monomer solution (0.08 M in THF, 0.50 mL, 0.040 mmol, 25 equiv), and precatalyst Pd(IPr)(3-Clpy)Cl₂ (0.01 M in THF, 0.160 mL, 0.00160 mmol, 1.00 equiv) and stirred at rt for 15 min before taking aliquots (see below for details) for end-capping experiment/control reactions. The remaining solution was removed from the glovebox, quenched with aq. HCl (12 M, 1 mL), and worked up for GC, GPC, and MALDI-TOF/MS analysis.

End-capping control (capping agent only) reaction: An aliquot (0.50 mL, 0.0020 mmol, 1.0 equiv) of the polymerization was added to the end-capping control solution and stirred for 1 h before removing from the glovebox, quenching with aq. HCl (12 M, 1 mL), and working up for analysis GPC and MALDI-TOF/MS analysis.

End-capping experiment reaction: An aliquot (3.0 mL) of the polymerization was moved to the first capping/M(0) scavenging agent solution (ec1, Table S9) and stirred for 1 h. Then, two-thirds of the solution was moved to the subsequent end-capping experiment solution (ec2, Table S9). The remaining mother liquor (of ec1) was immediately removed from the glovebox and quenched with aq. HCl (12 M, 3 mL) and worked up for analysis. This process was repeated for 7 end-capping condition experiment solutions.

Table A1-10. GC data from the polymerization of P3DT before end-capping experiments via Pd(IPr)(3-Clpy)Cl₂. Initial ratio of Grignard isomers is 4:1 (major:minor).

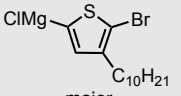
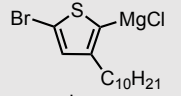
	 major (% conv.)	 minor (% conv.)
Run 1	quant.	75%
Run 2	quant.	76%

Table A1-11. M_n and \bar{D} from the control, capping, and capping/competition experiments for Pd(IPr)(3-Clpy)Cl₂ and P3DT.

Run 1	M_n (kg/mol)	\bar{D}	Run 2	M_n (kg/mol)	\bar{D}
P3DT	7.78	1.19	P3DT	7.83	1.19
cap only	7.73	1.19	cap only	7.86	1.19
ec1	7.71	1.19	ec1	7.78	1.18
ec2	7.79	1.17	ec2	7.66	1.17
ec3	7.83	1.16	ec3	7.61	1.18
ec4	7.70	1.19	ec4	7.65	1.19
ec5	7.46	1.18	ec5	7.45	1.18
ec6	7.70	1.17	ec6	7.78	1.17
ec7	7.61	1.17	ec7	7.70	1.17

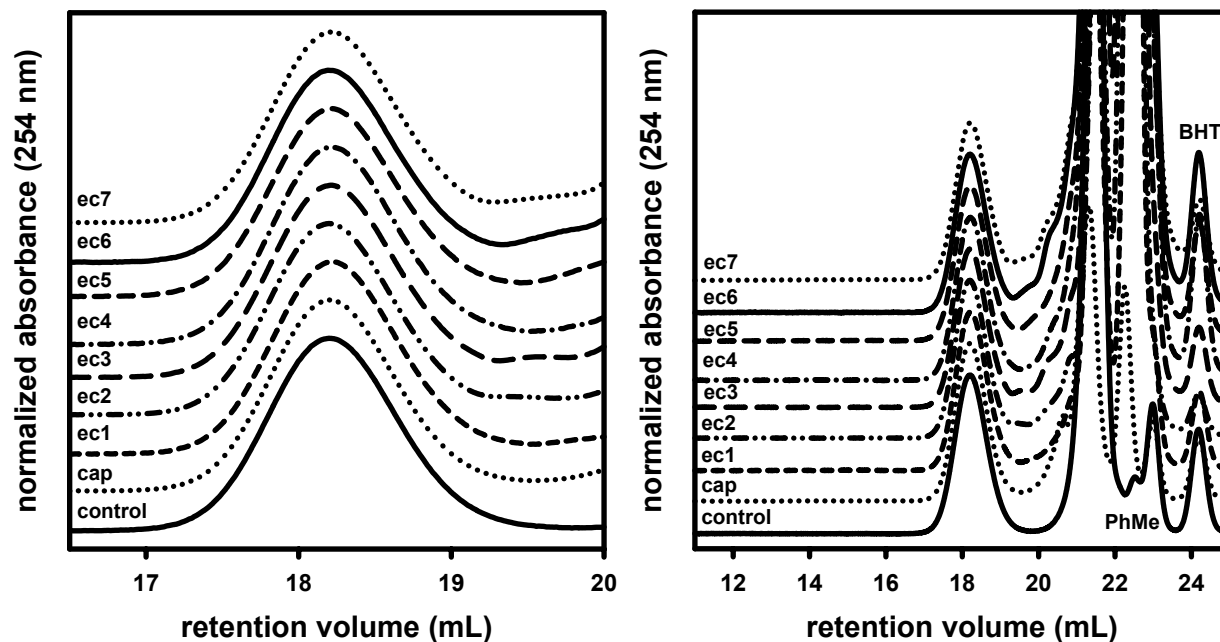


Figure A1-25. GPC traces from the control, end-capping control, and end-capping experiments for Pd(IPr)(3-Clpy)Cl₂ and P3DT. (Left = zoomed, right = full GPC trace from Run 1).

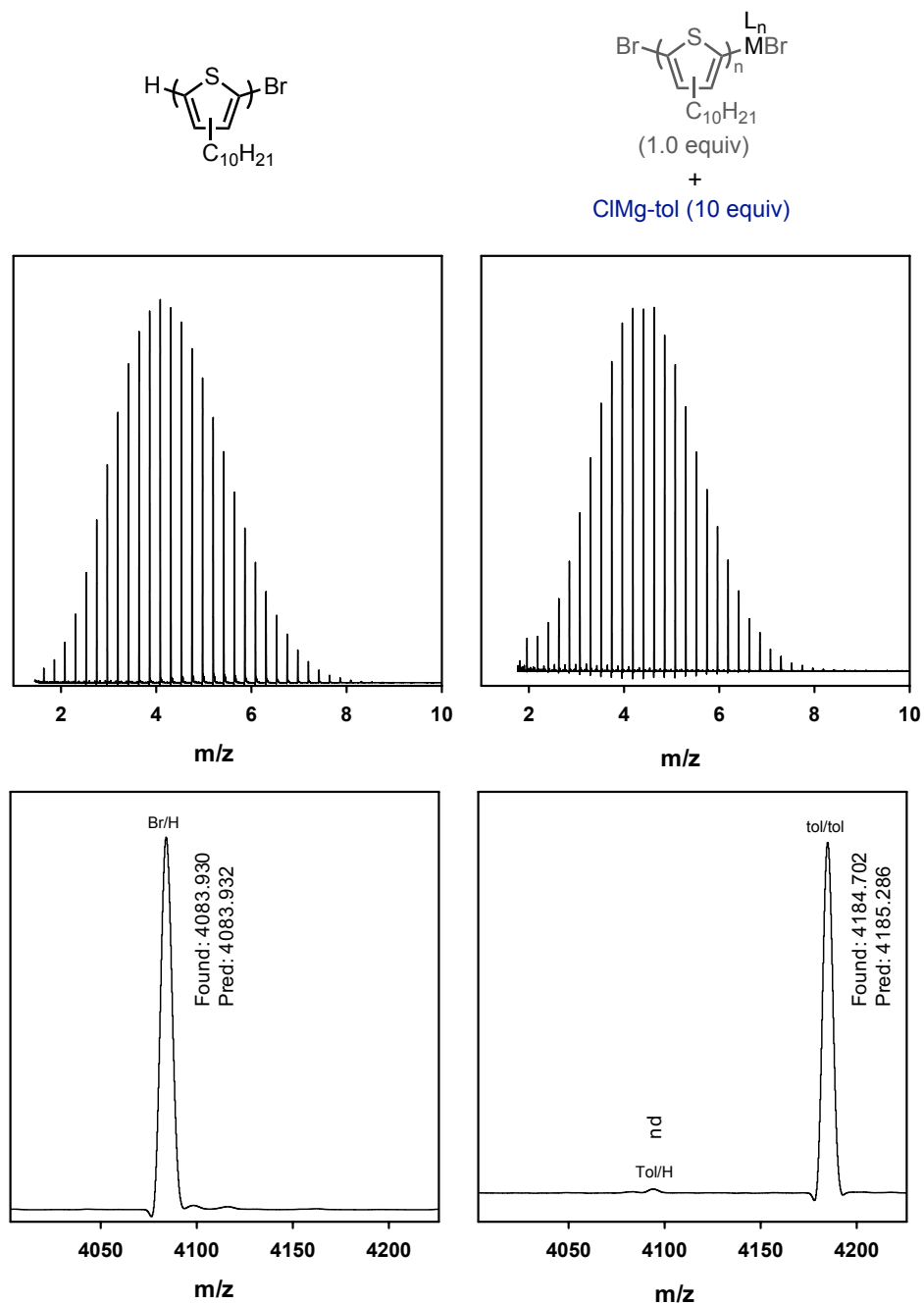


Figure A1-26. MALDI-TOF/MS traces from P3DT (before end-capping) and end-capping control (only capping agent) experiments for $Pd(I\text{Pr})(3\text{-Clpy})Cl_2$ and P3DT from Run 1. Values calculated using an average mass method, nd = not detected at signal-to-noise = 2. The degree of polymerization shown is 18.

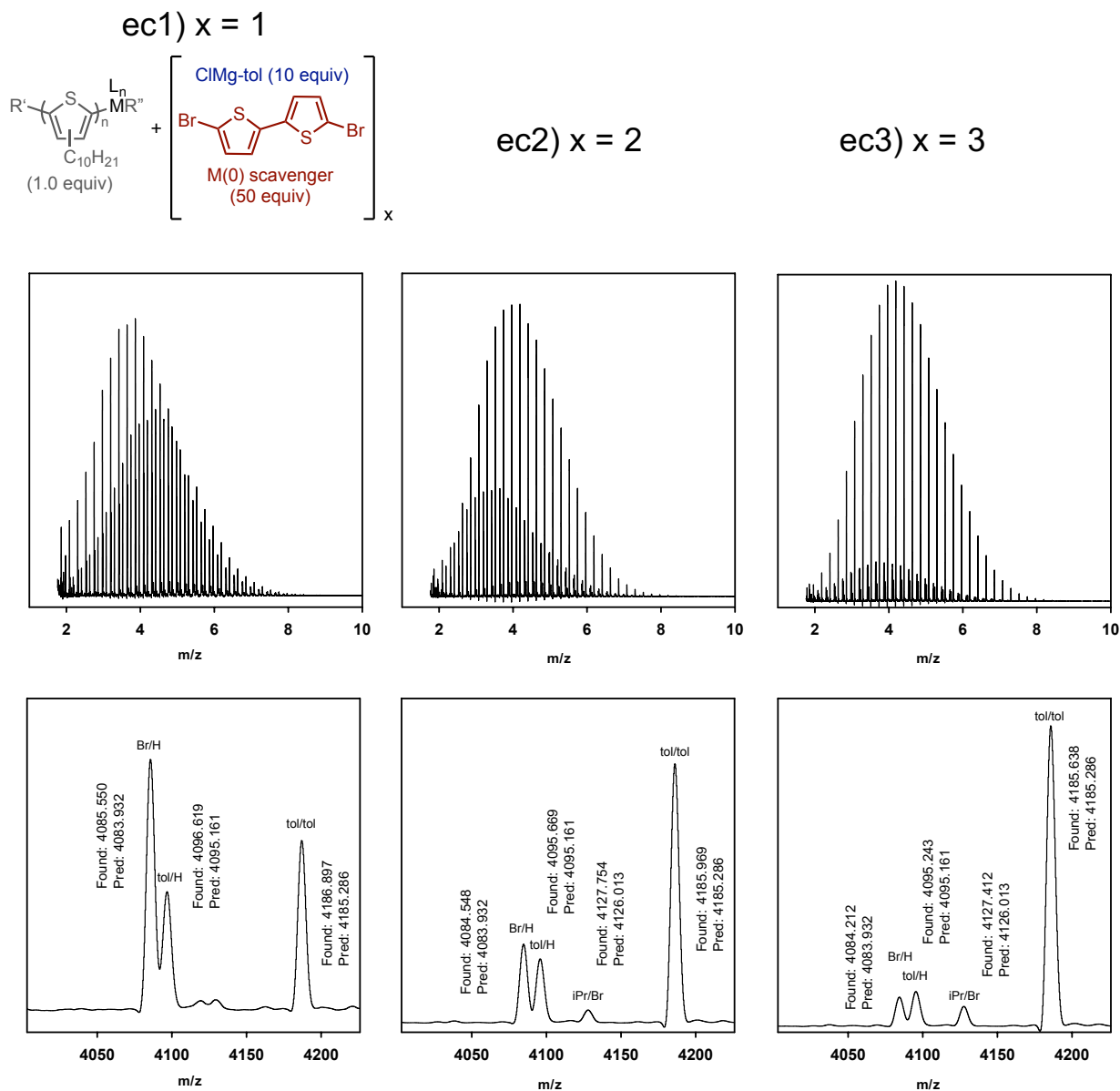


Figure A1-27. MALDI-TOF/MS traces from end-capping experiments (ec1, ec2, and ec3) for $Pd(iPr)(3-Clpy)Cl_2$ and P3DT from Run 1. Values calculated using an average mass method, signal-to-noise = 2. The degree of polymerization shown is 18.

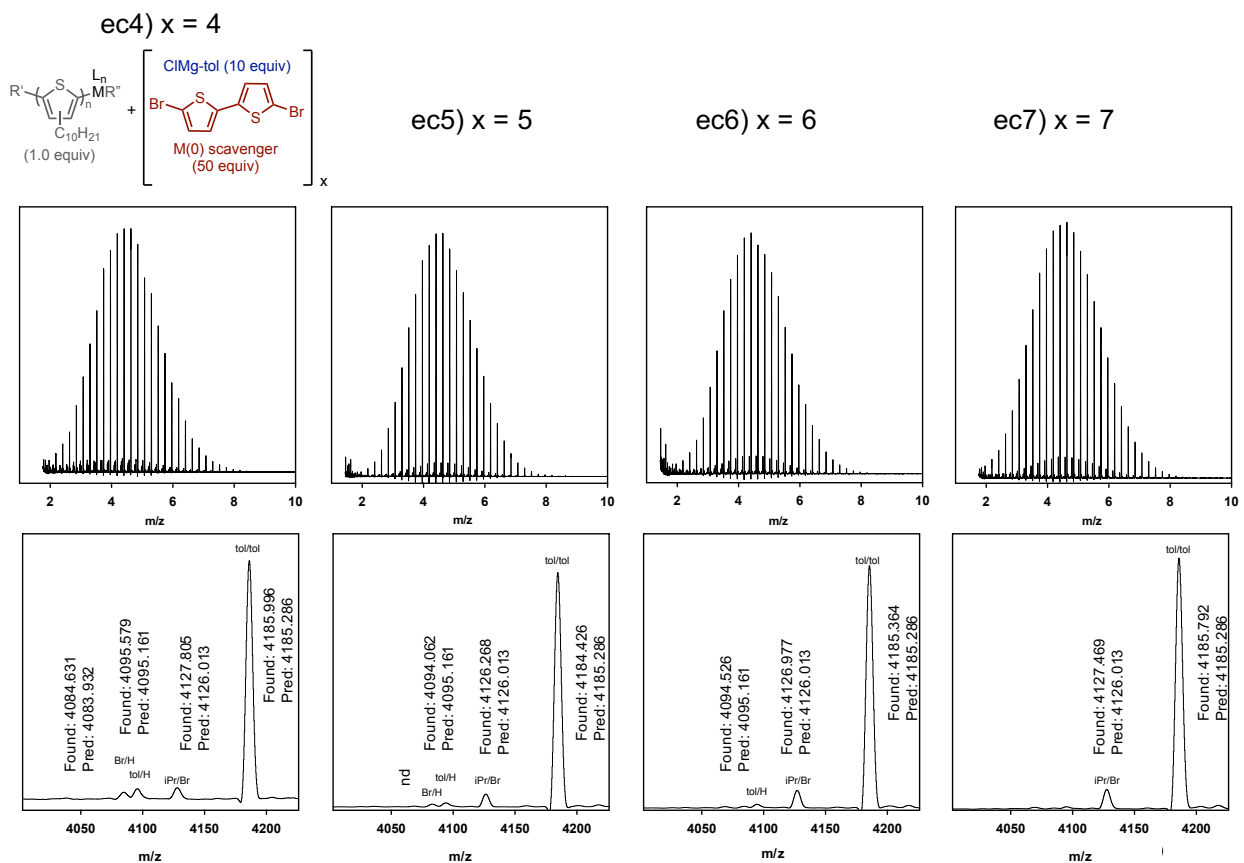
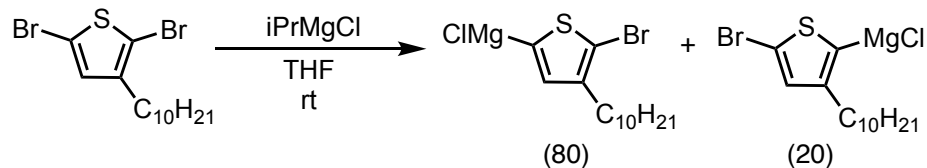


Figure A1-28. MALDI-TOF/MS traces from end-capping experiments (ec4, ec5, ec6, and ec7) for Pd(IPr)(3-Clpy)Cl₂ and P3DT from Run 1. Values calculated using an average mass method, nd = not detected at signal-to-noise = 2. The degree of polymerization shown is 18.

iii. General Procedure for Ni(dppp)Cl₂ - 1 h end-capping



Monomer activation: In a glovebox, *i*PrMgCl (2.0 M in THF, 76.4 μ L, 0.153 mmol, 0.800 equiv) was added to a stirring solution of DB3DT (73.0 mg, 0.191 mmol, 1.00 equiv) in THF (1.83 mL) and stirred for 30 min at rt.

Preparing stock solution:

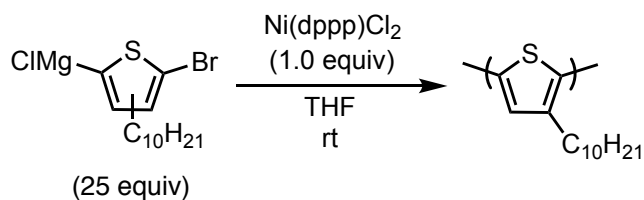
M(0) scavenger solution: To a 4 mL vial was added 5,5'-dibromo-2,2'-bithiophene (9.4 mg, 0.029 mmol) and then was dissolved in THF (1.16 mL) for an overall concentration of 0.025 M.

Preparing end-capping vial experiments:

(equiv are relative to the catalyst/polymer (1.0 equiv) that will be added to each vial)

End-capping experiment vial: *p*-Toluenemagnesium chloride (0.26 M in THF, 15.4 μ L, 10.0 equiv, 0.00400 mmol), 5,5'-dibromo-2,2'-bithiophene (0.025 M in THF, 0.800 mL, 0.0200 mmol, 50.0 equiv) and THF (0.36 mL).

End-capping control vial: *p*-Toluenemagnesium chloride (0.26 M in THF, 15.4 μ L, 10.0 equiv, 0.00400 mmol) and THF (1.16 mL).



Polymerization: Freshly prepared Grignard monomer (0.08 M in THF, 0.969 mL, 0.0775 mmol, 30.0 equiv) was added to a 20 mL vial containing precatalyst Ni(dppp)Cl_2 (1.4 mg, 0.0026 mmol, 1.0 equiv) and THF (5.60 mL) and stirred for 30 min at rt.

In situ end-capping: Two aliquots (1.0 mL each containing 0.00040 mmol catalyst, 1.0 equiv) were removed from the polymerization vial and added to the end-capping control/experiment vials (1.0 mL to each vial). The remaining polymer solution was immediately removed from the glovebox and quenched with aq. HCl (12 M, 1 mL). The end-capping control/experiment experiments were stirred for either 1 or 18 h before quenching outside the glovebox with 12 M aq. HCl (1 mL). The quenched solutions were worked up for GC, GPC, MALDI-TOF/MS.

Table A1-12. GC data from the polymerization of P3DT before end-capping experiments via Ni(dppp)Cl_2 . Initial ratio of Grignard isomers is 4:1 (major:minor).

	 major (% conv.)	 minor (% conv.)
Run 1	85	3%
Run 2	86	4%

Table A1-13. M_n and \mathcal{D} from P3DT (before end-capping), end-capping experiment (ec), and end-capping control (only capping agent) ($t = 1$ h) experiments for Ni(dppp)Cl₂ and P3DT.

Run 1	M_n (kg/mol)	\mathcal{D}	Run 2	M_n (kg/mol)	\mathcal{D}
P3DT	4.50	1.17	P3DT	6.67	1.13
cap only	4.65	1.16	cap only	6.91	1.13
ec	4.23	1.17	ec	6.61	1.13

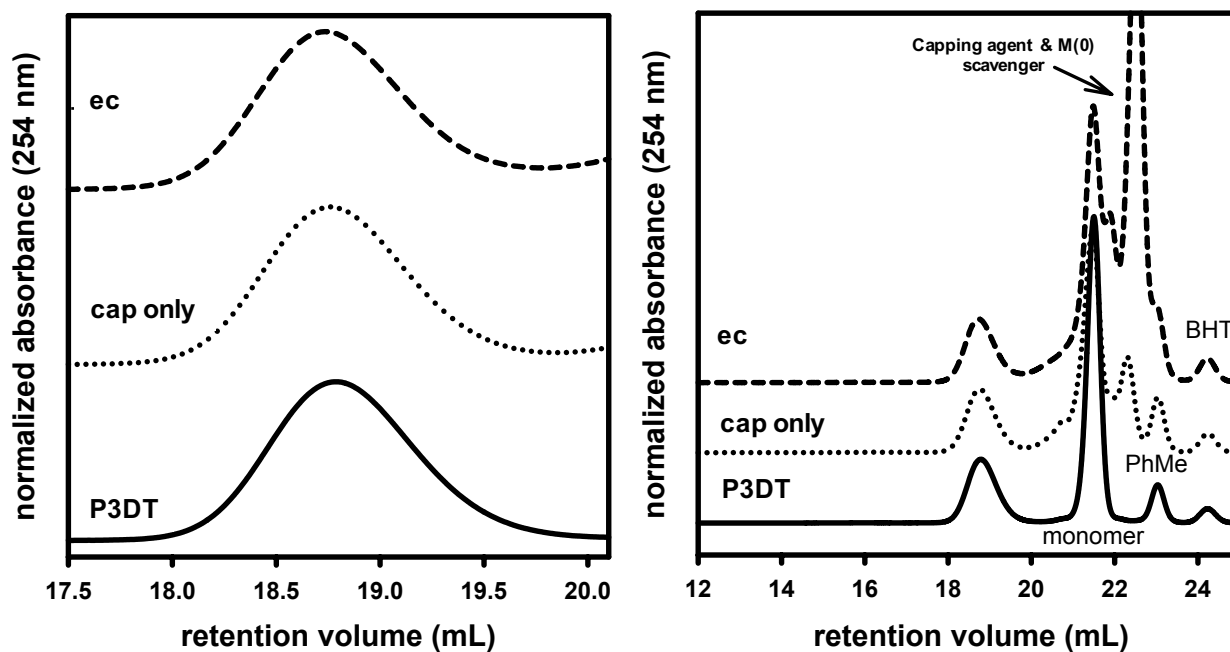


Figure A1-29. GPC traces of P3DT (before end-capping), end-capping experiment, and end-capping control (only capping agent) ($t = 1$ h) experiments for Ni(dppp)Cl₂ and P3DT. (Left = zoomed, right = full GPC trace from Run 1).

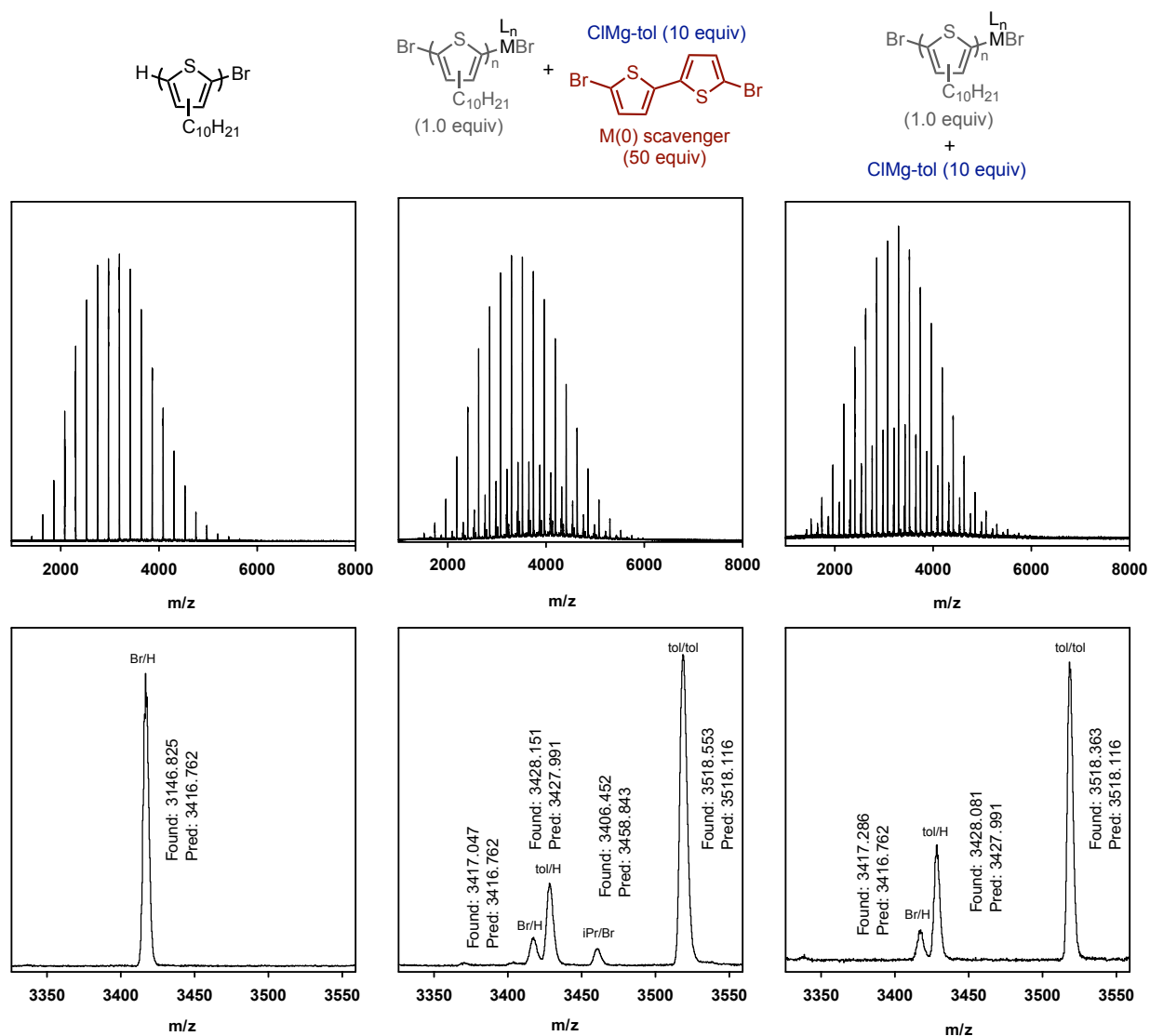


Figure A1-30. MALDI-TOF/MS traces from P3DT (before end-capping), end-capping experiment, and end-capping control (only capping agent) experiments ($t = 1$ h) for $Ni(dppp)Cl_2$ and P3DT from Run 1. Values calculated using an average mass method, signal-to-noise = 2. The degree of polymerization shown is 15.

iii. Ni(dppp)Cl₂ - 18 h end-capping

Table A1-14. GC data from the polymerization of P3DT before end-capping experiments via Ni(dppp)Cl₂. Initial ratio of Grignard isomers is 4:1 (major:minor).

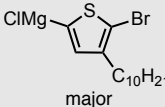
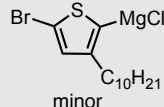
	 major (% conv.)	 minor (% conv.)
Run 1	75	2%
Run 2	82	0%

Table A1-15. M_n and \bar{D} from P3DT (before end-capping), end-capping experiment (ec), and end-capping control (only capping agent) experiments (t = 18 h) for Ni(dppp)Cl₂ and P3DT.

Run 1	M_n (kg/mol)	\bar{D}	Run 2	M_n (kg/mol)	\bar{D}
P3DT	9.26	1.11	P3DT	7.16	1.13
cap only	9.13	1.13	cap only	7.42	1.26
ec	9.41	1.15	ec*	7.56	1.14
			ec**	8.07	1.29

*/** are from the same sample not including/including a high molecular weight shoulder (possibly from a quenching error).

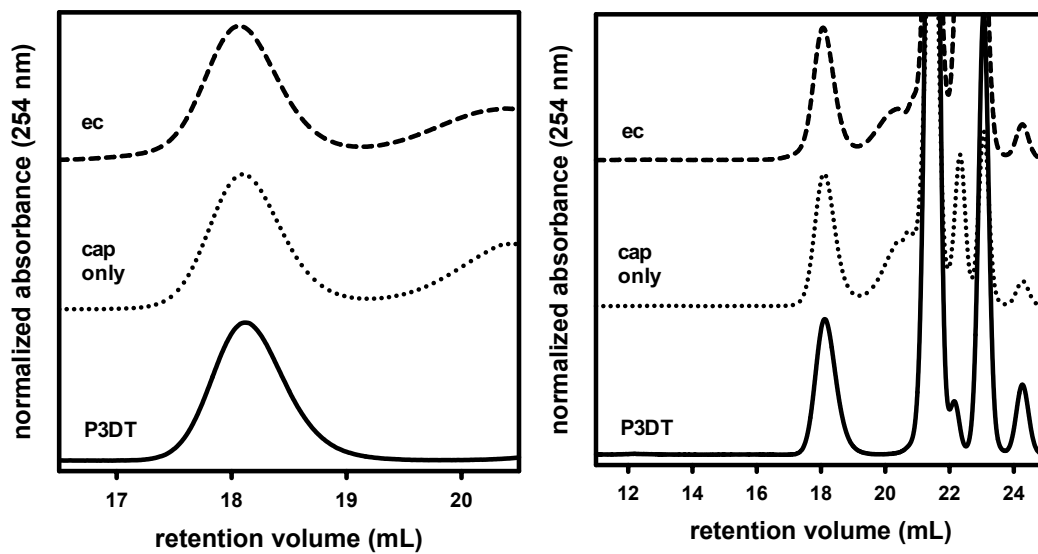


Figure A1-31. GPC traces from P3DT (before end-capping), end-capping experiment, and end-capping control (only capping agent) experiments ($t = 18$ h) for Ni(dppp)Cl₂ and P3DT. (Left = zoomed, right = full GPC trace from Run 1).

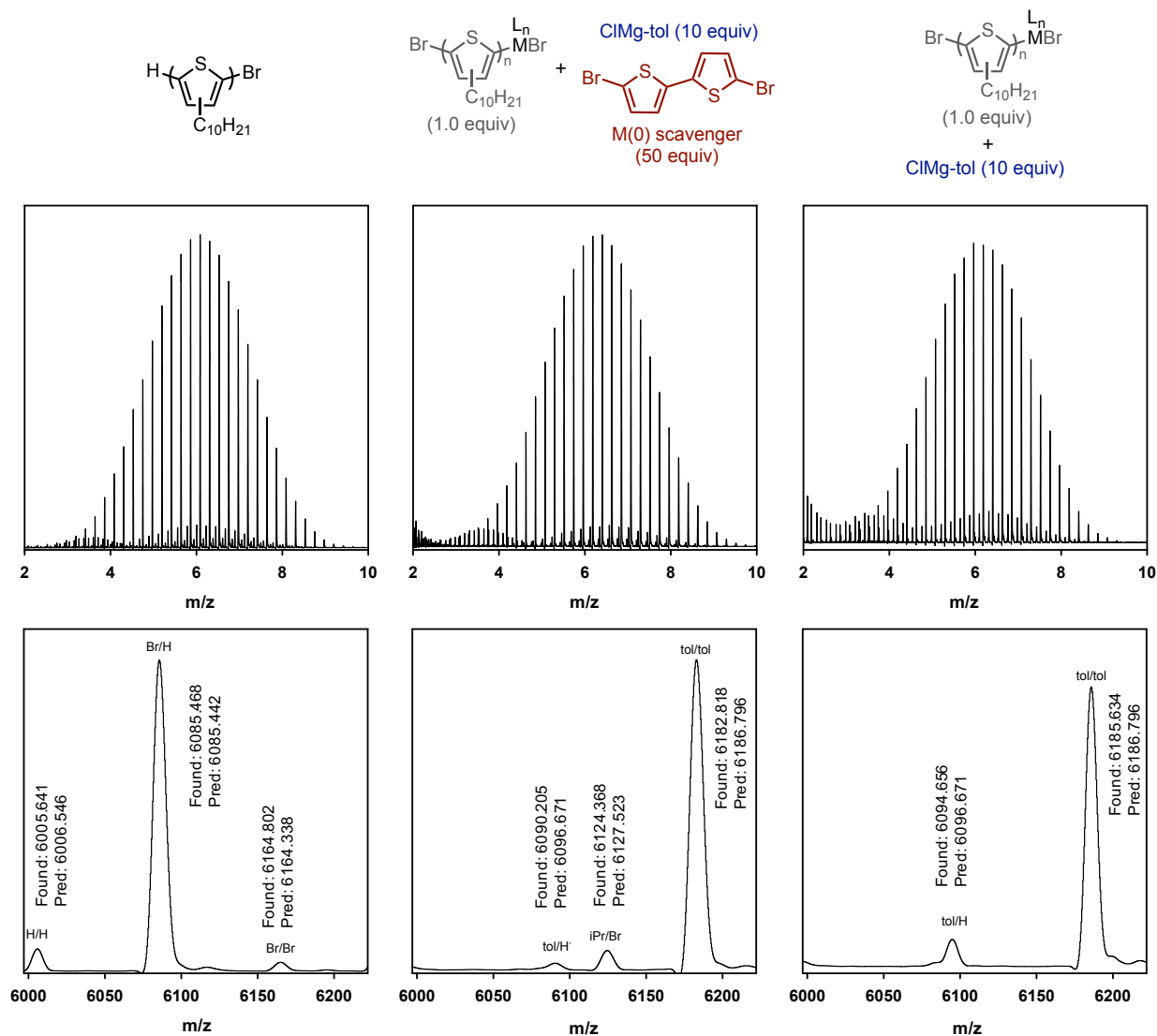
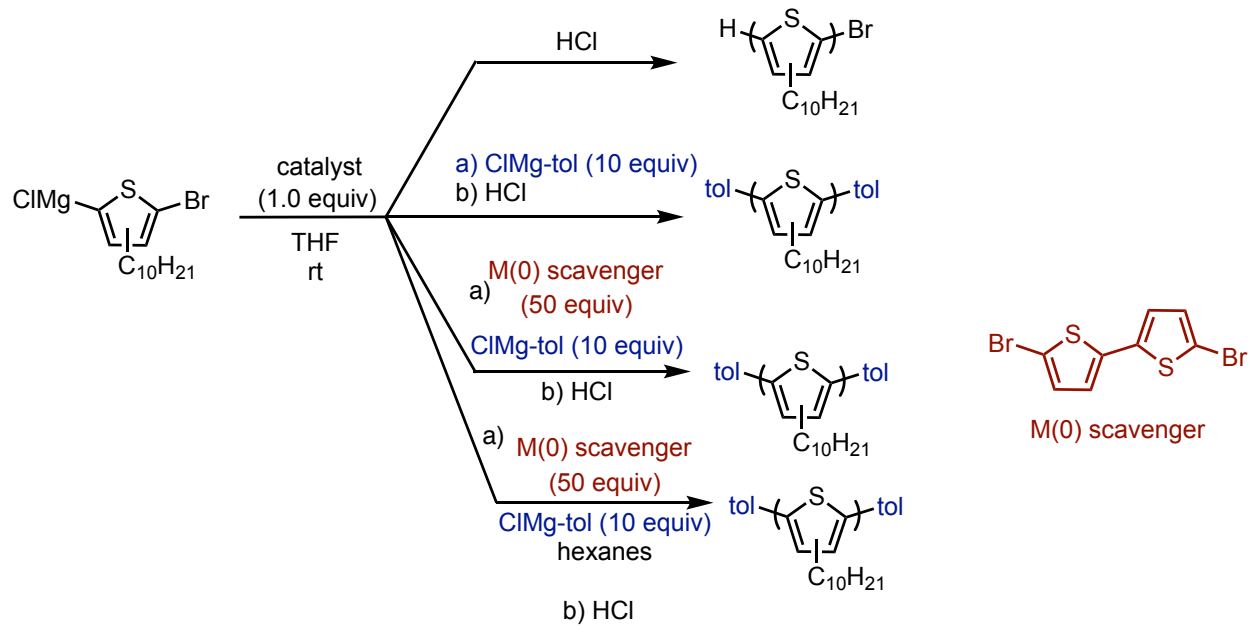
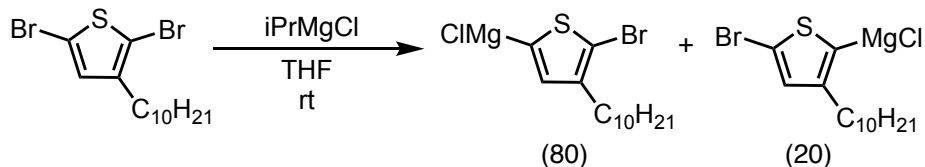


Figure A1-32. MALDI-TOF/MS traces from P3DT (before end-capping), end-capping experiment, and end-capping control (only capping agent) experiments ($t = 18$ h) for $\text{Ni}(\text{dppp})\text{Cl}_2$ and P3DT from Run 1. Values calculated using average mass method, signal-to-noise = 2. The degree of polymerization shown is 27.

iv. Evaluating the influence of solvent (hexane) on 3-decylthiophene end-capping experiments





Monomer activation: In a glovebox, iPrMgCl (2.2 M in THF, 0.112 mL, 0.247 mmol, 0.800 equiv) was added to a solution of DB3DT (118 mg, 0.309 mmol, 1.00 equiv) in THF (2.98 mL) and stirred for 30 min at rt.

Preparing precatalysts:

Pd(IPr)(3-Clpy)Cl₂: To an 8 mL vial was added Pd(IPr)(3-Clpy)Cl₂ (12.4 mg, 0.0182 mmol) and dissolved in THF (1.82 mL) for a [0.01 M] solution.

Ni(IPr)(PPh₃)Cl₂: To an 8 mL vial was added Ni(IPr)(PPh₃)Cl₂ (4.2 mg, 0.0054 mmol) and dissolved in THF (0.54 mL) for a [0.01 M] solution.

Ni(dppp)Cl₂: To a 20 mL vial was added Ni(dppp)Cl₂ (2.2 mg, 0.0041 mmol).

Preparing stock solution:

M(0) scavenger solution: To a 4 mL vial was added 5,5'-dibromo-2,2'-bithiophene (21.4 mg, 0.0660 mmol) and then was dissolved in THF (1.32 mL) for an overall concentration of 0.050 M.

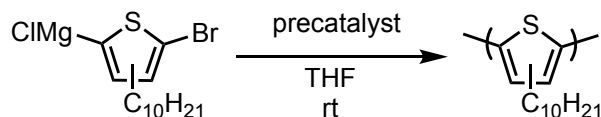
Preparing end-capping vial experiments:

(equiv are relative to the catalyst/polymer (1.0 equiv) that will be added to each vial)

End-capping experiment vial (THF only): *p*-Toluenemagnesium chloride (0.26 M in THF, 15.4 μ L, 10.0 equiv, 0.00400 mmol), 5,5'-dibromo-2,2'-bithiophene (0.050 M in THF, 0.400 mL, 0.0200 mmol, 50.0 equiv) and THF (0.76 mL).

End-capping experiment vial (THF and hexanes): *p*-Toluenemagnesium chloride (0.26 M in THF, 15.4 μ L, 10.0 equiv, 0.00400 mmol), 5,5'-dibromo-2,2'-bithiophene (0.050 M in THF, 0.400 mL, 0.0200 mmol, 50.0 equiv) and hexanes (0.76 mL).

End-capping control vial: *p*-Toluenemagnesium chloride (0.26 M in THF, 15.4 μ L, 10.0 equiv, 0.00400 mmol) and THF (1.16 mL).



Polymerization:

For Ni(IPr)(PPh₃)Cl₂: Freshly prepared Grignard monomer (0.08 M in THF, 0.90 mL, 0.072 mmol, 25 equiv) was diluted with THF (6.14 mL) then precatalyst (0.01M in THF, 0.288 mL, 0.00288 mmol, 1.00 equiv) and stirred for 5 min at rt.

For Pd(IPr)(3-Clpy)Cl₂: Freshly prepared Grignard monomer (0.08 M in THF, 0.50 mL, 0.040 mmol, 25 equiv) was diluted with THF (3.41 mL) then precatalyst (0.01M in THF, 0.160 mL, 0.00160 mmol, 1.00 equiv) and stirred for 15 min at rt.

For Ni(dppp)Cl₂: Freshly prepared Grignard monomer (0.08 M in THF, 1.52 mL, 0.122 mmol, 30.0 equiv) was diluted with THF (8.81 mL). An aliquot of the diluted monomer (0.0138 M in

THF, 1.03 mL, 0.0143 mmol, 2.87 equiv relative to Ni) was added to precatalyst Ni(dppp)Cl₂ (2.2 mg, 0.041 mmol, 1.0 equiv) and stirred for 60 s to preinitiate the solid precatalyst. Then, the remaining diluted monomer solution was added to the preinitiated catalyst and stirred for 30 min at rt.

In situ end-capping: Aliquots (1.0 mL each containing 0.00040 mmol catalyst, 1.0 equiv) were removed from each polymerization vial and added to the end-capping control/experiment vials (1.0 mL to each vial). The remaining polymer solution was immediately removed from the glovebox and quenched with aq. HCL (12 M, 1 mL). The end-capping control/experiment experiments were stirred for either 1 h (for Ni(IPr)(PPh₃)Cl₂ and Pd(IPr)(3-Clpy)Cl₂) or 18 h (for Ni(dppp)Cl₂) before quenching outside the glovebox with 12 M aq. HCl (1 mL). The quenched solutions were worked up for GC, GPC, MALDI-TOF/MS.

Table A1-16. GC data from the polymerization of P3DT before end-capping experiments via Ni(IPr)(PPh₃)Cl₂, Pd(IPr)(3-Clpy)Cl₂, and Ni(dppp)Cl₂. Initial ratio of Grignard isomers is 4:1 (major:minor).

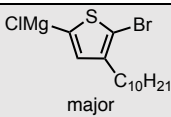
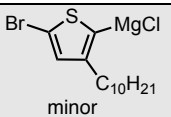
	 major (% conv.)	 minor (% conv.)
Ni(IPr)(PPh ₃)Cl ₂	97%	98%
Pd(IPr)(3-Clpy)Cl ₂	quant.	50%
Ni(dppp)Cl ₂	86%	0%

Table A1-17. M_n and \bar{D} from P3DT (before end-capping), end-capping control (capping agent only), end-capping (ec), and end-capping with hexanes (ec (hex)) experiments for Ni(IPr)(PPh₃)Cl₂, Pd(IPr)(3-Clpy)Cl₂, and Ni(dppp)Cl₂.

Ni(IPr)(PPh ₃)Cl ₂	M_n (kg/mol)	\bar{D}	Pd(IPr)(3-Clpy)Cl ₂	M_n (kg/mol)	\bar{D}	Ni(dppp)Cl ₂	M_n (kg/mol)	\bar{D}
P3DT	7.67	1.15	P3DT	7.49	1.18	P3DT	5.62	1.19
cap only	7.27	1.23	cap only	7.20	1.18	cap only	5.78	1.32
ec	10.73	1.14	ec	8.11	1.20	ec	7.29	1.42
ec (hex)	10.60	1.14	ec (hex)	8.99	1.23	ec (hex)	7.23	1.36

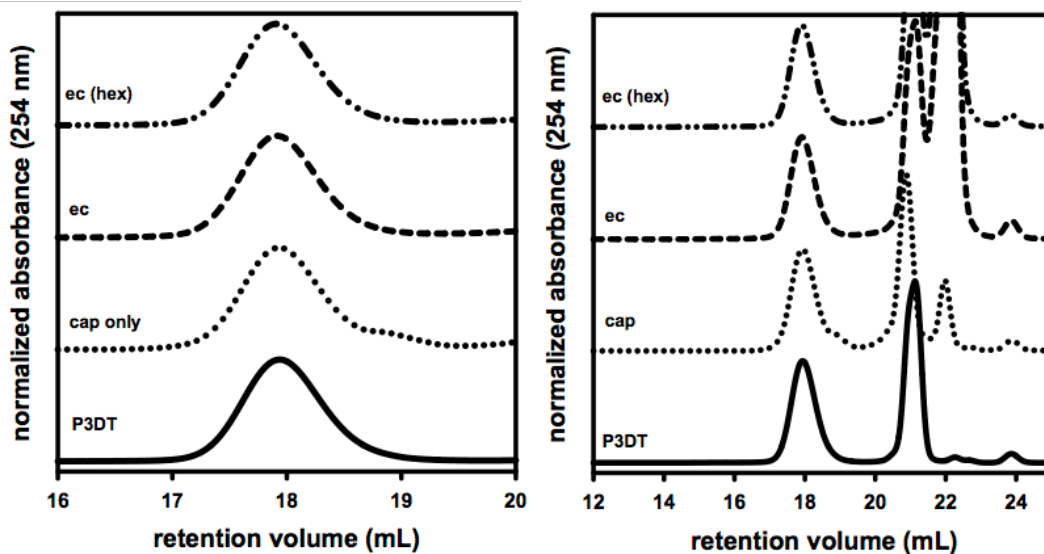


Figure A1-33. GPC traces from P3DT (before end-capping), end-capping control (only capping agent), end-capping (ec), and end-capping with hexane (ec (hex)) experiments for $\text{Ni}(\text{IPr})(\text{PPh}_3)\text{Cl}_2$. (Left = zoomed, right = full GPC trace). Note that M(0) scavenging agent and residual monomer elute from 20.5–22 min, PhMe elutes at 23.1 min and BHT elutes at 23.8 min.

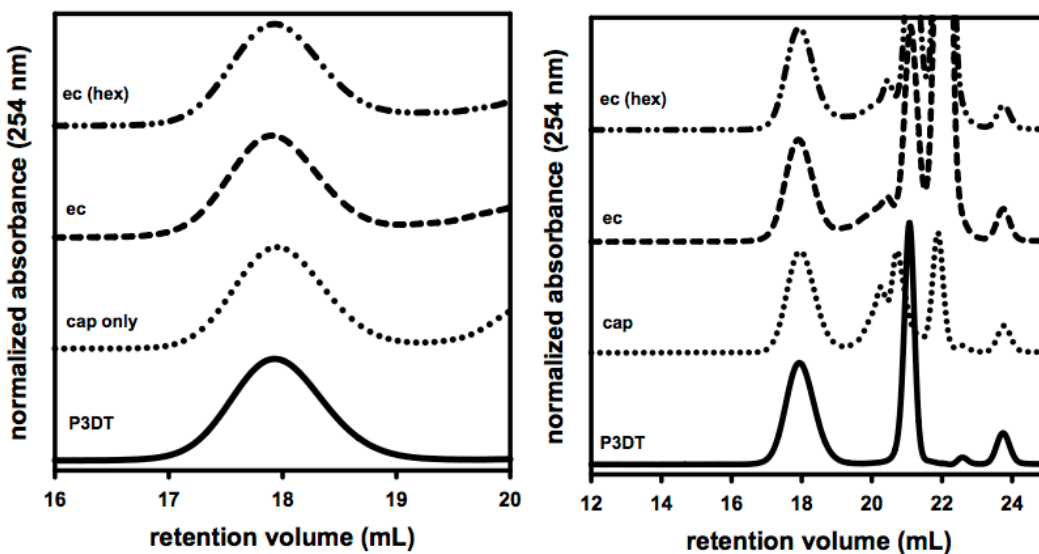


Figure A1-34. GPC traces from P3DT (before end-capping), end-capping control (only capping agent), end-capping (ec), and end-capping with hexane (ec (hex)) experiments for $\text{Pd}(\text{IPr})(3\text{-Clpy})\text{Cl}_2$. (Left = zoomed, right = full GPC trace). Note that M(0) scavenging agent and residual monomer elute from 20.5–22 min, PhMe elutes at 23.1 min and BHT elutes at 23.8 min.

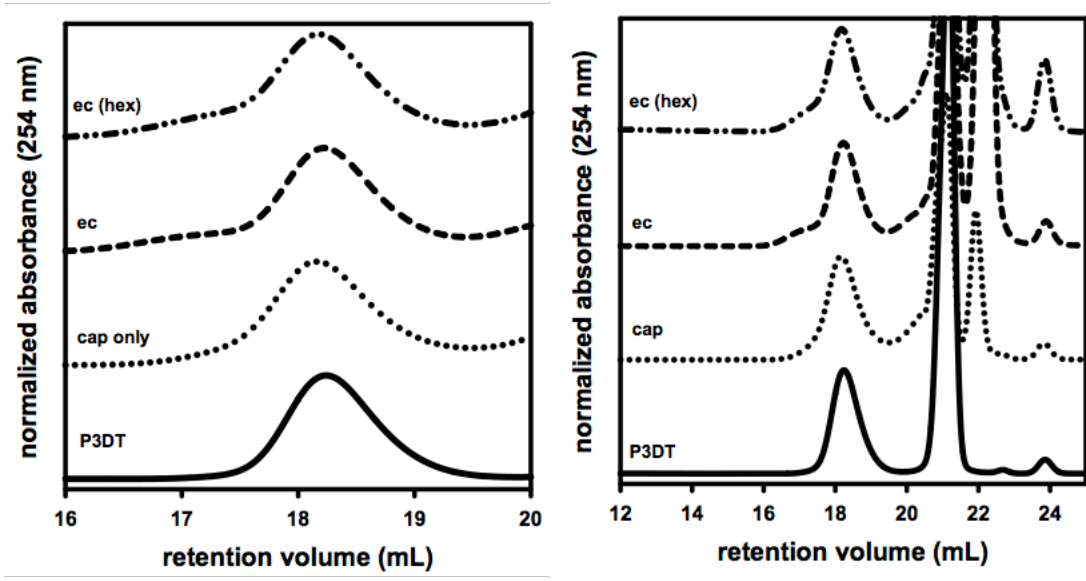


Figure A1-35. GPC traces from P3DT (before end-capping), end-capping control (only capping agent), end-capping (ec), and end-capping with hexane (ec (hex)) experiments for Ni(dppp)Cl₂. (Left = zoomed, right = full GPC trace). Note that M(0) scavenging agent and residual monomer elute from 20.5–22 min, PhMe elutes at 23.1 min and BHT elutes at 23.8 min.

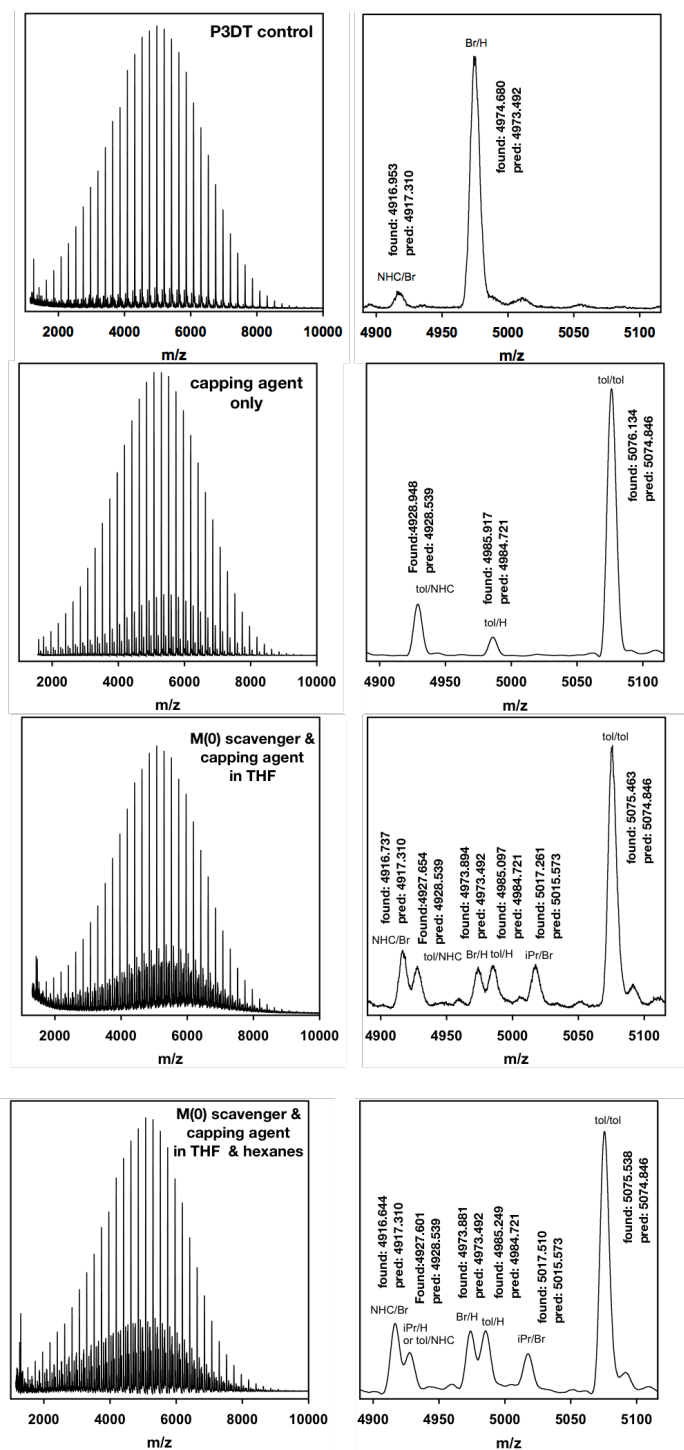


Figure A1-36. MALDI-TOF/MS traces from P3DT (before end-capping), end-capping experiments (THF alone, and THF & hexanes), and end-capping control (only capping agent) experiments for Ni(IPr)(PPh₃)Cl₂. Values calculated using average mass method signal-to-noise = 2. The repeat unit shown is 22. (Note that to reach complete tol/tol-end capped polymers 2 iterations of CIMg–tol and M(0) scavenger should be used).

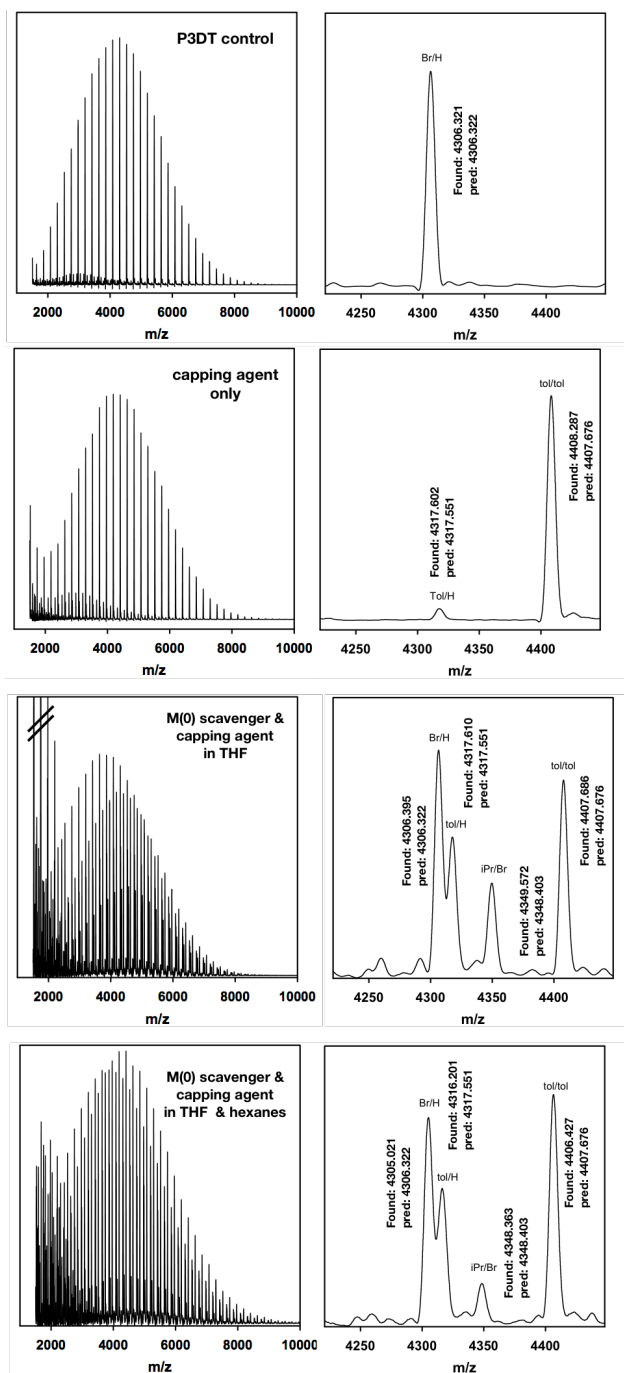


Figure A1-37. MALDI-TOF/MS traces from P3DT (before end-capping), end-capping experiments (THF alone, and THF & hexanes), and end-capping control (only capping agent) experiments for Pd(IPr)(3-Clpy)Cl₂. Values calculated using average mass method signal-to-noise = 2. The repeat unit shown is 19. (Note that to reach complete tol/tol-end capped polymers 6 iterations of CIMg-tol and M(0) scavenger should be used).

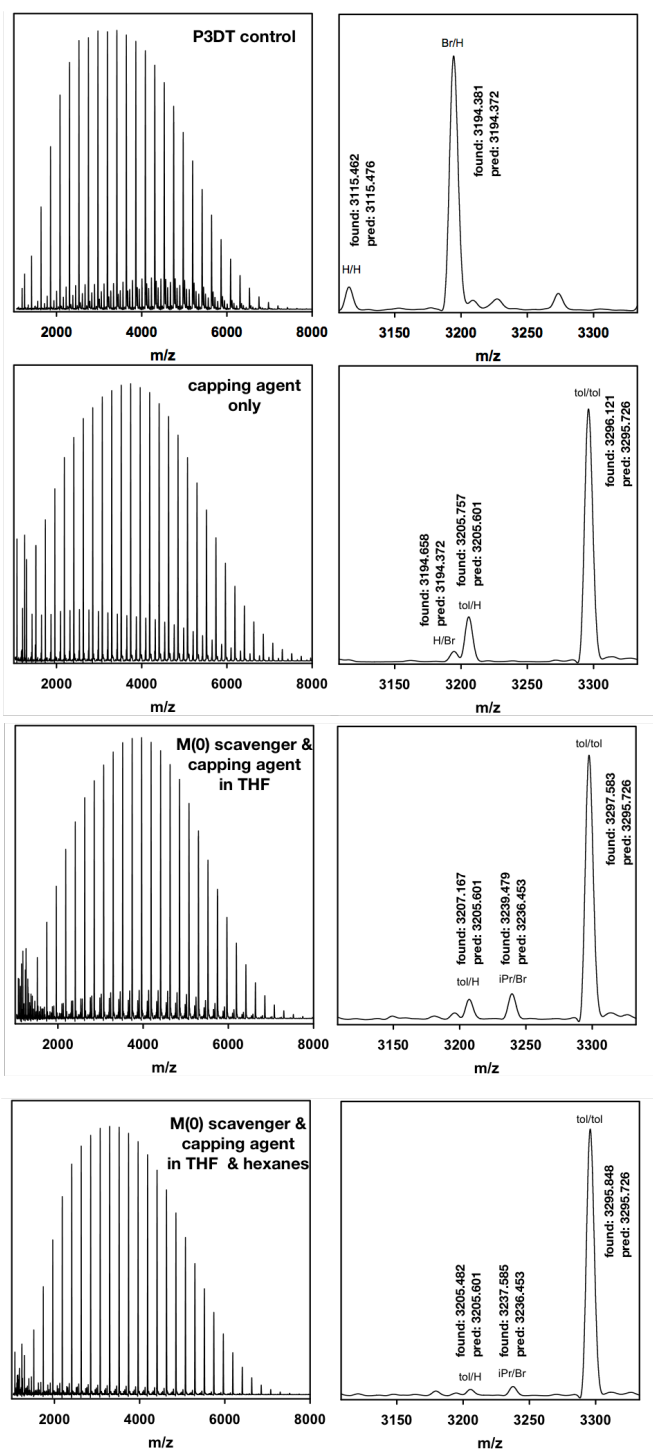
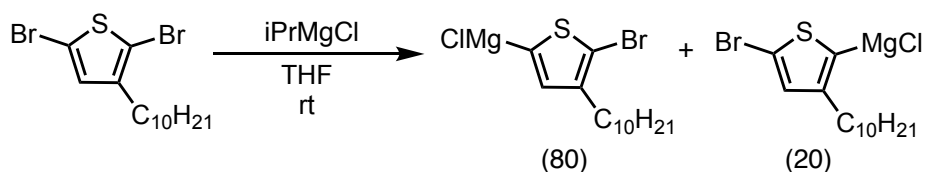


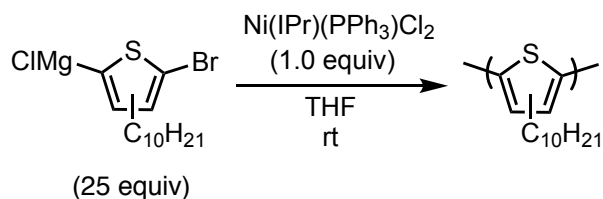
Figure A1-38. MALDI-TOF/MS traces from P3DT (before end-capping), end-capping experiments (THF alone, and THF & hexanes), and end-capping control (only capping agent) experiments for Ni(dppp)Cl₂. Values calculated using average mass method signal-to-noise = 2. The repeat unit shown is 14.

A1.5.6 3-Decylthiophene polymerization via Ni(IPr)(PPh₃)Cl₂ generating NHC/Br-polymers



Monomer activation: In a glovebox, $iPrMgCl$ (2.0 M in THF, 0.069 mL, 0.14 mmol, 0.80 equiv) was added to a solution of DB3DT (65.9 mg, 0.172 mmol, 1.00 equiv) and $C_{22}H_{46}$ (as an internal standard, ~4 mg) in THF (1.65 mL) and stirred for 30 min at rt.

Precatalyst stock solution: To a 4 mL vial was added $Ni(IPr)(PPh_3)Cl_2$ (6.0 mg, 0.0077 mmol) and THF (0.77 mL) for an overall concentration of 0.01 M.



Polymerization: Freshly prepared Grignard monomer (0.08 M in THF, 1.20 mL, 0.0960 mmol, 25.0 equiv) was diluted with THF (8.20 mL) in a 20 mL vial equipped with a stirbar. Then, precatalyst stock solution (0.01 M in THF, 0.384 mL, 0.00384 mmol, 1.00 equiv) was added to the diluted monomer solution. After stirring at rt for 5 min, an aliquot of the polymerization (2.0 mL) was removed from the glovebox and quenched with aq. HCl (12 M, 5 mL), and extracted with $CHCl_3$ (3 x 3 mL). The remaining polymerization solution was stirred for ≥ 9 h before being removed from the glovebox, quenched with aq. HCl (12 M, 8 mL), and extracted with $CHCl_3$ (3 x 3 mL). The crude polymer samples were worked up for GC, GPC, MALDI-TOF/MS (see

general experimental). For ^1H NMR spectroscopic analysis, the polymers (in CHCl_3) were concentrated under reduced pressure, redissolved in a minimal amount of CHCl_3 (~0.1 mL), precipitated in MeOH (10 mL), transferred to a centrifuge tube, and spun for 15 min generating a purple solid with a clear supernatant. The supernatant was decanted and the solid was washed, by shaking to break up the solid, with MeOH (15 mL) and centrifuged again. The supernatant was decanted and the solid was dried under reduced pressure.

Table A1-18. GC data from the polymerization of 3-decylthiophene at rt via Ni(IPr)(PPh₃)Cl₂. Initial ratio of Grignard isomers is 4:1 (major:minor).

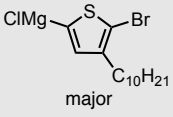
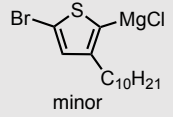
	 major (% conv.)	 minor (% conv.)
Run 1	99	99
Run 2	quant.	quant.

Table A1-19. M_n and \bar{D} from the polymerization of 3-decylthiophene at rt via Ni(IPr)(PPh₃)Cl₂.

Run 1	M_n (kg/mol)	\bar{D}	Run 2	M_n (kg/mol)	\bar{D}
5 min	8.56	1.14	5 min	9.85	1.19
20 h	5.52	1.52	9 h	5.33	2.11

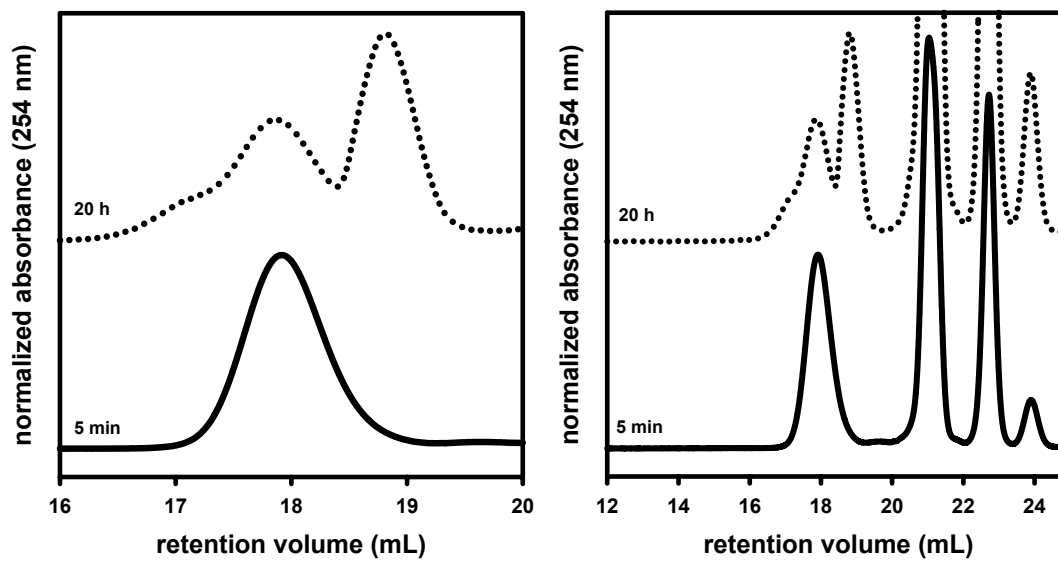


Figure A1-39. GPC traces from the polymerization of 3-decylthiophene at rt via $\text{Ni}(\text{IPr})(\text{PPh}_3)\text{Cl}_2$. (Left = zoomed, right = full GPC trace from Run 1).

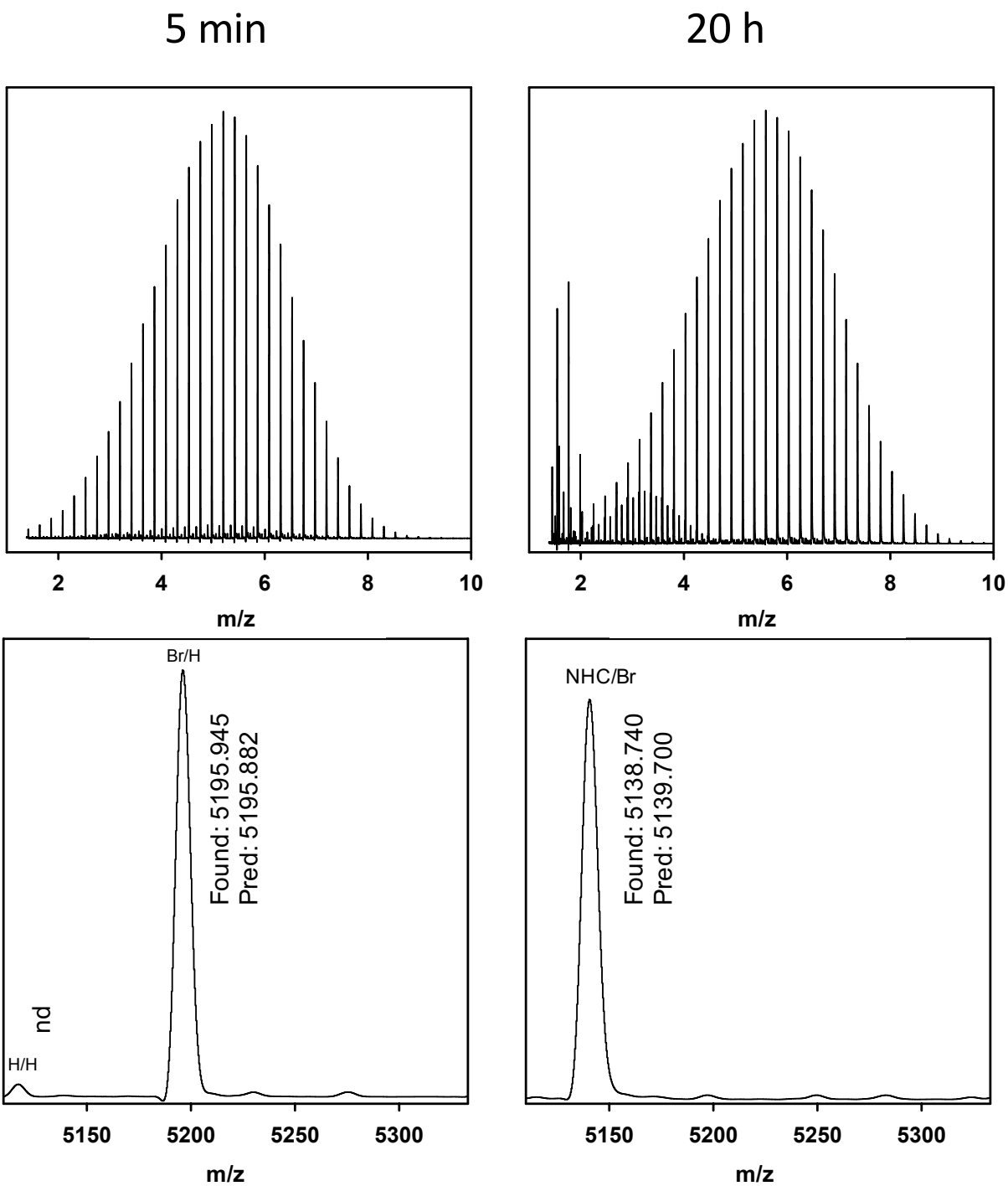


Figure A1-40. MALDI-TOF/MS traces from the polymerization of 3-decylthiophene at rt via Ni(IPr)(PPh₃)Cl₂ from Run 1. Values calculated using an average mass method, signal-to-noise = 2. The degree of polymerization shown is 23.

According to the MALDI-TOF/MS spectrum, the average degree of polymerization (m) is 23.

The chemdraw below shows the theoretical ^1H -distribution under the $m = 23$ assumption.

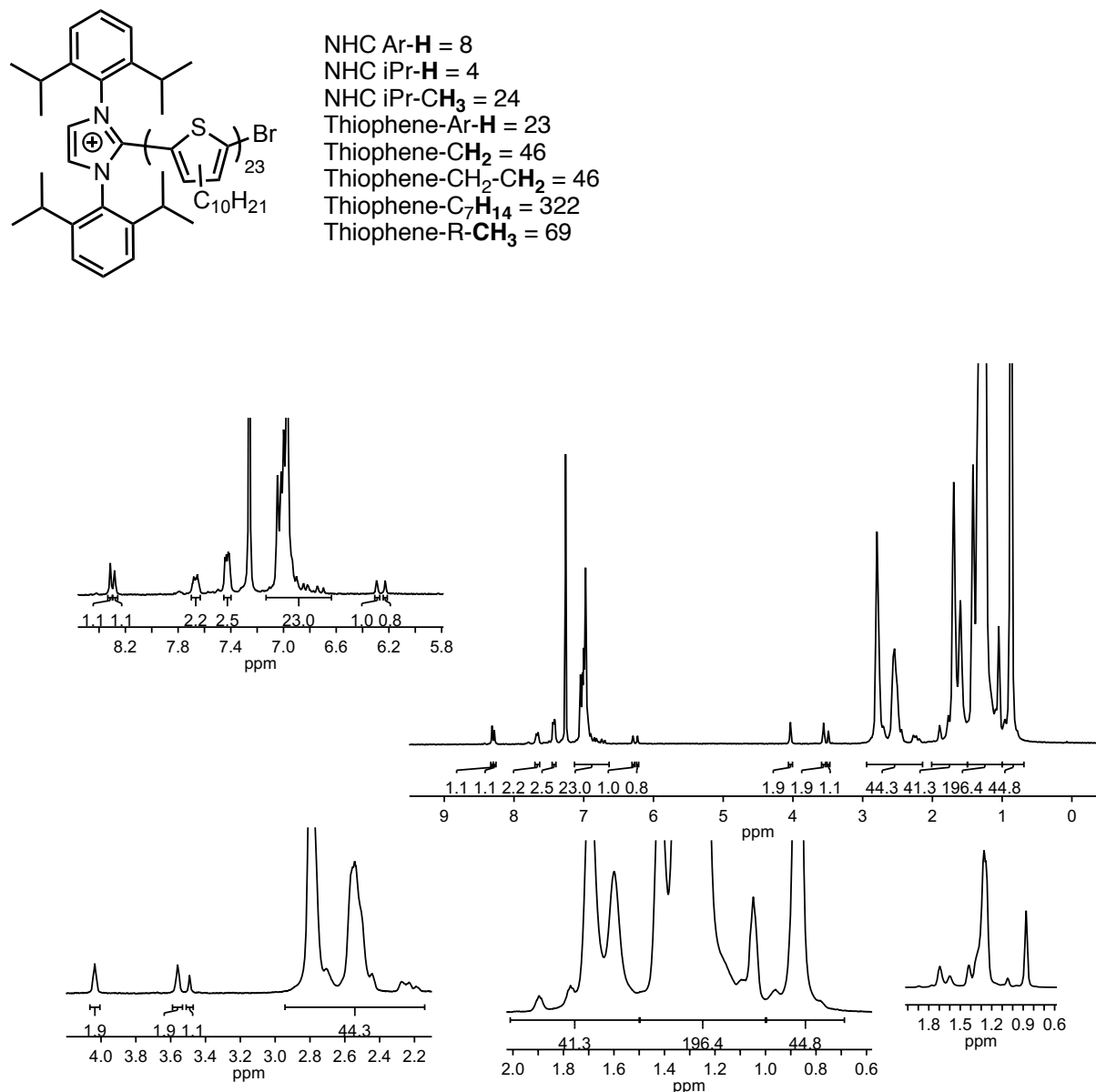


Figure A1-41. ^1H NMR spectra from the polymerization of 3-decylthiophene at rt via $\text{Ni}(\text{IPr})(\text{PPh}_3)\text{Cl}_2$ after 20 h (relaxation delay = 2 s). ^1H NMR (700 MHz, CDCl_3) δ 8.31 (s, 1H), 8.28 (s, 1H), 7.70–7.63 (m, 2H), 7.45–7.40 (m, 3H), 7.14–6.63 (multiple peaks, 23H), 6.29 (s, 1H), 6.23 (s, 1H), 4.06–4.01 (m, 2H), 3.59–3.54 (m, 2H), 3.49 (s, 1H), 2.95–2.15 (multiple peaks, 44H), 2.01–1.50 (multiple peaks, 41H), 1.50–1.01 (multiple peaks, 196H), 1.01–0.69 (multiple peaks, 45H).

A1.6 Phenylene

A1.6.1. Confirming MALDI-TOF/MS provides an accurate and quantitative description of end-group distributions for poly(2,5-bisalkoxyphenylene).

A1.6.2. Synthesis of H/Br-polymer for end-capping control reactions

A1.6.3. End-capping control reactions

i. Ni(IPr)(PPh₃)Cl₂

ii. Pd(IPr)(3-Clpy)Cl₂

iii. Ni(dppp)Cl₂

A1.6.4. Evaluating the impact of entangled chains

A1.6.5. End-capping reactions

i. Ni(IPr)(PPh₃)Cl₂

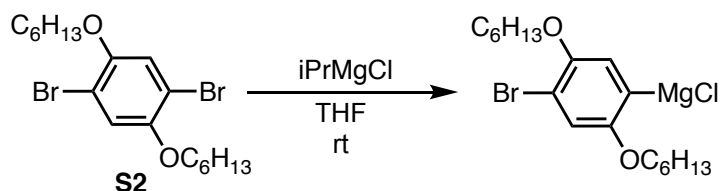
ii. Pd(IPr)(3-Clpy)Cl₂

iii. Ni(dppp)Cl₂

iv. Evaluating the impact of solvent (hexanes) on end-capping experiments

A1.6.6. 2,5-Bisalkoxyphenylene polymerization via Pd(IPr)(3-Clpy)Cl₂ generating NHC/Br-polymers

A1.6.1 Confirming MALDI-TOF/MS provides an accurate and quantitative description of end-group distributions for poly(2,5-bisalkoxyphenylene).



Monomer activation: In a glovebox, $i\text{PrMgCl}$ (2.2 M in THF, 1.393 mL, 0.003093 mol, 0.8000 equiv) was added to a stirring solution of **S2** (1.69 g, 0.00387 mmol, 1.00 equiv) in THF (6.3 mL) and stirred for 17 h at rt. Titrating the resulting solution against salicylaldehyde phenylhydrazone (see general experimental) revealed the $[\text{Grignard}] = 0.291 \text{ M}$.

For the polymers used in this experiment, $\text{Pd}(\text{IPr})(3\text{-Clpy})\text{Cl}_2$ was used to generate the end-capped-PBHP and $\text{Ni}(\text{IPr})(\text{PPh}_3)\text{Cl}_2$ was used to generate Br/H-PBHP.

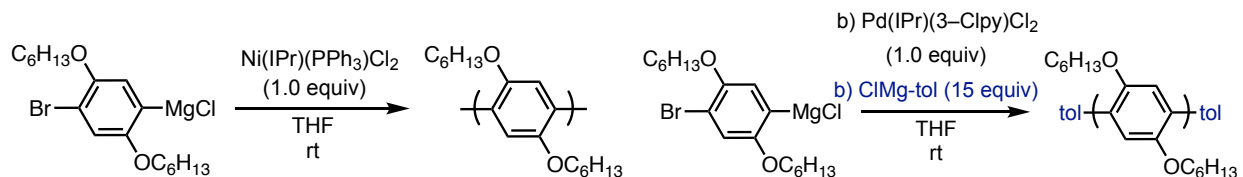
Precatalyst solutions:

$\text{Pd}(\text{IPr})(3\text{-Clpy})\text{Cl}_2$: To an 8 mL vial was added $\text{Pd}(\text{IPr})(3\text{-Clpy})\text{Cl}_2$ (11.7 mg, 0.0172 mmol) and dissolved in THF (1.72 mL) for a [0.01 M] solution.

$\text{Ni}(\text{IPr})(\text{PPh}_3)\text{Cl}_2$: To an 8 mL vial was added $\text{Ni}(\text{IPr})(\text{PPh}_3)\text{Cl}_2$ (10.8 mg, 0.0138 mmol) and dissolved in THF (1.38 mL) for a [0.01 M] solution.

Reaction flask preparation:

In the glovebox, to a 25 mL Schlenk flask was added precatalyst (0.01M in THF, 1.2 mL, 0.012 mmol, 1.0 equiv), THF (8 mL), and a stirbar. The Schlenk flask was capped with a septum, secured with copper wire, removed from the glovebox, and immediately placed under N₂.



Polymerization: In the glovebox, Grignard monomer solution (0.291 M in THF, 0.825 mL, 0.240 mmol, 20.0 equiv) was drawn into a 3 mL syringe equipped with a long needle, headspace (~1.4 mL) was pulled and then the syringe/needle were removed from the glovebox. During transit, to the catalyst-containing flask, headspace (~1.0 mL) was evacuated from the needle before puncturing the septum. The monomer was added at once to the stirring precatalyst flasks. The polymerizations were stirred for 90 min under N₂. The polymerization via Ni was quenched with aq. HCl (12 M, 3 mL). An aliquot (1.0 mL, containing 0.0015 mmol Pd) of the Pd-catalyzed polymerization was added to an 8 mL vial capped with a septum-cap containing a stirring solution of *p*-toluenemagnesium chloride (1.11 M in THF, 0.0203 mL, 0.0225 mmol, 15.0 equiv *relative to added Pd*) in THF (0.5 mL) and stirred for 2 h under N₂ before being quenched with aq. HCl (12 M, 1 mL).

Work-up: The crude polymers were extracted with CHCl₃ (3 x 2 mL), dried over MgSO₄, filtered and analyzed by GPC and MALDI-TOF/MS. The remaining quenched polymer was concentrated under reduced pressure, redissolved in CHCl₃ (0.2 mL), and precipitated using MeOH (10 mL). The resulting heterogeneous mixture was added to a centrifuge tube and diluted with additional MeOH (to fill the centrifuge tubes). The polymers were spun for 15 min. The

clear supernatant was decanted, then fresh MeOH (15 mL) was added to the centrifuge tubes to break up the solid, washing it, then the tubes were spun for an additional 15 min. Then, the supernatant was decanted and the white solid was collected by transferring to a vial using CHCl₃. The polymer solution was concentrated under reduced pressure, yielding 3.5 mg of poly(2,5-bis(hexyloxy)phenylene) (Br/H–PBHP) and 3.6 mg tol/tol–terminated poly(2,5-bis(hexyloxy)phenylene) (tol/tol–PBHP). Note the mother liquor for these polymerizations were also used for additional experiments so yields were not calculated.

Polymer solutions for ¹H NMR spectroscopic analysis and MALDI-TOF/MS:

Br/H–PBHP (3.5 mg) was dissolved in CDCl₃ (0.70 mL), tol/tol–PBHP (3.6 mg) was dissolved in CDCl₃ (0.72 mL). An aliquot (0.3 mL) of each polymer solution was injected into a single NMR tube and analyzed by ¹H NMR spectroscopy using a 3s relaxation delay. The NMR solution was used to prepare the MALDI-TOF/MS samples (see general experimental). The ¹H NMR spectrum and MALDI-TOF/MS are in agreement with the polymers being in equal 1:1 (wt/wt) concentration as prepared.

Table A1-20. Percent PBHP end-groups based on MALDI-TOF/MS analysis.

	Br/H–PBHP (%)	end-capped PBHP (%)	combined (theo.) (%)	combined (observed) (%)
H/H	4.21	2.15	3.18	6.21
iPr/H	4.21	0	2.11	2.07
Br/H	89.47	0	44.73	41.89
iPr/Br	2.11	0	1.08	0.41
tol/H	0	2.15	1.05	0.31
tol/Br	0	3.23	1.61	2.07
tol/tol	0	89.25	44.62	44.46
NHC/Br	0	3.23	1.61	2.58

Table A1-21. M_n and \mathcal{D} from Br/H–PBHP and end-capped–PBHP.

Ni(IPr)(PPh ₃)Cl ₂	M_n (kg/mol)	\mathcal{D}	Pd(IPr)(3-Clpy)Cl ₂	M_n (kg/mol)	\mathcal{D}
Br/H–PBHP	5.78	1.23	end-capped–PBHP	7.61	1.18

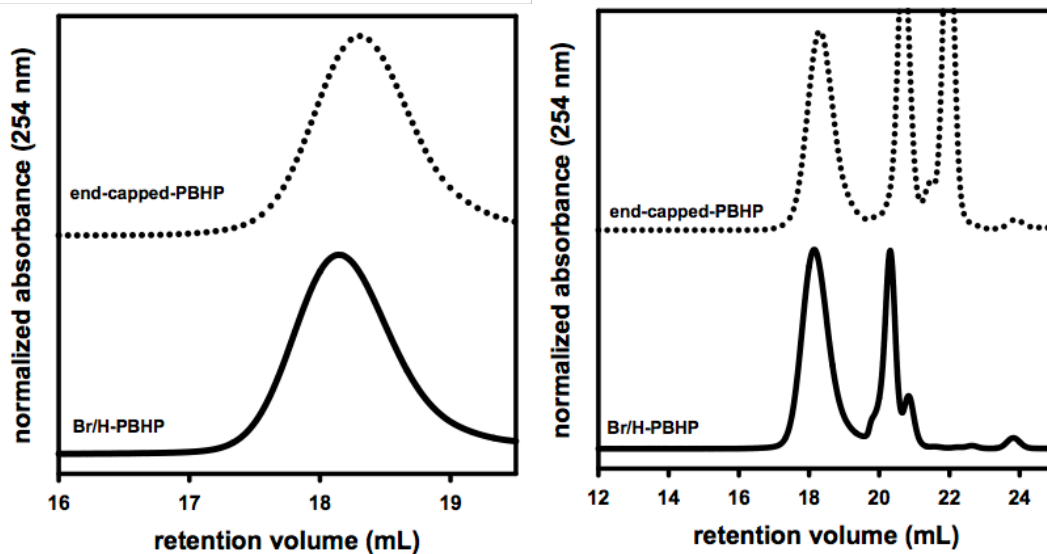


Figure A1-42. GPC traces from Br/H–PBHP and end-capped–PBHP (left = zoomed, right = full GPC trace of the set of samples). Note that residual monomer elutes from 20.5–22 min, PhMe elutes at 23.1 min and BHT elutes at 23.8 min.

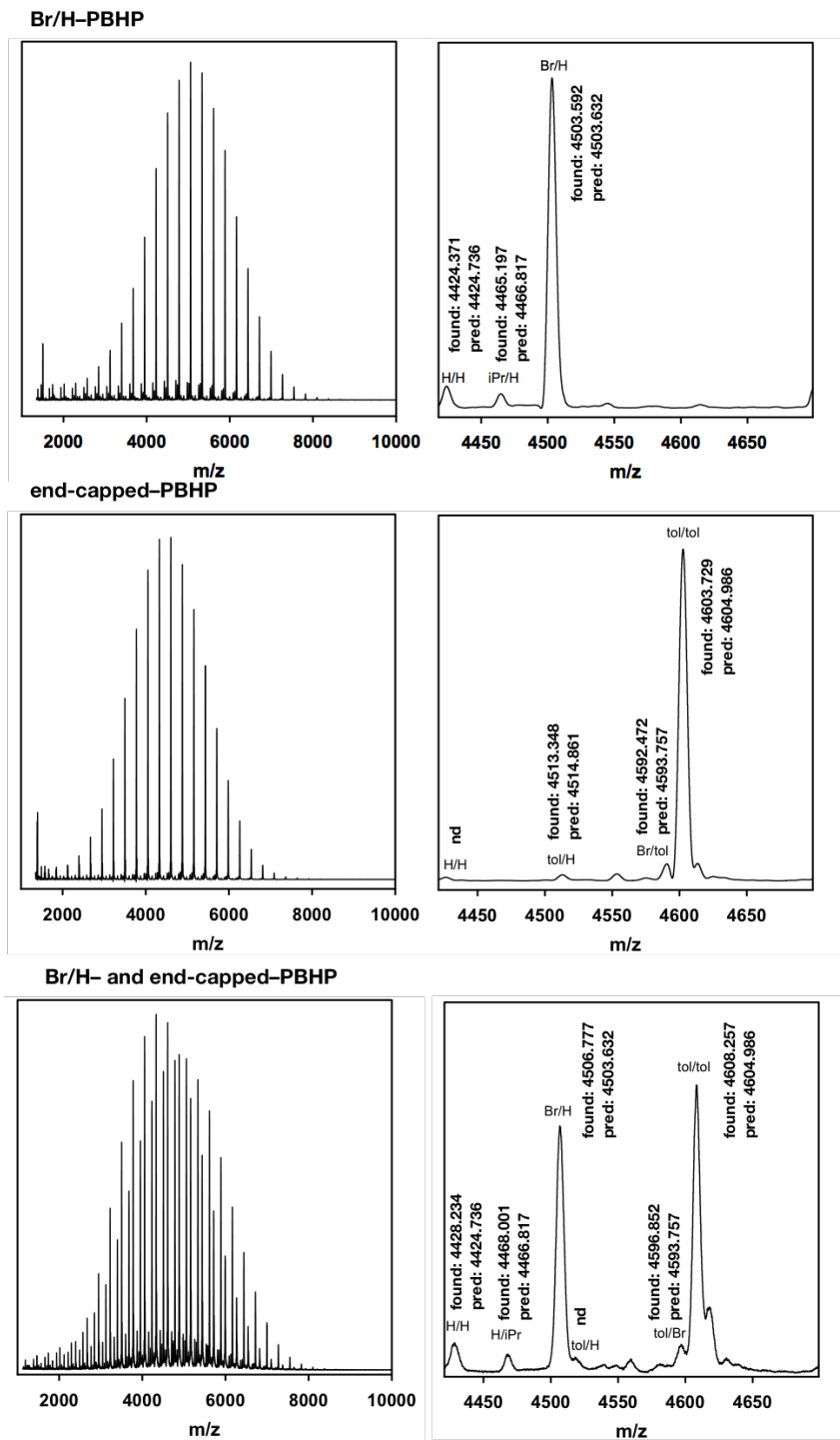


Figure A1-43. MALDI-TOF/MS spectra from Br/H-PBHP, end-capped-PBHP, and Br/H-PBHP combined with end-capped-PBHP in a 1:1 wt/wt ratio. Calculated using an average method, at signal-to-noise = 2. The degree of polymerization shown is 16.

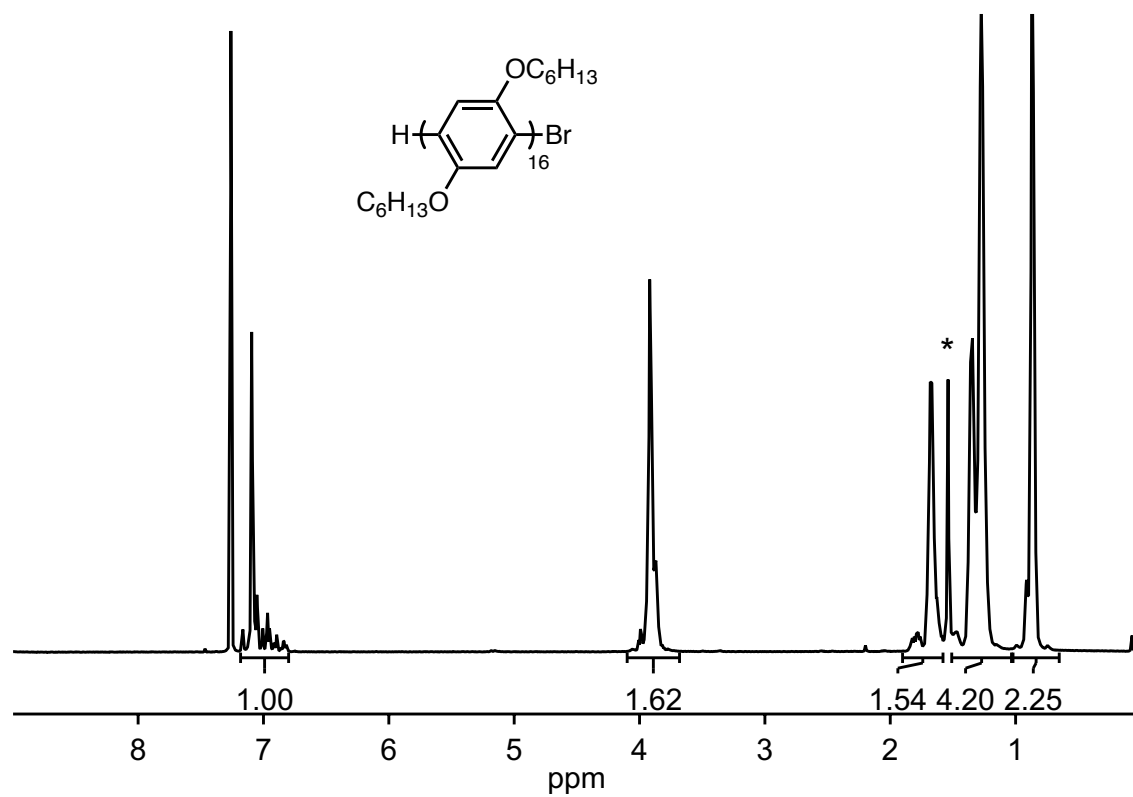


Figure A1-44. ^1H NMR spectrum of Br/H-PBHP (relaxation delay = 3s). ^1H NMR (500 MHz, CDCl_3-d) δ 7.18–6.78 (m, 1H), 4.10–3.68 (m, 2H), 1.91–1.59 (m, 2H), 1.51–1.02 (m, 4H), 1.02–0.65 (m, 2H).

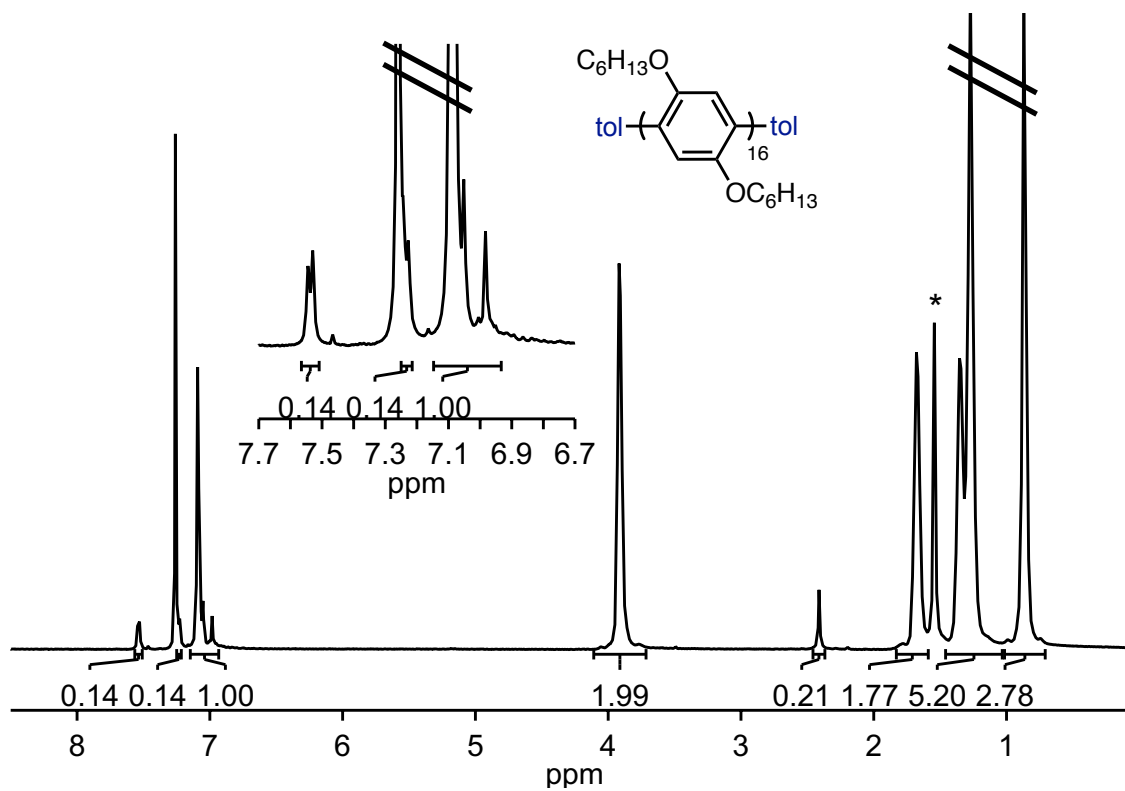


Figure A1-45. ^1H NMR spectrum of end-capped-PBHP (relaxation delay = 3s). ^1H NMR (500 MHz, CDCl_3 -*d*) δ 7.54 (d, $J = 7.5$ Hz, 0.14H), 7.24 (d, $J = 7.5$ Hz, 0.14H), 7.15–6.93 (m, 1H), 3.91 (q, $J = 5.8$ Hz, 2H), 2.41 (s, 0.21H), 1.83–1.58 (m, 2H), 1.45–1.02 (m, 5H), 0.86 (t, $J = 5.8$ Hz, 3H).

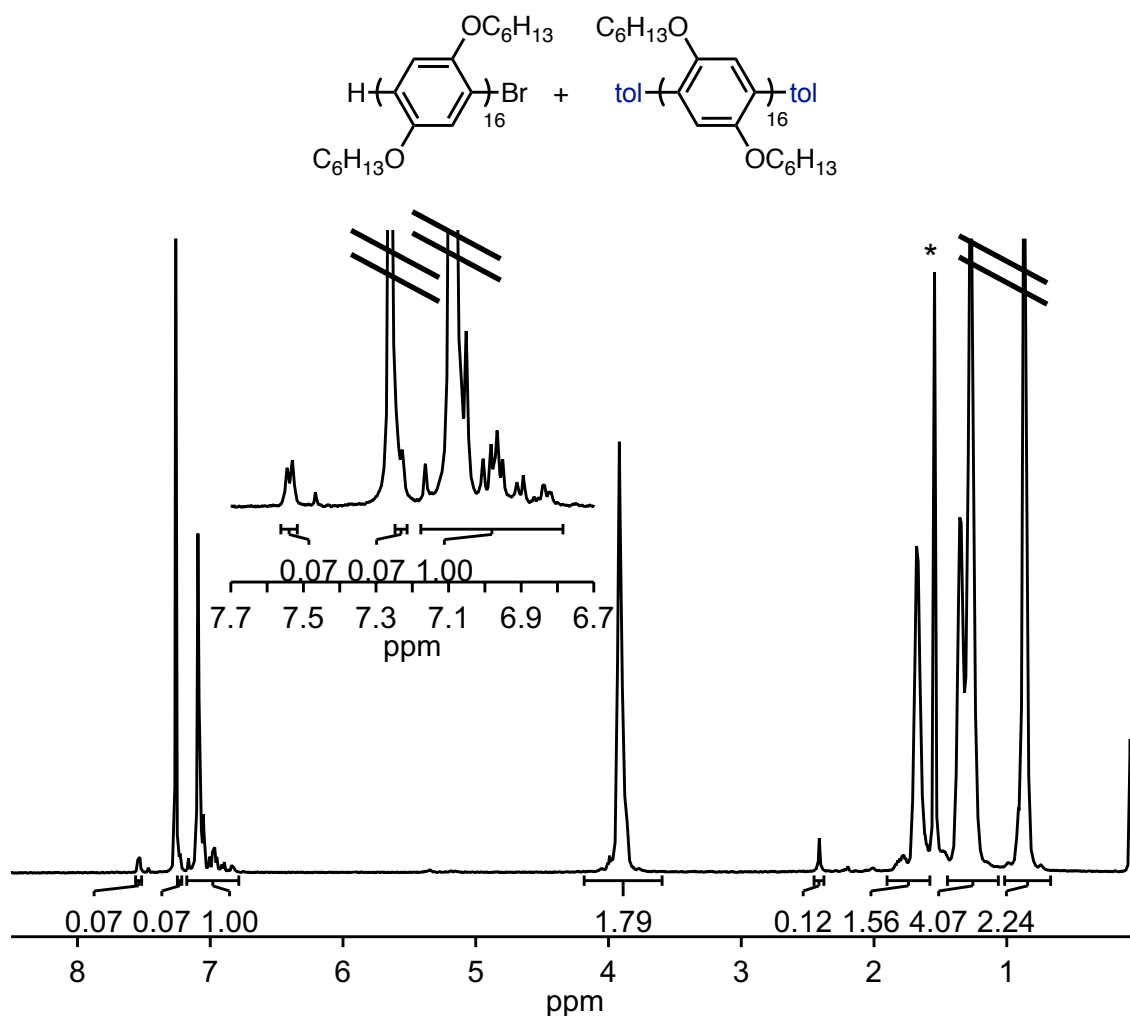
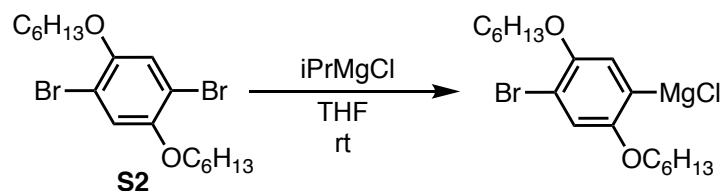


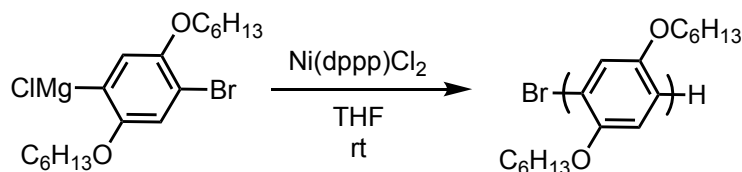
Figure A1-46. ^1H NMR spectrum of Br/H-PBHP combined with end-capped-PBHP in a 1:1 (wt/wt) ratio (relaxation delay = 3s). ^1H NMR (500 MHz, CDCl_3-d) δ 7.54 (d, $J = 7.6$ Hz, 0.7H), 7.23 (apparent s, 0.7H), 7.18–6.78 (m, 1H), 3.91 (q, $J = 5.9, 5.2$ Hz, wH), 2.41 (s, 0.12H), 1.90–1.57 (m, 2H), 1.45–1.07 (m, 4H), 0.87 (t, $J = 6.4$ Hz, 2H).

A1.6.2. Synthesis of H/Br-polymer for end-capping control reactions



Monomer activation: In a glovebox, iPrMgCl (2.0 M in THF, 0.526 mL, 1.05 mmol, 0.800 equiv) was added to a stirring solution of **S2** (574 mg, 1.32 mmol, 1.00 equiv) in THF (2.7 mL) and stirred for 17 h at rt. Titrating the resulting solution against salicylaldehyde phenylhydrazone (see general experimental) revealed the $[\text{Grignard}] = 0.272 \text{ M}$.

Precatalyst preparation: In the glovebox, to a 25 mL Schlenk flask was added Ni(dppp)Cl_2 (16 mg, 0.030 mmol, 1.0 equiv), THF (17.75 mL), and a stirbar. The Schlenk flask was capped with a septum, secured with copper wire, removed from the glovebox, and immediately placed under N_2 .



Polymerization: In the glovebox, Grignard monomer solution (0.272 M in THF, 2.20 mL, 0.598 mmol, 20.0 equiv) was drawn into a 3 mL syringe equipped with a long needle, headspace (~0.4 mL) was pulled and then the syringe/needle were removed from the glovebox. During transit, to the catalyst-containing flask, headspace (~0.2 mL) was evacuated from the needle before puncturing the septum. The monomer was added at once to the stirring catalyst heterogeneous mixture which turned from red solids to yellow solution within 30 s. The polymerization was stirred for 90 min under N_2 before being quenched with aq. HCl (12 M, 10 mL). The crude

polymer was extracted with CHCl_3 (3 x 10 mL), dried over MgSO_4 , filtered and analyzed by GC, GPC, and MALDI-TOF/MS. The remaining quenched polymer was concentrated under reduced pressure, redissolved in CHCl_3 (2 mL), and precipitated using MeOH (20 mL). The resulting heterogeneous mixture was divided equally into centrifuge tubes and diluted with additional MeOH (to fill the centrifuge tubes). The polymers were spun for 15 min. The clear supernatant was decanted and the white solid was collected by transferring to a vial using CHCl_3 . The polymer solution was concentrated under reduced pressure, yielding 113 mg of poly(2,5-bis(hexyloxy)phenylene) (PBHP) (68% yield).

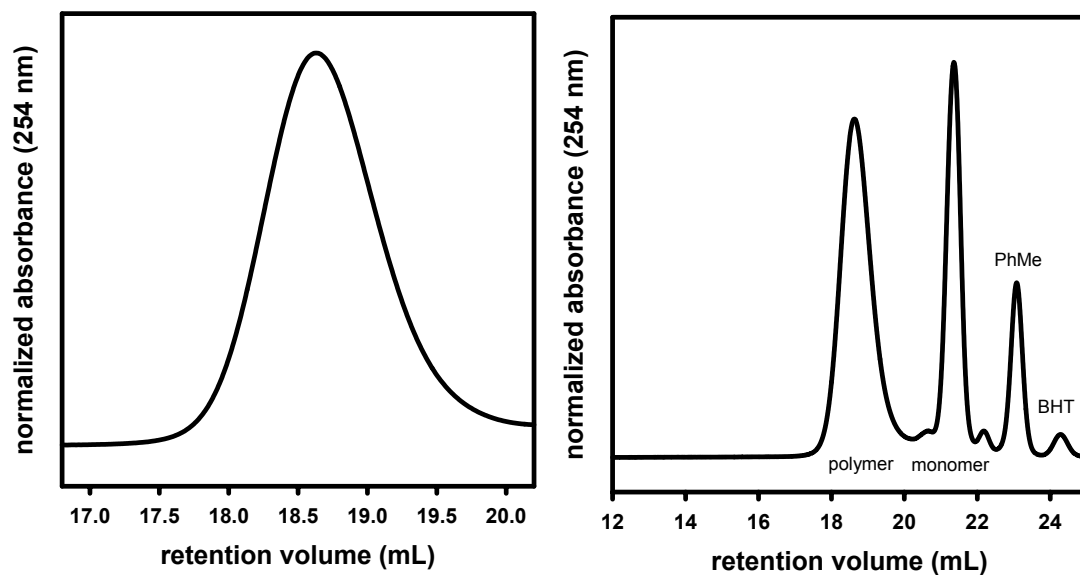


Figure A1-47. GPC trace of pre-precipitated PBHP synthesized via Ni(dppp)Cl₂. $M_n = 5.13$ kg/mol, $\bar{D} = 1.24$. (Left = zoomed, right = full GPC trace from the same sample).

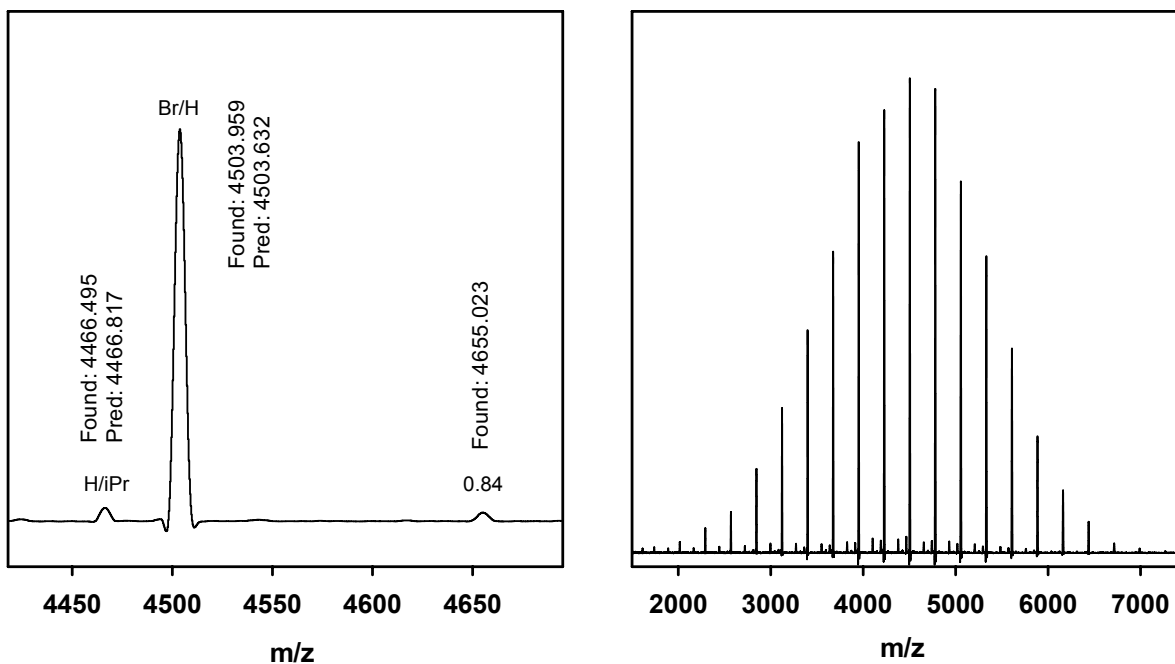


Figure A1-48. MALDI-TOF/MS spectrum of crude PBHP synthesized via Ni(dppp)Cl₂. The 0.84 fractional corresponds to an unknown impurity. Values calculated using an average mass method, signal-to-noise = 1. The degree of polymerization shown is 16.

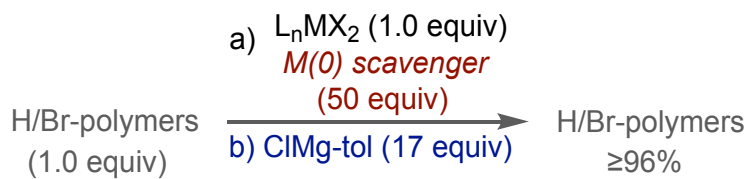
A1.6.3. End-capping control reactions

i. Ni(IPr)(PPh₃)Cl₂

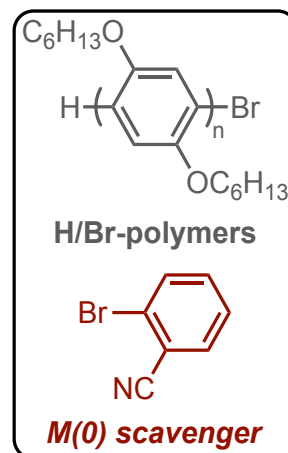
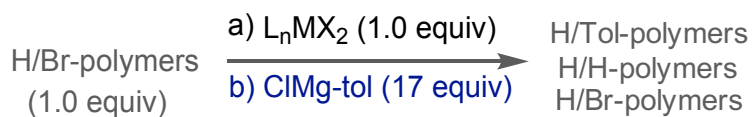
ii. Pd(IPr)(3-Clpy)Cl₂

iii. Ni(dppp)Cl₂

end-capping experiment control



end-capping control (capping agent only)



i. Ni(IPr)(PPh₃)Cl₂ (the following takes place in the glovebox until noted)

Polymer solution: PBHP ($M_n = 5057.159$ g/mol according to MALDI-TOF/MS, repeat unit = 276.42 Da, 113.0 mg) was dissolved in THF (13.63 mL) with mild heating (40 °C) for 5 min. Generating a [0.03 M] solution relative to repeat unit.

Vial preparation:

End-capping experiment vial: In a glovebox, to an 8 mL vial was added 1-bromo-2-cyanobenzene (7.4 mg, 0.041 mmol, 50. equiv), THF (0.279 mL), *p*-toluenemagnesium chloride (1.18 M in THF, 11.7 μL, 0.0138 mmol, 17.0 equiv) and a stirbar. The vial was capped with a septum cap and sealed with electrical tape.

End-capping control experiment (capping agent only) vial: In a glovebox, to an 8 mL vial was added THF (0.25 mL), *p*-toluenemagnesium chloride (1.18 M in THF, 10.8 μL, 0.0128 mmol, 17.0 equiv) and a stirbar. The vial was capped with a septum cap and sealed with electrical tape.

Experiments: In the glovebox, to an 8 mL vial equipped with a stirbar was added Ni(IPr)(PPh₃)Cl₂ (3.0 mg, 0.0038 mmol, 1.0 equiv), polymer solution (2.34 mL containing 19.4 mg polymer, 0.00384 mmol, 1.00 equiv), and THF (0.22 mL). The vial was capped with a septum cap and sealed with electrical tape, removed from the glovebox, and immediately placed under N₂. An aliquot (0.50 mL, i.e., 0.00075 mmol catalyst, 1.0 equiv) was removed from the polymer solution using a syringe and added to the capping agent only solution. A second aliquot (0.54 mL, i.e., 0.00081 mmol catalyst, 1.0 equiv) was removed from the polymer solution using a syringe and added to end-capping experiment vial. The solutions were stirred for 2 h under N₂

at rt and then an aliquot (0.2 mL) was removed and quenched directly into aq. HCl (12 M, 1 mL). The remaining solutions were stirred for 24 h under N₂ at rt before quenching with aq. HCl (12 M, 3 mL). After quenching, each solution was extracted with CHCl₃ (3 x 1 mL), dried over MgSO₄, and analyzed by MALDI-TOF/MS.

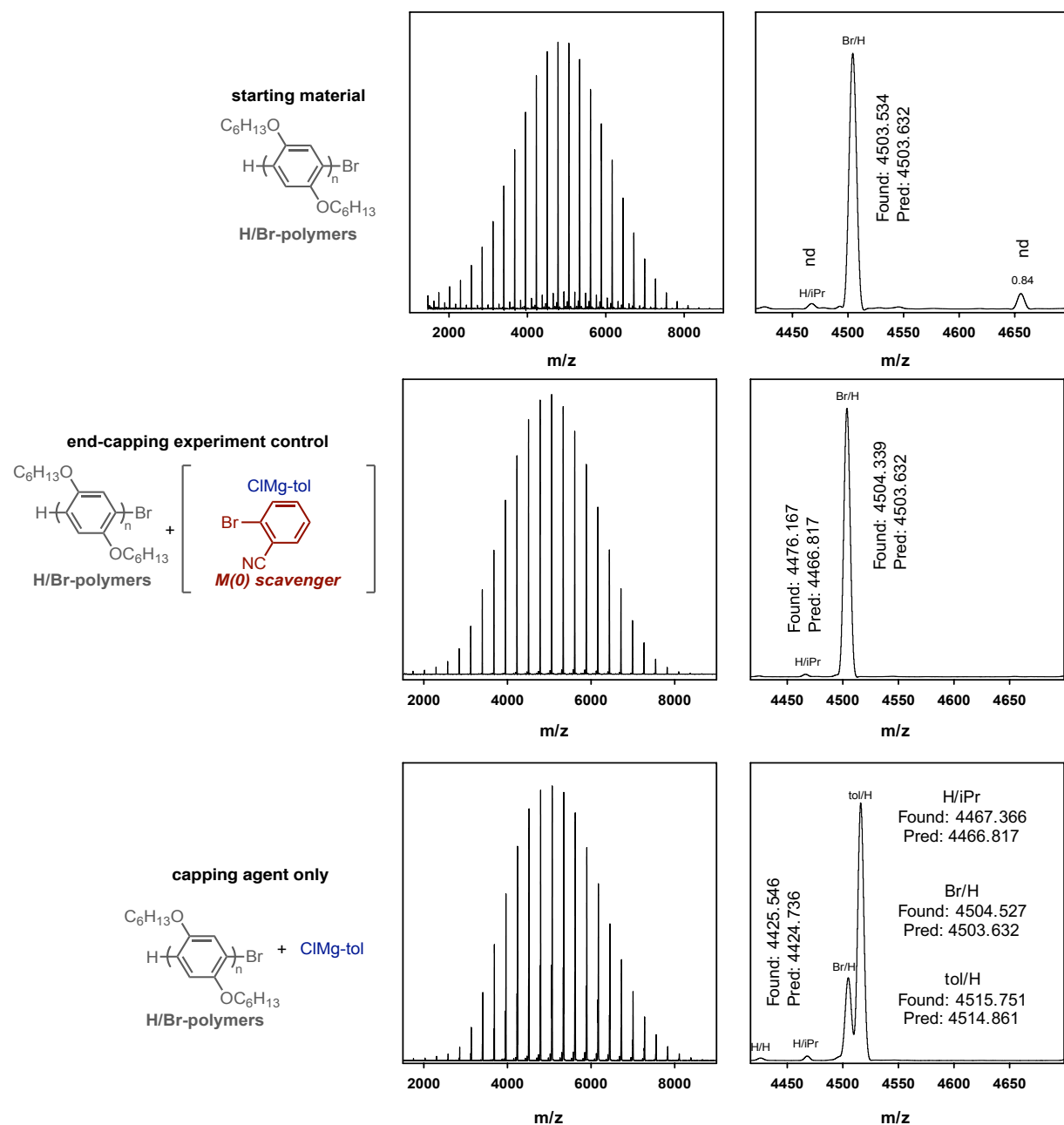


Figure A1-49. MALDI-TOF/MS spectra from end-capping control reactions for PBHP using $\text{Ni}(\text{IPr})(\text{PPh}_3)\text{Cl}_2$. The 0.84 fractional corresponds to an unknown impurity. Values calculated using an average mass method, signal-to-noise = 2. The degree of polymerization shown is 16.

ii. Pd(IPr)(3-Clpy)Cl₂ (the following takes place in the glovebox until noted)

Polymer solution: PBHP ($M_n = 5057.159$ g/mol according to MALDI-TOF/MS, repeat unit = 276.42 Da, 113.0 mg) was dissolved in THF (13.63 mL) with mild heating (40 °C) for 5 min. Generating a [0.03 M] solution relative to repeat unit.

Vial preparation:

End-capping experiment vial: In a glovebox, to an 8 mL vial was added 1-bromo-2-cyanobenzene (7.4 mg, 0.041 mmol, 50. equiv), THF (0.279 mL), *p*-toluenemagnesium chloride (1.18 M in THF, 11.7 μL, 0.0138 mmol, 17.0 equiv) and a stirbar. The vial was capped with a septum cap and sealed with electrical tape.

End-capping control experiment (capping agent only) vial: In a glovebox, to an 8 mL vial was added THF (0.25 mL), *p*-toluenemagnesium chloride (1.18 M in THF, 10.8 μL, 0.0128 mmol, 17.0 equiv) and a stirbar. The vial was capped with a septum cap and sealed with electrical tape.

Experiments: In the glovebox, to an 8 mL vial equipped with a stirbar was added Pd(IPr)(3-Clpy)Cl₂ (1.7 mg, 0.0025 mmol, 1.0 equiv), polymer solution (1.53 mL containing 12.6 mg polymer, 0.00250 mmol, 1.00 equiv), and THF (0.144 mL). The vial was capped with a septum cap and sealed with electrical tape, removed from the glovebox, and immediately placed under N₂. An aliquot (0.50 mL, i.e., 0.00075 mmol catalyst, 1.0 equiv) was removed from the polymer solution using a syringe and added to the capping agent only solution. A second aliquot (0.54 mL, i.e., 0.00081 mmol catalyst, 1.0 equiv) was removed from the polymer solution using a syringe and added to the end-capping experiment vial. Each solution was stirred for 2 h under N₂

at rt. The solutions were quenched with aq. HCl (12 M, 1 mL), extracted with CHCl₃ (3 x 1 mL), dried over MgSO₄, and analyzed by MALDI-TOF/MS.

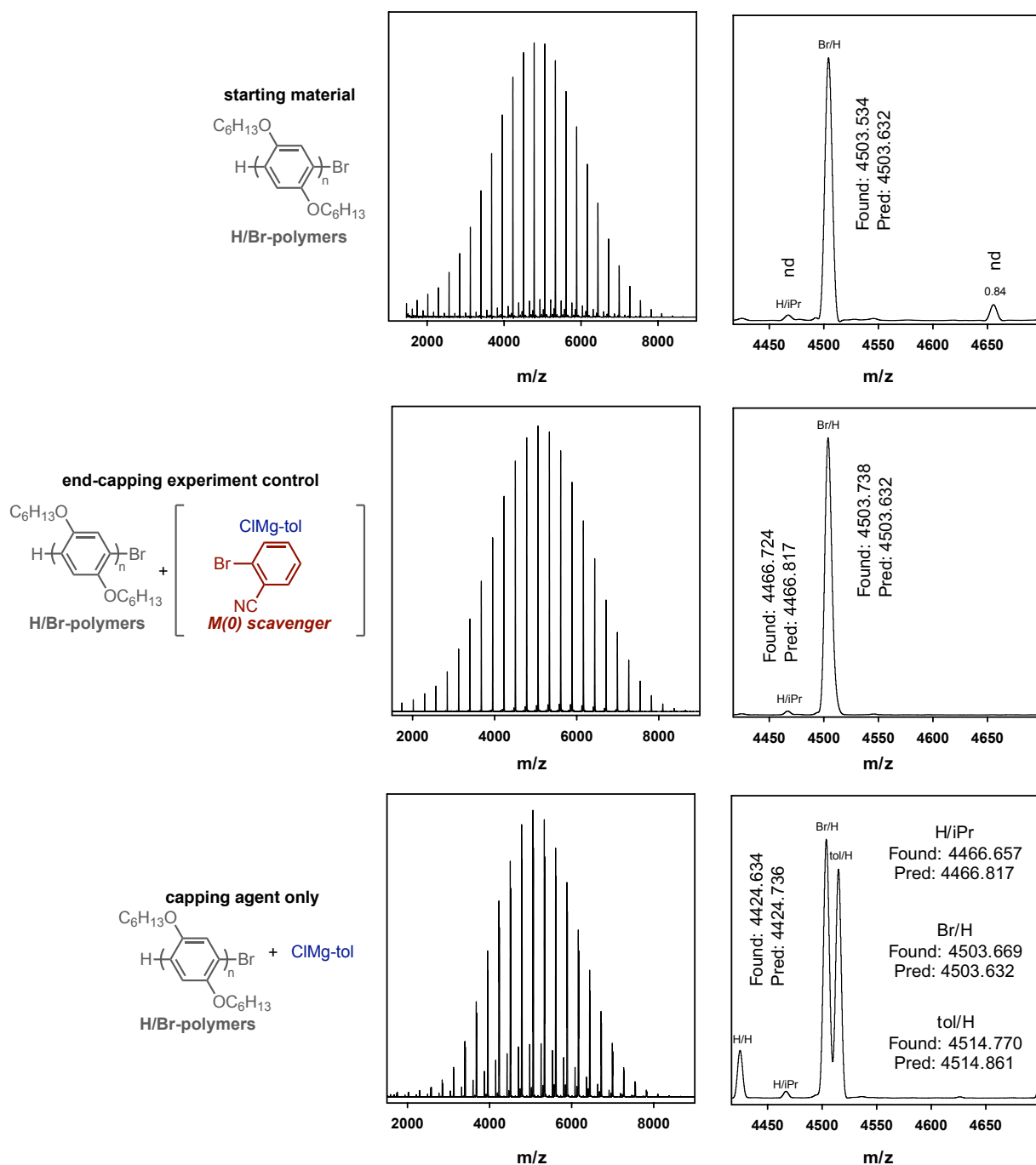


Figure A1-50. MALDI-TOF/MS spectra from end-capping control reactions for PHBP and $\text{Pd}(\text{IPr})(3\text{Clpy})\text{Cl}_2$. Values calculated using average mass method, nd = not detected at signal-to-noise = 1. The degree of polymerization shown is 16.

iii. Ni(dppp)Cl₂ (the following takes place in the glovebox until noted)

Polymer solution: PBHP ($M_n = 5057.159$ g/mol according to MALDI-TOF/MS, repeat unit = 276.42 Da, 113.0 mg) was dissolved in THF (13.63 mL) with mild heating (40 °C) for 5 min. Generating a [0.03 M] solution relative to repeat unit.

Vial preparation:

End-capping experiment vial: In a glovebox, to an 8 mL vial was added 1-bromo-2-cyanobenzene (16.0 mg, 0.0879 mmol, 50.0 equiv), THF (0.572 mL), *p*-toluenemagnesium chloride (1.18 M in THF, 25.2 μL, 0.0297 mmol, 17.0 equiv) and a stirbar. The vial was capped with a septum cap and sealed with electrical tape.

End-capping control experiment (capping agent only) vial: In a glovebox, to an 8 mL vial was added THF (0.572 mL), *p*-toluenemagnesium chloride (1.18 M in THF, 25.2 μL, 0.0297 mmol, 17.0 equiv) and a stirbar. The vial was capped with a septum cap and sealed with electrical tape.

Experiments: In the glovebox, to an 8 mL vial equipped with a stirbar was added Ni(dppp)Cl₂ (4.3 mg, 0.0079 mmol, 1.0 equiv), polymer solution (4.84 mL containing 40.1 mg polymer, 0.00793 mmol, 1.00 equiv), and THF (0.447 mL). The vial was capped with a septum cap and sealed with electrical tape, removed from the glovebox, and immediately placed under N₂. An aliquot (1.17 mL, i.e., 0.00175 mmol catalyst, 1.00 equiv) was removed from the polymer/precatalyst flask using a syringe and added to the capping agent only solution. A second aliquot (1.17 mL, i.e., 0.00175 mmol catalyst, 1.00 equiv) was removed from the polymer/precatalyst flask using a syringe and added to the end-capping experiment vial. It should

be noted that Ni(dppp)Cl₂ is not completely dissolved in the polymer/THF solution when transferred; however, Ni(dppp)Cl₂ visibly enters (red solids into the clear solution) the reaction vials and the solution color immediately changes from clear and colorless (end-capping vials) to pale yellow and finally black over the course of the reaction, indicating catalyst is present and reacting. Each solution was stirred for 2 h under N₂ at rt. The solutions were quenched with aq. HCl (12 M, 3 mL), extracted with CHCl₃ (3 x 1 mL), dried over MgSO₄, and analyzed by MALDI-TOF/MS.

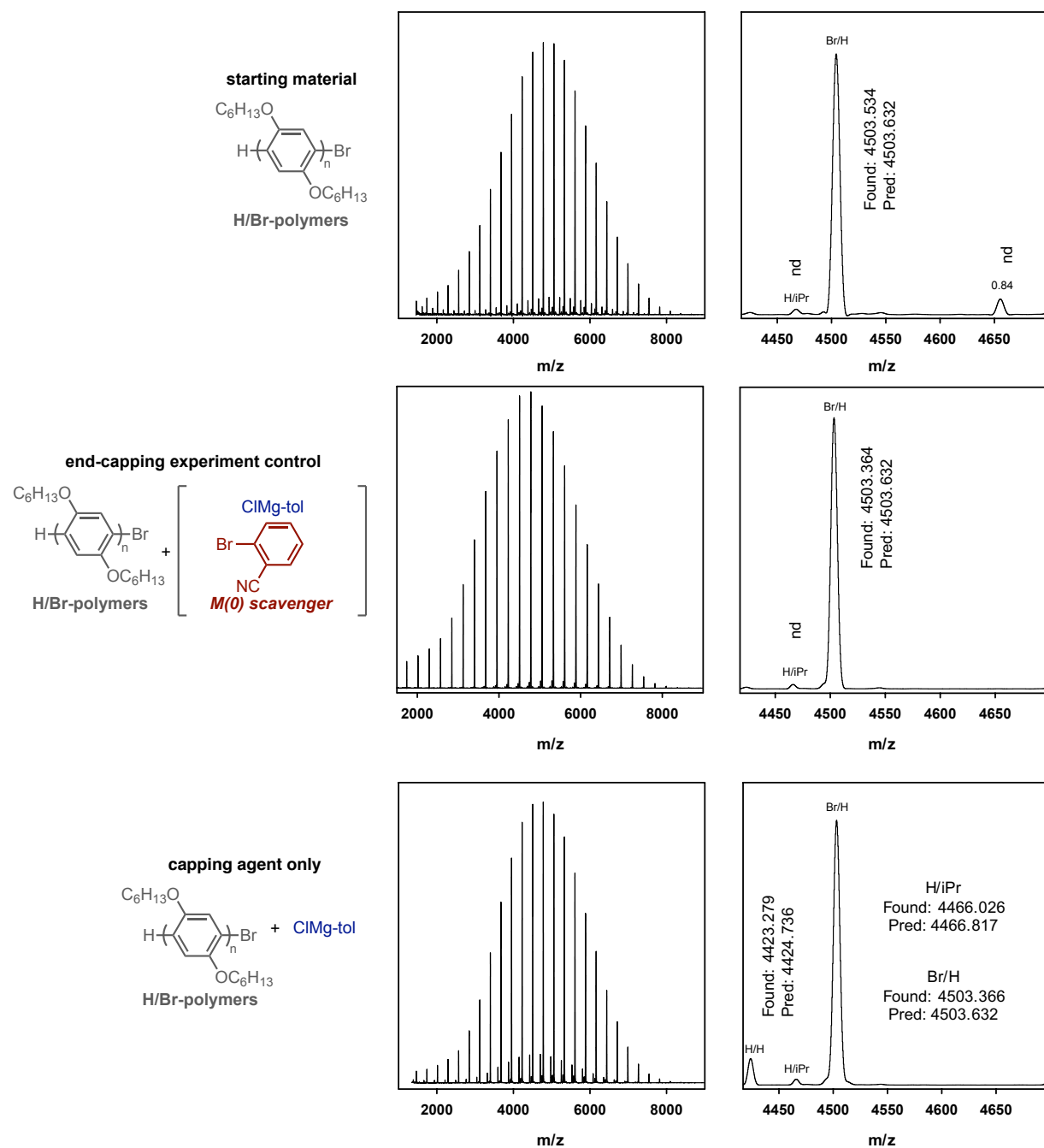
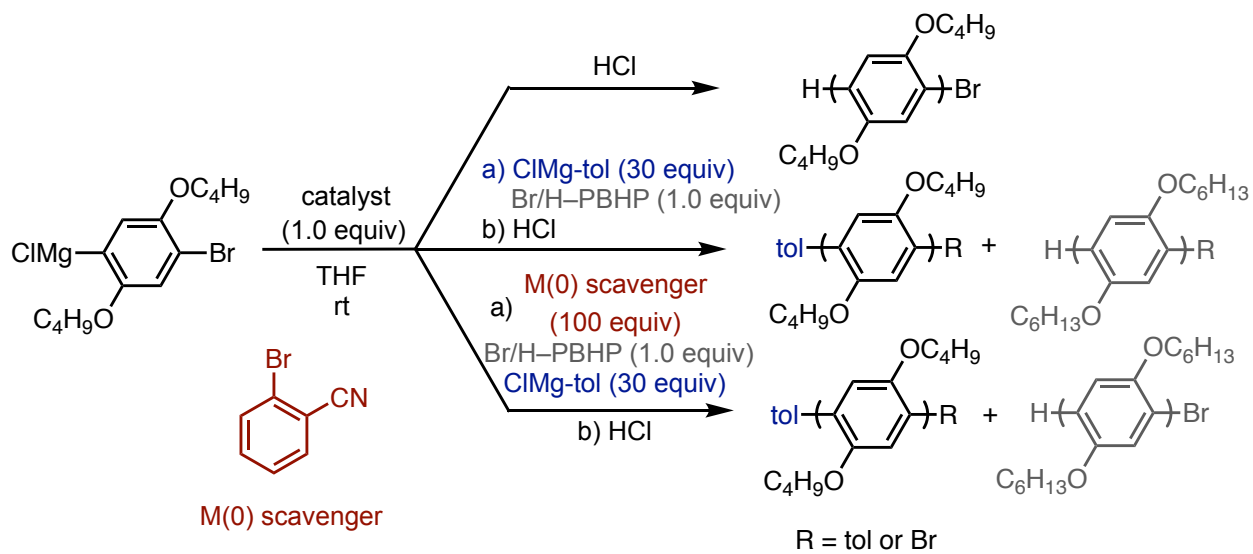
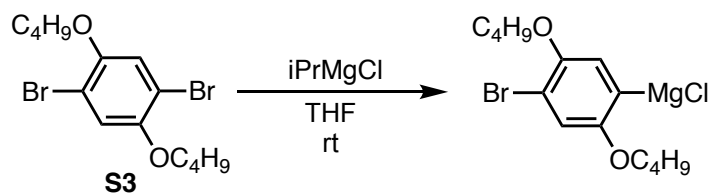


Figure A1-51. MALDI-TOF/MS spectra from end-capping control experiments for PBHP and $\text{Ni}(\text{dppp})\text{Cl}_2$. Values calculated using an average mass method, nd = not detected at signal-to-noise = 1. The degree of polymerization shown is 16.

A1.6.4. End-capping cross-over experiments to evaluate the impact of chain-entanglement for PBAP (A = alkoxy).





Monomer activation: In a glovebox, $i\text{PrMgCl}$ (2.2 M in THF, 0.912 mL, 2.01 mol, 0.800 equiv) was added to a stirring solution of **S3** (0.953 g, 2.51 mmol, 1.00 equiv) in THF (4.11 mL) and stirred for 17 h at rt. Titrating the resulting solution against salicylaldehyde phenylhydrazone (see general experimental) revealed the $[\text{Grignard}] = 0.299 \text{ M}$.

Preparing precatalysts:

$\text{Ni}(\text{IPr})(\text{PPh}_3)\text{Cl}_2$: To an 8 mL vial was added $\text{Ni}(\text{IPr})(\text{PPh}_3)\text{Cl}_2$ (7.7 mg, 0.0099 mmol) and dissolved in THF (0.99 mL) for a [0.01 M] solution.

Br/H–PBHP solution: Br/H–PBHP (MW calculated by MALDI-TOF/MS as 5057.159 g/mol, 41.0 mg, 0.00811 mmol) was dissolved in THF (5.41 mL) with mild heating (40 °C for 3 min) for a [0.0015 M] solution.

Preparing end-capping experiment vials:

(equiv are relative to the catalyst/polymer (1.0 equiv) that will be added to each vial)

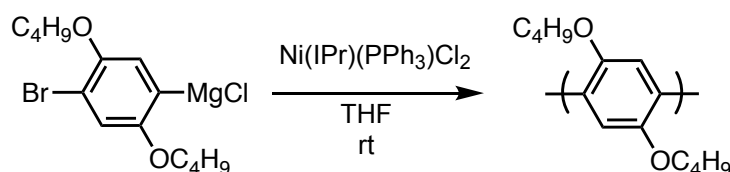
End-capping cross-over experiment vial: In a glovebox, to an 8 mL vial equipped with a stirbar was added 1-bromo-2-cyanobenzene (13.7 mg, 0.0750 mmol, 100.0 equiv), *p*-toluenemagnesium chloride (1.11 M in THF, 20.3 μL , 0.0225 mmol, 30.0 equiv), Br/H–PBHP (0.0015 M in THF, 0.50 mL, 0.00075 mmol, 1.0 equiv), and THF (0.5 mL). The vial was sealed with a septum-cap

and secured with electrical tape, upon removal from the glovebox the vial was immediately placed under N₂.

End-capping control vial (capping agent only): In a glovebox, in an 8 mL vial equipped with a stirbar was added *p*-toluenemagnesium chloride (1.11 M in THF, 20.3 μL, 0.0225 mmol, 30.0 equiv), Br/H–PBHP (0.0015 M in THF, 0.50 mL, 0.00075 mmol, 1.0 equiv), and THF (0.5 mL). The vial was sealed with a septum-cap and secured with electrical tape, upon removal from the glovebox the vial was immediately placed under N₂.

Reaction flask preparation:

Ni(IPr)(PPh₃)Cl₂: In the glovebox, to a 10 mL Schlenk flask was added precatalyst (0.498 mL, 0.00498 mmol, 1.00 equiv), THF (2.32 mL), and a stirbar. The Schlenk flask was capped with a septum, secured with copper wire, removed from the glovebox, and immediately placed under N₂.



Polymerization: In the glovebox, Grignard monomer solution (0.299 M in THF, 0.50 mL, 0.15 mmol, 30. equiv) was drawn into a 3 mL syringe equipped with a long needle, headspace (~1.4 mL) was pulled and then the syringe/needle were removed from the glovebox. During transit to the catalyst-containing flask, the headspace (~1.0 mL) was evacuated from the needle before puncturing the septum. The monomer was added at once to the stirring precatalyst flasks. The polymerizations were stirred for 90 min under N₂.

End-capping experiments: Aliquots (each 0.5 mL, containing 0.00075 mmol catalyst, 1.00 equiv catalyst) were added to the end-capping cross-over experiment and control vials and stirred under N₂ for 2 h before quenching with aq. HCl (12 M, 1 mL). Immediately after aliquots were removed from the polymerizations, the remaining polymer solution was quenched with aq. HCl (12 M, 3 mL). Samples were worked up for GC, GPC, and MALDI-TOF/MS.

Monomer conversion: 93%

Table A1-22. M_n and \mathcal{D} from PBBP (B = butyloxy) (before end-capping cross-over experiments), end-capping cross-over experiment (ec), end-capping cross-over control (only capping agent) experiment, and the added Br/H-PBHP via Ni(IPr)(PPh₃)Cl₂.

Ni(IPr)(PPh ₃)Cl ₂	M_n (kg/mol)	\mathcal{D}
PBBP	8.24	1.28
cap only	8.28	1.27
ec	7.54	1.27
added PBHP	6.48	1.25

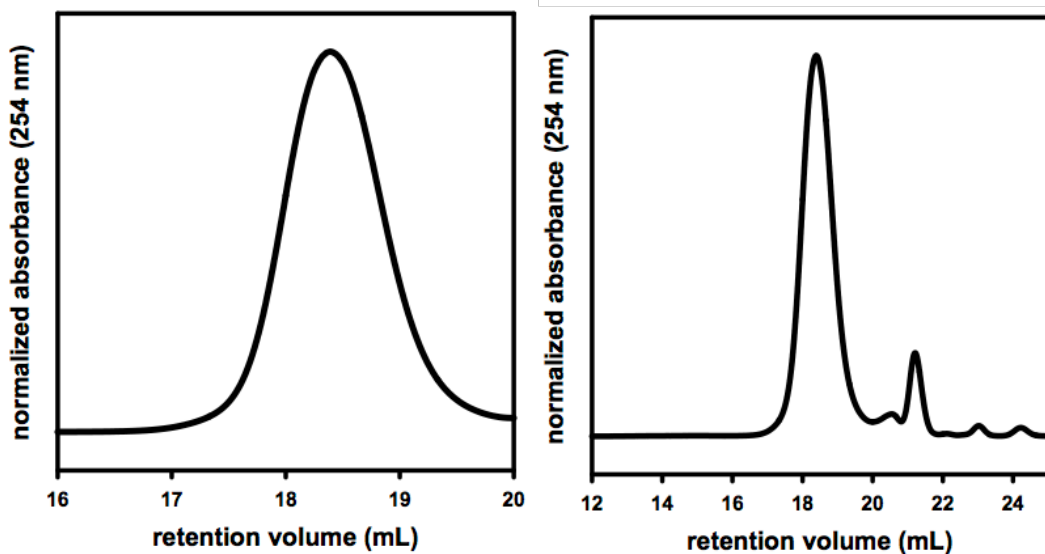


Figure A1-52. GPC traces from added Br/H-PBHP (left = zoomed, right = full GPC trace of the set of samples). Note that residual monomer elutes from 20.5–22 min, PhMe elutes at 23.1 min and BHT elutes at 23.8 min.

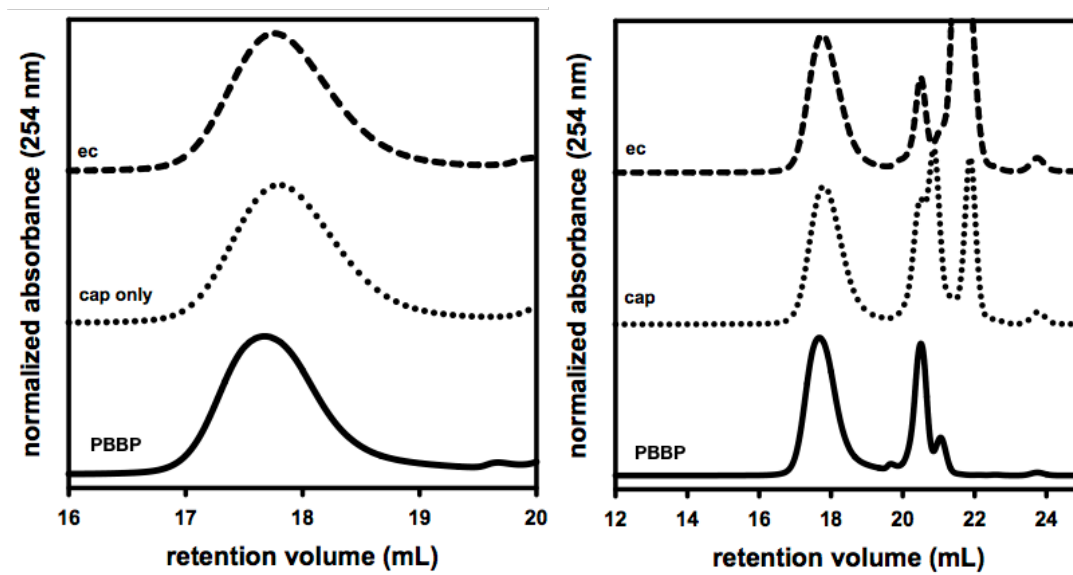


Figure A1-53. GPC traces from PBBP (before end-capping cross-over experiments), end-capping cross-over experiment (ec), and end-capping cross-over control (only capping agent) experiments via Ni(IPr)(PPh₃)Cl₂. Note that M(0) scavenging agent and residual monomer elute from 20.5–22 min, PhMe elutes at 23.1 min and BHT elutes at 23.8 min.

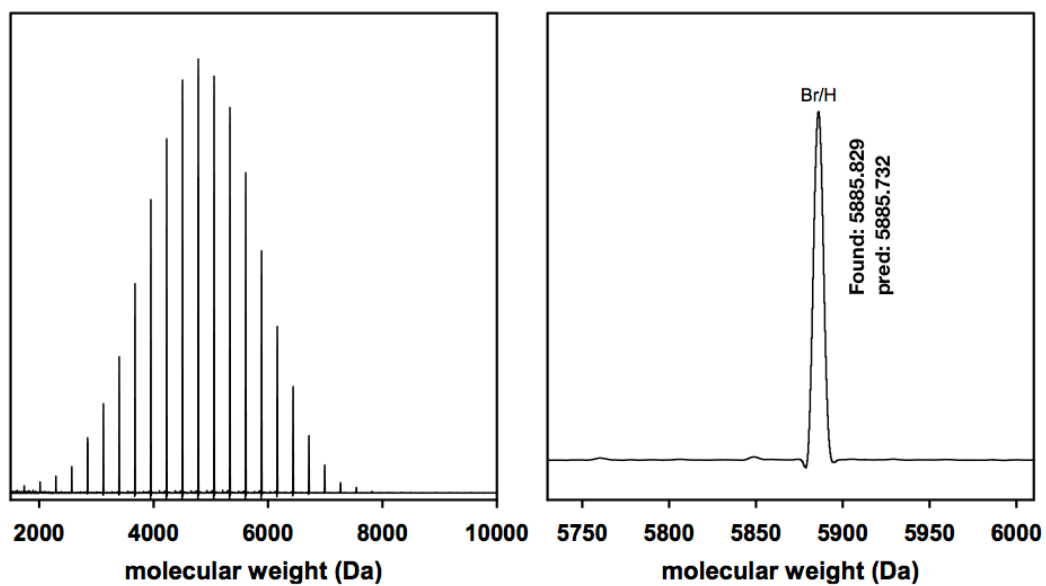


Figure A1-54. MALDI-TOF/MS traces from added Br/H-PBHP added polymer in cross-over experiment. Values calculated using average mass method at signal-to-noise = 2. The repeat unit shown is 21.

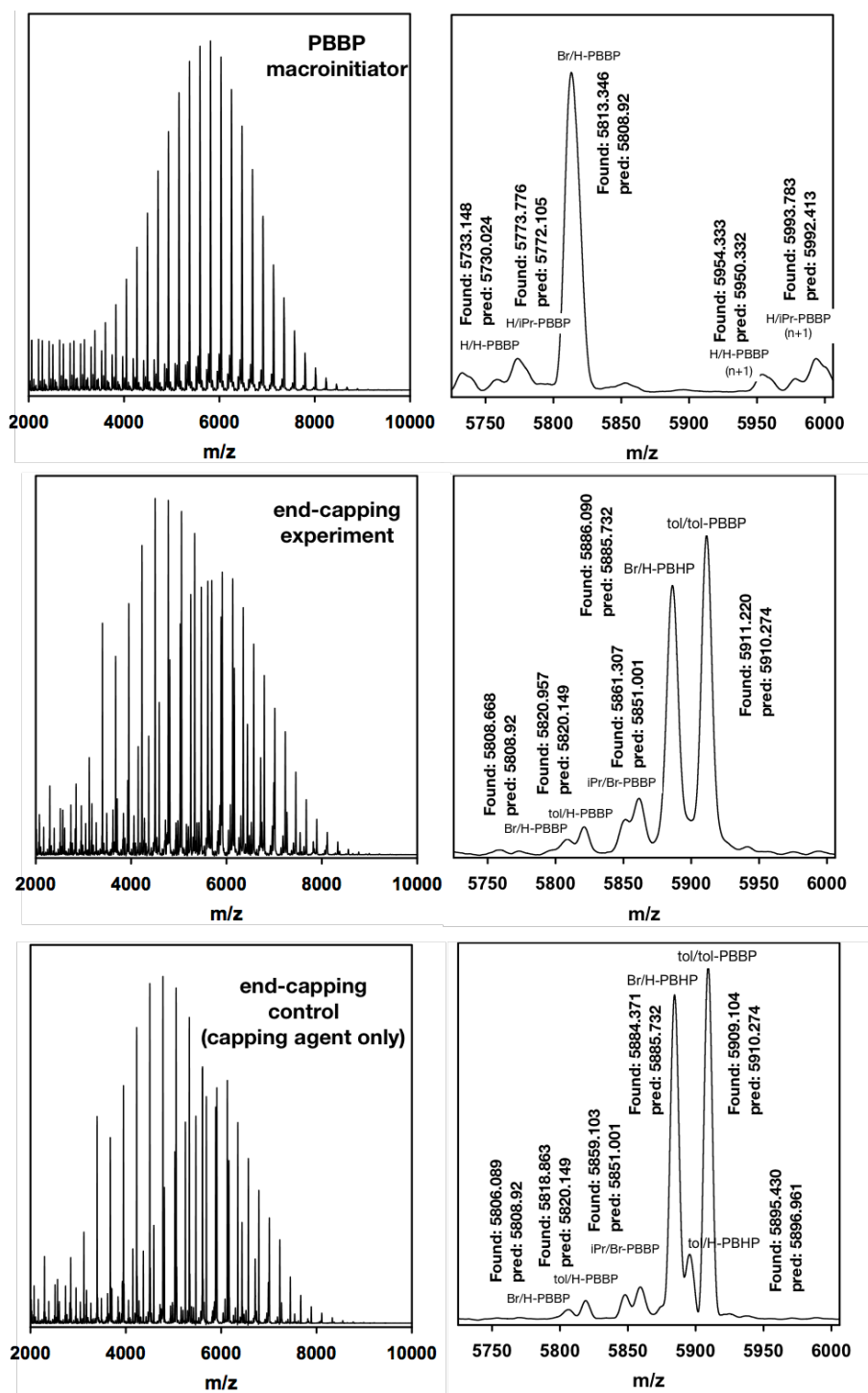


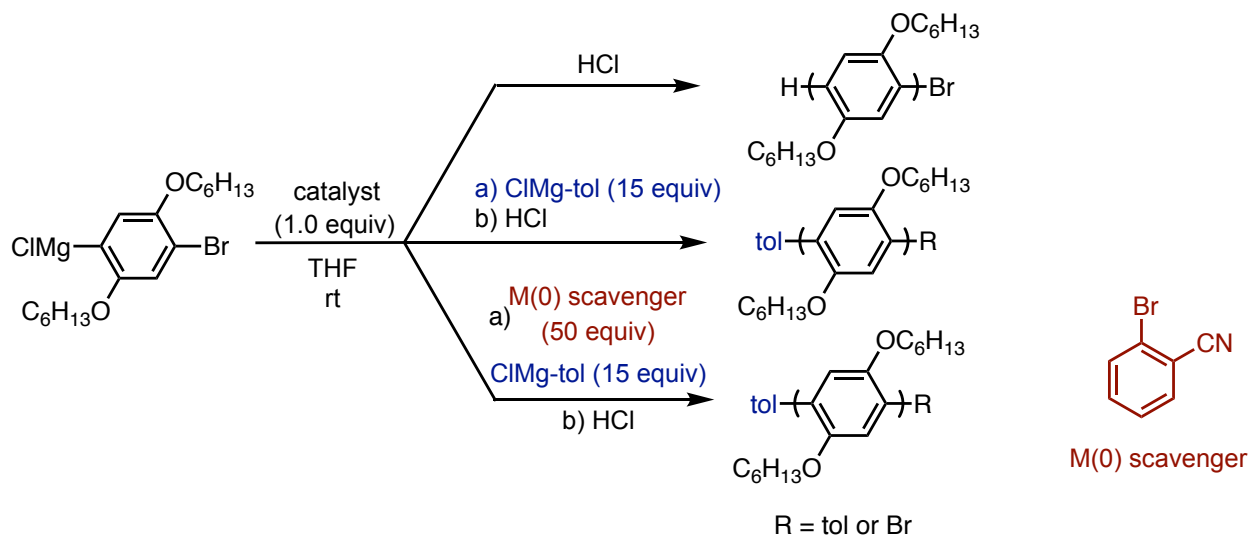
Figure A1-55. MALDI-TOF/MS traces from PBBP macroinitiator (before end-capping), end-capping cross-over experiment, and end-capping cross-over control (only capping agent) experiments for Ni(IPr)(PPh₃)Cl₂. Values calculated using average mass method at signal-to-noise = 2. The repeat unit shown is 26 for PBBP and 21 for PBHP.

A1.6.5. End-capping reactions

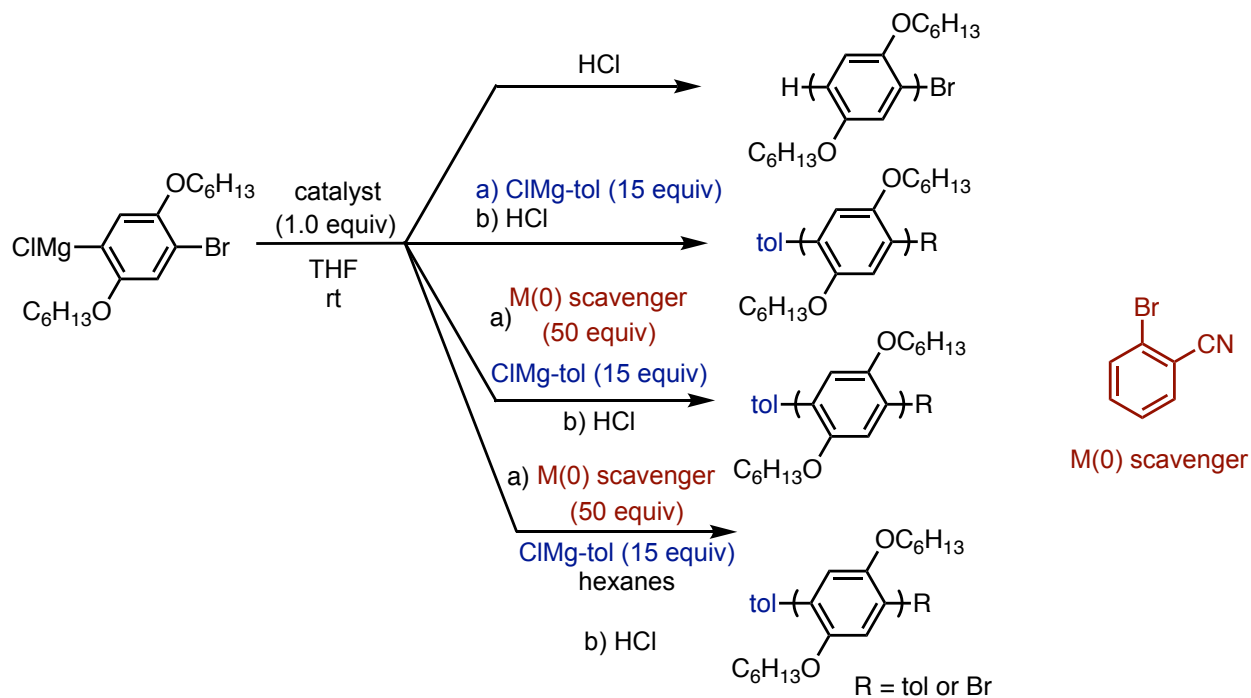
i. Ni(IPr)(PPh₃)Cl₂ (2 h end-capping and 24 h end-capping)

ii. Pd(IPr)(3-Clpy)Cl₂

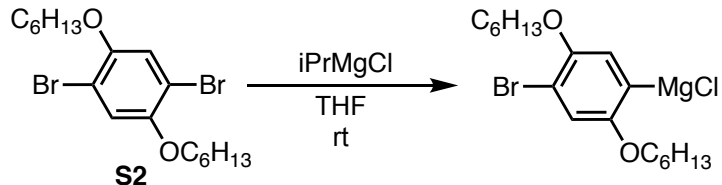
iii. Ni(dppp)Cl₂



iv. Evaluating the impact of solvent (hexane) on end-capping experiments



i. General Procedure for Ni(IPr)(PPh₃)Cl₂ - End-capping experiments for 2 h



Monomer activation: In a glovebox, **S2** (522.0 mg, 1.197 mmol, 1.000 equiv) was weighed into a 20 mL vial and dissolved in THF (1.92 mL). Then, iPrMgCl (2.0 M in THF, 479 μ L, 0.957 mmol, 0.800 equiv) and C₂₂H₄₆ (~8 mg, as an internal standard) were added and the solution was stirred for 17 h at rt. The activated monomer was titrated (see general experimental), revealing overall [Grignard] = 0.327 M.

Preparing stock solutions:

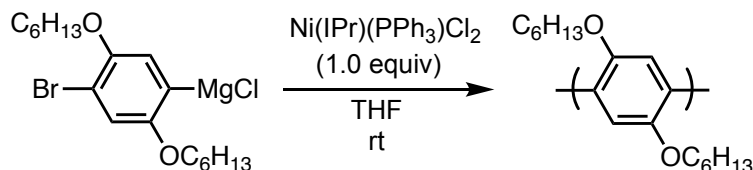
Precatalyst solution: In a glovebox, Ni(IPr)(PPh₃)Cl₂ (8.5 mg, 0.010 mmol) was weighed into a 4 mL vial and dissolved in THF (1.0 mL) for an overall concentration of 0.01 M.

Preparing end-capping control/experiment vials:

(equiv are relative to the catalyst/polymer (1.0 equiv) that will be added to each vial)

End-capping experiment vial: In a glovebox, to an 8 mL vial equipped with a stirbar was added 1-bromo-2-cyanobenzene (13.7 mg, 0.0750 mmol, 50.0 equiv), *p*-toluenemagnesium chloride (1.18 M in THF, 19.1 μ L, 0.0225 mmol, 15.0 equiv), and THF (0.5 mL). The vial was sealed with a septum-cap and secured with electrical tape, upon removal from the glovebox the vial was immediately placed under N₂.

End-capping control vial (capping agent only): In a glovebox, in an 8 mL vial equipped with a stirbar was added *p*-toluenemagnesium chloride (1.18 M in THF, 19.1 μ L, 0.0225 mmol, 15.0 equiv) and THF (0.5 mL). The vial was sealed with a septum-cap and secured with electrical tape, upon removal from the glovebox the vial was immediately placed under N₂.



Polymerization: In a glovebox, to a 15 mL Schlenk flask equipped with a stirbar was added precatalyst Ni(IPr)(PPh₃)Cl₂ (0.01 M in THF, 0.654 mL, 0.00654 mmol, 1.00 equiv) and THF (3.21 mL). The flask was capped with a septum, sealed with copper wire, removed from the glovebox, and immediately placed under N₂. The Grignard monomer (0.327 M in THF, 0.500 mL, 0.164 mmol, 25.0 equiv) was removed from the glovebox in a 1 mL syringe with a long needle and headspace (~0.4 mL). The monomer containing syringe was removed from the glovebox and during transit headspace (~0.25 mL) was evacuated before puncturing the Schlenk flask's septum with the needle. The Grignard monomer solution was added to the catalyst flask at once and stirred for 90 min at rt.

In situ end-capping: An aliquot (2.0 mL) was removed using a syringe and added in portions (1.0 mL/vial, 0.0015 mmol, 1.0 equiv) to i) the end-capping control solution and ii) the end-capping experiment solution. The remaining polymer solution was quenched with aq. HCl (12 M, 3 mL). The end-capping experiments were run for 2 h before quenching with aq. HCl (12 M, 1.0 mL). Samples were worked up for GC, GPC, and MALDI-TOF/MS.

Monomer conversion: Run 1: 87%, Run 2: 93%

Table A1-23. M_n , and \bar{D} from PBHP (before end-capping), end-capping experiment (ec), and end-capping control (only capping agent) experiments for Ni(IPr)(PPh₃)Cl₂ and PBHP.

Run 1	M_n (kg/mol)	\bar{D}	Run 2	M_n (kg/mol)	\bar{D}
PBHP	8.69	1.24	PBHP	8.11	1.25
cap control	8.82	1.26	cap control	8.28	1.24
ec	8.77	1.25	ec	8.17	1.25

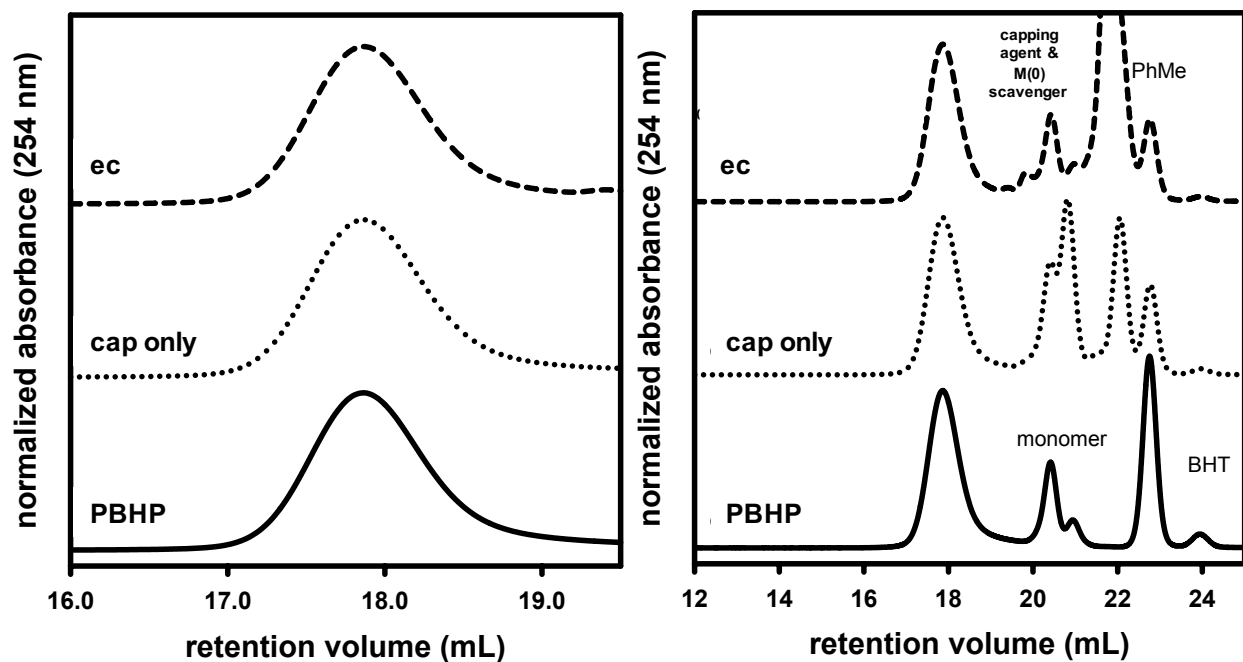


Figure A1-56. GPC traces from PBHP (before end-capping), end-capping experiment, and end-capping control (only capping agent) experiments for Ni(IPr)(PPh₃)Cl₂ and PBHP (t = 2 h). (Left = zoomed, right = full GPC trace from Run 1).

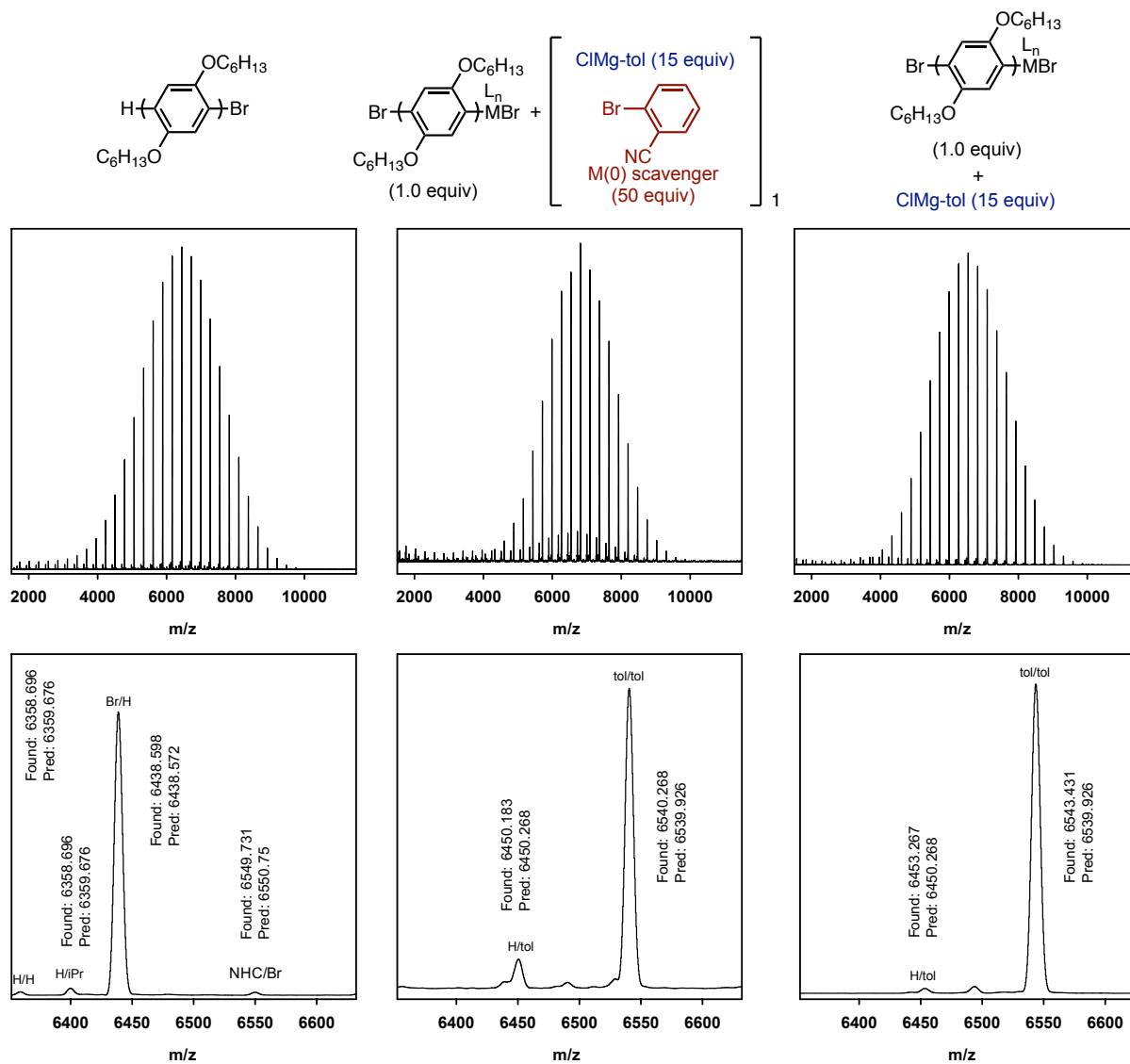


Figure A1-57. MALDI-TOF/MS traces from PBHP (before end-capping), end-capping experiment, and end-capping control (only capping agent) experiments ($t = 2$ h) for Ni(IPr)(PPh₃)Cl₂ and PBHP from Run 2. Values calculated using average mass method, signal-to-noise = 1. The degree of polymerization shown is 23.

i. Ni(IPr)(PPh₃)Cl₂ - End-capping experiments for 20 h

Monomer conversion: Run 1: 93%, Run 2: 93%

Table A1-24. M_n and \mathcal{D} from PBHP (before end-capping), end-capping experiment (ec), and end-capping control (only capping agent) experiments ($t = 20$ h) for Ni(IPr)(PPh₃)Cl₂ and PBHP.

Run 1	M_n (kg/mol)	\mathcal{D}	Run 2	M_n (kg/mol)	\mathcal{D}
PBHP	8.37	1.32	PBHP	8.11	1.25
cap control	8.69	1.32	cap control	8.04	1.28
ec	8.25	1.38	ec	8.21	1.25

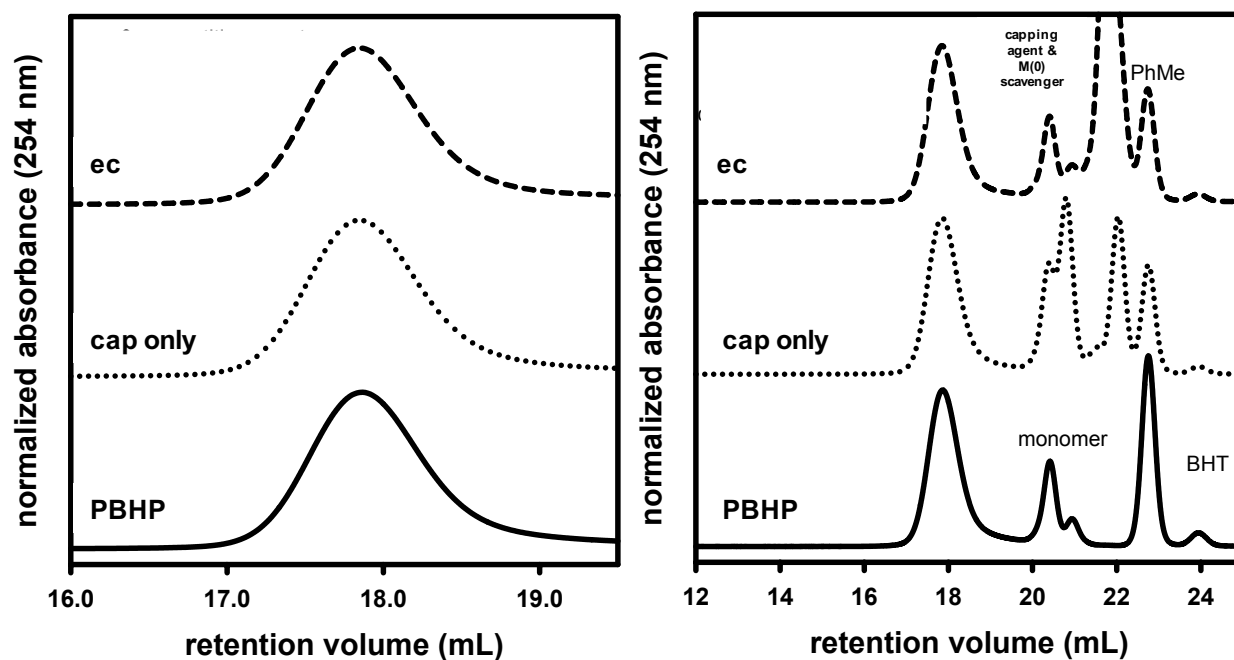


Figure A1-58. GPC traces from PBHP (before end-capping), end-capping experiment, and end-capping control (only capping agent) experiments ($t = 20$ h) for Ni(IPr)(PPh₃)Cl₂ and PBHP. (Left = zoomed, right = full GPC trace from Run 2).

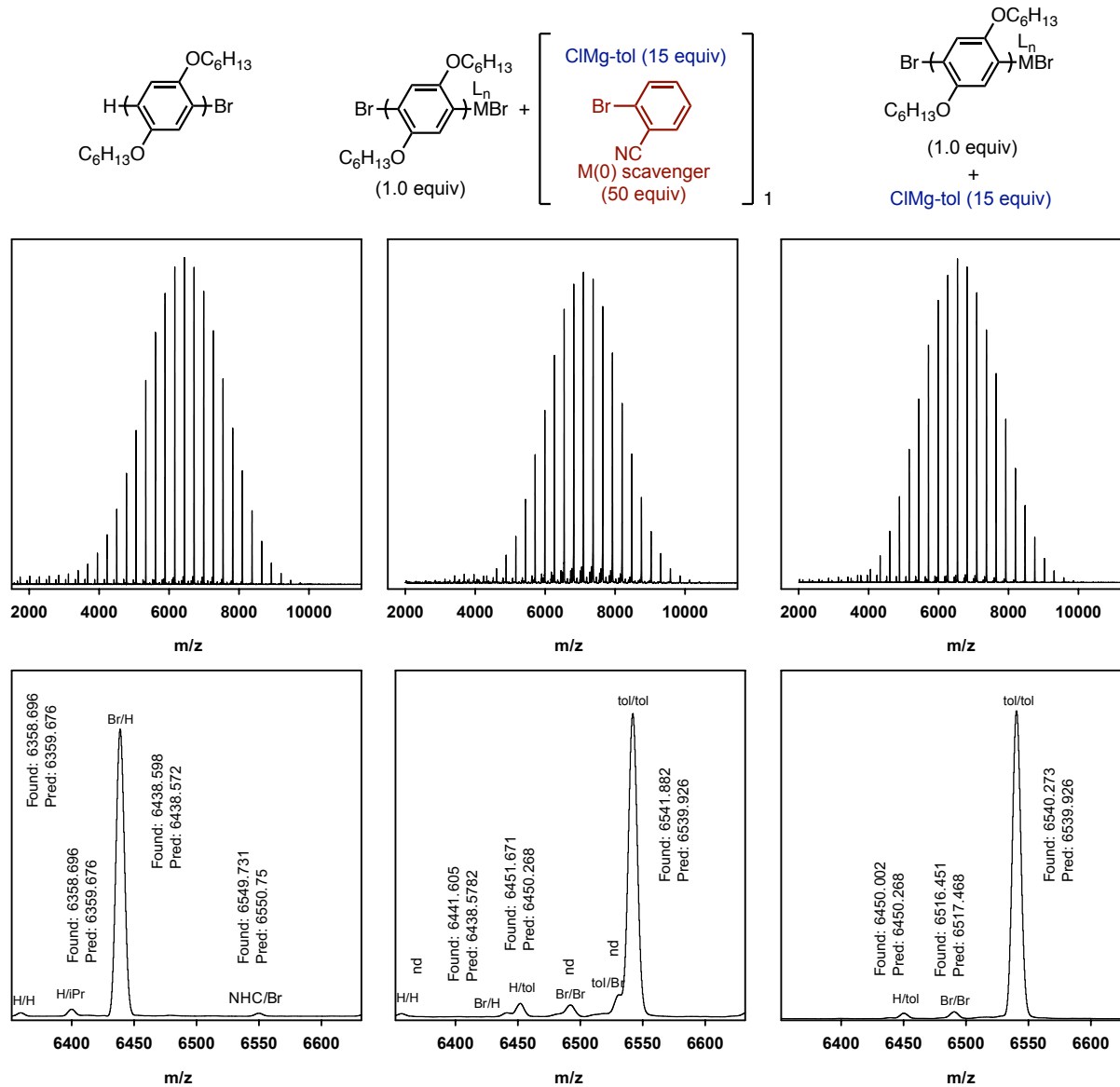
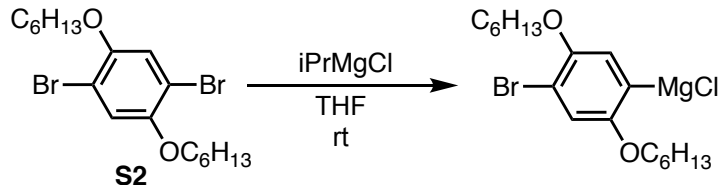


Figure A1-59. MALDI-TOF/MS traces from PBHP (before end-capping), end-capping experiment, and end-capping control (only capping agent) experiments ($t = 20$ h) for Ni(IPr)(PPh₃)Cl₂ and PBHP from Run 2. Values calculated using average mass method, nd = not detected at signal-to-noise = 1. The degree of polymerization shown is 23.

ii. General Procedure for Pd(IPr)(3-Clpy)Cl₂



Monomer activation: In a glovebox, **S2** (108 mg, 0.247 mmol, 1.00 equiv) was weighed into a 20 mL vial and dissolved in THF (0.474 mL). Then, iPrMgCl (2.0 M in THF, 98.8 μ L, 0.199 mmol, 0.800 equiv) and C₂₂H₄₆ (~4 mg, as an internal standard) were added and stirred for 15 h at rt. The Grignard monomer was titrated (see general experimental), revealing overall [Grignard] = 0.274 M.

Preparing stock solutions:

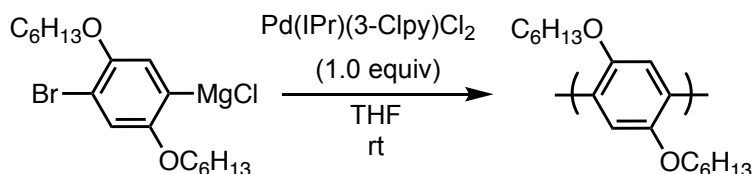
Precatalyst solution: In a glovebox, Pd(IPr)(3-Clpy)Cl₂ (6.8 mg, 0.010 mmol) was weighed into a 4 mL scintillation vial and dissolved in THF (1.0 mL) for an overall concentration of 0.01 M.

End-capping experiment vial preparation:

(equiv are relative to the catalyst/polymer (1.0 equiv) that will be added to each vial)

End-capping experiment vial: In a glovebox, to an 8 mL vial equipped with a stirbar were added 1-bromo-2-cyanobenzene (13.7 mg, 0.0750 mmol, 50.0 equiv), *p*-toluenemagnesium chloride (1.21 M in THF, 18.6 μ L, 0.0225 mmol, 15.0 equiv), and THF (0.50 mL). The vial was sealed with a septum-cap and secured with electrical tape, upon removal from the glovebox the vial was immediately placed under N₂.

End-capping control (only capping agent) vial: In a glovebox, to an 8 mL vial equipped with a stirbar *p*-toluenemagnesium chloride (1.21 M in THF, 18.6 μ L, 0.0225 mmol, 15.0 equiv) was diluted with THF (0.50 mL). The vial was sealed with a septum cap and secured with electrical tape, upon removal from the glovebox the vial was immediately placed under N₂.



Polymerization: In a glovebox, to a 15 mL Schlenk flask equipped with a stirbar was added Pd(IPr)(3-Clpy)Cl₂ (0.01 M in THF, 0.480 mL, 0.00480 mmol, 1.00 equiv) and THF (2.37 mL). The flask was capped with a septum and sealed with copper wire, removed from the glovebox and immediately placed under N₂. The Grignard monomer (0.274 M in THF, 0.30 mL, 0.082 mmol, 17 equiv) was removed from the glovebox in a 1 mL syringe with a long needle and headspace (~0.5 mL). During transit, headspace (~0.3 mL) was evacuated before puncturing the Schlenk flask's septum with the needle. The monomer solution was added at once to the precatalyst flask and stirred for 90 min at rt.

In situ end-capping: An aliquot (2.0 mL) was removed using a syringe and added in portions (1.0 mL/vial, 0.0015 mmol, 1.0 equiv) to a i) end-capping control vial and ii) end-capping experiment vial. The remaining polymer was quenched immediately with aq. HCl (12 M, 3 mL). The capping reactions were run for 2 h before quenching with aq. HCl (12 M, 1.0 mL). Samples were worked up for GC, GPC, and MALDI-TOF/MS analysis.

Note, 4 runs are presented to obtain overlapping values in the %ring-walking chart.

Monomer conversion: Run 1: 74%, Run 2: 69%, Run 3: 86%, Run 4: 85%

Table A1-25. M_n and \bar{D} from PBHP (before end-capping), end-capping experiment (ec), and end-capping control (only capping agent) experiments ($t = 2$ h) for Pd(IPr)(3-Clpy)Cl₂ and PBHP.

Run 1	M_n (kg/mol)	\bar{D}	Run 2	M_n (kg/mol)	\bar{D}	Run 3	\bar{D}	M_n (kg/mol)	Run 4	M_n (kg/mol)	\bar{D}
PBHP	3.45	1.22	PBHP	6.00	1.18	PBHP	1.20	4.67	PBHP	9.26	1.21
cap control	3.45	1.23	cap control	5.45	1.20	cap control	1.20	4.73	cap control	9.35	1.19
ec	3.45	1.22	ec	5.00	1.21	ec	1.19	4.82	ec	9.30	1.20

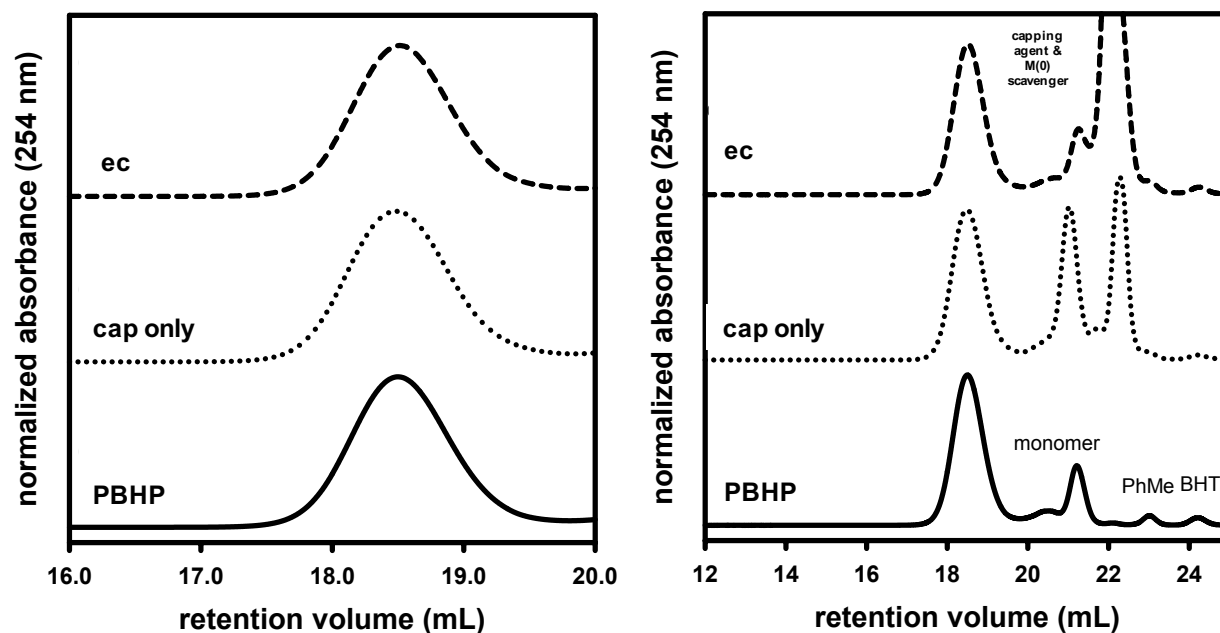


Figure A1-60. GPC traces from PBHP (before end-capping), end-capping experiment (ec), and end-capping control (only capping agent) experiments for Pd(IPr)(3-Clpy)Cl₂ and PBHP. (Left = zoomed, right = full GPC trace from Run 2).

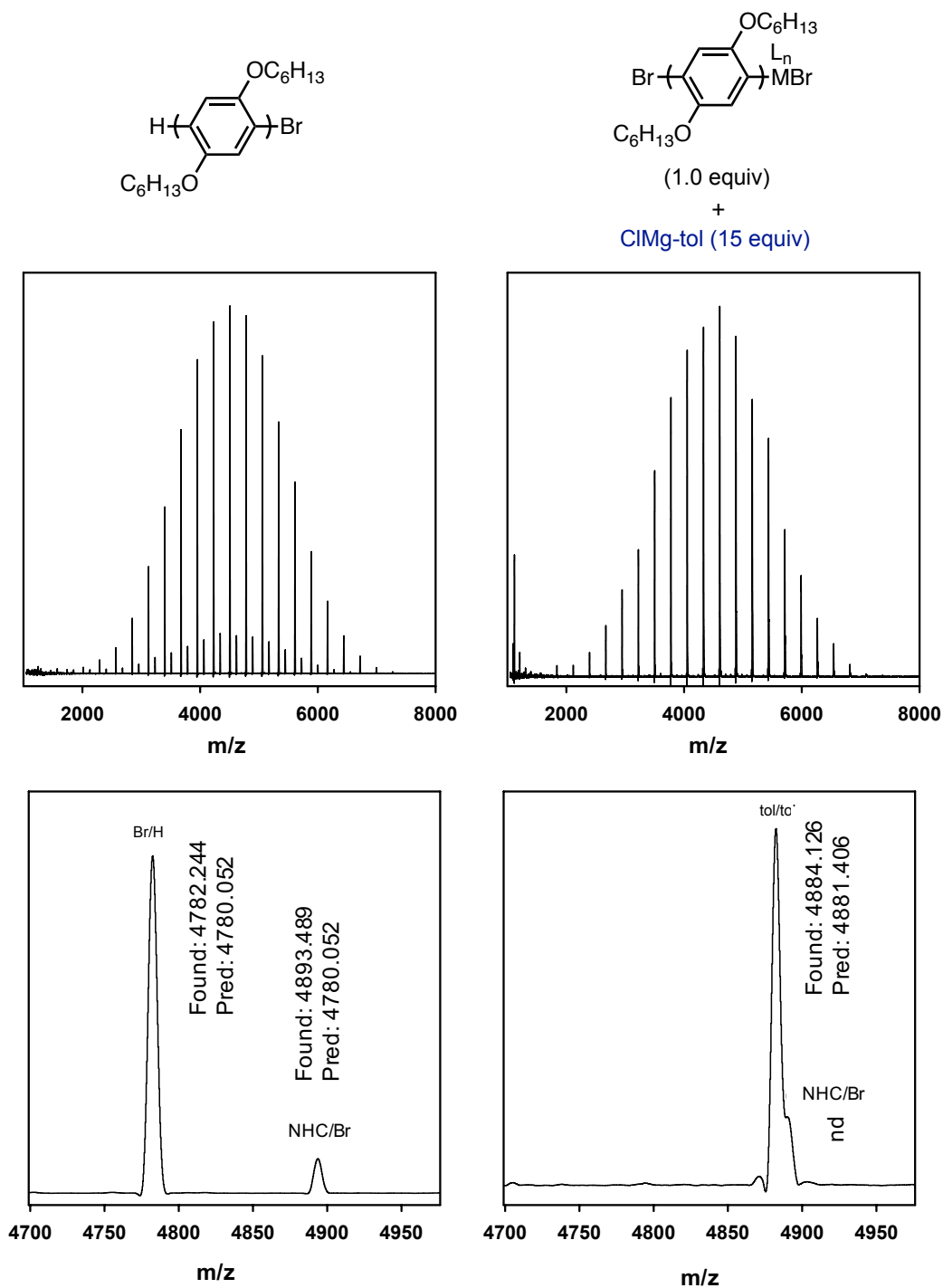


Figure A1-61. MALDI-TOF/MS traces from PBHP (before end-capping) and end-capping control (only capping agent) experiments for Pd(IPr)(3-Clpy)Cl₂ and PBHP from Run 2. Values calculated using an average mass method, nd = not detected at signal-to-noise = 2. The degree of polymerization shown is 17.

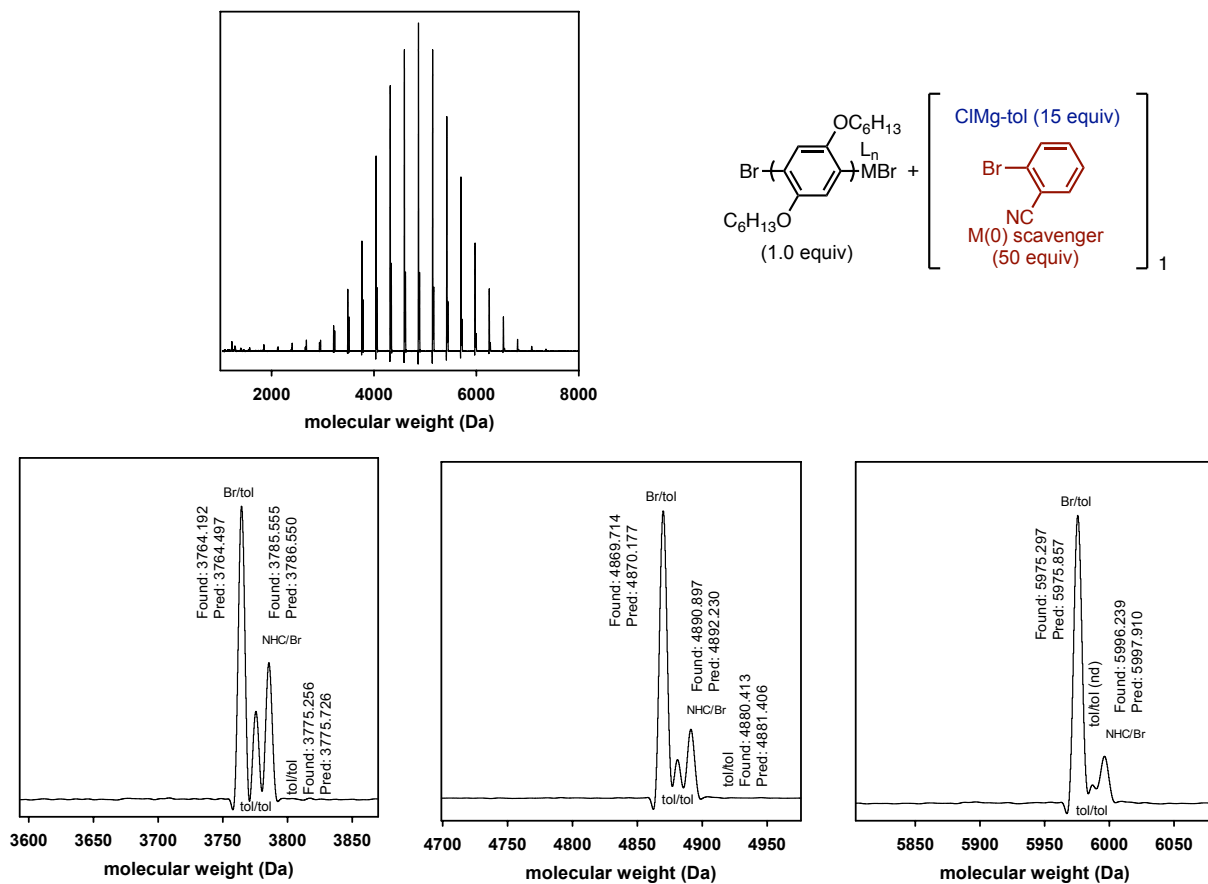
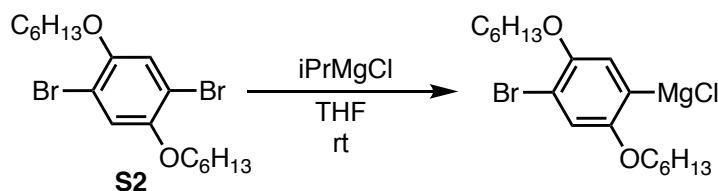


Figure A1-62. MALDI-TOF/MS traces from the end-capping experiment for $Pd(I\text{Pr})(3\text{-Clpy})Cl_2$ and PBHP. The zoomed MALDI-TOF/MS traces represent low–high molecular weight peaks to show a distribution of m from Run 2. Values calculated using average mass method, nd = not detected at signal-to-noise = 1. The degrees of polymerization shown are 13, 17, and 21 (from left to right).

iii. General Procedure for Ni(dppp)Cl₂



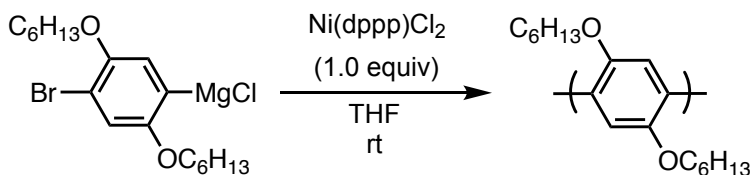
Monomer activation: In a glovebox, **S2** (199 mg, 0.456 mmol, 1.00 equiv) and C₂₂H₄₆ (4 mg, as an internal standard) were weighed into a 20 mL vial and dissolved in THF (0.871 mL). Then, iPrMgCl (1.8 M in THF, 203 μ L, 0.365 mmol, 0.800 equiv) was added and the solution was stirred for 14.5 h. The Grignard monomer was titrated (see general experimental) revealing a [Grignard] of 0.275 M.

End-capping experiment vial preparation:

(equiv are relative to the catalyst/polymer (1.0 equiv) that will be added to each vial)

End-capping experiment: In a glovebox, to an 8 mL vial equipped with a stirbar was added 1-bromo-2-cyanobenzene (13.7 mg, 0.0750 mmol, 50.0 equiv), *p*-toluenemagnesium chloride (1.21 M in THF, 18.6 μ L, 0.0225 mmol, 15.0 equiv), and THF (0.50 mL). The vial was sealed with a septum-cap and secured with electrical tape, upon removal from the glovebox the vial was immediately placed under N₂.

End-capping control (only capping agent) vial: In a glovebox, to an 8 mL vial equipped with a stirbar, *p*-toluenemagnesium chloride (1.21 M in THF, 18.6 μ L, 0.0225 mmol, 15.0 equiv) was diluted with THF (0.50 mL). The vial was sealed with a septum-cap and secured with electrical tape, upon removal from the glovebox the vial was immediately placed under N₂.



Polymerization: In a glovebox, to a 15 mL Schleck flask equipped with a stirbar was added precatalyst Ni(dppp)Cl₂ (3.0 mg, 0.0055 mmol, 1.0 equiv) and THF (3.17 mL). The flask was capped with a septum, sealed with copper wire, removed from the glovebox and immediately placed under N₂. The Grignard monomer (0.275 M in THF, 0.50 mL, 0.138 mmol, 25 equiv) was removed from the glovebox in a 1 mL syringe with a long needle and headspace (0.35 mL). During transit, headspace (0.2 mL) was evacuated before puncturing the precatalyst flask's septum with the needle. The monomer was added at once to the precatalyst flask and stirred for 90 min at rt.

In situ end-capping: Then, using a syringe an aliquot (2.0 mL) was removed using a syringe and was added in portions (1.0 mL/vial, 0.0015 mmol, 1.0 equiv) to a i) end-capping control vial and ii) end-capping experiment vial. The remaining polymer was quenched with aq. HCl (12 M, 3 mL). The capping reactions were run for 2 h before quenching with aq. HCl (12 M, 1.0 mL). Samples were worked up for GC, GPC, and MALDI-TOF/MS.

Monomer conversion: Run 1: 65%, Run 2: 74%

Table A1-26. M_n and \bar{D} from PBHP (before end-capping), end-capping experiment (ec), and end-capping control (only capping agent) experiments for Ni(dppp)Cl₂ and PBHP.

Run 1	M_n (kg/mol)	\bar{D}	Run 2	M_n (kg/mol)	\bar{D}
PBHP	3.32	1.26	PBHP	7.58	1.21
cap control	3.32	1.27	cap control	7.69	1.21
ec	3.30	1.26	ec	7.63	1.22

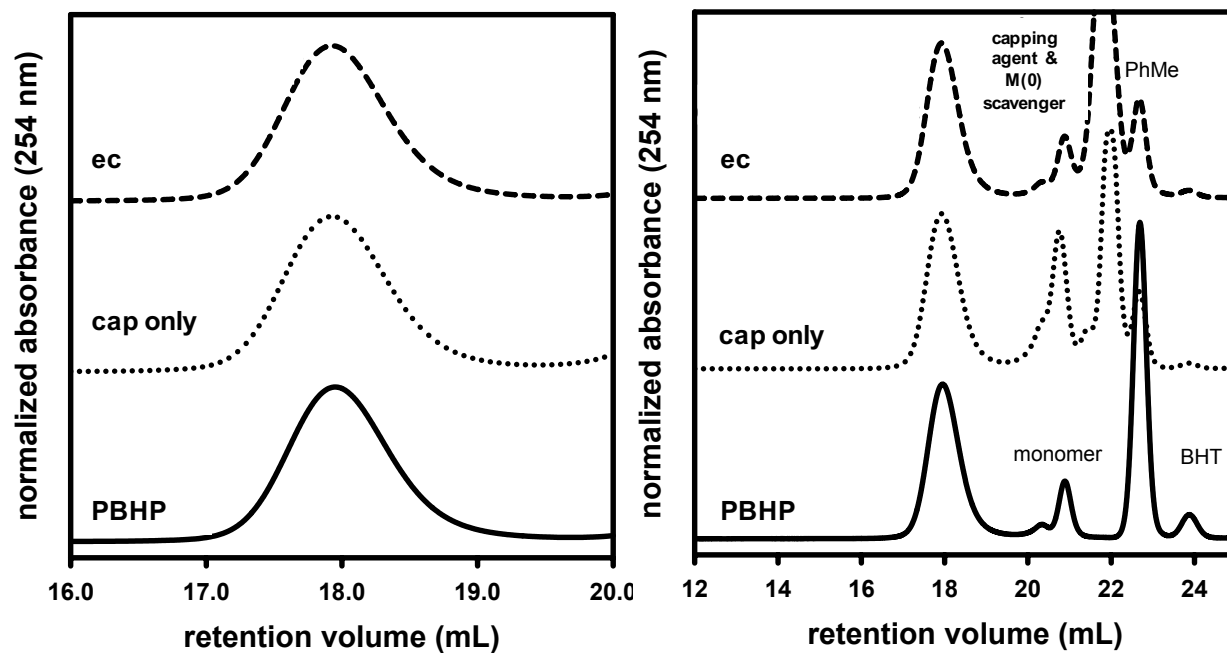


Figure A1-63. GPC traces from PBHP (before end-capping), end-capping experiment, and end-capping control (only capping agent) experiments for Ni(dppp)Cl₂ and PBHP. (Left = zoomed, right = full GPC trace from Run 2).

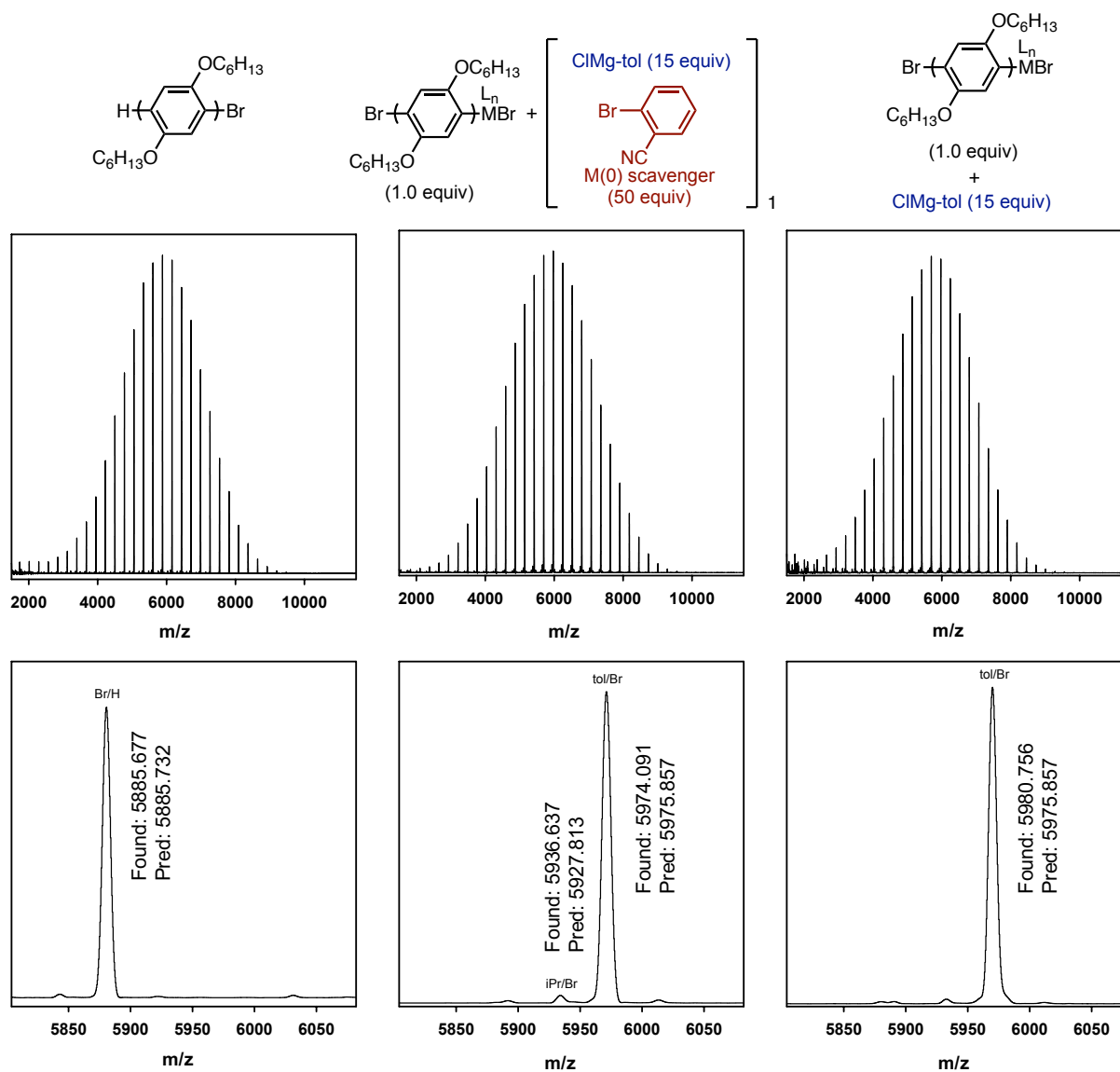
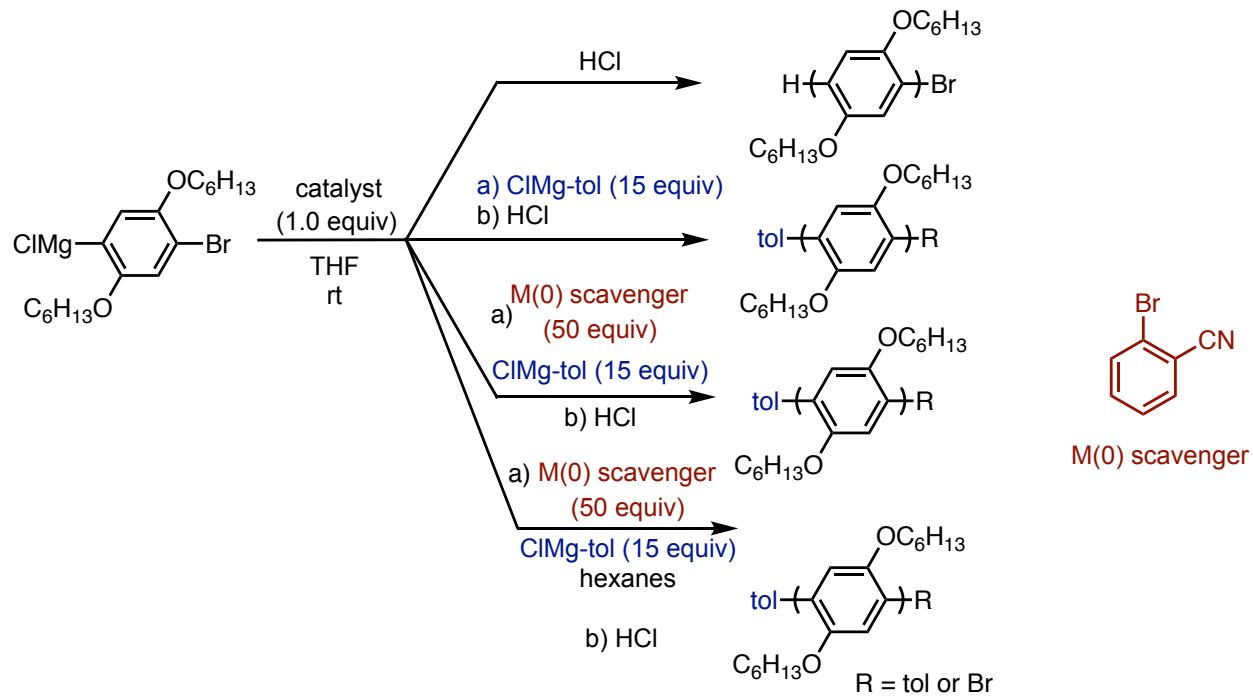
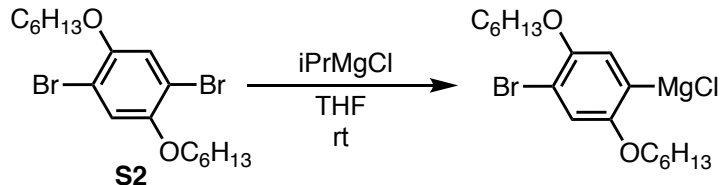


Figure A1-64. MALDI-TOF/MS traces from PBHP (before end-capping), end-capping experiment, and end-capping control (only capping agent) experiments for Ni(dppp)Cl₂ and PBHP from Run 2. Values calculated using average mass method signal-to-noise = 2. The degree of polymerization shown is 21.

iv. Evaluating the influence of solvent (hexane) on PBAP (A = alkoxy) end-capping experiments





Monomer activation: In a glovebox, iPrMgCl (2.2 M in THF, 1.393 mL, 0.003093 mol, 0.800 equiv) was added to a stirring solution of **S2** (1.69 g, 0.00387 mmol, 1.00 equiv) in THF (6.3 mL) and stirred for 17 h at rt. Titrating the resulting solution against salicylaldehyde phenylhydrazone (see general experimental) revealed the $[\text{Grignard}] = 0.291 \text{ M}$.

Preparing precatalysts:

$\text{Pd}(\text{IPr})(3\text{-Clpy})\text{Cl}_2$: To an 8 mL vial was added $\text{Pd}(\text{IPr})(3\text{-Clpy})\text{Cl}_2$ (11.7 mg, 0.0172 mmol) and dissolved in THF (1.72 mL) for a [0.01 M] solution.

$\text{Ni}(\text{IPr})(\text{PPh}_3)\text{Cl}_2$: To an 8 mL vial was added $\text{Ni}(\text{IPr})(\text{PPh}_3)\text{Cl}_2$ (10.8 mg, 0.0138 mmol) and dissolved in THF (1.38 mL) for a [0.01 M] solution.

Preparing end-capping control/experiment vials:

(equiv are relative to the catalyst/polymer (1.0 equiv) that will be added to each vial)

End-capping experiment vial (*THF only*): In a glovebox, to an 8 mL vial equipped with a stirbar was added 1-bromo-2-cyanobenzene (13.7 mg, 0.0750 mmol, 50.0 equiv), *p*-toluenemagnesium chloride (1.11 M in THF, 20.3 μL , 0.0225 mmol, 15.0 equiv), and THF (0.50 mL). The vial was

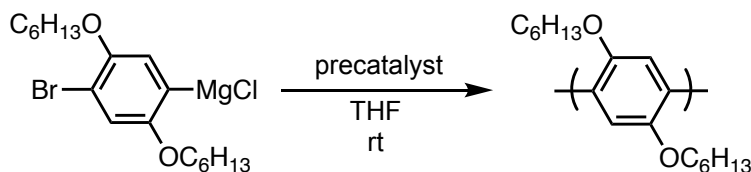
sealed with a septum-cap and secured with electrical tape, upon removal from the glovebox the vial was immediately placed under N₂.

End-capping experiment vial (*THF and hexanes*): In a glovebox, to an 8 mL vial equipped with a stirbar was added 1-bromo-2-cyanobenzene (13.7 mg, 0.0750 mmol, 50.0 equiv), *p*-toluenemagnesium chloride (1.11 M in THF, 20.3 μL, 0.0225 mmol, 15.0 equiv), hexanes (0.20 mL) and THF (0.30 mL). The vial was sealed with a septum-cap and secured with electrical tape, upon removal from the glovebox the vial was immediately placed under N₂. Note this hexane/THF ratio included the highest percentage of hexanes that did not result in a heterogeneous mixture when added to the Grignard capping agent alone. A heterogeneous mixture was avoided to ensure all Grignard capping agent was active.

End-capping control vial (capping agent only): In a glovebox, in an 8 mL vial equipped with a stirbar was added *p*-toluenemagnesium chloride (1.11 M in THF, 20.3 μL, 0.0225 mmol, 15.0 equiv) and THF (0.5 mL). The vial was sealed with a septum-cap and secured with electrical tape, upon removal from the glovebox the vial was immediately placed under N₂.

Reaction flask preparation:

In the glovebox, to a 25 mL Schlenk flask was added catalyst (1.2 mL, 0.012 mmol, 1.0 equiv), THF (8 mL), and a stirbar. The Schlenk flask was capped with a septum, secured with copper wire, removed from the glovebox, and immediately placed under N₂.



Polymerization: In the glovebox, Grignard monomer solution (0.291 M in THF, 0.825 mL, 0.240 mmol, 20.0 equiv) was drawn into a 3 mL syringe equipped with a long needle, headspace (~1.4 mL) was pulled and then the syringe/needle were removed from the glovebox. During transit, to the catalyst-containing flask, headspace (~1.0 mL) was evacuated from the needle before puncturing the septum. The monomer was added at once to the stirring precatalyst flasks. The polymerizations were stirred for 90 min under N₂.

End-capping experiments: Aliquots (each 1.0 mL, containing 0.0015 mmol catalyst, 1.00 equiv catalyst) were added to the end-capping experiment and control vials and stirred under N₂ for 2 h (for Pd experiments) and for 24 h (for Ni experiments) before quenching with aq. HCl (12 M, 1 mL). Immediately after aliquots were removed from the polymerizations, the remaining polymer solution was quenched with aq. HCl (12 M, 3 mL). Samples were worked up for GC, GPC, and MALDI-TOF/MS.

Table A1-27. GC data from the polymerization of PBAP before end-capping experiments via Ni(IPr)(PPh₃)Cl₂, Pd(IPr)(3-Clpy)Cl₂, and Ni(dppp)Cl₂.

	(% monomer conv.)
Ni(IPr)(PPh ₃)Cl ₂ (PBHP)	90%
Pd(IPr)(3-Clpy)Cl ₂ (PBHP)	89%
Ni(dppp)Cl ₂ (PBBP)	74%

Table A1-28. M_n and \bar{D} from PBAP (before end-capping), end-capping control (only capping agent), end-capping (ec), and end-capping with hexanes (ec (hex)) experiments for Ni(IPr)(PPh₃)Cl₂, Pd(IPr)(3-Clpy)Cl₂, and Ni(dppp)Cl₂.

Ni(IPr)(PPh ₃)Cl ₂	M_n (kg/mol)	\bar{D}	Pd(IPr)(3-Clpy)Cl ₂	M_n (kg/mol)	\bar{D}	Ni(dppp)Cl ₂	M_n (kg/mol)	\bar{D}
PBHP	5.78	1.23	PBHP	5.36	1.22	PBBP	6.35	1.45
cap only	8.31	1.21	cap only	7.61	1.18	cap only	7.47	1.31
ec	7.61	1.19	ec	8.15	1.18	ec	7.78	1.31
ec (hex)	8.31	1.21	ec (hex)	8.28	1.19	ec (hex)	7.88	1.30

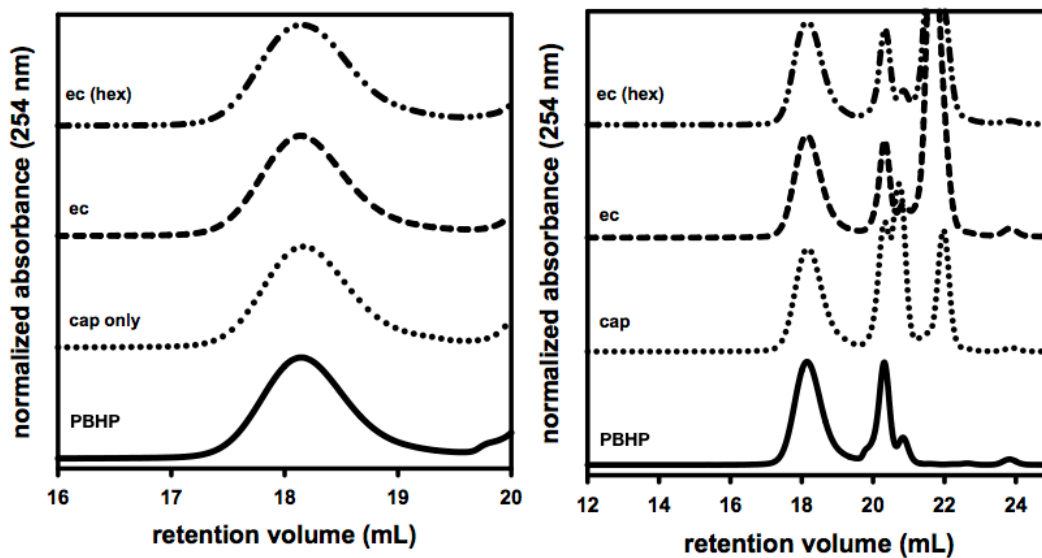


Figure A1-65. GPC traces from PBHP (before end-capping), end-capping control (only capping agent), end-capping (ec), and end-capping with hexane (ec (hex)) experiments for $\text{Ni}(\text{IPr})(\text{PPh}_3)\text{Cl}_2$. (Left = zoomed, right = full GPC trace). Note that $\text{M}(0)$ scavenging agent and residual monomer elute from 20.5–22 min, PhMe elutes at 23.1 min and BHT elutes at 23.8 min.

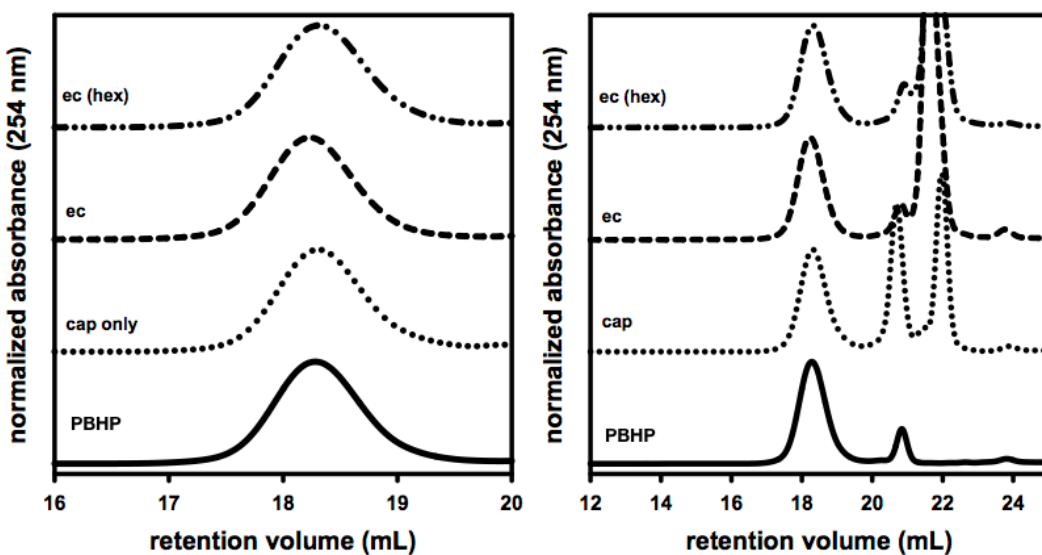


Figure A1-66. GPC traces from PBHP (before end-capping), end-capping control (only capping agent), end-capping (ec), and end-capping with hexane (ec (hex)) experiments for $\text{Pd}(\text{IPr})(3\text{-Clpy})\text{Cl}_2$. (Left = zoomed, right = full GPC trace). Note that $\text{M}(0)$ scavenging agent and residual monomer elute from 20.5–22 min, PhMe elutes at 23.1 min and BHT elutes at 23.8 min.

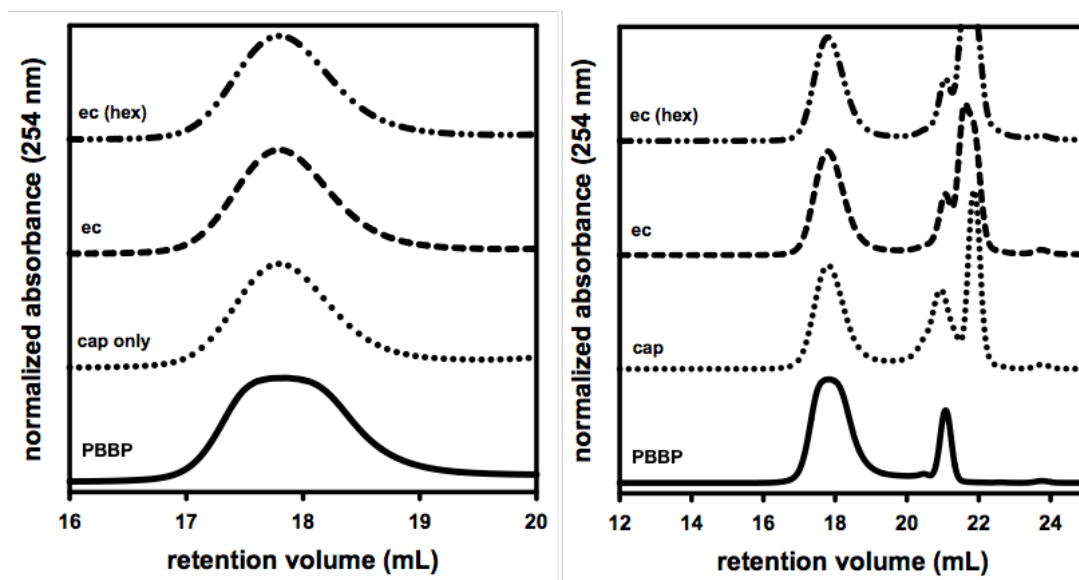


Figure A1-67. GPC traces from PBBP (before end-capping), end-capping control (only capping agent), end-capping (ec), and end-capping with hexane (ec (hex)) experiments for Ni(dppp)Cl₂. (Left = zoomed, right = full GPC trace). Note that M(0) scavenging agent and residual monomer elute from 20.5–22 min, PhMe elutes at 23.1 min and BHT elutes at 23.8 min.

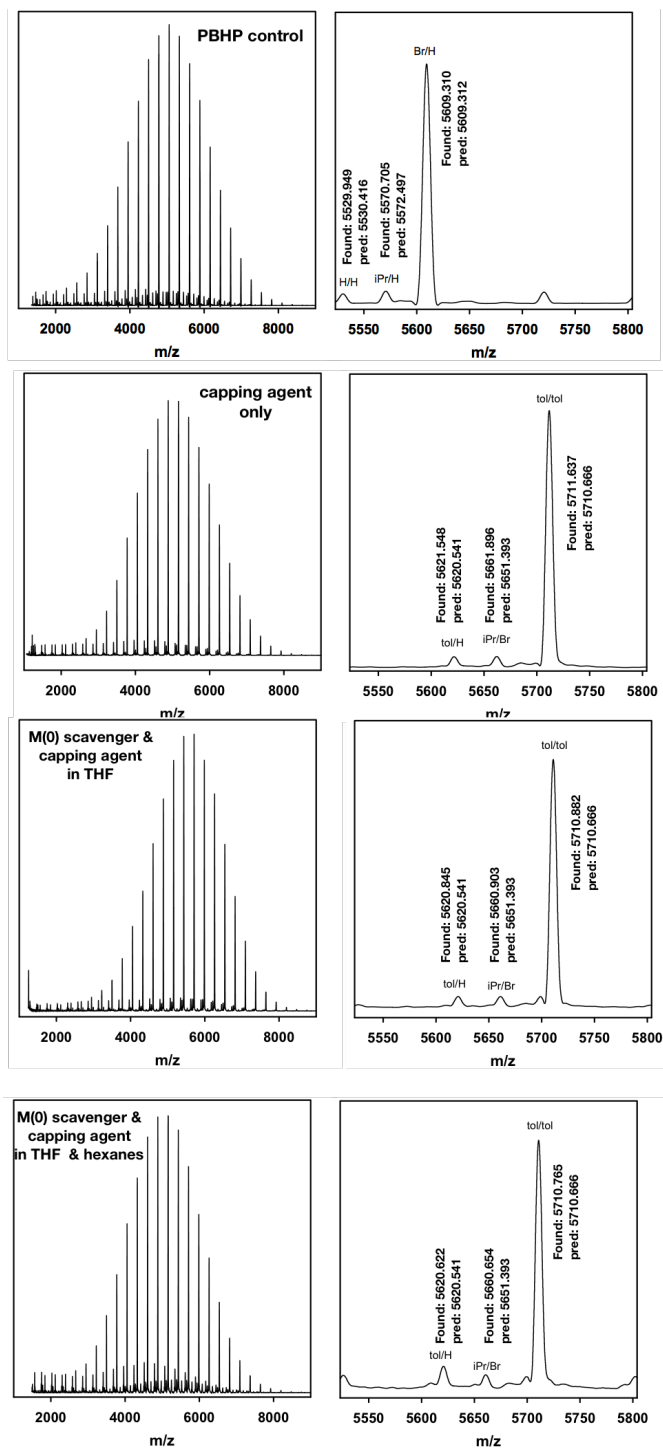


Figure A1-68. MALDI-TOF/MS traces from PBHP (before end-capping), end-capping experiments (THF alone, and THF & hexanes), and end-capping control (only capping agent) experiments for Ni(IPr)(PPh₃)Cl₂ and PBHP. Values calculated using average mass method signal-to-noise = 2. The degree of polymerization shown is 20.

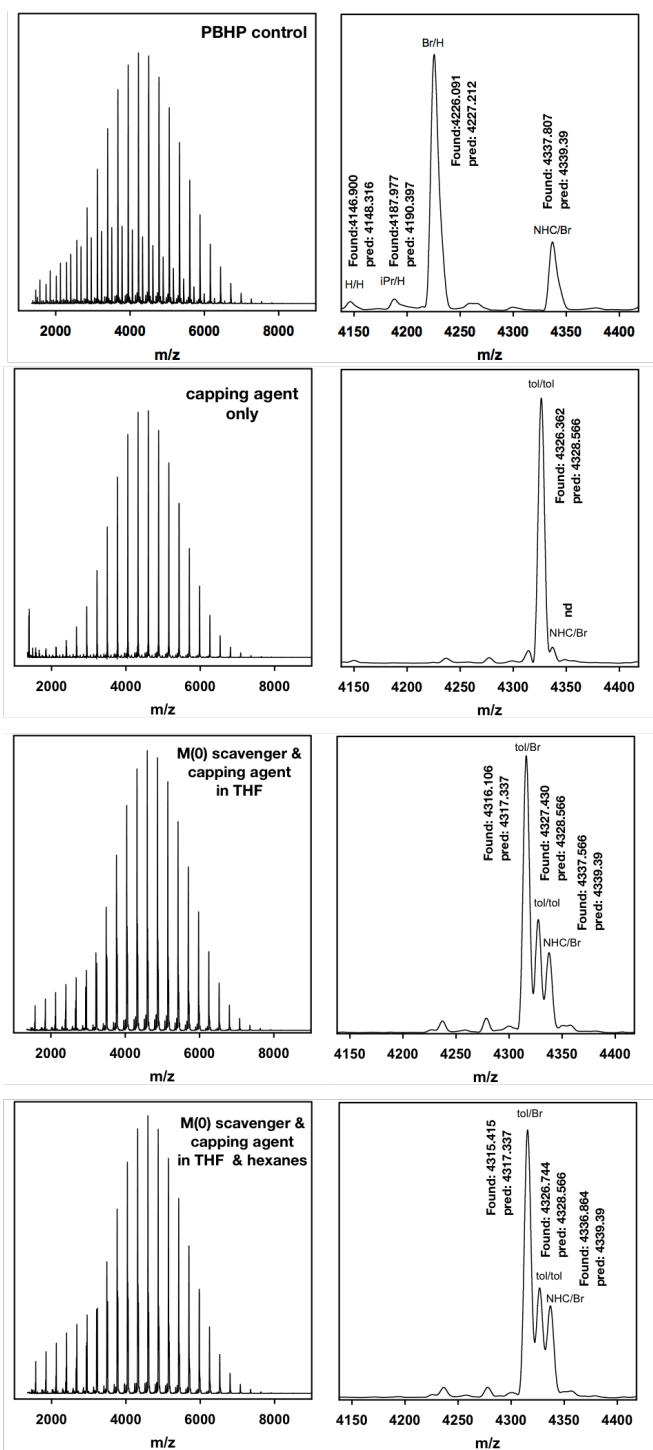


Figure A1-69. MALDI-TOF/MS traces from PBHP (before end-capping), end-capping experiments (THF alone, and THF & hexanes), and end-capping control (only capping agent) experiments for Pd(IPr)(3-Clpy)Cl₂ and PBHP. Values calculated using an average mass method signal-to-noise = 2. The degree of polymerization shown is 15.

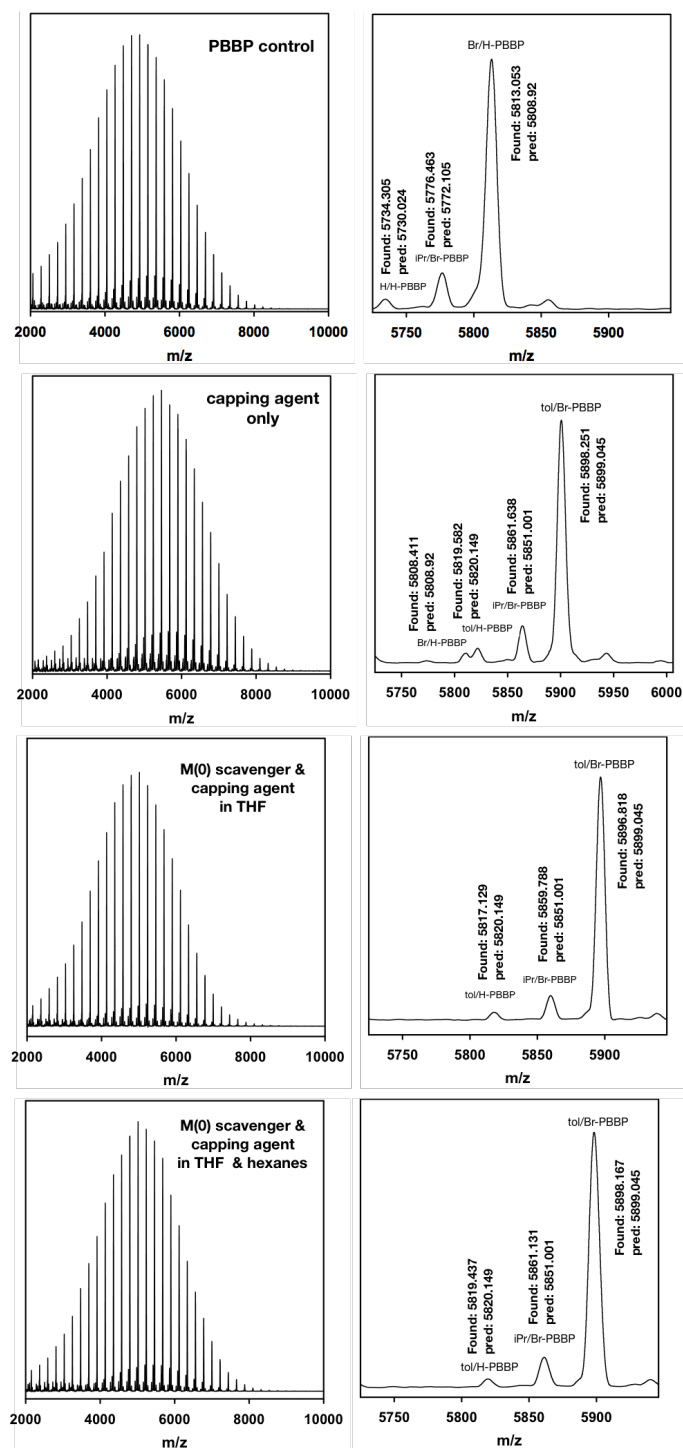
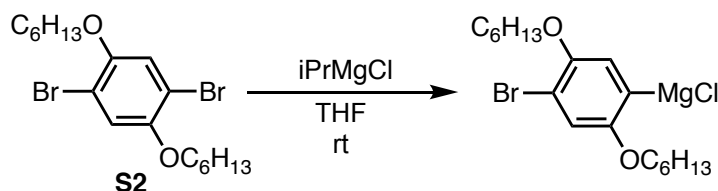
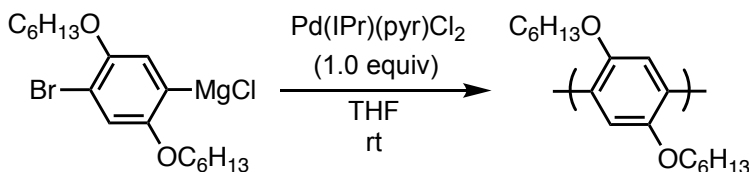


Figure A1-70. MALDI-TOF/MS traces from PBBP (before end-capping), end-capping experiments (THF alone, and THF & hexanes), and end-capping control (only capping agent) experiments for Ni(dppp)Cl₂ and PBBP. Values calculated using an average mass method signal-to-noise = 2. The degree of polymerization shown is 26.

A1.6.6. 2,5-Bis(hexyloxy)phenylene polymerization via Pd(IPr)(3-Clpy)Cl₂ generating NHC/Br-polymers



Monomer activation: In a glovebox, **S2** (1.016 mg, 0.00233 mol, 1.00 equiv) and C₂₂H₄₆ (10 mg, as an internal standard) were weighed into a 20 mL vial and dissolved in THF (3.73 mL). Then, iPrMgCl (2.0 M in THF, 932 μ L, 0.00186 mol, 0.800 equiv) was added and the solution was stirred for 20 h. The Grignard monomer was titrated (see general experimental) revealing a [Grignard] of 0.317 M.



Polymerization: In a glovebox, to a 50 mL Schlenk flask equipped with a stirbar was added Pd(IPr)(3-Clpy)Cl₂ (26.9 mg, 0.0396 mmol, 1.00 equiv) and THF (26.4 mL). The flask was capped with a septum and sealed with copper wire, removed from the glovebox and immediately placed under N₂. The Grignard monomer (0.317 M in THF, 2.50 mL, 0.793 mmol, 20.0 equiv) was removed from the glovebox in a 6 mL syringe with a long needle and headspace (~2.5 mL). During transit, headspace (~2.3 mL) was evacuated before puncturing the Schlenk flask's septum with the needle. The monomer solution was added at once to the precatalyst flask and stirred for 90 min at rt. Then, aliquot (3.0 mL) was removed using a syringe and quenched with aq. HCl (12 M, 3 mL). The capping reactions were run for 2 h before quenching with aq. HCl (12 M, 1.0

mL). After 6.5 h (total polymerization time) the remaining solution was quenched with aq. HCl (12 M, 10 mL). In each case, the crude polymer was extracted with CHCl₃ (3 x 5 mL), dried over MgSO₄ and worked up for GC, GPC, and MALDI-TOF/MS. For ¹H NMR spectroscopic analysis, polymers were concentrated under reduced pressure, re-dissolved in CHCl₃ (minimal, ~0.5 mL) with mild heating, precipitated with MeOH (20 mL) and divided into centrifuge tubes and spun for 15 min, resulting in a white precipitate and a clear supernatant which was decanted. The polymers were washed with MeOH (10 mL per tube), shaking, re-centrifuging, and decanting the supernatant. The polymers were collected and dried under reduced pressure.

Monomer conversion: 90 min = 90%, 6.5 h = 95%

Table A1-29. M_n and \mathcal{D} from PBHP t = 90 min and t = 6.5 h via Pd(IPr)(3-Clpy)Cl₂.

	M_n (kg/mol)	\mathcal{D}
90 min	6.01	1.21
6.5 h	5.84	1.27

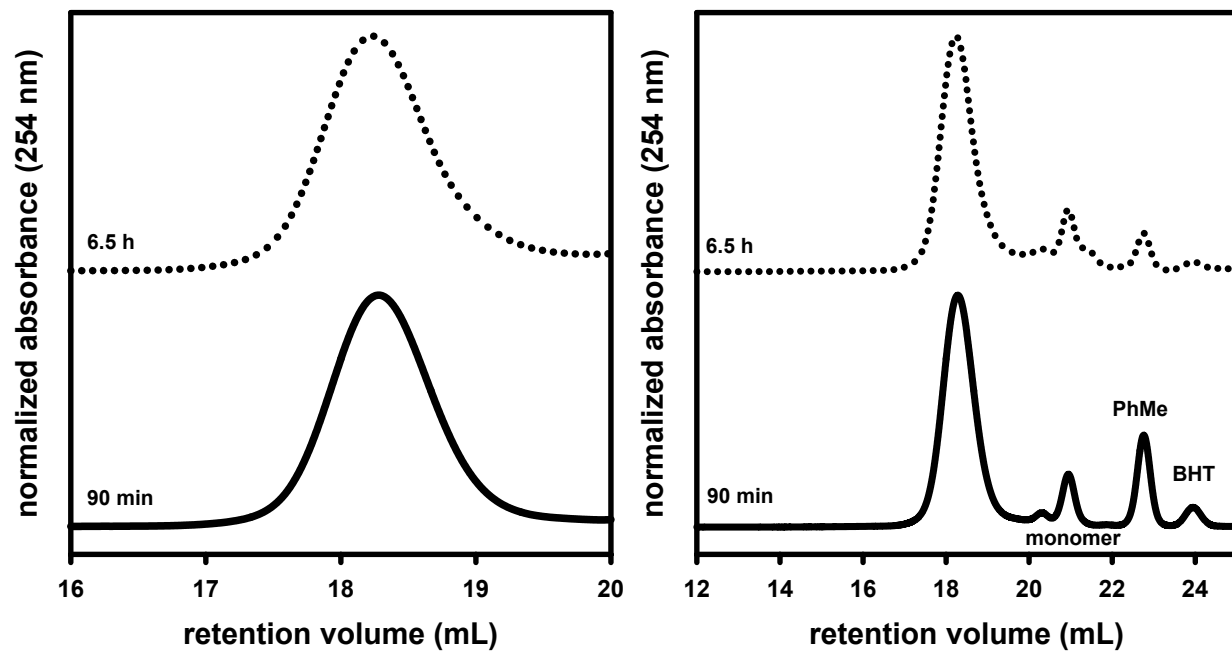


Figure A1-71. GPC traces from PBHP $t = 90$ min and $t = 6.5$ h via $\text{Pd}(\text{IPr})(3\text{-Clpy})\text{Cl}_2$. (Left = zoomed, right = full GPC trace from the same experiment).

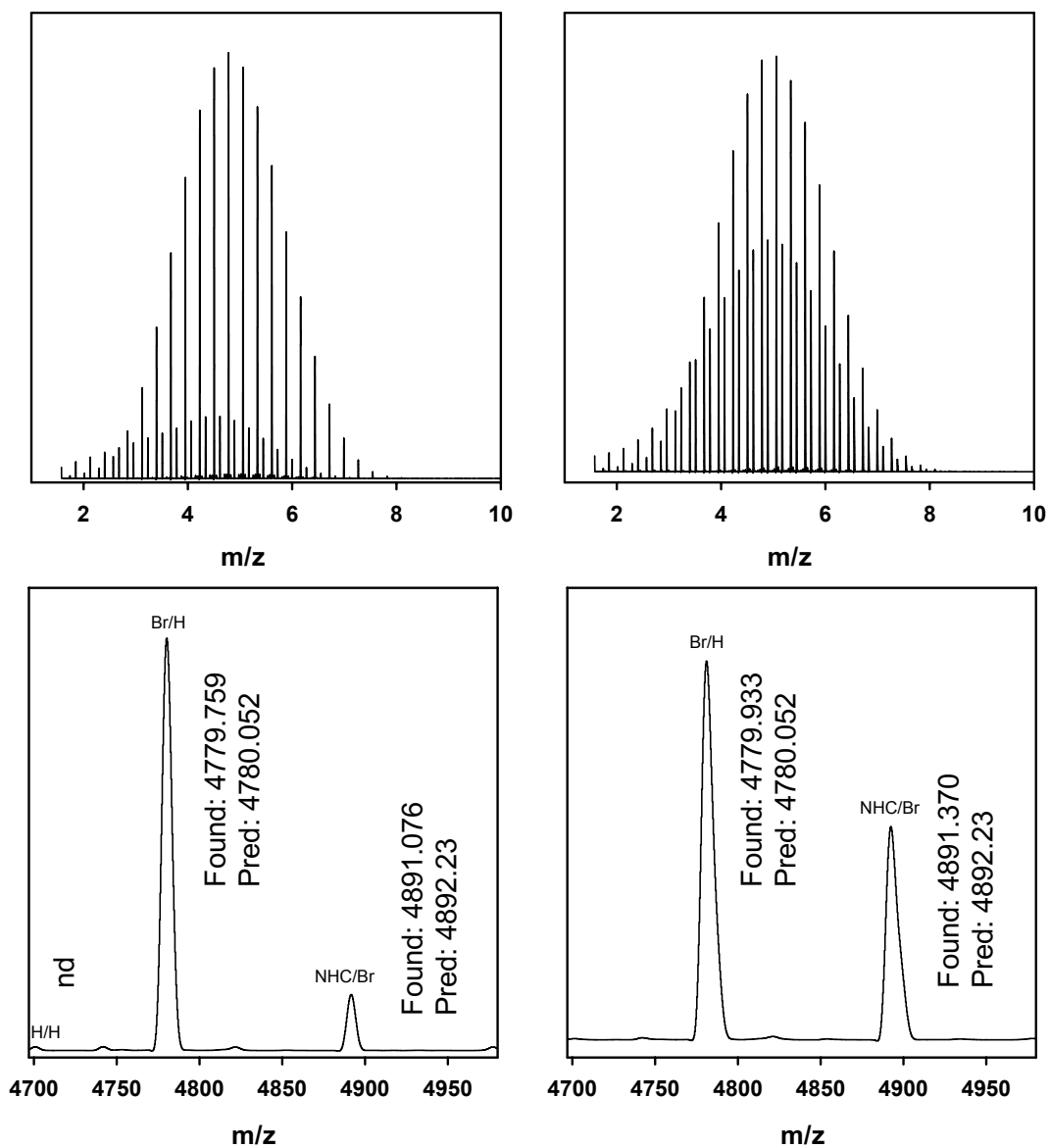
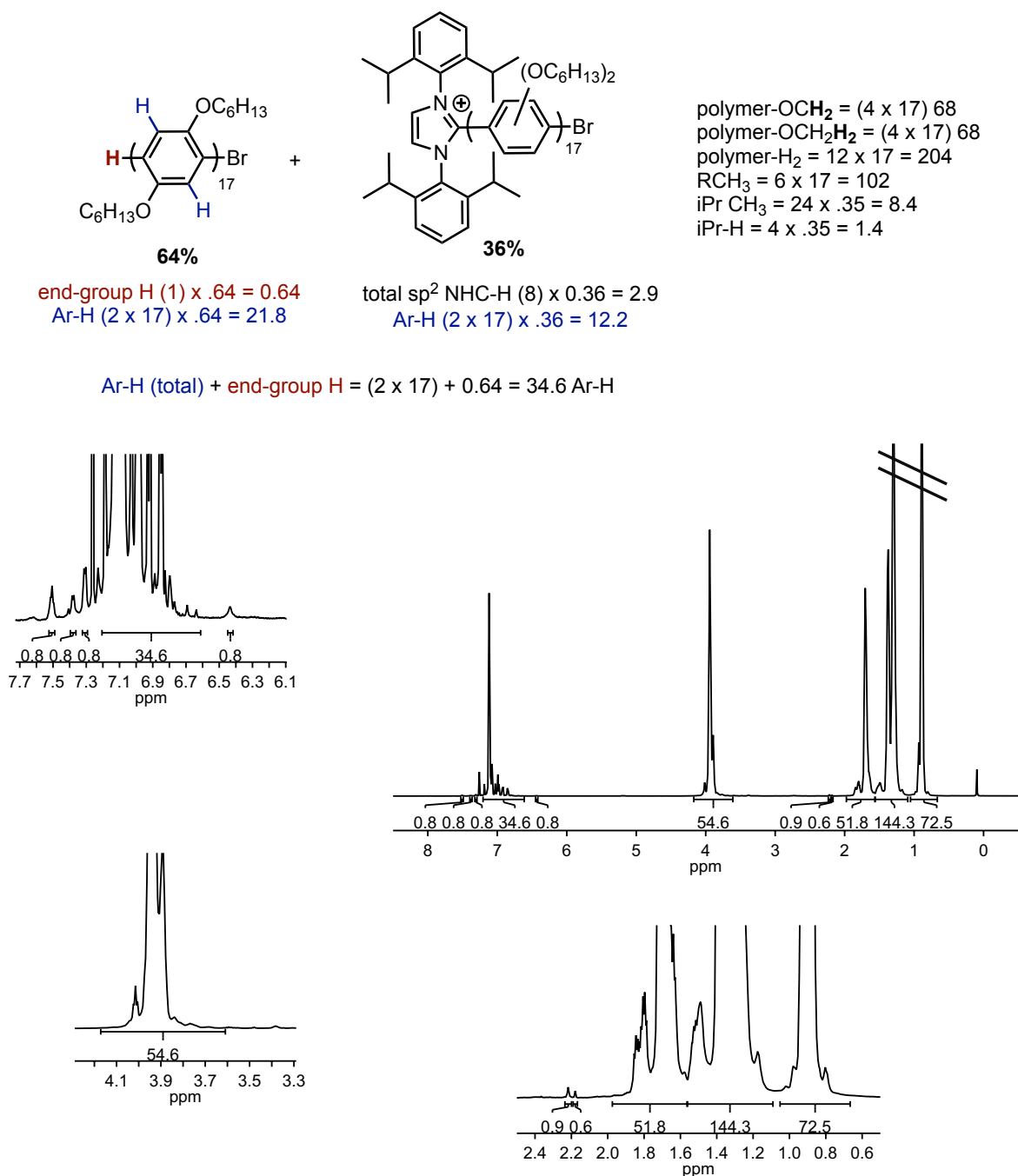


Figure A1-72. MALDI-TOF/MS traces from PBHP $t = 90$ min (left) and $t = 6.5$ h (right) via $\text{Pd}(\text{IPr})(3\text{-Clpy})\text{Cl}_2$. Values calculated using an average mass method signal-to-noise = 3.

The NMR were integrated according to the MALDI-TOF/MS ratio of H/Br- (61%) to NHC/Br- (35%) polymers with the average degree of polymerization 17.



A1.7. Values for the %ring-walking charts

Percent ring-walking was calculated using MALDI-TOF/MS peak picking at either signal-to-noise = 1 or 2. Percent ring-walking only considers tol/tol (efficient ring-walking) and tol/Br (failed ring-walking) end-groups. End-groups from unproductive pathways (e.g., NHC/Br) were not considered because these polymers imply catalysts were not active. The H/tol-terminated polymers were not considered because they could arise from multiple pathways not all of which would arise from ring-walking (i.e., an acid-quenched Grignard chain-end which would form an H-end group in the H/tol-terminated polymer). The %-ring-walking equals $(\text{tol/tol})/[(\text{tol/tol})+(\text{Br/tol})]$ with each peak on the MALDI-TOF/MS plot corresponding to the % ring-walking for that degree of polymerization (m).



% ring-walking = (tol/tol)/(tol/tol) + (tol/Br)								
	Ni(dppp)Cl ₂ /3DT				Ni(dppp)Cl ₂ /BHP			
m	Run 1	Run 2	avg	error	Run 1	Run 2	avg	error
4					0			
5					0	0	0	0
6					0	0	0	0
7					0	0	0	0
8					0	0	0	0
9					0	0	0	0
10					0	0	0	0
11					0	0	0	0
12					0	0	0	0
13					0	0	0	0
14	100	100	100	0	0	0	0	0
15	100	100	100	0	0	0	0	0
16	100	100	100	0	0	0	0	0
17	100	100	100	0	0	0	0	0
18	100	100	100	0	0	0	0	0
19	100	100	100	0	0	0	0	0
20	100	100	100	0	0	0	0	0
21	100	100	100	0	0	0	0	0
22	100	100	100	0		0		
23	100	100	100	0		0		
24	100	100	100	0		0		
25	100	100	100	0		0		
26	100	100	100	0		0		
27	100	100	100	0		0		
28	100	100	100	0		0		
29	100	100	100	0		0		
30	100	100	100	0		0		
31	100	100	100	0		0		
32	100	100	100	0		0		
33	100	100	100	0		0		
34	100	100	100	0		0		
35		100				0		
36		100						
37		100						
38		100						
39		100						
40		100						
41		100						



% ring-walking = (tol/tol)/(tol/tol) + (tol/Br)								
m	Ni(IPr)(PPh ₃)Cl ₂ /3DT				Ni(IPr)(PPh ₃)Cl ₂ / BHP			
	Run 1	Run 2	avg	error	Run 1	Run 2	avg	error
4								
5								
6	93.8				100			
7	100				100			
8	100	100	100	0	100			
9	100	100	100	0	100			
10	100	100	100	0	100			
11	100	100	100	0	100			
12	100	100	100	0	100			
13	100	100	100	0	100	100	100	0
14	100	100	100	0	100	100	100	0
15	100	100	100	0	100	100	100	0
16	100	100	100	0	100	100	100	0
17	100	100	100	0	100	100	100	0
18	100	100	100	0	100	100	100	0
19	100	100	100	0	100	100	100	0
20	100	100	100	0	100	100	100	0
21	100	100	100	0	100	100	100	0
22	100	100	100	0	100	100	100	0
23	100	100	100	0	98	100	99	1
24	100	100	100	0	100	100	100	0
25	100	100	100	0	100	100	100	0
26	100	100	100	0	100	100	100	0
27	100	100	100	0	100	100	100	0
28	100	100	100	0	100	100	100	0
29	100	100	100	0	100	100	100	0
30	100	100	100	0	100	100	100	0
31	100	100	100	0	100	100	100	0
32	100	100	100	0	100	100	100	0
33	100	100	100	0	100	100	100	0
34	100	100	100	0	100	100	100	0
35	100	100	100	0	100	100	100	0
36		100	100	0	100	100	100	0
37		100						

Pd(IPr)(3-Clpy)Cl₂

% ring-walking = (tol/tol)/(tol/tol) + (tol/Br)										
	Pd(IPr)(3-Clpy)Cl ₂ /3DT				Pd(IPr)(3Clpy)Cl ₂ /BHP					
m	Run1	Run 2	avg	error	Run 1	Run 2	Run 3	Run 4	avg	error
4										
5					100		100	100	100	0
6					100		100	100	100	0
7					86.4		92.7	100	93.03	3.93
8					71		85.8	100	85.6	8.37
9	100	100	100	0	56		74.7	*	65.35	9.35
10	100	100	100	0	43		63	42	49.33	6.84
11	100	100	100	0	35		50.8	35.2	40.33	5.23
12	100	100	100	0	27.5		42	27.4	32.3	4.85
13	100	100	100	0	21.5		34.8	20.3	25.53	4.65
14	100	100	100	0	16.6	17.8	29	19.1	20.63	2.84
15	100	100	100	0	13.1	16.6	24.1	15	17.2	2.41
16	100	100	100	0	0	13.2	21.1	13.2	11.88	4.37
17	100	100	100	0	0	11.6	17.2	12	10.2	3.63
18	100	100	100	0		10.3	14.8	11.1	12.07	1.39
19	100	100	100	0		9.3	11.9	10.6	10.6	0.75
20	100	100	100	0		0	11.2	9.5	6.9	3.48
21	100	100	100	0		0	0	0	0	0
22	100	100	100	0		0	0	0	0	0
23	100	100	100	0		0	0	0	0	0
24	100	100	100	0				0		
25	100	100	100	0				0		
26	100	100	100	0				0		
27	100	100	100	0				0		
28	100	100	100	0				0		
29	100	100	100	0				0		
30	100	100	100	0				0		
31	100	100	100	0				0		
32	100	100	100	0				0		
33	100	100	100	0				0		
34	100	100	100	0				0		
35	100	100	100	0				0		
36	100	100	100	0						
37		100								
38										
39										
40										
41										

*indicates that no tol/tol or tol/Br peaks were identified at a signal-to-noise > 1.

A1.8. Figures from the manuscript with found and predicted m/z.

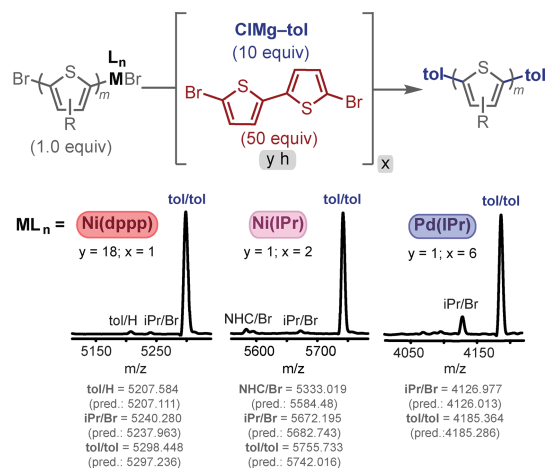


Figure A1-74. (Top) Reaction conditions for 3DT end-capping experiments, involving x iterations of capping/scavenger reagents over y hours. (Bottom) MALDI-TOF/MS data for 3DT polymerization followed by end-capping. (Values calculated using an average mass method signal-to-noise = 1 or 2)

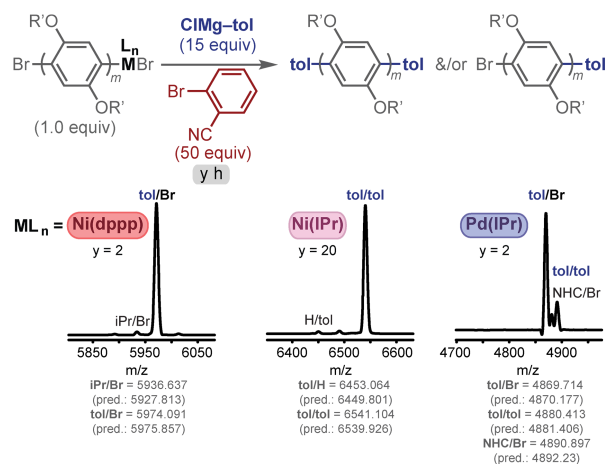


Figure A1-75. (Top) Reaction conditions for BHP end-capping experiments over y hours. (Bottom) MALDI-TOF/MS data for BHP polymerization followed by end-capping. (Values calculated using an average mass method signal-to-noise = 1 or 2. In the Ni(IPr) plot Br/Br was not detected)

A1.9 References

- (1) Love, B. E.; Jones, E. G. The Use of Salicylaldehyde Phenylhydrazone as an Indicator for the Titration of Organometallic Reagents. *J. Org. Chem.* **1999**, *64*, 3755–3756.
- (2) Lanni, E. L.; McNeil, A. J. Mechanistic Studies on Ni(dppe)Cl₂-catalyzed Chain-Growth Polymerizations: Evidence for Rate-Determining Reductive Elimination. *J. Am. Chem. Soc.* **2009**, *131*, 16573–16579.
- (3) Bryan, Z. J.; McNeil, A. J. Evidence for a Preferential Intramolecular Oxidative Addition in Ni-Catalyzed Cross-Coupling Reactions and Their Impact on Chain-Growth Polymerizations. *Chem. Sci.* **2013**, *4*, 1620–1624.

Appendix 2: Supporting Information for Chapter 3. Mechanistic Insight into Thiophene Catalyst-Transfer Polymerization Mediated by Nickel Diimine Catalysts

A2.1. Materials

Flash chromatography was performed on SiliCycle silica gel (40–63 μm). Thin layer chromatography was performed on Merck TLC plates (pre-coated with silica gel 60 F254). $i\text{PrMgCl}$ (2 M in THF) was purchased from Aldrich and titrated using salicylaldehyde phenylhydrazone (see General Experimental S3). 2,5-Dibromo-3-hexylthiophene was purchased from Ark Pharm and purified via column chromatography (100% hexanes as eluent). N-Bromosuccinimide was purchased from Aldrich and was recrystallized from hot water. All other reagent grade materials and solvents were purchased from Aldrich, Acros, or Fisher and were used without further purification unless otherwise noted. THF was dried and deoxygenated using an Innovative Technology (IT) solvent purification system composed of activated alumina, copper catalyst, and molecular sieves. The glovebox in which specified procedures were carried out was an MBraun LABmaster 130 with a N_2 atmosphere.

A2.2. General experimental

NMR Spectroscopy: Unless otherwise noted, ^1H , and ^{13}C NMR spectra for all compounds were acquired at rt. Chemical shift data are reported in units of δ (ppm) relative to tetramethylsilane (TMS) and referenced with residual solvent. Multiplicities are reported as follows: singlet (s), doublet (d), doublet of doublets (dd), triplet (t), quartet (q), multiplet (m), broad signal (br).

Residual water is denoted by an asterisk (*). Compounds **S1**,¹ **C1_{tBu}**,¹ **S2**,¹ **C2**,² **S3**,¹ **S4**,³ **C3_{Me}**,³ **C4_{Me}**,⁴ and **C4_{CF3}**⁴ were prepared according to modified literature procedures.

Mass Spectrometry: High-resolution mass spectrometry data were obtained on a Micromass AutoSpec Ultima Magnetic Sector mass spectrometer.

Gel-Permeation Chromatography (GPC): Polymer molecular weights were determined by comparison with polystyrene standards (Varian, EasiCal PS-2 MW 580–377,400) at 40 °C in THF on a Malvern Viscotek GPCMax VE2001 equipped with two Viscotek LT- 5000L 8 mm (ID) × 300 mm (L) columns and analyzed with Viscotek TDA 305 (with RI, UV-PDA Detector Model 2600 (190–500 nm), RALS/LALS, and viscometer). Data presented correspond to the absorbance at 254 nm normalized to the highest peak. Samples were dissolved in THF/toluene (99:1) (with mild heating), and passed through a polytetrafluoroethylene (PTFE, 0.2 μm) filter prior to analysis.

Gas Chromatography: Gas chromatography (GC) was carried out using a Shimadzu GC 2010 containing a Shimadzu SHRX5 (crossbound 5% diphenyl – 95% dimethyl polysiloxane; 15 m, 0.25 mm ID, 0.25 μm df) column.

Matrix-Assisted Laser Desorption/Ionization Mass Spectrometry: Matrix-assisted laser desorption/ionization Mass Spectrometry (MALDI-TOF-MS) was carried out on a Bruker AutoFlex Speed MALDI-TOF in positive-ion reflectron mode using *trans*-2-[3-(4-*tert*-butylphenyl)-2-methyl-2-propenylidene]malononitrile (DCTB) as a matrix. Samples were

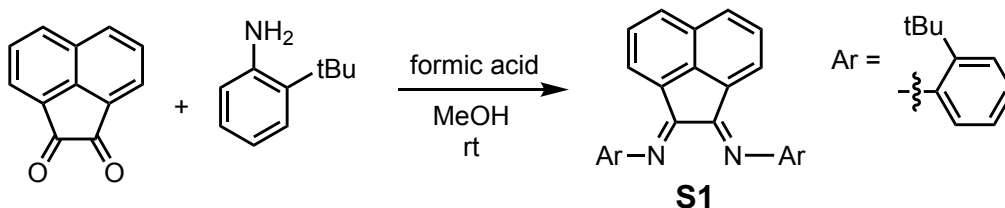
prepared by mixing polymer dissolved in THF/toluene (99:1 v/v) (~1 mg polymer/1 mL THF, 2.5 μ L) with DCTB dissolved in CHCl_3 (~1 M, 2.5–10 μ L). Samples were diluted with varying polymer/DCTB ratios (to ensure good signal/noise) and then spotted on a MALDI 96-well plate and air dried. The data were analyzed using flexAnalysis.

iPrMgCl titration: In a glovebox, salicylaldehyde phenylhydrazone⁵ (106 mg, 0.500 mmol) was dissolved in THF (5 mL) to make a 0.1 M solution. For titration, iPrMgCl was added dropwise using a 100 μ L syringe into a known amount of the salicylaldehyde phenylhydrazone solution. Titration was complete when the solution turned bright orange.

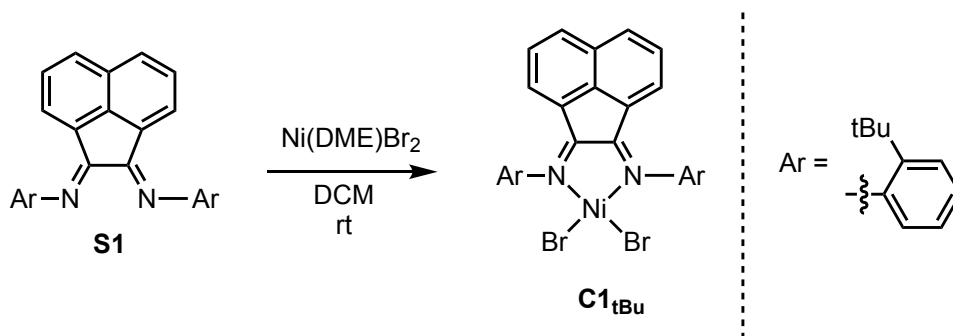
Polymer work-up for GC: Polymerizations were quenched using aq. HCl (12 M). The organic layer was extracted with CHCl_3 , dried over MgSO_4 , and filtered through a PTFE (0.2 μ m) filter into a GC vial.

Polymer work-up for GPC: Polymer samples worked-up for GC analysis were concentrated yielding a purple solid, which was redissolved in THF/toluene (99:1 v/v) with mild heating, then filtered through a PTFE (0.2 μ m) filter into a GPC vial.

A2.3. Synthetic procedures

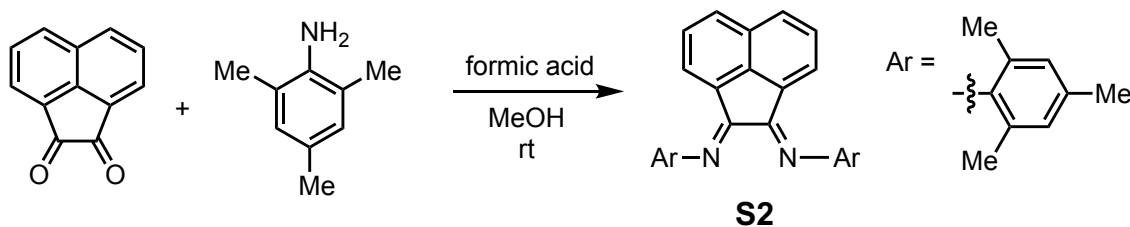


ArN=(An)=NAr (Ar = 2-*t*-butylphenyl, An = acenaphthylene) (S1).¹ In a 10 mL round-bottom flask equipped with a stir bar, *o*-*tert*-butylaniline (174 μ L, 1.12 mmol, 2.04 equiv) was added drop-wise to a solution of acenaphthenequinone (100. mg, 0.549 mmol, 1.00 equiv), formic acid (58 μ L, 1.5 mmol, 2.8 equiv.), and MeOH (1.5 mL). The reaction was stirred at rt for 18 h. Then, the heterogeneous mixture was filtered over a fine frit and washed with cold MeOH (3 x 10 mL) and cold pentane (3 x 10 mL). The solid was collected and re-dissolved in DCM (3 mL), layered with pentane (8 mL), and placed in a -20 °C freezer. After 18 h, the resulting solid was collected by filtration over a fine frit and washed with cold pentane (3 x 10 mL) to give 158 mg of S1 as orange powder (65% yield). HRMS (ESI⁺): Calcd. for C₃₂H₃₂N₂ [M+H]⁺ 445.2638; found 445.2641.



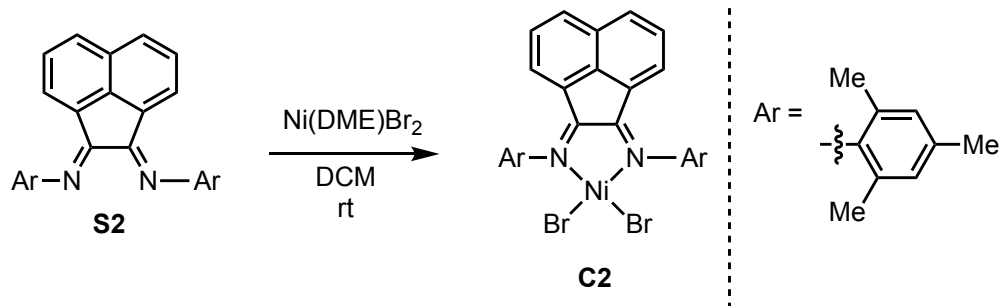
ArN=(An)=NArNiBr₂ (Ar = 2-*t*-butylphenyl, An = acenaphthylene) (C1_{tBu}).¹ To a 50 mL round-bottom flask, Ni(II) bromide ethylene glycol dimethyl ether (Ni(DME)Br₂, 66 mg, 0.21 mmol, 1.1 equiv) was added to a stirring solution of diimine S1 (86 mg, 0.19 mmol, 1.0 equiv) in dry DCM (6.4 mL) at rt. After 20 h, the solution was concentrated and washed with anh. Et₂O (2

x 10 mL). The resulting brown solid was dried under reduced pressure to give 118 mg of C1_{tBu} (92% yield).

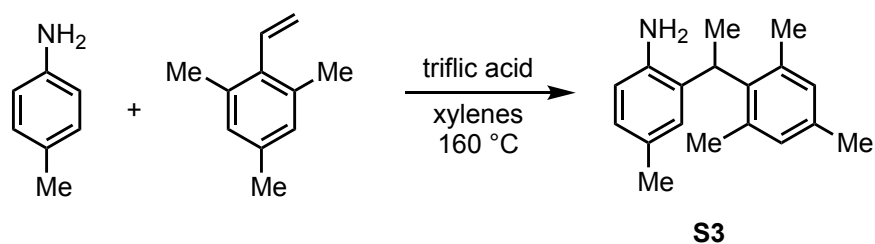


ArN=(An)=NAr (Ar = 2,4,6-trimethylphenyl, An = acenaphthylene) (S2).²

Acenaphthenequinone (100. mg, 0.549 mmol, 1.00 equiv) was added to a solution containing formic acid (11 μ L, 0.29 mmol, 0.52 equiv) in MeOH (1.45 mL) in a 10 mL round-bottom flask equipped with a stir bar. Subsequently, 2,4,6-trimethylaniline (170 μ L, 1.2 mmol, 2.2 equiv) was added to the stirring solution. After 18 h at rt, the reaction flask was placed in a -20 °C freezer where an orange solid precipitated from the solution over 24 h. The orange solid was collected via filtration over a fine frit, washed with cold MeOH (3 x 10 mL) and cold pentane (3 x 10 mL), then collected and dried under reduced pressure. The filtrate was transferred to a 100 mL round-bottom with DCM (10 mL), concentrated, re-dissolved in DCM (4 mL) filtered through glass wool and cooled to -20 °C to recrystallize. The orange solid was collected by filtration over a fine frit, washed with cold MeOH (3 x 10 mL) and cold pentane (3 x 10 mL), and dried under reduced pressure. The solids from each crystallization were combined, resulting in 174 mg of S2 as orange powder (76% yield). HRMS (ESI⁺): Calcd. for C₃₀H₂₈N₂ [M+H]⁺ 417.2325; found 417.2326.

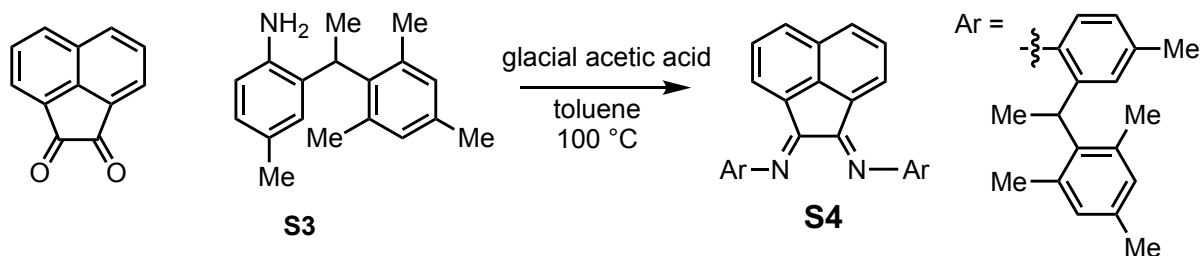


(ArN=(An)=NAr)NiBr₂ (Ar = **2,4,6-trimethylphenyl**, An = **acenaphthylene**) (**C2**).² In a 50 mL round-bottom flask, S2 (145 mg, 0.348 mmol, 1.00 equiv) was dissolved in DCM (9.5 mL). Then, Ni(DME)Br₂ (113 mg, 0.365 mmol, 1.05 equiv) was added and the reaction mixture was stirred for 20 h at rt. Overnight, a purple precipitate formed, which was collected by filtration over a fine frit and washed with cold MeOH (3 x 10 mL) and cold pentane (3 x 10 mL). The solid was collected and re-dissolved in DCM (3 mL), filtered through glass wool into a 20 mL vial, layered with pentanes (6 mL), and cooled to -20 °C. After 24 h, dark purple crystals were collected and washed with cold MeOH (3 x 10 mL) and cold pentanes (3 x 10 mL) to give 116 mg of C2 as dark purple crystals (53% yield).

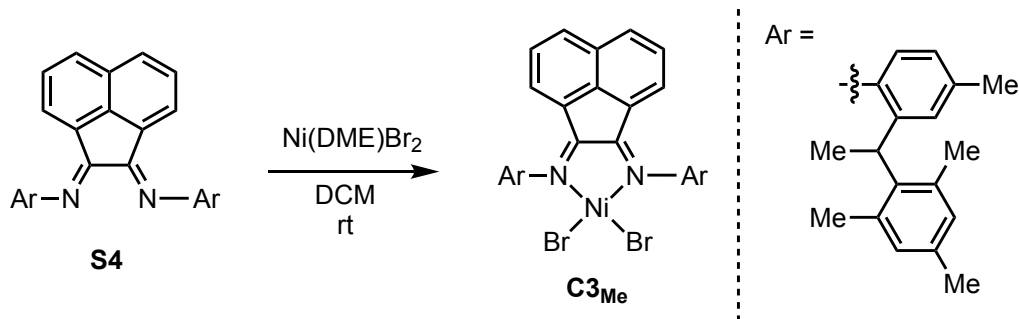


4-Methyl-2-(sec-(2,4,6-trimethylphenethyl)aniline (S3).³ To a 15 mL bomb flask equipped with a stir bar, *p*-toluidine (1.36 g, 12.7 mmol, 1.46 equiv) was dissolved in xylenes (1.1 mL). Subsequently, 2,4,6-trimethylstyrene (1.40 mL, 8.67 mmol, 1.00 equiv) and triflic acid (200. μL , 2.25 mmol, 0.260 equiv) were added to the reaction flask, which was sealed and placed behind a blast shield. After 17 h at 160 °C, the heterogeneous mixture was transferred to a 250 mL round-

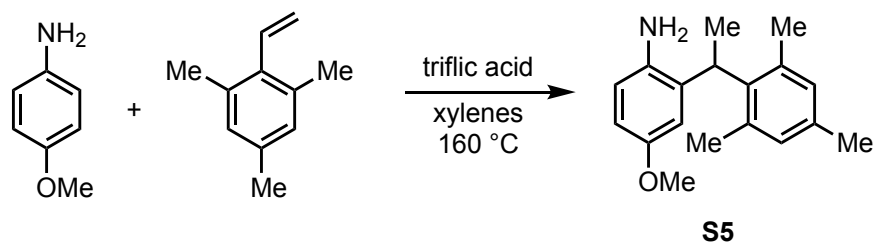
bottom flask with EtOAc (50 mL), concentrated, and purified via column chromatography on silica gel (100% hexanes to 80/20 hexanes/EtOAc) to give a brown oil which was recrystallized in 10/1 hexanes/EtOAc, yielding 1.25 g of S3 as a white solid (57% yield). HRMS (ESI+): Calcd. for C₁₈H₂₃N [M+H]⁺ 254.1903; found 254.1899.



Rac-ArN=(An)=NAr (Ar = 4-methyl-2-(sec-(2,4,6-trimethylphenethyl)phenyl; An = acenaphthylene) (**S4**).³ To a 20 mL vial equipped with a stir bar, acenaphthenequinone (438 mg, 2.41 mmol, 0.490 equiv) and amine S3 (1.25 mg, 4.92 mmol, 1.00 equiv.) were dissolved in toluene (2.8 mL) and glacial acetic acid (5.5 mL, 96 mmol, 19 equiv). After 3 h at 100 °C, the resulting heterogeneous mixture was filtered over a fine frit, washed with cold MeOH (3 x 10 mL) and cold hexanes (3 x 10 mL) and dried under reduced pressure, to give 1.13 g of S4 as a yellow powder (72% yield). HRMS (ESI+): Calcd. for C₄₈H₄₈N₂ [M+H]⁺ 653.3890; found 653.3897.

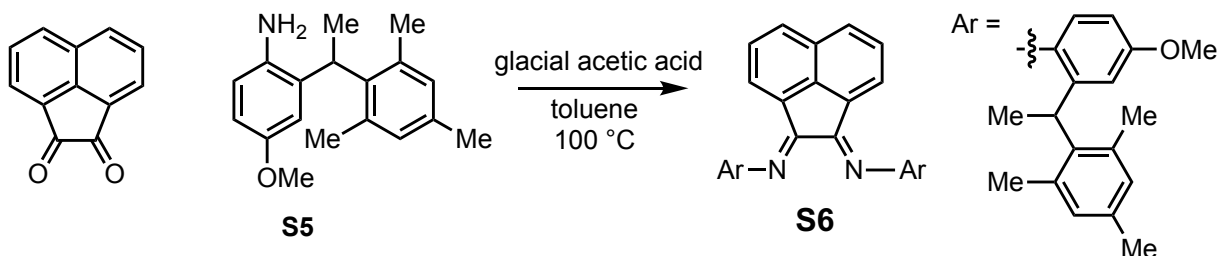


Rac-(ArN=(An)=NAr)NiBr₂ (Ar = 4-methyl-2-(sec-(2,4,6-trimethylphenethyl))-phenyl; An = acenaphthylene) (**C3_{Me}**).³ In a 50 mL Schlenk flask equipped with a stir bar, Ni(DME)Br₂ (156 mg, 0.505 mmol, 1.10 equiv.) and diimine S4 (300. mg, 0.460 mmol, 1.00 equiv) were dissolved in DCM (15 mL) and stirred at rt under N₂ for 16 h. Then, the dark maroon liquid was concentrated, dissolved in DCM (20 mL), filtered through a celite plug, layered with pentane (60 mL), and cooled to -20 °C. The resulting solid was collected by filtration over a coarse frit, washed with cold pentane (3 x 10 mL), and dried under reduced pressure to give 338 mg of C3_{Me} as a dark maroon solid (90% yield).

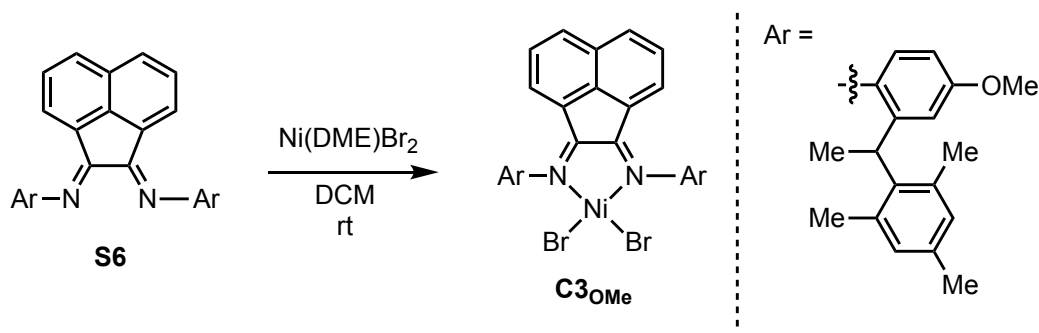


4-Methoxy-2-(sec-(2,4,6-trimethylphenethyl)aniline (S5). To a 15 mL bomb flask equipped with a stir bar, *p*-anisidine (1.65 g, 13.4 mmol, 1.55 equiv) was dissolved in xylenes (1.2 mL). Subsequently, 2,4,6-trimethylstyrene (1.40 mL, 8.64 mmol, 1.00 equiv) and triflic acid (150 μL, 1.7 mmol, 0.20 equiv) were added to the reaction flask, which was sealed and placed behind a shield. After 24 h at 160 °C, the reaction was transferred to a 250 mL round-bottom flask with EtOAc (50 mL), concentrated in vacuo, and purified via column chromatography on silica gel

(97.5:2.5 hexanes/EtOAc to 80:20 hexanes/EtOAc (v/v)) to give 941 mg of **S5** as a green-brown solid (40% yield). HRMS (EI): Calcd. for $C_{18}H_{23}NO$ $[M]^+$ 269.1800; found 269.1780.

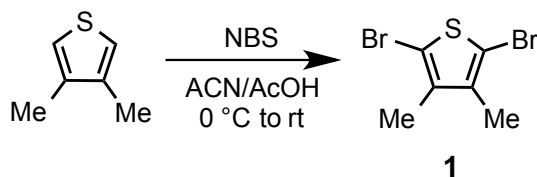


Rac-ArN=(An)=NAr (Ar = 4-methoxy-2-(sec-(2,4,6-trimethylphenethyl)phenyl); An = acenaphthylene) (**S6**). To a 20 mL vial equipped with a stir bar, acenaphthenequinone (143 mg, 0.785 mmol, 1.00 equiv.) and amine **S5** (433 mg, 1.61 mmol, 2.05 equiv) were dissolved in toluene (0.92 mL) and glacial acetic acid (1.9 mL, 33 mmol, 42 equiv). After 3 h at 100 °C, the resulting heterogeneous mixture was filtered over a fine frit, washed with cold MeOH (3 x 10 mL) and cold hexanes (3 x 10 mL) and dried under reduced pressure to give 159 mg of **S6** as a neon orange powder (30% yield). HRMS (ESI+): Calcd. for $C_{48}H_{48}N_2O_2$ $[M+H]^+$ 685.3789; found 686.3822.

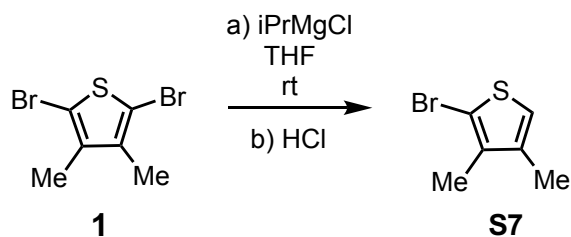


Rac-(ArN=(An)=NAr)NiBr₂ (Ar = 4-methoxy-2-(sec-(2,4,6-trimethylphenethyl)-phenyl; An = acenaphthylene) (**C3_{OMe}**). In a 50 mL Schlenk flask equipped with a stir bar, Ni(DME)Br₂ (145 mg, 0.469 mmol, 1.00 equiv) and diimine **S6** (385 mg, 0.562 mmol, 1.20 equiv) were

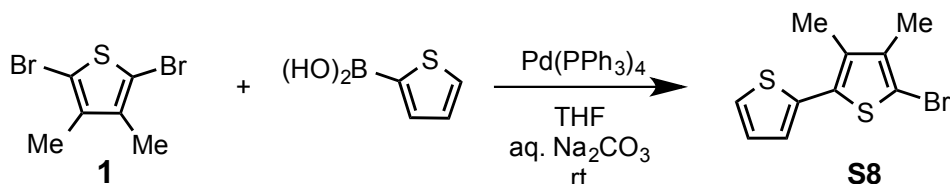
dissolved in DCM (14.2 mL). The heterogeneous mixture was stirred at rt under N₂. After 20 h, the dark maroon liquid was concentrated in vacuo to give a dark maroon solid, which was dissolved in DCM (3 mL), layered with pentane (8 mL), and cooled to -20 °C. The resulting solid was collected by filtration over a coarse frit, washed with cold pentane (3 x 10 mL), and dried under reduced pressure to give 275 mg of **C3_{OMe}** as a dark maroon solid (65 % yield).



2,5-Dibromo-3,4-dimethylthiophene (1). In a 50 mL round-bottom flask, 3,4-dimethylthiophene (0.89 g, 7.9 mmol, 1.0 equiv) was dissolved in dry ACN/AcOH (24 mL/1.4 mL) and cooled to 0 °C using an ice-water bath for 5 min. Then, NBS (3.10 g, 17.4 mmol, 2.20 equiv) was added over 5 min. The stirring solution was warmed to rt over 2.5 h, and then transferred to a separatory funnel using Et₂O (20 mL). The organic layer was washed with sat. aq. Na₂CO₃ (3 x 15 mL) and brine (3 x 20 mL), then dried over MgSO₄, concentrated, and purified by filtering through a silica plug and a neutral alumina pipette plug using hexanes. Drying under reduced pressure resulted in 1.73 g of **1** as a clear, colorless oil (82% yield). HRMS (EI): Calcd. for C₆H₆Br₂S [M]⁺ 267.8557; found 267.8566.

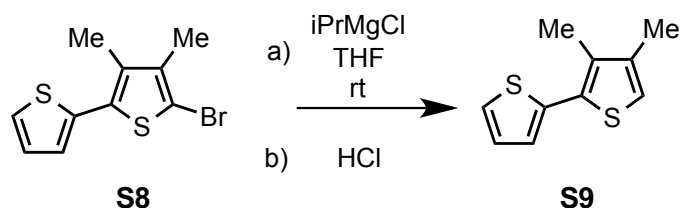


2-Bromo-3,4-dimethylthiophene (S7). In a glovebox in a 20 mL round-bottom flask equipped with a stir bar, thiophene derivative **1** (44.1 mg, 0.165 mmol, 1.00 equiv) was dissolved in THF (1.56 mL). Then, *i*PrMgCl (1.8 M in THF, 91.6 μ L, 0.165 mmol, 1.00 equiv) was added and the reaction stirred for 30 min at rt. The reaction was quenched outside the glovebox using aq. 12 M HCl (1 mL). The organic layer was extracted with CHCl_3 (3 x 3 mL), dried over MgSO_4 , filtered, concentrated using rotary evaporation, and purified using a silica plug with hexanes as the eluent yielding 12.2 mg of **S7** as a clear, colorless oil (39% yield). MS (EI+) Calcd for $\text{C}_6\text{H}_7\text{BrS}$ 189.9; found 189.8. Note **S7** was too volatile to obtain HRMS data.



5-Bromo-3,4-dimethyl-2,2'-bithiophene (S8). Solvents were sparged with N_2 for 20 min before using in this reaction. A 50 mL Schlenk flask was cooled under reduced pressure, filled with N_2 , then evacuated and refilled with N_2 3x. Sequentially, thiophene derivative **1** (200. mg dissolved in THF (3 mL), 0.747 mmol, 1.33 equiv), thiophen-2-ylboronic acid (71.7 mg, 0.560 mmol, 1.00 equiv), $\text{Pd(PPh}_3)_4$ (43 mg, 0.037 mmol, 0.067 equiv), THF (5.5 mL), and aq. Na_2CO_3 (2 M, 5.75 mL) were added. The reaction was stirred at rt for 20 h under N_2 . The heterogeneous mixture was then transferred to a separatory funnel using Et_2O (10 mL). The organic layer was separated

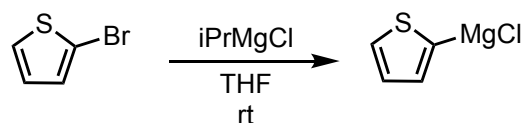
and washed with DI H₂O (20 mL) and brine (2 x 20 mL). The organic layer was collected and dried over MgSO₄, filtered, concentrated using rotary evaporation, and purified by column chromatography using hexanes (100%) as the eluent. The resulting white oil was dried under reduced pressure to yield 32.5 mg of **S8** as a white solid (21% yield). HRMS (EI) Calcd. for C₁₀H₉BrS₂ [M]⁺ 271.9329; found 271.9328.



3,4-dimethyl-2,2'-bithiophene (S9). In a glovebox, sequentially, **S8** (18.5 mg, 0.0677 mmol, 1.00 equiv), THF (0.62 mL), and iPrMgCl (1.8 M in THF, 56.7 μ L, 0.102 mmol, 1.50 equiv) were combined in a 20 mL vial and stirred at rt for 45 min, then removed from the glovebox and quenched with aq. 12 M HCl (1 mL). The organic layer was extracted with CHCl₃ (3 x 3 mL), dried over MgSO₄, filtered, concentrated, and purified using a silica plug with hexanes (100%) as the eluent. Drying under reduced pressure yielded 9.5 mg of **S9** as a clear oil (72% yield). HRMS (EI) Calcd. for C₁₀H₁₀S₂ [M]⁺ 194.0224; found 194.0223.

3',4'-Diimethyl-2,2':5',2''-terthiophene (**2**).

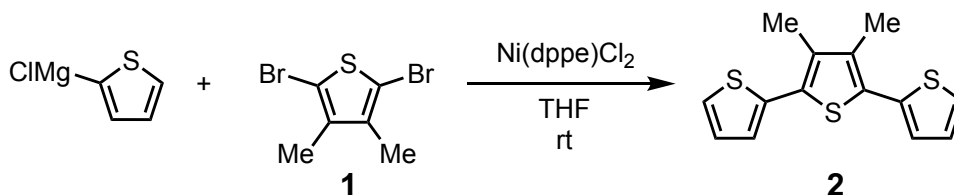
Preparing thiophene Grignard solution.



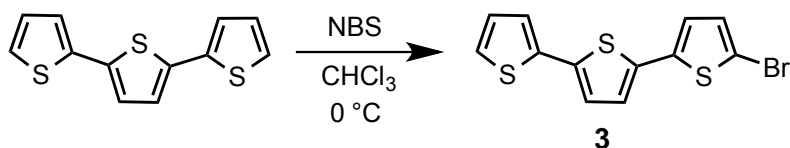
The following reactions were carried out in a glovebox. Thiophen-2-ylmagnesium chloride was prepared by reacting 2-bromothiophene (69.5 mg, 0.426 mmol, 1.00 equiv) with iPrMgCl (1.85

M in THF, 20.7 μ L, 0.384 mmol, 0.900 equiv) in THF (4.0 mL) for 30 min at rt. Subsequent titration revealed a 0.096 M solution.

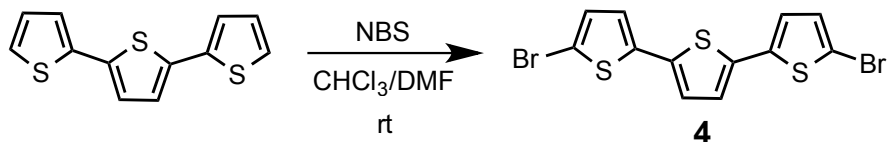
Synthesizing compound 2.



In the following order, freshly prepared thiophen-2-ylmagnesium chloride solution (1.68 mL, 0.161 mmol, 2.10 equiv) and Ni(dppe)Cl₂ (dppe = 1,2-bis(diphenylphosphino)ethane, 3.4 mg, 0.0064 mmol, 0.083 equiv) were added to a solution of **1** (20.6 mg, 0.0769 mmol, 1.00 equiv) in THF (2.0 mL) in a 20 mL vial and stirred for 2 h at rt. The red solution was removed from the glovebox and quenched using aq. 12 M HCl (1 mL). The organic layer was extracted with DCM (3 x 3 mL), dried over MgSO₄, filtered, and concentrated. The crude product was purified using column chromatography with hexanes (100%) as the eluent. Drying under reduced pressure yielded 18 mg of **2** as a white solid (84 % yield). HRMS (ESI+) Calcd. for C₁₄H₁₂S₃ [M+H]⁺ 277.0174; found 277.0176.



5-bromo-2,2':5',2''-terthiophene (3). In a 20 mL vial equipped with a stir bar, 2,2':5',2''-terthiophene (300. mg, 1.21 mmol, 1.00 equiv) was dissolved in CHCl_3 (4 mL). NBS (210. mg, 1.18 mmol, 0.975 equiv) was added over 2 min, and stirred for 2.5 h at 0 °C. The solution was washed with sat. aq. Na_2CO_3 (1 x 5 mL) and brine (2 x 5 mL), the organic layer was dried over MgSO_4 , filtered, concentrated, and purified by column chromatography with hexanes (100%) as the eluent, yielding 156 mg of **3** as a pale green solid (40% yield). HRMS (EI) Calcd. for $\text{C}_{12}\text{H}_6\text{BrS}_3$ $[\text{M}]^+$ 325.8893; found 325.8889.



5,5''-dibromo-2,2':5',2''-terthiophene (4). In a 20 mL vial equipped with a stir bar, 2,2':5',2''-terthiophene (300. mg, 1.21 mmol, 1.00 equiv) was dissolved in CHCl_3/DMF (9/2, 11 mL). NBS (434 mg, 2.44 mmol, 2.02 equiv) was added over 2 min, and the reaction was stirred for 13 h at rt. The solution was washed with sat. aq. Na_2CO_3 (10 mL), the organic layer was extracted with CHCl_3 (3 x 2 mL), dried over MgSO_4 , filtered, and concentrated. The resulting green solid was redissolved in CHCl_3 (4 mL with mild heating), filtered over a glass wool plug then layered with hexanes (10 mL), and placed in a -20 °C freezer for 15 h to effect crystallization. The resulting yellow-green crystals were collected by filtration over a frit and washing with cold hexanes (3 mL) to yield 392 mg of **4** (80% yield). HRMS (EI) Calcd. for $\text{C}_{12}\text{H}_6\text{Br}_2\text{S}_3$ $[\text{M}]^+$ 403.7998; found 403.7988.

A2.4. NMR Spectra

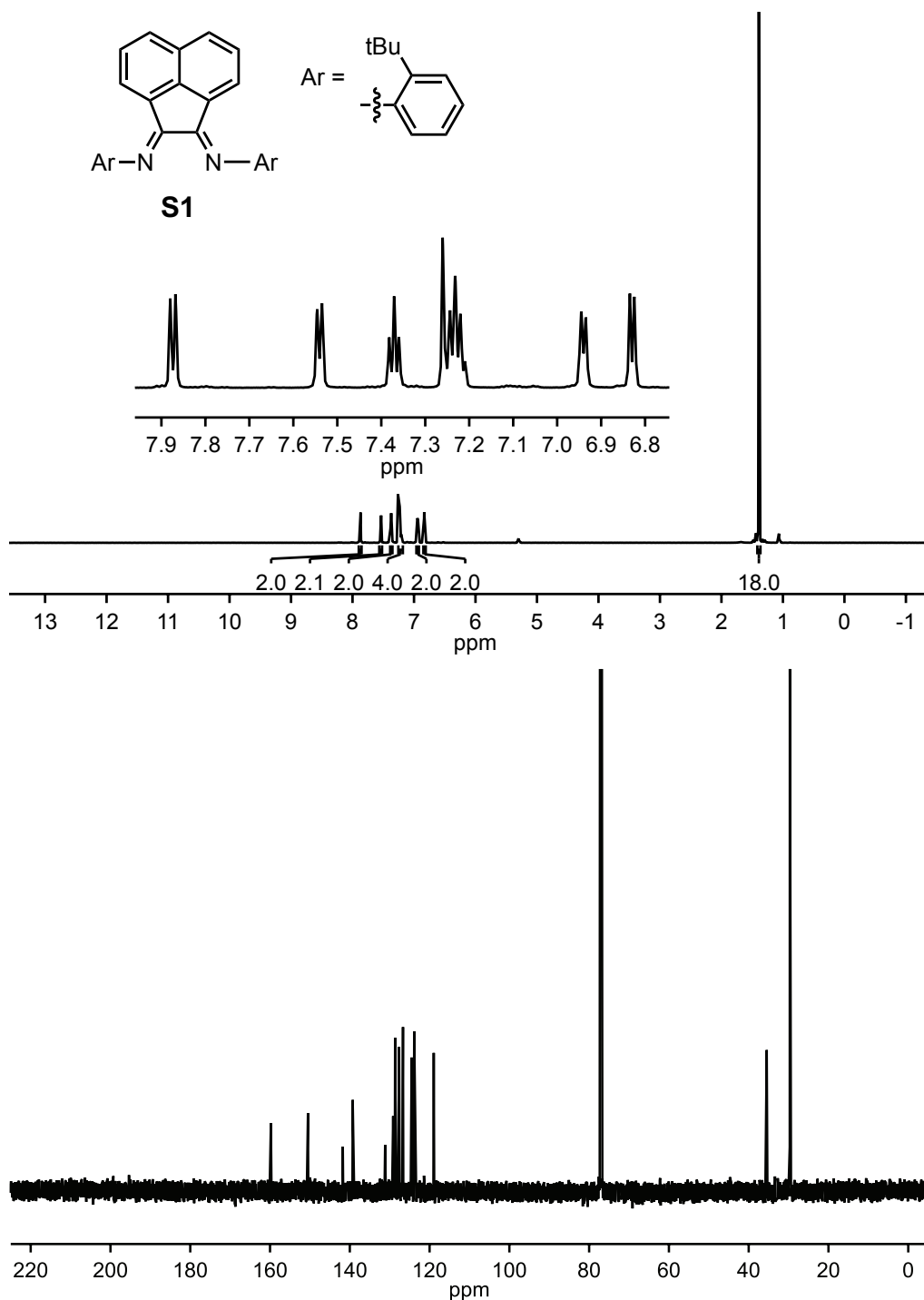


Figure A2-1. ¹H and ¹³C NMR Spectra of S1. ¹H NMR (700 MHz, CDCl₃) δ 7.87 (d, *J* = 8.2 Hz, 2H), 7.54 (d, *J* = 7.7 Hz, 2H), 7.37 (t, *J* = 7.7 Hz, 2H), 7.25–7.20 (m, 4H), 6.94 (d, *J* = 7.3 Hz, 2H), 6.83 (d, *J* = 7.3 Hz, 2H), 1.39 (s, 18H). ¹³C NMR (176 MHz, CDCl₃) δ 159.78, 150.50, 141.75, 139.27, 131.15, 129.14, 128.65, 127.64, 126.76, 126.66, 124.50, 123.86, 118.95, 35.48, 29.69.

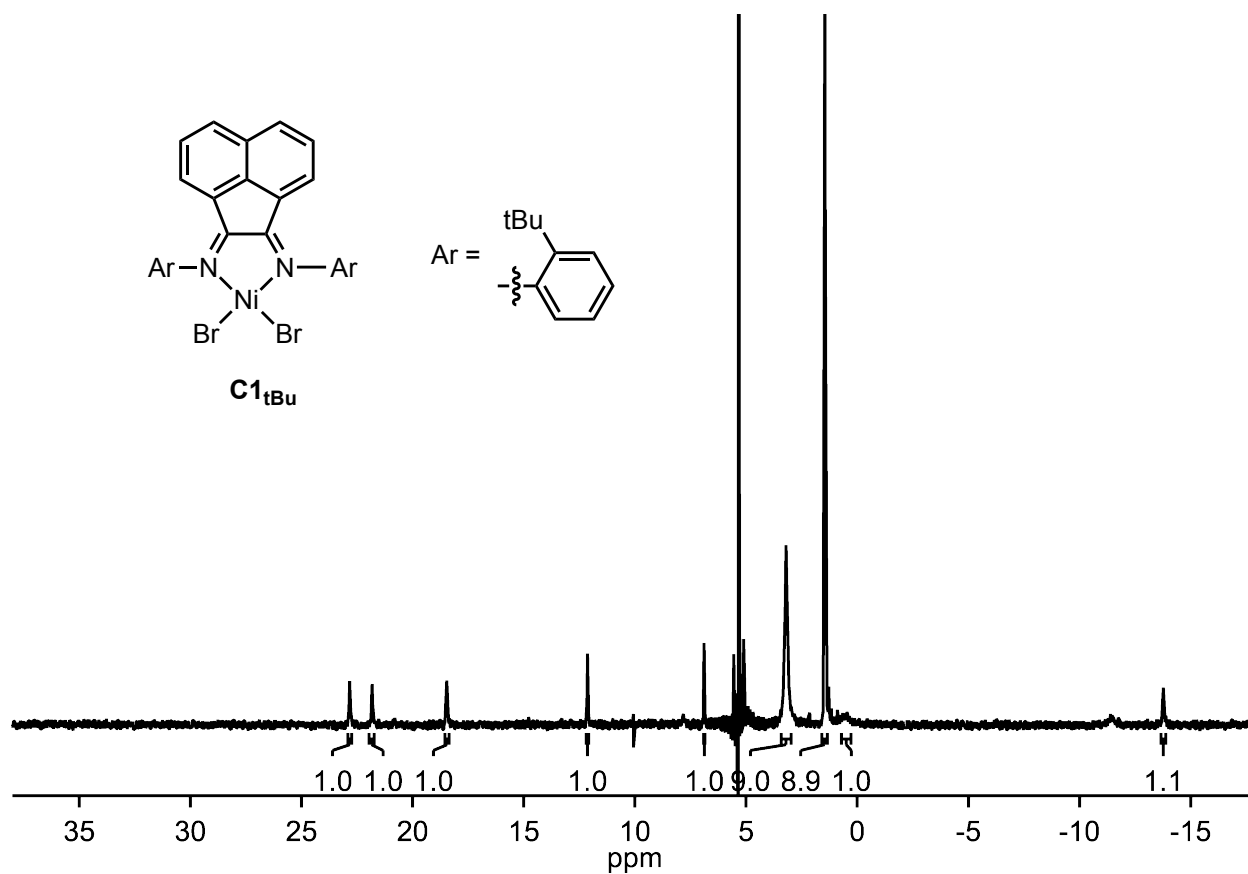


Figure A2-2. 1H NMR Spectrum of $C1_{tBu}$. 1H NMR (400 MHz, CD_2Cl_2 , rd = 0.005 s, at = 0.05 s) δ 22.83 (s, 1H), 21.82 (s, 1H), 18.46 (s, 1H), 12.14 (d, $J = 7.5$ Hz, 1H), 6.92–6.85 (m, 1H), 3.20 (s, 9H), 1.45 (s, 9H), 0.41 (broad s, 1H), -13.77 (s, 1H). Unaccounted for hydrogens (8 H) due to peak broadening.

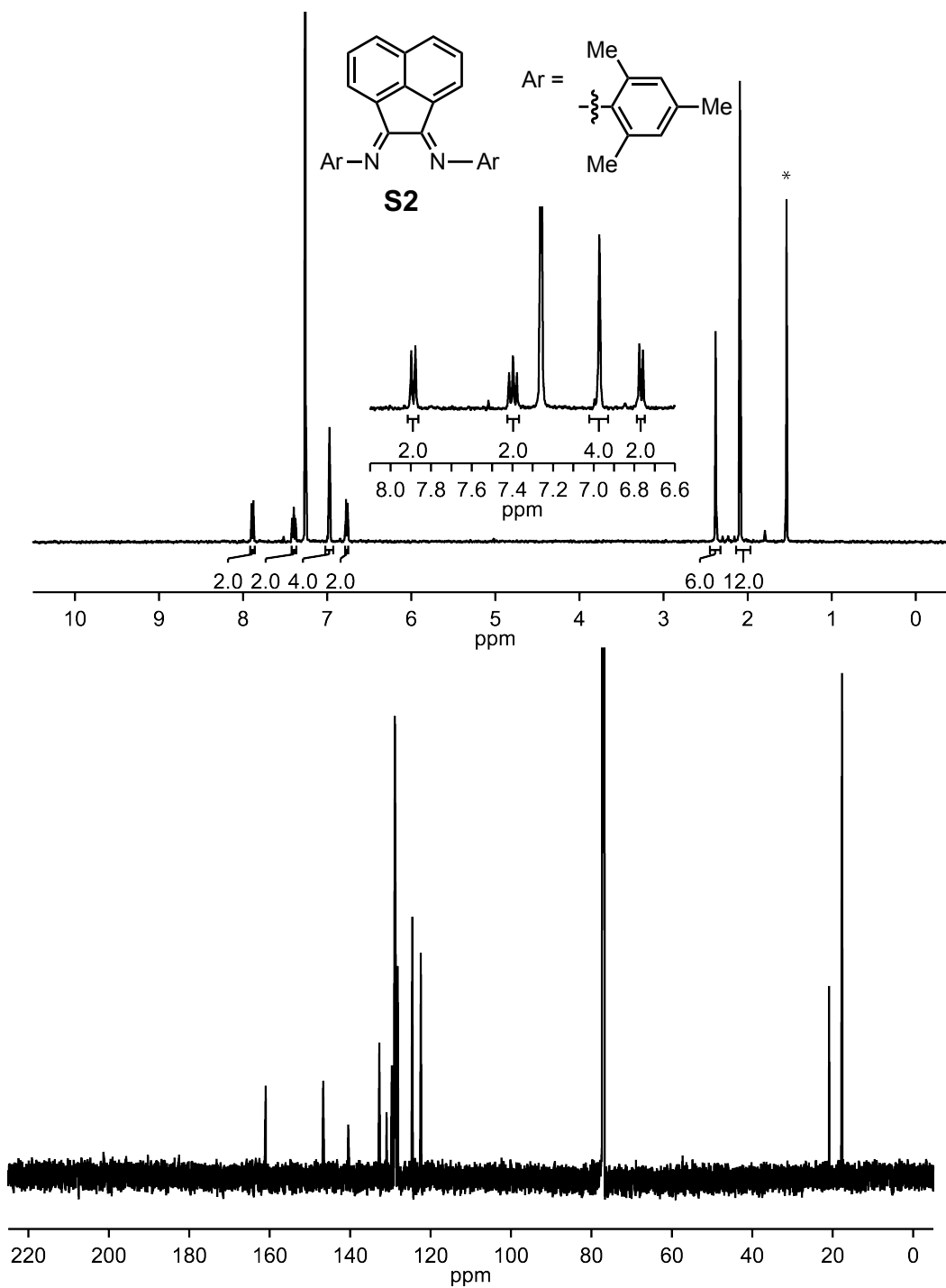


Figure A2-3. ^1H and ^{13}C NMR Spectra of **S2**. ^1H NMR (400 MHz, CDCl_3) δ 7.87 (d, $J = 8.3$ Hz, 2H), 7.38 (t, $J = 7.3$, 2H), 6.96 (s, 4H), 6.75 (d, $J = 7.3$ Hz, 2H), 2.36 (s, 6H), 2.07 (s, 12H). ^{13}C NMR (176 MHz, CDCl_3) δ 161.01, 146.73, 140.50, 132.76, 130.96, 129.67, 128.88, 128.72, 128.19, 124.55, 122.44, 20.92, 17.70.

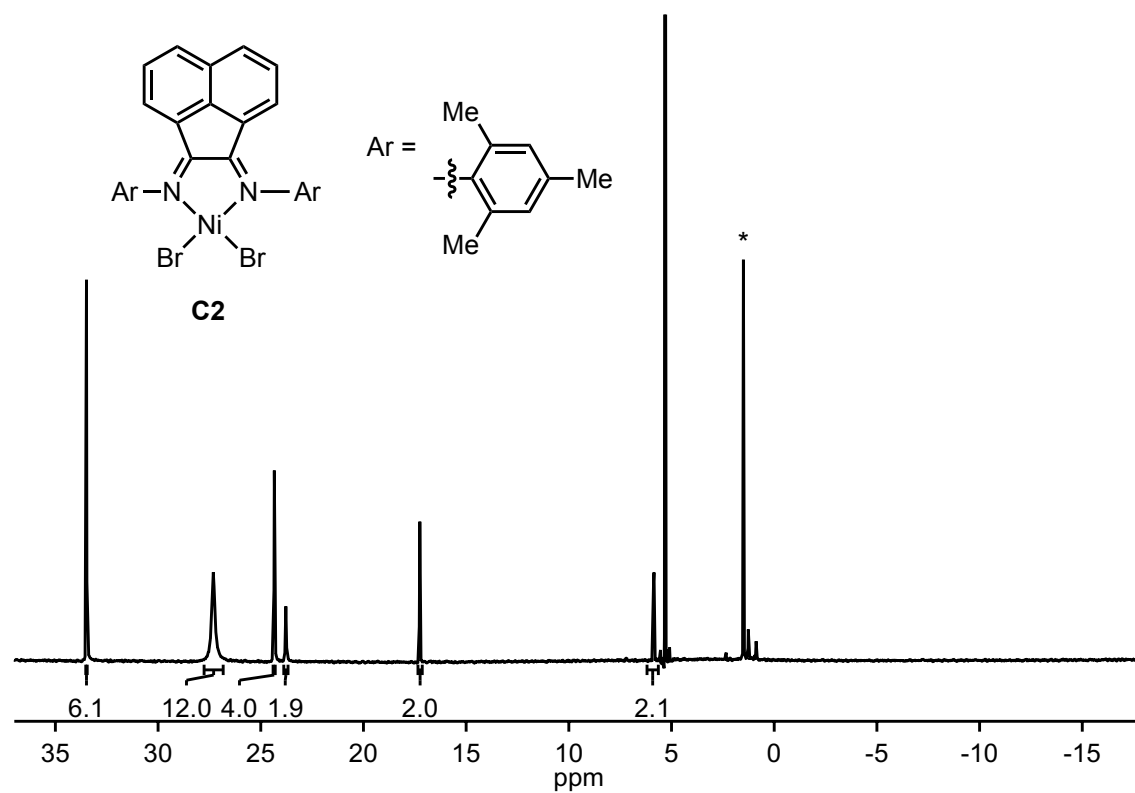


Figure A2-4. ^1H NMR Spectrum of **C2**. ^1H NMR (400 MHz, CD_2Cl_2 , rd = 0.005 s, at = 0.05 s δ 33.77 (s, 6H), 27.54 (s, 12H), 24.49 (s, 4H), 23.93 (s, 2H), 17.35 (d, $J = 7.9$ Hz, 2H), 5.85 (s, 2H).

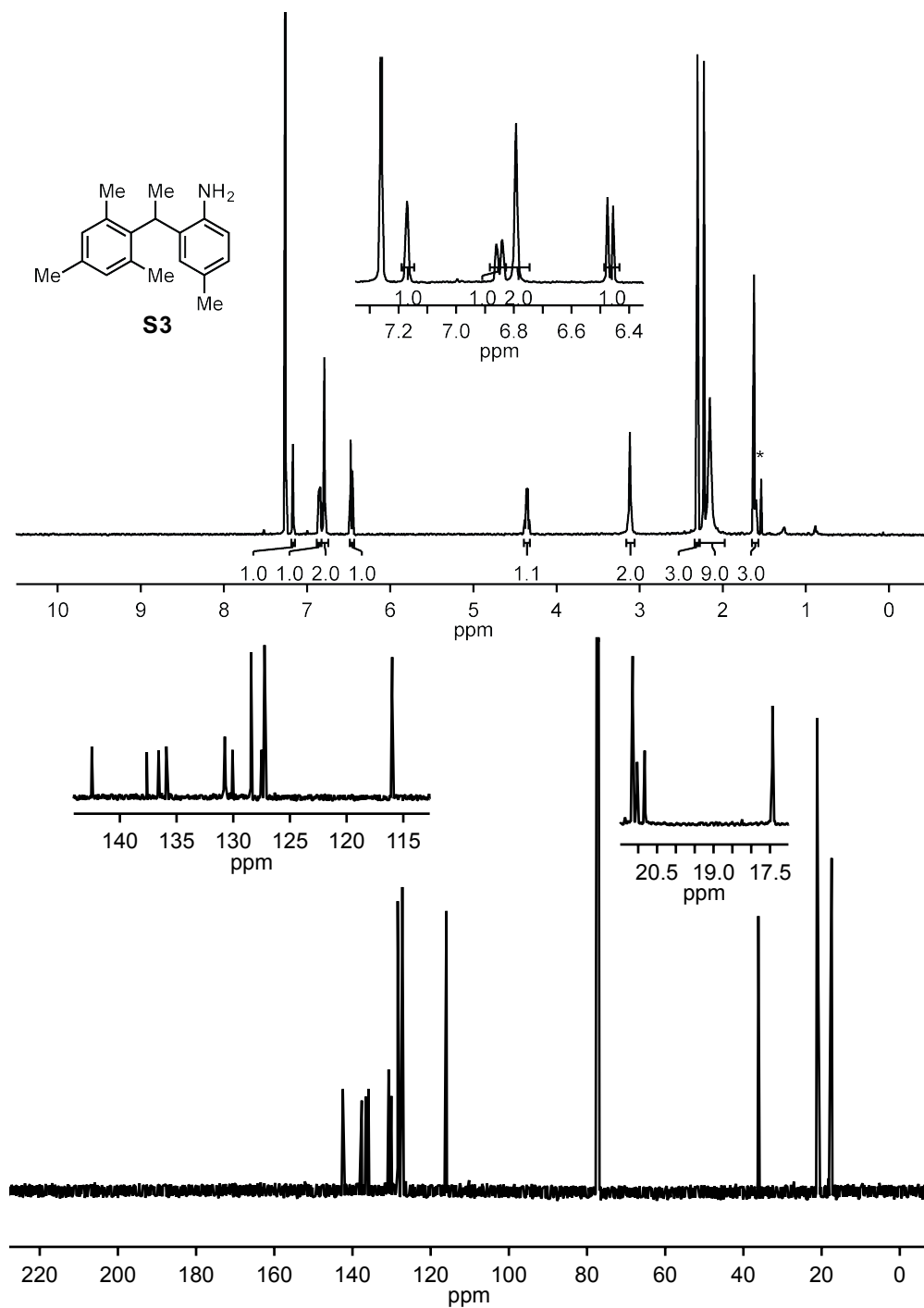


Figure A2-5. ¹H and ¹³C NMR Spectra of S3. ¹H NMR (500 MHz, CDCl₃) δ 7.17 (s, 1H), 6.85 (dd, *J* = 7.9, 1.9 Hz, 1H), 6.80 (s, 2H), 6.47 (d, *J* = 7.9 Hz, 1H), 4.35 (q, *J* = 7.3 Hz, 1H), 3.12 (s, 2H), 2.30 (s, 3H), 2.19 (overlapping peaks, 9H), 1.61 (d, *J* = 7.3 Hz, 3H). ¹³C NMR (126 MHz, CDCl₃) δ 142.48, 137.63, 136.58, 135.90, 130.75, 130.07, 128.43, 127.50, 127.24, 115.98, 36.17, 21.15, 21.03, 20.83, 17.43.

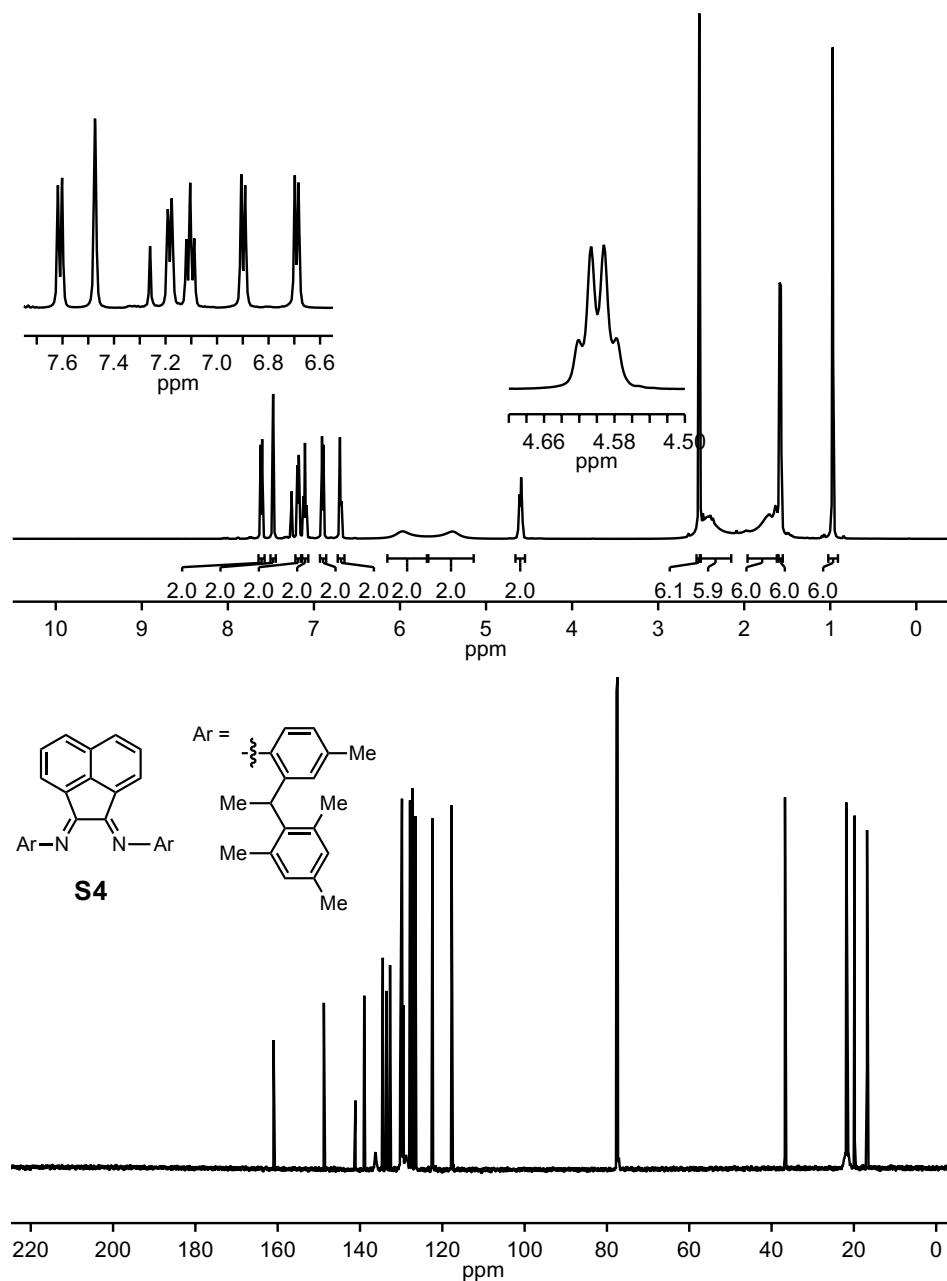


Figure A2-6. ^1H and ^{13}C NMR spectra of S4. ^1H NMR (500 MHz, CDCl_3) δ 7.61 (d, J = 8.2 Hz, 2H), 7.47 (s, 2H), 7.18 (d, J = 7.7 Hz, 2H), 7.10 (t, J = 7.7 Hz, 2H), 6.90 (d, J = 7.8 Hz, 2H), 6.69 (d, J = 7.2 Hz, 2H), 5.97 (br s, 2H), 5.39 (br s, 2H), 4.60 (q, J = 7.4 Hz, 2H), 2.52 (s, 6H), 2.41 (br s, 6H), 1.62 (br s, 6H), 1.58 (d, J = 7.4 Hz, 6H), 0.97 (s, 6H). ^{13}C NMR (126 MHz, CDCl_3) δ 161.00, 148.78, 141.11, 138.97, 136.22 (br), 134.46, 133.56, 132.70, 130.25, 129.80, 129.48, 128.78 (br), 127.85, 127.28, 126.57, 122.40, 117.77, 36.74, 21.84, 21.65 (br), 19.80, 16.80.

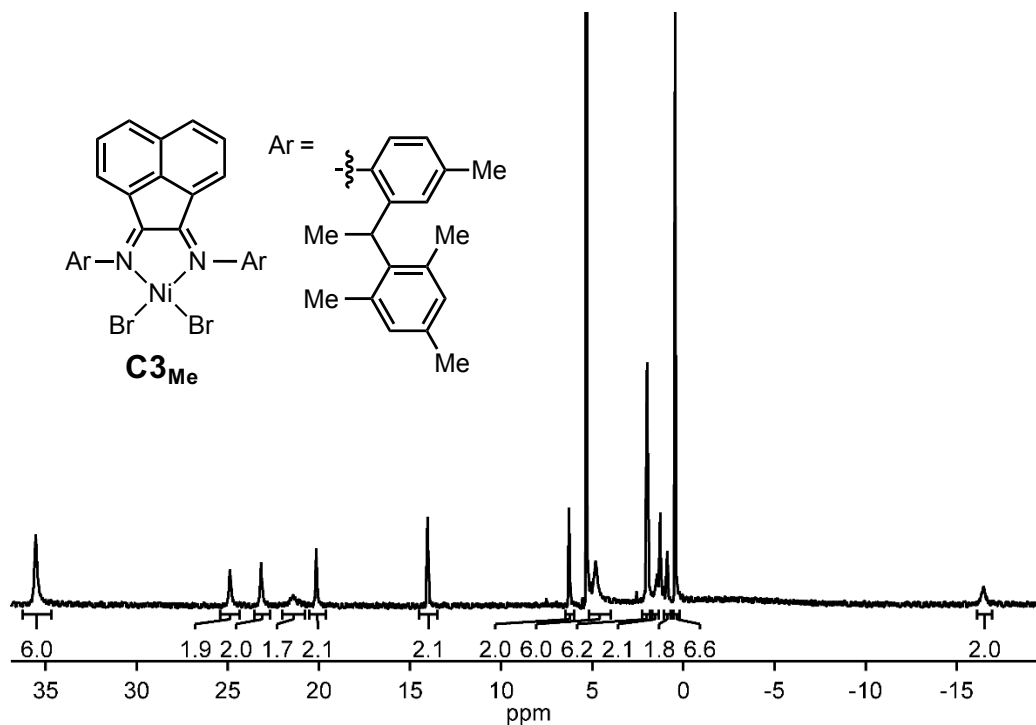


Figure A2-7. ^1H NMR Spectrum of C3_{Me} . ^1H NMR (500 MHz CD_2Cl_2) δ 35.53 (s, 6H), 24.88 (s, 2H), 23.17 (s, 2H), 21.45 (br s, 2H), 20.14 (s, 2H), 14.03 (s, 2H), 6.27 (s, 2H), 4.82 (br s, 6H), 1.99 (s, 6H), 1.44 (s, 2H), 0.87 (s, 2H), 0.45 (s, 6H), -16.43 (br s, 2H). Unaccounted for hydrogens (6H) due to peak broadening. Spectrum matches literature precedent.³

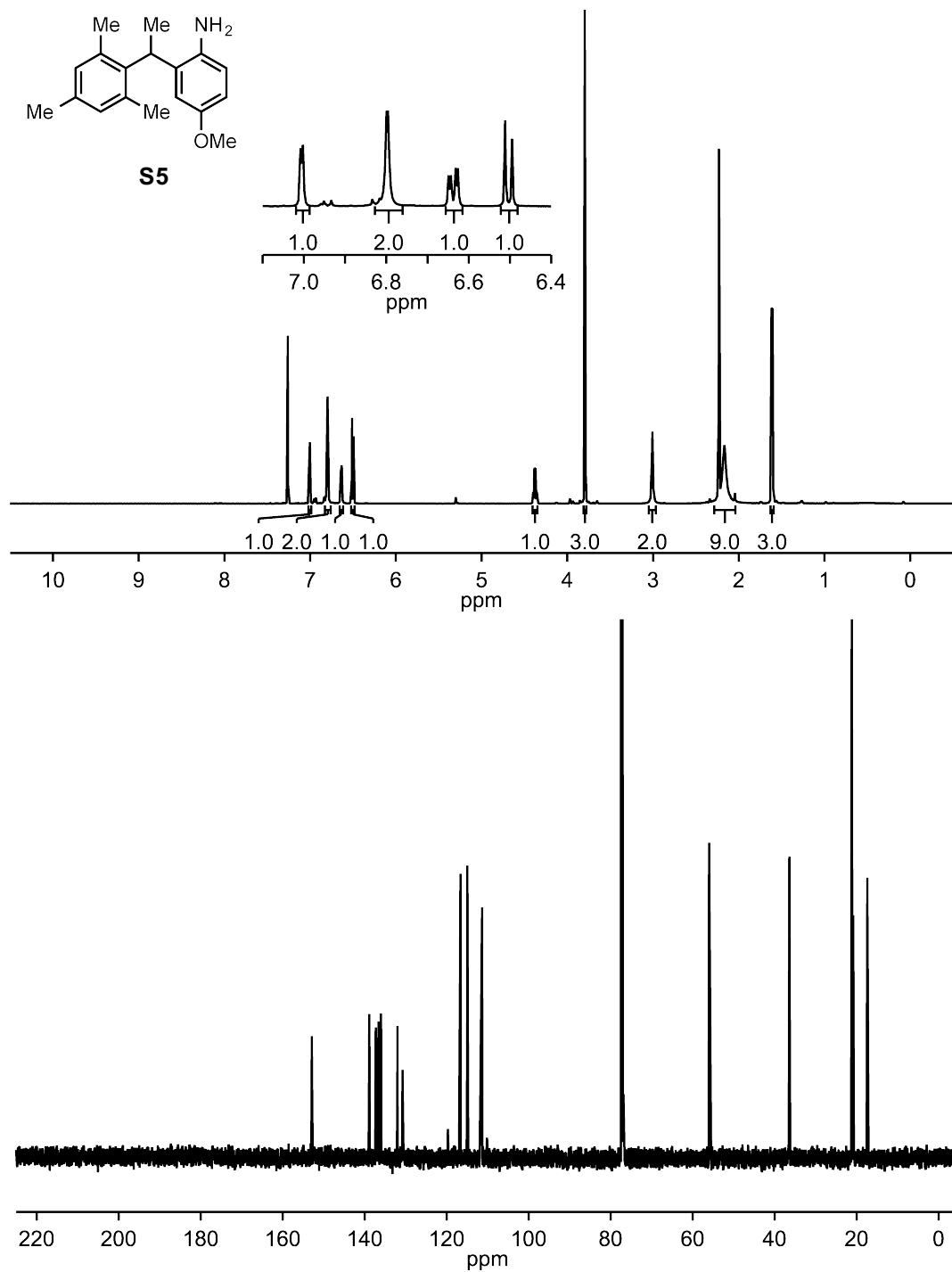


Figure A2-8. ^1H and ^{13}C NMR spectra of S5. ^1H NMR (500 MHz, CDCl_3) δ 7.02–6.98 (m, 1H), 6.80 (s, 2H), 6.64 (dd, $J = 8.5, 2.8$ Hz, 1H), 6.50 (d, $J = 8.5$ Hz, 1H), 4.38 (q, $J = 7.3$ Hz, 1H), 3.80 (s, 3H), 3.01 (s, 2H), 2.32–1.99 (m, 9H), 1.61 (d, $J = 7.3$ Hz, 3H). ^{13}C NMR (126 MHz, CDCl_3) δ 152.72, 138.69, 137.12, 136.44, 135.83, 131.81, 119.54, 116.45, 114.78, 111.18, 55.81, 36.23, 21.02, 20.66, 17.22.

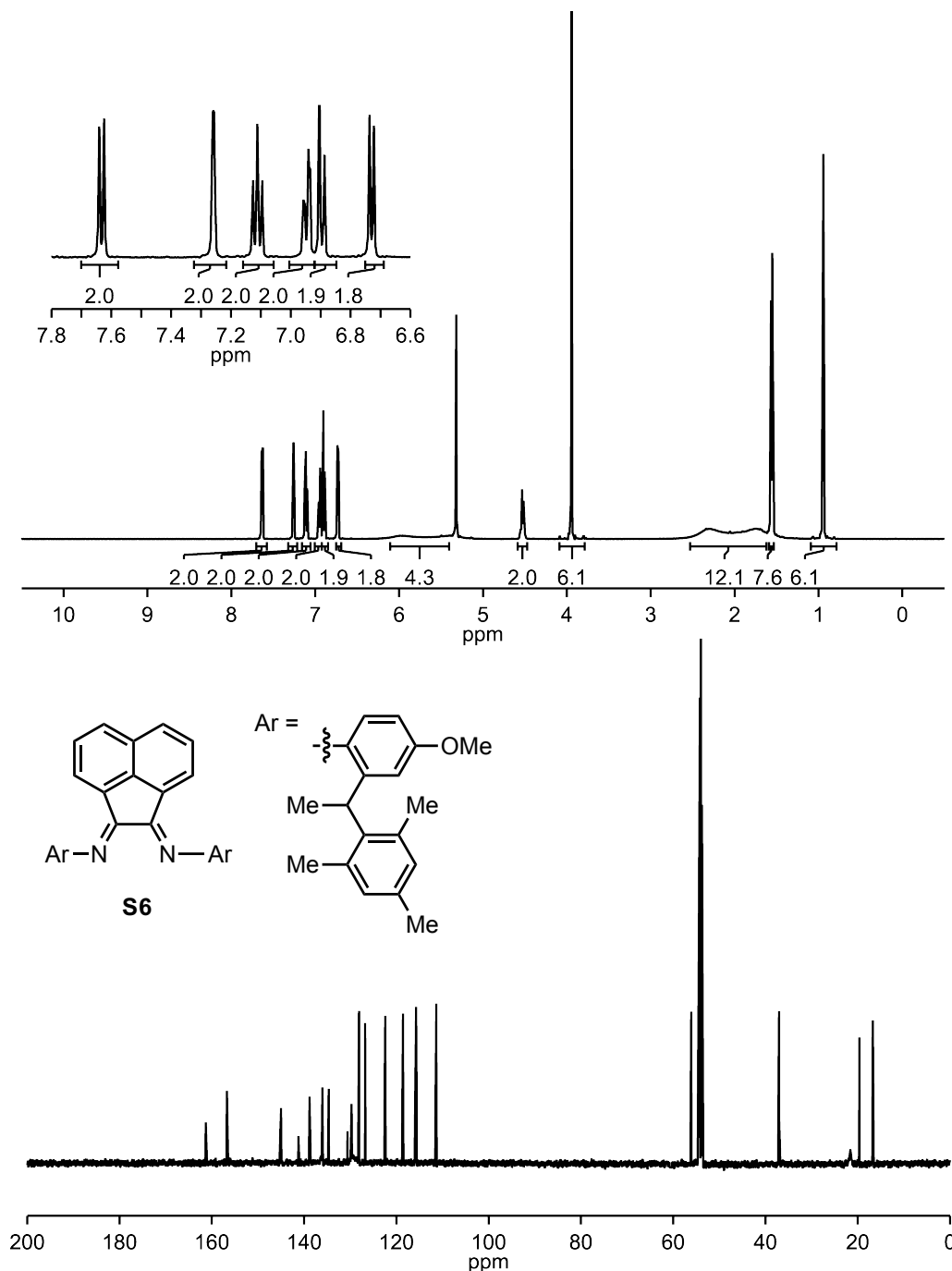


Figure A2-9. ^1H and ^{13}C NMR Spectra of S6. ^1H NMR (500 MHz, CD_2Cl_2) δ 7.63 (d, J = 8.2 Hz, 2H), 7.33–7.20 (m, 2H), 7.11 (ddd, J = 8.2, 7.2, 1.2 Hz, 2H), 6.95 (dd, J = 8.2, 2.6 Hz, 2H), 6.92–6.86 (m, 2H), 6.75–6.71 (m, 2H), 6.21–5.39 (m, 4H), 4.53 (q, J = 7.4 Hz, 2H), 3.94 (s, 6H), 2.61–1.62 (m, 12H), 1.56 (d, J = 7.7 Hz, 6H), 0.94 (s, 6H). ^{13}C NMR (126 MHz, CD_2CD_2) δ 160.71, 156.13, 144.39, 140.63, 140.63, 138.22, 135.44, 134.07, 130.00, 129.11, 127.49, 127.49, 126.17, 121.82, 117.97, 115.12, 110.75, 55.50, 36.47, 21.02, 19.07, 16.14.

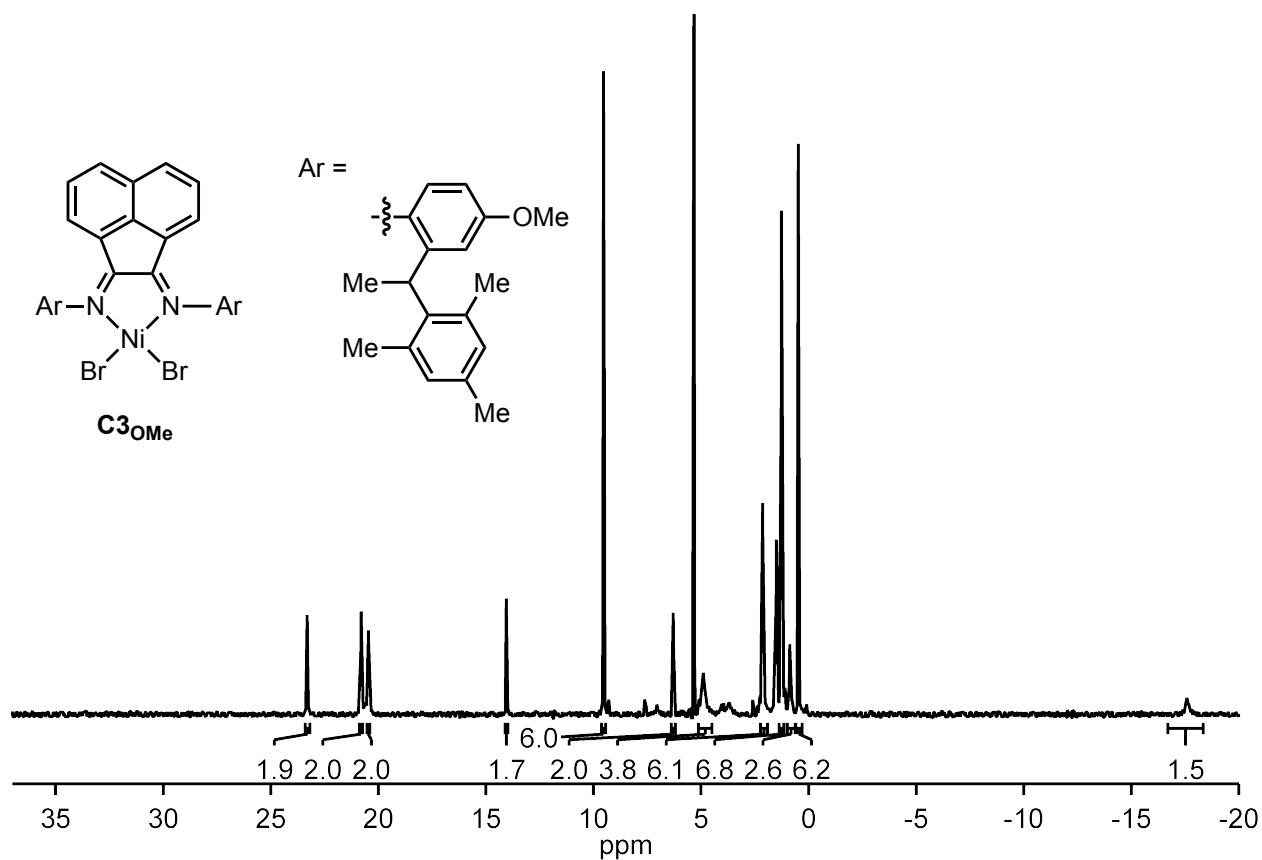


Figure A2-10. ¹H NMR Spectrum of C3_{OMe}. ¹H NMR (400 MHz, CD₂Cl₂, rd = 0.005 s, at = 0.05 s) δ 23.31 (s, 2H), 20.80 (s, 2H), 20.46 (s, 2H), 14.04 (d, J = 7.7 Hz, 2H), 9.53 (s, 6H), 6.29 (s, 2H), 4.89 (s, 4H), 2.14 (s, 7H), 1.27 (d, J = 4.1 Hz, 6H), 0.87 (s, 1H), 0.49 (d, J = 4.9 Hz, 6H), -17.60 (s, 2H). Unaccounted for hydrogens (6 H) due to peak broadening.

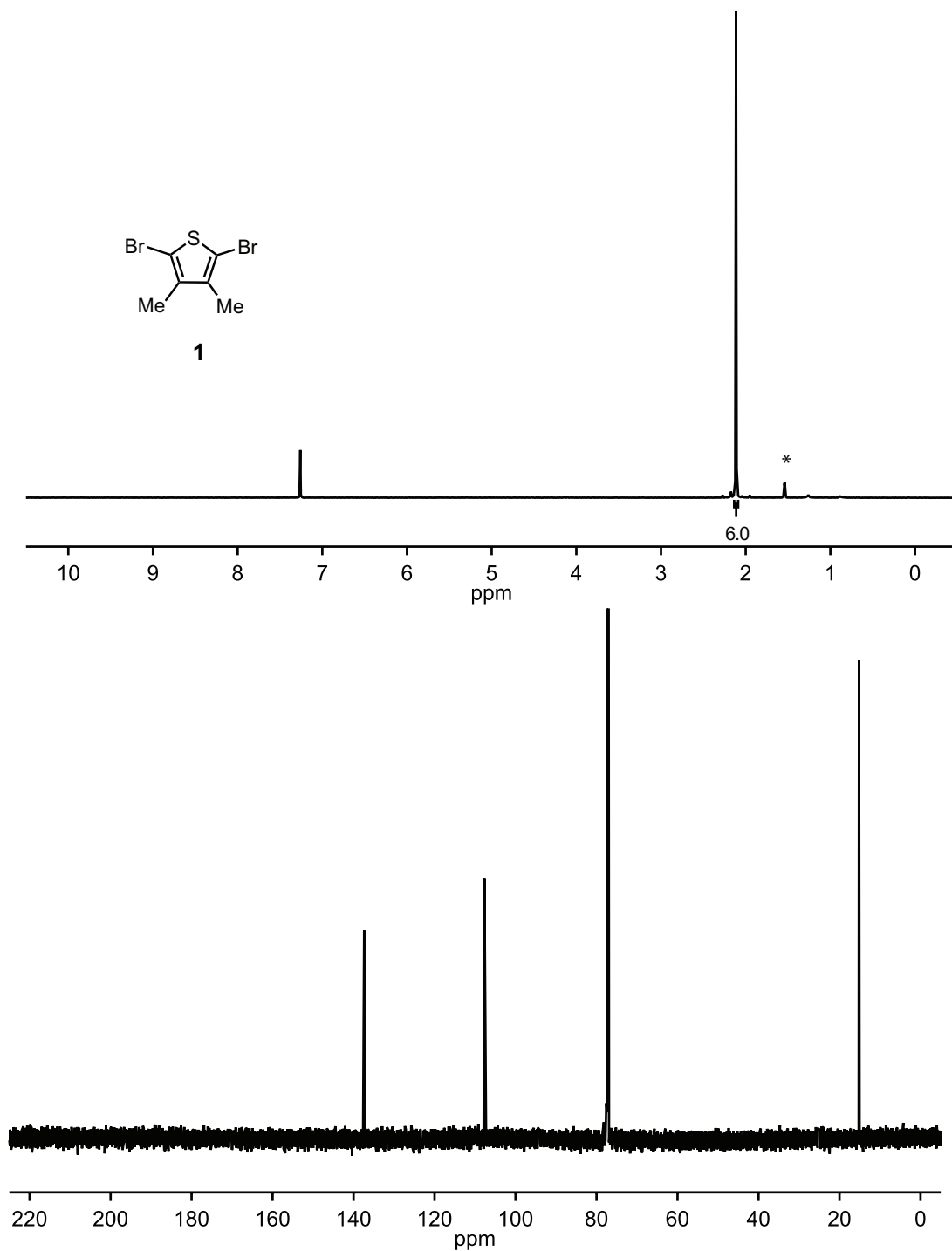


Figure A2-11. ^1H and ^{13}C NMR Spectra of **1**. ^1H NMR (400 MHz, CDCl_3) δ 2.11 (s, 6H). ^{13}C NMR (176 MHz, CDCl_3) δ 137.38, 107.68, 15.19.

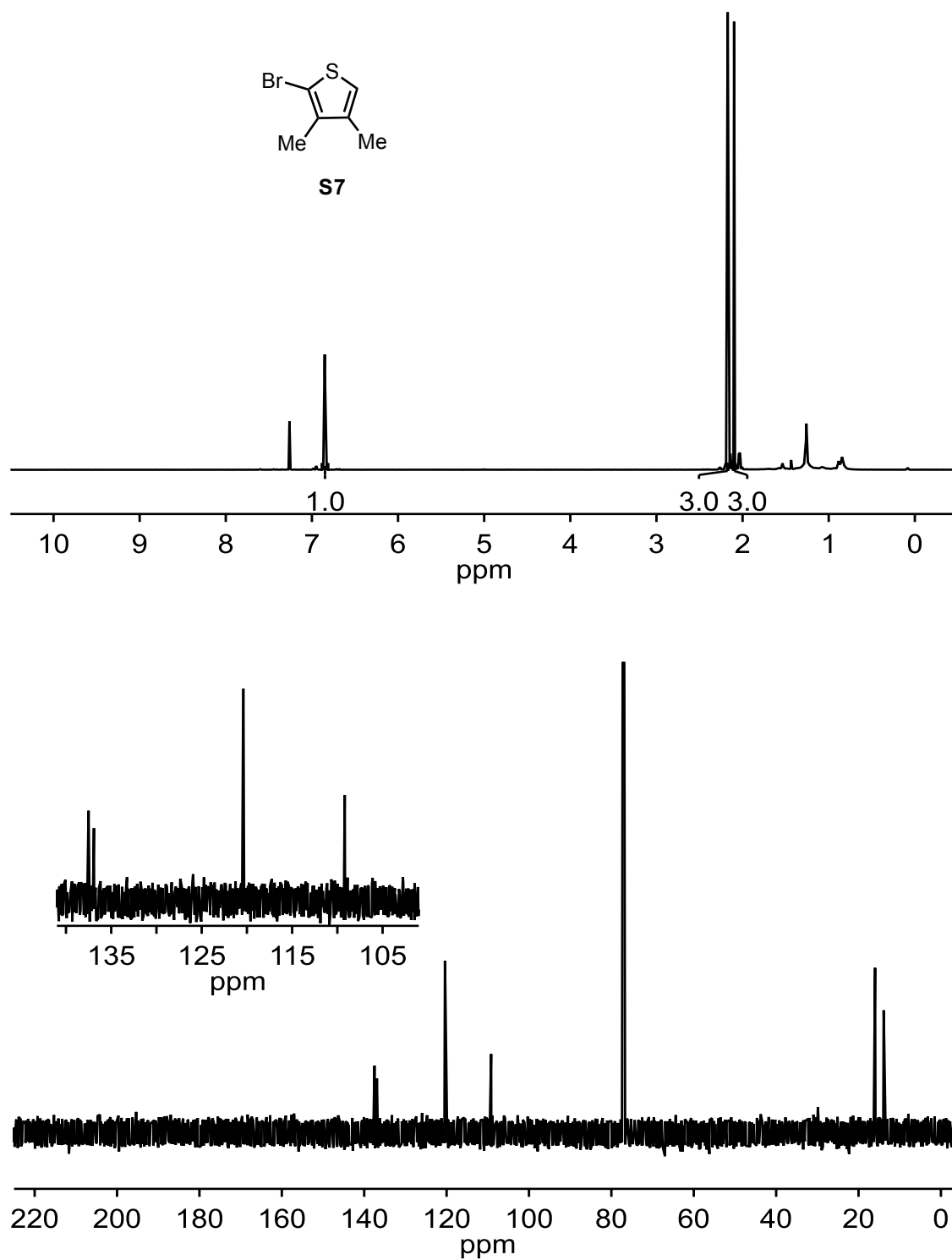


Figure A2-12. ^1H and ^{13}C NMR Spectra of S7. ^1H NMR (700 MHz, CDCl_3) δ 6.85 (s, 1H), 2.17 (s, 3H), 2.10 (s, 3H). ^{13}C NMR (176 MHz, CDCl_3) δ 137.50, 136.92, 120.39, 109.18, 15.98, 13.89.

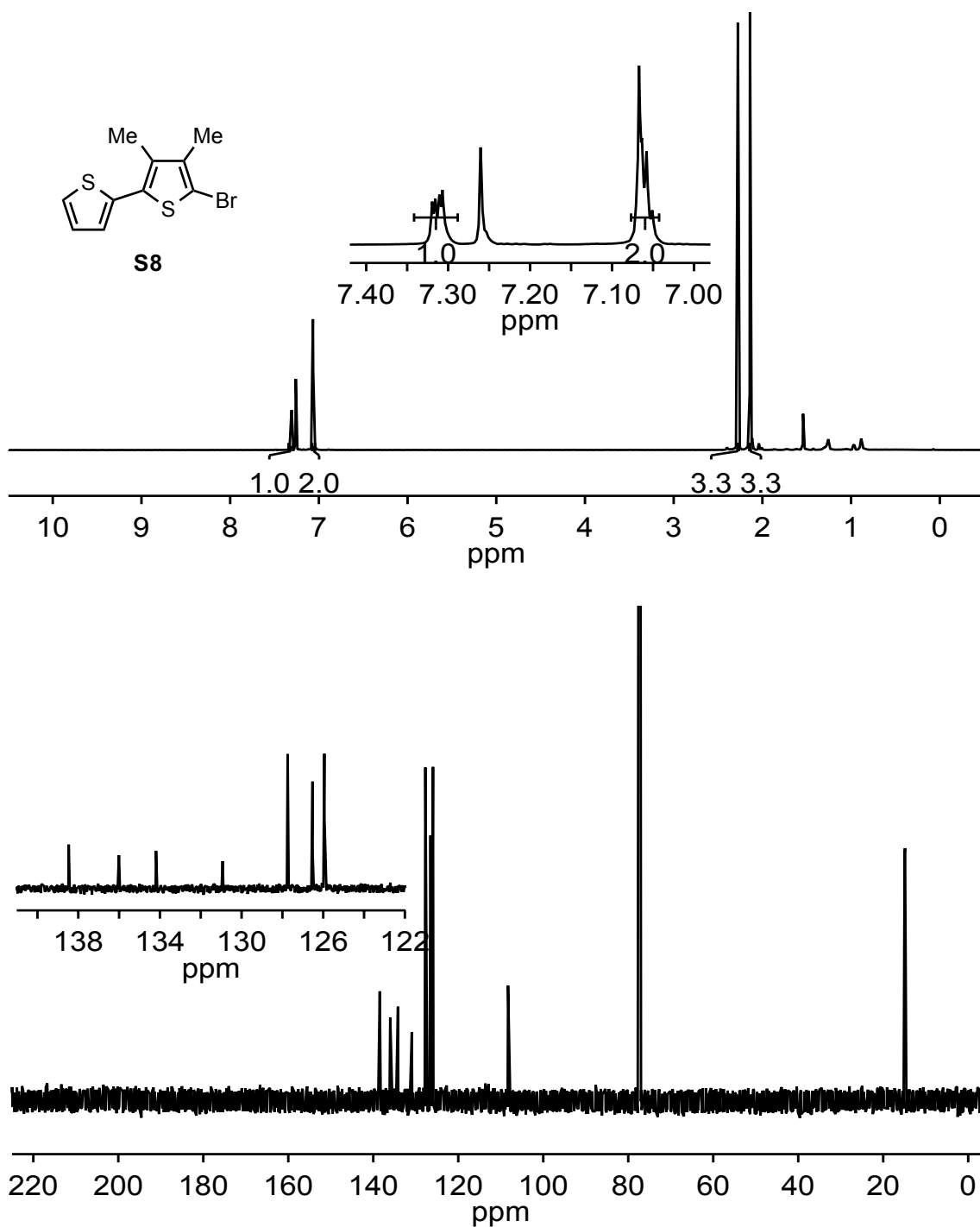


Figure A 2-13. ^1H and ^{13}C NMR Spectra of **S8**. ^1H NMR (500 MHz, CDCl_3) δ 7.31 (dd, $J = 4.4$, 1.9 Hz, 1H), 7.08–7.03 (multiple peaks, 2H), 2.28 (s, 3H), 2.14 (s, 3H). ^{13}C NMR (176 MHz, CDCl_3) δ 138.47, 136.01, 134.19, 130.93, 127.74, 126.52, 125.94, 108.28, 14.95, 14.86.

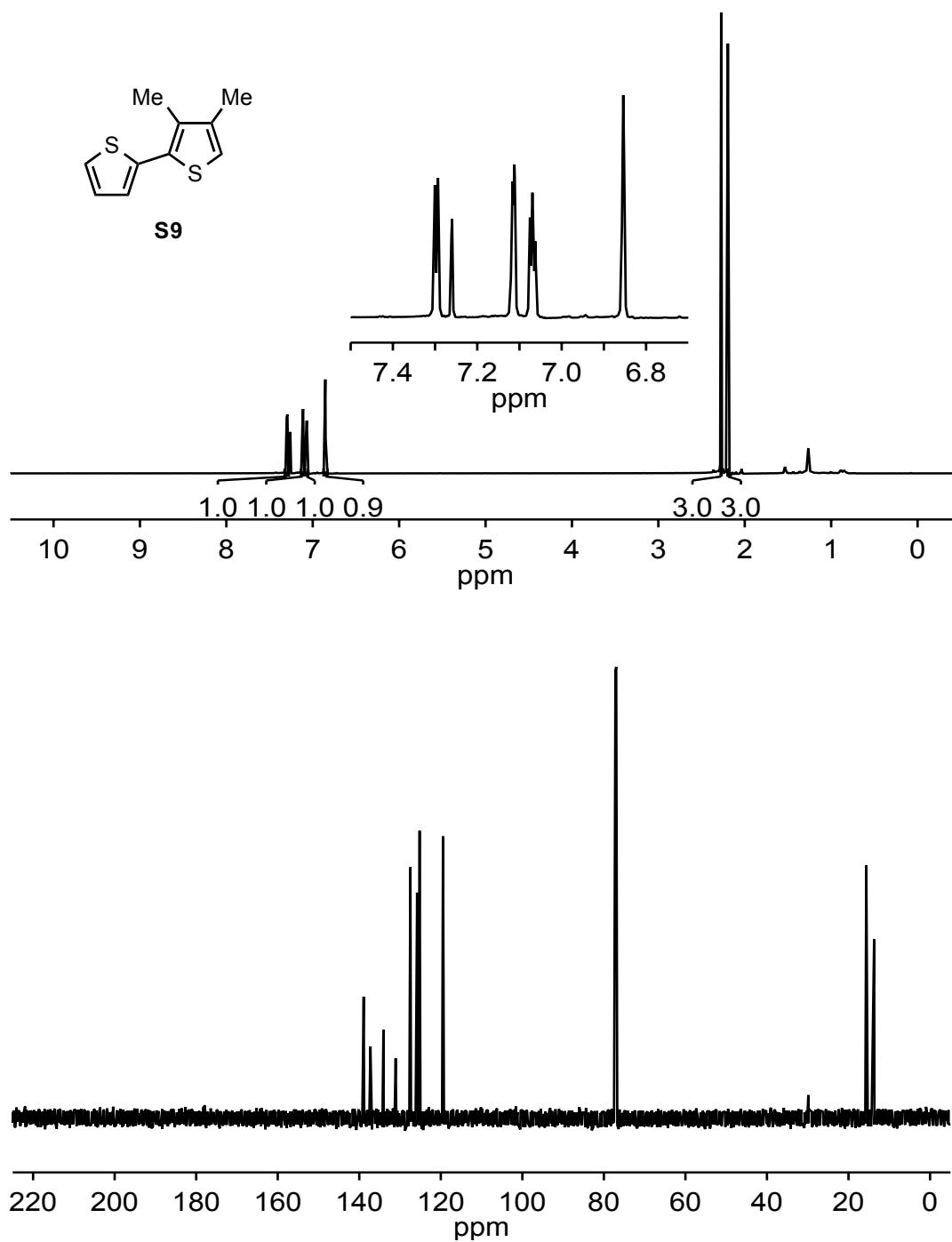


Figure A2-14. ¹H and ¹³C NMR Spectra of S9. ¹H NMR (700 MHz, CDCl₃) δ 7.30 (dd, *J* = 5.2, 1.3 Hz, 1H), 7.14–7.10 (m, 1H), 7.09–7.06 (m, 1H), 6.85 (s, 1H), 2.27 (s, 3H), 2.20 (s, 3H). ¹³C NMR (176 MHz, CDCl₃) δ 139.10, 137.44, 134.25, 131.25, 127.64, 125.99, 125.38, 119.64, 15.82, 13.90.

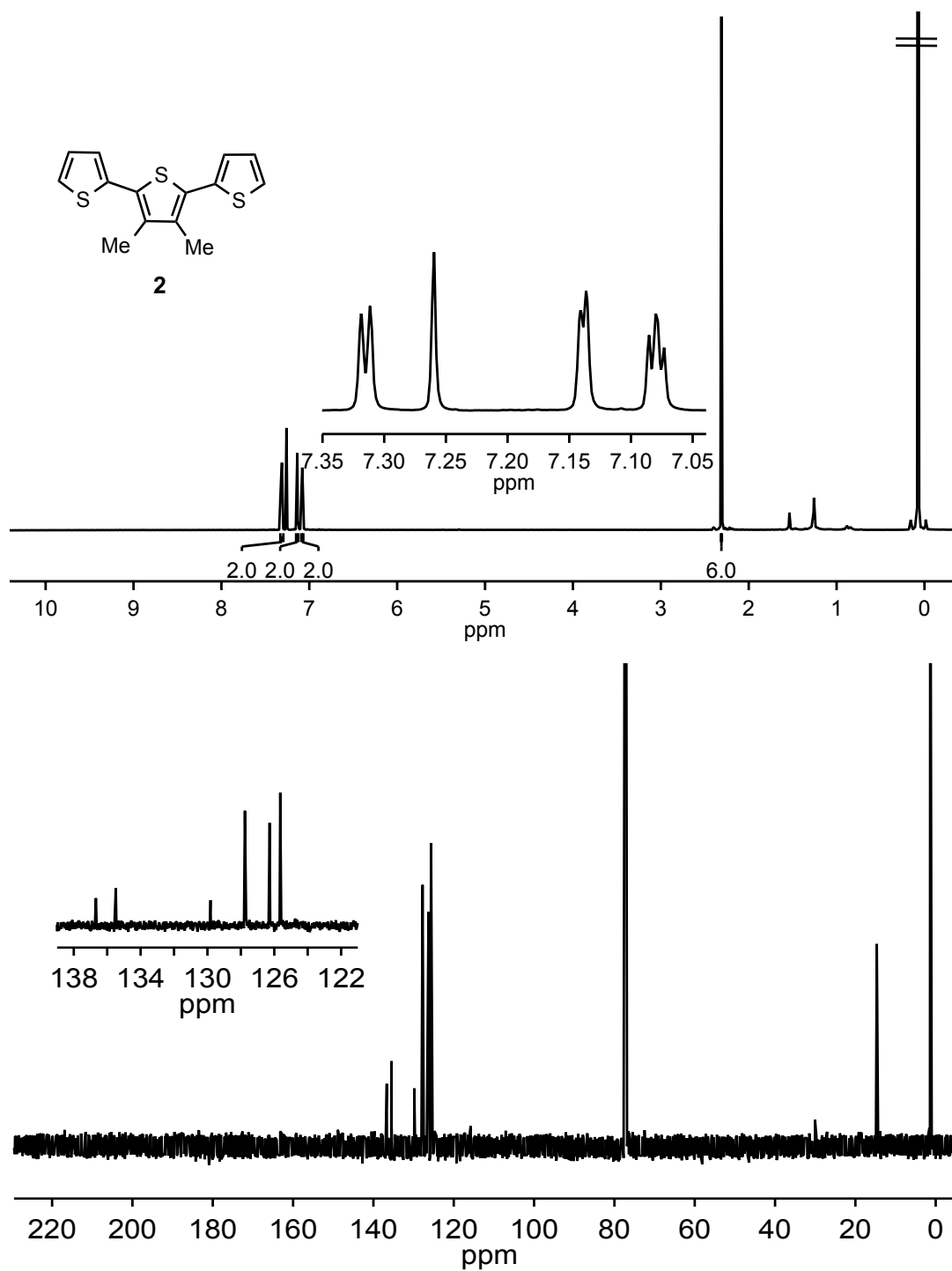


Figure A2-15. ¹H and ¹³C NMR Spectra of **2**. ¹H NMR (700 MHz, CDCl₃) δ 7.31 (d, *J* = 5.2 Hz, 2H), 7.14 (d, *J* = 3.6 Hz, 2H), 7.08 (dd, *J* = 5.2, 3.6 Hz, 2H), 2.31 (s, 6H). ¹³C NMR (176 MHz, CDCl₃) δ 136.67, 135.49, 129.82, 127.76, 126.28, 125.64, 14.66.

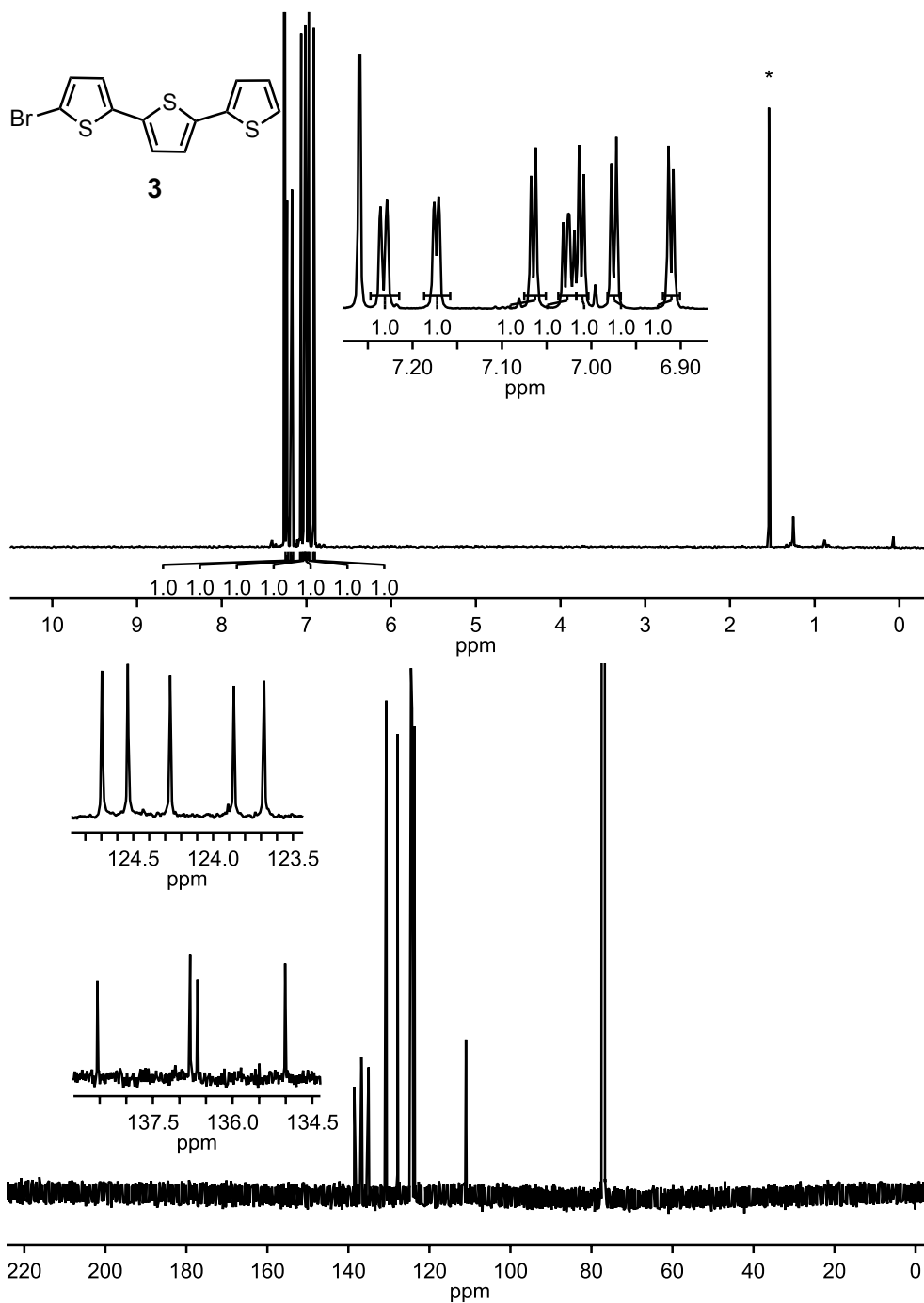


Figure A2-16. ^1H and ^{13}C NMR Spectra of 3. ^1H NMR (700 MHz, CDCl_3) δ 7.23 (d, $J = 5.1$ Hz, 1H), 7.17 (dd, $J = 3.6, 1.1$ Hz, 1H), 7.06 (d, $J = 3.8$ Hz, 1H), 7.03 (dd, $J = 5.1, 3.6$ Hz, 1H), 7.01 (d, $J = 3.8$ Hz, 1H), 6.97 (d, $J = 3.8$ Hz, 1H), 6.91 (d, $J = 3.8$ Hz, 1H). ^{13}C NMR (176 MHz, CDCl_3) δ 138.54, 136.80, 136.66, 135.01, 130.64, 127.89, 124.70, 124.53, 124.27, 123.87, 123.68, 110.99.

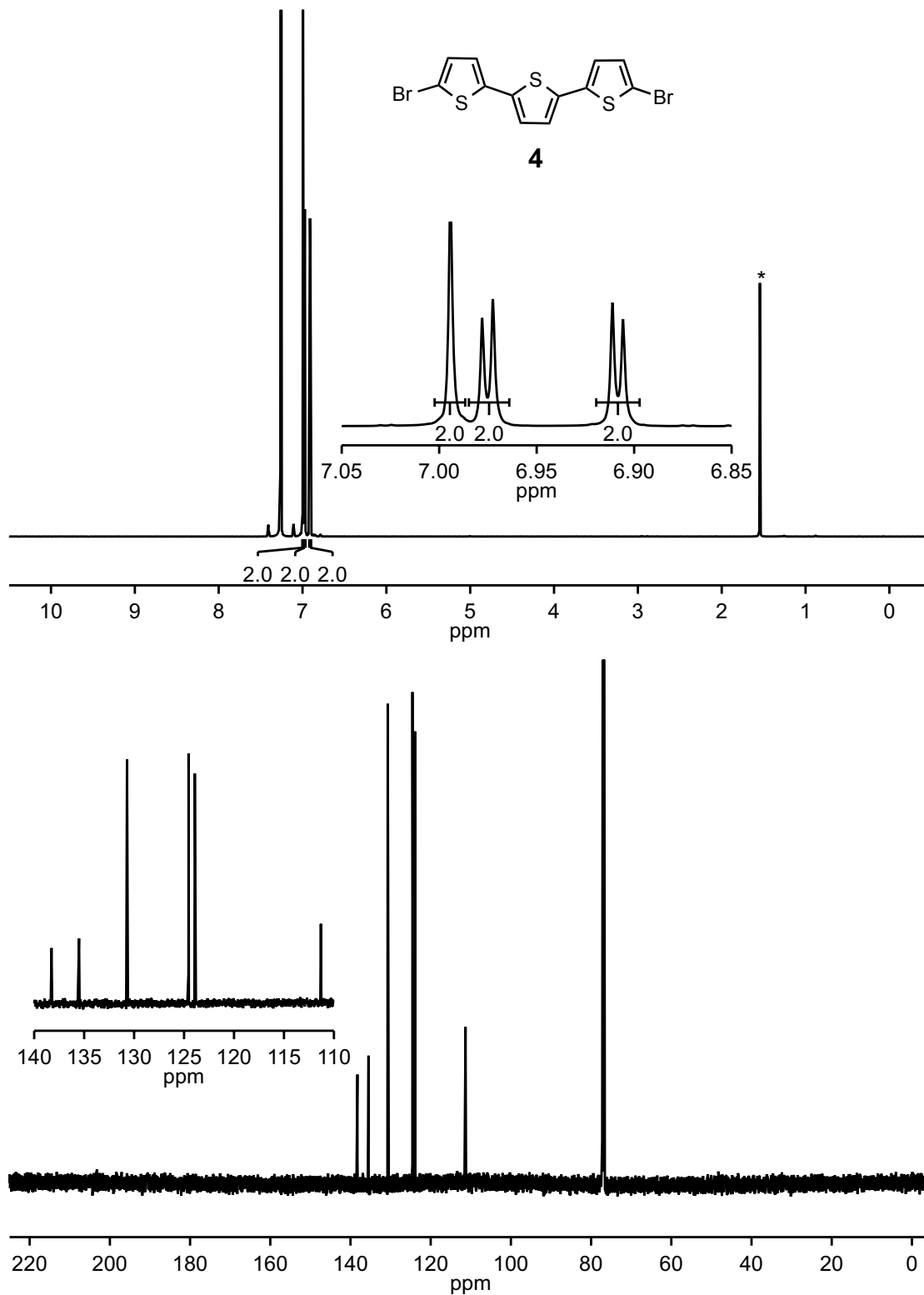
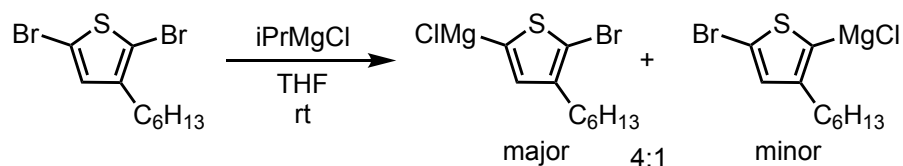


Figure A2-17. ¹H and ¹³C NMR Spectra of **4**. ¹H NMR (700 MHz, CDCl₃) δ 6.99 (s, 2H), 6.98 (d, *J* = 3.8 Hz, 2H), 6.91 (d, *J* = 3.8 Hz, 2H). ¹³C NMR (176 MHz, CDCl₃) δ 138.24, 135.49, 130.69, 124.53, 123.90, 111.29.

A2.5. Polymerizations at rt

General procedure for monomer activation:

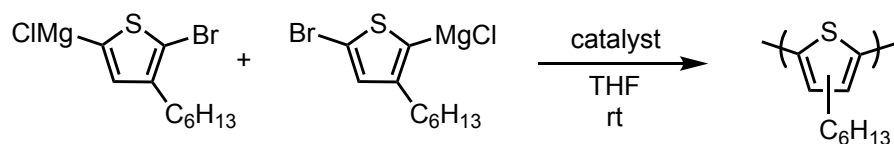


In a glovebox, $i\text{PrMgCl}$ (titrated 1.5–2.0 M in THF, 0.70–0.90 equiv) was added to a stirring solution of 2,5-dibromo-3-hexylthiophene (0.010 M, 1.0 equiv) and $\text{C}_{22}\text{H}_{46}$ (as an internal standard, ~2 mg) in THF and stirred for 30 min at rt. An aliquot of the resulting Grignard stock solution (~0.2 mL) is quenched with aq. HCl (12 M, ~0.5 mL) outside of the glovebox and worked up for GC as an initial time reference. The resulting GC trace reveals a ratio of regioisomers in a 4:1 ratio. Fresh monomer was prepared for each polymerization.

General procedure for rt polymerizations:

Preparing precatalyst solutions (0.005 M): In a glovebox, 4 mL vials were prepared by dissolving the respective precatalyst in THF.

catalyst (mg, mmol)	THF (mL)
C1 _{tBu} (5.5, 0.0083)	1.5
C2 (6.0, 0.0094)	1.9
C3 _{Me} (5.4, 0.0062)	1.2
C3 _{OMe} (9.0, 0.0010)	2.0
C4 _{Me} (3.0, 0.0036)	0.72
C4 _{CF₃} (2.8, 0.0030)	0.60



General procedure for rt polymerization: In a glovebox, 20 mL vials equipped with a stir bar were prepared as follows: Freshly prepared Grignard monomer solution (see monomer activation *General Experimental*) (0.075 M in THF, 0.75 mL, 0.056 mmol, 1.0 equiv), THF (2.9 mL), and precatalyst stock solution (90. μ L, 4.5×10^{-4} mmol, 0.0080 equiv). After 30 min each polymerization was quenched outside of the glovebox with aq. HCl (12 M, 2 mL), the organic layer was extracted with CHCl₃ (5 mL), dried over MgSO₄, and prepared for GC, GPC, and MALDI-TOF-MS analyses.

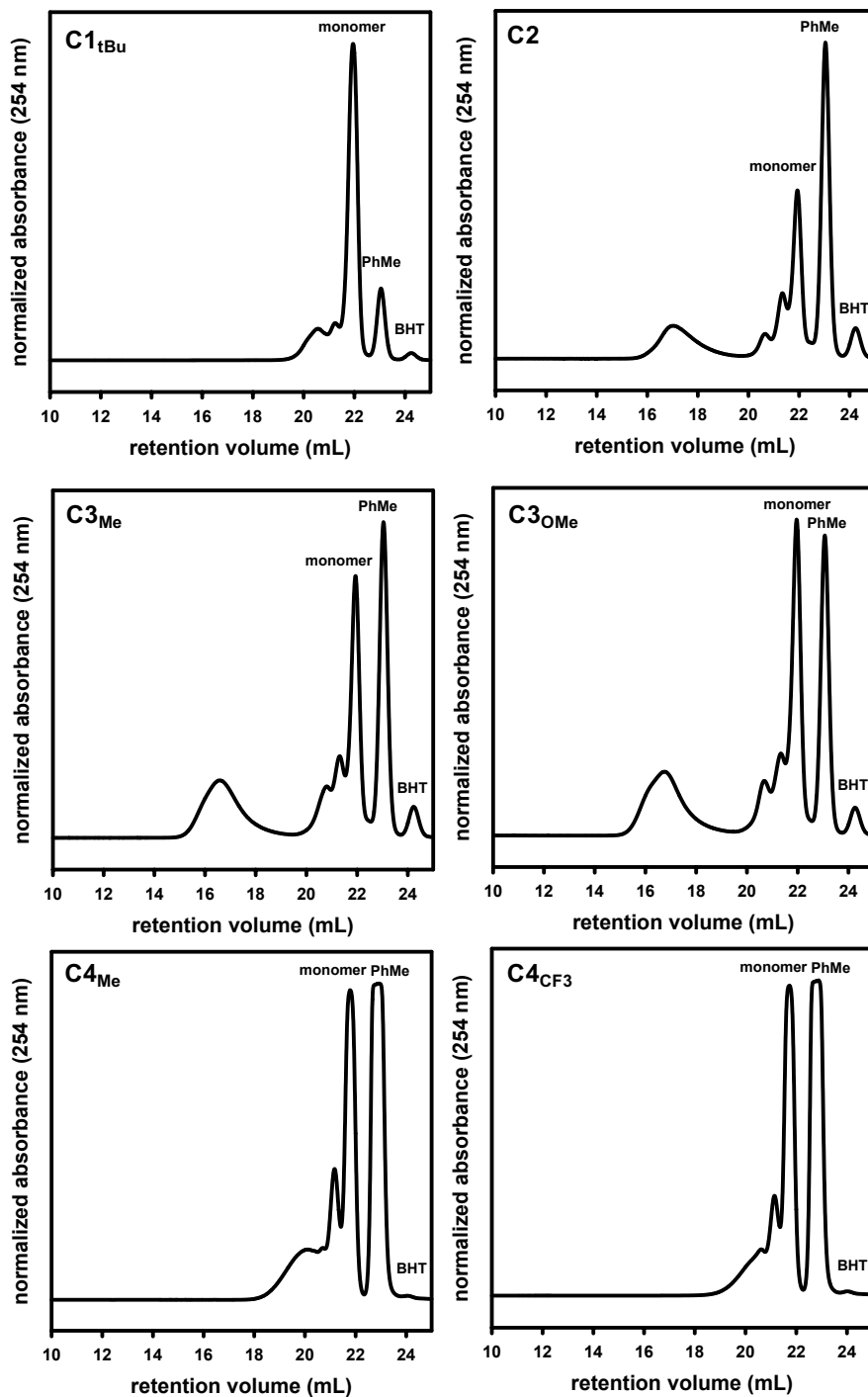


Figure A2-18. GPC traces of poly(3-hexylthiophene) (P3HT) generated at rt via (diimine)NiBr₂ precatalysts C1_{tBu}, C2, C3_{Me}, C3_{OMe}, C4_{Me}, and C4_{CF3}.

Table A2-1. GC and GPC data from the polymerization of 3-hexylthiophene at rt via (diimine)NiBr₂ precatalysts (C1_{tBu}, C2, C3_{Me}, and C3_{OMe}). Initial ratio of Grignard isomers is 4:1 (a:b).

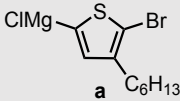
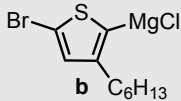
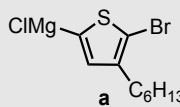
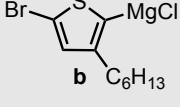
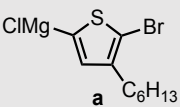
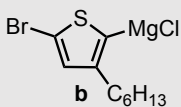
catalyst	 a C ₆ H ₁₃	 b C ₆ H ₁₃	<i>M_n</i> (kg/mol)	Đ
	(% conv.)	(% conv.)		
C1 _{tBu}	19.5	17.6	1.90	1.90
C2	93.5	15.1	14.0	1.77
C3 _{Me}	94.1	21.5	23.8	1.75
C3 _{OMe}	68.4	92.1	22.3	1.75

Table A2-2. GC and GPC data from the polymerization of 3-hexylthiophene at rt via (diimine)NiBr₂ precatalysts (C4_{Me} and C4_{CF3}). Initial ratio of Grignard isomers is 4:1 (a:b).

catalyst	 a C ₆ H ₁₃	 b C ₆ H ₁₃	 a C ₆ H ₁₃	 b C ₆ H ₁₃	<i>M_n</i> (kg/mol) (24 h)	Đ (24 h)
	(% conv., 30 min)	(% conv., 30 min)	(% conv., 24 h)	(% conv., 24 h)		
C4 _{Me}	25.9	28.5	50.6	25.7	0.26	2.78
C4 _{CF3}	5.7	9.1	16.0	17.1	0.24	2.00

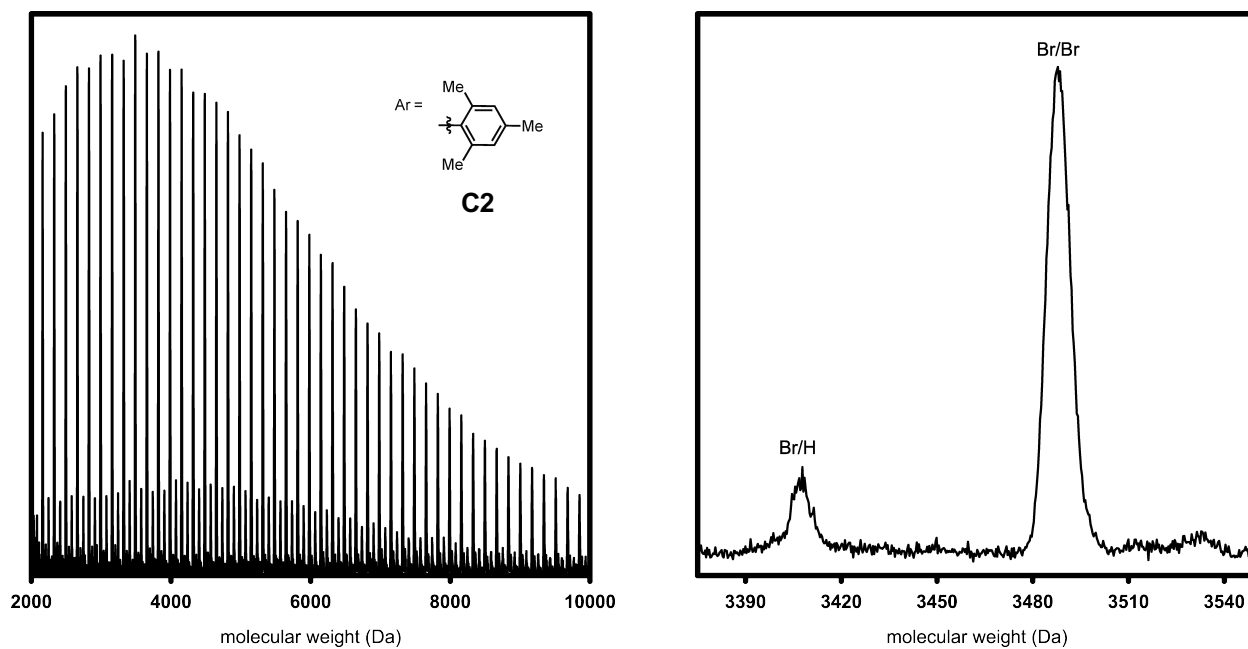


Figure A2-19. MALDI-TOF-MS spectra of P3HT via **C2** at rt, aliquot taken at 30 min.

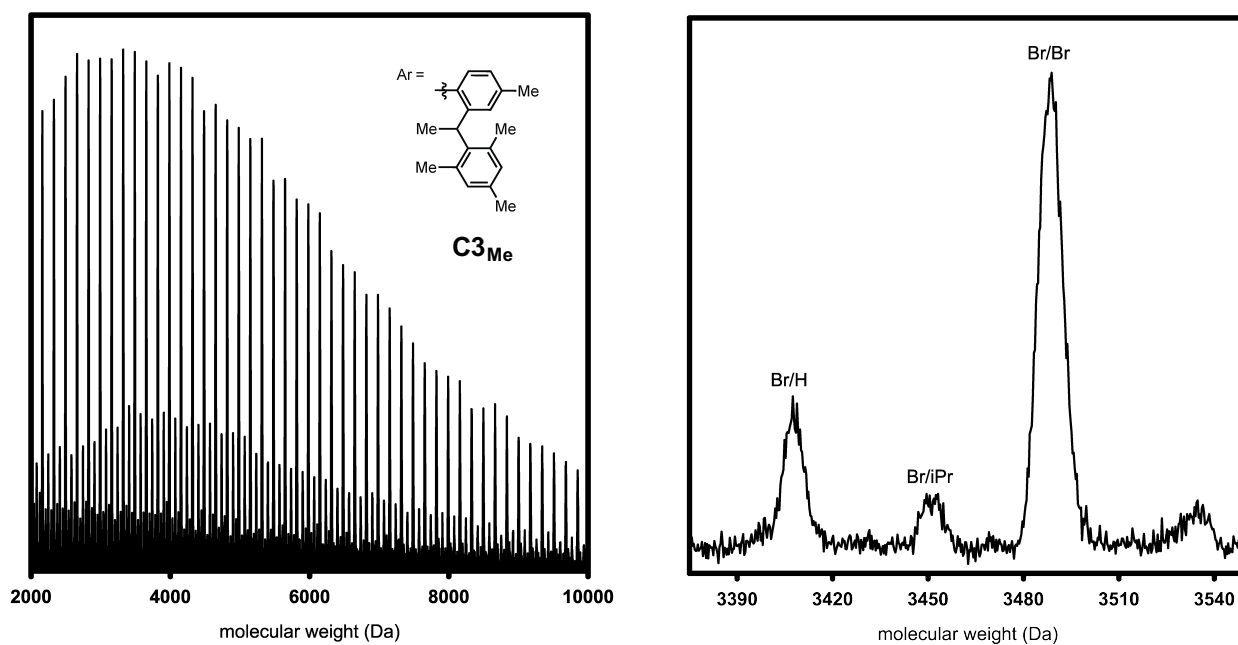


Figure A2-20. MALDI-TOF-MS spectra of P3HT via **C3_{Me}** at rt, aliquot taken at 30 min.

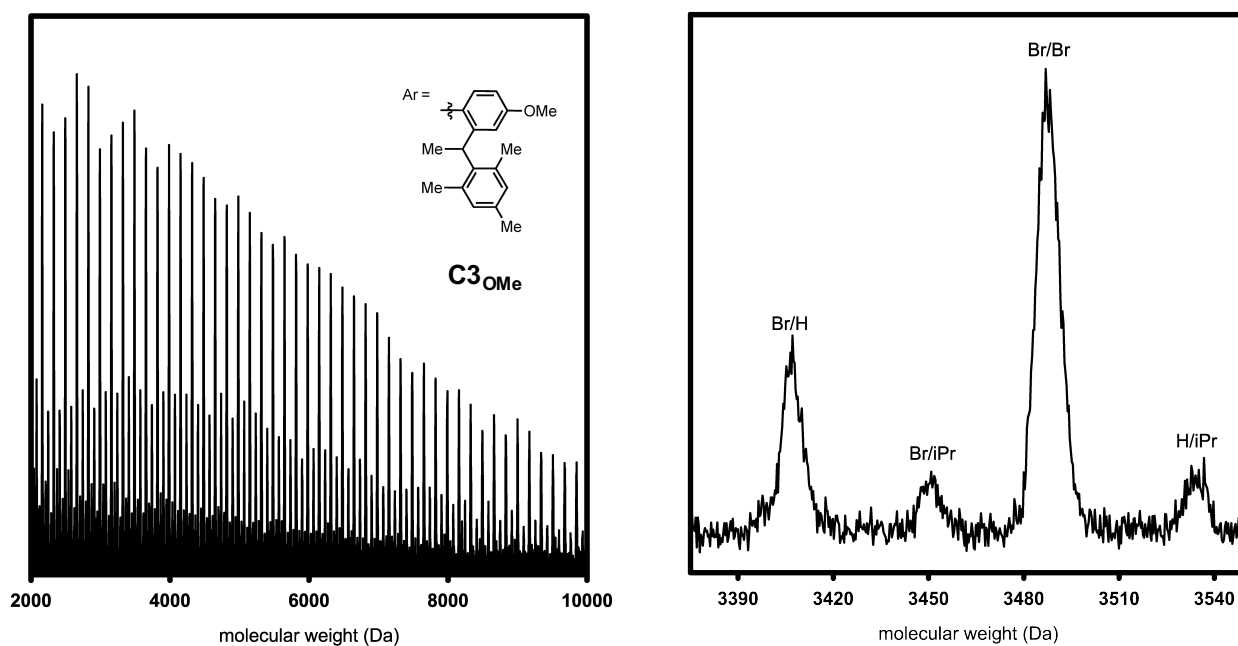
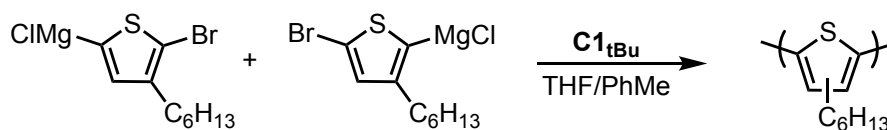


Figure A 2-21. MALDI-TOF-MS spectra of P3HT via **C3_{OMe}** at rt, aliquot taken at 30 min.

Preparing precatalyst solutions (0.005 M): In a glovebox, an 8 mL vial was prepared by dissolving the respective precatalyst in THF.

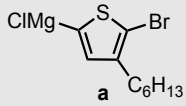
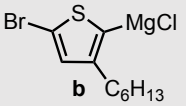
catalyst (mg, mmol)	THF (mL)
C1_{tBu} (14.4, 0.0217)	4.34



General procedure for rt polymerization: In a glovebox, 20 mL vials equipped with a stir bar were prepared as follows: Freshly prepared Grignard monomer solution (see monomer activation p.S3) (0.086 M in THF, 2.0 mL, 0.17 mmol, 1.0 equiv), PhMe (2.0 mL), and precatalyst stock

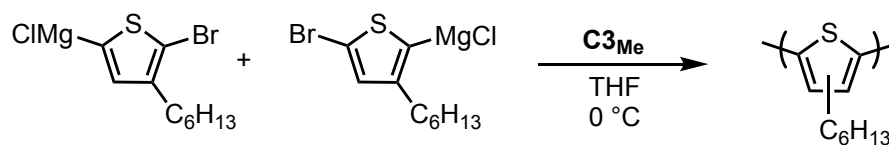
solution (55. μL , 0.00028 mmol, 0.00016 equiv). After 30 min and 20 h an aliquot (~ 0.4 mL) was quenched outside of the glovebox with aq. HCl (12 M, 2 mL), the organic layer was extracted with CHCl_3 (5 mL), dried over MgSO_4 , and prepared for GC and GPC.

Table A2-3. GC and GPC data from the polymerization of 3-hexylthiophene at rt via Cl_{tBu} . Initial ratio of Grignard isomers is 4:1 (a:b).

time	 a C_6H_{13} (% conv.)	 b C_6H_{13} (% conv.)	M_n (kg/mol)	\mathcal{D}
30 min	3.6	0.3	0.9	1.2
20 h	11.4	6.4	1.4	1.7

A2.6. M_n versus conversion at 0 °C

General procedure for M_n versus conversion at 0 °C



In a glovebox, freshly prepared Grignard monomer (0.07 M in THF, 1.2 mL, 0.084 mmol, 80. equiv) was diluted in THF (7.0 mL) in a Schlenk tube (25 mL) equipped with a stir bar. To a second Schlenk tube (25 mL) was added freshly prepared C3Me stock solution (0.005 M in THF, 6.5 mg, 0.0075 mmol in THF (1.5 mL)). The Schlenk tubes were sealed, removed from the glovebox, and immediately placed under N_2 . The Schlenk tube containing monomer was cooled to 0 ± 2 °C using an ice-water/brine bath (90:10 v/v). Subsequently, C3Me (0.210 mL, 0.00105 mmol, 1.00 equiv) was added to the stirring monomer solution via syringe. Aliquots (~0.3 mL) were removed from the polymerization via syringe and quenched by adding into a 4 mL vial containing aq. HCl (12 M, 0.5 mL), capped and shaken vigorously. The organic layer was extracted with CHCl_3 (2 x 5 mL), dried over MgSO_4 , and prepared for GC, GPC, and MALDI-TOF-MS.

Table A2-4. GC and GPC data from M_n versus conversion at 0 °C for polymerizations via precatalyst C3_{Me} (monomer/catalyst = 80/1).

Run 1 (MALDI-TOF-MS data was not acquired for this series)			Run 2			Run 3 (series acquired for MALDI-TOF-MS analysis)		
conv. (%)	M_n (kg/mol)	\bar{D}	conv. (%)	M_n (kg/mol)	\bar{D}	conv. (%)	M_n (kg/mol)	\bar{D}
39.8	3.6	1.16	19.1	3.6	1.17	26.6	4.3	1.21
43.9	5.7	1.20	45.4	5.8	1.19	32.3	6.2	1.41
53.8	7.5	1.23	54.0	7.2	1.24	92.4	16.6	1.58
63.4	8.2	1.50	55.0	8.0	1.49			
64.3	10.0	1.60	74.6	9.7	1.57			
82.3	11.5	1.67	79.9	11.6	1.61			
quant.	13.9	1.56	93.1	12.2	1.66			
			quant.	14.4	1.51			

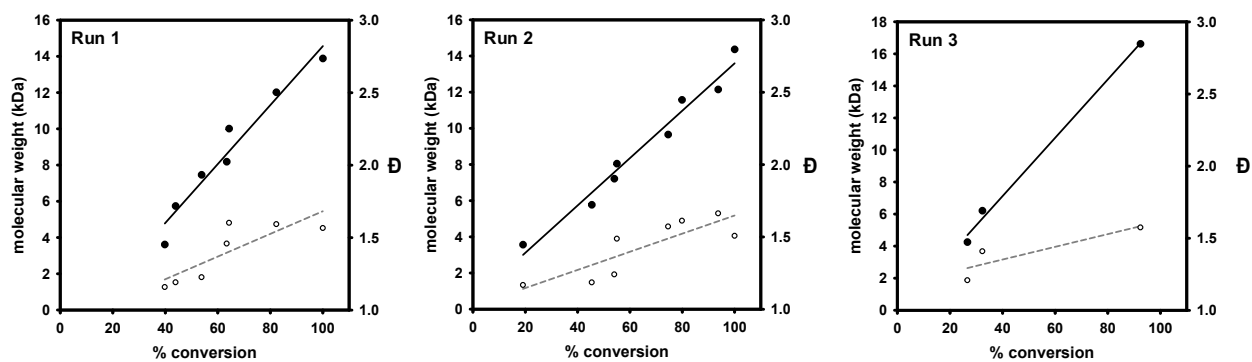


Figure A2-22. Plots of M_n versus conversion at 0 °C for polymerizations via precatalyst C3_{Me}.

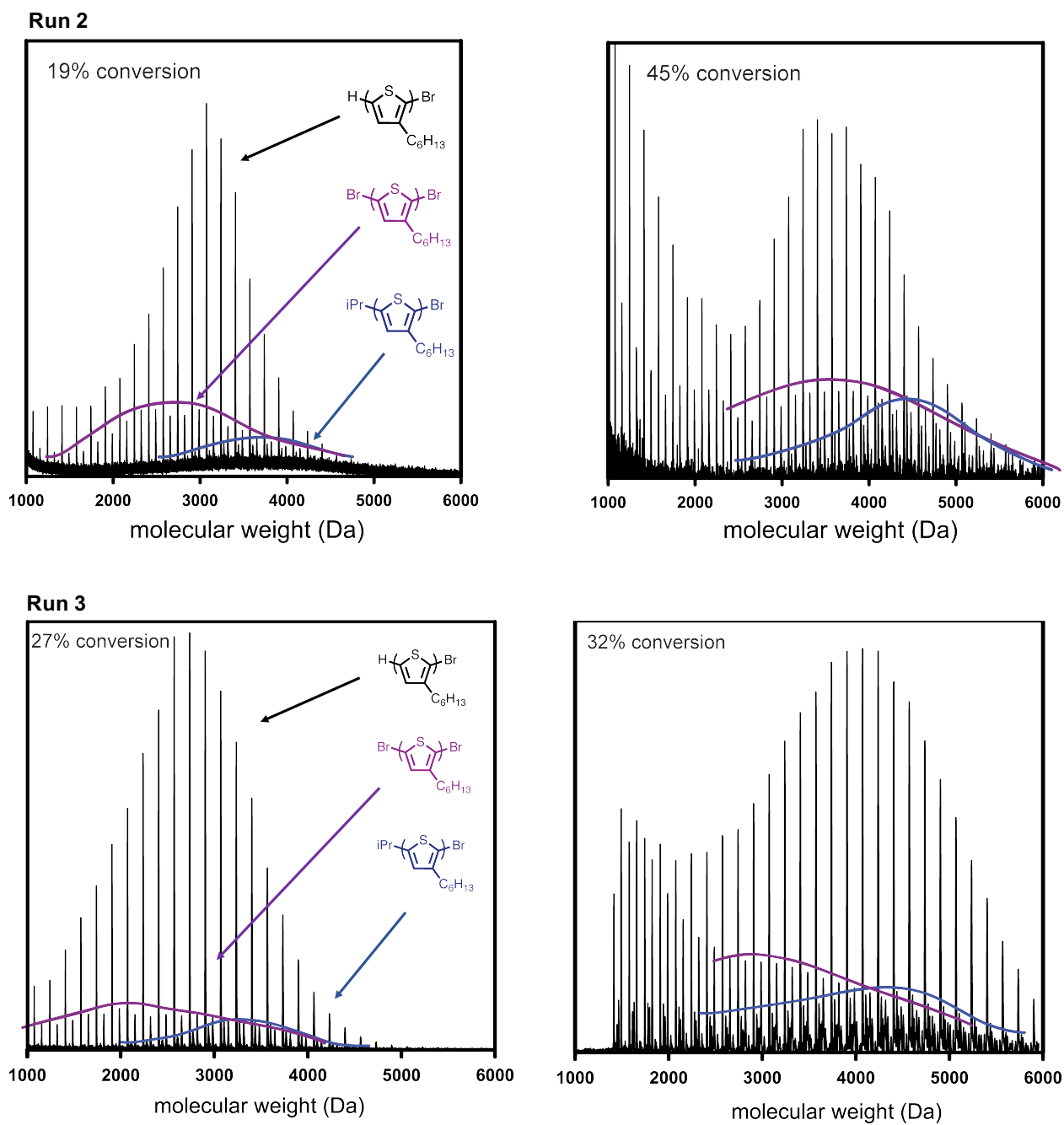


Figure A2-23. MALDI-TOF-MS data from M_n versus conversion at 0 °C for polymerizations via precatalyst C3_{Me} for the first two aliquots analyzed.

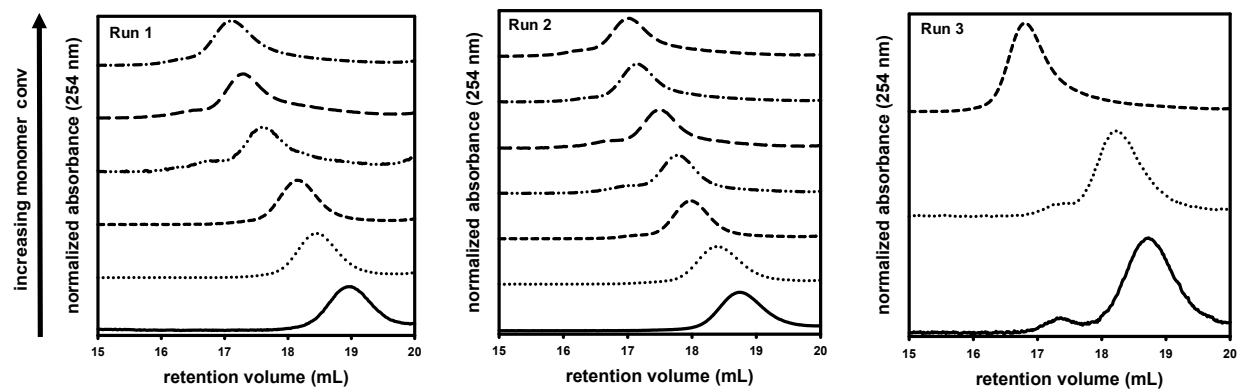
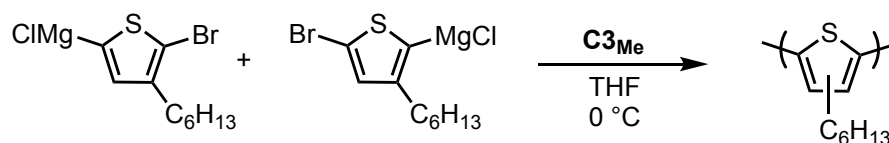


Figure A2-24. GPC traces from M_n versus conversion at 0 °C for polymerizations via precatalyst $C3_{Me}$ with increasing monomer conversion from bottom to top of plots.

A2.7. M_n versus Monomer/catalyst ratios at 0 °C

General procedure for comparing M_n versus monomer/catalyst ratios at 0 °C



In a glovebox, to 3 Schlenk tubes (25 mL) containing a stir bar were added freshly prepared Grignard monomer (0.07 M in THF, 1.0 mL, 0.070 mmol, 50–127 equiv (see below)) diluted in THF (6 mL). To a fourth Schlenk tube (25 mL) was added freshly prepared C3Me stock solution (0.005 M in THF, 10.3 mg, 0.0118 mmol dissolved in THF (2.36 mL)). The Schlenk tubes were sealed, with a septum and copper wire, removed from the glovebox, and immediately placed under N_2 . The Schlenk tubes containing monomer solution were cooled to 0 ± 2 °C using an ice-water/brine (90:10 v/v) bath. Subsequently, catalyst solution (0.005 M in THF, 0.11–0.28 mL, 0.00056–0.0014 mmol (see below), 1.00 equiv) was added to the stirring monomer solution via syringe. After 30 min, an aliquot (~1 mL) was removed from the polymerization using a pipette and quenched into a 4 mL vial containing aq. HCl (12 M, 0.5 mL), capped and shaken vigorously. The organic layer was extracted with CHCl_3 (2 x 5 mL), dried over MgSO_4 , and prepared for GC and GPC analyses.

Table A2-5. Monomer/catalyst details, GC, and GPC data from 0 °C polymerizations via precatalyst C3_{Me}.

monomer equiv	catalyst added (mL, mmol)	Run 1			Run 2		
		monomer conv. (%)	M_n (kg/mol)	\bar{D}	monomer conv. (%)	M_n (kg/mol)	\bar{D}
127	0.11, 0.00056	quant.	20.6	1.47	quant.	19.3	1.60
82	0.17, 0.00085	quant.	15.6	1.42	93.4	15.9	1.43
50	0.28, 0.0014	88.0	13.8	1.58	79.4	13.2	1.39

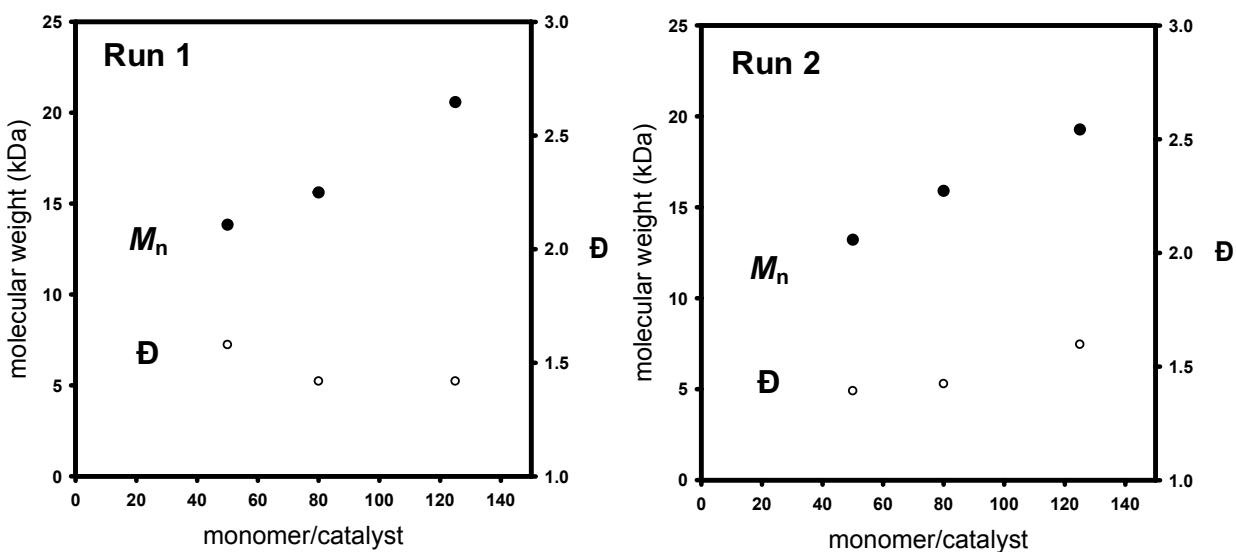
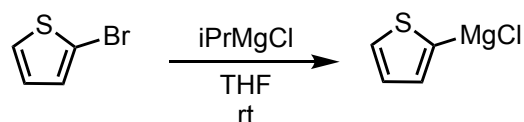


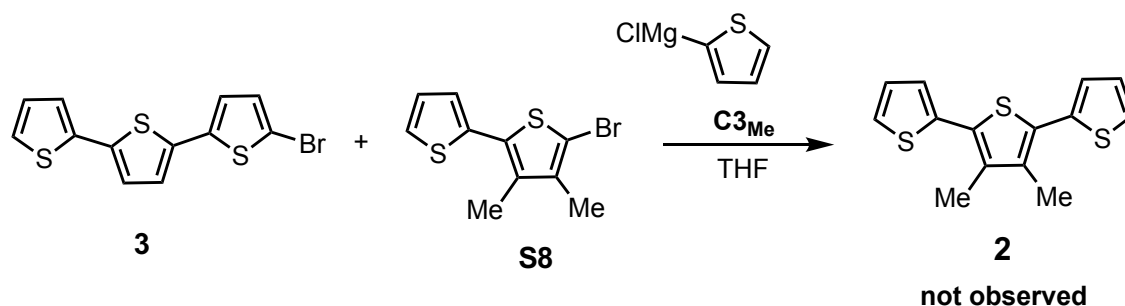
Figure A2-25. Plots of M_n versus monomer/catalyst ratio from 0 °C polymerizations via precatalyst C3_{Me} ($M_n = \bullet$, $\bar{D} = \circ$).

A2.8. Intramolecular competition experiment

General procedure for **3** versus **S8** reactivity control with stoichiometric **C3_{Me}**



Preparing thiophene-2-ylmagnesium chloride: In a glovebox, a solution of 2-bromothiophene (51.3 mg, 0.315 mmol, 1.00 equiv), THF (3.01 mL), and iPrMgCl (1.85 M in THF, 136 μ L, 0.252 mmol, 0.800 equiv) was stirred in a 20 mL vial for 30 min at rt.



Competition experiment: In a glovebox, to a 4 mL vial equipped with stir bar was added **3** (commercial source, 5.0 mg, 0.015 mmol, 5.0 equiv), **S8** (0.01 M in THF, 0.31 mL, 0.0031 mmol, 1.0 equiv), internal standard C₂₂H₄₆ (0.10 M in THF, 0.010 mL), and THF (0.2 mL). An aliquot (~0.1 mL) was removed for an initial time point. Subsequently, **C3_{Me}** (0.01 M in THF, 0.31 mL, 0.0031 mmol, 1.0 equiv) and freshly prepared thiophene-2-ylmagnesium chloride (0.08 M in THF, 107 μ L, 0.00857 mmol, 2.80 equiv) were added to the reaction vial and stirred for 10 min before quenching outside of the glovebox with aq. 12 M HCl (1 mL). The organic layer was extracted with CHCl₃ (3 x 1 mL), dried over MgSO₄, and filtered through glass wool for GC analysis. Samples were concentrated and redissolved in CDCl₃ for NMR spectroscopic analysis. Based on these GC and ¹H NMR spectroscopic data, **2** was not observed (Figure S26 & Figure S27).

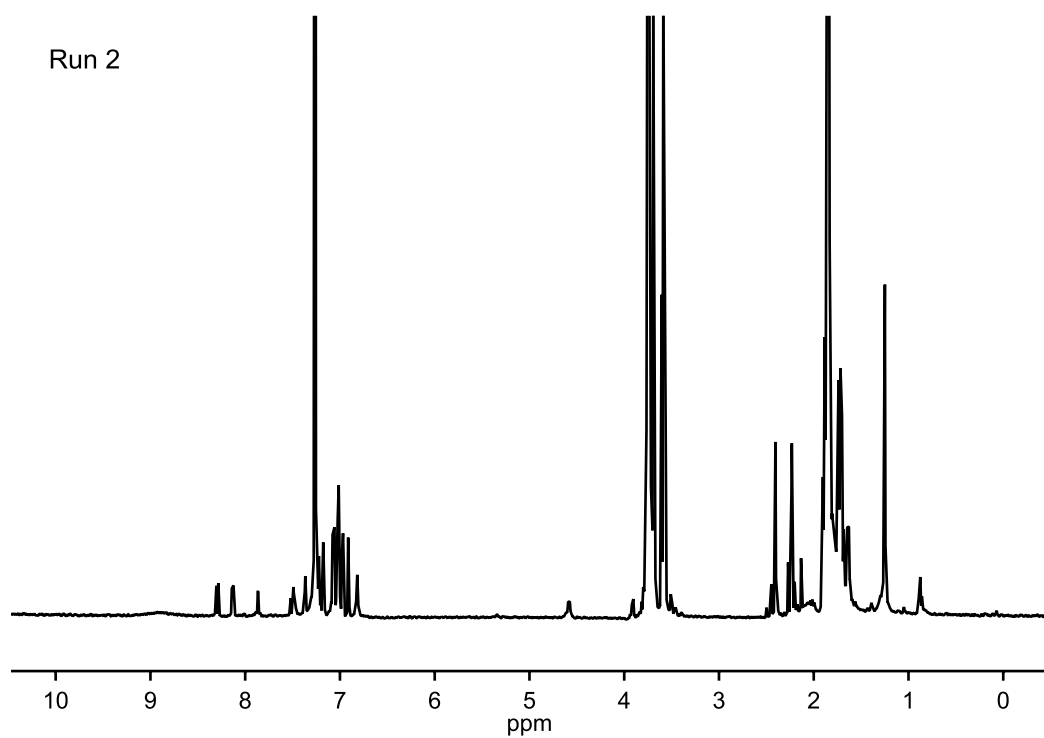
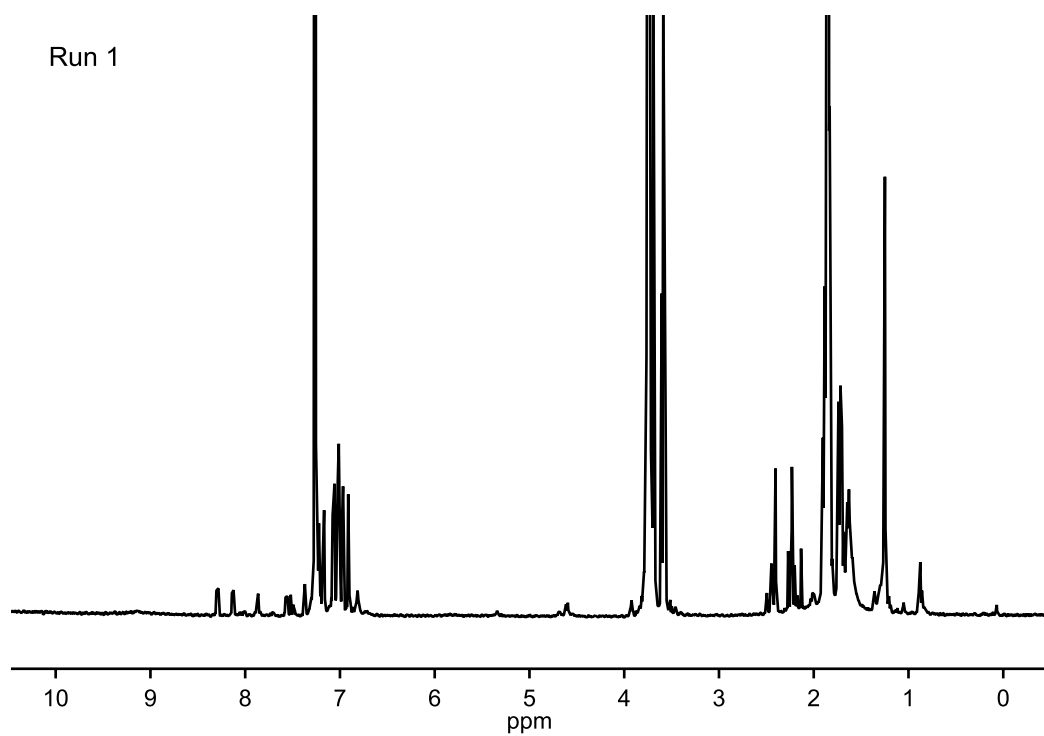


Figure A2-26. Full ^1H NMR spectra from the reaction of **3**, **S8**, and thiophene-2-ylmagnesium chloride with precatalyst C3Me_6 showing no formation of compound **2**.

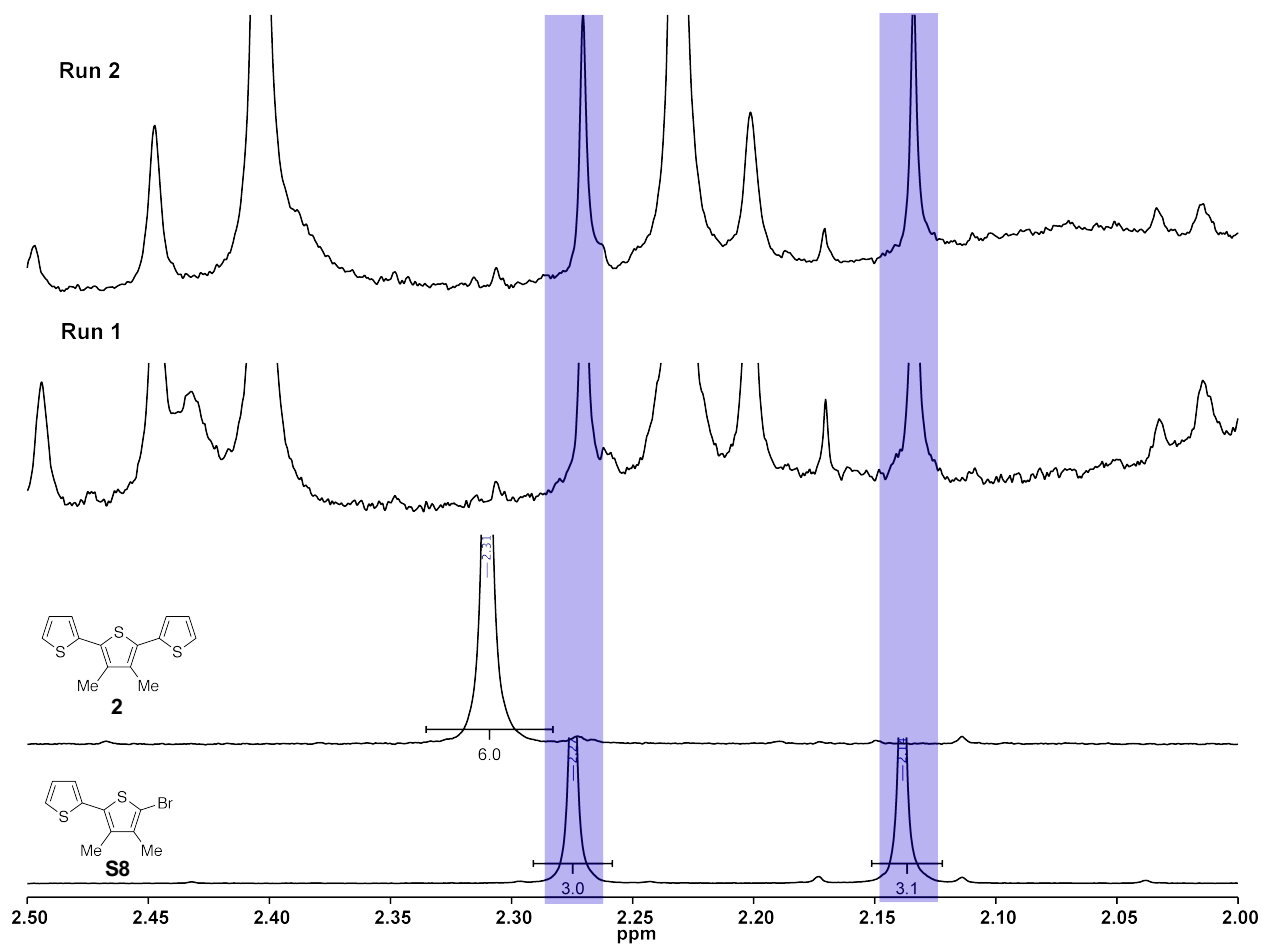
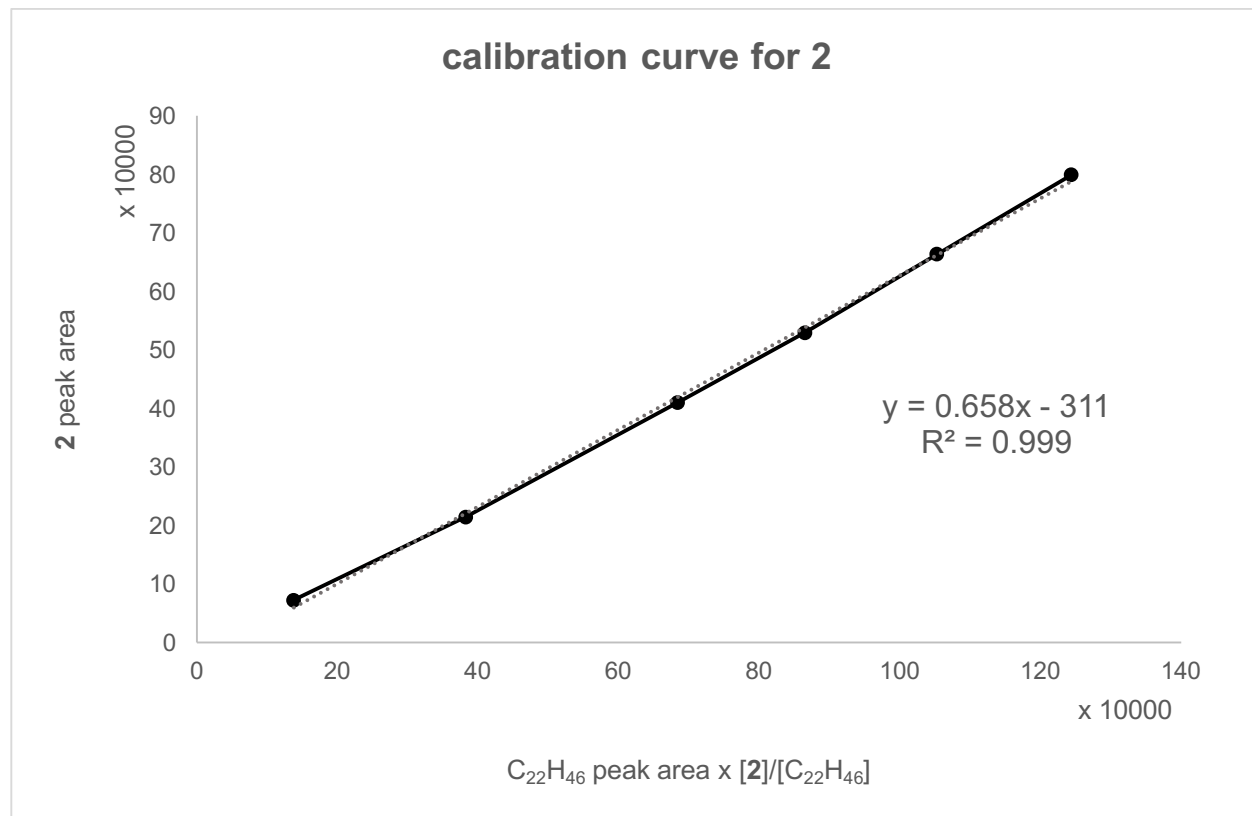


Figure A2-27. Zoomed-in regions of the ¹H NMR spectra (see Figure A2-26) from the reaction of **3**, **S8**, and thiophene-2-ylmagnesium chloride with precatalyst **C3_{Me}** showing no formation of compound **2**.

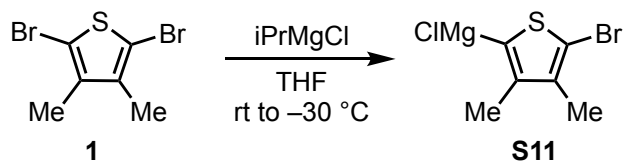
Calibration curve for trimer 2

Chart A2-1. Calibration curve of 2 relative to C₂₂H₄₆ using GC analysis.



General Procedure: Inter- versus intramolecular pathway competition experiments

Preparing reactant solutions:



Preparing S11. In a glovebox, a solution of **1** (26.4 mg, 0.0986 mmol, 1.00 equiv) and iPrMgCl (1.78 M in THF, 49.8 μL , 0.0890 mmol, 0.900 equiv) in THF (0.93 mL) was stirred for 30 min at rt and then cooled to $-30\text{ }^\circ\text{C}$ for 10 min.

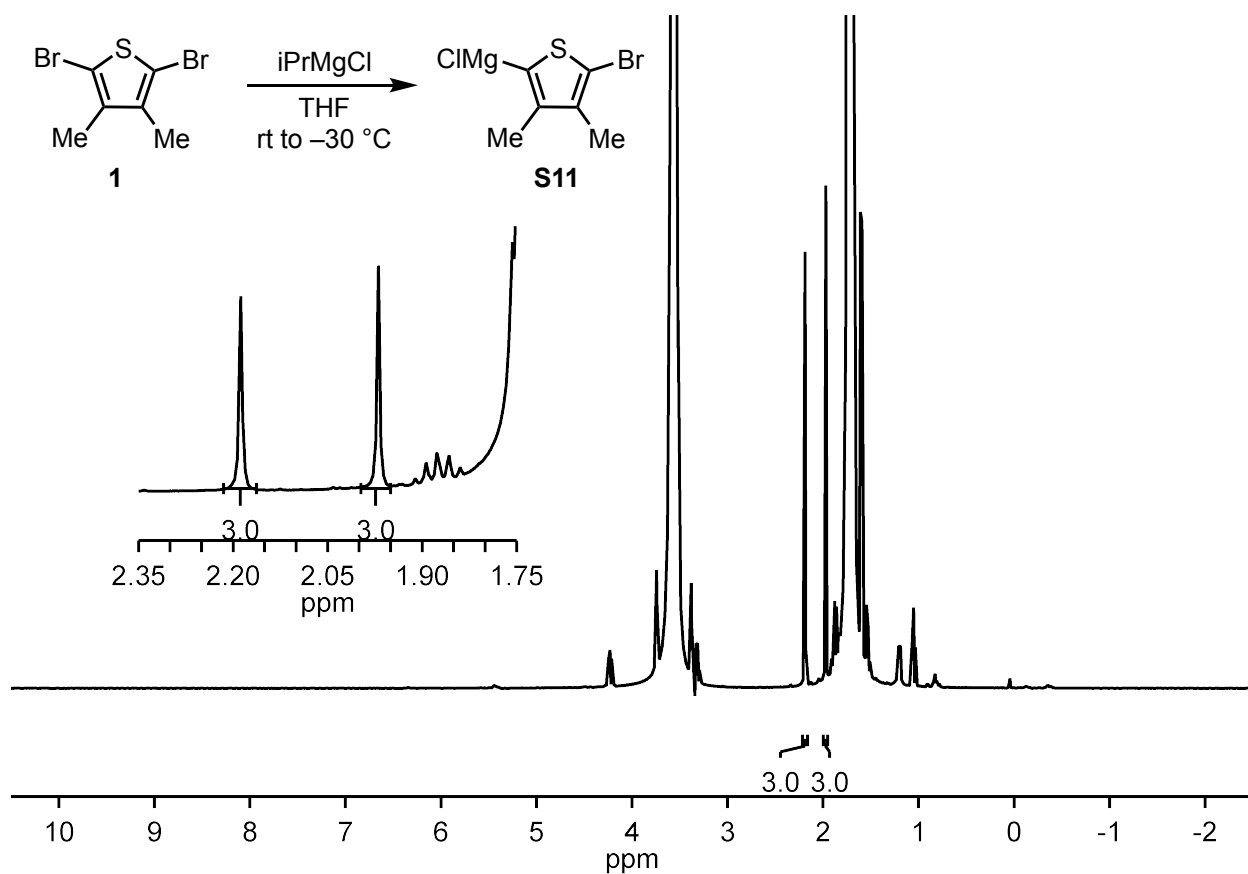
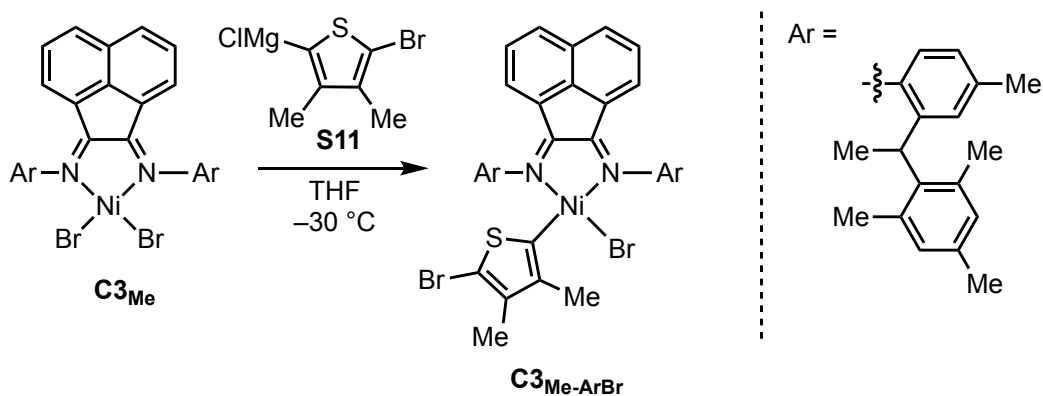


Figure A2-28. $^1\text{H NMR}$ spectrum for the reaction of **1** with $i\text{PrMgCl}$. $^1\text{H NMR}$ (400 MHz, $\text{THF-}d_8$) δ 2.19 (s, 3H), 1.97 (s, 3H).



Synthesis of C3_{Me-ArBr}. In a glovebox, to a 20 mL vial, **C3_{Me}** (37.8 mg, 0.0434 mmol, 1.00 equiv) was dissolved in THF (2.5 mL) and cooled to $-30\text{ }^\circ\text{C}$ for 10 min. Then, the freshly

prepared, cold S11 (0.09 M in THF, 482 μL , 0.0434 mmol, 1.00 equiv) was added dropwise to the C3_{Me} solution. After 1 min, the solution changed from red to blue at which time it was moved to the $-30\text{ }^{\circ}\text{C}$ freezer for 30 min. The solution was divided (20%, 40%, 40%) into pre-weighed 20 mL vials by filtering through a glass filter paper pipette plug and concentrated under reduced pressure. The 20% aliquot was dissolved in $\text{THF-}d_8$, transferred to a J-Young tube which was sealed and removed from the glovebox for spectroscopic analysis. Spectroscopic analysis revealed complete consumption of S11, indicated by the absence of singlets at 2.19 and 1.17 ppm (Figure S29). The remaining aliquots were used for the competition experiment.

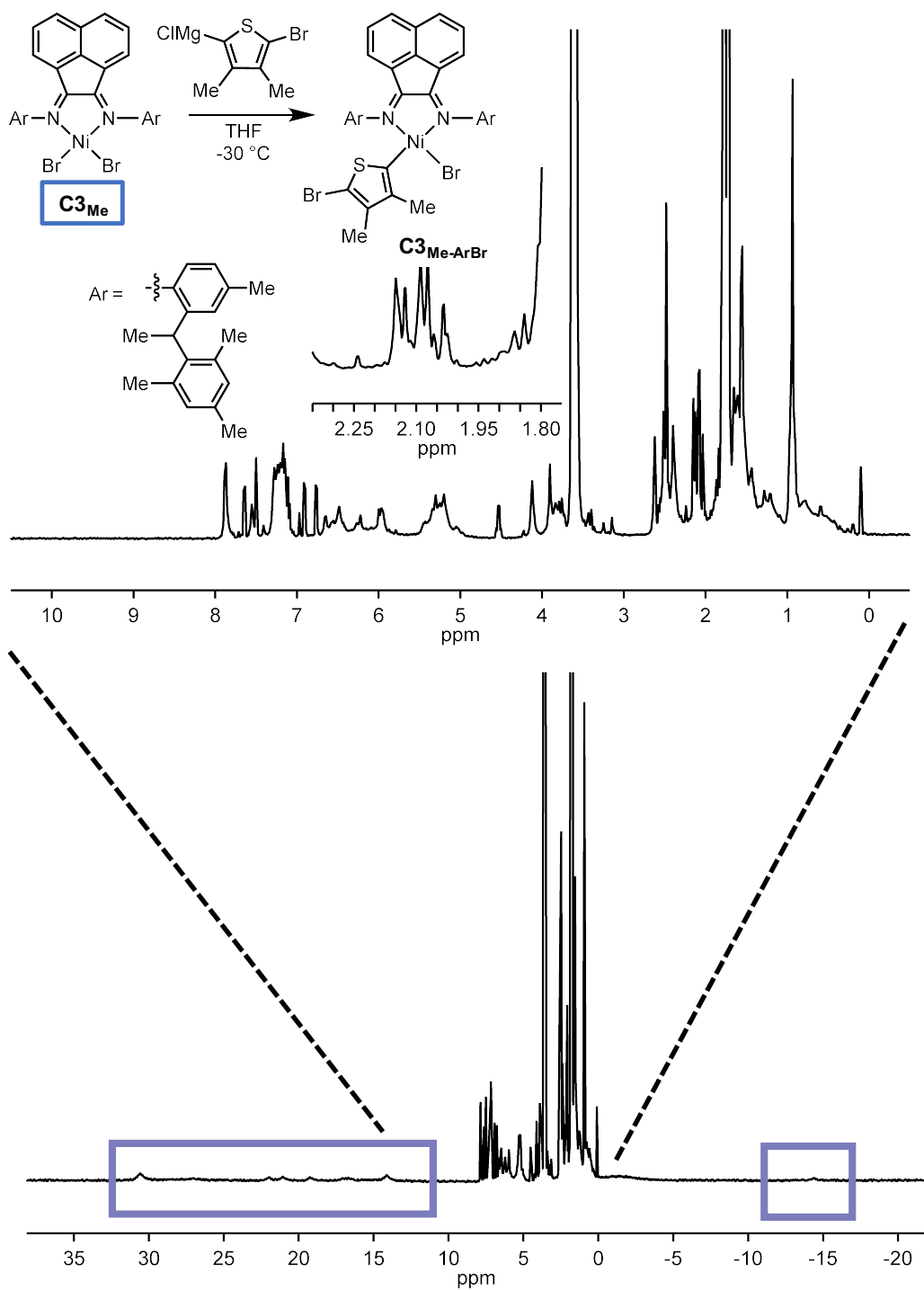
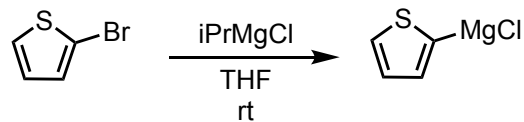
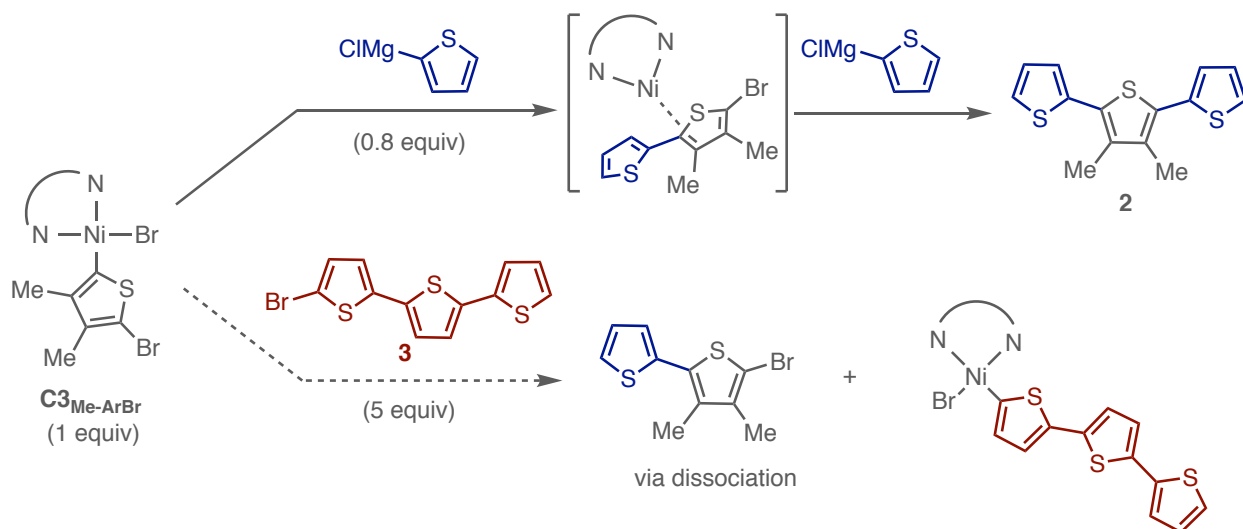


Figure A2-29. ^1H NMR spectra for the reaction of S11 with C3_{Me} . Full spectrum (bottom), zoomed-in region (top). No observed pair of singlets at 2.19 and 1.97 suggests complete conversion of S11. Paramagnetic peaks (boxed in blue) indicate unreacted C3_{Me} .



Preparing (thiophene-2-yl)magnesium chloride. A solution of 2-bromothiophene (31 mg, 0.19 mmol, 1.0 equiv) and *i*PrMgCl (1.78 M in THF, 106 μ L, 0.191 mmol, 1.00 equiv) in THF (2.28 mL) was stirred at rt for 2 h.

Competition Experiment:



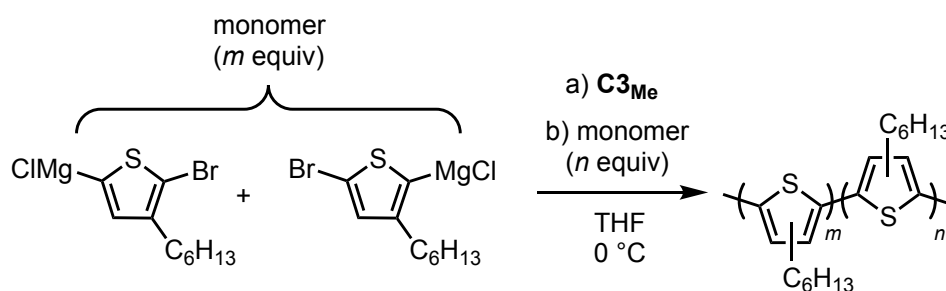
Competition experiment. In a 20 mL vial, $\text{C}3_{\text{Me-ArBr}}$ (17.0 mg, 0.0174 mmol, 1.00 equiv), **3** (28.4 mg, 0.0868 mmol, 5.00 equiv), and internal standard $\text{C}_{22}\text{H}_{46}$ (0.1 M in THF, 0.100 mL) were dissolved in THF (1.7 mL). An initial aliquot (~ 0.25 mL) was removed from the solution and transferred to a 4 mL vial, and quenched outside of the glovebox with aq. HCl (12 M, ~ 0.3 mL), the organic layers were extracted using CHCl_3 (3 x 1 mL), dried over MgSO_4 , and filtered through a PTFE (0.2 μm) filter for GC analysis as an initial time reference. Then, thiophene-2-

ylmagnesium chloride (0.08 M in THF, 174 μ L, 0.0139 mmol, 0.800 equiv) was added to the stirring C3_{Me-ArBr} solution. After 2 min, an aliquot (~0.4 mL) was removed from the solution using a needle and was directly quenched into a GC vial containing MeOH (1 mL) and shaken. The remaining solution was stirred for 5 min at rt before being removed from the glovebox and quenched with aq. HCl (12 M, 1 mL). Organic layers were extracted using CHCl₃ (3 x 1 mL), dried over MgSO₄, and filtered through a PTFE (0.2 μ m) filter for GC analysis. Calculating yield relative to a GC calibration curve reveals the formation of 2 in 74.6 \pm 0.01% (0.01 = standard error, standard deviation = 0.02) yield relative to (thiophene-2-yl)magnesium chloride.

A2.9. Chain-extension polymerizations at 0 °C

General procedure for chain-extension polymerizations at 0 °C

Catalyst stock solution. In a vial a solution of C3_{Me} (7.4 mg, 0.0085 mmol) in THF (0.85 mL) was prepared to give an overall [C3_{Me}] = 0.01 M.



In a glovebox, to a Schlenk tube (ST1, 50 mL) equipped with a stir bar was added freshly prepared Grignard monomer (0.07 M in THF, 1.0 mL, 0.07 mmol, 1.0 equiv) and THF (2.2 mL). To a second Schlenk tube (ST2, 25 mL) was added freshly prepared Grignard monomer (0.07 M in THF, 2.5 mL, 0.18 mmol, 2.57 equiv) and THF (4.4 mL). To a third Schlenk tube (ST3, 25 mL) was added freshly prepared C3_{Me} stock solution (0.85 mL). The 3 Schlenk tubes were sealed, with a septum and copper wire, removed from the glovebox and immediately placed under N₂. The 50 mL Schlenk tube (ST1) was cooled to 0 ± 2 °C for 5 min using an ice-water/brine bath (90:10 v/v), then C3_{Me} solution from ST3 (0.28 mL, 0.0028 mmol, 0.04 equiv relative to first monomer addition) was added using a syringe. After 10 min, an aliquot (~0.4 mL) was removed from the polymerization using a syringe and added to aq. HCl (12 M, 1 mL) capped and shaken (indicated as T1). Subsequently, diluted Grignard monomer solution from ST2 (0.0025 M in THF, 5.6 mL, 0.014 mmol, 2.0 equiv) was added to the polymerization Schlenk tube (ST1) using a syringe. Note the second Grignard monomer solution was rt but the addition needle was pressed against the inside of polymerization Schlenk tube (ST1) to cool the solution during addition. After 30 min an aliquot (~1.0 mL) was removed using a pipette and

added to aq. HCl (12 M, 1.5 mL) capped and shaken (indicated as T2). The aliquots were worked up for GC and GPC analyses.

Table A2-6. Monomer conversion, M_n , and \bar{D} of P3HT ($m = 25$, $n = 50$) chain-extension experiments at 0 °C via precatalyst **C3_{Me}**.

$m = 25$ $n = 50$	Run 1			Run 2		
	monomer conv. (%)	M_n (kg/mol)	\bar{D}	monomer conv. (%)	M_n (kg/mol)	\bar{D}
T1	85	9.30	1.34	89	8.39	1.40
T2	93	21.3	1.81	93	20.2	1.82

Table A2-7. Monomer conversion, M_n , and \bar{D} of thiophene ($m = 10$, $n = 70$) chain-extension experiments at 0 °C via (diimine)NiBr₂ precatalyst **C3_{Me}**.

$m = 10$ $n = 70$	Run 1			Run 2		
	monomer conv. (%)	M_n (kg/mol)	\bar{D}	monomer conv. (%)	M_n (kg/mol)	\bar{D}
T1	82	5.08	1.23	87	4.89	1.20
T2	60.	19.0	1.81	81	18.2	1.92

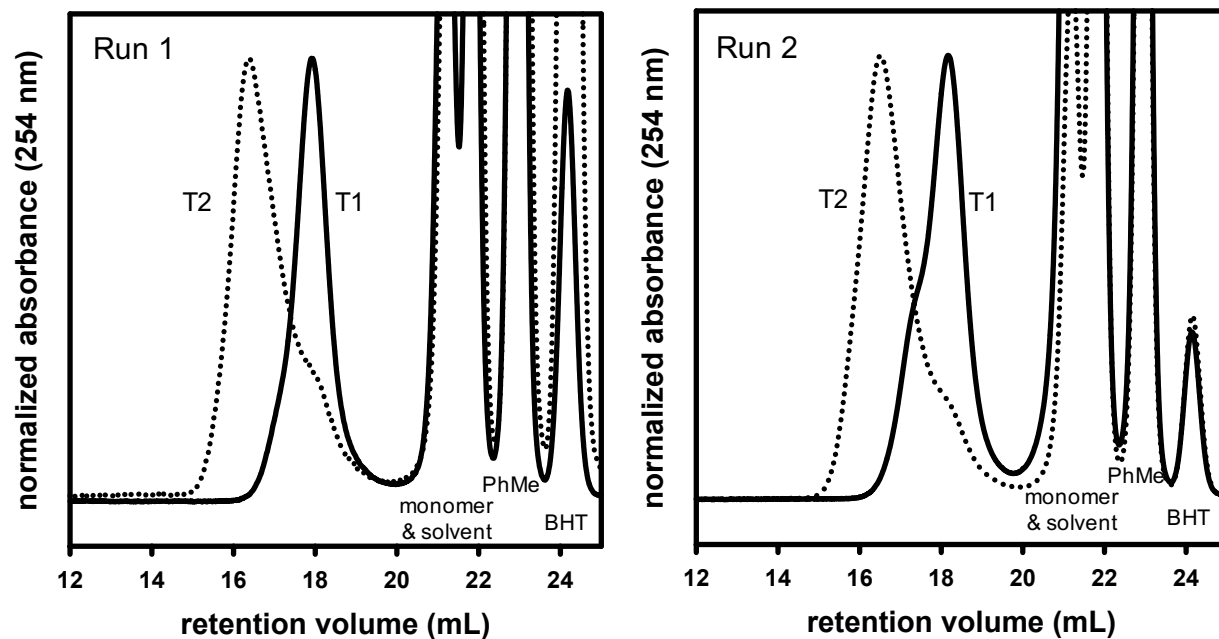


Figure A2-30. GPC traces of P3HT ($m = 25, n = 50$) chain-extension experiments at $0\text{ }^{\circ}\text{C}$ via precatalyst C3_{Me} .

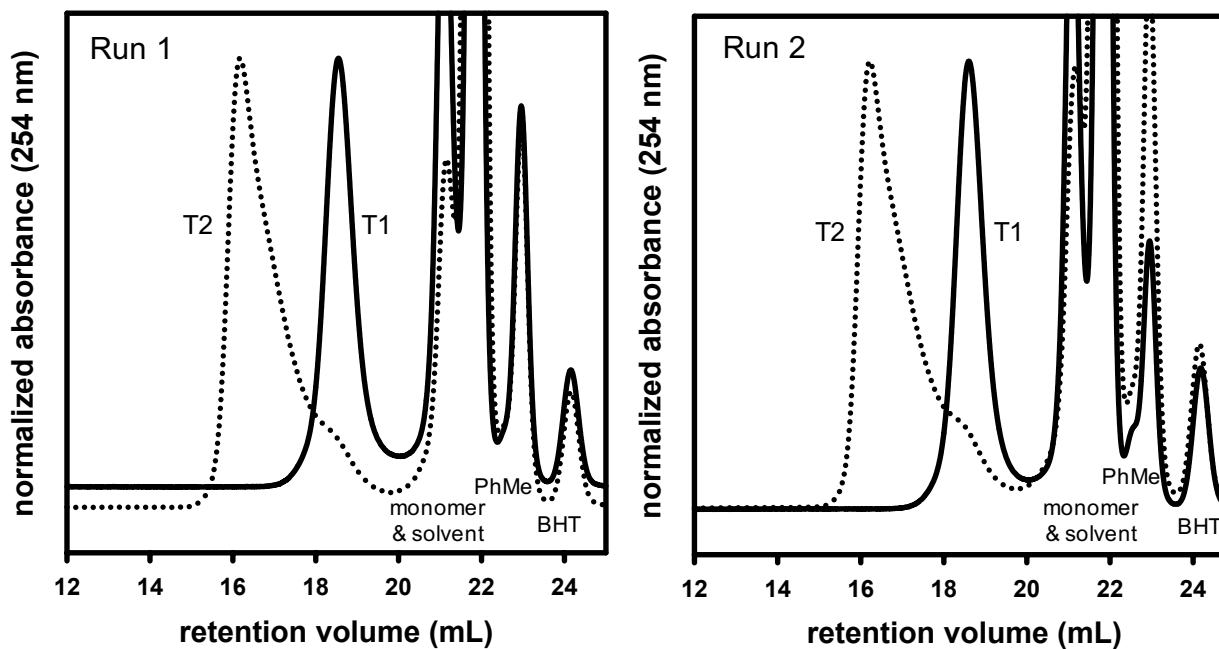
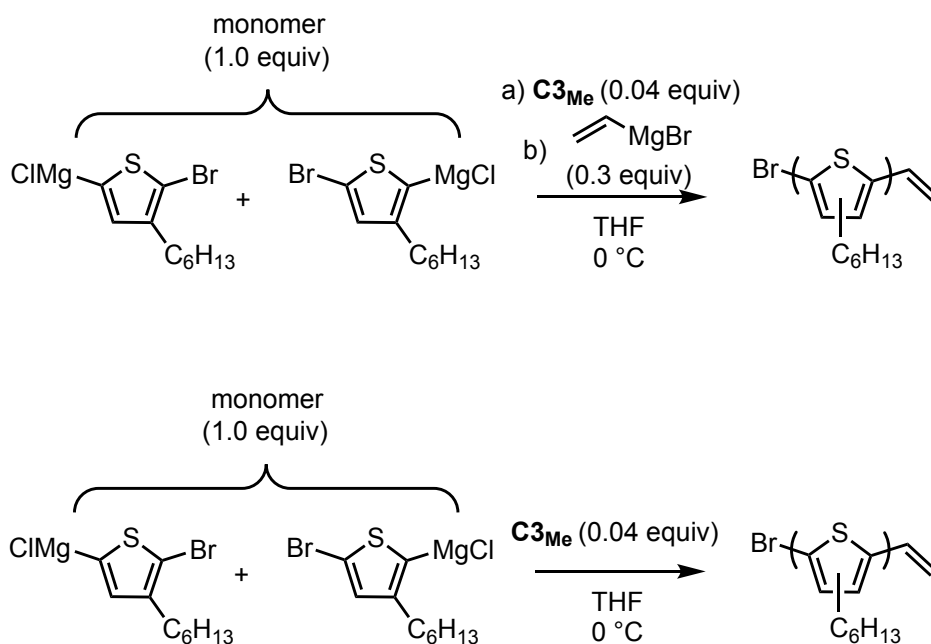


Figure A2-31. GPC traces of P3HT ($m = 10, n = 70$) chain-extension experiments at $0\text{ }^{\circ}\text{C}$ via precatalyst C3_{Me} .

A2.10. Vinyl end-capped polymerizations at 0 °C

General procedure for vinyl end-capped polymerizations at 0 °C



In a glovebox, to two Schlenk tubes (50 mL) each containing a stir bar was added freshly prepared Grignard monomer solution (0.07 M in THF, 1.75 mL, 0.123 mmol, 1.00 equiv) that was diluted with THF (3.9 mL). To a third Schlenk tube (25 mL) was added freshly prepared C3_{Me} stock solution (0.01 M in THF, 20.2 mg, 0.00232 mmol in THF (2.32 mL)). The Schlenk tubes were sealed with a septum and copper wire, removed from the glovebox, and immediately placed under N_2 . The Schlenk tubes containing monomer was cooled to 0 ± 2 °C using an ice-water/brine bath (90:10 v/v). Then, C3_{Me} stock solution (0.49 mL, 0.0049 mmol, 0.040 equiv) was added to each monomer solution using a syringe, and stirred for 8 min 45 s. One polymerization was quenched by adding 12 M aq. HCl (3 mL), then MeOH (4 mL) was added to precipitate the polymer. To the second polymerization was added vinyl MgBr (0.7 M in THF, 52.5 μL , 0.0368 mmol, 0.300 equiv) using a syringe and then stirred for 10 min (at 0 °C) before

precipitating with MeOH (4 mL). The polymers were transferred to centrifuge tubes, and spun for 15 min. The supernatant was decanted leaving a purple solid, which was collected, and analyzed by GPC and MALDI-TOF-MS.

Table A2-8. GPC data from vinyl end-capping polymerizations at 0 °C via precatalyst C3_{Me}.

	Run 1		Run 2	
quench	M_n (kg/mol)	\bar{D}	M_n (kg/mol)	\bar{D}
HCl	6.48	1.35	8.27	1.33
Vinyl MgBr	7.11	1.32	8.21	1.27

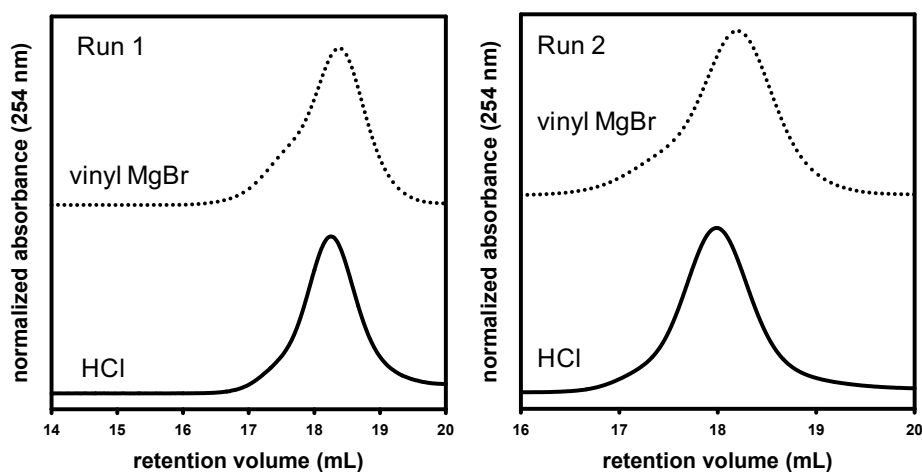
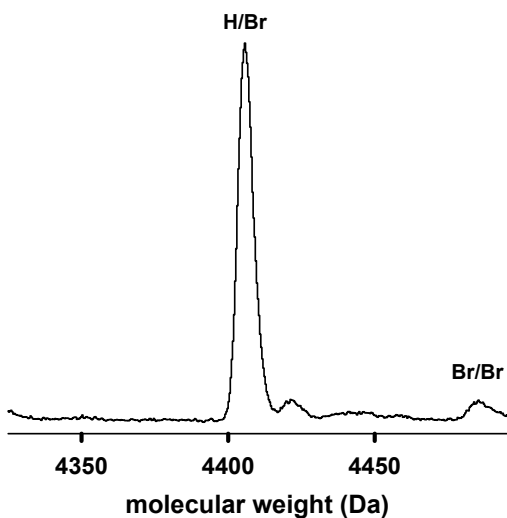
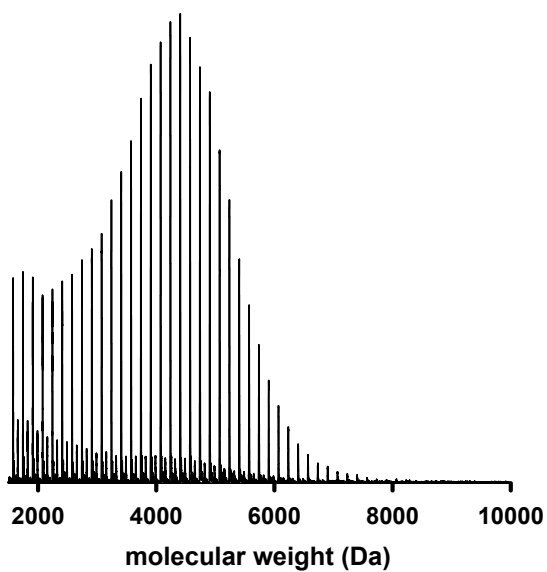
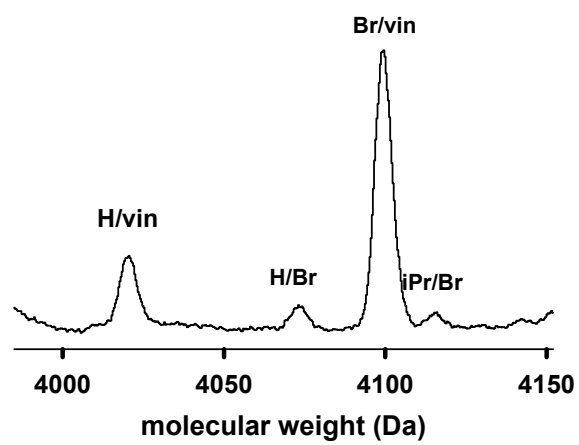
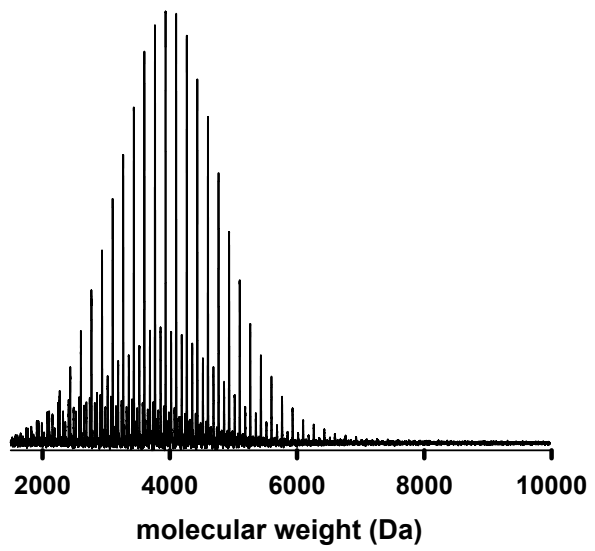


Figure A2-32. GPC traces from vinyl end-capping polymerizations at 0 °C via precatalyst C3_{Me}.

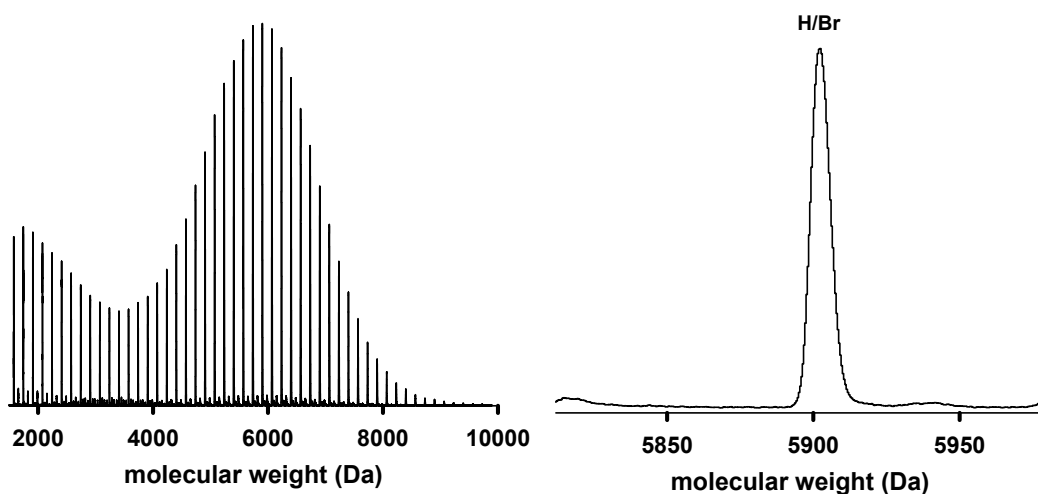
Run 1: HCl quench



Run 1: vinyl MgBr quench



Run 2: HCl quench



Run 2: vinyl MgBr quench

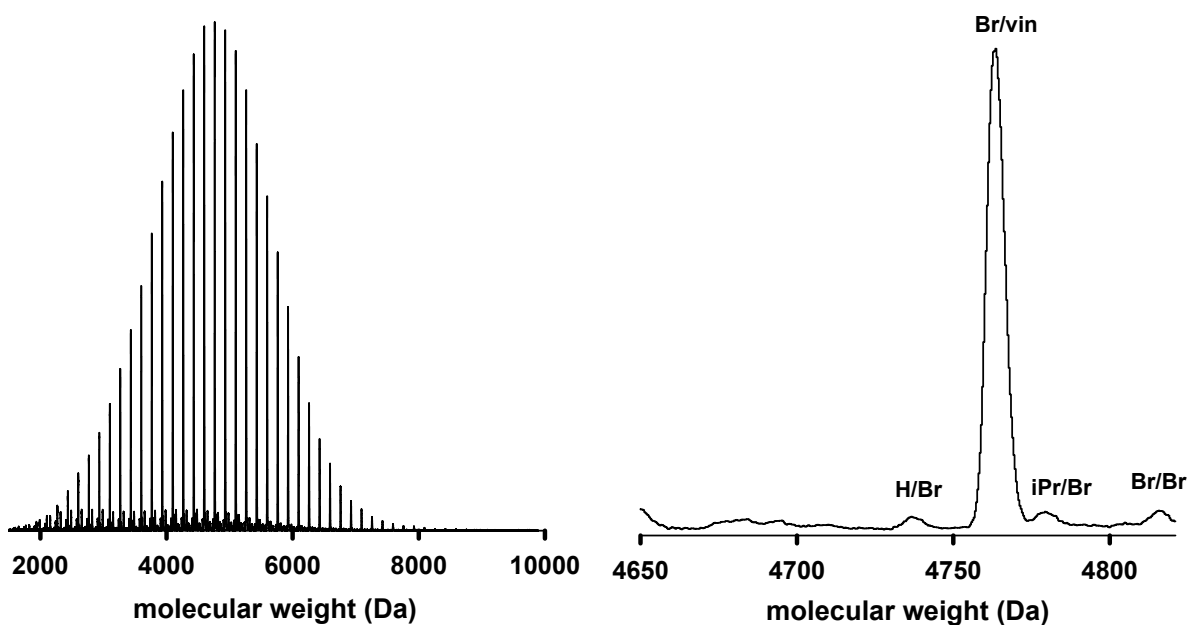
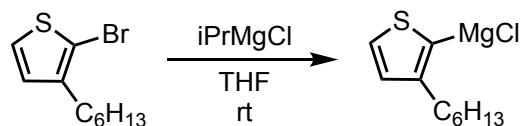


Figure A2-33. MALDI-TOF-MS data from vinyl end-capping polymerizations at 0 °C via precatalyst $C3_{Me}$.

A2.11. Mono/terthiophene reactivity experiment

General Procedure for comparing the reactivity of mono/terthiophene molecules

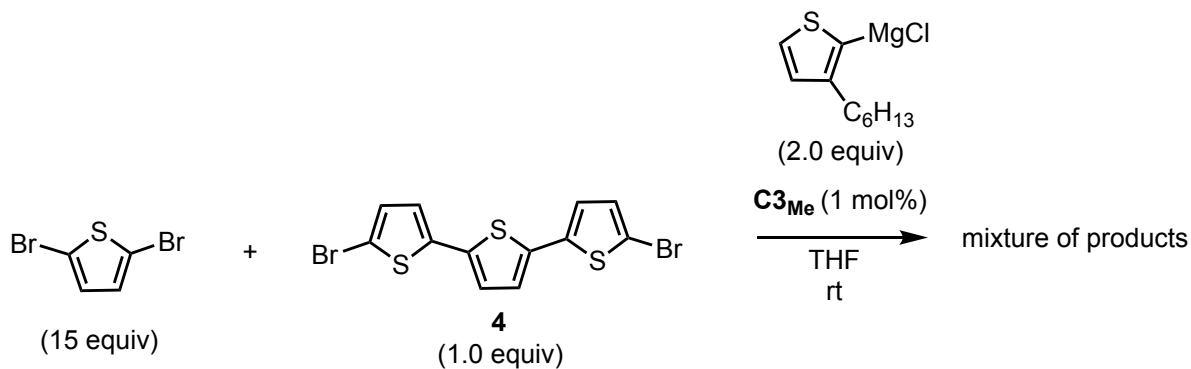
Preparing reactant solutions:



Preparing (3-hexylthiophen-2-yl)magnesium chloride. In a glovebox, to a 20 mL vial was added, 2-bromo-3-hexylthiophene (64.0 mg, 0.259 mmol, 1.00 equiv) and THF (2.46 mL). Then iPrMgCl (1.85 M in THF, 0.133 mL, 0.246 mmol, 0.950 equiv) was added and stirred for 30 min at rt.

Preparing C3_{Me} stock solution. Catalyst C3_{Me} (11.1 mg, 0.0127 mmol) was dissolved in THF (2.56 mL) to generate an overall [C3_{Me}] of 0.005 M.

Competition experiment:



Competition experiments. In a glovebox, to a 4 mL vial the following were sequentially added: 4 (6.0 mg, 0.015 mmol, 1.0 equiv), THF (1.1 mL for an overall [4] of 0.01 M), C₂₂H₄₆ as an internal standard (0.014 mL of 0.1 M in THF), 2,5-dibromothiophene (25 μ L, 0.22 mmol, 15 equiv), and freshly prepared (3-hexylthiophen-2-yl)magnesium chloride (0.095 M in THF, 0.311

mL, 0.0295 mmol, 2.00 equiv). An aliquot (~0.1 mL) was removed for an initial time reference. Then, freshly prepared $C3_{Me}$ (0.005 M in THF, 29.5 μ L, 0.00015 mmol, 0.01 equiv) was added to the mother liquor. The initial time aliquot was quenched with aq. HCl (12 M, ~0.3 mL) and worked up for GC analysis. After 2 h the reaction was quenched with aq. HCl (12 M, ~1 mL), extracted with $CHCl_3$ (2 x 3 mL), and worked up for GC analysis.

Table A2-9. GC data from the reaction of excess 2,5-dibromothiophene, **4**, and (3-hexylthiophen-2-yl)magnesium chloride with precatalyst $C3_{Me}$. Note that 2,5-dibromothiophene flies with solvent on the GC, hence conversion could not be measured

	Run 1	Run 2
Grignard conv. (%)	54	53
4 conv. (%)	12	19

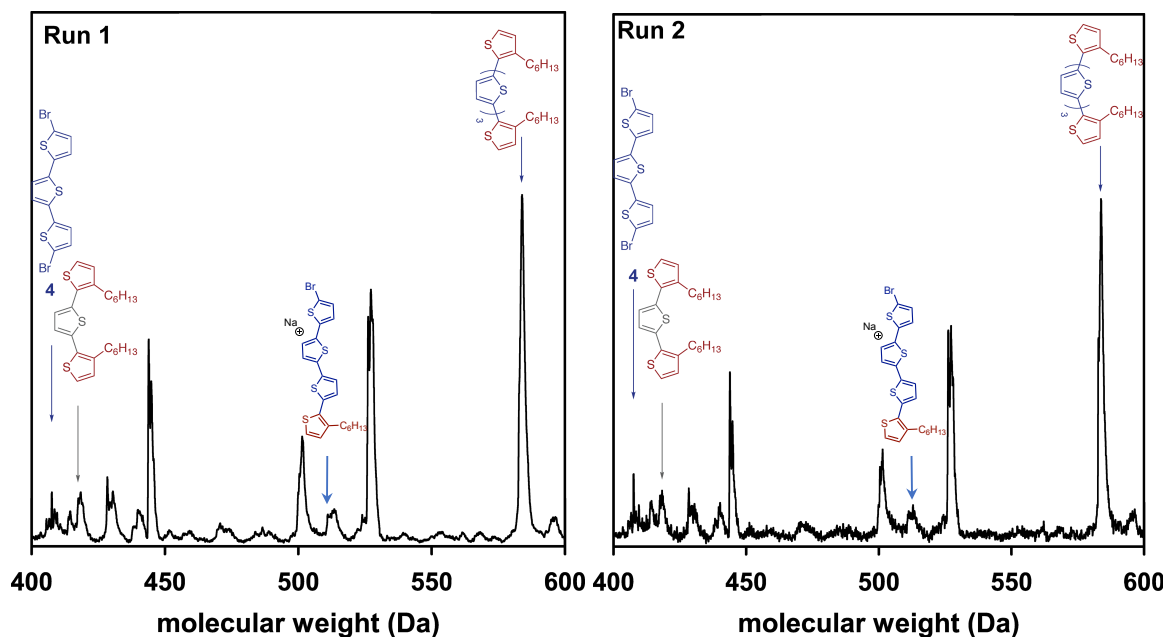


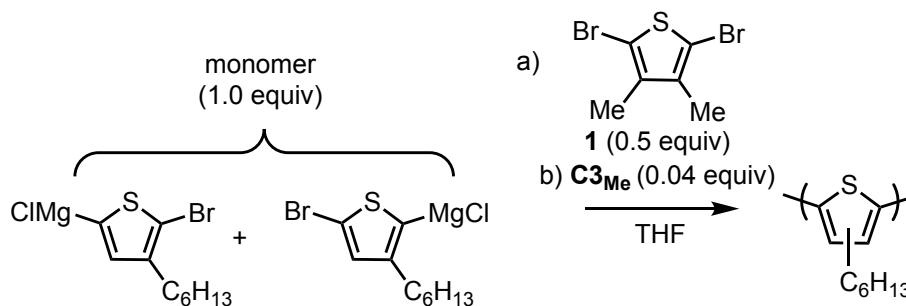
Figure A2-34. MALDI-TOF-MS spectrum from the reaction of excess 2,5-dibromothiophene, **4**, and (3-hexylthiophen-2-yl)magnesium chloride with precatalyst $C3_{Me}$.

A2.12. Monomer analogue addition polymerizations at rt

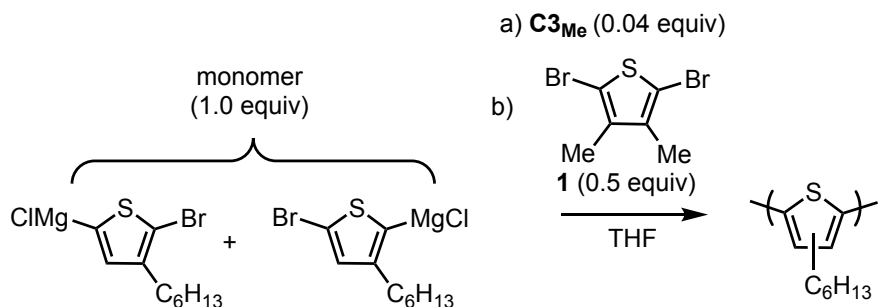
General procedure for adding monomer analogue (1) to thiophene polymerizations

Catalyst stock solution. In the glovebox, in a 4 mL vial, a solution of $C3_{Me}$ (8.5 mg, 0.0098 mmol) in THF (0.98 mL) was prepared to give an overall $[C3_{Me}] = 0.01$ M

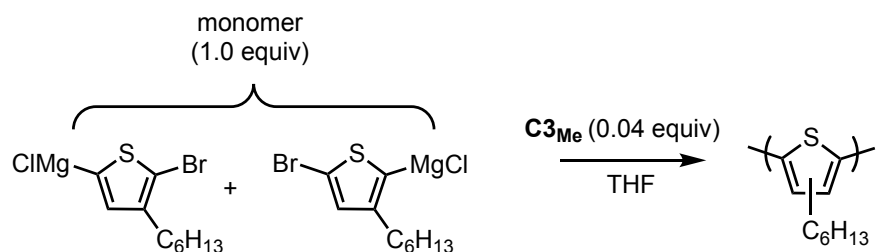
Monomer analogue (1) stock solution. In the glovebox, in a 4 mL vial, a solution of 1 (11.8 mg, 0.0441 mmol) and internal standard $C_{20}H_{44}$ (6.2 mg) in THF (0.44 mL) was prepared to give an overall $[1] = 0.1$ M.



Additive before polymerization: In a glovebox, to a 4 mL vial equipped with a stir bar, monomer analogue 1 (0.1 M in THF, 87.5 μ L, 0.00875 mmol, 0.500 equiv) and freshly prepared Grignard monomer solution (0.07 M in THF, 0.250 mL, 0.0175 mmol, 1.00 equiv) were diluted in THF (3.25 mL). Freshly prepared $C3_{Me}$ (0.01 M in THF, 0.070 mL, 0.00070 mmol, 0.040 equiv) was added. The reactions stirred for 8 min before being quenched with aq. HCl (12 M, 0.5 mL) outside of the glovebox.



Additive during polymerization: In a glovebox, to a 4 mL vial equipped with a stir bar, freshly prepared Grignard monomer solution (0.07 M in THF, 0.250 mL, 0.0175 mmol, 1.00 equiv) was diluted in THF (3.25 mL). Freshly prepared **C3_{Me}** (0.01 M in THF, 0.070 mL, 0.00070 mmol, 0.040 equiv) was added. After 90 s, monomer analogue **1** (0.1 M in THF, 87.5 μ L, 0.00875 mmol, 0.500 equiv) was added. The reactions stirred for 8 min before being quenched with aq. HCl (12 M, 0.5 mL) outside of the glovebox.



Control polymerization: In a glovebox, to a 4 mL vial equipped with a stir bar, freshly prepared Grignard monomer solution (0.07 M in THF, 0.250 mL, 0.0175 mmol, 1.00 equiv) was diluted in THF (3.25 mL). Freshly prepared **C3_{Me}** (0.01 M in THF, 0.070 mL, 0.00070 mmol, 0.040 equiv) was added. An aliquot (~0.3 mL) was removed and quenched outside of the glovebox with aq. 12 M HCl (0.5 mL) at 90 s. After 8 min the polymerization was quenched with 12 M aq. HCl (2 mL) outside of the glovebox.

All polymerizations were worked up for GC, GPC, and MALDI-TOF-MS (refer to *General experimental* for details).

Table A2-10. GC and GPC data from rt polymerizations with and without monomer analogue **1** added prior to initiation via precatalyst **C3_{Me}**.

	Run 1	control	Run 2	control
1 (X equiv)	0.5	0	0.5	0
1 conv. (%)	0	-	0	-
monomer conv. (%)	78.7	95.0	92.4	98.5
M_n (kg/mol)	8.5	9.3	10.6	13.2
Đ	1.54	1.59	1.52	1.59

Table A2-11. GC and GPC data from rt polymerization via precatalyst **C3_{Me}** with and without monomer analogue **1** added after 90s.

	Run 1	Run 2	control (90 s)	control (final)
1 (X equiv)	0.5	0.5	0	0
1 conv. (%)	4.8	3.1	-	-
monomer conv. (%)	89.4	90.0	84.7	98.4
M_n (kg/mol)	11.3	11.0	6.9	11.5
Đ	1.57	1.60	1.20	1.58

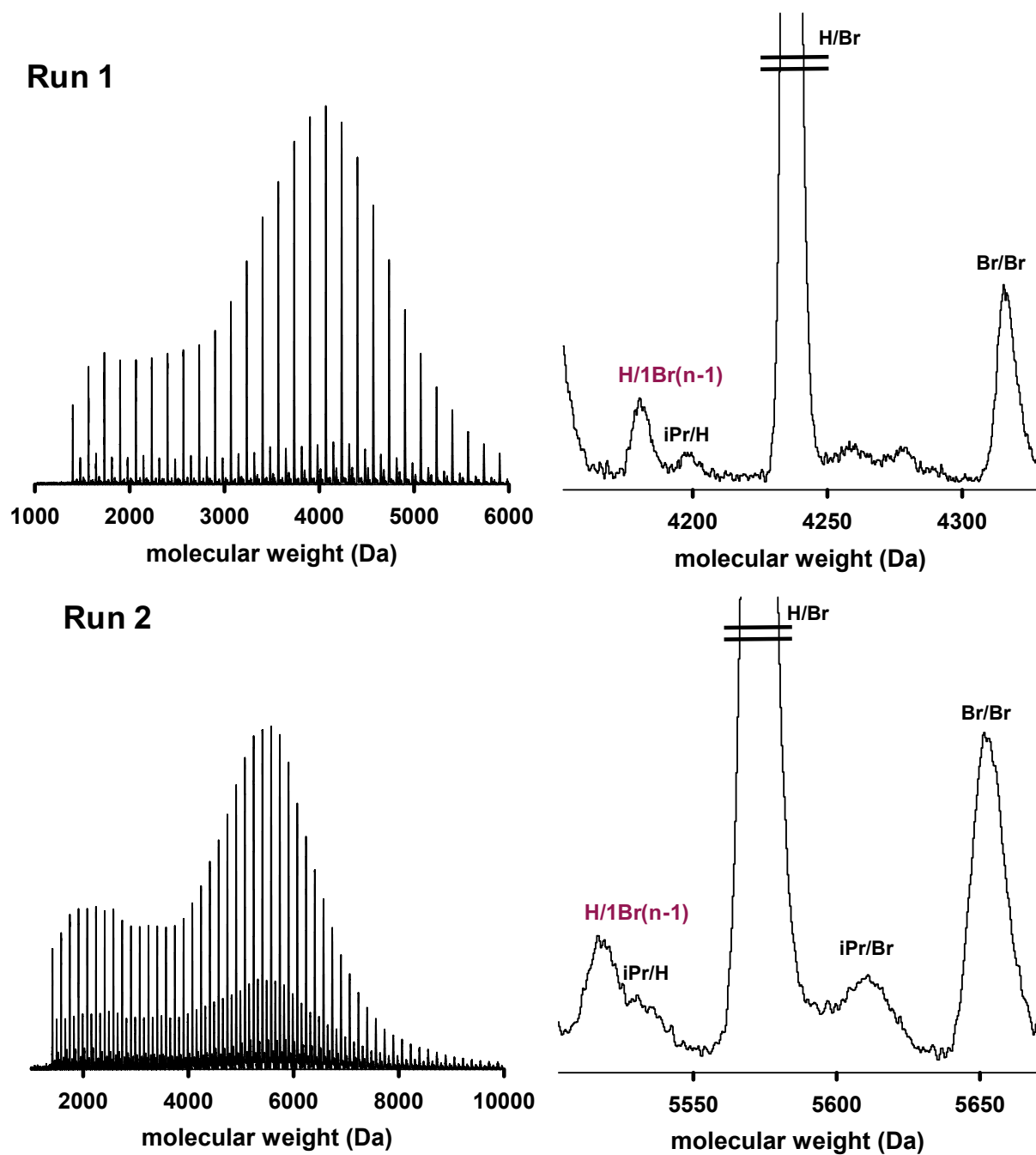


Figure A2-35. MALDI-TOF-MS spectra of the rt polymerization with monomer analogue **1** added before initiation via precatalyst $C3_{Me}$.

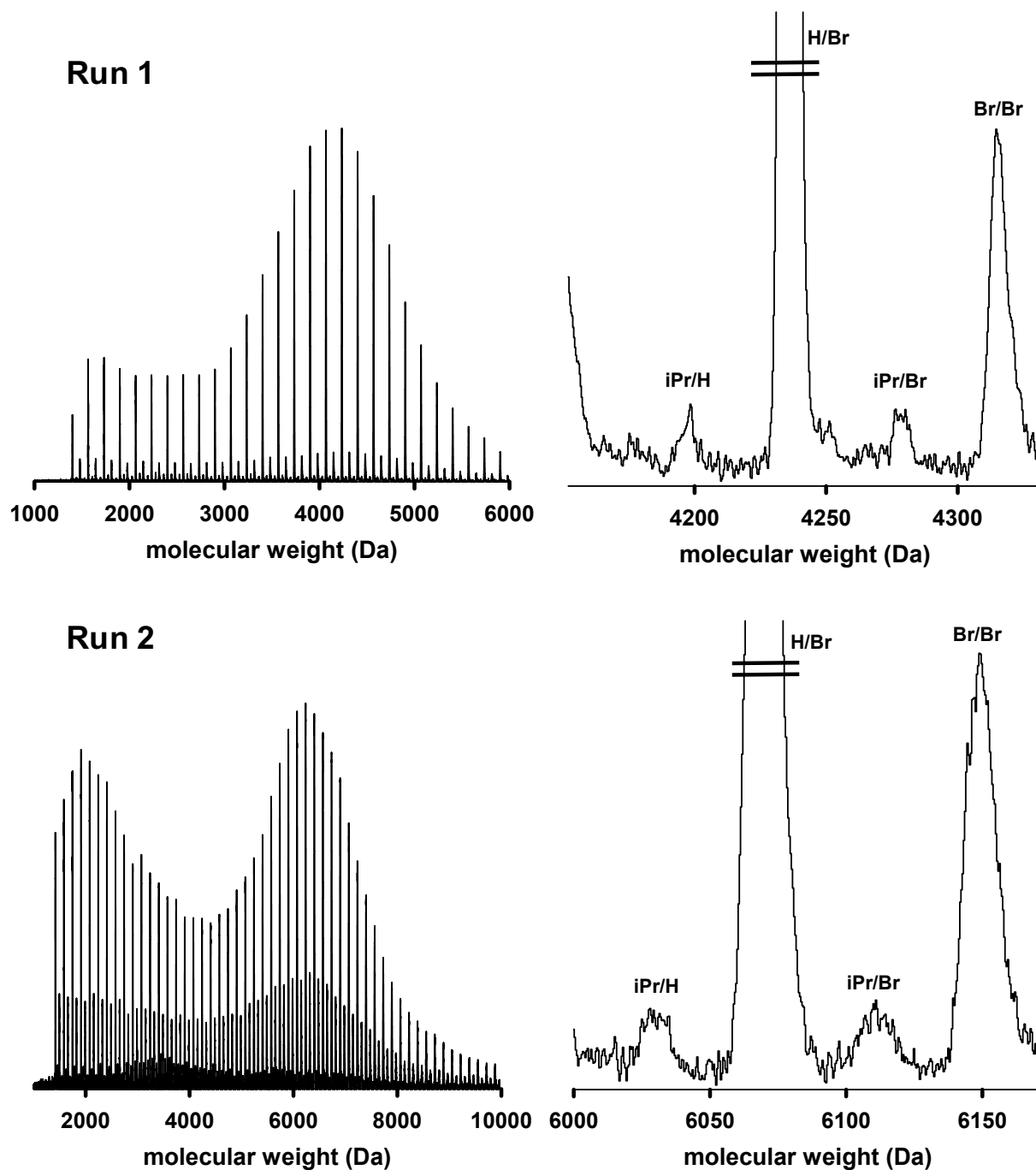


Figure A2-36. MALDI-TOF-MS spectra of rt polymerizations via precatalyst $C3_{Me}$ after 8 min (control polymerization).

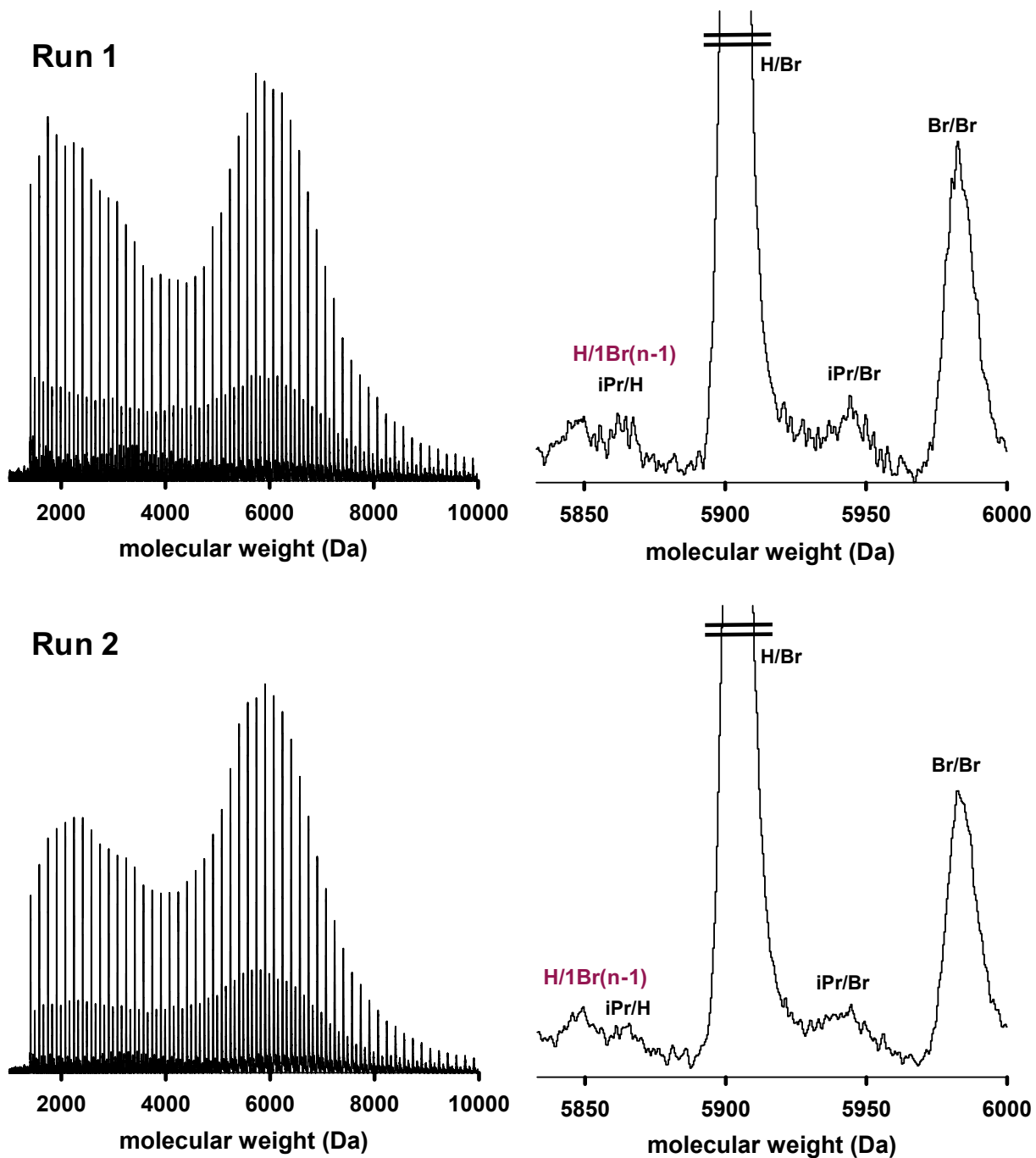


Figure A2-37. MALDI-TOF-MS spectra of rt polymerizations with monomer analogue (1) added after 90s at rt via precatalyst C3_{Me} after 8 min.

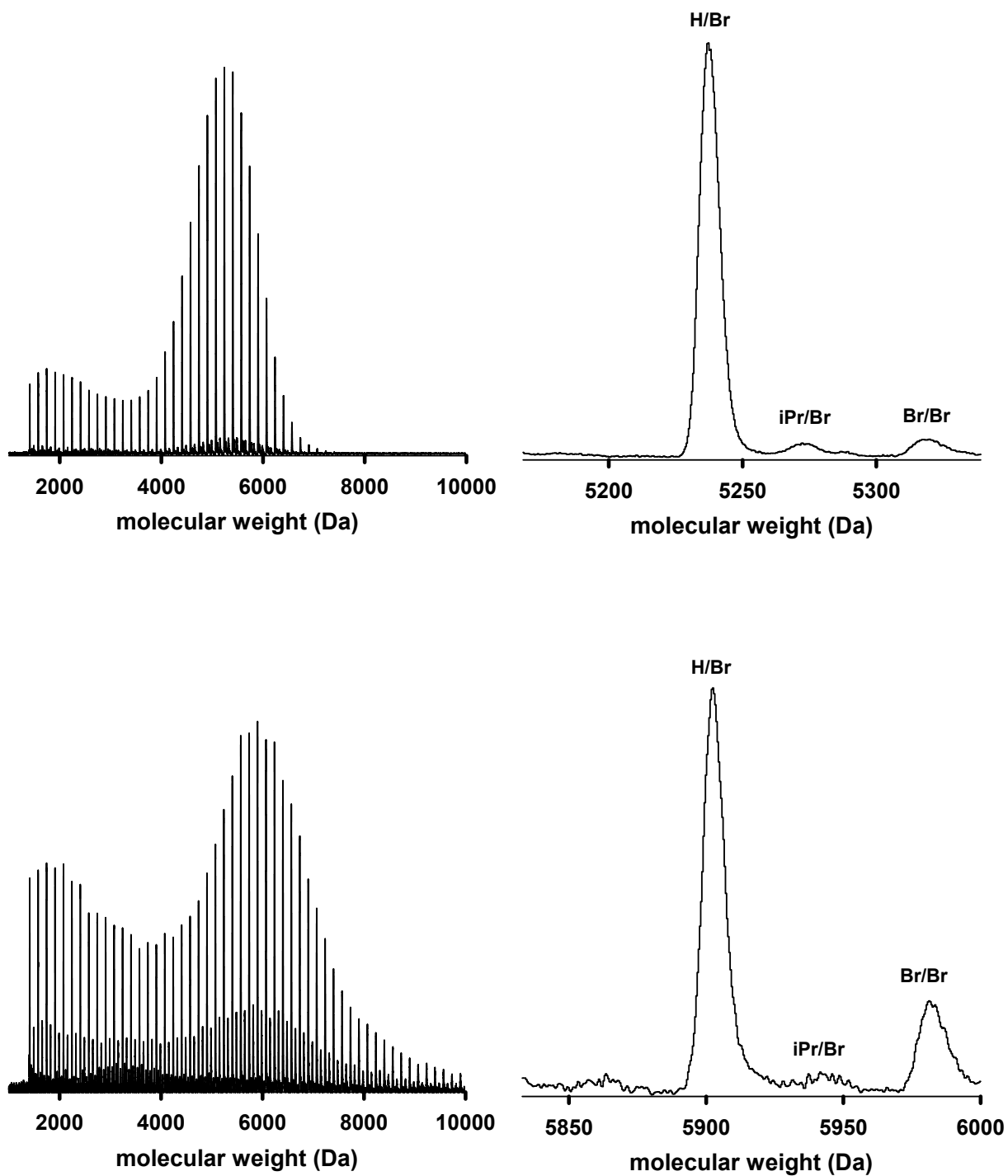


Figure A2-38. MALDI-TOF-MS spectra of the polymerization of thiophene at rt via precatalyst $C3_{Me}$ after 90 s (top) and 8 min (bottom) (control polymerization).

A2.13. Computational Details

All quantum chemical calculations were performed by density functional theory (DFT) using the Q-Chem 4.3 quantum chemistry package. The B3LYP density functional^{6,7} with singlet spin and the restricted framework was used with the LANL2DZ basis set and core potential^{8,9} to acquire gas phase energies for the intermediates discussed. The ω B97X-D density functional¹⁰ and the triple-zeta, polarized cc-pVTZ basis set¹¹ were used to calculate energies with the SMD solvation model¹² using THF as the implicit solvent. The hexyl group of the 3-hexylthiophene Grignard monomer was substituted with a methyl group to reduce computational cost. Thermodynamic corrections were applied to the solvated energies at a temperature of 298 K.

Catalyst	Species	Ni Mulliken Charge
C3_{Me}	CW_{rct}	0.180
	CW_{prd}	0.305
C3_{OMe}	CW_{rct}	0.208
	CW_{prd}	0.308

*Performed with ω B97X-D/cc-pVTZ/SMD(THF)

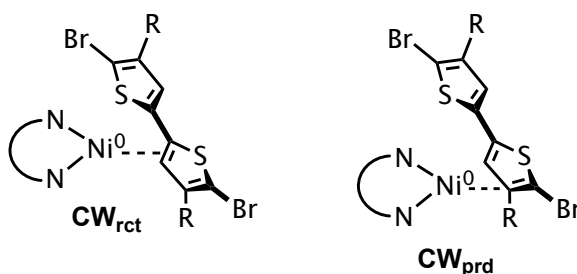


Figure A2-39. Ni Mulliken Charge Calculations for **C3_{Me}** and **C3_{OMe}**

XYZ coordinates and Gibbs Free Energy (in Hartree) for all reported structures

All XYZ coordinates for structures used to calculate catalyst dissociation and chain-walking (Scheme 3-2) are provided below. Total electronic energies and free energy corrections are provided in Hartree. See online Supplementary Information for specific details.

A2.14 References

- (1) Killian, C. M.; Tempel, D. J.; Johnson, L., K.; Brookhart, M. Living Polymerization of α -Olefins Using NiII- α -Diimine Catalysts. Synthesis of New Block Polymers Based on α -Olefins. *J. Am. Chem. Soc.* **1996**, *118*, 11664–11665.
- (2) McLain, S., J.; Feldman, J.; McCord, E., F.; Gardner, K. H.; Teasley, M. F.; Coughlin, E. B.; Sweetman, K. J. Addition Polymerization of Cyclopentene with Nickel and Palladium Catalysts. *Macromolecules* **1998**, *31*, 6705–6707.
- (3) Cherian, A. E.; Rose, J. M.; Lobkovsky, E. B.; Coates, G. W. A C₂-Symmetric, Living α -Diimine Ni(II) Catalyst: Regioblock Copolymers from Propylene. *J. Am. Chem. Soc.* **2005**, *127*, 13770–13771.
- (4) Vaidya, T.; Klimovica, K.; LaPointe, A. M.; Keresztes, I.; Lobkovsky, E. B.; Daugulis, O.; Coates, G. W. Secondary Alkene Insertion and Precision Chain-Walking: A New Route to Semicrystalline “Polyethylene” from α -Olefins by Combining Two Rare Catalytic Events. *J. Am. Chem. Soc.* **2014**, *136*, 7213–7216.
- (5) Love, B. E.; Jones, E. G. The Use of Salicylaldehyde Phenylhydrazone as an Indicator for the Titration of Organometallic Reagents. *J. Org. Chem.* **1999**, *64*, 3755–3756.
- (6) Becke, A. D. Density-Functional Thermochemistry. III. The Role of Exact Exchange. *J. Chem. Phys.* **1993**, *98*, 5648–5652.
- (7) Lee, C.; Yang, W.; Parr, R. G. Development of the Colle-Salvetti Correlation-Energy Formula into a Functional of the Electron Density. *Phys. Rev. B.* **1988**, *37*, 785–789.
- (8) Hay, P. J.; Wadt, W. R. Ab Initio Effective Core Potentials for Molecular Calculations. Potentials for K to Au Including the Outermost Core Orbitals. *J. Chem. Phys.* **1985**, *82*, 299–310.

- (9) Hay, P. J.; Wadt, W. R. Ab Initio Effective Core Potentials for Molecular Calculations. Potentials for the Transition Metal Atoms Sc to Hg. *J. Chem. Phys.* **1985**, *82*, 270–283.
- (10) Chai, J.-D.; Head-Gordon, M. Systematic Optimization of Long-Range Corrected Hybrid Density Functionals. *J. Chem. Phys.* **2008**, *128*, 084106–084106.
- (11) Kendall, R. A.; Dunning Jr., T. H.; Harrison, R. J. Electron Affinities of the First-Row Atoms Revisited. Systematic Basis Sets and Wave Functions. *J. Chem. Phys.* **1992**, *96*, 6796–6806.
- (12) Marenich, A. V.; Cramer, C. J.; Truhlar, D.G. Universal Solvation Model Based on Solute Electron Density and on a Continuum Model of the Solvent Defined by the Bulk Dielectric Constant and Atomic Surface Tensions. *J. Phys. Chem. B.* **2009**, *113*, 6378–6396.

Appendix 3: Supporting Information for Chapter 4. Progress Towards Thiophene/Olefin Block Copolymers using an in-situ Ligand-Exchange Approach

A3-1. Materials

Flash chromatography was performed on SiliCycle silica gel (40–63 μm). Thin layer chromatography was performed on Merck TLC plates (pre-coated with silica gel 60 F254). $i\text{PrMgCl}$ (2 M in THF) was purchased from Aldrich and titrated using salicylaldehyde phenylhydrazone.¹ 2,5-Dibromo-3-decylthiophene (DB3DT) and 2,5-dibromo-3-hexylthiophene (DB3HT) were purchased from TCI America and purified by column chromatography with hexanes as the eluent. Methylmagnesium chloride (3 M in Et_2O) was purchased from Sigma Aldrich. 5,5'-Dibromo-2,2'-bithiophene was purchased from Ark Pharm Inc. Compounds **S1**,² **C2**,² **S2**,³ **S3**,³ and **S4**³ were prepared according to modified literature procedures. All other reagent grade materials and solvents were purchased from Aldrich, Acros, or Fisher and were used without further purification unless otherwise noted. Tetrahydrofuran (THF) and diethyl ether (Et_2O) were dried and deoxygenated using an Innovative Technology (IT) solvent purification system composed of activated alumina, copper catalyst, and molecular sieves. The glovebox in which specified procedures were carried out was an MBraun LABmaster 130 with a N_2 atmosphere.

A3.2 General Experimental

NMR Spectroscopy: Unless otherwise noted, ^1H , and ^{13}C NMR spectra for all compounds were acquired at rt. Chemical shift data are reported in units of δ (ppm) relative to tetramethylsilane (TMS) and referenced with residual solvent. Multiplicities are reported as follows: singlet (s), doublet (d), doublet of doublets (dd), triplet (t), quartet (q), multiplet (m), broad resonance (br). Residual water is denoted by an asterisk (*).

Mass Spectrometry: High-resolution mass spectrometry data were obtained on a Micromass AutoSpec Ultima Magnetic Sector mass spectrometer.

Gel-Permeation Chromatography (GPC): Polymer molecular weights were determined by comparison with polystyrene standards (Varian, EasiCal PS-2 MW 580–377,400) at 40 °C in THF on a Malvern Viscotek GPCMax VE2001 equipped with two Viscotek LT- 5000L 8 mm (ID) \times 300 mm (L) columns and analyzed with Viscotek TDA 305 (with RI, UV-PDA Detector Model 2600 (190–500 nm), RALS/LALS, and viscometer). Data presented correspond to the absorbance at 254 nm normalized to the highest peak. Peaks are normalized to the polymer peak, when traces are presented in series, the normalized peaks are offset vertically. The peaks at ~21 min represent monomer which include unreacted, quenched Grignard monomers and/or unactivated dibromo monomer (see monomer activation procedures).

Polymer work-up for GPC: Polymerizations were quenched using aq. HCl (12 M). The organic layer was extracted with CHCl_3 , dried over MgSO_4 , and filtered through a PTFE filter (0.2 μm), concentrated under reduced pressure to dryness and then redissolved (~0.5 mg polymer/mL) in

THF/toluene (99:1 v/v) with mild heating and filtered through a PTFE filter (0.2 μm) into a GPC vial.

Gas Chromatography: Gas chromatographic (GC) analysis was done using a Shimadzu GC 2010 containing a Shimadzu SHRX5 (crossbound 5% diphenyl – 95% dimethyl polysiloxane; 15 m, 0.25 mm ID, 0.25 μm df) column.

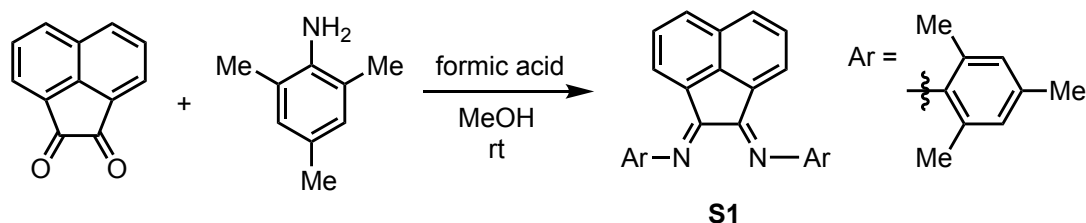
Polymer work-up for GC: Polymerizations were quenched using aq. HCl (12 M). The organic layer was extracted with CHCl_3 , dried over MgSO_4 , and filtered through a PTFE filter (0.2 μm) into a GC vial.

Matrix-Assisted Laser Desorption/Ionization Mass Spectrometry: Matrix-assisted laser desorption/ionization mass spectrometry (MALDI-TOF/MS) was done on a Bruker AutoFlex Speed MALDI-TOF in positive-ion reflectron mode using *trans*-2-[3-(4-*tert*-butylphenyl)-2-methyl-2-propenylidene]malononitrile (DCTB) as a matrix. Samples were prepared by mixing polymer dissolved in THF/toluene (99:1 v/v) (~1 mg polymer/1 mL THF) with DCTB dissolved in CHCl_3 (~1 M). Samples were made with varying polymer/DCTB ratios ([2.5–10 μL]/[2.5 μL] to ensure good signal/noise) and then spotted on a MALDI 96-well plate and air-dried. The data were analyzed using flexAnalysis. The MALDI-TOF/MS spectra shown represent the polymer distribution as well as a zoomed spectrum from the center of the curve unless otherwise noted.

iPrMgCl titration:¹ In a glovebox, a precise amount (10–20 mg) of salicylaldehyde phenylhydrazone was dissolved in a precise amount of THF (0.3–0.5 mL). For titration, iPrMgCl

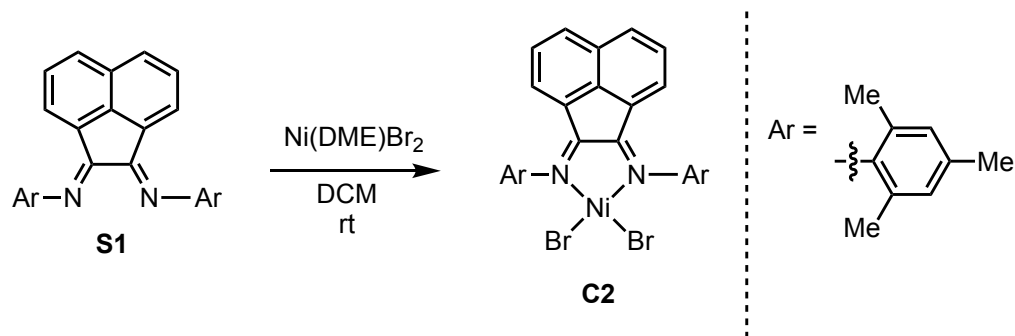
was added dropwise using a 100 μL syringe into the salicylaldehyde phenylhydrazone solution. Titration was complete when the solution turned bright orange.

A3.3 Synthetic Procedures

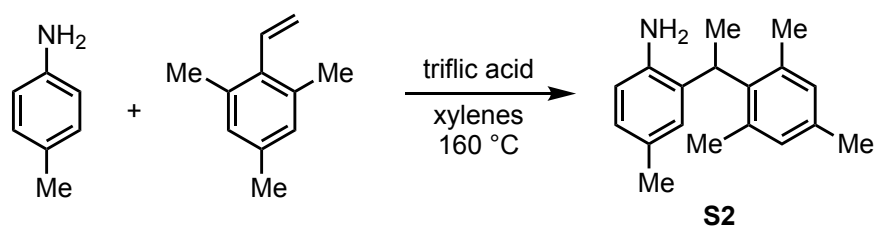


$\text{ArN}=(\text{An})=\text{NAr}$ (Ar = 2,4,6-trimethylphenyl, An = acenaphthylene) (**S1**).²

Acenaphthenequinone (100. mg, 0.549 mmol, 1.00 equiv) was added to a solution containing formic acid (11 μL , 0.29 mmol, 0.52 equiv) in MeOH (1.45 mL) in a 10 mL round-bottom flask equipped with a stir bar. Subsequently, 2,4,6-trimethylaniline (170 μL , 1.2 mmol, 2.2 equiv) was added to the stirring solution. After 18 h at rt, the reaction flask was placed in a $-20\text{ }^\circ\text{C}$ freezer where an orange solid precipitated from the solution over 24 h. The orange solid was collected via filtration over a fine frit, washed with cold MeOH (3 x 10 mL) and cold pentane (3 x 10 mL), then collected and dried under reduced pressure. The filtrate was transferred to a 100 mL round-bottom flask with DCM (10 mL), concentrated, re-dissolved in DCM (4 mL) filtered through glass wool and cooled to $-20\text{ }^\circ\text{C}$ to recrystallize. The orange solid was collected by filtration over a fine frit, washed with cold MeOH (3 x 10 mL) and cold pentane (3 x 10 mL), and dried under reduced pressure. The solids from each crystallization were combined, resulting in 174 mg of **S1** as an orange powder (76% yield). HRMS (ESI⁺): Calcd. for $\text{C}_{30}\text{H}_{28}\text{N}_2$ $[\text{M}+\text{H}]^+$ 417.2325; found 417.2326.

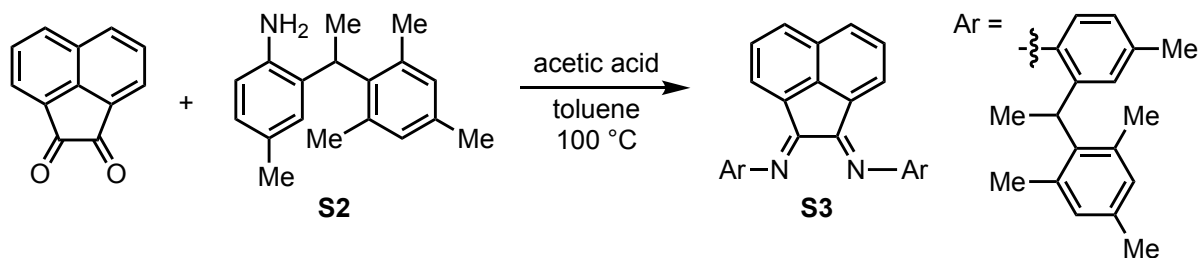


(ArN=(An)=NAr)NiBr₂ (Ar = 2,4,6-trimethylphenyl, An = acenaphthylene) (**C2**).² In a 50 mL round-bottom flask, **S1** (145 mg, 0.348 mmol, 1.00 equiv) was dissolved in DCM (9.5 mL). Then, Ni(DME)Br₂ (113 mg, 0.365 mmol, 1.05 equiv) was added and the reaction mixture was stirred for 20 h at rt. Overnight, a purple precipitate formed, which was collected by filtration over a fine frit and washed with cold MeOH (3 x 10 mL) and cold pentane (3 x 10 mL). The solid was collected and re-dissolved in DCM (3 mL), filtered through glass wool into a 20 mL vial, layered with pentanes (6 mL), and cooled to -20 °C. After 24 h, dark purple crystals were collected and washed with cold MeOH (3 x 10 mL) and cold pentanes (3 x 10 mL) to give 116 mg of **C2** as dark purple crystals (53% yield).

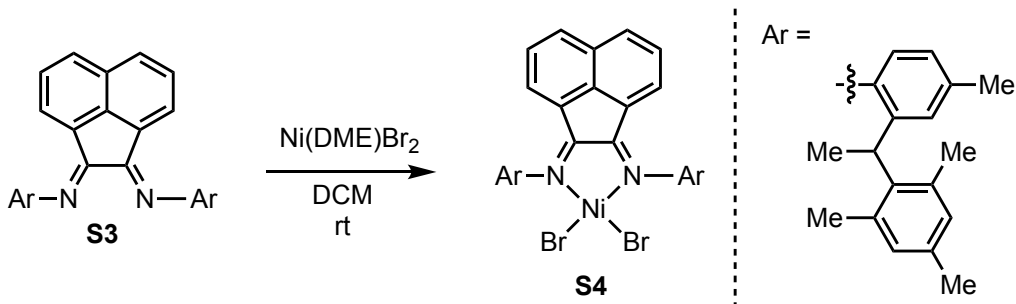


4-Methyl-2-(sec-(2,4,6-trimethylphenethyl)aniline (S2).³ To a 15 mL bomb flask equipped with a stir bar, *p*-toluidine (1.36 g, 12.7 mmol, 1.46 equiv) was dissolved in xylenes (1.1 mL). Subsequently, 2,4,6-trimethylstyrene (1.40 mL, 8.67 mmol, 1.00 equiv) and triflic acid (200. μL, 2.25 mmol, 0.260 equiv) were added to the reaction flask, which was sealed and placed behind a blast shield. After 17 h at 160 °C, the heterogeneous mixture was transferred to a 250 mL round-

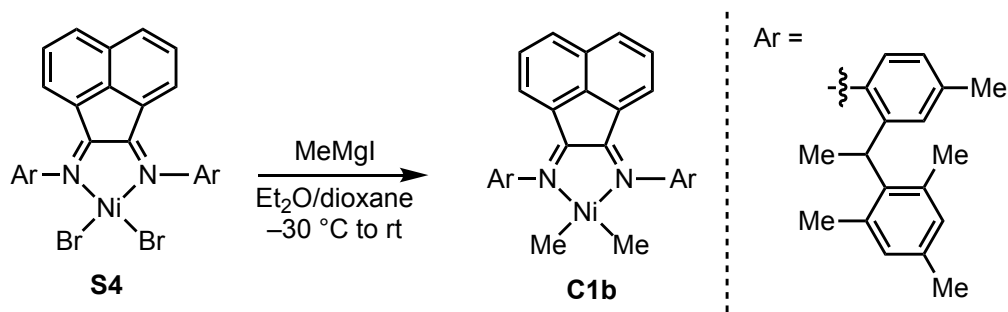
bottom flask with EtOAc (50 mL), concentrated, and purified via column chromatography on silica gel (100% hexanes to 80/20 hexanes/EtOAc) to give a brown oil which was recrystallized in 10/1 hexanes/EtOAc, yielding 1.25 g of **S2** as a white solid (57% yield). HRMS (ESI+): Calcd. for C₁₈H₂₃N [M+H]⁺ 254.1903; found 254.1899.



Rac-ArN=(An)=NAr (Ar = 4-methyl-2-(sec-(2,4,6-trimethylphenethyl))phenyl; An = acenaphthylene) (**S3**).³ To a 20 mL vial equipped with a stir bar, acenaphthenequinone (438 mg, 2.41 mmol, 0.490 equiv) and amine **S2** (1.25 mg, 4.92 mmol, 1.00 equiv.) were dissolved in toluene (2.8 mL) and glacial acetic acid (5.5 mL, 96 mmol, 19 equiv). After 3 h at 100 °C, the resulting heterogeneous mixture was filtered over a fine frit, washed with cold MeOH (3 x 10 mL) and cold hexanes (3 x 10 mL) and dried under reduced pressure, to give 1.13 g of **S3** as a yellow powder (72% yield). HRMS (ESI+): Calcd. for C₄₈H₄₈N₂ [M+H]⁺ 653.3890; found 653.3897.



***Rac*-(ArN=(An)=NAr)NiBr₂** (Ar = 4-methyl-2-(sec-(2,4,6-trimethylphenethyl)-phenyl; An = acenaphthylene) (**S4**).³ In a 50 mL Schlenk flask equipped with a stir bar, Ni(DME)Br₂ (156 mg, 0.505 mmol, 1.10 equiv.) and diimine **S3** (300. mg, 0.460 mmol, 1.00 equiv) were dissolved in DCM (15 mL) and stirred at rt under N₂ for 16 h. Then, the dark maroon liquid was concentrated, dissolved in DCM (20 mL), filtered through a celite plug, layered with pentane (60 mL), and cooled to -20 °C. The resulting solid was collected by filtration over a coarse frit, washed with cold pentane (3 x 10 mL), and dried under reduced pressure to give 338 mg of **S4** as a dark maroon solid (90% yield).



***Rac*-(ArN=(An)=NAr)NiMe₂** (Ar = 4-methyl-2-(sec-(2,4,6-trimethylphenethyl)-phenyl; An = acenaphthylene) (**C1b**). In the glovebox, **S4** (300. mg, 0.340 mmol, 1.00 equiv) and diethyl ether (40 mL) were added to a 100 mL Schlenk flask equipped with a stirbar. The red suspension was cooled in the freezer (-30 °C) for 10 min. Then, MeMgI (2.6 M in Et₂O, 0.28 mL, 0.72 mmol, 2.2 equiv) was added dropwise at -30 °C. The red suspension immediately turned dark purple. The Schlenk flask was placed back in the freezer for 10 min. Then dioxane (2.7 mL,

0.043 mmol, 0.13 equiv) was added and stirred for 2 h at rt. Then, the solution was filtered through a frit, concentrated until ~10 mL remained. Pentanes (~10 mL) were added to the solution and then concentrated under reduced pressure until ~5 mL remained. The heterogeneous mixture was then filtered over a frit, washed with pentanes (3 x 5 mL) and dried under reduced pressure to yield **C1b** as a purple powder (130 mg, 52%).

A3.4 NMR Spectra

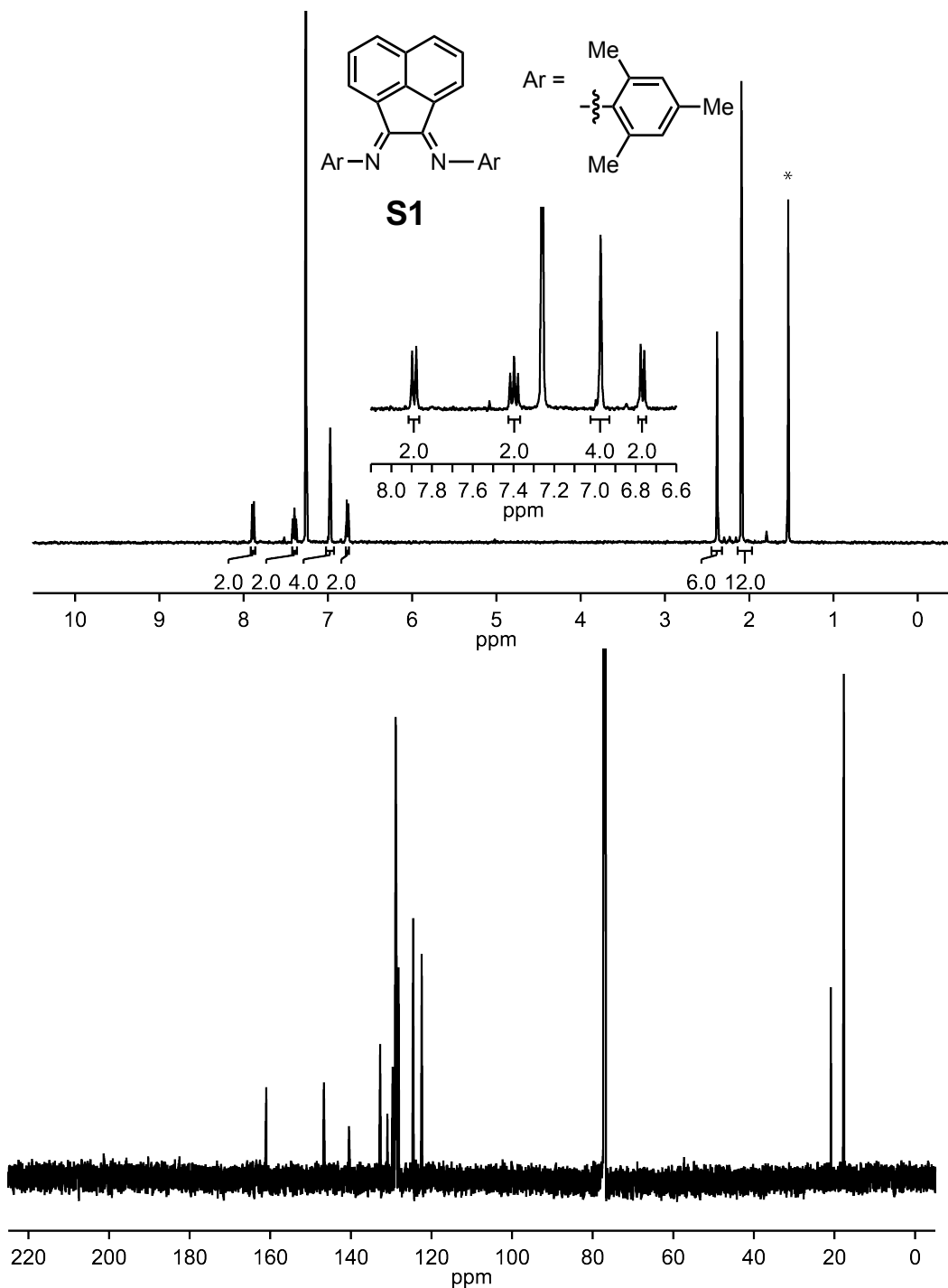


Figure A3-1. ^1H and ^{13}C NMR Spectra of **S1**. ^1H NMR (400 MHz, CDCl_3) δ 7.87 (d, $J = 8.3$ Hz, 2H), 7.38 (t, $J = 7.3$ Hz, 2H), 6.96 (s, 4H), 6.75 (d, $J = 7.3$ Hz, 2H), 2.36 (s, 6H), 2.07 (s, 12H). ^{13}C NMR (176 MHz, CDCl_3) δ 161.01, 146.73, 140.50, 132.76, 130.96, 129.67, 128.88, 128.72, 128.19, 124.55, 122.44, 20.92, 17.70.

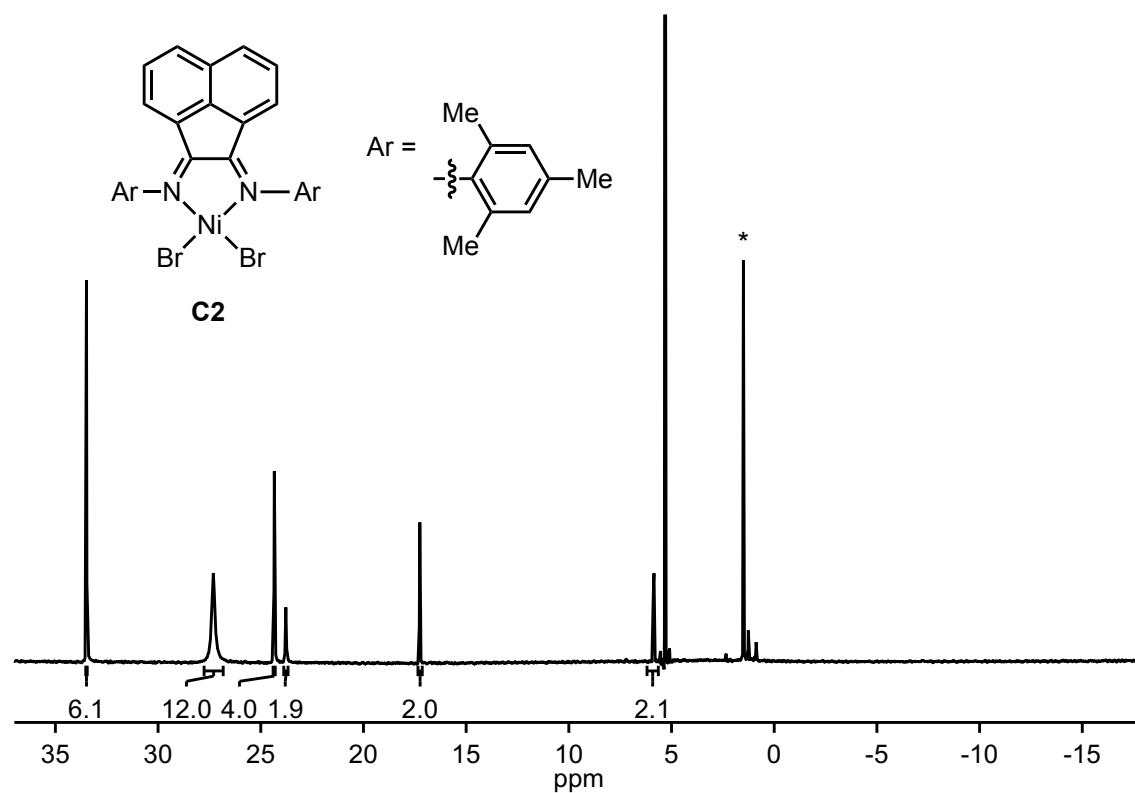


Figure A3-2. ^1H NMR Spectrum of **C2**. ^1H NMR (400 MHz, CD_2Cl_2 , rd = 0.005 s, at = 0.05 s) δ 33.77 (s, 6H), 27.54 (s, 12H), 24.49 (s, 4H), 23.93 (s, 2H), 17.35 (d, $J = 7.9$ Hz, 2H), 5.85 (s, 2H).

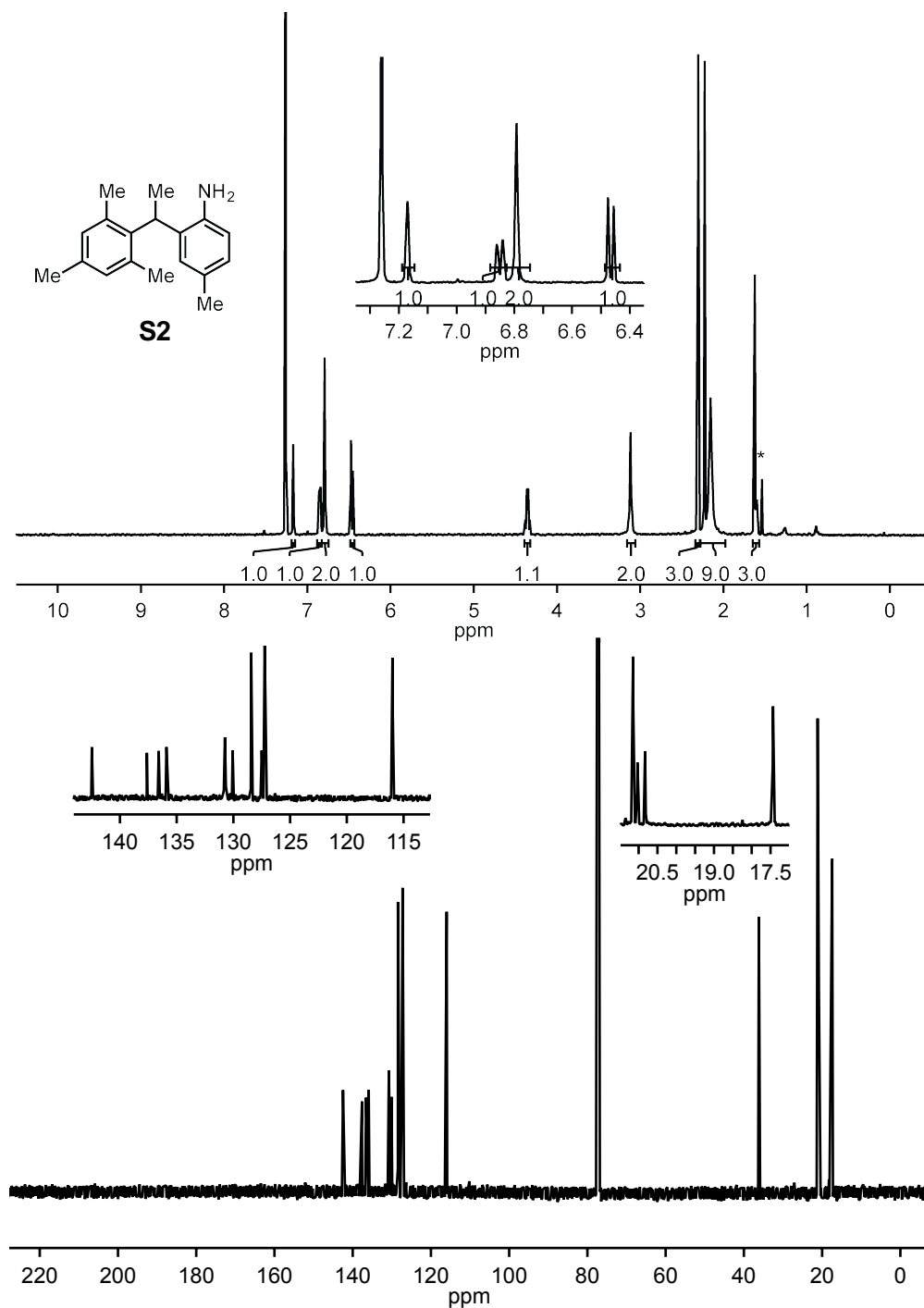


Figure A3-3. ¹H and ¹³C NMR Spectra of **S2**. ¹H NMR (500 MHz, CDCl₃) δ 7.17 (s, 1H), 6.85 (dd, *J* = 7.9, 1.9 Hz, 1H), 6.80 (s, 2H), 6.47 (d, *J* = 7.9 Hz, 1H), 4.35 (q, *J* = 7.3 Hz, 1H), 3.12 (s, 2H), 2.30 (s, 3H), 2.19 (overlapping peaks, 9H), 1.61 (d, *J* = 7.3 Hz, 3H). ¹³C NMR (126 MHz, CDCl₃) δ 142.48, 137.63, 136.58, 135.90, 130.75, 130.07, 128.43, 127.50, 127.24, 115.98, 36.17, 21.15, 21.03, 20.83, 17.43.

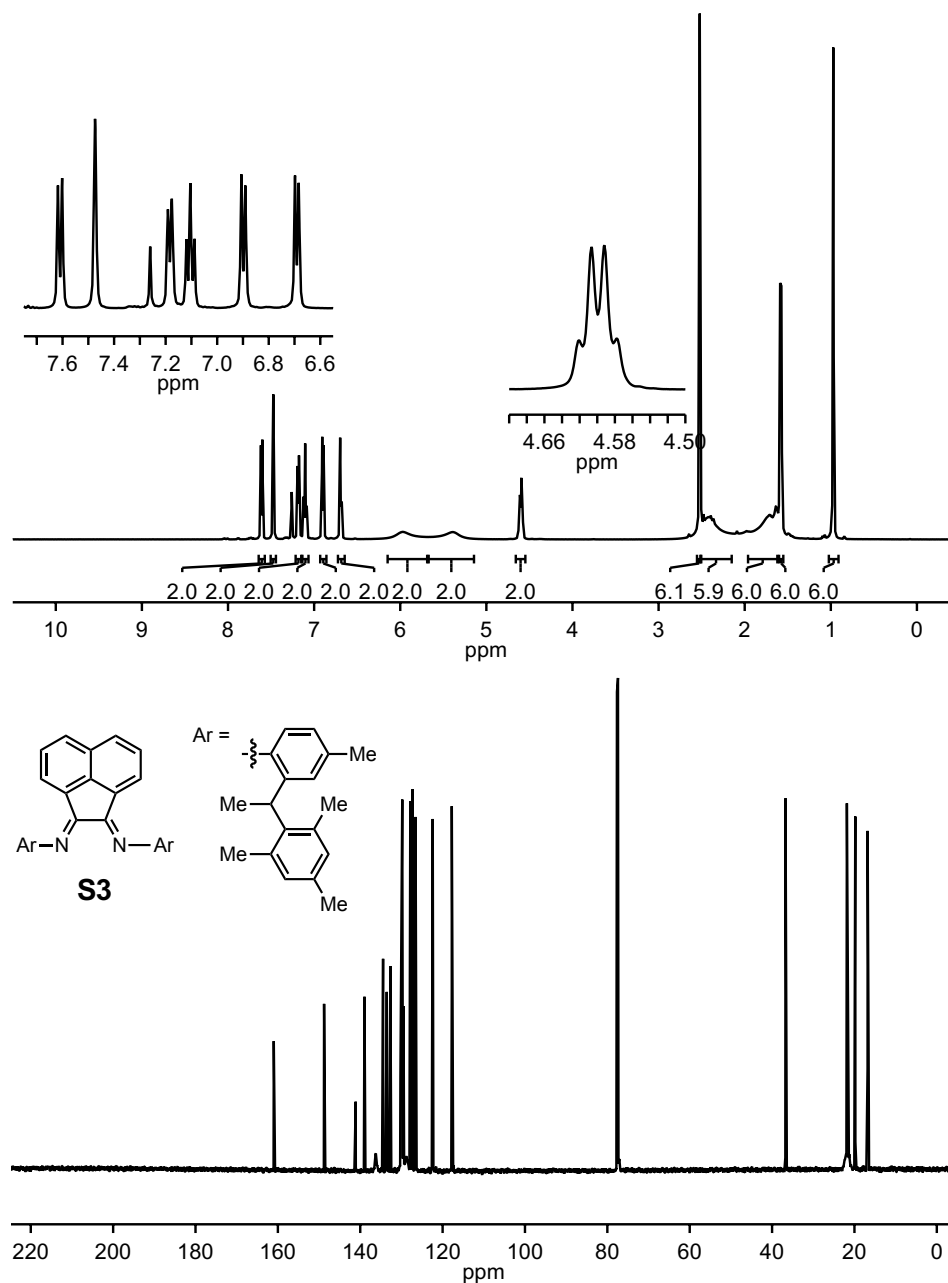


Figure A3-4. ^1H and ^{13}C NMR spectra of **S3**. ^1H NMR (500 MHz, CDCl_3) δ 7.61 (d, $J = 8.2$ Hz, 2H), 7.47 (s, 2H), 7.18 (d, $J = 7.7$ Hz, 2H), 7.10 (t, $J = 7.7$ Hz, 2H), 6.90 (d, $J = 7.8$ Hz, 2H), 6.69 (d, $J = 7.2$ Hz, 2H), 5.97 (br s, 2H), 5.39 (br s, 2H), 4.60 (q, $J = 7.4$ Hz, 2H), 2.52 (s, 6H), 2.41 (br s, 6H), 1.62 (br s, 6H), 1.58 (d, $J = 7.4$ Hz, 6H), 0.97 (s, 6H). ^{13}C NMR (126 MHz, CDCl_3) δ 161.00, 148.78, 141.11, 138.97, 136.22 (br), 134.46, 133.56, 132.70, 130.25, 129.80, 129.48, 128.78 (br), 127.85, 127.28, 126.57, 122.40, 117.77, 36.74, 21.84, 21.65 (br), 19.80, 16.80.

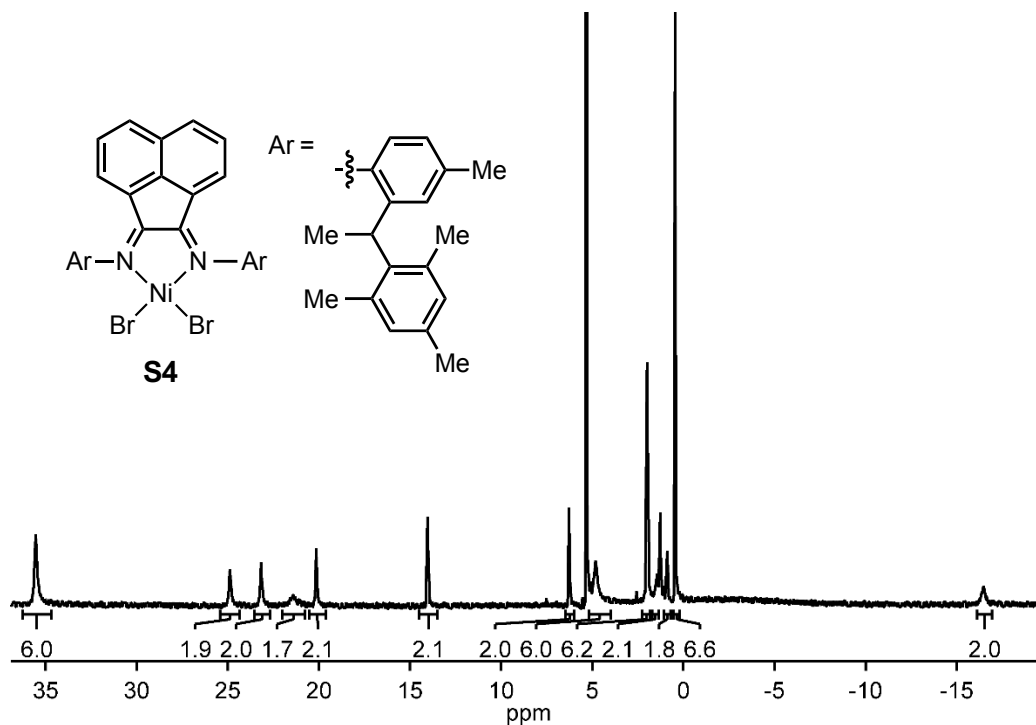
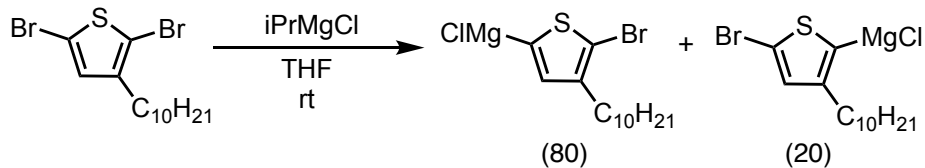


Figure A3-5. ^1H NMR Spectrum of **S4**. ^1H NMR (500 MHz, CD_2Cl_2) δ 35.53 (s, 6H), 24.88 (s, 2H), 23.17 (s, 2H), 21.45 (br s, 2H), 20.14 (s, 2H), 14.03 (s, 2H), 6.27 (s, 2H), 4.82 (br s, 6H), 1.99 (s, 6H), 1.44 (s, 2H), 0.87 (s, 2H), 0.45 (s, 6H), -16.43 (br s, 2H). Unaccounted for hydrogens (6H) due to peak broadening. Spectrum matches literature precedent.³

A3.5 Me-end capping experiments

A3.5.1 Precatalyst screen for ligand-switch



Monomer activation: In a glovebox, $i\text{PrMgCl}$ (2.2 M in THF, 204 μL , 0.448 mmol, 0.800 equiv) was added to a stirring solution of DB3DT (214.0 mg, 0.5599 mmol, 1.000 equiv) in THF (5.40 mL) and stirred for 30 min at rt.

Preparing precatalysts:

$\text{Ni}(\text{dppp})\text{Cl}_2$: $\text{Ni}(\text{dppp})\text{Cl}_2$ (5.5 mg, 0.0101 mmol) was weighed into a 4 mL vial with a stirbar.

$\text{Ni}(\text{IPr})(\text{PPh}_3)\text{Cl}_2$: $\text{Ni}(\text{IPr})(\text{PPh}_3)\text{Cl}_2$ (5.5 mg, 0.0071 mmol) was weighed into a 4 mL vial and dissolved in THF (0.71 mL) for an overall concentration of 0.01 M.

$\text{Pd}(\text{IPr})(3\text{-Clpyr})\text{Cl}_2$: $\text{Pd}(\text{IPr})(3\text{-Clpy})\text{Cl}_2$ (5.0 mg, 0.0074 mmol) was weighed into a 4 mL vial and dissolved in THF (0.74 mL) for an overall concentration of 0.01 M.

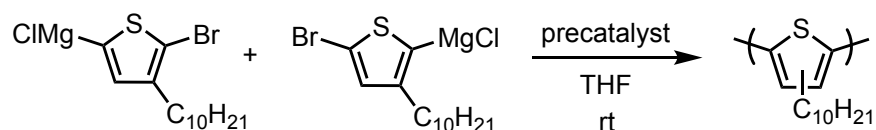
$\text{Pd}(\text{IPent})(3\text{-Clpyr})\text{Cl}_2$: $\text{Pd}(\text{IPent})(3\text{-Clpy})\text{Cl}_2$ (2.6 mg, 0.0033 mmol) was weighed into a 4 mL vial and dissolved in THF (0.33 mL) for an overall concentration of 0.01 M.

Preparing M(0) scavenger stock solution: 5,5'-Dibromo-2,2'-bithiophene (128 mg, 0.396 mmol) was dissolved in THF (5.27 mL) in a 4 mL vial for an overall concentration of 0.075 M.

End-capping experiment vials:

End-capping experiment vials: 5,5'-Dibromo-2,2'-bithiophene (0.075 M in THF, 0.80 mL, 0.060 mmol, 150 equiv – relative to the catalyst that will be added to this vial) and THF (0.36 mL) were added to a 20 mL vial equipped with a stirbar.

Polymerizations:



Polymerization procedure for precatalysts Ni(IPr)(PPh₃)Cl₂, Pd(IPr)(3-Clpyr)Cl₂, and Pd(IPent)(3-Clpyr)Cl₂: In a glovebox, to a 20 mL vial equipped with a stirbar was added THF (3.57 mL), Grignard monomer solution (0.080 M in THF, 0.50 mL, 0.040 mmol, 25 equiv), and precatalyst (0.01 M in THF, 0.160 mL, 0.00160 mmol, 1.00 equiv) and stirred at rt for the following times Ni(IPr)(PPh₃)Cl₂ (5 min), Pd(IPr)(3-Clpyr)Cl₂ (15 min), and Pd(IPent)(3-Clpyr)Cl₂ (30 min).

Polymerization procedure for precatalyst Ni(dppp)Cl₂: In a glovebox, Ni(dppp)Cl₂ (5.5 mg, 0.010 mmol) was preinitiated by stirring with activated monomer (0.08 M in THF, 0.379 mL, 0.0303 mmol, 3.0 equiv) for 60 s. The preactivated catalyst solution ([Ni] = 0.027 M in THF, 0.068 mL, 0.0018 mmol, 1.0 equiv) was added to a 20 mL vial equipped with a stirbar containing THF (3.50 mL) and Grignard monomer solution (0.080 M in THF, 0.50 mL, 0.040 mmol, 22 equiv) and stirred at rt for 30 min.

In situ end-capping: An aliquot (1.0 mL each containing 0.00040 mmol catalyst, *new* 1.0 equiv) was removed from the polymerization and added to the end-capping experiment reaction vial. Then MeMgI (0.24 M in Et₂O, 50. μL, 0.012 mmol, 30. equiv) was added (note that adding MeMgI after the polymer was added was necessary to avoid forming a white precipitate, which forms if MeMgI is stirred in THF in the absence of catalyst). The remaining polymerization solution was removed from the glovebox, quenched with aq. HCl (12 M, 2 mL), and worked up for analysis by GC, GPC, and MALDI-TOF/MS analysis (see general experimental). Unless otherwise noted, the end-capping experiment reactions were stirred for 1 h (the end-capping reaction with Ni(dppp)Cl₂ was stirred for 14 h) before quenching outside the glovebox with aq. HCl (12 M, 1 mL) and working up for GPC and MALDI-TOF/MS.

Table A3-1. GC data from the polymerization of 3-decylthiophene at rt via Ni and Pd precatalysts before end-capping experiments.

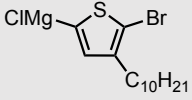
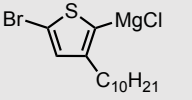
	 (% conv.)	 (% conv.)
Ni(dppp)Cl ₂	72	0
Ni(IPr)(PPh ₃)Cl ₂	quant.	quant.
Pd(IPr)(3-Clpyr)Cl ₂	quant.	49
Pd(IPent)(3-Clpyr)Cl ₂	71	33

Table A3-2. GPC data from the polymerization of 3-decylthiophene at rt via Ni and Pd precatalysts before and after end-capping experiments.

	before end-capping		after end-capping	
	M_n (kg/mol)	\mathcal{D}	M_n (kg/mol)	\mathcal{D}
Ni(dppp)Cl ₂	10.15	1.14	9.45	1.15
Ni(IPr)(PPh ₃)Cl ₂	8.42	1.17	8.94	1.15
Pd(IPr)(3-Clpyr)Cl ₂	7.34	1.18	7.38	1.24
Pd(IPent)(3-Clpyr)Cl ₂	5.26	1.35	4.73	1.76

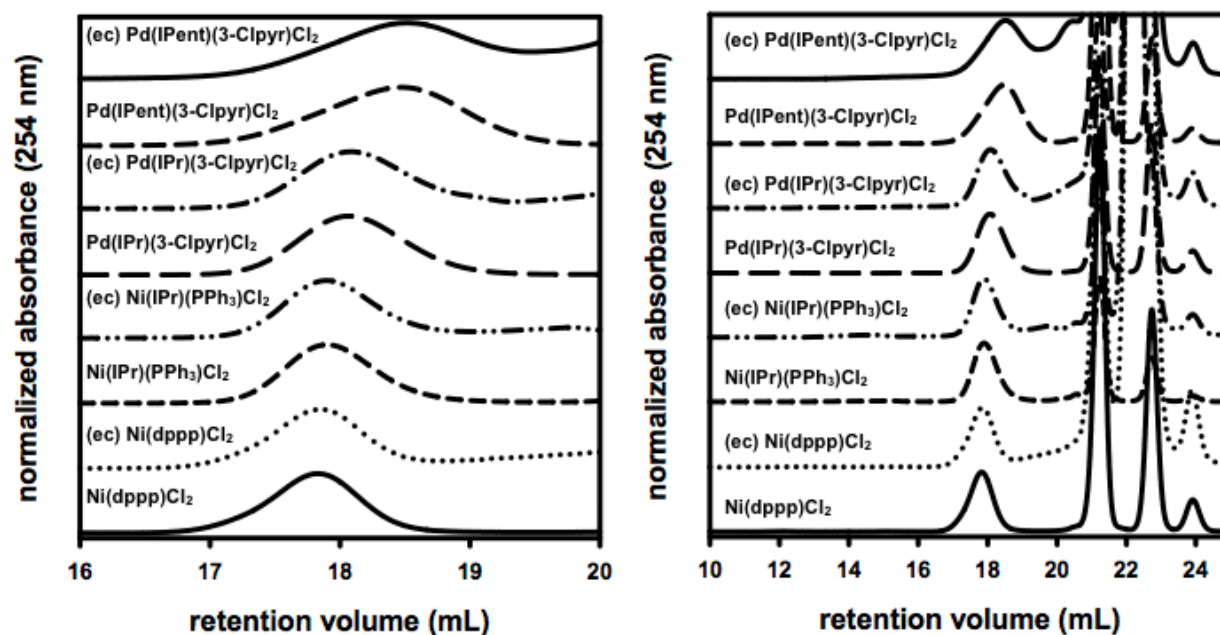


Figure A3-6. GPC data from the polymerization of 3-decylthiophene at rt via Ni and Pd precatalysts before and after end-capping experiments (ec). Zoomed (left) and full traces (right) of the same experiment. Note that M(0) scavenging agent and residual monomer elute from 20.5–22 min, PhMe elutes at 23.1 min, and BHT elutes at 23.8 min.

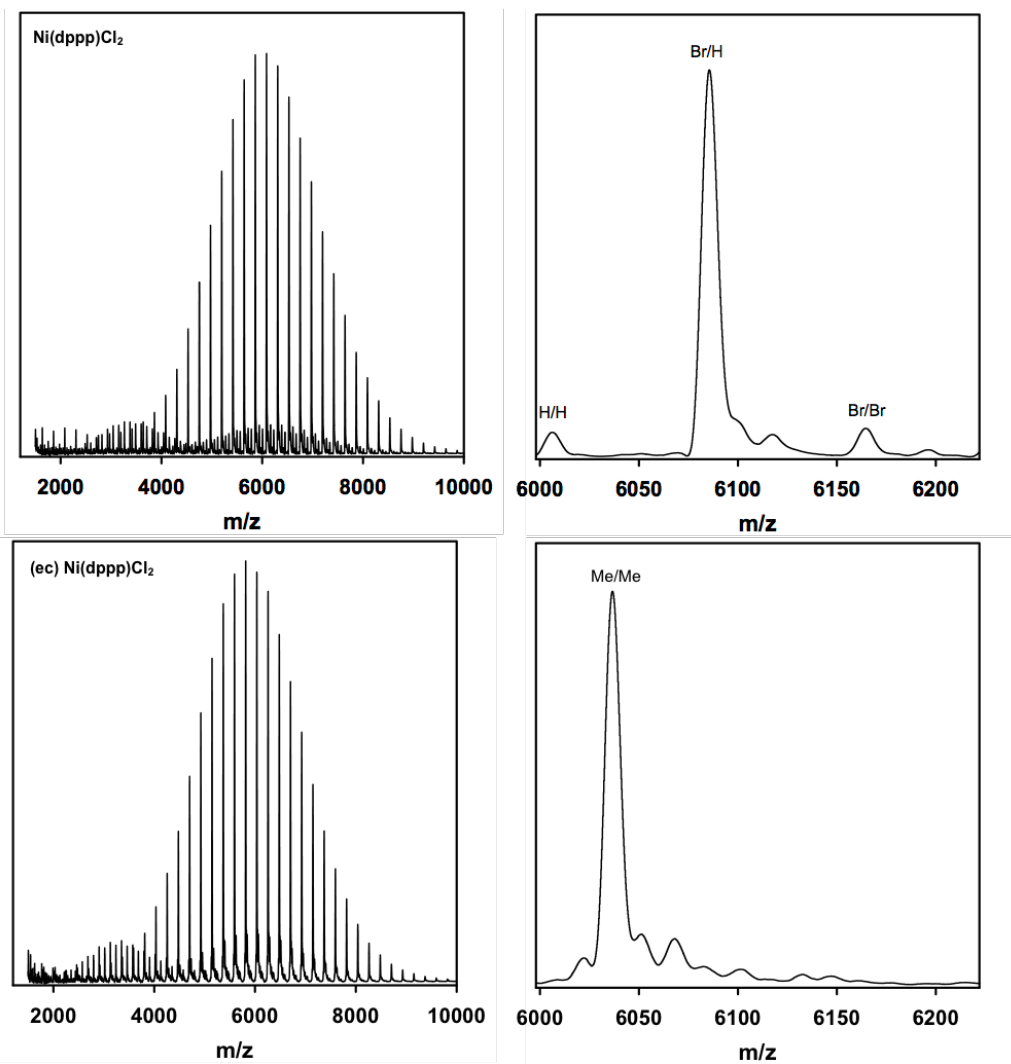


Figure A3-7. MALDI-TOF/MS spectra the polymerization of 3-decylthiophene at rt via Ni(dppp)Cl₂ before and after end-capping experiments (ec). Full trace (left) zoomed image (right). Values calculated using average mass method, signal-to-noise = 2. The degree of polymerization shown is 27.

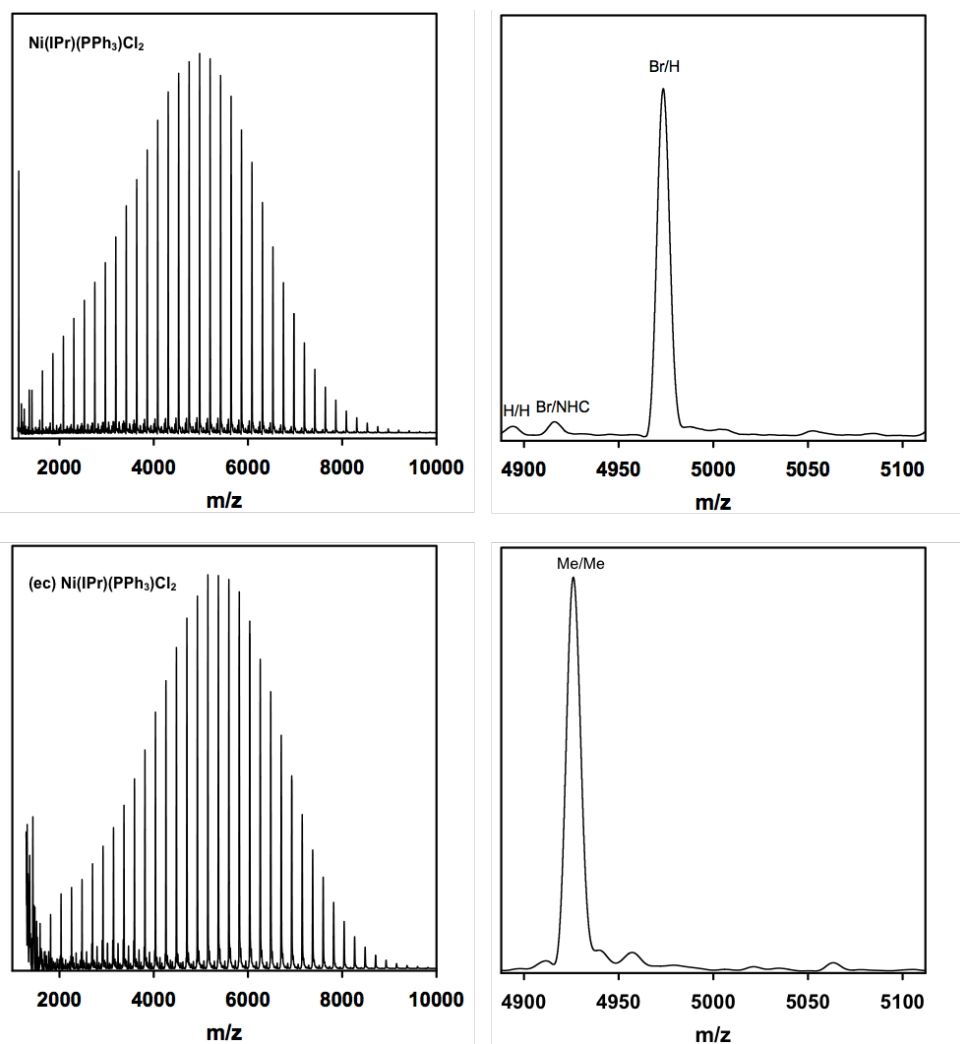


Figure A3-8. MALDI-TOF/MS spectra the polymerization of 3-decylthiophene at rt via Ni(IPr)(PPh₃)Cl₂ before and after end-capping experiments (ec). Full trace (left) zoomed image (right). Values calculated using average mass method, signal-to-noise = 2. The degree of polymerization shown is 22.

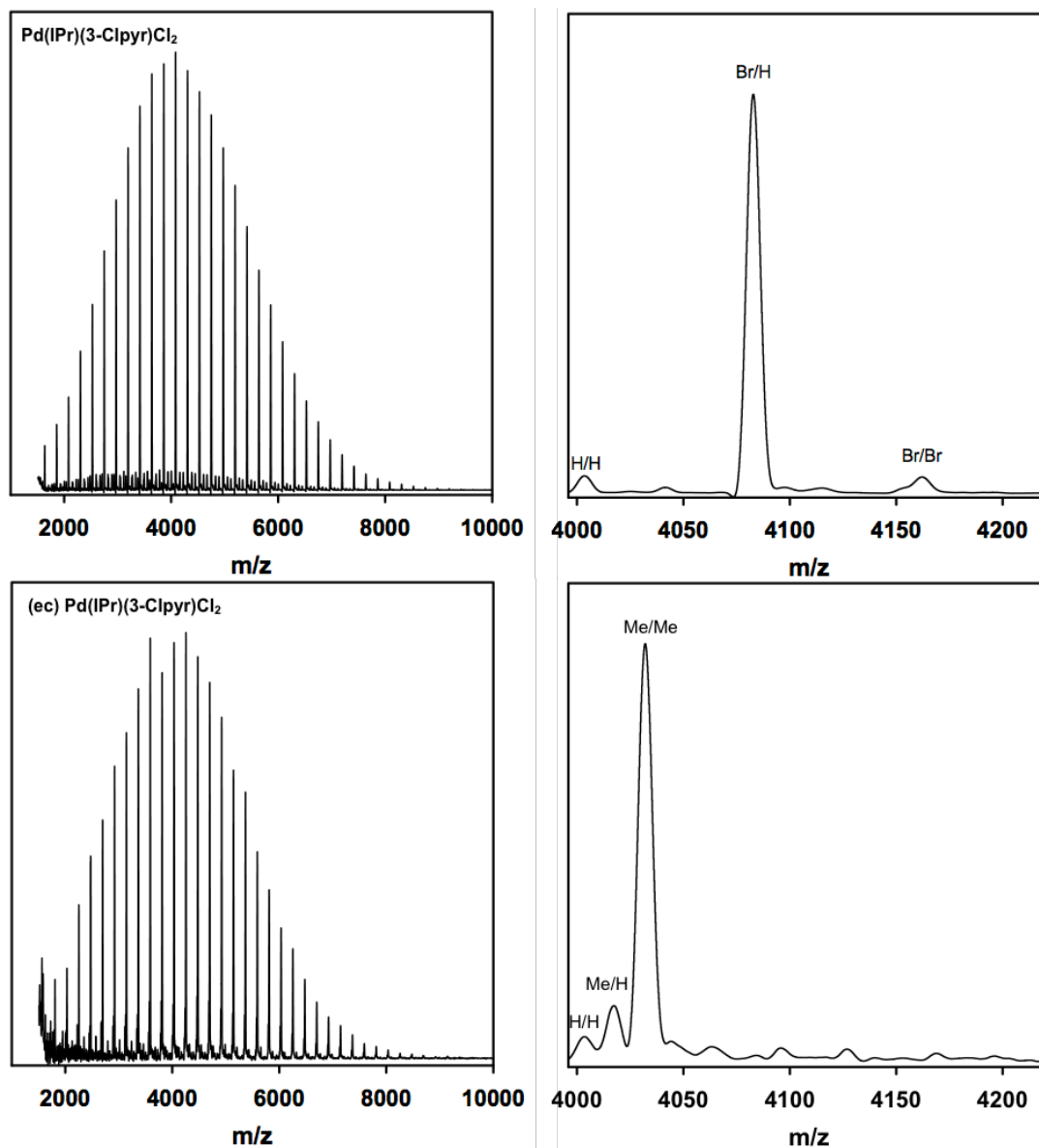


Figure A3-9. MALDI-TOF/MS spectra the polymerization of 3-decylthiophene at rt via Pd(IPr)(3-Clpyr)Cl₂ before and after end-capping experiments (ec). Full trace (left) zoomed image (right). Values calculated using average mass method, signal-to-noise = 2. The degree of polymerization shown is 18.

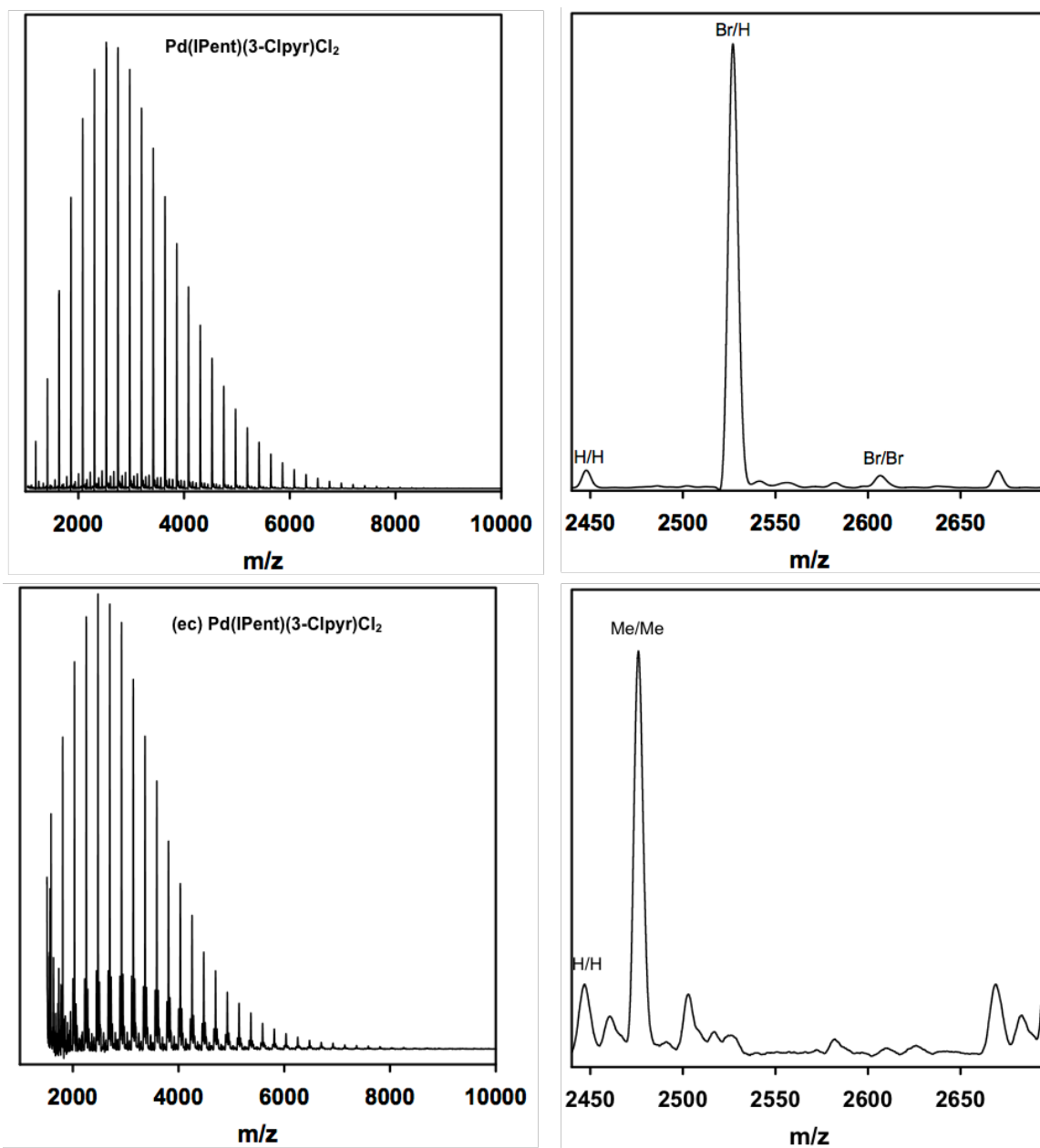
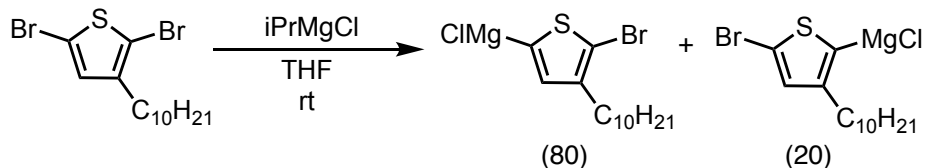


Figure A3-10. MALDI-TOF/MS spectra the polymerization of 3-decylthiophene at rt via $\text{Pd(IPent)(3-Clpyr)Cl}_2$ before and after end-capping experiments (ec). Full trace (left) zoomed image (right). Values calculated using average mass method, signal-to-noise = 2. The degree of polymerization shown is 11.

A3.5.2 Ligand Switch thiophene polymerization followed by end-capping



Monomer activation: In a glovebox, iPrMgCl (2.2 M in THF, 140. μ L, 0.307 mmol, 0.800 equiv) was added to a stirring solution of DB3DT (147 mg, 0.384 mmol, 1.00 equiv) in THF (3.7 mL) and stirred for 30 min at rt.

Preparing stock solutions:

C2: C2 (11.0 mg, 0.0173 mmol) was weighed into a 4 mL vial and dissolved in THF (1.73 mL) for an overall concentration of 0.01 M.

IPr: IPr (6.0 mg, 0.015 mmol) was weighed into a 4 mL vial and dissolved in THF (1.5 mL) for an overall concentration of 0.01 M.

PPh₃: PPh₃ (4.3 μ L, 0.016 mmol) was weighed into a 4 mL vial and dissolved in THF (1.6 mL) for an overall concentration of 0.01 M.

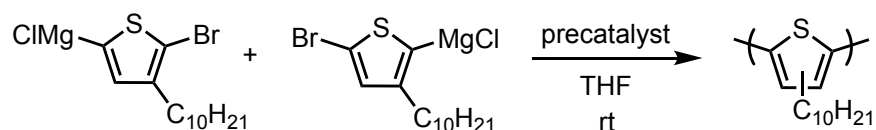
pyr: pyr (20 μ L, 0.248 mmol) was weighed into a 4 mL vial and dissolved in THF (2.28 mL) for an overall concentration of 0.1 M.

M(0) scavenger: 5,5'-Dibromo-2,2'-bithiophene (110.8 mg, 0.3419 mmol) was dissolved in THF (4.56 mL) in an 8 mL vial for an overall concentration of 0.075 M.

End-capping experiment vials:

End-capping experiment vials: 5,5'-Dibromo-2,2'-bithiophene (0.075 M in THF, 0.80 mL, 0.060 mmol, 150 equiv – relative to the catalyst that will be added to this vial) and THF (0.36 mL) were added to a 20 mL vial equipped with a stirbar.

Polymerizations:



Polymerization procedures:

C2 only: In a glovebox, to a 20 mL vial equipped with a stirbar was added THF (3.57 mL) and **C2** (0.01 M in THF, 0.160 mL, 0.00160 mmol, 1.00 equiv) and stirred for 15 min (to be consistent with the following reactions). Then, Grignard monomer solution (0.080 M in THF, 0.50 mL, 0.040 mmol, 25 equiv) was added and stirred at rt for 6 min.

C2 and IPr only: In a glovebox, to a 20 mL vial equipped with a stirbar was added THF (3.38 mL), **C2** (0.01 M in THF, 0.160 mL, 0.00160 mmol, 1.00 equiv) and IPr (0.01 M in THF, 0.192 mL, 0.00192 mmol, 1.20 equiv) were combined and stirred for 15 min. Then, Grignard monomer solution (0.080 M in THF, 0.50 mL, 0.040 mmol, 25 equiv) was added and stirred at rt for 6 min.

C2, IPr, and PPh₃: In a glovebox, to a 20 mL vial equipped with a stirbar was added in the following order, THF (3.19 mL), **C2** (0.01 M in THF, 0.160 mL, 0.00160 mmol, 1.00 equiv), IPr (0.01 M in THF, 0.192 mL, 0.00192 mmol, 1.20 equiv), and PPh₃ (0.01 M in THF, 0.192 mL,

0.00192 mmol, 1.20 equiv) and stirred for 15 min. Then, Grignard monomer solution (0.080 M in THF, 0.50 mL, 0.040 mmol, 25 equiv) was added and stirred at rt for 6 min.

C2, IPr, and pyr: In a glovebox, to a 20 mL vial equipped with a stirbar was added in the following order, THF (3.36 mL), **C2** (0.01 M in THF, 0.160 mL, 0.00160 mmol, 1.00 equiv), pyr (0.1 M in THF, 0.0192 mL, 0.00192 mmol, 1.20 equiv), and IPr (0.01 M in THF, 0.192 mL, 0.00192 mmol, 1.20 equiv) and stirred for 15 min. Then, Grignard monomer solution (0.080 M in THF, 0.50 mL, 0.040 mmol, 25 equiv) was added and stirred at rt for 6 min.

C2, IPr, pyr, and 1-hexene: In a glovebox, to a 20 mL vial equipped with a stirbar was added in the following order, THF (2.86 mL), 1-hexene (0.5 mL, ~2500 equiv relative to Ni), **C2** (0.01 M in THF, 0.160 mL, 0.00160 mmol, 1.00 equiv), pyr (0.1 M in THF, 0.0192 mL, 0.00192 mmol, 1.20 equiv), and IPr (0.01 M in THF, 0.192 mL, 0.00192 mmol, 1.20 equiv) and stirred for 15 min. Then, Grignard monomer solution (0.080 M in THF, 0.50 mL, 0.040 mmol, 25 equiv) was added and stirred at rt for 6 min.

In situ end-capping:

An aliquot (1.0 mL containing 0.00040 mmol catalyst, 1.0 equiv) was removed from the polymerization and added to the end-capping experiment reaction vial. Then, MeMgI (0.24 M in Et₂O, 50. μ L, 0.012 mmol, 30. equiv) was added (note that adding MeMgI after the polymer was necessary to avoid forming a white precipitate, which forms if MeMgI is stirred in THF in the absence of catalyst). The remaining polymerization solution was removed from the glovebox, quenched with aq. HCl (12 M, 2 mL), and worked up for analysis by GC, GPC, and MALDI-

TOF/MS analysis (see general experimental). The end-capping experiments were stirred for 1 h before quenching outside the glovebox with aq. HCl (12 M, 1 mL) and working up for GPC and MALDI-TOF/MS.

Table A3-3. GC data from the polymerization of 3-decylthiophene to evaluate IPr ligand-switching effectiveness. GC data is acquired from the polymerizations before end-capping is done.

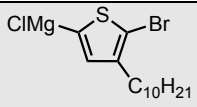
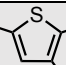
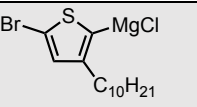
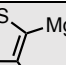
	 ClMg  Br C ₁₀ H ₂₁	 Br  MgCl C ₁₀ H ₂₁
	(% conv.)	(% conv.)
C2	quant.	quant.
C2 and IPr	quant.	quant.
C2, IPr, and PPh₃	quant.	quant.
C2, IPr, and pyr	84	49
C2, IPr, pyr, and 1-hexene	59	38

Table A3-4. GPC data from the polymerization of 3-decylthiophene to evaluate IPr ligand-switching effectiveness. GPC data is acquired from the polymerizations before and after end-capping is done.

	before end-capping		after end-capping	
	M_n (kg/mol)	\mathcal{D}	M_n (kg/mol)	\mathcal{D}
C2	9.99	1.72	8.58	1.68
C2 and IPr	11.04	1.92	8.88	1.82
C2, IPr, and PPh₃	5.64*	3.23*	5.01**	17.12**
C2, IPr, and pyr	5.52	1.22	4.29	1.23
C2, IPr, pyr, and 1-hexene	5.79	1.23	4.39	1.21

*bimodal or **trimodal GPC trace

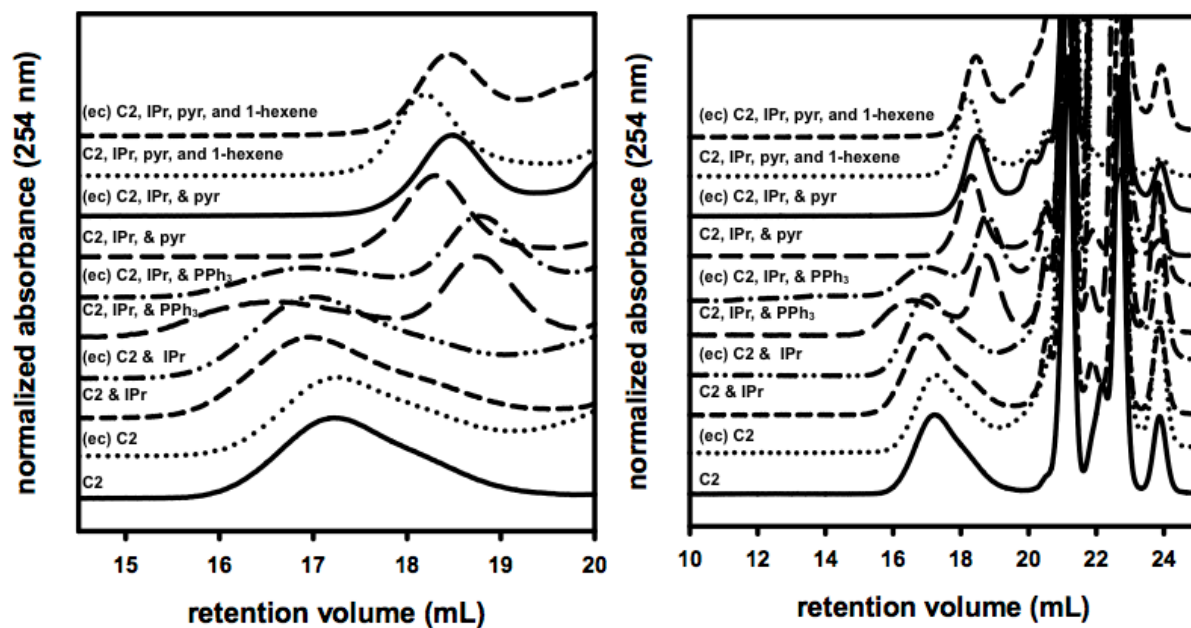


Figure A3-11. GPC data from the polymerization of 3-decylthiophene to evaluate IPr ligand-switching effectiveness before and after (ec) end-capping experiments. Zoomed (left) and full traces (right) of the same experiment. Note that M(0) scavenging agent and residual monomer elute from 20.5–22 min, PhMe elutes at 23.1 min and BHT elutes at 23.8 min.

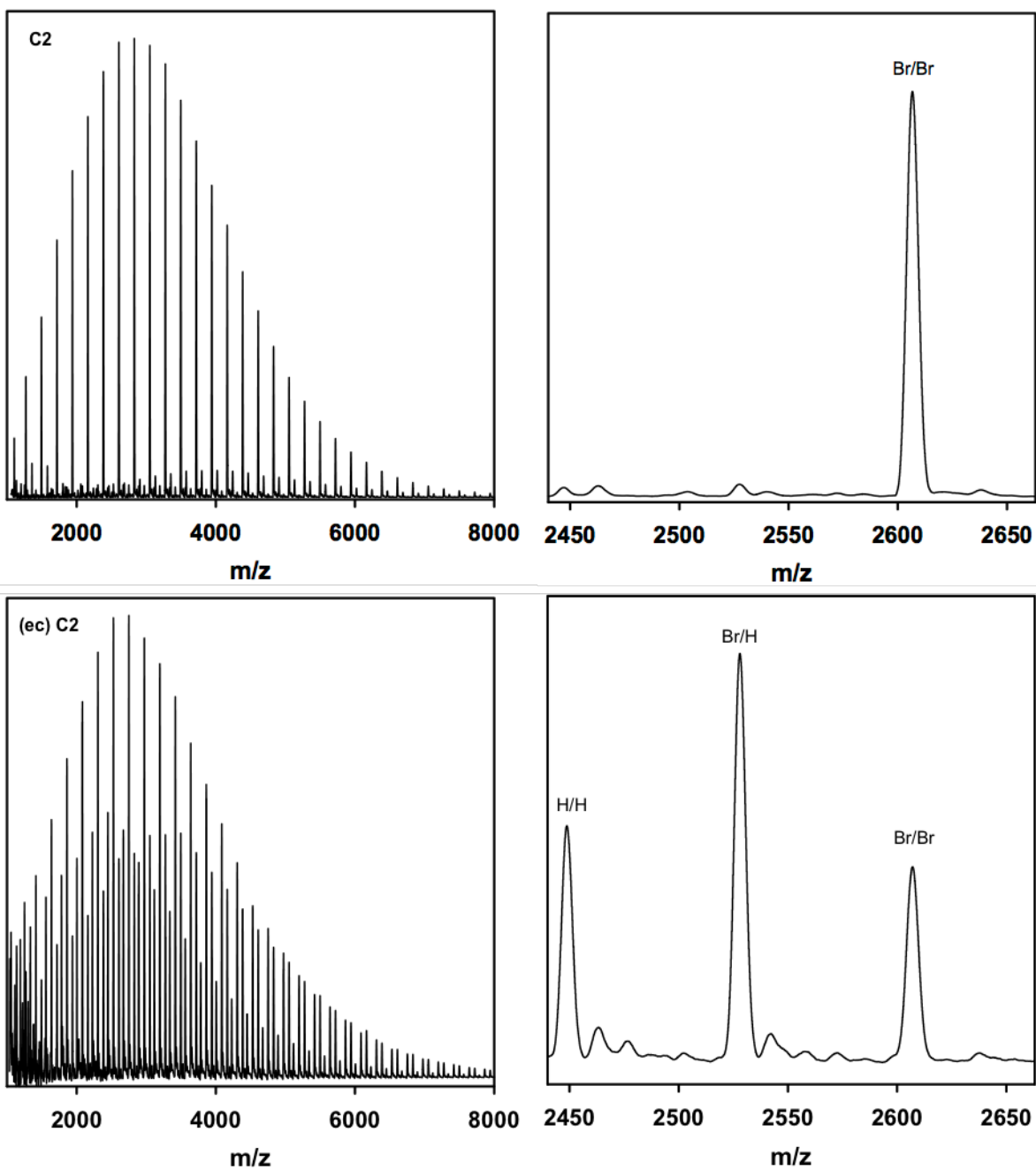


Figure A3-12. MALDI-TOF/MS data from the polymerization of 3-decylthiophene using precatalyst **C2** before and after (ec) end-capping experiments. Full traces (left) and zoomed (right) of the same experiment. Values calculated using average mass method, signal-to-noise = 2. The degree of polymerization shown is 11.

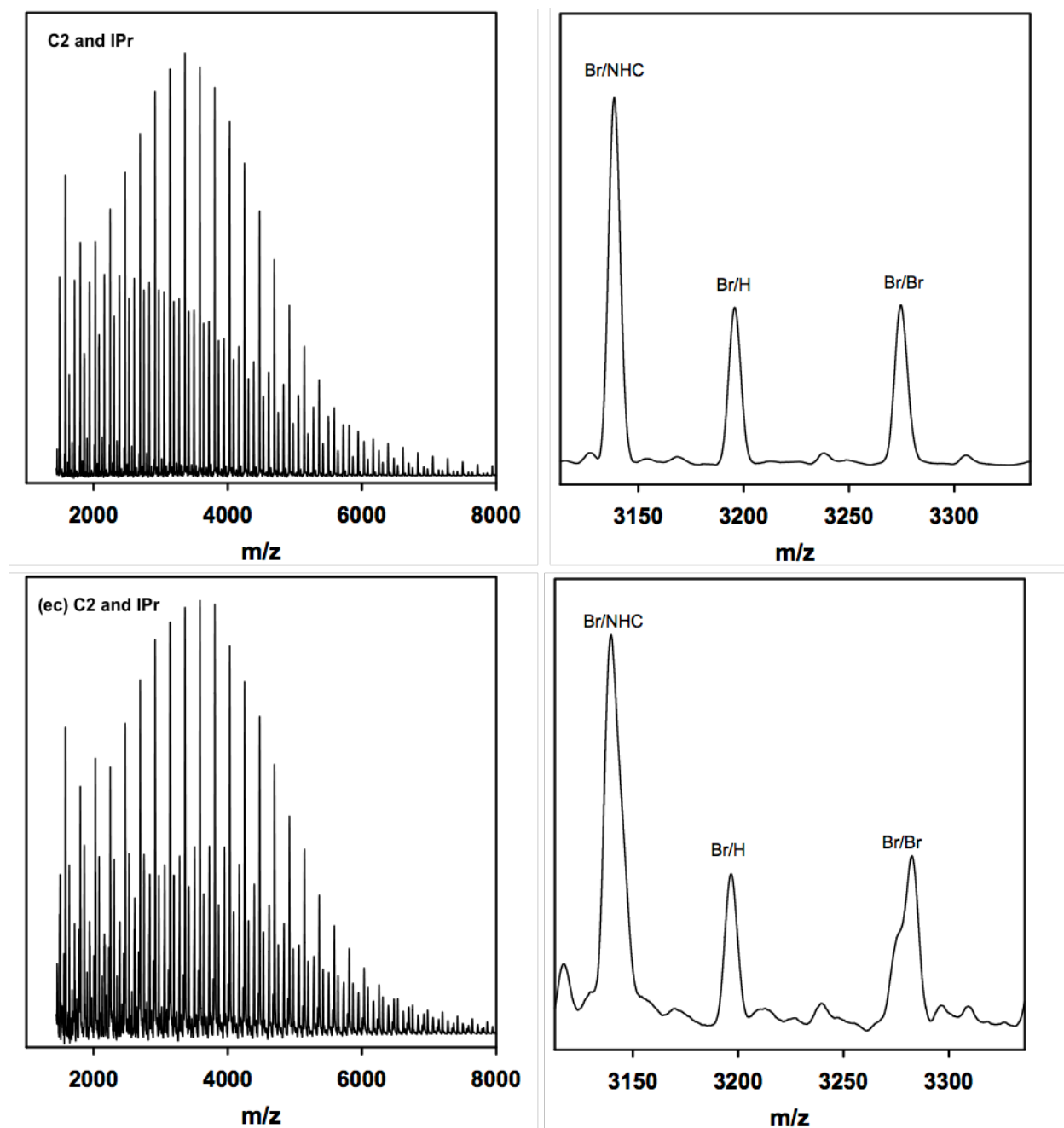


Figure A3-13. MALDI-TOF/MS data from the polymerization of 3-decylthiophene using precatalyst **C2** treated with IPr before and after (ec) end-capping experiments. Full traces (left) and zoomed (right) of the same experiment. Values calculated using average mass method, signal-to-noise = 2. The degree of polymerization shown is 14.

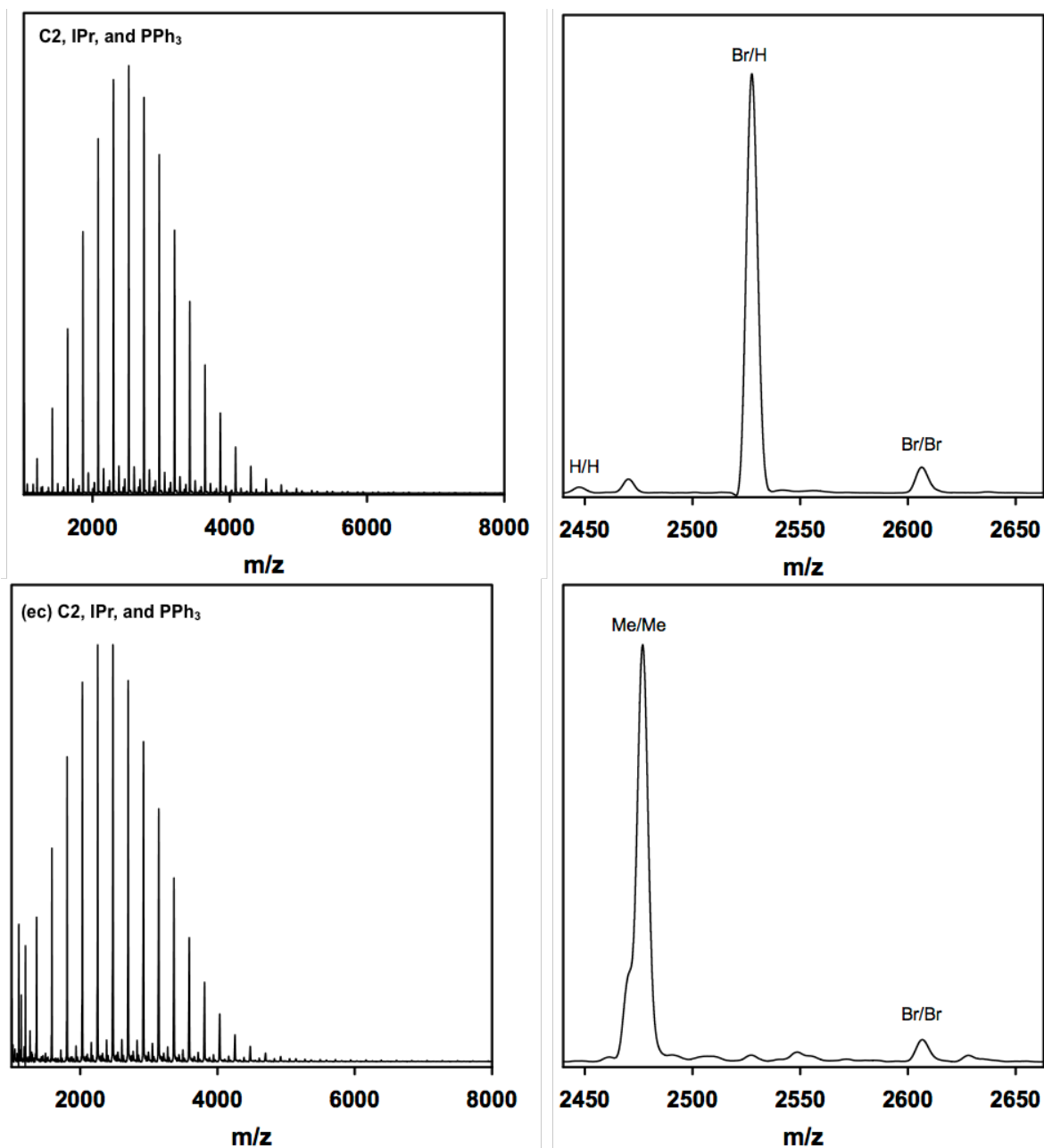


Figure A3-14. MALDI-TOF/MS data from the polymerization of 3-decylthiophene using precatalyst **C2** treated with IPr and PPh₃ before and after (ec) end-capping experiments. Full traces (left) and zoomed (right) of the same experiment. Values calculated using average mass method, signal-to-noise = 2. The degree of polymerization shown is 11. Note that the GPC trace indicates high molecular weight polymer was formed however these polymers did not ionize here.

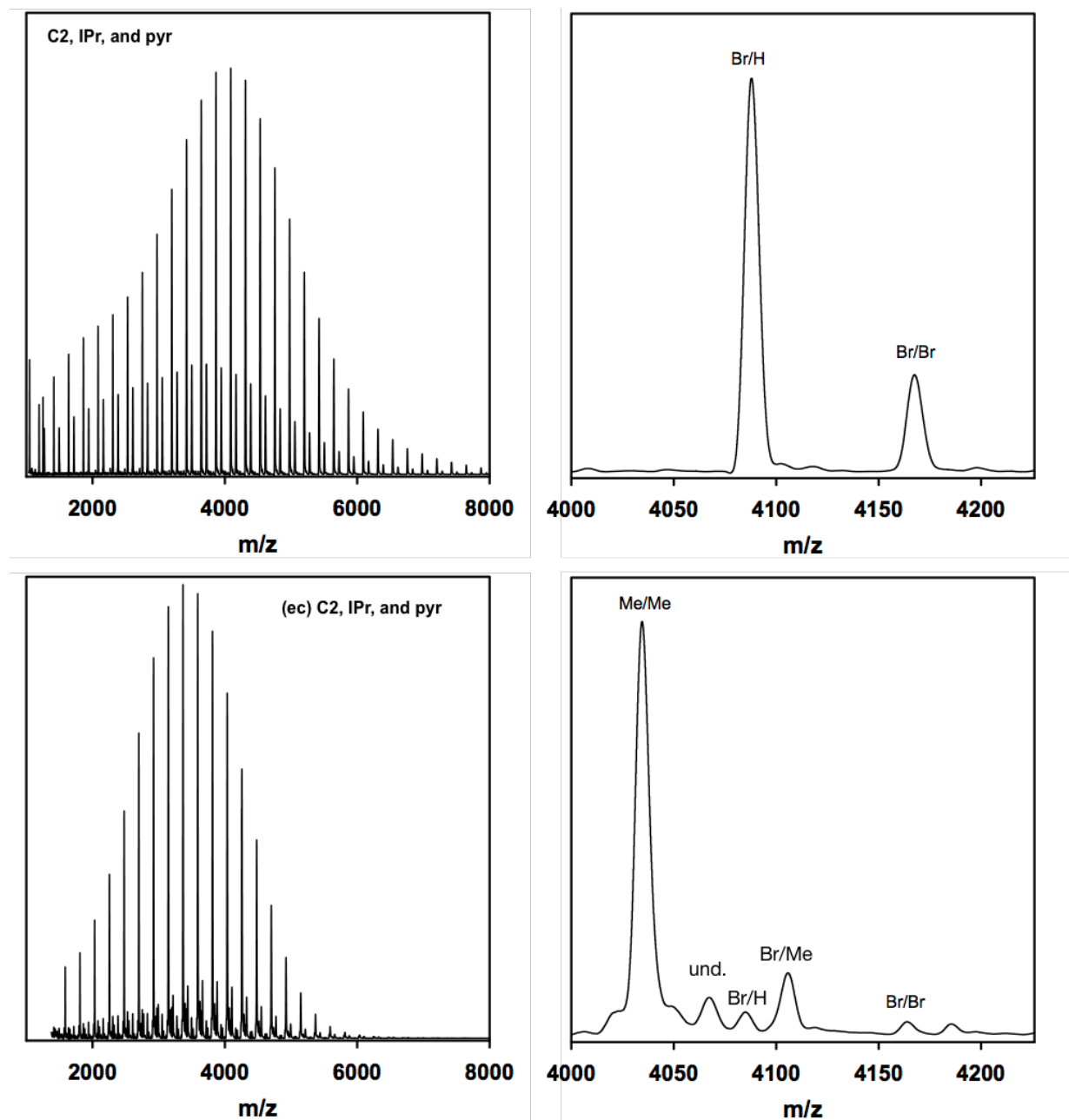


Figure A3-15. MALDI-TOF/MS data from the polymerization of 3-decylthiophene using precatalyst **C2** treated with pyr and IPr before and after (ec) end-capping experiments. Full traces (left) and zoomed (right) of the same experiment. Values calculated using average mass method, signal-to-noise = 2. The degree of polymerization shown is 18.

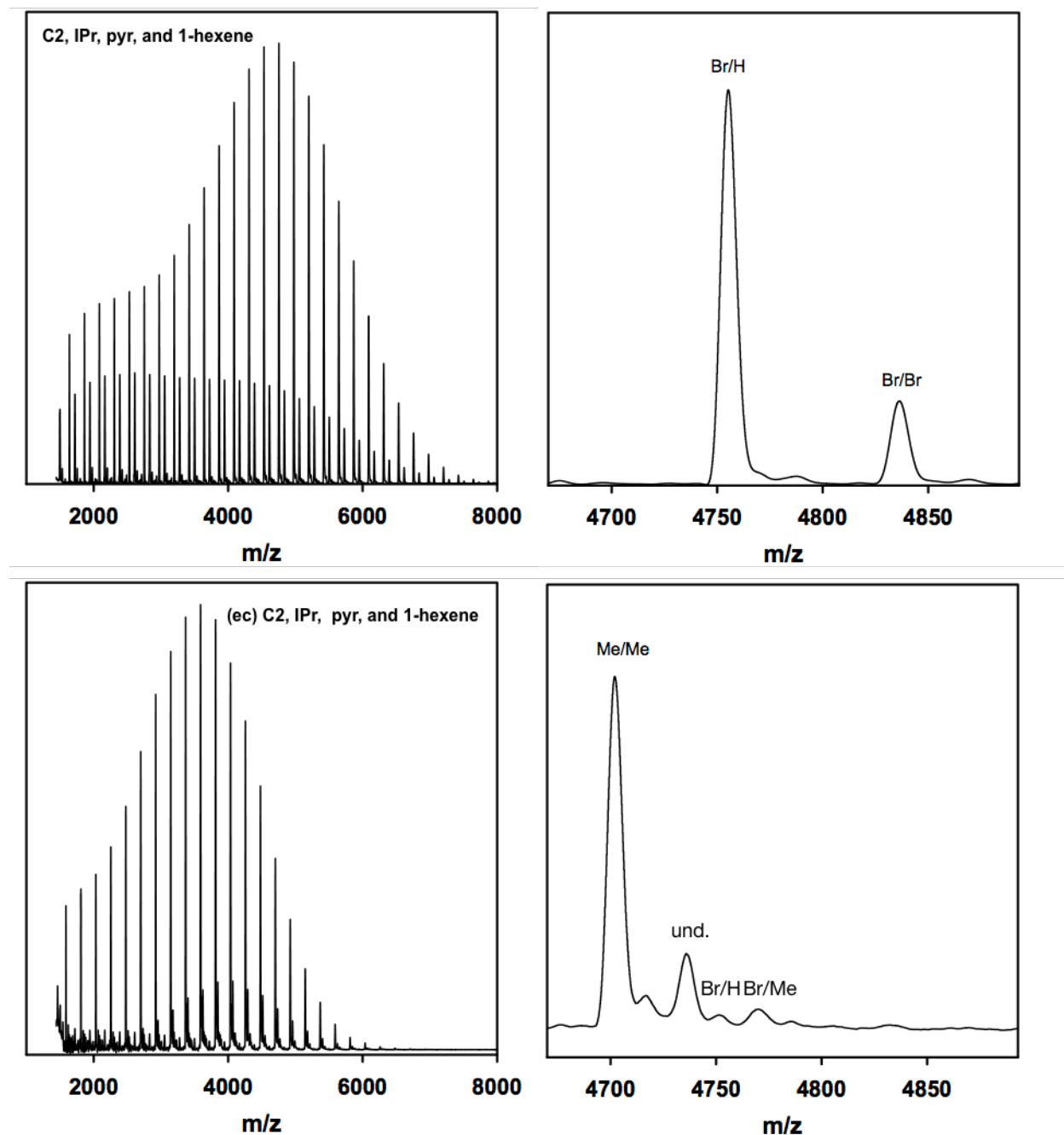


Figure A3-16. MALDI-TOF/MS data from the polymerization of 3-decylthiophene in the presence of 1-hexene using precatalyst **C2** treated with pyr and IPr before and after (ec) end-capping experiments. Full traces (left) and zoomed (right) of the same experiment. Values calculated using average mass method, signal-to-noise = 2. The degree of polymerization shown is 21.

A3.6. Attempting copolymerization



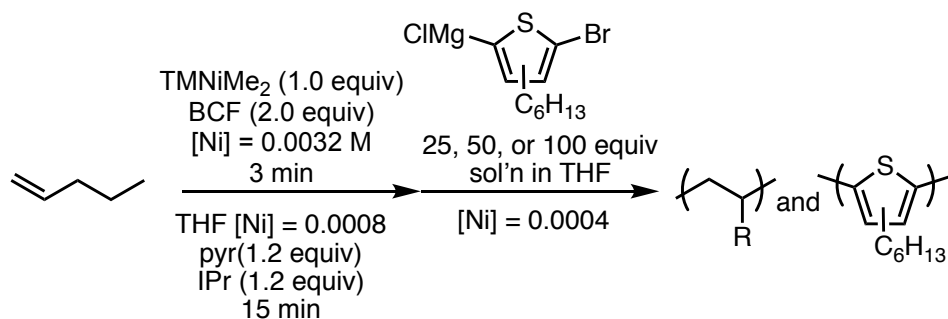
Thiophene monomer activation: In a 20 mL vial equipped with a stirbar, DB3HT (92.7 mg, 0.284 mmol, 1.00 equiv) was dissolved in THF (2.73 mL) and reacted with *i*PrMgCl (2.1 M in THF, 108 μ L, 0.227 mmol, 0.800 equiv) and stirred for 30 min at rt.

Preparing stock solutions:

*i*Pr (4.8 mg, 0.0012 mmol) was dissolved in THF (1.2 mL) for an overall concentration of 0.01M, which is stored in the freezer ($-30\text{ }^{\circ}\text{C}$).

Pyridine (20 μ L, 0.0248 mmol) was dissolved in THF (2.28 mL) for an overall concentration of 0.1M.

Tris(pentafluoro) borane (BCF, 14.0 mg, 0.0273 mmol) was dissolved in 1-pentene (3.79 mL) for an overall concentration of 0.0072 M, which was placed in the freezer ($-30\text{ }^{\circ}\text{C}$).



Macroinitiator synthesis:

Precatalyst **C1b** (8.2 mg, 0.011 mmol) was dissolved in 1-pentene (0.40 mL) and placed in the freezer ($-30\text{ }^\circ\text{C}$) for 2 min. Then, while both **C1b** and BCF were still cold, BCF (0.0072 M in 1-pentene, 3.06 mL, 0.0221 mmol, 2.00 equiv) was added to the stirring catalyst, which were stirred for 3 min at rt. Overall $[\text{Ni}] = 0.0032 \text{ M}$ in 1-pentene. Then, THF (10.42 mL) was added to stall the polymerization. Overall $[\text{Ni}] = 0.0008 \text{ M}$ in 1-pentene/THF (total volume = 13.88 mL). An aliquot (2.0 mL) was removed from the glovebox and immediately quenched with MeOH (5 mL).

Ligand-switch: To the remaining macroinitiator solution (0.0095 mmol Ni remain), pyr (0.1 M in THF, 114 μL , 0.0114 mmol, 1.20 equiv) and IPr (0.01 M in THF, 0.114 mL, 0.0114 mmol, 1.20 equiv) were added and stirred for 15 min at rt. Overall $[\text{Ni}] = 0.00072 \text{ M}$ in 1-pentene/THF (total volume = 13.13 mL).

Thiophene addition: Three aliquots (0.0072 M Ni in THF/1-pentene, 1.50 mL each, 0.00109 mmol Ni, *new* 1.00 equiv) from the ligand-switched macroinitiator solution were added to stirring Grignard thiophene monomer solutions and stirred for 1 h before quenching outside of the glovebox with aq. HCl (12 M, 2 mL) and working up for GPC and MALDI-TOF/MS.

Vial 1) thiophene monomer (0.08 M in THF, 0.34 mL, 0.027 mmol, 25 equiv) in THF (0.89 mL).

Vial 2) thiophene monomer (0.08 M in THF, 0.68 mL, 0.055 mmol, 50. equiv) in THF (0.54 mL).

Vial 3) thiophene monomer (0.08 M in THF, 1.36 mL, 0.109 mmol, 100. equiv).

Table A3-5. GC data from the ligand-switch copolymerization experiments.

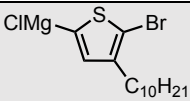
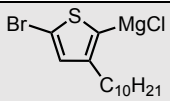
	 (% conv.)	 (% conv.)
Vial 1 (25 equiv thiophene)	6	0
Vial 2 (50 equiv thiophene)	19	4
Vial 3 (100 equiv thiophene)	20	6

Table A3-6. GPC data from the ligand-switch copolymerization experiments.

	before ligand-switch		after ligand switch	
	M_n (kg/mol)	\bar{D}	M_n (kg/mol)	\bar{D}
Poly(olefin) macroinitiator	21.10	1.31	21.27	1.33

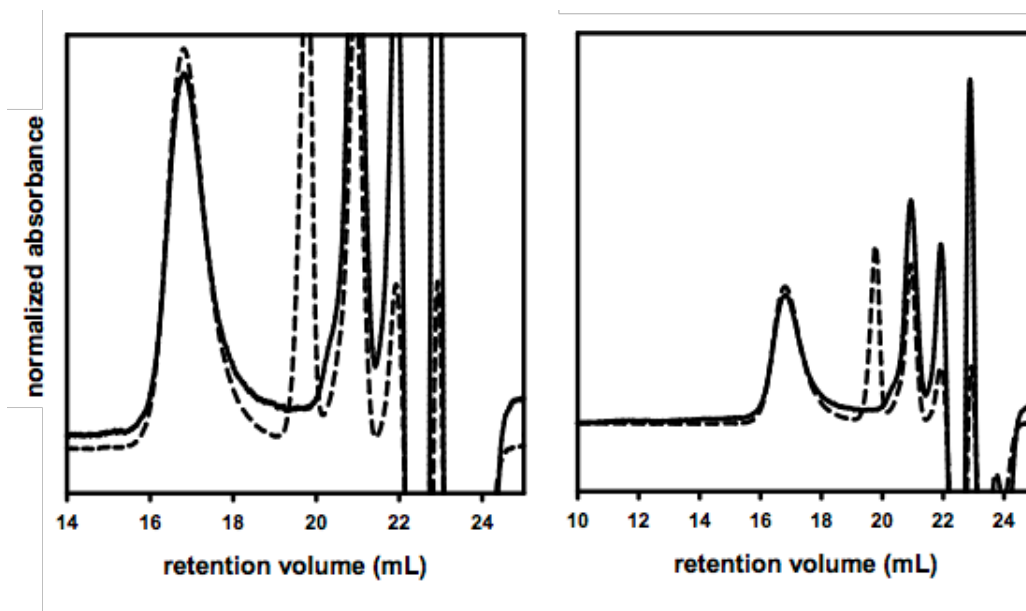


Figure A3-17. GPC data from the attempted ligand-switch copolymerization. Zoomed (left) and full traces (right) of the same experiment. The solid line represents poly(1-pentene) macroinitiator before ligand-switch. The dashed line line represents poly(1-pentene) macroinitiator after ligand-switch. The RI traces are shown, poly(olefin) does not absorb UV light. Note that BCF and residual monomer elute from 20.5–22 min, PhMe elutes at 23.1 min and BHT elutes at 23.8 min.

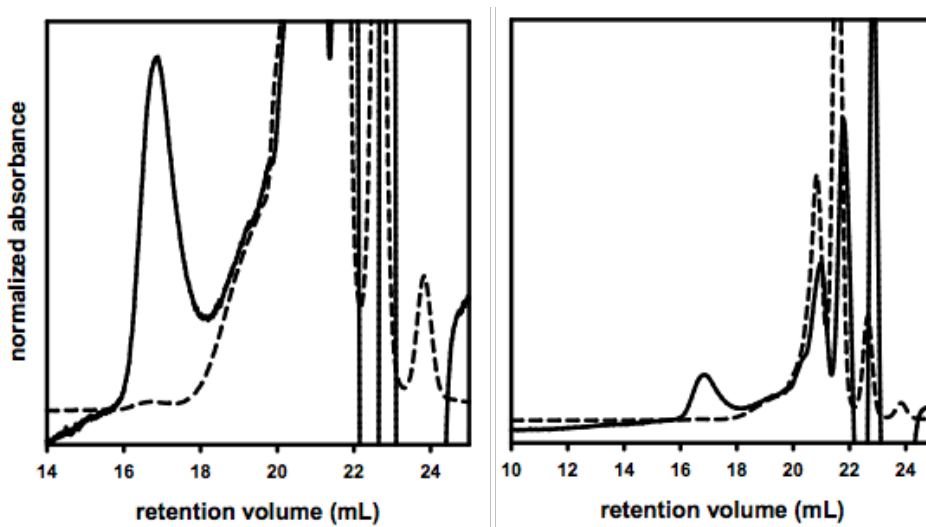


Figure A3-18. GPC data from the attempted ligand-switch copolymerization with thiophene monomer added (25 equiv.). Zoomed (left) and full traces (right) of the same experiment. The solid line represents the RI trace. The dashed line represents the UV trace. Note that BCF and residual monomer elute from 20.5–22 min, PhMe elutes at 23.1 min and BHT elutes at 23.8 min.

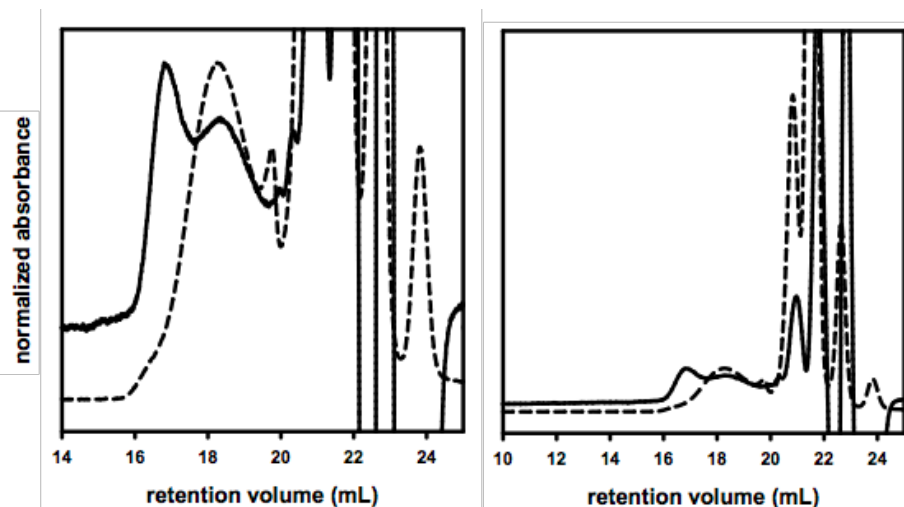


Figure A3-19. GPC data from the attempted ligand-switch copolymerization with thiophene monomer added (50 equiv.). Zoomed (left) and full traces (right) of the same experiment. The solid line represents the RI trace. The dashed line represents the UV trace. Note that BCF and residual monomer elute from 20.5–22 min, PhMe elutes at 23.1 min and BHT elutes at 23.8 min.

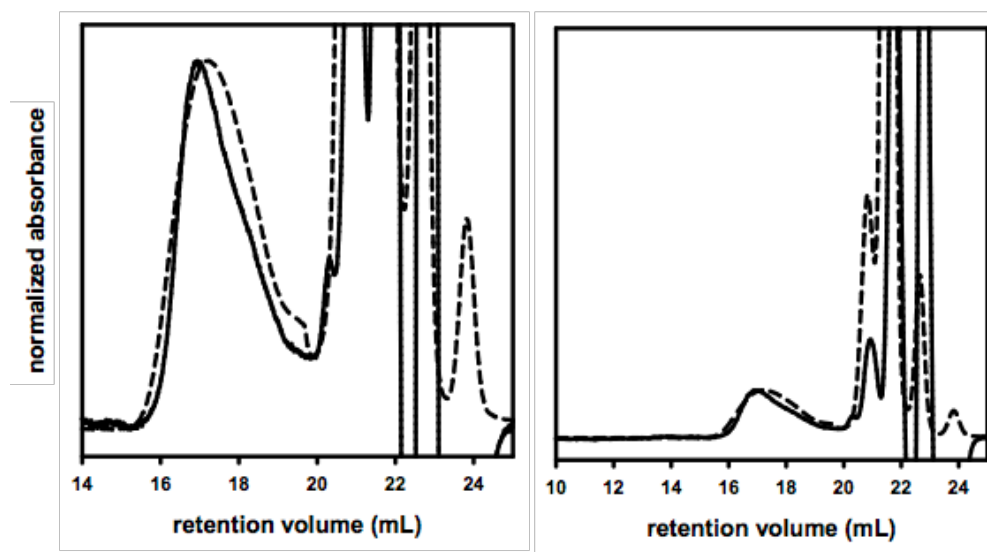


Figure A3-20. GPC data from the attempted ligand-switch copolymerization with thiophene monomer added (100 equiv.). Zoomed (left) and full traces (right) of the same experiment. The solid line represents the RI trace. The dashed line represents the UV trace. Note that BCF and residual monomer elute from 20.5–22 min, PhMe elutes at 23.1 min and BHT elutes at 23.8 min.

A3.7 References

- (1) Love, B. E.; Jones, E. G. The Use of Salicylaldehyde Phenylhydrazone as an Indicator for the Titration of Organometallic Reagents. *J. Org. Chem.* **1999**, *64*, 3755–3756.
- (2) McLain, S., J.; Feldman, J.; McCord, E., F.; Gardner, K. H.; Teasley, M. F.; Coughlin, E. B.; Sweetman, K. J. Addition Polymerization of Cyclopentene with Nickel and Palladium Catalysts. *Macromolecules* **1998**, *31*, 6705–6707.
- (3) Cherian, A. E.; Rose, J. M.; Lobkovsky, E. B.; Coates, G. W. A C₂-Symmetric, Living α -Diimine Ni(II) Catalyst: Regioblock Copolymers from Propylene. *J. Am. Chem. Soc.* **2005**, *127*, 13770–13771.